

Fundamental Modeling of Membrane Systems

Fundamental Modeling of Membrane Systems

Membrane and Process
Performance

Edited by

Patricia Luis



“To my daughters”

Elsevier

Radarweg 29, PO Box 211, 1000 AE Amsterdam, Netherlands
The Boulevard, Langford Lane, Kidlington, Oxford OX5 1GB, United Kingdom
50 Hampshire Street, 5th Floor, Cambridge, MA 02139, United States

© 2018 Elsevier Inc. All rights reserved.

No part of this publication may be reproduced or transmitted in any form or by any means, electronic or mechanical, including photocopying, recording, or any information storage and retrieval system, without permission in writing from the publisher. Details on how to seek permission, further information about the Publisher's permissions policies and our arrangements with organizations such as the Copyright Clearance Center and the Copyright Licensing Agency, can be found at our website: www.elsevier.com/permissions.

This book and the individual contributions contained in it are protected under copyright by the Publisher (other than as may be noted herein).

Notices

Knowledge and best practice in this field are constantly changing. As new research and experience broaden our understanding, changes in research methods, professional practices, or medical treatment may become necessary.

Practitioners and researchers must always rely on their own experience and knowledge in evaluating and using any information, methods, compounds, or experiments described herein. In using such information or methods they should be mindful of their own safety and the safety of others, including parties for whom they have a professional responsibility.

To the fullest extent of the law, neither the Publisher nor the authors, contributors, or editors, assume any liability for any injury and/or damage to persons or property as a matter of products liability, negligence or otherwise, or from any use or operation of any methods, products, instructions, or ideas contained in the material herein.

Library of Congress Cataloging-in-Publication Data

A catalog record for this book is available from the Library of Congress

British Library Cataloguing-in-Publication Data

A catalogue record for this book is available from the British Library

ISBN: 978-0-12-813483-2

For information on all Elsevier publications
visit our website at <https://www.elsevier.com/books-and-journals>



Working together
to grow libraries in
developing countries

www.elsevier.com • www.bookaid.org

Publisher: Susan Dennis

Acquisition Editor: Anita A. Koch

Editorial Project Manager: Karen R. Miller

Production Project Manager: Prem Kumar Kaliamoorthi

Cover Designer: Mark Rogers

Typeset by SPi Global, India

Introduction

Patricia Luis*Materials & Process Engineering (iMMC-IMAP), Catholic University of Louvain,
Louvain-la-Neuve, Belgium***CHAPTER OUTLINE**

1.1 General Overview of Technologies	1
1.2 Kind of Membranes and the Implications in Modeling	5
1.2.1 Polymeric Membranes	5
1.2.2 Inorganic Membranes	7
1.3 Mass Transfer in Laminar and Turbulent Flow	9
1.3.1 Laminar Flow or Stagnant Fluid Film	9
1.3.2 Turbulent Flow	12
1.4 Mass Transfer Through Membranes	13
1.5 Polarization and Fouling Phenomena	16
1.5.1 Concentration Polarization	17
1.5.2 Temperature Polarization	18
1.5.3 Membrane Fouling	19
1.5.4 In Situ Monitoring Techniques for Concentration Polarization and Fouling Phenomena in Membrane Filtration	20
References	22

1.1 GENERAL OVERVIEW OF TECHNOLOGIES

Membrane technology has become a strong competitor of conventional separation processes. Membranes have experienced a dramatic increase in applications in the last years and it seems that they are ready to conquer the world. Membranes have been proposed for environmental purposes to clean gas or liquid waste streams, or because of economic reasons, normally related to the reduction of energy consumption that using membranes involve instead of other conventional separation systems, such as the multiple variations of distillation. Key membrane processes that

are considered in this book are pressure-driven membrane processes, pervaporation, gas permeation, supported liquid membranes, membrane contactors, membrane bioreactors, and electro-driven processes. Each of them is characterized by a typical kind of membrane (dense or porous), present fluid phases (gas-gas, liquid-liquid, gas-liquid, or liquid-gas), and a specific driving force (concentration, temperature, pressure). [Table 1.1](#) presents a brief description of each membrane process with some key characteristics.

In spite of the differences in operation and application of those technologies, it is possible to make a general classification based on the selective or nonselective character of the membrane. Thereby, two main approaches can be considered ([Luis and Van der Bruggen, 2013](#)): (i) when the membrane acts as a selective barrier determining which compound will permeate faster through the membrane, and (ii) when the membrane does not give selectivity to the separation since it is only a physical barrier that separates two fluid phases (a gas and a liquid phase, or two immiscible liquid phases). The first situation happens typically when dense membranes or when porous membranes in which there is a mechanism of size exclusion are used. This is the case of most of the cited membrane processes except from membrane contactors. Membrane contactors present the characteristic of using a porous membrane that gives absolutely no selectivity to the separation. This means, for example, that if we use membrane distillation (in which membrane contactors are applied) to separate an azeotropic mixture, the feed mixture will be never separated because the azeotropic vapor phase will traverse the membrane pores without any separation. The azeotrope will be collected in the permeate.

The evaluation of membrane processes is experimentally based on the determination of the mass transfer through the membrane and the degree of separation. The former is normally expressed in terms of transmembrane flux, and the latter as a separation factor. The flux and the separation factor are characteristics that determine the process performance, which is key information to decide if a process is economically viable or not since the membrane area is determined by the flux and the separation efficiency. However, in membrane science, we are interested in the membrane performance, this is, what the effect of the membrane is. This is not evident in a process in which several factors are participating in the separation, such as differences in concentration, temperature, or pressure (driving force). An example is the separation of liquid mixtures with pervaporation. Commonly, the higher the temperature, the higher the flux. However, we should not say that the membrane performance is better at higher temperatures by checking only the flux. It may happen that the permeability is lower at high temperature. This situation may be due to the increase of the vapor pressure of the permeating compound, thus increasing the driving force. It is thus mandatory to remove the effect of the driving force from the calculations in order to determine the permeability of the pervaporation membrane and hence, the membrane performance. In this book, membrane performance and process performance are distinguished for each membrane technology, and modeling of membrane processes is proposed considering the kind of membranes used.

Table 1.1 Summary of membrane processes described in this book

Membrane process	Membrane structure	Present fluid phases	Driving force	Basic description	Disposition in this book
Microfiltration	Porous	Liquid-liquid	Pressure gradient	Pressure-driven membrane process in which membranes are used in the micrometer range, down to c. 0.1 μm . It require pressures typically below 1 bar	Chapter 2
Ultrafiltration	Porous	Liquid-liquid	Pressure gradient	Pressure-driven membrane process in which membranes are used in the nanometer range (2 nm to 100 nm); working pressures in the range of 1–6 bar	Chapter 2
Nanofiltration	Nanoporous	Liquid-liquid	Pressure gradient	Pressure-driven membrane process in which membranes have a pore size of 1 nm and below; operational pressures are 5–15 bar	Chapter 2
Reverse osmosis	Dense	Liquid-liquid	Pressure gradient	Pressure-driven membrane process in which membranes are dense and may operate at pressures of 20 bar or even below, in the absence of osmotic pressure. Pressures of 40–60 bar are needed in seawater desalination. Higher pressures go up to 100 bar in high pressure reverse osmosis	Chapter 2
Forward osmosis	Dense	Liquid-liquid	Osmotic pressure gradient	Membrane process that relies on osmotic pressure rather than on an applied pressure. Typical pressures are those used in reverse osmosis for desalination, since forward osmosis membranes are also dense	Chapter 2
Pervaporation	Dense/porous	Liquid-vapor	Partial pressure gradient	Membrane process in which selective permeation of components from a liquid mixture takes place through a dense membrane. Porous membranes are also possible but less common. Vacuum is applied in the permeate side in order to increase the driving force. The permeate is a vapor to be condensed	Chapter 3

Continued

Table 1.1 Summary of membrane processes described in this book —cont'd

Membrane process	Membrane structure	Present fluid phases	Driving force	Basic description	Disposition in this book
Gas permeation	Dense/ porous	Gas-gas	Partial pressure gradient	A gas mixture is separated by the selective transport of components through a dense or porous membrane. Pressure is required in the feed side to increase the driving force of the system	Chapter 4
Supported liquid membranes	Supported liquid in a porous membrane	Gas-gas or liquid-liquid or liquid-gas	Concentration (or partial pressure) gradient	Membrane process in which the pores of a porous membrane are filled with a liquid. Applications have been proposed to separate mixtures of gases or liquids	Chapter 4
Membrane contactors	porous	Liquid-liquid or gas-liquid	Concentration (or partial pressure)/ temperature gradient	Membrane process that uses a porous membrane as a barrier to separate two fluid phases (gas-liquid or two immiscible liquids). The membrane gives no selectivity to the separation. The liquid in the permeate side has to provide the required selectivity	Chapter 5
Membrane bioreactors (micro- and ultrafiltration membranes)	porous	Liquid-liquid	Pressure gradient	Membrane process that combines microfiltration or ultrafiltration with a biological wastewater treatment process (activated sludge process). Typically used for treatment of municipal and industrial wastewater	Chapter 6
Electromembrane processes	Ion-exchange dense membranes	Liquid-liquid	Electrical gradient	Membrane process that uses ion-exchange membranes (a stack of alternating anion exchange membranes and cation exchange membranes) and an electrical potential as a driving force. Typically applied in nonselective removal of salt from brackish water	Chapter 7

1.2 KIND OF MEMBRANES AND THE IMPLICATIONS IN MODELING

Membranes can be made from many different materials. In general, two main groups can be defined: organic (polymeric) and inorganic (ceramic, glass, zeolite, carbon based, metallic) membranes. The choice of material is limited by the operation conditions of the process. For example, very hard environments such as those at high temperature and/or with presence of organic solvents limit significantly the use of polymeric materials. Application of polymer membranes is often limited to temperatures below 200°C and to mixtures that are chemically inert. Operation at high temperatures and with chemically active mixtures requires membranes made of inorganic materials, such as microporous ceramics, metals, and carbon; and dense metals, such as palladium, that allow the selective diffusion of small molecules (e.g., hydrogen and helium) (Seader et al., 2013). In addition, the membrane material will determine the membrane structure, which will have a direct impact on the membrane performance. The use of selective or nonselective membranes (i.e., membrane contactors) is also an important aspect to take into account. In membrane contactors or microfiltration/ultrafiltration processes, the membrane material needs to provide a porous structure as well as chemical and mechanical resistance toward the feed mixture, temperature, and pressure applied to the system. On the other hand, for selective membranes (porous or dense membranes), the choice of the material directly affects the membrane permeability and selectivity. The type of material and structure will also determine the kind of mass transport through the membrane (solution, diffusion, Knudsen diffusion, convection, etc.) and therefore the mathematical model to be applied to describe the mass transfer (solution-diffusion model, pore-flow model, etc.).

1.2.1 POLYMERIC MEMBRANES

Polymeric membranes can be made of different kind of polymers. Polymers composed of linear-chain polymers soften with an increase in temperature and are soluble in organic solvents. These polymers are called thermoplastics. On the other hand, polymers composed of highly cross-linked chains decompose at high temperature and are not soluble in organic solvents. They are referred to as thermosetting polymers (Seader et al., 2013). In addition, polymers can be amorphous or crystalline. Amorphous polymers refer to a polymer that is glassy in appearance but lacks crystalline structure. A crystalline polymer is opaque but has a crystalline structure. When the temperature of a glassy polymer is increased so that it becomes rubbery, the glass transition temperature, T_g , is reached. If the temperature of a crystalline polymer is increased until melting, the melting point, T_m , is reached. On the other hand, thermosetting polymers never melt. Most polymers have a certain degree of crystallinity that varies from 5% to 90%, having both amorphous and crystalline regions. Then, they may have both T_g and T_m (Seader et al., 2013). Table 1.2 lists repeat units and values of glass transition

Table 1.2 Main polymeric materials used in membranes (Seader et al., 2013)

Polymer	Type	Representative repeat unit	T_g , °C	T_m , °C
Cellulose triacetate	Crystalline			300
Polyisoprene (natural rubber)	Rubbery		-70	
Aromatic polyamide	Crystalline			275
Polycarbonate	Glassy		150	
Polyimide	Glassy		310–365	
Polystyrene	Glassy		74–110	
Polysulfone	Glassy		190	
Polytetrafluoroethylene (Teflon)	Crystalline			327

T_g , glass transition temperature; T_m , melting temperature.

temperature (T_g) and/or melting temperature (T_m) for some of the many natural and synthetic polymers from which membranes have been fabricated. Included are crystalline, glassy, and rubbery polymers (Seader et al., 2013).

Polymer membranes can be dense or microporous. In dense membranes, diffusing species must dissolve into the polymer and then diffuse through the polymer between segments of macromolecular chains (Seader et al., 2013). Diffusion will occur almost exclusively through amorphous regions. The presence of crystalline regions will decrease the diffusion area and increase the diffusion path (Seader et al., 2013). Porous membranes are applied in microfiltration and ultrafiltration, for example, while dense membranes are applied in gas separation and pervaporation among others.

1.2.2 INORGANIC MEMBRANES

Four different types of inorganic materials are frequently used: ceramic membranes, glass membranes, zeolite membranes, metallic membranes, and carbon-based membranes (Mulder, 1998). Ceramic membranes are formed by the combination of a metal (e.g., aluminum, titanium, silicon, zirconium) with a nonmetal in the form of an oxide, nitride, or carbide. Examples are aluminum oxide or alumina ($\gamma\text{-Al}_2\text{O}_3$), and zirconium oxide or zirconia (ZrO_2). Ceramic membranes are the most used inorganic membranes and are characterized by a very high thermal, chemical, and mechanical stability. The melting points of ceramics are very high (Al_2O_3 : $T_m=2050^\circ\text{C}$; ZrO_2 : $T_m=2770^\circ\text{C}$; TiO_2 : $T_m=1605^\circ\text{C}$; SiC : $T_m=2500^\circ\text{C}$) (Wyatt and Dew-Hughes, 1974), hence, these membranes are very interesting for gas separation at high temperature. In addition, ceramic membranes present very high chemical stability since they can operate at any pH and with any organic solvent, which is important in applications in which chemical cleaning is required, such as ultrafiltration and microfiltration, or when organic solvents may be present, such as in membrane-based liquid extraction or pervaporation. Finally, mechanical stability is also high in ceramic membranes, which is of interest in processes working under pressure, such as ultrafiltration and microfiltration.

Glass membranes are made of silicon oxide or silica (SiO_2). Silica membranes can be used in many applications such as gas separation and pervaporation. They have good gas separation properties but may suffer from water sorption sensitivity at room temperature due to the hydrophilic nature of the silica surface (de Vos and Verweij, 1998; de Vos et al., 1999; Cheraitia et al., 2010), which can result in the degradation of the membrane due to pore blocking. In order to improve the hydrothermal stability of silica membranes, several strategies have been proposed in the literature, such as making the internal (pore) surfaces of the silica material more hydrophobic (de Vos et al., 1999) or modifying the membrane by the incorporation of carbon species (Park and Lee, 2003; Duke et al., 2004), inorganic additives such as Al_2O_3 , ZrO_2 , or TiO_2 (Guizard et al., 2002), and also Mg/Al or Pt (Nijmeyer, 1999), cobalt (Mori et al., 2006) and nickel.

Zeolites are crystalline microporous materials containing channels and cavities of molecular dimensions. They are composed of tetrahedral building units of TO_4

($T = \text{Si, Al, B, Ge, etc.}$), which are interconnected through oxygen atoms, forming a one-, two-, or three-dimensional network. The framework exhibits a negative charge that is compensated by a cation, either inorganic or organic (e.g., Na^+ , K^+ , Ca^{2+} , or H^+) (Sommer et al., 2005). The cations reside in the pores of the framework. The pore size of the zeolite channels is determined by the number of T atoms that form the ring. Small-pore zeolites include those structures made up of eight-member oxygen rings, medium-pore zeolites have 10-member rings, and large-pore zeolites have 12-member rings (Ockwig and Nenoff, 2007). Zeolite membranes combine pore size and selectivity with high chemical, thermal, and mechanical stability. The separation performance is determined by the effective pore size distribution when molecular size exclusion sieving is the dominant mechanism and no other diffusion pathways bypass the network of well-defined zeolitic pores/channels. Otherwise, viscous flow through grain boundaries prevails. However, the existence of intercrystal pores with sizes larger than the zeolitic pores is a major cause for decline in molecular separation efficiency (Ockwig and Nenoff, 2007). The disadvantages of using zeolite membranes are their cost and complex fabrication procedure. Thin and compact zeolite membranes should provide high flux and high selectivity. However, decreasing the membrane thickness leads to an increase in membrane fragility. In order to overcome this limitation, mixed matrix membranes (MMMs), which comprise polymeric and inorganic membranes, present an interesting approach for enhancing the separation performance (Feng et al., 2015).

Metallic membranes are typically dense sheets or films used in gas separation. The fundamental mechanism of action in dense metallic membranes requires the conduction of free electrons and the presence of specific catalytic surfaces to dissociate the target compound (e.g., H_2) on the raw feed stream side and reassociate the protons and electrons on the product side (Ockwig and Nenoff, 2007). Metallic membranes have been extensively proposed for the hydrogen separation since they provide very high selectivity due to their dense structure, which prevents the permeation of large atoms and molecules such as CO , CO_2 , O_2 , N_2 , and so on, in addition, they can operate at high operating temperatures. Typical metals are tantalum, niobium, vanadium, platinum, and palladium. Metals are deposited as thin layers on various supports (e.g., glasses, ceramics, or other metals) in order to increase the transmembrane flux and ensure a good mechanical strength, thermal stability, and reliability. The metallic coating can be a thin metal layer (dense or porous) formed on the surface and extraneous to the support, a thin metal layer formed on the walls within a porous support, a microporous ceramic layer formed on the supporting layer by finely distributing metal particles within the pores of the support, or a microporous ceramic layer formed on the supporting layer by sintering metal-coated particles onto the surface (Uemiya, 1999; Ockwig and Nenoff, 2007). Presence of defects, grain boundaries, thermal dilatation, and lattice defects lead to variations in the membrane performance due to the strong dominance of surface phenomena (Liu et al., 1997).

Carbon-based membranes can be produced from various precursor polymers, which are converted to pure carbon by treatment at high temperature in an inert atmosphere (carbonization) (Ismail et al., 2011). The most popular precursor for carbon

membranes is currently polyimide, which contributes largely to the high manufacturing cost (Ockwig and Nenoff, 2007). Carbon-based membranes can be categorized into three classes: carbon membranes, carbon molecular sieve membranes (CMSMs), and carbon nanotubes (CNTs). Both the chemistry of the material and the fabrication/implementation (i.e., module design) will determine the separation performance of each class of material (Ockwig and Nenoff, 2007). For solid carbon-based membranes, pore-flow mechanisms are often expected, but if the pores or channels are very small (~ 1 nm in size), conventional notions of pore flow may not apply. However, they suffer because of their fragile mechanical nature and high cost. Carbon-based membranes are promising for the separation of light gases (Ockwig and Nenoff, 2007) and they have been also proposed for wastewater treatment (Al-anzi and Siang, 2017). Recently, graphene oxide membranes and diamond-like carbon membranes have shown high flux to water and organic solvents, respectively (Paul, 2012).

The membrane material is directly related to the membrane structure and to possible interactions with the components to be separated. Thus it is an important decision in the design of a separation process.

1.3 MASS TRANSFER IN LAMINAR AND TURBULENT FLOW

Generally, three main mechanisms of mass transfer are identified in a fluid (Seader, 2013): (i) molecular diffusion by random and spontaneous microscopic movement of molecules due to thermal motion; (ii) eddy (turbulent) diffusion by random, macroscopic fluid motion; and (iii) bulk flow by the overall movement of fluid. Mass transfer will occur as the result of those three mechanisms and the molar flux of a species can be considered as the sum of the contribution of each mechanism. Thus if N_i is the molar flux of i with mole fraction x_i (Seader, 2013):

$$N_i = \text{molecular diffusion flux of } i + \text{eddy diffusion flux of } i + x_i N \quad (1.1)$$

where N is the total molar flux in moles per unit time per unit area in a direction perpendicular to a stationary plane across which mass transfer occurs, and $x_i N$ is the bulk-flow flux. Each term can be positive or negative depending on the direction of the flux, which may lead to situations in which the net mass transfer flux of a species is zero ($N_i = 0$) when the molecular and eddy diffusion fluxes are in one direction and N is in the opposite direction (molecular diffusion flux of i + eddy diffusion flux of $i = x_i N$).

1.3.1 LAMINAR FLOW OR STAGNANT FLUID FILM

A system operating under laminar flow or when there is a stagnant fluid film, only molecular diffusion and bulk flow need to be considered, with the latter often negligible. The mass transfer rates can be calculated using Fick's law of diffusion:

$$J_A = -D_{AB} \frac{dc_A}{dz} \quad (1.2a)$$

$$J_B = -D_{BA} \frac{dc_B}{dz} \quad (1.2b)$$

where J_A and J_B are the molar flux of A and B , respectively, by ordinary molecular diffusion relative to the molar average velocity of the mixture in the z -direction; D_{AB} and D_{BA} are the mutual diffusion coefficient or diffusivity of A in B and B in A , respectively; c_A and c_B are the molar concentration of A and B , respectively; and $\frac{dc_A}{dz}$ and $\frac{dc_B}{dz}$ are the concentration gradients (negative in the direction of diffusion) of A and B , respectively. The fluxes of A and B are in opposite directions. Correlations to calculate molecular diffusivities in gases, liquids, and porous solids can be found in [chapter 5 of Perry's Chemical Engineers' Handbook \(Green and Perry, 2007\)](#).

Then, Eq. (1.1) can be written as

$$N_A = -D_{AB} \frac{dc_A}{dz} + x_A N = -c \cdot D_{AB} \frac{dx_A}{dz} + x_A N \quad (1.3a)$$

and

$$N_B = -D_{BA} \frac{dc_B}{dz} + x_B N = -c \cdot D_{BA} \frac{dx_B}{dz} + x_B N \quad (1.3b)$$

where c is the total molar concentration, and x_A and x_B are the molar fractions of A and B , respectively.

If *equimolecular counterdiffusion* (EMD) takes place, the molar fluxes are equal but opposite in direction ($N_A = -N_B$):

$$N = N_A + N_B = 0 \quad (1.4)$$

Thus from Eqs. (1.3a), (1.3b), the diffusion fluxes are also identical but opposite in direction:

$$J_A = -J_B \quad (1.5)$$

Finally, it is obtained that

$$N_A = J_A = -c \cdot D_{AB} \frac{dx_A}{dz} \quad (1.6a)$$

and

$$N_B = J_B = -c \cdot D_{BA} \frac{dx_B}{dz} \quad (1.6b)$$

Integrating these equations leads to:

$$J_A = \frac{c \cdot D_{AB}}{z - z_1} (x_{A1} - x_A) \quad (1.7a)$$

$$J_B = \frac{c \cdot D_{BA}}{z - z_1} (x_{B1} - x_B) \quad (1.7b)$$

which shows that the concentration profiles of a stagnant film are linear under steady-state conditions ([Fig. 1.1A](#)).

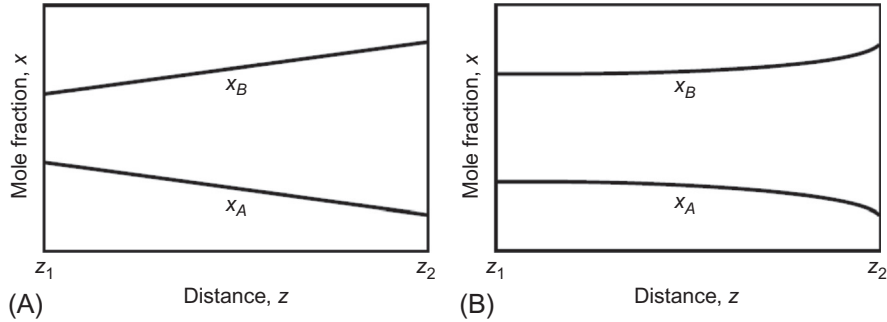


FIG. 1.1

Concentration profiles for limiting cases of ordinary molecular diffusion in binary mixtures across a stagnant film: (A) equimolar counterdiffusion (EMD); (B) unimolecular diffusion (UMD).

Reprinted with permission from Seader (2013).

In addition, the total concentration ($c = c_A + c_B$) does not change through the film. Thus

$$dc = 0 = dc_A + dc_B \quad (1.8)$$

or

$$dc_A = -dc_B \quad (1.9)$$

By combining Eqs. (1.2a), (1.2b), (1.5), (1.9), it is obtained that:

$$\frac{D_{AB}}{dz} = \frac{D_{BA}}{dz} \quad (1.10)$$

which indicates that diffusion coefficients are always equal in a binary mixture (Seader, 2013):

$$D_{AB} = D_{BA} \quad (1.11)$$

On the other hand, if *unimolecular diffusion* (UMD) occurs, only mass transfer of component *A* is taking place. In this case, $N_B = 0$, and $N = N_A$. Eq. (1.3a) becomes:

$$N_A = -c \cdot D_{AB} \frac{dx_A}{dz} + x_A N_A \quad (1.12)$$

which can be rearranged to:

$$N_A = -\frac{c \cdot D_{AB}}{(1 - x_A)} \frac{dx_A}{dz} = -\frac{c \cdot D_{AB}}{x_B} \frac{dx_A}{dz} \quad (1.13)$$

By integrating this equation, we obtain:

$$N_A = \frac{c \cdot D_{AB}}{(z - z_1)} \ln \left(\frac{1 - x_A}{1 - x_{A1}} \right) \quad (1.14)$$

And the variation of mole fraction with the distance is given by (see Fig. 1.1B):

$$x_A = 1 - (1 - x_{A1}) \exp \left[\frac{N_A(z - z_1)}{c \cdot D_{AB}} \right] \quad (1.15)$$

Eq. (1.14) can be also written considering log mean concentrations and $z = z_2$ (end of the stagnant film):

$$N_A = \frac{c \cdot D_{AB}}{z_2 - z_1} \ln \left(\frac{1 - x_{A2}}{1 - x_{A1}} \right) = \frac{c \cdot D_{AB} (x_{A1} - x_{A2})}{z_2 - z_1 (1 - x_A)_{LM}} \quad (1.16)$$

with

$$(1 - x_A)_{LM} = \frac{(1 - x_{A2}) - (1 - x_{A1})}{\ln[(1 - x_{A2})/(1 - x_{A1})]} = \frac{x_{A1} - x_{A2}}{\ln[(1 - x_{A2})/(1 - x_{A1})]} \quad (1.17)$$

1.3.2 TURBULENT FLOW

Turbulent flow is very common in industrial process due to high flow rates. In those cases, eddy diffusion should be considered. Eddies of fluid will mix with each other by moving from one region to another in fluctuating motion (Seader, 2013). Mass transfer can take place by molecular diffusion (slow), turbulent or eddy diffusion (rapid), and bulk flow, although the latter may not be significant. The mass transfer rate is then calculated from empirical correlations since there is not a fundamental theory that can be applied.

There is an analogy among the momentum, heat, and mass transfer fluxes since all of them are proportional to a driving force, which is the difference in velocity, temperature, and concentration, respectively, in the media of study. The proportionality is given by a diffusion coefficient, which can include the contribution related to the presence of turbulence:

$$\frac{\tau_{zx}}{\rho} = -(\vartheta + \epsilon_M) \frac{du_x}{dz} \quad (1.18a)$$

$$\frac{q_z}{C_p \rho} = -(\alpha + \epsilon_H) \frac{dT}{dz} \quad (1.18b)$$

$$N_{A_z} = -(D_{AB} + \epsilon_D) \frac{dC_A}{dz} \quad (1.18c)$$

where ϵ_M , ϵ_H , and ϵ_D are the momentum, heat, and mass eddy diffusivities, respectively; ϑ is the momentum diffusivity (kinematic viscosity, μ/ρ); and α is the thermal diffusivity, $k/\rho C_p$. The three eddy diffusivities may be assumed equal, good approximation for ϵ_H and ϵ_D , although experience indicates that $\epsilon_M/\epsilon_H = \epsilon_M/\epsilon_D$ is sometimes less than 1.0 and as low as 0.5 for turbulence in a free jet (Seader, 2013). Nevertheless, if the three eddy diffusivities are equal ($\epsilon_M = \epsilon_H = \epsilon_D$), and the molecular diffusivities are negligible or equal ($\vartheta = \alpha = D_{AB}$), the Reynolds analogy is obtained:

$$\frac{f}{2} = \frac{h}{\rho C_p \bar{u}_x} = \frac{k_C}{\bar{u}_x} \quad (1.19)$$

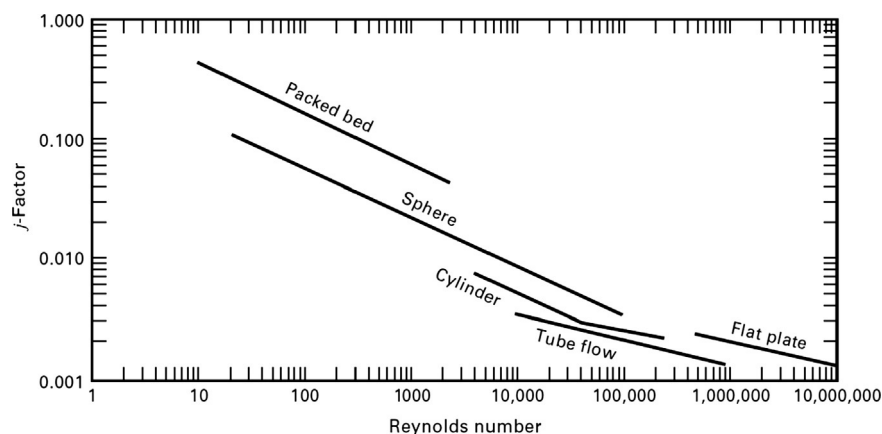


FIG. 1.2

Chilton-Colburn j -factor correlations.

Reprinted with permission from Seader (2013).

which allows the estimation of heat and mass transfer coefficients from values of the Fanning friction factor for turbulent flow. This analogy is only valid when $N_{Pr} = N_{Sc} = 1$ (i.e., $\nu/\alpha = \nu/D_{AB} = 1$). Due to the limited application of the Reynolds analogy, an extension was presented by Chilton and Colburn (1934) based on the empirical determination of the j -factors:

$$j_M \equiv \frac{f}{2} = j_H \equiv \frac{h}{G C_p} (N_{Pr})^{\frac{2}{3}} = j_D \equiv \frac{k_c \rho}{G} (N_{Sc})^{\frac{2}{3}} \quad (1.20)$$

Eq. (1.20) is known as the Chilton-Colburn analogy and allows estimating transport coefficients for turbulent flow. Fig. 1.2 shows values of j -factors for several geometries as a function of the Reynolds number.

This section has showed mass transfer in fluid systems under laminar or turbulent conditions. However, the presence of a membrane, or more generally, an interface, introduces aspects of fluid-fluid or fluid-solid equilibrium in the system that have to be taken into account.

1.4 MASS TRANSFER THROUGH MEMBRANES

Mass transfer in membrane systems takes place across interfaces between phases, which can be gas-membrane-gas, liquid-membrane-gas, gas-membrane-liquid, or liquid-membrane-liquid. For example, in gas separation, the membrane separates two gas phases and allows the preferential permeation of one or more of the components in the feed solution. In pervaporation, the liquid feed is separated from the permeate side (operating under vacuum) by a dense membrane, which also separates selectively the components in the feed. In membrane-based gas absorption, a component in a gaseous feed will be absorbed by a selective liquid that is separated by a porous nonselective membrane. In membrane-based liquid extraction, a porous membrane separates two immiscible liquids, and the mass transfer will take place from the feed solution to the extractant agent through the nonselective membrane.

The transmembrane flux through a membrane is proportional to the driving force. This statement is the basis of mass transfer modeling in membrane technology. It is not new and not special for membranes, as we have already seen how mass transfer takes place in fluid phases in the previous section. However, due to the evolution of each membrane system in a different discipline or application, the development of models has followed different paths even though the initial roots are the same. This leads to a different nomenclature depending on the membrane system and even different kinds of models. For example, mass transfer in dense membranes is typically described by a “solution-diffusion” model that leads to a key parameter called “permeability,” which is the proportionality coefficient between flux and driving force. On the other hand, in membrane contactors in which a porous membrane is used, this proportionality coefficient is called “mass transfer coefficient.” A reason to use different names for the same parameter is due to historical developments of applying each technology in different fields. For instance, microfiltration or membrane bioreactors were born as environmental technologies while pervaporation or membrane contactors were developed in a chemical engineering context. Thus each chapter of this book describes the fundamental modeling on mass (and heat transfer if relevant) applied to each specific membrane system, using the conventional nomenclature so that the reader is not confused by other reference sources. However, it is important to highlight the necessity of a common approach that allows unifying concepts and models to describe membranes with a multidisciplinary perspective.

Having said that, two main models are indicated in this section, which manifests the relevance of the membrane structure on the permeation mechanism: the solution-diffusion model, applied for dense membranes; and, the pore-flow model, applied for porous membranes. Fig. 1.3 shows the illustration of the mechanism of permeation for each kind of model. In the solution-diffusion model, it is considered that permeants dissolve in the membrane material and then diffuse through the membrane because of a concentration gradient. The differences in solubilities among permeants in the membrane and the differences in the diffusion rates through the membrane lead to their separation (Baker, 2004). In the pore-flow model, transport of permeants

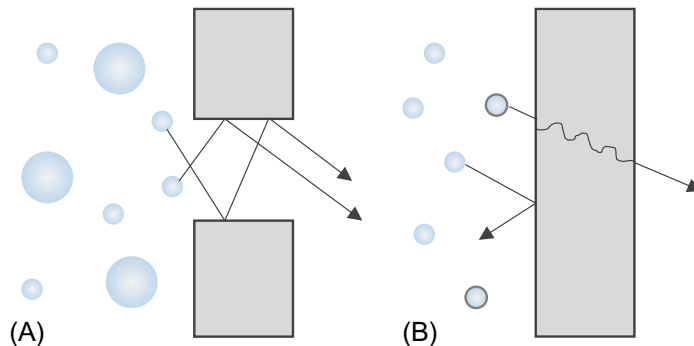


FIG. 1.3

Molecular transport through membranes can be described by (A) a flow through permanent pores or (B) the solution-diffusion mechanism (Baker, 2004).

is governed by a convective flow driven by pressure through tiny pores. One of the permeants will be excluded (filtered) from some of the pores in the membrane while other permeants will pass through. Then, the separation occurs. Thus one can imagine that dealing with porous or dense membranes means to have to use one or the other model. For this reason, choosing the membrane material is a very important step in the overall picture of applying membrane technology since it conditions the membrane structure and therefore the membrane performance.

Another kind of modeling that is extensively applied when using porous membranes is the resistances-in-series model. This model assumes that the resistance to mass transfer in the fluid phases is located in a film layer close to the membrane surface. The overall resistance is the sum of the individual resistances (i.e., the resistances in the feed phase, the membrane, and the permeate phase), which is an analogy taken from electrical circuits. Each resistance is represented mathematically by the inverse of the individual mass transfer coefficient. Fig. 1.4 shows a schematic representation of mass and heat transfer resistances in a porous membrane.

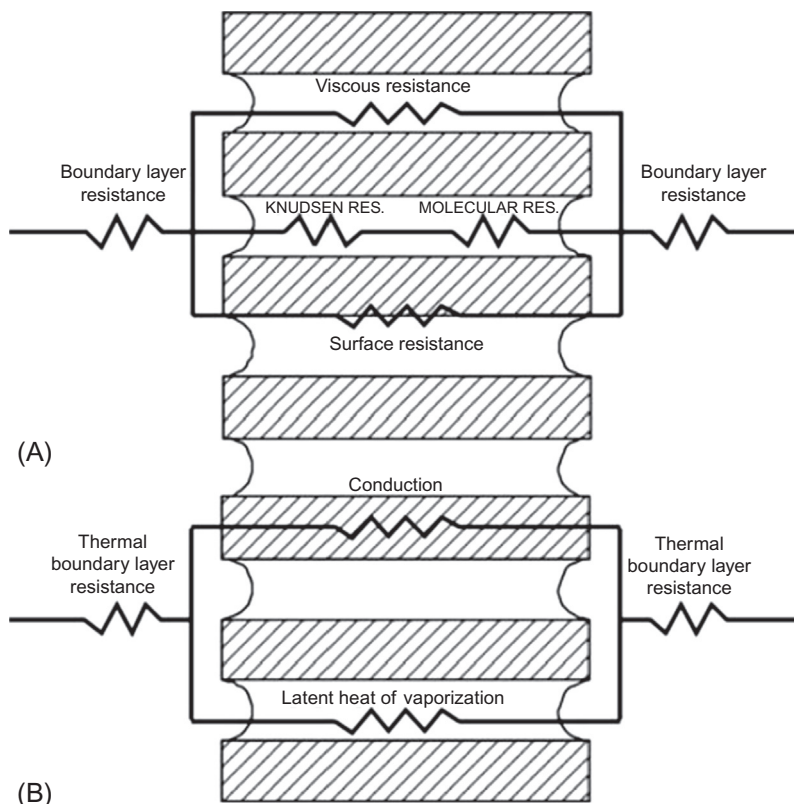


FIG. 1.4

Schematic representation of serial and parallel arrangement of resistances to mass (A) and heat (B) transfer in a porous membrane.

Reprinted with permission from Drioli, E., Curcio, E., Di Profio, G., 2005. State of the art and recent progresses in membrane contactors. *Chem. Eng. Res. Des.* 83(A3), 223–233.

Table 1.3 Membrane processes and mass transfer modeling

Membrane process	Membrane structure	Mass transfer model
Microfiltration	Porous	Resistances-in-series model
Ultrafiltration	Porous	Pore flow
Nanofiltration	Nanoporous	Solution-diffusion model
Reverse osmosis	Dense	Solution-diffusion model
Forward osmosis	Dense	Solution-diffusion model
Pervaporation	Dense/porous	Solution-diffusion model/pore-flow model
Gas permeation	Dense/porous	Solution-diffusion model/pore-flow model
Supported liquid membranes	Supported liquid in a porous membrane	Solution-diffusion model
Membrane contactors	Porous	Resistances-in-series model
Membrane bioreactors (micro- and ultrafiltration membranes)	Porous	Pore flow/fouling models
Electromembrane processes	Ion-exchange dense membranes	Extended Nernst-Planck

Table 1.3 shows a summary of the different membrane technologies addressed in this book and the corresponding models that are typically used to describe mass transfer. The reader is addressed to the corresponding chapter for more detailed information.

1.5 POLARIZATION AND FOULING PHENOMENA

The membrane performance, and consequently the process performance, may change dramatically with time due to a decrease of the transmembrane flux over time. This situation happens due to concentration polarization and fouling and may lead to a process that is technically and/or economically disadvantageous. Concentration polarization and fouling are two very different phenomena but they may be dependent on each other since fouling can result from polarization phenomena (Mulder, 1998). In addition, those processes driven by a thermal force such as membrane distillation may suffer of a similar phenomenon to concentration polarization, called temperature polarization. Those aspects are introduced generally in the next subsections. A more detailed explanation can be found in the respective chapter for the studied technology.

1.5.1 CONCENTRATION POLARIZATION

Concentration polarization occurs when the concentration of a specific component increases or decreases at the boundary layer close to the membrane surface due to the selective transport through the membrane. In case of pressure-driven processes such as microfiltration, ultrafiltration, nanofiltration, or reverse osmosis, the solute is typically retained by the membrane, leading to a concentration profile similar to Fig. 1.5A. This profile can be also found in processes such as membrane-based

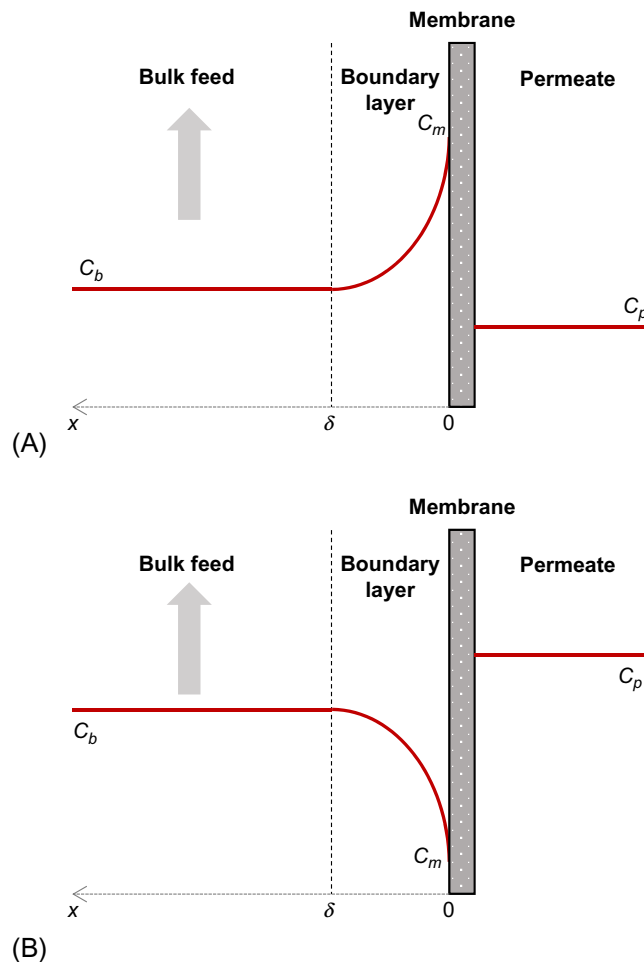


FIG. 1.5

Concentration profile with concentration polarization: (A) mass transfer limited by the membrane and (B) mass transfer limited by the boundary layer.

extraction or membrane-based absorption. In other membrane processes where the transport through the membrane takes place by diffusion rather than by convection, a concentration profile similar to Fig. 1.5B is obtained since the component will permeate faster through the membrane, being in the boundary layer where the transport is limited by diffusion. This concentration profile can thus appear in processes such as gas separation, pervaporation, dialysis, electro dialysis, membrane crystallization, membrane distillation, etc.

Concentration polarization produces a decline in the transmembrane flux, which may be very severe, such as in microfiltration or ultrafiltration, or negligible, such as in gas separation. Regarding the retention, it may lead to a lower retention if low molecular weight solutes (e.g., salts) are considered, or it may lead to a higher retention, which is the case of mixtures of macromolecular solutes. Concentration polarization can be mathematically described by a concentration polarization modulus or coefficient (see Chapter 2 or Chapter 4) or other more specific models that have been described in the literature, for example, gel layer model, osmotic pressure model, boundary layer resistance model (Mulder, 1998).

1.5.2 TEMPERATURE POLARIZATION

In nonisothermal processes, the temperature difference across the membrane generates a driving force that causes the mass transport through the membrane. Coupled heat and mass transfer may contribute toward temperature polarization. Membrane distillation is a typical case in which temperature polarization may take place since the feed solution is at higher temperature (higher vapor pressure) than the permeate side. Water molecules will evaporate within the membrane pores and will permeate from the warm side to the cold side where condensation will take place. The heat needed for the evaporation of water molecules is taken from the feed solution, and heat flux through the membrane will occur by diffusion of water vapor and by conduction through the membrane material and the pores, which are full of air in nonwetted conditions. Due to this heat transfer, a difference of temperature between the bulk of the feed solution and the membrane surface could appear, which can be represented by boundary layers, as shown in Fig. 1.6. This difference of temperatures is called temperature polarization.

Temperature polarization is a undesired phenomenon with economic implications. Increasing the temperature of the feed solution is in benefit of having higher driving force, thus higher transmembrane flux. The membrane area required for a specific process target would be then reduced. However, if temperature polarization takes place, not all the heat is being used efficiently to evaporate the water molecules, and increasing the driving force (i.e., increasing the feed temperature) will not lead to the expected increase in transmembrane flux. Heat is thus wasted in the process. Using membrane materials with very low conductivity would decrease temperature polarization. The mathematical description of temperature polarization can be found in Chapter 5 related to membrane distillation.

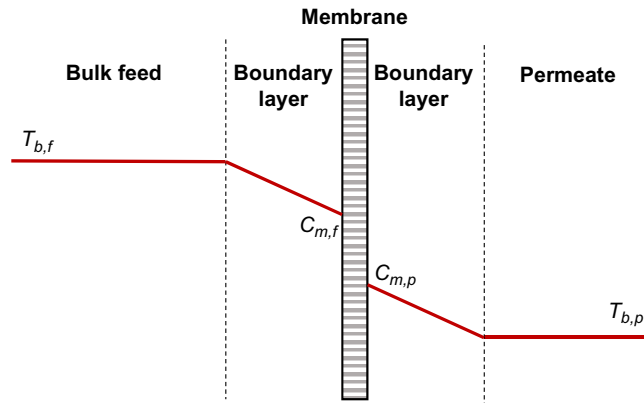


FIG. 1.6

Temperature profile when temperature polarization occurs.

1.5.3 MEMBRANE FOULING

Fouling may be defined as the (ir)reversible deposition of retained particles, colloids, emulsions, suspensions, macromolecules, salts, and so on, on or in the membrane (Mulder, 1998). The deposition of those components will lead to a decrease in flux over time. Foulants can be organic or inorganic components, leading to (bio)fouling and scaling, respectively. The main difference with the phenomena of concentration or temperature polarization is that in those cases, steady state is reached. However, membrane fouling leads to a decrease of flux over time in a nonsteady-state situation. Fig. 1.7 shows the variation of transmembrane flux as a function of time when polarization or fouling occurs. Fouling may be very significant in pressure-driven

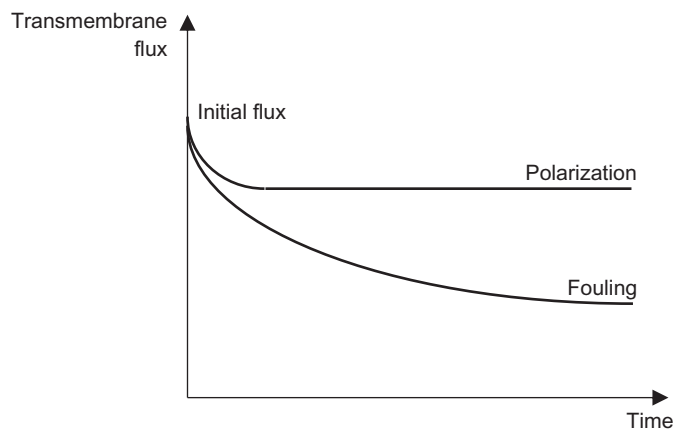


FIG. 1.7

Transmembrane flux as a function of time when polarization or fouling occur.

processes such as microfiltration and ultrafiltration where porous membranes susceptible to fouling are used. In pervaporation and gas separation, fouling is virtually absent (Mulder, 1998). Nevertheless, if fouling takes place, methods to reduce it are essential in order to keep the process performance. There are several strategies that are commonly applied but each case needs to be studied specifically since the kind of fouling will determine the required treatment. The most general approach is to be carried out by periodic cleaning of the membranes. The cleaning can be hydraulic (e.g., back flushing), mechanical cleaning (e.g., using oversized sponge balls), chemical cleaning (e.g., using acids or alkali salts, detergents, enzymes, complexing agents such as EDTA, disinfectants, steam and gas), or electric cleaning (e.g., by applying an electric field) (Mulder, 1998). Membrane fouling, if occurs, has to be reduced in order to keep the membrane process working under stable and optimal conditions.

1.5.4 IN SITU MONITORING TECHNIQUES FOR CONCENTRATION POLARIZATION AND FOULING PHENOMENA IN MEMBRANE FILTRATION

Understanding the concentration polarization and fouling phenomena has led to the development of novel, noninvasive, in situ quantification of physicochemical processes occurring during membrane filtration. Membrane fouling is commonly related to the formation of a cake or a gel on the membrane surface. The mechanisms in which cake formation and fouling occur are relatively poorly understood. Thus in situ measurements of fouling and direct observation of cake layer formation are necessary to understand the fundamental processes governing those phenomena. [Chen et al. \(2004\)](#) presented a complete review of the main in situ techniques available to evaluate concentration polarization and membrane fouling. A brief summary is presented as follows:

Techniques to determine concentration polarization ([Chen et al., 2004](#)):

- *Light deflection techniques*: they are based on the fact that the refractive index of a solution changes with concentration. Thus the change in deflection when light passes through a solution provides information about the concentration gradient along the light pathway.
- *Magnetic resonance imaging (MRI)*: high-resolution images are obtained by placing the test section in a static magnetic field. Magnetized protons (hydrogen nuclei) within the sample align and behave as magnets in this field. An oscillating magnetic field perpendicular to the main field is created by means of radio frequency pulses. The nuclei absorb energy from this field and move out of alignment with the static field, in an excited state. When the nuclei return from excitation to the equilibrium state, a signal induced in the receiver coil of the instrument by the nuclear magnetization can then be transformed by a series of algorithms into diagnostic images. ^1H nuclear magnetic resonance (NMR) images are generated from the distribution of mobile protons in the

sample weighted by the corresponding spin-spin and spin-lattice relaxation functions.

- *Electron diode array microscope*: A collimated, near infrared light parallel to the membrane surface and perpendicular to the flow direction is channeled through the filtration cell to a photodetector by microscopic lenses. An oscilloscope monitors the intensity pattern caused by the concentration gradient in the polarization layer that takes place due to absorption of the incident light.
- *Direct pressure measurements*: the evaluation of the pressure distribution across the concentration polarization layer gives additional information on the physicochemical transport process to understand the phenomena behind concentration polarization. The main disadvantage of this technique is that the pressure sensor disturbs the concentration polarization layer.

Techniques to determine membrane fouling (Chen et al., 2004):

- *Direct observation through the membrane*: Using an optical microscope is a simple method to observe fouling on the membrane surface. The microscope objective is positioned at the permeate side of a transparent membrane and particle deposition can be observed in real time by the microscope. A limitation of this technique is that an adequate membrane should be used, such as a transparent membrane that facilitates the observation of the membrane surface from the permeate side.
- *Direct visualization above the membrane*: Positioning the microscope above the membrane avoids the limitation of having to use transparent membranes and allows the observation of particle accumulation beyond a monolayer. Thus the microscope objective is mounted above the membrane to view particle deposition from the feed side.
- *Laser triangulometry*: a laser beam is directed onto a surface of varying elevation, as happens in a developing particle cake layer. A CCD camera captures the reflection of the laser beam off the surface. Since the elevation of the surface changes, the location where the reflected beam is imaged by the CCD array will shift. Measurement of the shift can then be directly related to the displacement of the elevation of the surface. In this way, the growth of a particle cake layer can be monitored during membrane filtration and the thickness of the cake layer can be measured.
- *Optical laser sensor*: the thickness of the cake layer during membrane filtration can be measured using optical laser sensor. The principle of this technique is that the formation of the deposit layer will absorb light from a bypassing laser beam. Since the deposit thickness is changing, the laser beam will detect a variation of the signal intensity. A calibration procedure with known values of cake layer thickness should be performed to extract the correlation.
- *Ultrasonic time-domain reflectometry (UTDR)*: UTDR measures the location of a moving or stationary interface by using sound waves. Information on the physical characteristics of the media through which the waves travel can be gathered with this technique. An ultrasonic transducer will detect reflected waves

produced when the ultrasonic waves encounter an interface between two media. The amplitude of the reflected wave relative to the incident wave is determined by the acoustic impedance difference between the two media as well as the topography of the interface. The time interval between the initiation of the incident wave and the detection of the reflected wave can be used to measure the distance between interfaces.

- *Electrical impedance spectroscopy*: this technique can be used for characterizing membrane properties and membrane fouling. Electrical contacts are connected with the edges of the membrane so that an alternating current is injected directly into the membrane. A metal layer sputtered onto the membrane surface is used to enhance conduction properties. The flow of the current across the membrane surface suffers dispersion due to the presence of the bulk solution and the membrane pores. This dispersion phenomenon is characterized by the capacitance and conductance of the membrane material and the bulk solution, and possible polarization or fouling layer. The changes in the capacitance dispersion of the system are a method to monitor in situ accumulation of particulates that could potentially foul the membrane.

REFERENCES

- Al-anzi, B.S., Siang, O.C., 2017. Recent developments of carbon based nanomaterials and membranes for oily wastewater treatment. *RSC Adv.* 7, 20981.
- Baker, R.W., 2004. *Membrane Technology and Applications*. Wiley.
- Chen, J.C., Li, Q., Elimelech, M., 2004. In situ monitoring techniques for concentration polarization and fouling phenomena in membrane filtration. *Adv. Colloid Interf. Sci.* 107, 83–108.
- Chilton, T.H., Colburn, A.P., 1934. *Ind. Eng. Chem.* 26, 1183–1187.
- Duke, M.C., Diniz da Costa, J.C., Lu, G.Q.M., Petch, M., Gray, P., 2004. *J. Membr. Sci.* 241, 325.
- Feng, C., Khulbe, K.C., Matsuura, T., Farnood1, R., Ismail, A.F., 2015. Recent progress in zeolite/zeotype membranes. *J. Membr. Sci. Res.* 1, 49–72.
- Green, D.W., Perry, R.H., 2007. *Perry's Chemical Engineers' Handbook*, eighth ed. McGraw-Hill, New York, NY.
- Guizard, C., Ayrat, A., Julbe, A., 2002. *Desalination*. vol. 147. p. 275.
- Ismail, A.F., Rana, D., Matsuura, T., Foley, H.C., 2011. *Carbon-Based Membranes for Separation Processes*. Springer-Verlag, New York.
- Liu, B.S., Li, H.X., Cao, Y., Deng, J.F., Sheng, C., Zhou, S.Y., 1997. *J. Membr. Sci.* 135, 33.
- Luis, P., Van der Bruggen, B., 2013. The role of membranes in postcombustion CO₂ capture. *Greenh. Gas Sci. Technol.* 3, 1–20.
- Mori H., S. Fujisaki, T. Siato, T. Sumino, Y. Iwamoto, in *Proceedings of the 9th International Conference on Inorganic Membranes, ICIM9, 2006*, Ed. by R. Bredesen, H. Raeder, pp. 382–385.

- Nijmeyer, A., 1999. Hydrogen-Selective Silica Membranes for Use in Membrane Steam Reforming. (Ph.D. Thesis). Twente University, The Netherlands.
- Park, H.B., Lee, Y.M., 2003. *J. Membr. Sci.* 213, 263.
- Paul, D.R., 2012. Creating new types of carbon-based membranes. *Science* 335 (6067), 413–414.
- Seader, J.D., Henley, E.J., Roper, D.K., 2013. *Separation Process Principles*, third ed. (978-0-470-48183-7).
- Uemiya, S., 1999. *Sep. Purif. Method* 28, 51.
- Wyatt, O.H., Dew-Hughes, D., 1974. *Metals, Ceramic and Polymers*. Cambridge University Press, London.

Microfiltration, ultrafiltration, nanofiltration, reverse osmosis, and forward osmosis

Bart Van der Bruggen*[†]

Department of Chemical Engineering, KU Leuven, Leuven, Belgium Faculty of Engineering and the Built Environment, Tshwane University of Technology, Pretoria, South Africa[†]*

CHAPTER OUTLINE

2.1 Introduction	25
2.2 Process Description and Operating Mode	27
2.3 General Overview of Applications	29
2.4 System Configuration	33
2.5 Hydraulic Resistance	36
2.6 Modeling of Microfiltration (MF)	37
2.7 Modeling of Ultrafiltration (UF)	41
2.8 Modeling of Nanofiltration (NF)	45
2.8.1 Uncharged Solutes	46
2.8.2 Charged Solutes	48
2.9 Modeling of Organic Solvent Nanofiltration (OSN)	49
2.10 Modeling of Reverse Osmosis (RO)	55
2.11 Modeling of Forward Osmosis (FO)	58
2.12 Module Performance	63
2.13 Conclusions	64
References	65
Further Reading	68

2.1 INTRODUCTION

Pressure-driven membrane filtration refers to the use of a transmembrane pressure difference as the driving force for permeation through a membrane (Van der Bruggen, 2017). This pressure can be low, for membranes with a very high porosity and pore size, or high, for nanoporous or dense membranes. According to this, a

classification is made resulting in distinguished processes depending on pore size, applied pressure and, as a consequence, application potential (Mulder, 1996). Microfiltration (MF) is a process in which membranes are used in the micrometer range, down to ca. 0.1 μm . They are denoted as porous membranes and require pressures typically below 1 bar. Ultrafiltration (UF) membranes have a smaller pore size, in the nanometer range (2–100 nm); the porosity is typically lower as well. This requires pressures in the range of 1–6 bar. Nanofiltration (NF) membranes have a pore size of 1 nm and below; operational pressures are 5–15 bar. The application of nanofiltration in organic solvents is typically described as a different process, that is, organic solvent nanofiltration (OSN) or solvent-resistant nanofiltration (SRNF); membranes fall in the NF range in terms of pore size, but membrane materials are different, and flux and rejection models are different as well. Reverse osmosis (RO) membranes are dense and may operate at pressures of 20 bar or even below, in the absence of osmotic pressure, or in the range of 40–60 bar for seawater desalination; in some applications, very high pressures are used, which can go up to 100 bar (“High Pressure Reverse Osmosis”). Forward osmosis (FO) is an outlier, because it relies on osmotic pressure rather than on an applied pressure; this is ideally in the range of pressures used in reverse osmosis for desalination, since FO membranes are also dense. They may be very similar or the same, even though the optimization of membrane properties is different for FO than for RO (Lutchmiah et al., 2014).

The performance of each of these processes is evidently related to these parameters. In microfiltration, nondissolved compounds with a size above the pore size, that is, in the micrometer range, are retained. Energy requirements, however, are low. For ultrafiltration, target compounds to retain are dissolved macromolecules, corresponding to the membranes’ pore size. Energy requirements are higher, as the price to pay for higher rejections.

On the high end of energy requirements is reverse osmosis. This is not only related to the membrane properties as such, but also to the generation of an osmotic pressure due to the rejection of salts (including NaCl). As a consequence, energy requirements are very high and even though this has been optimized over the years, the intrinsic occurrence of osmotic pressure gives a lower value for the optimized energy needs. Nanofiltration was developed as a variation on reverse osmosis (originally also referred to as “Loose Reverse Osmosis”) because it only partially retains monovalent ions, while still rejection multivalent ions nearly completely. This suppresses the osmotic pressure, so that the energy requirements are substantially lower.

Forward osmosis is a process with low energy requirements, since there is no external pressure to be applied. On the other hand, the rejection of salts is very similar to reverse osmosis. However, it should be understood that the outcome of forward osmosis is a (diluted) brine, which requires further processing; therefore the overall energy requirements should be considered rather than the forward osmosis operation alone.

Process modeling for pressure-driven membranes has several critical aspects. First of all, it allows for a comparison among different membranes available for applications, because the parameters that are derived from models give a clear indication of the expected performance. Second, it provides understanding in the mechanisms that govern permeation and separation; for various membrane processes this is still ill understood (which, in turn, also gives uncertainty with respect to available models). Third, modeling is essential for process monitoring. This aspect is especially crucial in the event of membrane fouling, which changes the performance characteristics; this is evident for the flux or permeability, but may also affect the rejection of solutes.

This chapter provides an overview of modeling approaches for microfiltration, ultrafiltration, nanofiltration, reverse osmosis, and forward osmosis, based on today's understanding of the operational principles of each of these processes.

2.2 PROCESS DESCRIPTION AND OPERATING MODE

Two operating modes are applied: dead-end filtration and cross-flow filtration. In dead-end filtration (Fig. 2.1), a feed is applied perpendicular to a membrane, without any flow along the membrane. Stirring is typically applied to reduce polarization effects and obtain a sufficiently high Reynolds number. In dead-end mode, an accumulation of rejected solutes occurs near the membrane surface, which influences the course of the separation. Fluxes may decrease due to the additional resistance of the accumulated compounds; the nature of these compounds is determined by the membrane itself so that the effect may be variable. For microfiltration in particular, the

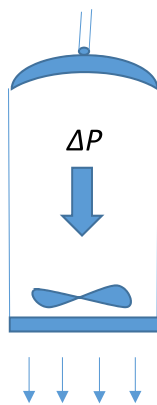


FIG. 2.1

Schematic representation of dead-end filtration.

rejected compounds are solids, which would form a cake layer on the membrane. This decreases the membrane's permeability and flux (often drastically). Thus dead-end filtration is simple in design, but not in operation. Filtration models should primarily take this effect into account and describe flux as a time-dependent function.

Dead-end filtration can be applied at constant flux and increasing pressure to compensate for flux reduction with time, or alternatively, at constant pressure and the flux decreasing with time.

Cross-flow filtration intends to improve the stability of flux and rejection by applying shear forces on the membrane surface, through a flow of the feed along the membrane. This is more energy intensive, and therefore in principle more costly although the improved performance may balance this. A schematic representation is shown in Fig. 2.2. The flow velocity should in principle be as high as possible; a good compromise with the process cost is obtained when applying flow velocities in the order of 1 m/s.

The energy needed for circulating the feed relative to the energy needed for providing the transmembrane pressure is high for microfiltration; for reverse osmosis, this is only a fraction of the required energy. Furthermore, the build-up of solute concentrations, salt concentrations in particular, would be too high for reverse osmosis when applied in dead-end mode; this is also the case for nanofiltration. At the same time, effects of fouling and concentration polarization can be effectively kept under control in cross-flow filtration. Therefore this is the only filtration mode for reverse osmosis and nanofiltration.

For microfiltration the preferred operation mode is dead-end filtration, as it is the most economical strategy. However, microfiltration may also be applied in cross-flow mode, for applications where the effect of fouling is too severe to apply dead-end filtration. Conversely, ultrafiltration is typically applied in cross-flow mode, but may also be used in dead-end mode as a more economical method.

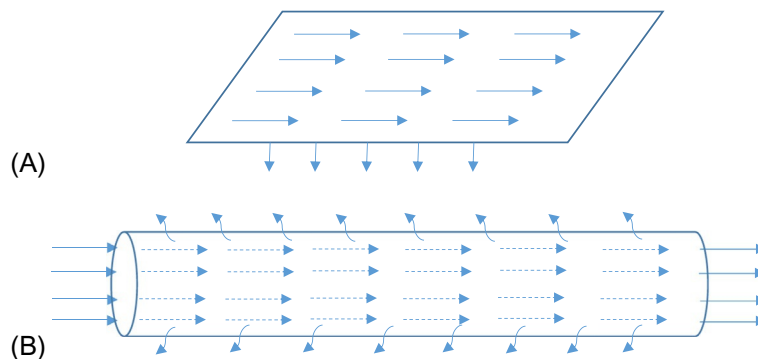


FIG. 2.2

Schematic representation of cross-flow filtration (A) for a flat sheet membrane and (B) for a tubular membrane.

A compromise between dead-end and cross-flow operation is a hybridization denoted as semidead-end operation. This intends to combine the advantage of a dead-end system in obtaining a very high permeate yield, and the advantage of a cross-flow system in having a more efficient control of fouling. A semidead-end system relies on a periodical backwash, that is, a reversal of the flow direction so that permeate returns to the feed side through the membrane, thereby flushing away foulants that have accumulated in the pores of the membrane. After a certain time of regular operation, the effect of fouling becomes significant; at this point, a backwash pump becomes active. The wash water is collected as a waste fraction. After the backwash, the flux is restored and normal filtration can continue. This approach is particularly of interest for the application of microfiltration and ultrafiltration in cases where dead-end operation is not possible due to the extent of membrane fouling.

2.3 GENERAL OVERVIEW OF APPLICATIONS

Applications of pressure-driven membrane processes are specific for the type of membrane; this defines to a large extent the difference between the various membrane processes. The principle is that the maximum pore size should be below the minimum size of the compounds to be retained, preferably by a factor 2. However, the pore size distribution is seldom known, nor is the size of the compounds to be retained; therefore a pragmatic approach is needed, which probably requires testing in order to determine the best membrane choice. General guidelines are limited to the type of process that fits with a given target for removal (shown in Fig. 2.3).

Microfiltration is applied for the removal of nondissolved matter with a size of at least $0.1\ \mu\text{m}$. This includes suspended solids, blood cells, large macromolecules,

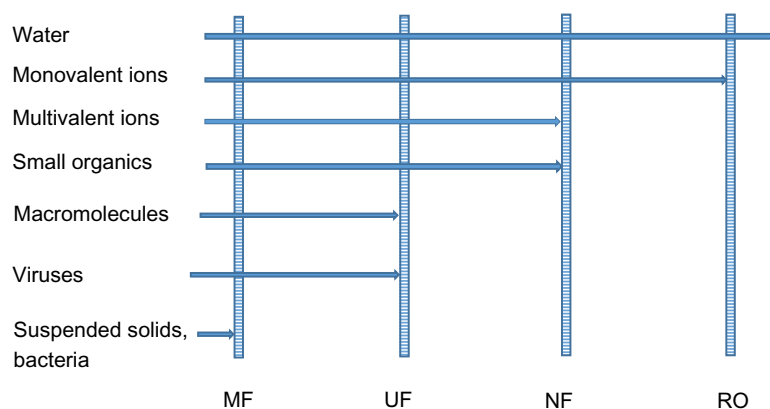


FIG. 2.3

Application scope of pressure-driven membrane processes (*MF*, microfiltration; *NF*, nanofiltration; *RO*, reverse osmosis; *UF*, ultrafiltration).

bacteria with special interest in large bacteria such as *Cryptosporidium* and *Giardia*, which are difficult to oxidize with chlorine. Microfiltration membranes often serve as pretreatment method, in order to avoid particulate fouling in a subsequent operation involving, for example, nanofiltration or reverse osmosis. Microfiltration yields a permeate entirely free of turbidity, which is a much better outcome than can be obtained with settling. However, the removal of dissolved compounds is minimal. Thus the point of reference is settling since this has the same removal targets. In this comparison, microfiltration easily wins in terms of technical performance. This explains its use in membrane bioreactors (MBRs), where the benefit compared to a classical activated sludge system with subsequent settling is indeed in the use of a microfiltration membrane. Similarly, microfiltration is used for harvesting of microalgae (Bilad et al., 2014). Another important application area is in the food technology, where microfiltration is used for clarification of fruit juices and beverages (Girard and Fukumoto, 2000). A specific example is wine filtration by cross-flow microfiltration (El Rayess et al., 2011).

An application with much impact is the treatment of oil-water emulsions. For separation of oil emulsions as an end-of-pipe treatment, membranes are more likely where process volumes are $<190\text{ m}^3$ per day. Membranes could also be useful in a hybrid system when combined with conventional chemical treatment systems to concentrate sludge (Cheryan and Rajagopalan, 1998). For this purpose, 3D printed membranes have been reported to be viable (Yuan et al., 2017).

Ultrafiltration has replaced microfiltration in several applications, or has become competitive with microfiltration for enhanced turbidity removal because of its gradually increased permeability, which yields a similar flux than with a microfiltration membrane in many cases, but with an enhanced removal potential. This is particularly the case for membrane bioreactors, where the trend is to use ultrafiltration membranes rather than microfiltration membranes; this is partly related to the target of water reuse, which has more potential when using ultrafiltration membranes since not only bacteria are effectively removed, but also viruses (which are smaller than bacteria, while they are in the size range for ultrafiltration set by the rule of thumb given previously). In a more general sense, ultrafiltration appeared to be a cost effective and efficient method of removing suspended solids and bacteria (Jamaly et al., 2014). The disinfection effect of an ultrafiltration is generally an important consideration for applications. Other applications include the separation of macromolecules, the color removal, the preconcentration of milk, the recovery of vaccines from fermentation, and the concentration of fruit juices.

Applications of *nanofiltration* define the scope of the process, rather than the separation principle or membrane type. Nanofiltration membranes were developed to retain small organic compounds and ions, but to a lower extent than reverse osmosis membranes, so that the osmotic pressure (and therefore the required transmembrane pressure) is lower. Membranes that were used for this purpose were made in the same way as reverse osmosis membranes, by the addition of an interfacially polymerized thin polyamide top layer on top of an asymmetric phase inversion membrane. Such nanofiltration membranes were then in fact reverse osmosis membranes with an

insufficient performance in desalination. The interest is in economical separations for applications where a complete rejection of salts, specifically monovalent salts, is not necessary or even desired. Desalination of seawater is not a target application; however, for many other water sources (in drinking water production), an adjustment of the concentration of (multivalent) ions and organic compounds is of interest. The key application is in a combined removal of natural organic matter and hardness from water (Van der Bruggen and Vandecasteele, 2003). This has a proven efficiency in many applications.

The same objectives were explored by optimizing membranes made with synthesis methods similar to ultrafiltration membranes, without an interfacially polymerized thin top layer. This led to a different type of nanofiltration membranes, which typically have a lower rejection of salts. Such membranes allowed to explore a new range of applications, that is, in fractionation of salts and organic solutes. A key application of this is the treatment of textile effluents, which often contain high concentrations of dyes and salts. By producing a permeate containing (most of) the salts, it can be directly reused in textile processing so that no salts are to be added, apart from a small fraction to compensate for the loss of salts in the concentrate. The concentrate contains the dyes, which in some cases can be recycled as well (Lin et al., 2015). The driver for applying nanofiltration is thus in the fractionation ability, which is unique for nanofiltration and allows for resource recovery. This can be applied for other wastewater streams as well; the objective of resource recycling can be also extended to conversion processes in biorefineries, which has much potential to produce valuable compounds but has high demands for fractionation. Membrane cascades based on nanofiltration membranes might solve these challenges (Caus et al., 2009a).

Organic solvent nanofiltration or *solvent-resistant nanofiltration* is similar to aqueous nanofiltration, but materials, mechanisms of transport, and models are different because of the strong influence of solvent properties and their interaction with the membrane material. Organic solvent nanofiltration was developed later than aqueous nanofiltration, mostly due to a lack of stability of polymeric membranes in organic solvents. Stable membranes have been developed since the end of the 1990s, which shifted the challenge to the development of a fundamental understanding of solvent nanofiltration. In addition, available membranes often have a limited scope in applicable solvents.

Organic solvent nanofiltration has a potential use in a broad range of applications (Marchetti et al., 2014), including solvent recovery in lube oil dewaxing, as well as use in the vegetable oil industry, in heterogeneous synthesis and in chemical processes requiring solvent exchange for solvent purification in the oil industry (Vandezande et al., 2008). Another significant application area is the preparation of active pharmaceutical ingredients (APIs) in the pharmaceutical industry. Several active compounds are obtained by organic synthesis (extraction from vegetable products, animal sources, or micro-organisms). Impurities present in solvents could have an impact on the stability and performance of the drugs, so that purification is an essential step. Organic solvent nanofiltration allows to recover and recycle organic

solvents during the process, which increases the production capacity and results in a considerable cost reduction for the in-line manufacturing of pharmaceuticals and drugs. Important economic and environmental benefits can be achieved, provided that stable membranes with good separation performance can be used (Geens et al., 2007).

Reverse osmosis has a dominant application in desalination. It has been applied for the first time in 1964 in Coalinga, California, USA, although the process was far from realistic in that moment due to the extremely high pressures to be applied, and the limited production of water. However, reverse osmosis membranes were gradually improved, and especially the use of thin film composite membranes, with a very thin top layer made by interfacial polymerization, drastically improved the performance of reverse osmosis in desalination. By the mid-1990s, reverse osmosis had become the most economical desalination process. This initiated applications on a massive scale. In Israel, for example, the Sorek desalination plant uses reverse osmosis to produce 150 million m³ water per year; the total capacity of RO desalination in Israel is over 600 million m³. For this reason, reverse osmosis is the membrane process used on the largest scale. This has further stimulated other applications; because membranes for reverse osmosis have become economically very competitive, this gave a large benefit for any other use of such membranes as well. Thus reverse osmosis has also become a standard process for the production of ultrapure water, and for water recycling either directly from wastewater, or indirectly by infiltration of permeates into aquifers for later use as drinking water (Van Houtte and Verbauwhe, 2013).

Forward osmosis is often referred to as a desalination process, but this is not correct. In forward osmosis, a draw solution is diluted by water extracted from a feed stream; the driving force for transport of water through the membrane is the osmotic pressure difference between the concentrated draw solution and the feed stream. Desalination of the feed stream is only obtained when the draw solution is regenerated by removal of the dilution water. When the draw solution is a brine, this is the real desalination process (which can be reverse osmosis or any other desalination process). Various processes for draw solution regeneration have been explored, as well as a large number of potential candidates to provide the osmotic pressure required in the draw solution. In addition, variations on forward osmosis such as pressure-assisted forward osmosis have been explored (Yun et al., 2012). However, none of these appeared to be energetically beneficial in the overall process. Integration of processes may overcome this problem; for example, extracting water from wastewater to dilute a stream intended for desalination would lower the osmotic pressure for the desalination process, which gives an energetic benefit. This is shown in Fig. 2.4 (Choi et al., 2017).

Forward osmosis was developed in 1976 as a method for fertigation (Kessler and Moody, 1976; Moody and Kessler, 1976). Such application does not require a regeneration of the draw solution, which is to be used as a diluted fertilizer. The rediscovery of forward osmosis fifteen years later overlooked this aspect and failed in finding solutions for the draw solution (Van der Bruggen and Luis, 2015) so that the process after two more decades has still not made a breakthrough.

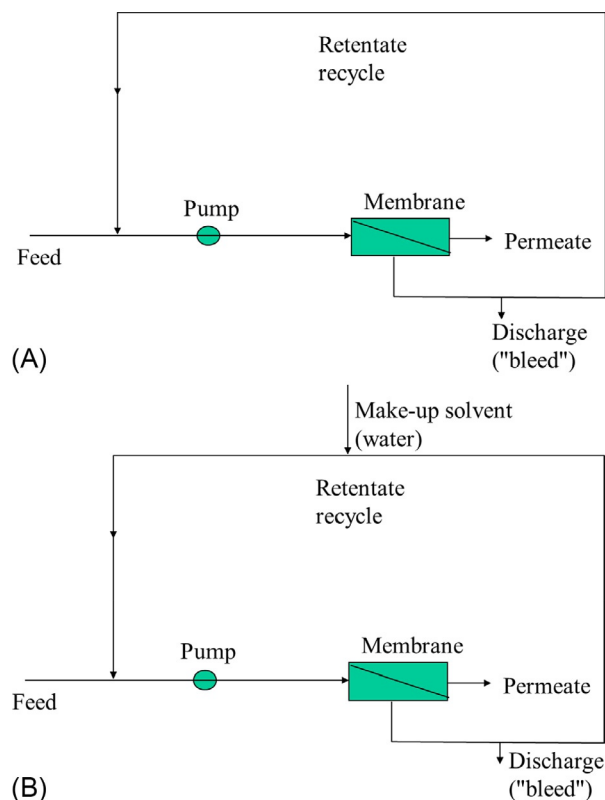


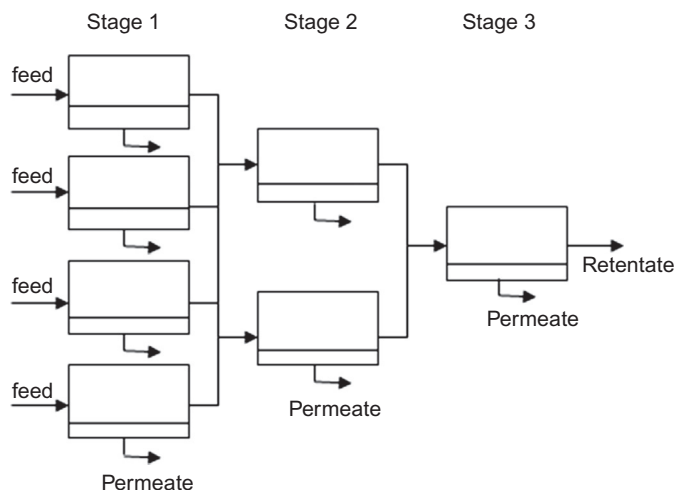
FIG. 2.5

Process configuration for (A) feed-and-bleed operation and (B) diafiltration.

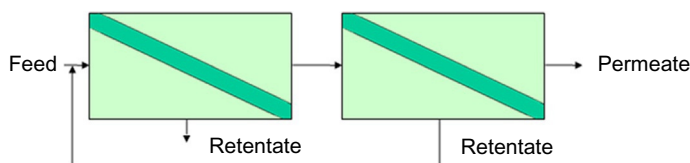
separation between two solutes is obtained. The obvious disadvantage of diafiltration is that the permeate flow is diluted.

In order to optimize the volume of permeate rather than its purity, the concentrate produced in a filtration module can be fed to a new module, producing more permeate (although at higher feed concentration). This yields the so-called Christmas tree configuration shown in Fig. 2.6: due to the decrease in remaining volume, less filtration modules are needed in every stage.

Finally, the configuration for an optimal performance is a membrane cascade. In this approach, the concentrate obtained in a second stage is recycled to the first stage, in order to enhance the overall permeate yield. A two-stage membrane cascade is shown in Fig. 2.7; this concept can be extended to more stages, although the cost of repressurizing the permeate is a limitation for applying membrane cascades in practice. It should be noted that while in the example in Fig. 2.7 the concentrate (retentate) is recycled, the same approach can be followed for a recycle of the permeate.

**FIG. 2.6**

Christmas tree configuration with further filtration of concentrate.

**FIG. 2.7**

Two-stage membrane cascade.

Membrane cascades are particularly of interest for nanofiltration, which is a process with much potential for fractionation. In aqueous solution, nanofiltration membranes have a significantly different rejection for monovalent salts than for multivalent salts. By using a membrane cascade, this difference can be enhanced to obtain a complete separation of monovalent ions (in the permeate) and multivalent ions (in the concentrate), of course depending on the composition of the feed stream and the exact ionic composition. This can also be applied for organic solutes such as micropollutants or dyes, aiming at permeating the salts while efficiently retaining the organics. The limitation is mostly in the cost of a two (or more) stage process, which is often not justified for water purification. However, for solutes in organic solvents this should not be a limitation, for example, in pharmaceutical synthesis, where a cascade can be used to fractionate two solutes with a difference in molar mass, or a difference in polarity (Renouard et al., 2018; Caus et al., 2009b; Peeva et al., 2014). The operation of a cascade is challenging because the flows are connected and should therefore be consistent in each stage (since permeabilities may be low

in some cases, and then yield insufficient feed for the subsequent stage). Thus a careful estimation of the performance of a cascade, and a good membrane selection, are essential.

2.5 HYDRAULIC RESISTANCE

The equilibrium between two phases separated by a membrane is defined by the electrochemical potential:

$$\mu_i = \mu_i^\circ + RT \ln a_i + V_i \cdot P + z_i F \psi \quad (2.1)$$

where, μ_i is the electrochemical potential of component i , μ_i° is the chemical potential of component i in reference conditions, R is the ideal gas constant, T is the temperature, a_i is the activity of component i , V_i is the molar volume of component i , P is the pressure, z_i is the ion valence ($=0$ in case of uncharged compounds), F is Faraday's constant, and ψ is the electrical potential.

It should be remarked that for phases separated by a membrane, thermal and mechanical equilibrium between the phases on each side of the membrane is not a condition, since the membrane can be used as an insulator, and can also sustain a difference in pressure between phases. Moreover, these two parameters appear in the equation for the electrochemical potential, so that they can be used to induce mass transfer from one phase to the other. The two remaining parameters that can be used for this purpose are the activity difference between two phases and a difference in electrical potential. Pressure-driven membrane processes are those in which the pressure is exploited as the driving force to transport mass through a membrane. This can be expressed by the following general equation:

$$N_i \sim \frac{dP}{dx} \quad (2.2)$$

in which N_i is the molar flux of a component i . Since the pressure gradient is the same for all components, the proportionality constant should be specific for each species i . Because a membrane is generally thin, the pressure gradient can be replaced by a pressure difference, while the denominator is the membrane thickness:

$$N_i = \frac{P_{M,i}}{l_M} \Delta P = \overline{P_{M,i}} \Delta P \quad (2.3)$$

in which $P_{M,i}$ is the permeability, and $\overline{P_{M,i}}$ is the permeance.

The equation is mostly used for describing transport of the solvent (water, or any other solvent in the case of organic solvent nanofiltration). The component i then refers to the solvent.

The (inverse) permeability or permeance can be represented as the hydraulic resistance against mass transport. However, the permeability depends not only on the membrane properties, but also on the feed viscosity: permeability is inversely proportional to viscosity. For this reason, the viscosity is represented as a separate factor in the flux equation and is not included in the hydraulic resistance R_M :

$$N = \frac{1}{R_M} * \frac{1}{\eta} * \Delta P \quad (2.4)$$

in which N is the solvent flux, and η is the viscosity of the feed flow.

For modeling the flux of a pure solvent, the hydraulic resistance R_M can be related to the membrane morphology and/or functional parameters of the membrane. By extending this approach, time dependency and membrane fouling can be introduced in the model as an additional resistance; this will lead to the resistance-in-series model, which will be further elaborated later.

2.6 MODELING OF MICROFILTRATION (MF)

Microfiltration models are focused on fluxes or permeabilities, rather than on rejection; this is due to the unavailability of data for particle sizes in feed solutions, and pore size distributions, as stated previously.

In microfiltration, transport of the solvent (which would be water in most cases) occurs by bulk flow. This assumes that the dimensions of the pore are sufficient to resemble a flow in which the pore wall is relatively far away. In the case of aqueous flow, the pore size is at least three orders of magnitude.

Thus known equations for macroscopic flow can be used as a starting point. Two cases may then be considered: flow through a cylinder, for pores with a cylindrical shape, and flow through a packed bed, for sintered structures. It should be noted that Reynolds numbers for the flow in a microfiltration membrane are normally below 2000 so that a laminar flow regime can be assumed.

For a cylinder, the velocity of the bulk flow, v , depends on the pressure drop, $(P_0 - P)$ over the membrane, the pore diameter D , the liquid viscosity, μ , and the length of the pore, L , as described by Hagen-Poiseuille's law:

$$v = \frac{D^2}{32\eta L} (P_0 - P) \quad (2.5)$$

The flow occurs only in the fraction of the surface occupied by pores, ε :

$$\varepsilon = n\pi \frac{D^2}{4} \quad (2.6)$$

in which n is the number of pores for a given surface area.

The flux N can be written as:

$$N = v \cdot \varepsilon \cdot \rho \quad (2.7)$$

in which ρ represents the density.

This then becomes:

$$N = \frac{n\pi\rho D^4}{128\eta L} (P_0 - P) \quad (2.8)$$

If the pores are not straight or cylindrical this equation should be adapted with a factor reflecting the tortuosity τ , the ratio between the real length of the pore and the minimum length, which assumes a straight cylinder. This corresponds to an increase of the pore length.

$$N = \frac{n\pi\rho D^4}{128\eta\tau L}(P_0 - P) = \frac{\varepsilon\rho D^2}{32\eta\tau L}(P_0 - P) \quad (2.9)$$

The tortuosity can differ from pore to pore, but for the overall flux equation an average value should be estimated. This can be done by measuring the flux at a given pressure difference, given the membrane thickness, porosity, and pore size as membrane parameters, and the viscosity and density as flow parameters:

$$\tau = \frac{\varepsilon\rho D^2(P_0 - P)}{32\eta L N} \quad (2.10)$$

For noncylindrical pores, the hydraulic diameter is given by:

$$d_h = 4 \cdot \left(\frac{\text{available volume}}{\text{total surface area of pores}} \right) \quad (2.11)$$

Based on the Ergun equation for flow in a packed bed, this yields:

$$N = \frac{\rho\varepsilon^4}{2\tau(1-\varepsilon)2a_v2\eta L}(P_0 - P) \quad (2.12)$$

in which a_v is the specific surface area of the pores.

An important aspect of modeling in microfiltration is to follow up the decrease of flux in conditions of membrane fouling. This is often done by using the resistance-in-series model (in contrast to pore blocking models, not considered here), which considers a foulant layer as an additional mass transfer resistance. The (volumetric) flux is then expressed as:

$$N = \frac{1}{\eta} \cdot \frac{\Delta P}{(R_m + R_c)} \quad (2.13)$$

with R_m the membrane resistance and R_c the additional resistance due to fouling.

The additional resistance for formation of a cake layer can be written as

$$R_c = K_1 \frac{c_F V (1 - \varepsilon_c)}{\rho_c A_M \varepsilon_c^3} \quad (2.14)$$

with ρ_c the density of the cake layer, ε_c the porosity of the cake layer, and V the volume filtered through the membrane.

The flux equation then becomes:

$$N = \frac{1}{\eta} \cdot \frac{\Delta P}{\left(R_m + K_1 \frac{c_F V (1 - \varepsilon_c)}{\rho_c A_M \varepsilon_c^3} \right)} \quad (2.15)$$

The properties of the cake are typically not known and do not contribute to the model since a proportionality factor, K_1 , is used. Thus the equation can be simplified to:

$$N = \frac{1}{\eta} \cdot \frac{\Delta P}{\left(R_m + K_2 \frac{c_F V}{A_M}\right)} \quad (2.16)$$

Microfiltration can be operated in two modes, as previously explained: with constant pressure, or with constant flux. If the flux is constant, the pressure is time dependent as follows:

$$\Delta P = N \cdot \eta \cdot (R_m + K_2 c_F N t) \quad (2.17)$$

With constant pressure, Eq. (2.16) should be integrated:

$$\int_0^V \left(R_m + K_2 \frac{c_F V}{A_M}\right) dV = \frac{A_M \Delta P}{\eta} \int_0^t dt \quad (2.18)$$

which yields

$$R_m V + \frac{K_2 c_F V^2}{2 A_M} = \frac{A_M \Delta P}{\eta} t \quad (2.19)$$

This can be solved for V :

$$V = -\frac{R_m A_M}{K_2 c_F} + \frac{A_M}{K_2 c_F} \left(R_m^2 + \frac{2 K_2 c_F \Delta P \cdot t}{\eta}\right)^{0.5} \quad (2.20)$$

And

$$N = \frac{1}{A_M} \frac{dV}{dt} = \frac{\Delta P}{\eta} \left(R_m^2 + \frac{2 K_2 c_F \Delta P \cdot t}{\eta}\right)^{-0.5} \quad (2.21)$$

Thus for constant flux (Eq. 2.17) as well as for constant pressure (Eq. 2.21), the (volumetric) flux can be described based on a single fitting parameter, K_2 , the membrane resistance in unfouled conditions as the only membrane parameter, and the viscosity and feed concentration as feed parameters.

The flux relative to the initial flux can be obtained by dividing Eq. (2.21) to the flux value at $t = 0$ (Romero and Davis, 1990; Davis, 1992):

$$\frac{N}{N_0} = \left(1 + \frac{2 R_c \Phi_c \Delta P \cdot t}{(\Phi_c - \Phi_b) \eta R_m^2}\right)^{-0.5} \quad (2.22)$$

in which the constant K_2 is related to the cake layer resistance R_c , the solid volume fraction in the suspension Φ_b , and the solid volume fraction in the cake Φ_c .

These equations can be applied as such in dead-end filtration. In cross-flow microfiltration, however, a shear stress is applied. In these conditions, a term should be included to express the transport away from the membrane due to the forces induced by shear stress. The difference between both is shown in Fig. 2.8.

The resistance-in-series model is then written as:

$$N = \frac{1}{\eta} \cdot \frac{\Delta P}{(R_m + \hat{R}_c \delta_c + R_f)} \quad (2.23)$$

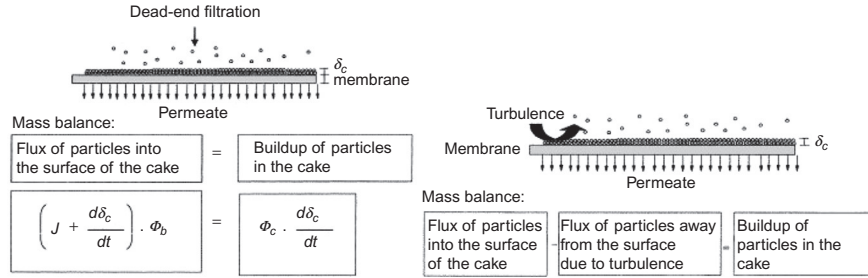


FIG. 2.8

Mass balance for dead-end microfiltration (left) and cross-flow microfiltration (right) (Silva et al., 2000).

in which the cake layer resistance is considered as a specific cake resistance multiplied by the cake thickness. The fouling resistance R_f can be due, for instance, to pore-blocking and adsorption phenomena (Silva et al., 2000).

The particle mass balance in the system shown in Fig. 2.8 is:

$$\left(N + \frac{d\delta_c}{dt}\right)\Phi_b - k_1 \left(\frac{dU}{dy}\right)\delta_c = \Phi_c \frac{d\delta_c}{dt} \quad (2.24)$$

The membrane pore size and suspended particle diameter distribution are considered uniform, and particles are retained completely by the membrane. Furthermore, concentration polarization is assumed to be completely eliminated by agitation (Wang et al., 2007).

Assuming that the membrane resistance and the fouling resistance are smaller than the cake layer resistance, Eqs. (2.23), (2.24) can be combined to

$$\frac{d\delta_c}{dt} = \frac{\Delta P \Phi_b}{\eta \hat{R}_c \delta_c (\Phi_c - \Phi_b)} - \frac{k_1 \left(\frac{dU}{dy}\right) \delta_c}{(\Phi_c - \Phi_b)} \quad (2.25)$$

Assuming that the cake thickness is 0 at the beginning of the filtration ($\delta_c = 0$ at $t = 0$); considering that the transmembrane pressure ΔP and the velocity gradient dU/dy are constant over the period of filtration, and assuming that \hat{R}_c is constant, that is, no significant changes in cake compression occur, Eq. (2.25) can be solved to

$$\delta_c(t) = \left(\frac{\Delta P \Phi_b}{\hat{R}_c k_1 \eta \left(\frac{dU}{dy}\right)} \left(1 - \exp \left(\frac{-2k_1 \left(\frac{dU}{dy}\right) t}{\Phi_c - \Phi_b} \right) \right) \right)^{0.5} \quad (2.26)$$

The flux then becomes (reintroducing R_m and R_f):

$$N(t) = \frac{\Delta P}{\left(\frac{\Delta P \Phi_b \eta \hat{R}_c}{k_1 \left(\frac{dU}{dy} \right)} \left(1 - \exp \left(\frac{-2k_1 \left(\frac{dU}{dy} \right) t}{\Phi_c - \Phi_b} \right) \right) \right)^{0.5}} + \eta \cdot (R_m + R_f) \quad (2.27)$$

The term dU/dy depends on the fluid behavior; for Newtonian liquids:

$$\frac{dU}{dy} = \frac{\tau_w}{\eta} \quad (2.28)$$

while for non-Newtonian liquids more complex equations have to be used.

Lastly, the compressibility of the cake layer can be taken into account by assuming

$$\hat{R}_c = \alpha_0 (\Delta P)^s \rho_s \Phi_c \quad (2.29)$$

where α_0 is a constant related to the size and shape of particles, s the cake compressibility, and ρ_s the mass density of solids comprising the cake (Silva et al., 2000).

2.7 MODELING OF ULTRAFILTRATION (UF)

The focus in models for ultrafiltration is in the ability to predict the separation performance of ultrafiltration membranes. Generally, only the molecular weight cutoff (MWCO) is used as a reference for the performance of an ultrafiltration membrane. The MWCO of a membrane is the molar mass of a solute retained for 90% by the membrane. The retention of a solute is defined as:

$$R_i = \left(1 - \frac{c_{p,i}}{c_{F,i}} \right) \cdot 100\% \quad (2.30)$$

where $c_{p,i}$ and $c_{F,i}$ are the concentration of solute i in the permeate and feed, respectively.

The MWCO is the molar mass of a compound i with retention 90%. This gives a (very) rough indication of the separation ability. However, there is no standardized procedure for the determination of the MWCO, so that the information given by suppliers is not always reliable. Furthermore, the MWCO does not provide sufficient information, not even qualitatively. This is shown in Fig. 2.9, where two rejection curves are compared, describing the rejection as a function of molar mass as a size indicator. The two membranes shown in this figure are different in MWCO, but also in the variation of rejections as a function of molecular size. These variations occur over several orders of magnitude, since the horizontal axis has a logarithmic scale. The curves indicate that the MWCO has very limited value in predicting the rejection of compounds with a molar mass different from the MWCO; even for solutes with a molar mass close to the MWCO a prediction is unreliable, because other characteristics such as the configuration of the molecule may also play a role.

A more detailed analysis can be made on the basis of sieving coefficients, which are defined as one minus the retention, or:

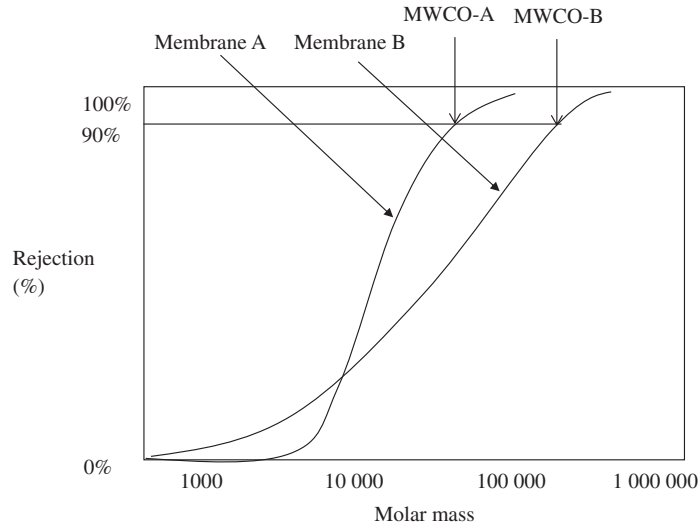


FIG. 2.9

Indicative rejection curves for two membranes A and B, with molecular weight cutoff values MWCO-A and MWCO-B.

$$S_i = \left(\frac{c_{p,i}}{c_{F,i}} \right) \quad (2.31)$$

For traditional ultrafiltration processes used for protein concentration, the selectivity Ψ is defined as the ratio of the flux of a small solute (e.g., a buffer component) to that of the product/protein of interest and is thus equal to the reciprocal of the protein sieving coefficient (assuming that the sieving coefficient of the small solute is equal to one) (Polyakov and Zydney, 2013).

$$\Psi_i = \frac{1}{S_i} \quad (2.32)$$

This selectivity (or separation factor) has a trade-off relationship with the hydraulic permeability, similar to the “upper bound” used in gas separation and denoted in the literature (Mehta and Zydney, 2005) with the worrisome term “line of death.” An example of this trade-off relationship for bovine serum albumin (BSA) with different UF membrane materials is shown in Fig. 2.10 (Mehta and Zydney, 2005).

Modeling of transport through ultrafiltration membranes is based on steady-state hydrodynamic equations describing hindered diffusion and convection of solutes and solvents. For the solute flux, the governing set of hydrodynamic equations for the motion of a single solute particle in a pore can be directly solved (Polyakov and Zydney, 2013). The role of the membrane in mass transport is in providing hindrances to diffusion and convection, which are due to solute steric restriction at the pore entrance and frictional drag caused by hydrodynamic interactions with the pore wall. This is described in modeling by simple hindrance factors; typically,

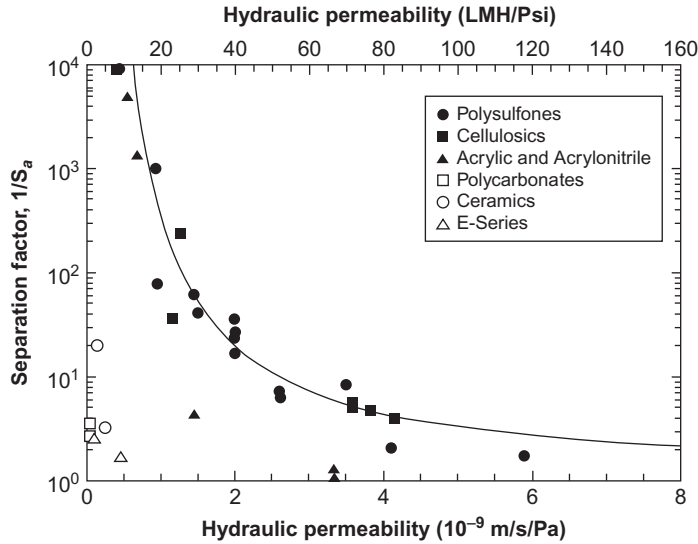


FIG. 2.10

Selectivity-permeability trade-off for ultrafiltration membranes using bovine serum albumin (BSA) as the model protein (Mehta and Zydney, 2005).

these hindrance factors are related to the ratio of the solute to pore radius. The position of the solute in the pore determines the hydrodynamic interactions with the wall; therefore all forces that influence the equilibrium particle position within the pore should be taken into account. Furthermore, the solute concentrations in the pore interior are related to the concentrations in the solution external to the membrane pores by the solute equilibrium partition coefficient (Polyakov and Zydney, 2013). The resulting transport and partition coefficients can be substituted into the differential equations obtained by equating the gradient in the chemical potential of the solute to the hydrodynamic drag force acting on the solute in the pore (Polyakov and Zydney, 2013).

The sieving coefficient is then obtained by applying the Spiegler-Kedem model over the length of the membrane pores (for a complete analysis the reader is referred to the work of Opong and Zydney (1991)):

$$S_i = \frac{\Phi K_c \exp(Pe_m)}{\Phi K_c + \exp(Pe_m) - 1} \quad (2.33)$$

in which Φ is the solute partition coefficient, K_c is the hindrance factor for solute convective transport, and Pe_m is the membrane pore Péclet number, defined as:

$$Pe_m = \frac{K_c N l_p}{K_d D_\infty} \quad (2.34)$$

in which K_d is the hindrance factor for solute diffusive transport, l_p is the membrane thickness (=pore length), and D_∞ is the solute diffusion coefficient in the free solution outside the pore.

For an uncharged, hard sphere in an uncharged cylindrical pore, the partition coefficient accounts for the steric exclusion of the solute from the region within one solute radius of the pore wall and is therefore (Polyakov and Zydney, 2013):

$$\Phi = (1 - \lambda)^2 \quad (2.35)$$

In this equation, λ is the ratio between solute size and pore size. For the partition coefficient for a charged hard sphere in a cylindrical pore with charged walls, other equations are available (Polyakov and Zydney, 2013).

For $\lambda < 0.8$:

$$K_c = (1 + 2\lambda - \lambda^2)(1.0 + 0.054\lambda - 0.988\lambda^2 + 0.441\lambda^3) \quad (2.36)$$

$$K_d = 1.0 - 2.30\lambda + 1.154\lambda^2 + 0.224\lambda^3 \quad (2.37)$$

Further extensions of this approach are in considering a pore size distribution instead of a single pore size, although it appears that the pore size distribution for typical ultrafiltration membranes has only a small effect on the permeability-selectivity trade-off.

For further considerations and other conditions, the reader is referred to Mochizuki and Zydney (Mochizuki and Zydney, 1992) and to Opong and Zydney (Opong and Zydney, 1991).

For fouled membranes, the permeability and sieving coefficients become time dependent. In the classical pore blocking model, in which it is assumed that all solutes are larger than the pore size and are therefore completely retained, an exponential decrease is predicted:

$$\frac{N}{N_0} = \exp(-k_G t) \quad (2.38)$$

in which k_G is an empirical fouling coefficient (in principle equal to the initial volumetric permeate flow rate G_0 times the initial concentration).

When the membrane has a distribution pore sizes, with minimum pore radius $r_{min p}$ and a maximum pore radius $r_{max p}$, the permeate flux is given by an integral over the pore size distribution, as follows:

$$N(t) = \frac{\pi \Delta P}{8 \eta l_p} \int_{r_p^{min}}^{r_p^{max}} n(t) f_n(r_p, t) r_p^4 dr_p \quad (2.39)$$

In this equation, $n(t)$ is the total number of open pores per m^2 at time t and $f_n(r_p, t)$ is the probability density function, which can be written as:

$$\int_{r_p^{min}}^{r_p^{max}} n(t) f_n(r_p, t) dr_p = 1 \quad (2.40)$$

The change in flux is depending on the kinetics of pore plugging:

$$\frac{dn(t)f_n(r_p, t)}{dt} = \frac{N(t)n(t)f_n(r_p, t)r_p^4}{\int_{r_p^{min}}^{r_p^{max}} n(t)f_n(r_p, t)r_p^4 dr_p} \int_{r_p}^{r_p^{max}} c(r_s) dr_s \quad (2.41)$$

where $c(r_s)$ is the solute concentration density. This should fulfill the following requirement:

$$c(r_s) dr_s = C f_s(r_s) dr_s \quad (2.42)$$

C is the total number of solutes per m^3 of solution (which is assumed to be constant) and $f_s(r_s)$ is the solute probability density function:

$$\int_{r_s^{min}}^{r_s^{max}} f_s(r_s) dr_s = 1 \quad (2.43)$$

Eq. (2.41) generalizes the classical pore blockage model in the sense that the pore plugging rate for pores of radius r_p is proportional to the permeate flux through those pores multiplied by the number concentration of hard sphere solutes with radii equal to or larger than r_p .

By combining Eqs. (2.39) and (2.41):

$$\frac{dn(t)f_n(r_p, t)}{dt} = -\frac{\pi\Delta P}{8\eta l_p} f_n(r_p, t) r_p^4 \int_{r_p}^{r_p^{max}} c(r_s) dr_s \quad (2.44)$$

This then eventually leads to the following flux equation:

$$N(t) = \frac{\pi\Delta P}{8\eta l_p} \int_{r_p^{min}}^{r_p^{max}} n(0)f_n(r_p, 0) \exp\left(-\frac{\pi\Delta P}{8\eta l_p} r_p^4 t \int_{r_p}^{r_p^{max}} c(r_s) dr_s\right) r_p^4 dr_p \quad (2.45)$$

For uniform pore and solute size distributions, Eq. (2.38) is found again.

The selectivity of the membrane is composed of two contributions. Solutes with a radius of at least r_p are completely retained, while smaller solutes are retained due to steric and/or electrostatic interactions.

For a compound with radius r_s the permeate solute concentration density $c_p(r_s, t)$ at time t then becomes:

$$c_p(r_s, t) = c(r_s) \frac{\int_{r_p}^{r_p^{max}} S_i\left(\frac{r_s}{r_p}\right) n(t)f_n(r_p, t) r_p^4 dr_p}{\int_{r_p^{min}}^{r_p^{max}} n(t)f_n(r_p, t) r_p^4 dr_p} \quad (2.46)$$

2.8 MODELING OF NANOFILTRATION (NF)

Nanofiltration modeling is complicated in the sense that steric effects are to be combined with charge interactions on a molecular scale. This entails a combination of transport by diffusive effects, convective flow, and electrostatic effects.

2.8.1 UNCHARGED SOLUTES

For uncharged molecules, transport is a combination of diffusion and convection. This is reflected by the transport equations of Spiegler and Kedem for the water flux and for the flux of a dissolved component (Spiegler and Kedem, 1996):

$$N_v = L_p(\Delta P - \sigma \cdot \Delta \pi) \quad (2.47)$$

$$N_s = P_s \Delta c + (1 - \sigma) N_v c \quad (2.48)$$

in which L_p is the hydraulic permeability of the membrane, P_s is a solute permeability coefficient equal to the diffusion coefficient evaluated in the pore divided by the membrane thickness, ΔP is the applied pressure difference, $\Delta \pi$ is the osmotic pressure difference (which will be described in more detail in the section on reverse osmosis), and σ is the reflection coefficient, indicating the fraction of the solute that is maximally retained by the membrane.

Solving this equation yields an expression for the rejection:

$$R_i = \frac{\sigma_i(1 - F)}{1 - \sigma_i F} \quad (2.49)$$

With

$$F = \exp\left(-\frac{1 - \sigma}{P_s} N_v\right) \quad (2.50)$$

The reflection coefficient σ of a given component is the maximal possible retention for that component. From Eqs. (2.49) and (2.50), it can be seen that this corresponds with the rejection at an infinite solvent flux. A model for σ would provide the necessary information about retention at relatively high solvent fluxes, and, correspondingly, at high pressures.

In the Steric Hindrance Pore (SHP) model the reflection coefficient is calculated based on the pore diameter and the diameter of the solute (Wang et al., 1997); it is assumed that all pores have the same diameter. Therefore this uniform pore size should not be considered a real value for the diameter of the pores. The calculated pore size is understood to be the pore size of an imaginary membrane with uniform pores, for which the retention of unchanged molecules is equal to the retention with the real membrane. In reality not every pore is cylindrical with the same diameter; the model is therefore an approximation of the membrane structure.

The reflection coefficient is approximated in a similar way as for ultrafiltration membranes:

$$\sigma = 1 - H_F S_F \quad (2.51)$$

in which H_F is a “wall-correction parameter” representing the effect of the pore wall; S_F is a parameter representing steric hindrance during transport through the pores.

Expressions for H_F and S_F are as follows:

$$H_F = 1 + (16/9)\lambda^2 \quad (2.52)$$

$$S_F = (1 - \lambda)^2 (2 - (1 - \lambda)^2) \quad (2.53)$$

in which λ is again the ratio between solute size and pore size.

In the log-normal model (Bruggen et al., 2000) the pore size is not assumed constant; a log-normal distribution is anticipated for the pore size. No steric hindrance in the pores or hydrodynamic lag is taken into account, but it is assumed that a molecule permeates through every pore that is larger than the diameter of the molecule. Moreover, the diffusion contribution to the transport through the membrane is considered to be negligible. Therefore the reflection coefficient becomes:

$$\sigma(r_s) = \int_0^{r_s} \frac{1}{S_p \sqrt{2\pi}} \cdot \frac{1}{r} \cdot \exp\left(\frac{-(\ln(r) - \ln(\bar{r}))^2}{2S_p^2}\right) dr \quad (2.54)$$

in which $r_s = d_s/2$. S_p is the standard deviation of the distribution, that is, a measure for the distribution of pore sizes. As the reflection curve (reflection coefficients as a function of solute size) corresponds to an integrated log-normal distribution, a small S_p represents a large slope of the reflection curve; a large S_p represents a small slope. The parameter \bar{r} is a mean pore size, that is, the size of a solute that is retained for 50%.

The final step in modeling the rejection of an uncharged solute is to calculate the rejection based on the reflection coefficient. This is done by first transforming Eq. (2.54) into an equation using readily available parameters, molar mass and the MWCO. This yields (Van der Bruggen and Vandecasteele, 2002):

$$\sigma(MW^*) = \int_0^{MW^*} \frac{1}{S_{MW} \sqrt{2\pi}} \cdot \frac{1}{MW} \cdot \exp\left(\frac{-(\ln(MW) - \ln(\overline{MW}) + 0.56S_{MW})^2}{2S_{MW}^2}\right) dMW \quad (2.55)$$

in which \overline{MW} is the MWCO of the membrane, and S_{MW} is a distribution parameter derived from S_p .

In this transformation, a relation of the form $d_c = A (MW)^B$ is assumed:

$$d_c = 0.065 (MW)^{0.438} \quad (2.56)$$

Once the reflection coefficient is known, the rejection can be determined by using Eq. (2.49). The parameter P_s can be deduced from the equation $P_s = D_s/\Delta x$. The diffusion coefficient is inversely proportional to the size of the molecule (Stokes' law): $D_s = A/d_s$, in which A is a constant. The equation for the permeability can thus be written as:

$$P_s = \frac{A}{\Delta x} \cdot \frac{1}{d_c} \quad (2.57)$$

The constant A and the membrane thickness can be brought together in one membrane specific diffusion parameter Ω :

$$P_s = \frac{\Omega}{d_c} \quad (2.58)$$

Ω can be determined for each membrane with one single experiment with a known solute (by preference a solute with a rejection that is not extremely high or low).

2.8.2 CHARGED SOLUTES

Modeling the rejection of ions by nanofiltration is complex, because it depends on charge interactions between the solution and the membrane. These interactions do not only depend on the specific ion that is considered alone, but also on the overall (ionic) composition of the feed flow. This complicates the models that have been developed. An excellent review of the detailed modeling approach for charged solutes is given by Yaroshchuk and Bruening (Yaroshchuk and Bruening, 2018); this chapter explores a simplified strategy outlining the main principles of such models.

The analysis of ion transport and rejection is typically based on irreversible thermodynamics, starting from the following equations (which are generalizations of Eqs. (2.47), (2.48)):

$$N_i = -\frac{P_i}{RT} c_i \frac{d\mu_i^{(e)}}{dx} + N_v \tau_i c_i \quad (2.59)$$

$$N_v = -\chi \cdot \left(\frac{dp}{dx} - \sum_i c_i \cdot (1 - \tau_i) \cdot \frac{d\mu_i^{(e)}}{dx} \right) \quad (2.60)$$

in which P_i is the ion permeability of i in the membrane, c_i is the concentration of ion I (which in reality represents a virtual concentration (Yaroshchuk and Bruening, 2018)), $\mu_i^{(e)}$ is the ion electrochemical potential, x is the membrane coordinate, τ_i is the ion transmission coefficients (corresponding to one minus the reflection coefficient), p is the hydrostatic pressure, and χ is the membrane hydraulic permeability defined at zero gradients of electrochemical potentials of all the ions.

The electrochemical potential is written as:

$$\mu_i^{(e)} = \mu_i^{(c)} + FZ_i\varphi \quad (2.61)$$

The electric current density I_e is given by:

$$I_e = F \sum_i Z_i N_i \quad (2.62)$$

Or

$$I_e = -g \left(\frac{d\varphi}{dx} + \frac{1}{F} \cdot \sum_i \frac{t_i}{Z_i} \frac{d\mu_i^{(c)}}{dx} \right) + \rho_{ek} N_v \quad (2.63)$$

with

$$g = \frac{F^2}{RT} \sum_i Z_i^2 c_i P_i \quad (2.64)$$

and t_i is the ion transport number at zero volume flow

$$t_i = \frac{Z_i^2 c_i P_i}{\sum_j Z_j^2 c_j P_j} \quad (2.65)$$

and the electrokinetic charge density:

$$\rho_{ek} = F \cdot \sum_i Z_i c_i \tau_i \quad (2.66)$$

In nanofiltration, J_e is zero, so that the actual electrical field is

$$E = -\frac{d\varphi}{dx} = \frac{1}{F} \cdot \sum_i \frac{t_i}{Z_i} \cdot \frac{d\mu_i^{(c)}}{dx} - \frac{\rho_{ek}}{g} \cdot N_v \quad (2.67)$$

As a result one obtains:

$$N_i = -\frac{P_i}{RT} c_i \left(\frac{d\mu_i^{(c)}}{dx} - Z_i \sum_i \frac{t_i}{Z_i} \cdot \frac{d\mu_i^{(c)}}{dx} \right) + N_v T_i c_i \quad (2.68)$$

where

$$T_i = \tau_i - \frac{t_i \rho_{ek}}{F Z_i c_i} \quad (2.69)$$

is the ion transmission coefficient at zero electric current, which includes ion movement due to the streaming potential gradient. This is equivalent to modeling transport using the extended Nernst-Planck equation, with some slight nuances; it is the basis for further modeling of ion transport in various cases.

Nanopore models provide a mechanistic approach to derive the coefficients in irreversible thermodynamics modeling. However, although mechanistic models provide insight into the thermodynamic coefficients, this approach may be based on incorrect assumptions, such as steric exclusion taking solute size into account but neglecting the finite size of solvent molecules, which is important in sub-nm pores.

The literature contains several variations on the approach highlighted here, which may be based on irreversible thermodynamics (extended Nernst-Planck equation) or on a mechanistic approach. Typically, all these models share a high complexity; the approach of Yaroshchuk and Bruening (Yaroshchuk and Bruening, 2018), however, is one of the few allowing to predict all experimental observations, including the occurrence of negative rejections.

2.9 MODELING OF ORGANIC SOLVENT NANOFILTRATION (OSN)

Organic solvent nanofiltration is considered separately from aqueous nanofiltration, because of the strong differences not only in membrane materials, but also in interactions that govern the permeability and the separation. Even when the size range of solutes to be separated is the same, and applied pressures are in the same range, the governing equations are different from those used in aqueous nanofiltration. For this reason, OSN is usually considered a separate process.

It is expected that membrane properties (hydrophilicity/hydrophobicity, swelling, presence of “nanovoids”, etc.) as well as solvent properties (viscosity, molar volume, polarity, solubility) play a role in the membrane performance. Thus a challenge is in developing a model applicable to different types of membranes (with varying degrees of hydrophilicity/hydrophobicity) and a wide range of solvents (polar and nonpolar) and solutes. In the literature, different mathematical models have been used to predict transport of solvents through polymeric OSN membranes. In most cases, solution-diffusion and pore flow models have been used to fit the experimental data (White, 2002; Yang et al., 2001; Stafie et al., 2005). Permeation of organic solvents through membranes does not simply follow the traditional models generally used in aqueous media. The origin of this deviation can be found in physicochemical interaction parameters occurring between the solvent and the membrane material (Darvishmanesh et al., 2009a).

A conventional approach in describing fluxes in OSN is in considering solvent transport through the membrane by solution-diffusion. The difference with aqueous NF is then in the estimation of the permeability coefficient, which only includes the solvent viscosity in the case of water. For solvents, several correlations have been proposed:

$$L_p \sim \left(\frac{V_m}{\eta} \right) \cdot \left(\frac{1}{\Phi^n \gamma_{sv}} \right) \quad (2.70)$$

in which η is the viscosity, V_m is the molar volume (as a measure for molecular size), γ_{sv} is the surface energy of the solid membrane material, and Φ^n is a sorption value (as a measure for membrane-solvent interactions) (Bhanushali et al., 2001).

In an alternative approach to consider solvent transport through the membrane by viscous flow, the permeability can be expressed as (Machado et al., 2000):

$$L_p \sim \left(\frac{1}{\lambda[(\gamma_c - \gamma_t) + f_1 \eta] + f_2 \eta} \right) \quad (2.71)$$

In this equation, the membrane is a combination of a nanofiltration top layer with an ultrafiltration sublayer; solvent independent parameters are used to characterize the NF (f_1) and UF sublayer (f_2). The parameter λ is a solvent-membrane dependence parameter that shows the porosity of the membrane surface. The affinity of the solvent and membrane is considered by including the difference between γ_c , the surface tension of the membrane material, and γ_t , the surface tension of the solvent.

In a hybrid modeling approach, the membrane can be considered as a parallel connection of a matrix having the solution-diffusion mechanism of solvent transport and of pores where the solvent is convectively transported without change of concentration (Darvishmanesh et al., 2009b). This is schematically shown in Fig. 2.11. The hybrid approach leads to the following flux equation:

$$N_v = \frac{a_0 \alpha}{\eta \exp(1 - \beta)} (\Delta P - \Delta \pi) + \frac{b_0}{\eta \exp(1 - \beta)} \Delta P \quad (2.72)$$

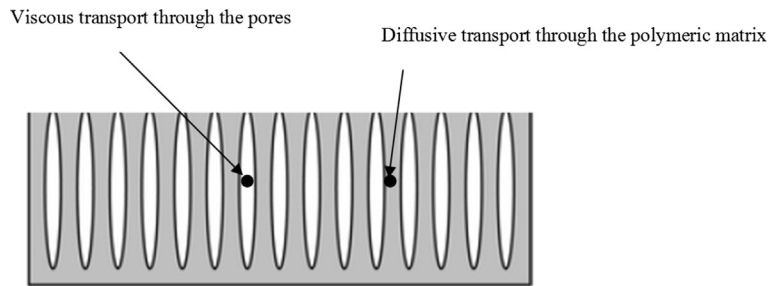


FIG. 2.11

Hybrid model for organic solvent nanofiltration, combining viscous transport with diffusive transport (Darvishmanesh et al., 2009b).

in which a_0 and b_0 are specific diffusivity and permeability values, and β is defined as:

$$\beta = \frac{\gamma_m}{\gamma_l} \quad (2.73)$$

with γ_m the surface tension of the membrane, and γ_l the surface tension of the liquid, in case of a hydrophobic membrane, and

$$\beta = \frac{\gamma_l}{\gamma_m} \quad (2.74)$$

in case of a hydrophilic membrane.

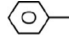
In spite of the efforts made to develop generally applicable models, these usually lack a broad predictive ability. They are able to predict the behavior of series of solvents (solvents of the same type, e.g., alcohols, ethers, etc.) for a given membrane, but they fail in providing a general prediction, and are unable to explain the performance of some of the solvents tested (Andecochea Saiz et al., 2018).

The role of solute-membrane interactions may, however, be crucial in transport modeling; it is known that equal solvent/membrane pairs show different results with different solutes (Rezaei Hosseinabadi et al., 2014). In the assessment of these interactions, the Hansen Solubility Parameter (HSP) plays a key role. This may explain solvent permeabilities beyond the models outlined previously (Buekenhoudt et al., 2013). Furthermore, the HSP approach may also qualitatively and even quantitatively predict solute fluxes and rejections in organic solvents. This, however, is restricted to nanoporous membranes. The HSP was used as a parameter together with the dielectric constant to predict separation factors in OSN (Li et al., 2014), without identifying the different components of the HSP.

The Hansen Solubility Parameter has three components: a dispersion, polarity, and hydrogen bonding component. These can be calculated by a group contribution method (Barton, 1991):

$$\delta_d = \frac{\sum F_d}{\sum V} \quad (2.75)$$

Table 2.1 Group contribution method for calculating the dispersion, polarity, and hydrogen bonding component of the Hansen Solubility Parameter (Barton, 1991)

Group	F_d ($\text{J}^{1/2} \text{cm}^{3/2} \text{mol}^{-1}$)	F_p ($\text{J}^{1/2} \text{cm}^{3/2} \text{mol}^{-1}$)	$-U_m$ (Jmol^{-1})	V ($\text{cm}^3 \text{mol}^{-1}$)
$>\text{CH}-$	80	0	0	-1.0
$=\text{CH}-$	200	0	0	13.5
$-\text{CH}_2-$	270	0	0	16.1
$\text{CH}_2=$	400	0	0	28.5
CH_3-	420	0	0	33.5
$=\text{C}<$	70	0	0	-5.5
$>\text{C}<$	-70	0	0	-19.2
$-\text{O}-$	100	400	3000	3.8
$-\text{CO}-$	290	770	2000	10.8
$-\text{COO}-$	390	490	7000	18
	1430	110	0	71.4
$-\text{OH}$	210	500	20,000	10
Plane of symmetry	-	$\times 0.5$	-	-

$$\delta_p = (\Sigma F_p^2)^{1/2} / \Sigma V \quad (2.76)$$

$$\delta_h = \left(\Sigma -U_m / \Sigma V \right)^{1/2} \quad (2.77)$$

Values for commonly occurring groups are given in Table 2.1 (Barton, 1991).

A ternary HSP diagram, also denoted as Teas plot (Teas, 1968), shows the three components of the HSP in a triangular diagram. The different components of the HSP are expressed as a percentage, with the sum of the three coordinates always 100%. For the dispersion axis, this is:

$$\%_{\delta_d \text{ Teas}} = \frac{\delta_d}{\delta_d + \delta_p + \delta_h} \cdot 100 \quad (2.78)$$

An example of such a Teas plot is given in Fig. 2.12, based on HSP values of solvents from the work of Hansen (Hansen, 2007). In a Teas plot, it can be visually assessed how close the HSP of two components are to one another; this is a basis to estimate whether their interactions are expected to be high. The closer two points are in the diagram, the greater the interactions (e.g., solvent miscibility in Fig. 2.12, which is

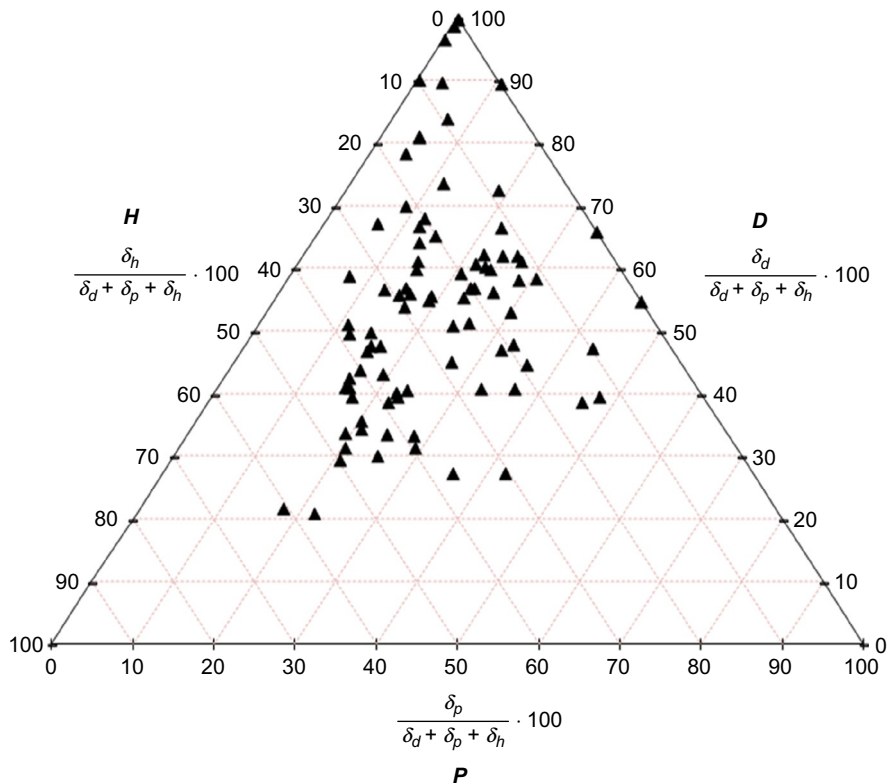


FIG. 2.12

Teas diagram for a set of common solvents (Andecochea Saiz et al., 2018).

the traditional application are of the Teas diagram). A compound with a predominant polarity component should be located in a similar place as another compound with a similar polarity predominance, although their absolute value of polarity might not be the same.

For OSN, it was observed that solvents with a similar permeability appear in the same area of the graph, that is, solvents with a similar HSP distribution have similar permeabilities and thus a similar level of interaction. The higher the flux, the higher the interactions and the closer the data points in the diagram. Therefore it can be assumed that the HSP distribution of the membrane would be in the area where high permeability solvents are plotted and thus the HSP distribution of the membrane is obtained (Andecochea Saiz et al., 2018). In some cases, the HSP of the membrane can be determined directly.

In order to describe rejections, it can be also considered that the solutes with a HSP closer to the one of the membrane have lower solute rejections. This can be

predicted by considering a relative affinity (solvent to solute) to the membrane (Andecochea Saiz et al., 2018):

$$\text{Relative affinity}_{\text{SoM-SM}} = \sqrt{(\delta_{d\text{So}} - \delta_{d\text{M}})^2 + (\delta_{p\text{So}} - \delta_{p\text{M}})^2 + (\delta_{h\text{So}} - \delta_{h\text{M}})^2} - \sqrt{(\delta_{d\text{S}} - \delta_{d\text{M}})^2 + (\delta_{p\text{S}} - \delta_{p\text{M}})^2 + (\delta_{h\text{S}} - \delta_{h\text{M}})^2} \quad (2.79)$$

For a small relative affinity, representing a high affinity of the membrane to the solute compared with the affinity to the solvent, rejections are predicted to be low. This is observed when the membrane has much more affinity for the solute and higher rejections occur when it has much more affinity for the solvent.

The general procedure to use the HSP for modeling OSN is shown in Fig. 2.13 (Andecochea Saiz et al., 2018).

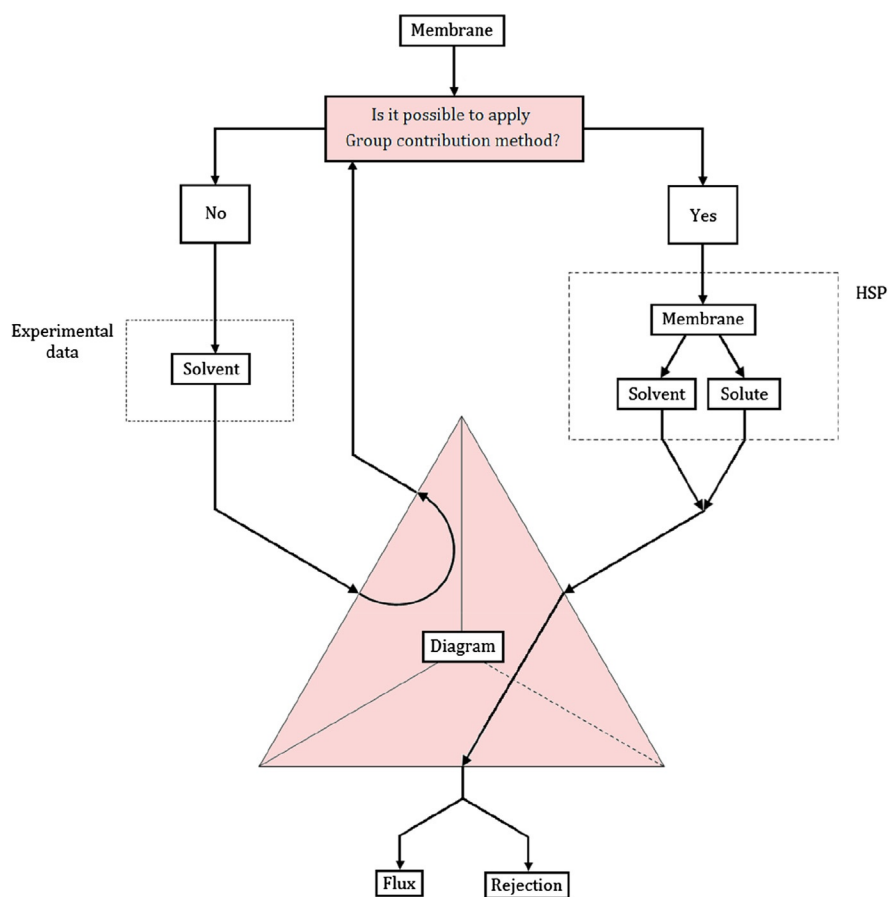


FIG. 2.13

General procedure for using the Hansen Solubility Parameter for modeling organic solvent nanofiltration (Andecochea Saiz et al., 2018).

2.10 MODELING OF REVERSE OSMOSIS (RO)

For reverse osmosis, the permeability is described by Eq. (2.47). The reflection coefficient is sometimes not taken into account, as it is assumed to be equal to one:

$$N_v = L_p(\Delta P - \Delta\pi) \quad (2.80)$$

Typical RO membranes have a NaCl rejection of at least 98% at operational pressure, so that the approximation does not invoke a large error. The difficulty, however, is in a correct calculation of the osmotic pressure. The occurrence of osmotic pressure is typical for reverse osmosis and originates from the fact that the two phases separated by the membrane are directed toward chemical equilibrium, but not toward mechanical or thermal equilibrium. As a result, the concentrated phase (the feed) is diluted, which increases the pressure on feed side until the chemical potential is equal on both sides as indicated in Eq. (2.1). Thus the effective pressure is the applied pressure minus this osmotic pressure, as indeed appears in Eq. (2.80). Calculating the osmotic pressure can be carried out for simple systems based on van't Hoff's equation:

$$\Delta\pi = \nu_i c_i \frac{RT}{MW} \quad (2.81)$$

in which ν_i is the number of ions in the dissociated salt, c_i the concentration (in g/L units), and MW the molar mass of the ion. This is of course equivalent to Eq. (2.82), with molar concentrations:

$$\Delta\pi = \nu_i c_i RT \quad (2.82)$$

It is obvious that osmotic pressure is only significant when small solutes are retained, since molar mass is in the denominator. This is the case for reverse osmosis and partly for nanofiltration, but not for ultrafiltration or microfiltration.

The van't Hoff equation is built up in a form that reminds of the ideal gas law derived in thermodynamics. Indeed the van't Hoff equation is based on the same thermodynamic functions (considering the entropy of mixing), in order to calculate the energy associated with the mixing of two or more components in a solution while neglecting nonideal interactions. Thus both equations are only considering the concentrations of the components present in the solution; interactions or the overall composition are not taken into account. However, ideality is a reasonable approximation only for dilute salt solutions, much below the concentrations found in seawater. At seawater concentrations, the difference between the Van't Hoff equation and measured values becomes significant.

For higher concentrations, as is also the case for example, industrial brines, a more detailed calculation can be obtained with the Pitzer model (Pitzer, 1973). This model calculates the osmotic pressure on the base of interactions between ions. The osmotic pressure is expressed as:

$$\Delta\pi = \Phi RT \sum_i \gamma_i c_i \quad (2.83)$$

This requires the calculation of activity coefficients (γ_i); ϕ in this equation is an osmotic pressure coefficient, indicating the deviation from the Van't Hoff model. ϕ can be calculated (for a 2–1 electrolyte) with the following equation:

$$\phi - 1 = |z_m z_X| f^\phi + m \left(\frac{2v_m v_X}{v} \right) B_{MX}^\phi + m^2 \left(\frac{2(v_m v_X)^{3/2}}{v} \right) C_{MX}^\phi \quad (2.84)$$

where the fugacities and the interaction coefficients can be obtained from theoretical considerations and experimental values:

$$\phi - 1 = 2 \cdot f^\phi + m \frac{4}{3} B_{MX}^\phi + m^2 \frac{2^{(5/2)}}{3} C_{MX}^\phi \quad (2.85)$$

$$= 2 \cdot -A_\phi \frac{I^{1/2}}{1 + bI^{1/2}} + m \left(\frac{4}{3} \beta^{(0)} + \frac{4}{3} \beta^{(1)} \exp(-\alpha I^{-1/2}) \right) + m^2 \frac{2^{(5/2)}}{3} C_{MX}^\phi \quad (2.86)$$

More detailed explanations on the application of the Pitzer model can be found in the literature.

Although several models have been developed for transport in reverse osmosis (models based on irreversible thermodynamics, Maxwell-Stefan-based models, hydrodynamic or pore models) (Malaeb and Ayoub, 2011), the generally accepted theory is solution-diffusion (Wijmans and Baker, 1995). In this approach, a three-step mechanism is assumed. First, the solutes present on the feed side partition into a polymeric membrane; second, the solutes diffuse through the membrane phase; and third, the solutes desorb to the permeate stream. The solution-diffusion process is schematically shown in Fig. 2.14 (Wang et al., 2014).

Fig. 2.15 shows the changes in pressure, chemical potential, and activity in and around the membrane phase. Based on these assumptions, an analysis can be made.

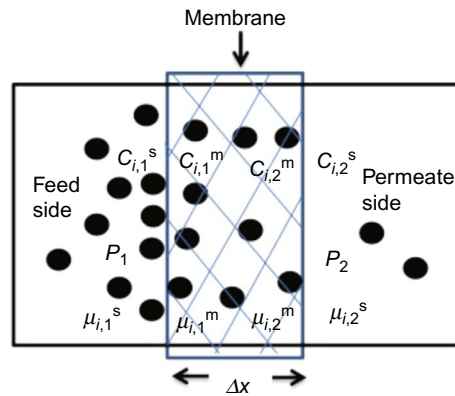


FIG. 2.14

Solution-diffusion in a dense membrane, with solutes partitioning into the membrane material at the feed side and diffusing across the membrane (Wang et al., 2014).

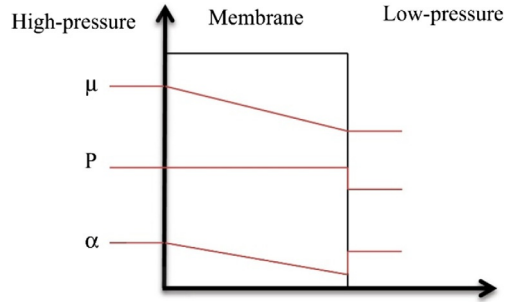


FIG. 2.15

Pressure-driven permeation of a one-component solution through a membrane according to the solution-diffusion model.

On the feed side, components partition into the membrane phase:

$$c_{i,o(m)} = K_i c_{i,o} \quad (2.87)$$

with $c_{i,o(m)}$ the concentration of i inside the membrane, and $c_{i,o}$ the concentration in the liquid on the feed side, at the membrane interface.

At the permeate side, there is a pressure difference, but the chemical potentials should be equal:

$$\mu_{i,l(m)} = \mu_{i,l} \quad (2.88)$$

Or

$$\mu_i^0 + RT \ln(\gamma_{i,l} c_{i,l}) + v_i(p_l - p_{i,sat}) = \mu_i^0 + RT \ln(\gamma_{i,l(m)} c_{i,l(m)}) + v_i(p_0 - p_{i,sat}) \quad (2.89)$$

Thus it can be deduced that

$$c_{i,l(m)} = K_i c_{i,l} \exp\left(-\frac{v_i(p_0 - p_l)}{RT}\right) \quad (2.90)$$

This can be used in Fick's law to describe diffusion through the membrane:

$$N_i = \frac{D_i(c_{i,o(m)} - c_{i,l(m)})}{\Delta x} \quad (2.91)$$

which gives:

$$N_i = \frac{D_i K_i}{\Delta x} \left(c_{i,o} - c_{i,l} \exp\left(-\frac{v_i(p_0 - p_l)}{RT}\right) \right) \quad (2.92)$$

When the applied hydrostatic pressure balances the water activity gradient, in the point of osmotic equilibrium, $N_i = 0$ so that

$$c_{i,l} = c_{i,o} \exp\left(\frac{v_i(\Delta\pi)}{RT}\right) \quad (2.93)$$

So that

$$N_i = \frac{D_i K_i c_{i,o}}{\Delta x} \left(1 - \exp \left(- \frac{v_i [(p_0 - p_l) - \Delta\pi]}{RT} \right) \right) \quad (2.94)$$

The second term with the exponential function is small. For small values of x , the function $(1 - \exp(x))$ can be approximated by x . This gives then

$$N_i = \frac{D_i K_i c_{i,o}}{\Delta x} \cdot \frac{v_i [\Delta P - \Delta\pi]}{RT} \quad (2.95)$$

which can be simplified to

$$N_i = A \cdot [\Delta P - \Delta\pi] \quad (2.96)$$

which is again Eq. (2.47), with σ intrinsically taken into account by only considering the nonrejected compounds in the osmotic pressure.

For the solute, Eq. (2.92) can also be simplified by observing that the exponential function is close to unity ($v_i(p_0 - p_l)$) is small:

$$N_i = \frac{D_i K_i}{\Delta x} (c_{i,o} - c_{i,l}) \quad (2.97)$$

which can be written as

$$N_i = B (c_{i,o} - c_{i,l}) \quad (2.98)$$

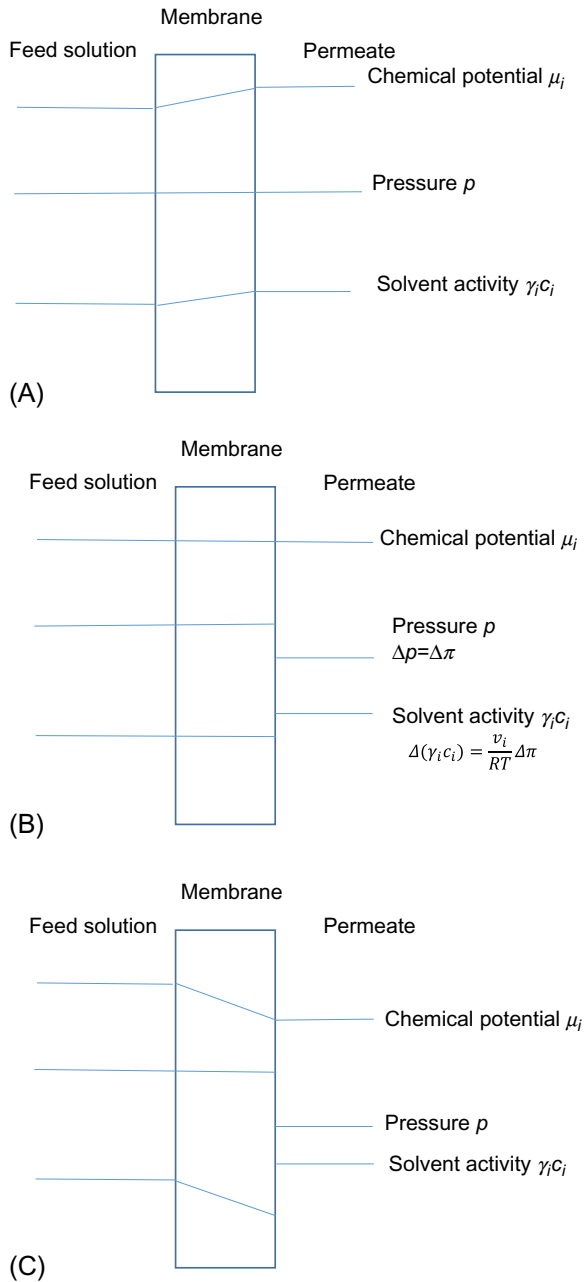
in which B is the salt permeability:

$$B = \frac{D_i K_i}{\Delta x} \quad (2.99)$$

For a more detailed description of the use of the solution-diffusion model, the reader is referred to [Wijmans and Baker \(1995\)](#).

2.11 MODELING OF FORWARD OSMOSIS (FO)

Forward osmosis makes use of the same principles as reverse osmosis, but with transport occurring in the natural, “osmotic” direction. The relation between (forward) osmosis and reverse osmosis is shown in [Fig. 2.16](#). This indicates that the direction of changes in parameters is different, but the transport by solution-diffusion is the same. Thus it could be assumed that the same transport equations could be used with different parameters. However, a dominant aspect to be taken into account for forward osmosis is concentration polarization. Forward osmosis membranes are used with the active layer of the membrane directed to the feed side, in order to optimize the separation performance of the membrane (which is the aim of the process). The permeate side of the membrane has now a concentrated draw solution, and this solution contacts the support layer of the membrane. This causes a concentration profile inside the porous support, which cannot be easily controlled by turbulence promoters or stirring, since it occurs inside the membrane structure. This effect is denoted as “internal concentration polarization” (or ICP) and affects the performance of the

**FIG. 2.16**

Changes in chemical potential, pressure, and activity for osmosis, osmotic equilibrium, and reverse osmosis.

Redrawn based on Wijmans, J.G., Baker, R.W., 1995. *The solution-diffusion model: a review. J. Membr. Sci.* 107, 1–21.

process. Thus models for forward osmosis should take ICP into account. External concentration polarization (ECP) is added to this. The concentration changes due to polarization are shown in Fig. 2.17.

Pressure-retarded osmosis is similar to forward osmosis, but since the objective is in energy generation and not in purification, the active side of the membrane is normally directed toward the draw solution. Transport through the membrane again occurs according to the same fundamental principles, with similar effects of concentration polarization.

To account for external concentration polarization, the concentration polarization modulus CP can be used:

$$CM = \frac{c_m}{c_f} = (1 - R_r) + R_r \exp\left(\frac{N_w}{k_f}\right) \quad (2.100)$$

in which R_r is the rejection, N_w is the water flux, and k_f is the mass transfer coefficient of the feed channel.

The mass transfer coefficient k_f can be written as (Manickam and McCutcheon, 2017):

$$k_f = \frac{D_s^e / \tau}{\Delta x} = \frac{D_s}{S} \quad (2.101)$$

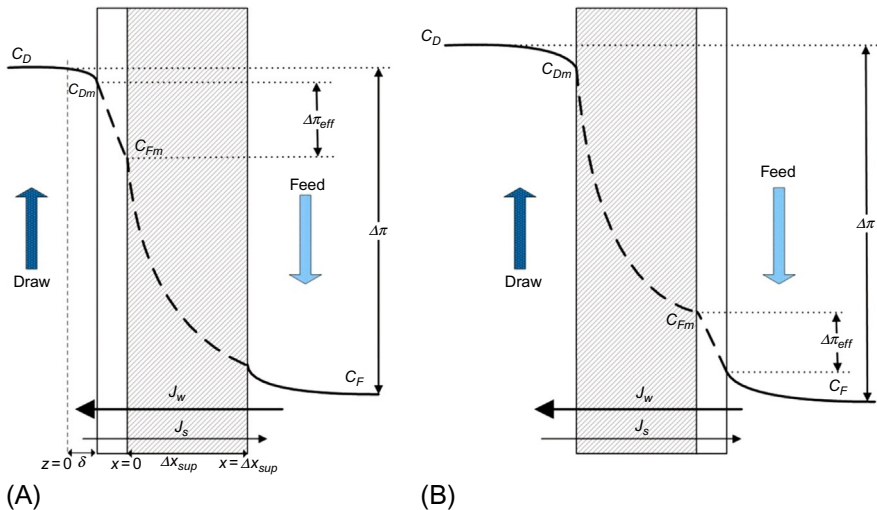


FIG. 2.17

Concentration profiles through an asymmetric membrane used for FO/PRO, illustrating the reduction in the osmotic pressure difference due to (A) concentrative ICP in PRO mode and (B) dilutive ICP in FO mode (Wang et al., 2014).

With

$$S = \frac{\Delta x \cdot \tau}{\epsilon} \quad (2.102)$$

S is denoted as the “structural parameter” of the membrane. Membranes with low S values are preferred in order to reduce the severity of ICP (Manickam and McCutcheon, 2017), since these membranes would have a better mass transfer characteristic, as appears from Eq. (2.101).

The effect of ECP appears in the actual osmotic pressure, which is lower than suggested by the equations given previously. The real osmotic pressure is:

$$\Delta\pi_{eff} = \Delta\pi \cdot R_f \exp\left(\frac{N_w}{k_f}\right) \quad (2.103)$$

where the osmotic pressure is calculated by van ‘t Hoff’s equation (Eq. 2.82) or by the Pitzer model.

The water flux is then determined from

$$N_w = A(\Delta\pi_{eff} - \Delta P) \quad (2.104)$$

In order to account for internal concentration polarization, the actual concentration inside the membrane, in between the support layer and the active layer, should be determined. This concentration is not a measureable quantity, but it can be related to salt flux across the support membrane:

$$N_s = -D_s \frac{dc(x)}{dx} - N_w c(x) \quad (2.105)$$

In this equation, D_s is the diffusivity of the solute in the porous support layer of the composite membrane.

The salt flux can also be determined from the transport equation through the active layer, which can be equalized:

$$-D_s \frac{dc(x)}{dx} - N_w c(x) = B(c_{Dm} - c_{Fm}) \quad (2.106)$$

The resulting equations for water flux and solute flux are then obtained as follows (Wang et al., 2014):

$$N_w = A \left[\frac{\pi_D \exp\left(-\frac{N_w}{k_f}\right) - \pi_F \exp(N_w K)}{1 + \frac{B}{N_w} \left[\exp(N_w K) - \exp\left(-\frac{N_w}{k_f}\right) \right]} - \Delta P \right] \quad (2.107)$$

And

$$N_s = B \left[\frac{\pi_D \exp\left(-\frac{N_w}{k_f}\right) - \pi_F \exp(N_w K)}{1 + \frac{B}{N_w} \left[\exp(N_w K) - \exp\left(-\frac{N_w}{k_f}\right) \right]} \right] \quad (2.108)$$

where K is a parameter to quantify the extent of ICP called resistance to solute diffusion by the porous substructure, which depends on the orientation of the membrane. For PRO mode and deionized water as the feed solution:

$$K = \frac{1}{N_w} \ln \left(\frac{B + A\pi_D - N_w}{B + A\pi_F} \right) \quad (2.109)$$

And for FO mode:

$$K = \frac{1}{N_w} \ln \left(\frac{B + A\pi_F}{B + A\pi_D - N_w} \right) \quad (2.110)$$

Typically, the water and salt permeabilities, that is, the coefficients A and B used in calculating K and, consequently, S , are determined from experiments evaluation FO/PRO membranes in reverse osmosis, which implies that the membrane is operated at elevated pressure. This would not represent the actual transport conditions in FO operation. Thus transport and structural parameters of FO membranes should be determined from FO experiments, for example, by using a range of concentrations of the draw solution.

For a complete overview of transport modeling in FO and PRO, the reader is referred to Manickam and McCutcheon (Manickam and McCutcheon, 2017). It should be remarked that current models for FO and PRO may not be fully able to predict the performance of a membrane under process conditions; this is, for example, clear through the observation of negative rejections (D'Haese et al., 2018), which cannot be predicted by the currently accepted models. Such effects are suggested to be caused by adsorption of the solutes to the membrane followed by coupled transport (D'Haese et al., 2018).

Some authors also remark that convective transport plays a nonnegligible role (Amamiya et al., 2017). The mass transfer equations explained previously indeed do not take a convective term into account, as typical for solution-diffusion. This could be solved by applying nonequilibrium thermodynamics to introduce the convection effect. Such approach may indeed be of practical use to understand the reverse salt flux, that is, the salt flux from the draw solution to the feed solution, which is usually assumed to be a diffusive flux. Although typically neglected, it was found that the effects of the reverse draw solute flux and ECP were not negligible for predicting the water flux in some operating conditions, such as in a feed solution with a high solute concentration (Suh and Lee, 2013). Adjusted operating modes such as Pressure-Assisted Osmosis (PAO) are to overcome current limitations of forward osmosis such as the reverse salt flux (Kim et al., 2017). The reverse flux of the draw solution is of course largely dependent on the nature of the draw solution; much experimental work is carried out with NaCl as the draw solute, while for practical applications this may not make much sense, and larger solutes with a lower reverse flux are explored as potential candidates.

2.12 MODULE PERFORMANCE

When the performance of a membrane for a given application (fluxes and separation) is determined, this is often done by considering a small membrane sample in laboratory conditions. This gives an impression of the potential of a membrane, but may not reflect the actual performance of a module. This is because concentrations in the feed flow change due to the selective removal of compounds through the membrane; when the solvent permeates and solutes are retained, the concentration of these solutes increases gradually during the flow through the module. Considering that the intrinsic rejection of a membrane would remain the same, a higher feed concentration would also translate in a higher permeate concentration. Thus the permeate composition should vary along the module, by definition; the overall product that is obtained is an average composition taken from the entire module.

The overall mass balance over the entire module is:

$$q_f = q_p + q_r \quad (2.111)$$

with q_f , q_p , and q_r are the overall flow of feed, permeate, and retentate, respectively.

The mass balance for a solute is:

$$q_f c_f = q_p c_p + q_r c_r \quad (2.112)$$

From Eqs. (2.111), (2.112), it can be calculated that

$$c_r = \frac{c_f - S c_p}{1 - S} \quad (2.113)$$

With

$$S = \frac{q_p}{q_f} \quad (2.114)$$

In order to assess the overall module performance, these mass balances should be considered for each infinitesimal segment of the module (see Fig. 2.18):

$$c'_r = \frac{c_f - S' c'_p}{1 - S'} \quad (2.115)$$

In which S' , c'_p , and c'_r are local yields and concentrations.

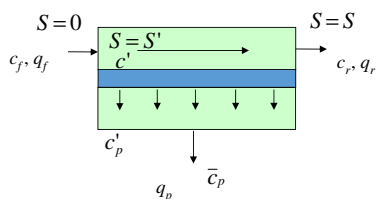


FIG. 2.18

Segmentation of a module in order to determine the overall module performance.

By integrating over the module from 0 to the position that is considered, c'_p can be calculated:

$$c'_p = \frac{1}{S'} \int (1-R)c' dS \quad (2.116)$$

Combine and derive to S' :

$$\frac{dc'}{dS'} = \frac{R \cdot c'}{1-S'} \quad (2.117)$$

This equation can be solved by:

$$\int \frac{dc'}{c'} = \int \frac{RdS'}{1-S'} \quad (2.118)$$

Which yields

$$c_r = c_f(1-S)^{-R} \quad (2.119)$$

and

$$c_p = c_f(1-R)(1-S)^{-R} \quad (2.120)$$

This is the final concentration of the permeate at the end of the module, not the average concentration. For the average concentration:

$$\bar{c}_p = \frac{c_f}{S} \left(1 - (1-S)^{1-R} \right) \quad (2.121)$$

which eventually gives the overall module performance based on the yield S and the rejection R .

2.13 CONCLUSIONS

Process modeling for pressure-driven membrane processes is highly dependent on the specific aspects of the process and the intended separation. In microfiltration, a process typically applied in dead-end mode, the variation of the flux is emphasized. Due to the rejection of nondissolved material, a cake layer may form on the membrane, which either results in a decrease of the flux, or an increase in the pressure required to sustain the flux. This may be further complicated by the occurrence of biofouling, which is difficult to adequately predict. This makes a pragmatic process monitoring necessary, in order to verify the expected effects of flux decline.

In ultrafiltration, models describe the separation by steric exclusion (the sieving effect); this relates to the membrane selectivity, while the flux variations are described by pragmatic fouling models.

Nanofiltration models have two focal points: (1) the description of the steric exclusion, which is similar to ultrafiltration but for smaller molecules, on nanometer scale, and (2) the prediction of charge interactions leading to the rejection of ions. Models for organic solvent nanofiltration are different and should consider the interaction effects between the membrane, the solvent, and the solutes, which can be

described by several parameters; the Hansen Solubility Parameter gives the best (qualitative) appraisal of solvent and solute transport, but models still lack a quantification that is valid for all membrane-solvent-solute combinations.

In reverse osmosis, the transport mechanism by solution-diffusion is well understood, and the main challenge in models is in a correct estimation of the osmotic pressure. The description of other osmotic processes such as forward osmosis (but also pressure-retarded osmosis and pressure assisted osmosis) is based on the solution-diffusion approach as well, but has specific attention for effects of internal and external concentration polarization.

REFERENCES

- Amamiya, S., Ohashi, H., Yamaguchi, T., 2017. Non-equilibrium thermodynamic model of a highly permeable forward osmosis membrane. *J. Chem. Eng. Jpn.* 50 (8), 618–631.
- Andecochea Saiz, C., Darvishmanesh, S., Buekenhoudt, A., Van der Bruggen, B., 2018. Short-cut applications of the Hansen solubility parameter for organic solvent nanofiltration. *J. Membr. Sci.* 546, 120–127.
- Barton, A.F.M., 1991. *Handbook of Solubility Parameters and Other Cohesion Parameters*, second ed. CRC Press Inc., Boca Raton.
- Bhanushali, D., Kloos, S., Kurth, C., Bhattacharyya, D., 2001. Performance of solvent-resistant membranes for non-aqueous systems: solvent permeation results and modeling. *J. Membr. Sci.* 189 (1), 1–21.
- Bilad, M.R., Arafat, H.A., Vankelecom, I.F.J., 2014. Membrane technology in microalgae cultivation and harvesting: a review. *Biotechnol. Adv.* 32 (7), 1283–1300.
- Van der Bruggen, B.; Schaep, J.; Vandecasteele, C.; Wilms, D. A comparison of models to describe the maximal retention of organic molecules. *Sep. Sci. Technol.* 2000, 35 (2), 169–182.
- Buekenhoudt, A., Bisignano, F., De Luca, G., Vandezande, P., Wouters, M., Verhulst, K., 2013. Unravelling the solvent flux behaviour of ceramic nanofiltration and ultrafiltration membranes. *J. Membr. Sci.* 439, 36–47.
- Caus, A., Vanderhaegen, S., Braeken, L., Van der Bruggen, B., 2009a. Integrated nanofiltration cascades with low salt rejection for complete removal of pesticides in drinking water production. *Desalination* 241 (1–3), 111–117.
- Caus, A., Braeken, L., Boussu, K., Van der Bruggen, B. The use of integrated countercurrent nanofiltration cascades for advanced separations. *J. Chem. Technol. Biotechnol.* 2009b, 84 (3), 391–398
- Cheryan, M., Rajagopalan, N., 1998. Membrane processing of oily streams. Wastewater treatment and waste reduction. *J. Membr. Sci.* 151 (1), 13–28.
- Choi, B.G., Zhan, M., Shin, K., Lee, S., Hong, S., 2017. Pilot-scale evaluation of FO-RO osmotic dilution process for treating wastewater from coal-fired power plant integrated with seawater desalination. *J. Membr. Sci.* 540, 78–87.
- D’Haese, A.K.H., De Leersnyder, I., Vermeir, P., Verliefde, A.R.D., 2018. On negative rejection of uncharged organic solutes in forward osmosis. *J. Membr. Sci.* 548, 22–31.
- Darvishmanesh, S., Buekenhoudt, A., Degreève, J., Van der Bruggen, B., 2009a. Coupled series-parallel resistance model for transport of solvent through inorganic nanofiltration membranes. *Sep. Purif. Technol.* 70 (1), 46–52.

- Darvishmanesh, S., Buekenhoudt, A., Degrève, J., Van der Bruggen, B., 2009b. General model for prediction of solvent permeation through organic and inorganic solvent resistant nanofiltration membrane. *J. Membr. Sci.* 334 (1–2), 43–49.
- Davis, R.H., 1992. Modeling of fouling of crossflow microfiltration membranes. *Sep. Purif. Methods* 21 (2), 75–126.
- El Rayess, Y., Albasi, C., Bacchin, P., Taillandier, P., Raynal, J., Mietton-Peuchot, M., Devatine, A., 2011. Cross-flow microfiltration applied to oenology: a review. *J. Membr. Sci.* 382 (1–2), 1–19.
- Geens, J., De Witte, B., Van der Bruggen, B., 2007. Removal of API's (active pharmaceutical ingredients) from organic solvents by nanofiltration. *Sep. Sci. Technol.* 42 (11), 2435–2449.
- Girard, B., Fukumoto, L.R., 2000. Membrane processing of fruit juices and beverages: a review. *Crit. Rev. Food Sci. Nutr.* 40 (2), 91–157.
- Hansen, C.M., 2007. *Hansen Solubility Parameters A User's Handbook*, second ed. CRC Press Inc., Boca Raton.
- Jamaly, S., Darwish, N.N., Ahmed, I., Hasan, S.W., 2014. A short review on reverse osmosis pretreatment technologies. *Desalination* 354, 30–38.
- Kessler, J.O., Moody, C.D., 1976. Forward osmosis extractors. *Desalination* 18 (3), 297–306.
- Kim, B., Gwak, G., Hong, S., 2017. Analysis of enhancing water flux and reducing reverse solute flux in pressure assisted forward osmosis process. *Desalination* 421, 61–71.
- Li, J.D., Wang, M.M., Huang, Y.C., Luo, B.B., Zhang, Y., Yuan, Q.P., 2014. Separation of binary solvent mixtures with solvent resistant nanofiltration membranes part B: process modeling. *RSC Adv.* 4, 37375–37380.
- Lin, J., Ye, W., Zeng, H., Yang, H., Luis, P., Sotto, A., Van der Bruggen, B., 2015. Fractionation of direct dyes and salts in aqueous solution using loose nanofiltration membranes. *J. Membr. Sci.* 477, 183–193.
- Lutchmiah, K., Verliefde, A.R.D., Roest, K., Rietveld, L.C., Cornelissen, E.R., 2014. Forward osmosis for application in wastewater treatment: a review. *Water Res.* 58, 179–197.
- Machado, D.R., Hasson, D., Semiat, R., 2000. Effect of solvent properties on permeate flow through nanofiltration membranes: part II. Transport model. *J. Membr. Sci.* 166 (1), 63–69.
- Malaeb, L., Ayoub, G.M., 2011. Reverse osmosis technology for water treatment: state of the art review. *Desalination* 267, 1–8.
- Manickam, S.S., McCutcheon, J.R., 2017. Understanding mass transfer through asymmetric membranes during forward osmosis: a historical perspective and critical review on measuring structural parameter with semi-empirical models and characterization approaches. *Desalination* 421, 110–126.
- Marchetti, P., Solomon, M.F.J., Szekely, G., Livingston, A.G., 2014. Molecular separation with organic solvent Nanofiltration: a critical review. *Chem. Rev.* 114 (21), 10735–10806.
- Mehta, A., Zydny, A.L., 2005. Permeability and selectivity analysis for ultrafiltration membranes. *J. Membr. Sci.* 249 (1–2), 245–249.
- Mochizuki, S., Zydny, A.L., 1992. Dextran transport through asymmetric ultrafiltration membranes: comparison with hydrodynamic models. *J. Membr. Sci.* 68, 21–41.
- Moody, C.D., Kessler, J.O., 1976. Drinking water from seawater by forward osmosis. *Desalination* 18 (3), 283–295.
- Mulder, M., 1996. *Basic Principles of Membrane Technology*, second ed. Kluwer Academic, Dordrecht.

- Opong, W.S., Zydney, A.L., 1991. Diffusive and convective protein transport through asymmetric membranes. *AIChE J.* 37, 1497–1510.
- Peeva, L., Bursal, J.D., Valtcheva, I., Livingston, A.G., 2014. Continuous purification of active pharmaceutical ingredients using multistage organic solvent nanofiltration membrane cascade. *Chem. Eng. Sci.* 116, 183–194.
- Pitzer, K.S., 1973. Thermodynamics of electrolytes I. Theoretical basis and general equations. *J. Phys. Chem.* 77, 268–277.
- Polyakov, Y.S., Zydney, A.L., 2013. Ultrafiltration membrane performance: effects of pore blockage/constriction. *J. Membr. Sci.* 434, 106–120.
- Renouard, T., Lejeune, A., Rabiller-Baudry, M., 2018. Separation of solutes with an organic solvent nanofiltration cascade: designs, simulations and systematic study of all configurations. *Sep. Purif. Technol.* 194, 111–122.
- Rezaei Hosseiniabadi, S., Wyns, K., Meynen, V., Carleer, R., Adriaensens, P., Buekenhoudt, A., Van der Bruggen, B., 2014. Organic solvent nanofiltration with Grignard functionalised ceramic nanofiltration membranes. *J. Membr. Sci.* 454, 496–504.
- Romero, C.A., Davis, R.H., 1990. Transient model of crossflow microfiltration. *Chem. Eng. Sci.* 45 (1), 13–25.
- Silva, C.M., Reeve, D.W., Husain, H., Rabie, H.R., Woodhouse, K.A., 2000. Model for flux prediction in high-shear microfiltration systems. *J. Membr. Sci.* 173 (1), 87–98.
- Spiegler, K.S., Kedem, O., 1996. Thermodynamics of hyperfiltration (reverse osmosis): criteria for efficient membranes. *Desalination* 1, 311.
- Stafie, N., Stamatialis, D.F., Wessling, M., 2005. Effect of PDMS cross-linking degree on the permeation performance of PAN/PDMS composite nanofiltration membranes. *Sep. Purif. Technol.* 45 (3), 220–231.
- Suh, C., Lee, S., 2013. Modeling reverse draw solute flux in forward osmosis with external concentration polarization in both sides of the draw and feed solution. *J. Membr. Sci.* 427, 365–374.
- Teas, J.P., 1968. Graphic analysis of resin solubilities. *J. Paint Technol.* 40, 19–25.
- Van der Bruggen, B., 2017. Membrane technology. In: *Kirk-Othmer Encyclopedia of Chemical Technology*. John Wiley & Sons.
- Van der Bruggen, B., Luis, P., 2015. Forward osmosis: understanding the hype. *Rev. Chem. Eng.* 31 (1), 1–12.
- Van der Bruggen, B., Vandecasteele, C., 2002. Modelling of the retention of uncharged molecules with nanofiltration. *Water Res.* 36 (5), 1360–1368.
- Van der Bruggen, B., Vandecasteele, C., 2003. Removal of pollutants from surface water and groundwater by nanofiltration: overview of possible applications in the drinking water industry. *Environ. Pollut.* 122 (3), 435–445.
- Van Houtte, E., Verbauwhe, J., 2013. Long-time membrane experience at Torreele's water re-use facility in Belgium. *Desalin. Water Treat.* 51 (22–24), 4253–4262.
- Vandezande, P., Gevers, L.E.M., Vankelecom, I.F.J., 2008. Solvent resistant nanofiltration: Separating on a molecular level. *Chem. Soc. Rev.* 37, 365–405.
- Wang, X.L., Tsuru, T., Nakao, S., Igmura, S., 1997. The electrostatic and steric-hindrance model for the transport of charged solutes through nanofiltration membranes. *J. Membr. Sci.* 135, 19–32.
- Wang, Z., Chu, J.S., Zhang, X.M., 2007. Study of a cake model during stirred dead-end microfiltration. *Desalination* 217, 127–138.

- Wang, J.W., Dlamini, D.S., Mishra, A.K., Pendergast, M.T.M., Wong, M.C.Y., Freger, V., Verliefde, A.R.D., Hoek, E.M.V., 2014. A critical review of transport through osmotic membranes. *J. Membr. Sci.* 454, 516–537.
- White, L.S., 2002. Transport properties of a polyimide solvent resistant nanofiltration membrane. *J. Membr. Sci.* 205 (1–2), 191–202.
- Wijmans, J.G., Baker, R.W., 1995. The solution-diffusion model: a review. *J. Membr. Sci.* 107, 1–21.
- Yang, X.J., Livingston, A.G., Freitas dos Santos, L., 2001. Experimental observations of nanofiltration with organic solvents. *J. Membr. Sci.* 190 (1), 45–55.
- Yaroshchuk, A., Bruening, M.L., 2018. Modeling nanofiltration. (Chapter 6) In: *Nanofiltration, Principles and Applications*. Elsevier.
- Yuan, S.S.; Strobbe, D.; Kruth, J.P.; Van Puyvelde, P.; Van der Bruggen, B. Superhydrophobic 3D printed polysulfone membrane with a switchable wettability by self-assembled candle soot for efficient gravity-driven oil/water separation. *J. Mater. Chem. A* 2017, 5, 25401–25409.
- Yun, T.G., Kim, Y.J., Lee, S., Hong, S.K., 2012. Pressure assisted forward osmosis: effect of membrane materials and operating conditions. *Euromembrane conference. Procedia Eng.* 44, 1906.

FURTHER READING

Microfiltration

- Piron, E., René, F., Latrille, E., 1995. A cross-flow microfiltration model based on integration of the mass transport equation. *J. Membr. Sci.* 108, 57–70.
- Seminario, L., Rozas, R., Borquez, R., Toledo, P.G., 2002. Pore blocking and permeability reduction in cross-flow microfiltration. *J. Membr. Sci.* 209, 121–142.
- Kramadhati, N.N., Mondor, M., Moresoli, C., 2002. Evaluation of the shear-induced diffusion model for the microfiltration of polydisperse feed suspension. *Sep. Purif. Technol.* 27, 11–24.
- Bacchin, P., Si-Hassen, D., Starov, V., Clifton, M.J., Aimar, P., 2002. A unifying model for concentration polarization, gel-layer formation and particle deposition in cross-flow membrane filtration of colloidal suspensions. *Chem. Eng. Sci.* 57, 77–91.
- Hanspal, N.S., Waghode, A.N., Nassehi, V., Wakeman, R., 2009. Development of a predictive mathematical model for coupled stokes/Darcy flows in cross-flow membrane filtration. *Chem. Eng. J.* 149, 132–142.
- Polyakov, Y.S., 2008. Depth filtration approach to the theory of standard blocking: Prediction of membrane permeation rate and selectivity. *J. Membr. Sci.* 322, 81–90.
- Wang, Z., Chu, J.S., Zhang, X.M., 2007. Study of a cake model during stirred dead-end microfiltration. *Desalination* 217, 127–138.

Ultrafiltration

- Kim, J.H., DiGiano, F., 2009. Fouling models for low-pressure membrane systems. *Sep. Purif. Technol.* 68, 293–304.
- Kanani, D.M., Fissell, W.H., Roy, S., Dubnisheva, A., Fleischman, A., Zydney, A.L., 2010. Permeability–selectivity analysis for ultrafiltration: Effect of pore geometry. *J. Membr. Sci.* 349, 405–410.

- Nakatsuka, S., Michaels, A.S., 1992. Transport and separation of proteins by ultrafiltration through sorptive and non-sorptive membranes. *J. Membr. Sci.* 69, 181–211.
- Nakao, S.I., Kimura, S., 1982. Models of membrane transport phenomena and their applications for ultrafiltration data. *J. Chem. Eng. Jpn.* 15 (3), 200–205.

Nanofiltration

- Hilal, N., Al-Zoubi, H., Darwish, N.A., Mohammad, A.W., Abu Arabi, M., 2004. A comprehensive review of nanofiltration membranes: treatment, pretreatment, modeling, and atomic force microscopy. *Desalination* 170, 281–308.
- Bhattacharjee, S., Chen, J.C., Elimelech, M., 2001. Coupled model of concentration polarization and pore transport in crossflow Nanofiltration. *AIChE J.* 47 (12), 2733–2745.
- Palmeri, J., Blanc, P., Larbot, A., David, P., 1999. Theory of pressure-driven transport of neutral solutes and ions in porous ceramic nanofiltration membranes. *J. Membr. Sci.* 160, 141–170.
- Geraldes, V., Semiao, V., de Pinho, M.N., 2001. Flow and mass transfer modeling of nanofiltration. *J. Membr. Sci.* 191, 109–128.
- Szymczyk, A., Zhu, H.C., Balanec, B., 2010. Pressure-driven ionic transport through nanochannels with inhomogenous charge distributions. *Langmuir* 26 (2), 1214–1220.

Organic solvent nanofiltration

- Darvishmanesh, S., Van der Bruggen, B., 2016. Mass transport through nanostructured membranes: toward a predictive tool. *Membranes*. 6 (4). art. 49.
- Blumenschein, S., Bocking, A., Katzel, U., Postel, S., Wessling, M., 2016. Rejection modeling of ceramic membranes in organic solvent nanofiltration. *J. Membr. Sci.* 510, 191–200.
- Malakhov, A., Volkov, A., 2015. Application of coupled solution-diffusion model in organic solvent nanofiltration: positive and negative rejection of solutes. *Sep. Sci. Technol.* 50 (14), 2198–2210.
- Marchetti, P., Livingston, A.G., 2015. Predictive membrane transport models for organic solvent nanofiltration: how complex do we need to be? *J. Membr. Sci.* 476, 530–553.
- Peshev, D., Livingston, A.G., 2013. OSN designer, a tool for predicting organic solvent nanofiltration technology performance using aspen one, MATLAB and CAPE OPEN. *Chem. Eng. Sci.* 104, 975–987.
- Siew, W.E., Livingston, A.G., Ates, C., Merschaert, A., 2013. Molecular separation with an organic solvent nanofiltration cascade—augmenting membrane selectivity with process engineering. *Chem. Eng. Sci.* 90, 299–310.
- Kim, J.F., da Silva, A.M.F., Valtcheva, I.B., Livingston, A.G., 2013. When the membrane is not enough: a simplified membrane cascade using organic solvent nanofiltration (OSN). *Sep. Purif. Technol.* 116, 277–286.

Reverse osmosis

- Hall, M.S., Starov, V.M., Lloyd, D.R., 1997. Reverse osmosis of multicomponent electrolyte solutions. Part I. Theoretical development. *J. Membr. Sci.* 128, 23–37.
- Paul, D.R., 2004. Reformulation of the solution-diffusion theory of reverse osmosis. *J. Membr. Sci.* 241, 371–386.
- Geise, G.M., Paul, D.R., Freeman, B.D., 2014. Fundamental water and salt transport properties of polymeric materials. *Progr. Polym. Sci.* 39, 1–42.

Murthy, Z.V.P., Gupta, S.K., 1997. Estimation of mass transfer coefficient using a combined nonlinear membrane transport and film theory model. *Desalination* 109, 39–49.

Forward osmosis and pressure retarded osmosis

Manickam, S.S., Ramon, G.Z., McCutcheon, J.R., 2017. Modeling the effect of film-pore coupled transport on composite forward osmosis membrane performance. *J. Membr. Sci.* 523, 533–541.

D’Haese, A.K.H., Motsa, M.M., Van der Meeren, P., Verliefde, A.R.D., 2017. A refined draw solute flux model in forward osmosis: theoretical considerations and experimental validation. *J. Membr. Sci.* 522, 316–331.

McCutcheon, J.R., Elimelech, M., 2007. Modeling water flux in forward osmosis: implications for improved membrane design. *AICHE J.* 53 (7), 1736–1744.

Kang, P.K., Lee, W., Lee, S., Kim, A.S., 2017. Origin of structural parameter inconsistency in forward osmosis models: a pore-scale CFD study. *Desalination* 421, 47–60.

Field, R.W., Wu, J.J., 2018. On boundary layers and the attenuation of driving forces in forward osmosis and other membrane processes. *Desalination* 429, 167–174.

Rong, K., Zhang, T.C., 2018. Forward osmosis: mass transmission coefficient-based models for evaluation of concentration polarization under different conditions. *J. Environ. Eng.* 144 (2). art. 04017095.

Pervaporation

Patricia Luis

*Materials & Process Engineering (iMMC-IMAP), Catholic University of Louvain,
Louvain-la-Neuve, Belgium*

CHAPTER OUTLINE

3.1 Process Description	71
3.2 General Overview of Applications	74
3.3 Mass Transfer in Pervaporation	75
3.3.1 Solution-Diffusion Model	76
3.3.2 Pore-Flow Model	80
3.4 Interpretation of Pervaporation Results	81
3.5 McCabe-Thiele Diagram	86
3.6 Coupling Effects	88
3.6.1 Modified Solution-Diffusion Models	89
3.6.2 Hansen Solubility Approach	91
3.6.3 Examples of Application	97
3.7 Concluding Remarks	100
References	101

3.1 PROCESS DESCRIPTION

Pervaporation is a technique oriented to the separation of liquid mixtures that are characterized by a reasonable volatility. Originally, the term pervaporation is a combination of the words “permselective” and “evaporation,” first reported in 1917 by [Kober \(1917\)](#). The reason of this name states in the operating mode since the components present in a liquid stream in contact with a dense membrane permeate selectively through the membrane to the permeate side, where they are collected in a vapor phase. Thus, permeation and evaporation are taking place somewhere inside the membrane. The main interest of pervaporation is that the separation is not based on the thermodynamic equilibrium between the vapor and liquid phase, as occurs in distillation. This means that the concentration of the permeate is not defined by

the vapor-liquid equilibrium but by the permeability of the compounds through the membrane, which depends on their solubility and diffusion rate in the membrane. This makes pervaporation an alternative technology to distillation when the energy penalty becomes very high due to the presence of azeotropes or close-boiling point components. Also, the recovery of small quantities of impurities and the enhancement of equilibrium reactions are typical attractive areas for pervaporation. In addition to being less energy-intensive technology and thus more economical, pervaporation is safe and ecofriendly and it is considered as a clean technology.

In the pervaporation process, the feed solution is kept at a specific temperature and pressure that ensure a liquid phase during the operation (i.e., temperature lower than the boiling point and pressure higher than the bubble point of the feed). A dense membrane is required to perform the separation since it is the membrane that gives selectivity to the process. This means that the membrane is the key factor in the separation and the efficiency of pervaporation to separate a specific compound from the mixture depends on the selectivity provided by the membrane. The components that permeate through the membrane vaporize somewhere inside the membrane until reaching the other side, that is, the permeate side. The permeate side is kept normally under vacuum so that a large driving force is ensured. The use of a sweep gas is not very common and the components that have permeated (the “permeate”) are condensed and collected again in a liquid phase. The liquid stream that did not permeate through the membrane is called “the retentate” and is concentrated in the less permeant species. The driving force for the separation is the difference in the partial pressures of the components at the two sides of the membrane. The selectivity of the separation is given by different transport rates of the molecules through the membrane as a result of different solubilities and diffusivities of the components. [Fig. 3.1](#) shows a schema of the pervaporation process and the two regions, the liquid and vapor phase zones, formed during the permeation of compounds through the membrane ([Seader et al., 2013](#)). The vapor-liquid interface may be located at any place inside the membrane or even very close to the feed or permeate sides.

Evaluating the mass transfer in pervaporation is performed in two ways: (i) determining the transmembrane flux (total flux and individual flux for each compound) and the separation factor; and (ii) applying mathematical models that try to describe the mass transfer through the membrane, leading to the calculation of the main mass transfer coefficient, that is, the permeability (or permeance), and the selectivity. The first approach consists of calculating the transmembrane flux and the separation factor from experimental results when testing the membrane under specific conditions of temperature, pressure, and feed composition and will give us information on the membrane area that we need to perform a specific separation and the permeate purity. Thus we will have information on the process performance. On the other hand, the second approach allows going deeper and evaluating to which extent the membrane is enhancing the permeance of one or other compound, and if the selected membrane is a good choice or the operation is not optimal. Thus we will have information on the membrane performance. These two different approaches

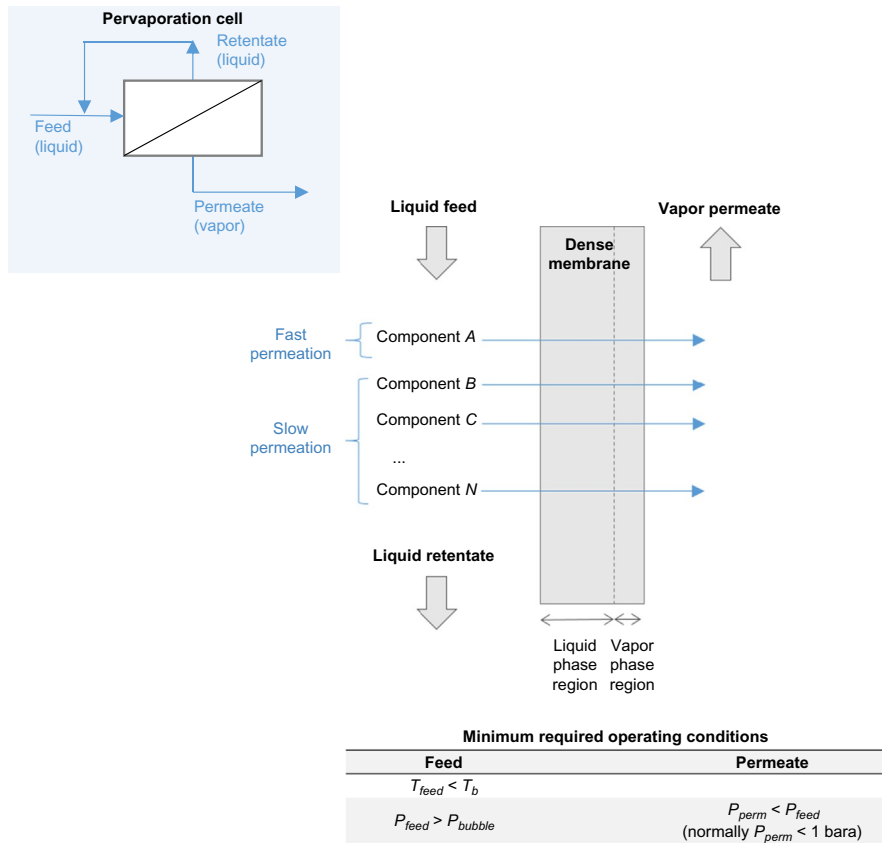


FIG. 3.1

Pervaporation process of a multicomponent mixture with N components. T_{feed} , feed temperature; T_b , boiling point of the feed solution; P_{feed} , feed pressure; P_{bubble} , bubble point of the feed solution; P_{perm} , permeate pressure.

give complementary information and both are essential to finally have the overall picture on the efficiency of the separation and the best operating conditions that should be applied (and the penalty of not working under those conditions).

Based on this reasoning and after giving a general overview of applications, the following sections will provide with the essential information that has to be evaluated when using pervaporation as the separation technique as well as when synthesizing membranes for a specific separation target. Understanding the difference between the use of parameters such as permeability and selectivity and more applicable variables such as transmembrane flux and separation factor is critical to give projection to pervaporation at industrial level (Luis and Van der Bruggen, 2015a).

3.2 GENERAL OVERVIEW OF APPLICATIONS

Pervaporation is reaching industrial maturity due to the accumulated experience in membrane manufacture and operation of pervaporation units. Several applications concerning end-of-pipe processes are industrially well established, such as solvent recovery (e.g., dehydration of ethanol/water and isopropanol/water azeotropes), but the number of applications has dramatically increased in the last years, integrating pervaporation in the production process (e.g., separation of reaction mixtures containing azeotropes). Thus the major fields of current application can be generally classified as follows:

- Separation of water from aqueous/organic mixtures. This application includes the separation of water, which is the low concentration component in the feed mixture, from organic solvents (dehydration); the separation of water-organic azeotropes (e.g., water/ethanol, water/isopropanol, etc.); and the enhancement of equilibrium-limited reactions that include water as a reaction product (e.g., esterification reactions), by shifting the reaction equilibrium due to water removal. The common membranes in this application are hydrophilic membranes to enhance the permeation of water (the low concentration compound) from the mixture. Hydrophilic membranes are designed to incorporate attractive interactions between water and the membrane material such as dipole-dipole interactions, hydrogen bonding, and ion-dipole interaction (Semenova et al., 1997). Most developed materials for dehydration applications are poly(vinyl alcohol), chitosan, alginate, polysulfone, polyimides, polyamides, polyelectrolyte membranes, polyaniline, ceramics, zeolites, and mixed-matrix membranes (Chapman et al., 2008).
- Removal of (volatile) organic compounds from aqueous streams. This application can have an environmental purpose, such as treating wastewater contaminated with organics (Lipski and Côté, 1990), or an economic one, such as the recovery of valuable organic compounds from process side streams (Kashemekat et al., 1981). Examples include (Kujawski, 2000) the removal of chlorinated hydrocarbons; the separation of organics from the fermentation broth; the separation of aroma compounds, wine and beer dealcoholization; and the removal of volatile organic compounds from air. Hydrophobic membranes are normally used to favor the permeance of the less hydrophilic (organic) compound.
- Separation of organic/organic mixtures. This application is showing an increasing attention and interest by researchers and industry due to the economic advantage that pervaporation can offer if the membrane can afford this challenging separation. Examples include the separation of azeotropes (e.g., ethanol/cyclohexane, methanol/methylacetate, methanol/MTBE, etc.); the separation of isomers (e.g., xylenes); the separation of products from equilibrium-limited reactions, such as transesterification reactions (e.g., methanol/butyl acetate in the transesterification of n-butanol with methyl acetate;

ethanol/methyl acetate in the transesterification of methanol with ethyl acetate) (Luis et al., 2013). For organic-organic separations, polymeric membranes are mainly chosen on the basis of relative solubility parameter of the organics and the membranes (Ray et al., 1997), although hydrophilic membranes are also used, for example, for the separation of a smaller amount of methanol from others like MTBE (Ray et al., 1999).

Pervaporation may be proposed as a stand-alone technology, meaning that the pervaporation unit is only responsible for the separation of the mixture. However, this involves having a membrane that covers all the necessities of the separation, providing the required permeate composition and flux to work under economically feasible conditions, mainly in terms of membrane area. In this case, pervaporation is replacing the distillation column and the reaction mixture is sent to the pervaporation unit and the retentate is returned (if required) to the reactor. Reactive pervaporation has been also proposed, in which the reaction takes place inside the pervaporation unit, for example, using catalytic membranes. Reaction and pervaporation are integrated in a single unit. However, when pervaporation alone is not able to separate economically a mixture with a specific feed concentration, combination of pervaporation with conventional distillation is considered. The reaction mixture is then first sent to a distillation column in which an azeotropic or a close-boiling point mixture is obtained, and then, this mixture is sent to the pervaporation unit to break the azeotrope or separate the target compounds to a target purity. A widely implemented case is the separation of alcohol/water azeotropes.

Pervaporation is thus reaching a more relevance in an industrial scenario in which a high energy penalty is not an option for the future. What can be expected from commercial and underdevelopment membranes is the key factor to design the appropriate process (stand-alone pervaporation, reactive pervaporation, hybrid distillation-pervaporation) and orientate further research. The transmembrane flux, separation factors, permeability (or permeance), and selectivity are thus the most relevant data to evaluate the technical and economic viability of pervaporation.

3.3 MASS TRANSFER IN PERVAPORATION

Several mass transfer models are commonly applied in pervaporation, depending on the membrane material and structure. Diffusion through a dense membrane (normally polymeric membranes) is typically described by means of the solution-diffusion model while for porous membranes (normally inorganic membranes), the pore-flow model defines different microscopic transport regimes, depending on pore size (Luis and Van der Bruggen, 2015a). As a rough rule of thumb, the transition between permanent (pore-flow) and transient (solution-diffusion) flow appears to be in the range 5–10 Å diameter (Wijmans and Baker, 1995). Both models have been demonstrated to lead to good approximations of mass transfer when binary mixtures are considered as feed solution. Mass transfer of multicomponent mixtures

involves interactions among components and membrane, which can be described by more complex models such as the Maxwell-Stefan theory or by considering coupling effects.

3.3.1 SOLUTION-DIFFUSION MODEL

The flux of a component i through a dense pervaporation membrane is normally described by the solution-diffusion model (Lonsdale et al., 1965; Merten, 1966; Mulder and Smolders, 1984), which defines the flux as the product of concentration, mobility, and driving force (gradient in the chemical potential):

$$J_i = -c_i B_i \frac{d\mu_i}{dx} \quad (3.1)$$

where $\frac{d\mu_i}{dx}$ is the gradient in chemical potential of component i and B is the mobility ($\text{mmol s}^{-1} \text{N}^{-1}$). At constant temperature, Eq. (3.1) may be written as:

$$J_i = -c_i B_i \left(RT \frac{d \ln a_i}{dx} + \bar{V}_i \frac{dP}{dx} \right)_T \quad (3.2)$$

The pressure gradient in pervaporation can be neglected with respect to the activity gradient since the pressure difference between the upstream and downstream phase is around 0.1 MPa. Thus Eq. (3.2) becomes

$$J_i = -c_i (B_i RT) \frac{d \ln a_i}{dx} \quad (3.3)$$

And with $D_i = B_i RT$

$$J_i = -c_i D_i \frac{d \ln a_i}{dx} \quad (3.4)$$

where D_i is the diffusion coefficient of component i in the polymer. The process that governs pervaporation consists of three stages: (1) solution of molecules in the upstream surface of the membrane, (2) diffusion of the dissolved species across the membrane matrix, and (3) desorption of the dissolved species in the downstream face of the membrane (Shao and Huang, 2007). Following these three main steps involved in the mass transfer through a dense membrane, the solution-diffusion describes mathematically the membrane flux of components i , J_i ($\text{kg s}^{-1} \text{m}^{-2}$) as:

$$J_i = \frac{D_i \cdot C_i}{a_i} \cdot \frac{1}{l} \cdot (a_{F,i} - a_{P,i}) \quad (3.5)$$

where D_i is the Fickian diffusion coefficient of component i in the membrane ($\text{m}^2 \text{s}^{-1}$); C_i is the concentration of component i in the membrane (kg m^{-3}); l is the membrane thickness (active layer) (m); and $a_i, a_{F,i}$, and $a_{P,i}$ are the activities of component i in membrane, feed, and permeate (–), respectively. The determination of D_i , C_i , and a_i involves uncertainties and difficulties to obtain those values experimentally, thus the permeability P_i is defined as:

$$P_i = \frac{D_i \cdot C_i}{a_i} \quad (3.6)$$

Thus a more applied equation that relates the flux with the driving force can be written as:

$$J_i = \frac{P_i}{l} \cdot (a_{F,i} - a_{P,i}) \quad (3.7)$$

This equation present mass units and a conversion of units is desired following the advice by Baker et al. (2010) in order to work with molar flux for each component J_i ($\text{cm}^3(\text{STP})\text{cm}^{-2} \text{s}^{-1}$). Ignoring simple conversion terms, m^2 to cm^2 , L to cm^3 , h to s, the following equation can be used:

$$j_i = \frac{J_i \cdot v_i^G}{m_i} \quad (3.8)$$

where v_i^G is the molar volume of gas i ($22.4 \text{ L}(\text{STP})\text{mol}^{-1}$) and m_i is the molecular weight of component i .

J_i is an experimental value determined by $J_i = J \cdot y_i$, in which J is the total flux measured experimentally by weighing the mass of permeate w (kg) that is obtained during the collecting time Δt (s), $J = \frac{w}{\Delta t \cdot A}$, with A as the effective surface area, y_i is the mass fraction of component i in the permeate, m_i is the molecular weight of the mixture, and v_i^G is the molar volume of gas i ($22.4 \text{ L}(\text{STP})\text{mol}^{-1}$) (Baker et al., 2010; Luis et al., 2013).

The permeability P_i can be calculated as:

$$\frac{P_i}{l} = \frac{J_i}{(x_i \cdot \gamma_i \cdot P_i^o - y_i \cdot P_p)} \quad (3.9)$$

where γ_i is the activity coefficient for the component i , x_i is the molar fraction in the feed solution, and P_i^o is the vapor pressure. The total pressure in the permeate side is P_p . If the thickness of the dense layer that is responsible for the separation (l) is unknown, then, one can determine the permeance, $\frac{P_i}{l}$. The term $(x_i \cdot \gamma_i \cdot P_i^o - y_i \cdot P_p)$ is the driving force of the separation, which is based on the difference in partial pressures between the feed side and the permeate side. Thus working in terms of permeance (or permeability) allows eliminating the effect of the driving force from the calculations and determining the real separation effect by the membrane. The permeance is normally expressed in GPU units ($1 \text{ GPU} = 1 \cdot 10^{-6} \text{ cm}^3(\text{STP})/(\text{cm}^2 \text{ s cmHg}) = 7.5005 \cdot 10^{-12} \text{ ms}^{-1} \text{ Pa}^{-1}$).

The permeance or permeability should be constant at different feed compositions. However, the solubility or the diffusivity of a component in the membrane is not only dependent on itself but also on the other components, meaning that thermodynamic interaction between the components and the membrane may take place, leading to coupling effects (see Section 3.6) (Cao et al., 2000). If no coupling effects take place, the permeance of component i in the mixture would be the same as the permeance of the pure compound, being independent of its composition of the mixture of that of the other components.

In order to determine the degree of separation, two experimental values can be calculated: the separation factor, $\beta_{i/j}$, and the selectivity, $\alpha_{i/j}$.

The separation factor is calculated as the ratio of the molar component concentrations in the permeate (y_i) and feed (x_i) solutions:

$$\beta_{i/j} = \frac{\frac{y_i}{x_i}}{\frac{y_j}{x_j}} = \frac{y_i/(1-y_i)}{x_i/(1-x_i)} \quad (3.10)$$

The selectivity of the membrane is calculated from the ratio between permeances or permeabilities:

$$\alpha_{i/j} = \frac{\frac{P_i}{l}}{\frac{P_j}{l}} = \frac{P_i}{P_j} \quad (3.11)$$

Values of $\alpha_{i/j} = 1$ indicate that the membrane is nonselective toward the studied compounds i and j , if molar units are used (Baker et al., 2010). In addition, by combining Eqs. 3.9–3.11, and considering a maximum driving force achieved by a pressure at the permeate side close to zero ($P \approx 0$) the relationship between separation factor and selectivity is obtained (Luis and Van der Bruggen, 2015a):

$$\alpha_{i/j} = \frac{y_i/(1-y_i)}{x_i/(1-x_i)} \cdot \frac{\gamma_j P_j^o \cdot v_i^G}{\gamma_i P_i^o \cdot v_j^G} = \beta_{i/j} \cdot \frac{\gamma_j P_j^o \cdot v_i^G}{\gamma_i P_i^o \cdot v_j^G} \quad (3.12)$$

From Eq. (3.12), the main difference between selectivity and separation factor can be easily inferred. The separation factor is giving information about the general performance in the separation, that is, which component is more abundant in the permeate. However, this information does not indicate that the membrane is selective toward that major component. The separation factor does not give information on the separation caused by the membrane itself since the components with higher volatility will have preference to be in the vapor phase regardless of the membrane. On the other hand, the selectivity considers the volatility of the compounds and their interaction in solution via the ratio of vapor pressures and activity coefficients, respectively. Thus the selectivity should be calculated to determine (and compare) the degree of separation caused by the membrane while the separation factor should be used to evaluate the general separation once the (best) membrane has been selected (Luis and Van der Bruggen, 2015a).

The temperature dependency of the permeance can be analyzed using an Arrhenius-type equation:

$$\frac{P_i}{l} = \frac{P_{i,\infty}}{l} \cdot \exp\left(-\frac{1000 \cdot E_a}{RT}\right) \quad (3.13)$$

where P_i/l is the permeance of the compound i , $P_{i,\infty}/l$ is the preexponential factor of permeance (i.e., permeance for temperatures approaching infinity), R is the gas

constant ($\text{J mol}^{-1} \text{K}^{-1}$), T is the temperature (K), and E_a is the activation energy (kJ mol^{-1}). By plotting the logarithmized permeability ($\ln P_i$) or permeance ($\ln P_i/l$) versus $1000/RT$, the values of the preexponential factor and the activation energy can be obtained from the origin coordinate and the slope, respectively. A negative activation energy suggests that the permeance of the component decreases with temperature, while the partial flux increases normally with temperature. This can be explained considering that the activation energy of pervaporation is the sum of the activation energy of diffusion ($E_{D,i}$) and the enthalpy of sorption ($\Delta H_{s,i}$) (Berendsen et al., 2006):

$$E_{a,i} = E_{D,i} + \Delta H_{s,i} \quad (3.14)$$

$E_{D,i}$ is generally positive and $\Delta H_{s,i}$ is usually negative for the exothermic sorption process (Feng and Huang, 1996). Thus when the enthalpy of sorption is larger than the energy of diffusion, a negative value of $E_{a,i}$ is obtained, indicating that the membrane permeance decreases with increasing temperature (Feng and Huang, 1996; Luis et al., 2013). Examples of this behavior can be observed in Fig. 3.2. In both cases, increasing the temperature plays against a better membrane performance even though the transmembrane fluxes may increase.

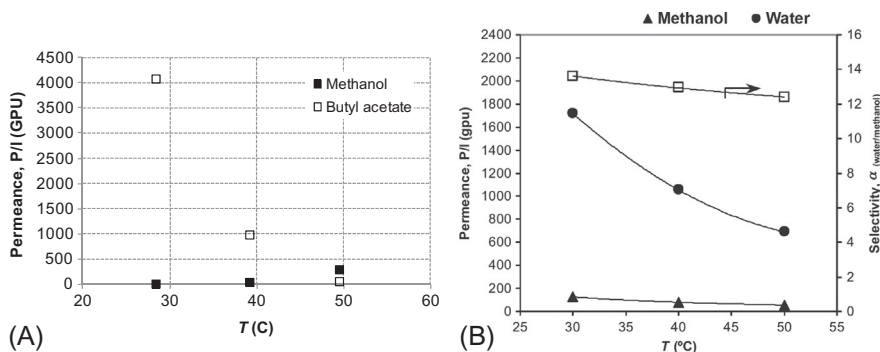


FIG. 3.2

Effect of temperature on permeance for: (A) the separation of 50 mol% methanol/butyl acetate mixtures using the membrane Pervap 1201 from Sulzer Chemtech, Switzerland. (B) the separation of 10 wt% water/methanol mixtures in self-made poly(3-hydroxybutyrate) membranes.

(A) Reproduced with permission from Luis, P., Degrève, J., Van der Bruggen, B., 2013. Separation of methanol-*n*-butyl acetate mixtures by pervaporation: potential of 10 commercial membranes. *J. Membr. Sci.* 429, 1–12.

(B) Published with permission from Villegas, M., Castro Vidaurre, E.F., Gottifredi, J.C., 2015. Sorption and pervaporation of methanol/water mixtures with poly(3-hydroxybutyrate) membranes. *Chem. Eng. Res. Des.* 94, 254–265.

3.3.2 PORE-FLOW MODEL

Applying the pore-flow model involves considering a convective flow transport within the pores due to a pressure gradient. The pore-flow model is thus applied to describe the mass transfer in porous pervaporation membranes.

Developed by Okada and Matsuura in 1991 (Okada and Matsuura, 1991), the pore-flow model assumes that the membrane is like a bundle of straight cylindrical pores distributed across its surface layer. The length of the pores is considered equal to the thickness of the selective layer of the membrane. The liquid penetrates partially into the pores of the membrane and the remaining pore volume is occupied by the vapor phase. Evaporation of compounds takes place at the liquid-vapor interface, which is inside the membrane (notice that in the solution-diffusion model, the vapor-liquid interface is considered at the boundary between the liquid phase and the membrane). A pressure difference between the liquid-vapor interface (saturated vapor pressure) and the vapor phase (normally kept under vacuum) is the driving force of the process. When the pressure inside the membrane falls below the saturated vapor pressure, a phase change occurs (Lipnizki and Trägårdh, 2001). Pervaporation is then described as liquid permeation followed by vapor permeation through small pores, due to a pressure difference over the membrane (Luis and Van der Bruggen, 2015a).

The mass transport through the pores consists of three steps (George and Thomas, 2001): (i) liquid transport from the pore inlet to a liquid-vapor phase boundary, (ii) evaporation at the phase boundary, and (iii) vapor transport from the boundary to the pore outlet. The pore-flow model assumes that the concentrations of solvent and solute within a membrane are uniform and that the chemical potential gradient across the membrane is expressed only as a pressure gradient (Wijmans and Baker, 1995). For a simple component, the mass transport in the liquid part of the membrane is equal to that in the vapor part:

$$J = J_{liquid} = J_{vapor} \quad (3.15)$$

$$J = \frac{A^{pore}}{l_{liquid}} \cdot (p^{liquid} - p^{sat}) = \frac{B^{pore}}{l_{vapor}} \cdot (p^{sat} - p^{vapor}) \quad (3.16)$$

where l_{liquid} is the length of the liquid-filled proportion of the pore (m) and l_{vapor} length of the vapor-filled proportion of the pore (m). Hence, the overall flux of a component can be determined by (Lipnizki and Trägårdh, 2001):

$$J = \frac{A^{pore}}{l} \cdot (p^{liquid} - p^{sat}) + \frac{B^{pore}}{l} \cdot \left((p^{sat})^2 - (p^{vapor})^2 \right) \quad (3.17)$$

with the constants A^{pore} , defined according to Darcy's Equation for liquid transport through cylindrical pores, and B^{pore} , from the simplification of Henry's law and monolayer adsorption:

$$A^{pore} = \frac{\pi \cdot r_{pore}^4 \cdot \rho_i \cdot N_I}{8 \cdot \eta_i \cdot M_i} \quad (3.18)$$

$$B^{pore} = \frac{\pi \cdot (2 \cdot r_{pore} \cdot l_{Ad} - l_{Ad}^2)^2 \cdot l_{Ad} \cdot N_t \cdot R \cdot T}{8 \cdot r_{pore} \cdot \mu_i} (k'_{D,i})^2 \quad (3.19)$$

where ρ_i is the density of component i (kg m^{-3}), N_t is the total number of pores per effective membrane area ($-$), η_i is the liquid viscosity of component i (Pa s), M_i is the molar weight of component i (kg kmol^{-1}), l_{Ad} is the thickness of the adsorption monolayer (m), r_{pore} is the pore radius (m), and $k'_{D,i}$ is the Henry's law constant referring to component i (bar^{-1}). These constants A_{pore} and B_{pore} can be also treated as empirical parameters, fitting their value to the experimental results (flux vs driving force).

For binary mixtures and assuming that l_{liquid} is negligible (pore diameter small and low swelling of the membrane), the flux for each component can be calculated as:

$$J_i = \frac{B_i^{pore}}{l} \cdot \left((p_i^{sat})^2 - (p_i^{vapor})^2 \right) \quad (3.20)$$

$$J_j = \frac{B_j^{pore}}{l} \cdot \left((p_j^{sat})^2 - (p_j^{vapor})^2 \right) \quad (3.21)$$

Eqs. (3.20) and (3.21) allow the calculation of the transmembrane flux of each component. The constants determined for pervaporation of a single component are not transferable to two-component pervaporation and the effect of flux coupling has to be accounted for by additional experiments (Lipnizki and Trägårdh, 2001).

3.4 INTERPRETATION OF PERVAPORATION RESULTS

Pervaporation results can be discussed in terms of transmembrane fluxes, permeances or permeabilities, separation factors, and selectivities, according to the models shown in Section 3.3. However, it is of utmost importance to understand the meaning of each variable and parameter so that a correct interpretation and application of results is done. Highlighting the difference between process performance and membrane performance is the main objective of this section. Process performance is a measure of how efficient or effective a process is. When using membrane technology, the objective when evaluating the process performance is to know if a separation is technically possible and under which process conditions. The economic factor appears as well when determining the total membrane area to achieve the target separation. Thus we are focusing on the overall process. Instead, membrane performance focuses specifically on the membrane. The thermodynamic equilibrium between a liquid and a vapor leads to the separation of mixtures. This is the basis of distillation and related processes. The presence of a membrane should show a clear effect on the degree of separation, for example, enhancing the mass transfer of a target compound through the membrane and “blocking” the other compounds. The effect of the driving force, mainly due to the differences in vapor pressures

of the components in the feed mixture, should not be taken into account when evaluating the performance of the membrane. These two different perspectives have to be evaluated differently.

The evaluation of process performance should be done in terms of transmembrane fluxes and separation factors. In this case, we are interested in the overall efficiency of the separation, that is, to which extent we can perform the desired separation under realistic operating conditions and affordable cost. The transmembrane flux is a key factor since it will determine the required membrane area, which is the major investment cost in pervaporation. In this sense, we can firmly say that the larger the flux, the better since the required area for a given process feed stream is inversely proportional to the flux. Thus high fluxes mean small area. In addition, the separation factor will give a clear indication of which components are transferred through the membrane easier and faster. Normally, those components will be found at high concentration in the permeate. The transmembrane flux and the separation factor is the information that we need to evaluate or design a process and to determine the best operating conditions (i.e., temperature) for a maximum efficiency.

The evaluation of the membrane performance has to be done in terms of permeances (or permeabilities) and selectivities. The reason is that the transmembrane flux does not give information about the ability of the membrane to separate a mixture. As said before, the thermodynamic equilibrium between the liquid phase and the vapor phase is already establishing a degree of separation and this happens with or without membrane. If this effect is not removed from the calculations and we work only with the transmembrane flux, the real effect caused by the presence of the membrane cannot be determined. In order to eliminate the influence of the driving force in the results, permeances (or permeabilities) have to be used. When done, the real separation due to the membrane will be seen. This may involve situations in which the less volatile compound is permeating preferably (it has highest permeance or permeability) in spite of presenting the lowest transmembrane flux. Regarding the membrane selectivity, Eq. (3.12) in Section 3.3 showed the main difference with the separation factor. The selectivity allows evaluating the separation caused only by the membrane, since it is the ratio of permeances (or permeabilities). Thus if the selectivity α_{ij} is higher than 1, component i permeates preferably through the membrane in comparison to j , even if the permeate presents a composition in which j is the major component. Using permeances (or permeabilities) and selectivities is hence the appropriate way to evaluate the degree of separation given by the membrane. This is critical in the synthesis of novel membranes based on new materials or new structures.

Examples of clear differences between the fluxes and permeances, and separation factors and selectivities can be found in the literature. Baker et al. (2010) used the separation of ethanol/water mixtures as a case study to show those differences. Fig. 3.3 includes the results obtained with a 10- μm thick mixed-matrix membrane consisting of 60 wt% ZSM-5 zeolite dispersed in a silicone rubber matrix. The concentration of ethanol in the feed solution has an important effect on both the flux and the permeability of both components, mainly those of ethanol. However, the

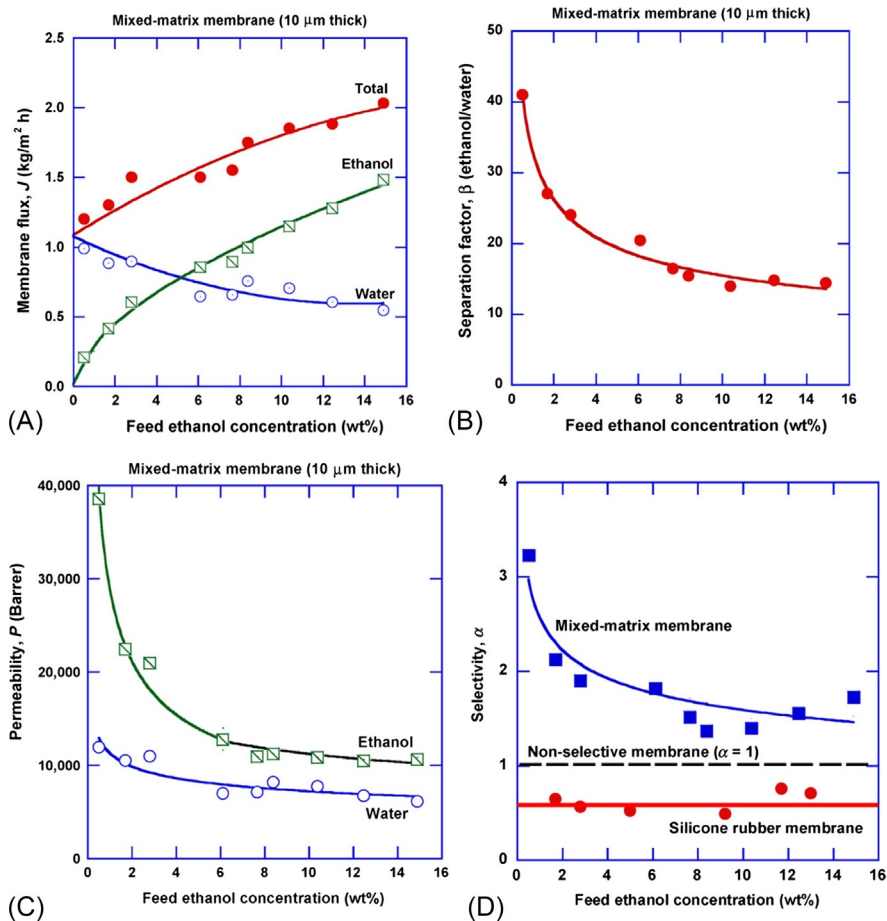


FIG. 3.3

Flux (A), ethanol/water separation factor (B), permeability (C), and selectivity (D) obtained with a 10- μm zeolite (60wt%)—silicone rubber mixed-matrix membrane.

Reproduced with permission from Baker, R.W., Wijmans, J.G., Huang, Y., 2010. Permeability, permeance and selectivity: a preferred way of reporting pervaporation performance data. *J. Membr. Sci.* 348, 346–352.

observed trend is different for the case of ethanol. The higher the concentration of ethanol, the higher the flux but a lower permeability is obtained. Thus once the effect of the driving force is removed, the separation given by the membrane can be observed. The membrane is very selective toward ethanol at low concentrations of this compound, while losing selectivity when higher concentrations of ethanol are used.

Villegas et al. (2015) studied the separation of methanol/water mixtures by using poly(3-hydroxybutyrate) membranes. Fig. 3.4 shows the trends of flux, permeance,

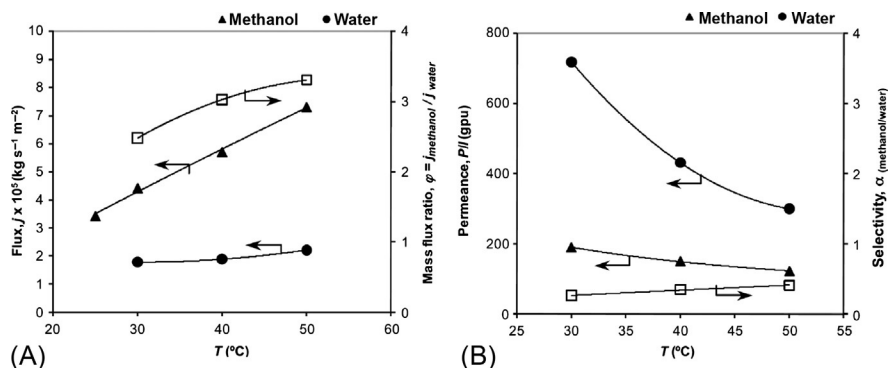


FIG. 3.4

Effect of feed temperature in single methanol and water pervaporation tests in PHB membranes: (A) flux and mass flux ratio and (B) permeance and selectivity.

Reproduced with permission from Villegas, M., Castro Vidaurre, E.F., Gottifredi, J.C., 2015. Sorption and pervaporation of methanol/water mixtures with poly(3-hydroxybutyrate) membranes. *Chem. Eng. Res. Des.* 94, 254–265.

separation factor, and selectivity as a function of the temperature. It can be observed as an increasing flux with temperature, with methanol having the highest flux. On the other hand, permeance results show that water presents a preferential transfer through the membrane. It is not a surprise that methanol flux is higher than that of water since its vapor pressure is higher and the thermodynamic equilibrium plays in its advantage, leading to a larger driving force for methanol. When the effect of the driving force is removed, the real separation ability of the membrane is shown, indicating that water permeance is enhanced. Those results are obtained for pure solutions of each component, thus no coupling effects are taking place.

A third example is the application of pervaporation for the separation of an equimolar quaternary mixture composed of methanol, methyl acetate, butanol, and butyl acetate. The separation of this mixture is energetically very consuming due to the presence of two azeotropes: methanol-methyl acetate and butanol-butyl acetate. Pervaporation has been proposed by Luis et al. (Luis et al., 2013; Luis and Van der Bruggen, 2015b) to face this separation and minimize the energy consumption. Fig. 3.5 shows the results obtained with the commercial membrane Pervap 2255-50 (Sulzer Chemtech, Switzerland). All the compounds present an increasing flux with temperature, being methanol the compound with the largest flux (Fig. 3.5A). Regarding the permeance, the effect of temperature is much less remarkable (Fig. 3.5B). Only butanol shows a significant decrease of permeance when the temperature increases. Butanol is also the compound that permeates preferably through the membrane, thus the membrane is selective to butanol (Fig. 3.5C). Again the driving force is playing an important role in the process performance and it is critical to remove its effect in order to evaluate the membrane performance.

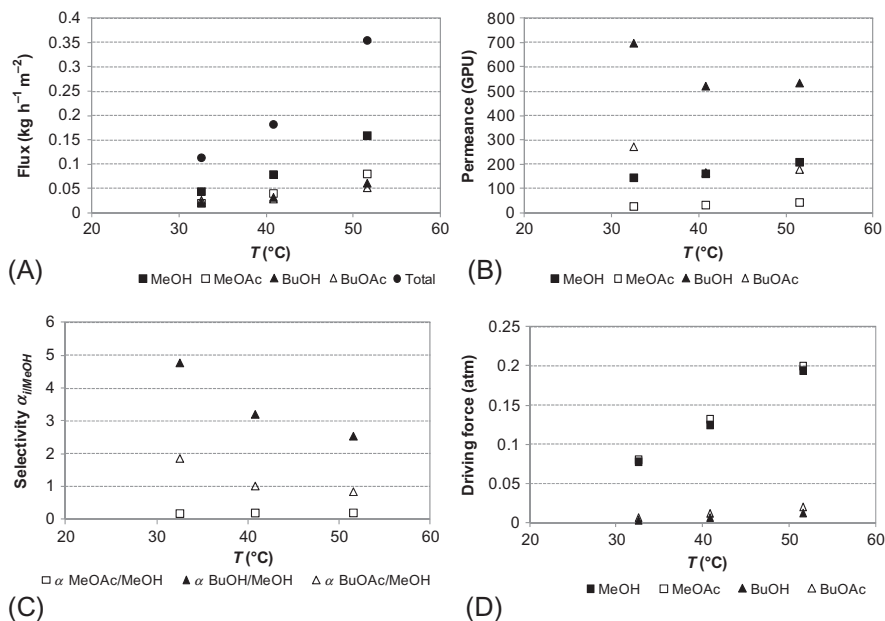


FIG. 3.5

Permeance (A), selectivity (B), transmembrane flux (C), and driving force (D) of a quaternary mixture of methanol (MeOH), methyl acetate (MeOAc), butanol (BuOH), and butyl acetate (BuOAc) on the commercial membrane Pervap 2255-50 from Sulzer Chemtech, Switzerland.

Reproduced with permission from Luis, P., Van der Bruggen, B., 2015a. Pervaporation modeling: state of the art and future trends. In: Basile, A., Figoli, A., Khayet, M. (Eds.), *Pervaporation, Vapour Permeation and Membrane Distillation. Principles and Applications. A Volume in Woodhead Publishing Series in Energy* pp. 87–106. ISBN: 978-1-78242-246-4; Luis, P., Van der Bruggen, B., 2015b. The driving force as key element to evaluate the pervaporation performance of multicomponent mixtures. *Sep. Purif. Technol.* 148, 94–102.

The examples shown previously confirm the large differences that can be found between transmembrane flux and permeance, and separation factors and selectivities, among compounds. Having high permeability for a compound with low flux is a paradox that appears frequently in pervaporation. Then, the question arises: what should be the priority, the process performance, or the membrane performance? The more rational answer would be to use membranes that are working under their maximum performance for a specific separation. This means that using a membrane that mainly enhances the permeation of a compound with the lowest flux (highest selectivity for the compound with low flux) is not a good approach since the membrane is operating against the driving force (having a low process efficiency), which will increase the overall cost significantly.

In order to determine the best membranes for a specific separation, Luis and Van der Bruggen (2015b) suggested a prior evaluation of the driving force. The membranes that would benefit of the effect of the driving force by permeating the species with the highest driving force should be preferably selected so that pervaporation

is applied under conditions of maximum performance from the point of view of the membrane as well as the process. Following the example of Fig. 3.5, Fig. 3.5B showed that the compound that permeates preferably through the membrane is butanol, showing also the highest selectivity (Fig. 3.5C). A fast conclusion would be then that this membrane is useful for the separation of butanol from a mixture. However, if one analyses the driving force as done in Fig. 3.5D, the evidence of a very low driving force for butanol appears. From Eq. (3.9), it can be seen that compounds with higher vapor pressure will normally present a higher driving force for the separation. In this example, methanol and methyl acetate present the highest driving force. Thus the selected membrane should enhance the permeance of one or both of these compounds so that the driving force is used in favor of the separation. However, the membrane of this example is “blocking” the methanol and the methyl acetate and enhancing the permeation of butanol. In other words, the membrane is not taking advantage of the existing driving force but acting against it. A membrane that enhances the permeation of methanol or methyl acetate would be the best choice. In general terms, we could say that the membrane should increase the permeance of those compounds that already have a preference due to the favorable driving force so that the membrane is operating under maximum performance. Starting from a simple analysis of the driving force for each compound would allow determining the objective of pervaporation and the requirements of the membrane (Luis and Van der Bruggen, 2015b).

3.5 MCCABE-THIELE DIAGRAM

An interesting study that completes the evaluation of the membrane performance is the comparison of the separation achieved via distillation with that obtained via pervaporation. This can be done easily using McCabe-Thiele diagrams in which the concentration of one of the components in the liquid phase (feed) is represented in the x -axis, and the concentration of that component in the vapor phase (permeate in pervaporation) is represented in the y -axis. By comparing the vapor-liquid equilibrium (distillation curve) with the pervaporation results (pervaporation curve), it is possible to see easily if pervaporation is achieving a better separation than distillation. Fig. 3.6A shows an example for the separation of the binary mixture methanol/butyl acetate. Fig. 3.6B represents the separation of the quaternary mixture methanol/methyl acetate/butanol/butyl acetate. The point related to distillation indicates the separation achieved when a liquid mixture of equimolar concentration enters a flash equilibrium unit, modeled with the NRTL thermodynamic model, and using Aspen Plus v8.4 to perform the simulation (Luis and Van der Bruggen, 2015b). Two aspects should be discussed when evaluating those diagrams. First, the relative position of the pervaporation points for each membrane. Being close to the diagonal means no separation (i.e., same composition of liquid and vapor phase); the further the concentration of one compound from the dotted line and from other compounds, the better the separation. In addition, their position in the graph allows comparison

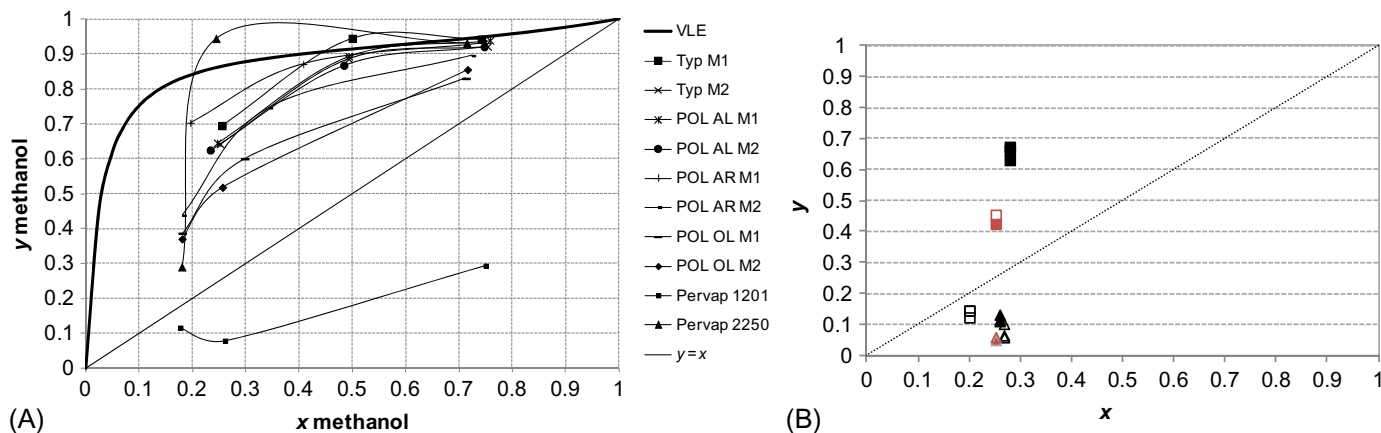


FIG. 3.6

McCabe-Thiele separation diagram. Comparison of pervaporation selectivity with distillation selectivity (vapor-liquid equilibrium) for the systems: (A) methanol/butyl acetate and (B) methanol/methyl acetate/butanol/butyl acetate. The lines for the membrane data have been added to guide the eye. The distillation data have been obtained when a liquid mixture of equimolar concentration enters a flash equilibrium unit, modeled with the NRTL thermodynamic model and using the commercial simulator Aspen Plus.

Reproduced with permission from Luis, P., Degève, J., Van der Bruggen, B., 2013. Separation of methanol-*n*-butyl acetate mixtures by pervaporation: potential of 10 commercial membranes. *J. Membr. Sci.* 429, 1–12 and Luis, P., Van der Bruggen, B., 2015b. The driving force as key element to evaluate the pervaporation performance of multicomponent mixtures. *Sep. Purif. Technol.* 148, 94–102, respectively.

among different membranes so that the membrane with the richest permeate can be easily pointed. Second, the position of the pervaporation points regarding the distillation points. In this way, it is possible to determine the competitive character of pervaporation with the conventional process.

In Fig. 3.6A, several pervaporation membranes are compared with the distillation curve. Most of the membranes are below the distillation curve, indicating that they enhance the enrichment of the vapor phase with butyl acetate, opposite tendency to distillation. As discussed by Luis et al. (2013), the membrane Pervap 1201 produces a very significant effect on the separation, achieving a permeate enriched in butyl acetate. The membranes Pervap 2255-50 and Typ M1 show a high concentrated permeate in methanol since the y - x pairs are above the VLE curve. On the other hand, Fig. 3.6B shows that pervaporation using the membrane Pervap 2255-50 leads to a permeate richer in methanol in spite of the preference of this membrane for butanol as discussed in the previous section, showing a clear difference with the distillation results (red points in the figure). Thus using McCabe-Thiele separation diagrams is an interesting way to compare the separation character of different membranes as well as the performance against distillation, which is essential information to determine the real applicability of pervaporation (Luis et al., 2013; Luis and Van der Bruggen, 2015b).

3.6 COUPLING EFFECTS

Coupling effects in the mass transfer of compounds through the pervaporation membrane have been repeatedly observed in the literature. Coupling effects are considered when a component permeates more or less when it is in a feed mixture with other components than when it is alone (the feed solution is the pure component). It is thus not a surprise that researchers try to understand and explain why and how this phenomenon is taking place. Two types of coupled transport have been described, that is, the thermodynamic, and the kinetic coupling (Mulder and Smolders, 1984). The thermodynamic coupling is caused by the interaction between the dissolved species in the membrane. The change in concentration of one component in the membrane due to the presence of another component is caused by mutual interactions between the permeants in the membrane as well as by interactions between the individual components and the membrane material (Mulder and Smolders, 1984). The Gibbs free energy of one species can be affected by the presence of other species, and the change in the free energy can lead to changes in the partition/sorption capacity of species in the membrane (Shao and Huang, 2007). Kinetic coupling is due to the dependence of the concentration on the diffusion coefficients of low molecular weight components in polymers, particularly in glassy polymers (Mulder and Smolders, 1984), thus it may be linked to changes in the diffusion coefficient caused by the plasticization of the membrane. When low molecular weight components are dissolved in polymers below their glass transition (e.g., cellulose acetate, polysulfone, polyacrylonitrile) at room temperature, the mobility of the polymer chains increases that explains the plasticizing effect and the enhanced

mobility of the components through the membrane (Mulder and Smolders, 1984). Since it is the combined effect of all the plasticizants in the membrane that changes the free volume of the polymer, the diffusion of the transporting species in the polymer matrix is interdependent (Shao et al., 2007).

3.6.1 MODIFIED SOLUTION-DIFFUSION MODELS

Several researchers have developed transport models to take into account these coupling effects in pervaporation. Mulder and Smolders (1984) presented a modified solution-diffusion model which combines both the thermodynamic and the kinetic (diffusive) aspects of the pervaporation process, considering coupling of fluxes, whereas in the original solution-diffusion model each component dissolved in the membrane and diffused through it independently. Thus the activity of each component in the membrane is described by Flory-Huggins thermodynamics (Flory, 1953). For a binary system:

$$\ln a_1 = \frac{\Delta\mu_1}{RT} = \ln v_1 + \left(1 - \frac{V_1}{V_2}\right)v_2 + \chi_{12}v_2^2 \quad (3.22)$$

$$\ln a_2 = \frac{\Delta\mu_2}{RT} = \ln v_2 + \left(1 - \frac{V_2}{V_1}\right)v_1 + \chi_{12}\frac{V_2}{V_1}v_1^2 \quad (3.23)$$

The Flory-Huggins interaction parameter χ_{12} is a binary interaction parameter between the components 1 and 2 and it is a dimensionless quantity characterizing the difference in interaction energy of a solvent molecule immersed in pure polymer compared with one in pure solvent, reflecting the intermolecular forces between the molecules in solution (Flory, 1953; Mulder and Smolders, 1984). Flory-Huggins theory is applied to calculate the solubility of liquids in amorphous polymers that are in rubbery or gel-like state (Tang et al., 2013). For glassy polymers, empirical sorption models for correlation of solubility of gases and vapors are applied (Tang et al., 2013).

In the case of a polymeric membrane and a binary liquid mixture, a ternary system, the activities a_1 and a_2 of liquid components 1 and 2 in the polymeric membrane are given by (Flory, 1953):

$$\ln a_1 = \ln \varphi_1 + (1 - \varphi_1) - \varphi_2 \frac{V_1}{V_2} - \varphi_3 \frac{V_1}{V_3} + (\chi_{12}\varphi_2 + \chi_{13}\varphi_3)(\varphi_2 + \varphi_3) - \chi_{23} \frac{V_1}{V_2} \varphi_2 \varphi_3 \quad (3.24)$$

$$\ln a_2 = \ln \varphi_2 + (1 - \varphi_2) - \varphi_1 \frac{V_2}{V_1} - \varphi_3 \frac{V_2}{V_3} + \left(\chi_{12}\varphi_1 \frac{V_2}{V_1} + \chi_{23}\varphi_3\right)(\varphi_1 + \varphi_3) - \chi_{13} \frac{V_2}{V_1} \varphi_1 \varphi_3 \quad (3.25)$$

$$J_1 = -\varphi_1 D_1(\varphi_1, \varphi_2) \frac{d}{dx} \left[\ln \varphi_1 + (1 - \varphi_1) - \varphi_2 \frac{V_1}{V_2} - \varphi_3 \frac{V_1}{V_3} + (\chi_{12}\varphi_2 + \chi_{13}\varphi_3)(\varphi_2 + \varphi_3) - \chi_{23} \frac{V_1}{V_2} \varphi_2 \varphi_3 \right] \quad (3.26)$$

$$J_2 = -\varphi_2 D_2(\varphi_1, \varphi_2) \frac{d}{dx} \left[\ln \varphi_2 + (1 - \varphi_2) - \varphi_1 \frac{V_2}{V_1} - \varphi_3 \frac{V_2}{V_3} + \left(\chi_{12} \varphi_1 \frac{V_2}{V_1} + \chi_{23} \varphi_3 \right) (\varphi_1 + \varphi_3) - \chi_{13} \frac{V_2}{V_1} \varphi_1 \varphi_3 \right] \quad (3.27)$$

These equations allow the calculation of the transmembrane flux of each component as a function of the concentration of the other component. The estimation of the binary interaction parameters χ_{12} , χ_{13} , and χ_{23} can be done from the equations in Table 3.1 (Mulder and Smolders, 1984). In general, the smaller the value of χ for the polymer-solvent combination (close to 0.5 but not below), the greater will be the interaction between the polymer and the liquid species (Ravindra et al., 2000).

Since the diffusion coefficient of a species is affected by the presence of other compounds (plasticizants), several researchers have adapted the solution-diffusion model by modifying the calculation of the diffusion coefficient. Vrentas and Duda (Vrentas and Duda, 1977a,b; Vrentas et al., 1986) developed the free volume theory in this sense. For a ternary system consisting of two components and the membrane, the diffusion coefficient can be calculated according to Eq. (3.34) in Table 3.2. Other expressions have been suggested (Shao and Huang, 2007): Eqs. (3.35)–(3.37) in Table 3.2.

Brun et al. (1985) proposed the “six coefficients” model (D_{i0} , D_{j0} , α_{ii} , α_{ij} , β_{jj} , β_{ij}) for a ternary system, which is obtained after dividing the permeation fluxes of the components i and j through the membrane and assuming zero concentrations of both the species at the downstream membrane face (Eqs. 3.31, 3.32), leading to Eq. (3.33):

$$N_i = -D_{i0} \exp(\alpha_{ii} C_i + \beta_{ij} C_j) \frac{dC_i}{d\delta} \quad (3.31)$$

$$N_j = -D_{j0} \exp(\alpha_{ij} C_i + \beta_{jj} C_j) \frac{dC_j}{d\delta} \quad (3.32)$$

$$\frac{N_i}{N_j} = \frac{D_{i0} (\beta_{jj} - \beta_{ij}) [\exp((\alpha_{ii} - \alpha_{ij}) C_{mi}) - 1]}{D_{j0} (\alpha_{ii} - \alpha_{ij}) [\exp((\beta_{jj} - \beta_{ij}) C_{mj}) - 1]} \quad (3.33)$$

Table 3.1 Estimation of binary interaction parameters

Equation	Ref
$\chi_{12} = \frac{1}{m_1 v_2} \left[m_1 \ln \frac{m_1}{v_1} + m_2 \ln \frac{m_2}{v_2} + \frac{\Delta G^E}{RT} \right] \quad (3.28)$	Mulder and Smolders, 1984
$\chi_{12} = \frac{\Delta G^E}{RT m_1 m_2} \quad (3.29)$	Dondos et al., 1970
$\chi = - \frac{[\ln(1 - v_p) + v_p]}{v_p^2} \quad (3.30)$	Flory, 1953
v_p is the volume fraction of polymer	

Table 3.2 Main equations suggested to estimate diffusions coefficients using a modified solution-diffusion model due to coupling effects (Shao et al., 2007)

$D = D_0 \exp\left(-\frac{E_a}{RT}\right) \times \exp\left[\gamma \left(\frac{\omega_1 \hat{V}_1^* + \omega_2 \hat{V}_2^* \xi}{\hat{V}_{FH}}\right)\right]$	(3.34)
<p>With $V_{FH} = \omega_1 K_{11}(K_{21} - T_{g1} + T) + \omega_2 K_{12}(K_{22} - T_{g2} + T)$ D_0: diffusion coefficient at infinite dilution E_a: diffusion activation energy \hat{V}_i^*: specific critical hole free volume required for a diffusive jump of the component i R: universal gas constant T: absolute temperature γ: overlap factor ω_i: weight fraction of the component i ($i = 1, 2$) ξ: ratio of the critical volume of the solvent per mole to that of the polymer \hat{V}_{FH}: specific hole free volume of the polymer-solvent system K_{1i} and K_{2i}: the free volume parameters T_{gi}: glass transition temperature of component i ($i = 1, 2$).</p>	
$D_i = D_{i0} \exp(\alpha_i C_i + \beta_j C_j)$	(3.35)
<p>D_{i0}: diffusion coefficients of species i at infinite dilution C_i, C_j: local concentrations of the species of i and j in the membrane, respectively α, β: plasticization coefficients of the two species for the membrane, respectively</p>	
$D_i = D_{i0}(1 + \alpha_i C_i + \beta_j C_j)$	(3.36)
<p>For glassy polymers</p>	
$D_i = D_{i0}(C_i + a C_j)$	(3.37)

3.6.2 HANSEN SOLUBILITY APPROACH

Coupling effects may be also evaluated in terms of the Hansen solubility approach. Solubility of solvents in the polymeric membrane is going to determine the overall concentration gradient, which is the driving force for the diffusion process. Thus it makes sense that the diffusion, and therefore, the permeability of species through the membrane, is going to be affected by the solubility of those species into the polymer. The Hansen solubility parameters for the solvent and the polymer can be used to determine which compounds will “like” the polymer (those with similar parameters than the polymer), leading to swelling of the membrane, changes in diffusivities and coupling effects; and which components will not “like” the polymer (those with different parameters than the polymer), which would mean that their permeability through the membrane is more limited. When mixtures of solvents are considered, the Hansen solubility parameters of the mixture can be very different from those of the pure compounds, thus pure solvents could have no affinity with the membrane polymer but as a mixture, they could even dissolve the polymer. This is the great potential of this approach to evaluate coupling effects: pure solvents may be rejected by the membrane but the same solvents in a mixture could have a great affinity

(solubility) with the membrane, or with other words, a pure solvent may have a very low (or zero) permeability through the membrane but in combination with another solvent, it will permeate significantly.

The Hansen solubility parameter is calculated as the square root of the cohesive energy density for all liquids whose vapors can be considered ideal (Hansen, 1967):

$$\delta = (\text{cohesive energy density})^{1/2} = \left(\frac{\Delta E}{V_m}\right)^{1/2} \quad (3.38)$$

where ΔE is the energy of evaporation of the solvent (cal), and V_m is the molar volume (cm^3).

ΔE includes the energies arising from all modes of interaction which hold the liquid together: dispersion (London) forces, polar forces, and hydrogen bonding.

Hansen (1967) assumed that ΔE is given by the simple sum of the energies arising from dispersion forces, ΔE_d , polar forces, ΔE_p , and hydrogen bonding forces, ΔE_h . Thus Eq. (3.38) can be written as:

$$\delta = \left(\frac{\Delta E_d}{V_m}\right) + \left(\frac{\Delta E_p}{V_m}\right) + \left(\frac{\Delta E_h}{V_m}\right) = \delta_d + \delta_p + \delta_h \quad (3.39)$$

Thus the Hansen solubility parameter can be represented by three components: δ_d : the contribution of the dispersion interaction; δ_p : the contribution of the polar interaction; and δ_h : the contribution of the hydrogen bonding. This means that each solvent can be located in a three-dimensional system as a fixed point with coordinates agreeing with Eq. (3.39). The axes of the system are the dispersion axis, δ_d ; the polar axis, δ_p ; and the hydrogen bonding axis, δ_h . The system can be represented for a given volume of interaction by a sphere in a 3D space or by circles taking pairs of parameters in a 2D space. Hansen (1967) also observed that the volumes of solubility are not spherical when plotting is done with equal unit distances for δ_d , δ_p , and δ_h . However, if the scale of the dispersion axis, δ_d , is doubled, spherical volumes of solubility are found. The reason is that the polar and hydrogen bonding interactions are of a similar nature, arising from molecular, permanent dipole-permanent dipole interactions; but the dispersion interactions are fundamentally different, arising from atomic, induced dipole-induced dipole interactions (Hansen, 1967). Hansen solubility approach has been experimentally validated based on a “trial-and-error” method, and obtained results up to date show the success of its application.

Fig. 3.7 shows the spherical representation of the Hansen solubility approach. The radius of the solubility sphere is usually called the interaction radius, R_0 , and it is experimentally determined from solubility tests. This value determines the radius of the sphere in Hansen space and its center is the three Hansen parameters. Table 3.3 presents values of R_0 for several polymers and resins (Hansen, 1967) and Table 3.4 presents the Hansen solubility parameters for different solvents. Solvents that are located inside the sphere, are expected to dissolve the polymer (center of the sphere), and those outside the sphere will not dissolve it. A mathematical

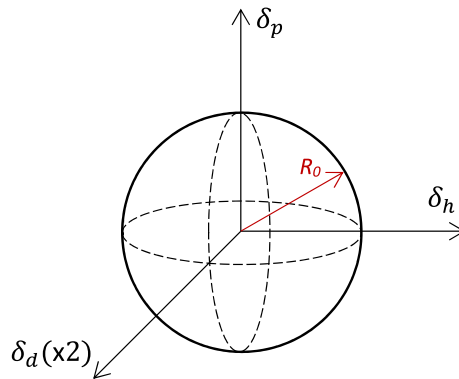


FIG. 3.7

General representation of the Hansen solubility sphere (δ_d : contribution of the dispersion interaction; δ_p : contribution of the polar interaction; δ_h : contribution of the hydrogen bonding; R_0 : interaction radius).

Table 3.3 Characteristic parameters for polymers and resins

Solute	δ_o	δ_{d0}	δ_{p0}	δ_{h0}	δ_{a0}	R_{A0}	Comments
A	10.8	9.2	5.3	2.1	5.7	5.3	
B	11.3	9.2	5.0	4.2	6.5	4.0	
C	11.5	8.5	5.5	5.5	7.8	4.7	
D	9.4	8.5	2.5	3.0	3.9	5.3	δ_d Arbitrary
E	11.2	9.4	3.2	5.1	6.0	5.0	Some deviations
F	11.0	8.5	4.3	5.5	7.0	4.8	
G	9.8	8.6	3.0	2.0	3.6	3.5	
H	11.3	9.3	5.0	4.0	6.4	4.9	A few deviations
I	12.1	9.5	4.0	6.4	7.5	4.7	
J	10.8	7.0	7.0	4.3	8.2	5.5	
K	10.2	9.3	3.7	2.1	4.3	4.2	
L	12.7	9.5	6.0	6.0	8.5	4.5	Radius of strong interaction
M	11.3	9.0	4.0	5.5	6.8	6.4	Too soluble, inaccurate
N	13.1	9.4	5.3	7.4	9.1	5.5	
O	10.1	8.9	3.0	3.8	4.8	4.5	
P	11.7	8.5	4.7	6.5	8.0	5.0	
Q	12.1	9.3	6.2	4.7	7.8	4.2	
R	10.5	9.2	4.5	2.6	5.2	5.0	
S	12.5	8.8	7.0	5.5	8.9	6.0	Low M.W. solute, liquid
T	9.0	8.7	1.8	1.8	2.5	3.5	
U	10.5	9.3	4.5	2.0	4.9	4.7	
V	8.8	8.5	1.5	1.5	2.1	3.4	

Continued

Table 3.3 Characteristic parameters for polymers and resins —cont'd

Solute	δ_0	δ_{d0}	δ_{p0}	δ_{h0}	δ_{a0}	R_{A0}	Comments
X	8.6	7.8	1.0	3.5	3.6	4.0	High M.W. rubber
Y	9.2	8.8	2.5	1.2	2.8	3.8	
Z	10.2	8.2	0.8	5.7	3.2	2.9	Some deviations
\bar{A}	9.7	8.7	2.5	3.5	4.3	4.2	
\bar{B}	11.7	9.5	4.0	5.5	6.8	7.0	Too soluble, inaccurate
\bar{C}	8.8	8.5	1.0	2.0	2.2	3.4	
\bar{D}	11.6	9.2	5.8	4.2	7.2	5.0	Liquid, hard to place
\bar{E}	8.8	8.5	1.5	1.8	2.3	2.6	
\bar{F}	11.0	9.4	4.5	3.5	5.7	3.2	Radius of strong interaction
\bar{G}	9.6	8.8	2.7	2.7	3.9	4.0	
\bar{L}	15.6	10.8	7.0	8.8	11.2	7.1	

A: Lucite 2042-poly (ethyl methacrylate), E. I. du Pont de Nemours & Co., Inc.

B: Poly (methyl methacrylate), Rohm and Haas Co.

C: Epikote 1001-epoxy, Shell Chemical Co.

D: Plexal P65-66% oil length alkyd, Polyplex.

E: Pentalyne 830-alcohol soluble rosin resin, Hercules Incorporated.

F: Butvar B76-poly (vinyl butyral), Shawinigan Resins Co.

G: Polystyrene LG, Badische Anilin- und Soda Fabrik.

H: Mowilith 50-poly (vinyl acetate), Farbwerke Hoechst.

I: Plastopal H-urea formaldehyde resin, Badische Anilin- und Soda Fabrik.

J: 1/2 Sec. Nitrocellulose-H 23, A. Hagedorn and Co., Osnabrück, W. Germany.

K: Parlon P10-chlorinated poly(propylene), Hercules Incorporated.

L: Cellulose acetate, Cellidora A-Bayer AG.

M: Super Beckacite 1001-Pure Phenolic Resin, Reichhold Chemicals Co.-Hamburg.

N: Phenodur 373U-phenol-resol resin, Chemische Werke Albert-Wiesbaden.

O: Cellolyn 102-modified pentaerythritol ester of rosin, Hercules Incorporated.

P: Pentalyne 255-alcohol soluble resin, Hercules Incorporated.

Q: Suprasec F5100-blocked isocyanate (phenol), Imperial Chemical Ind. Ltd.

R: Plexal C34-34% coconut oil-phthalic anhydride alkyd, Polyplex.

S: Desmophen 850, Polyester-Farbenfabriken Bayer AG. Leverkusen.

T: Polysar 5630-styrene-butadiene (SBR) raw elastomer, Polymer Corp.

U: Hycar 1052-acrylonitrile-butadiene raw elastomer, B. F. Goodrich Chemical Corp.

V: Cariflex IR 305-isoprene raw elastomer, Shell Chemical Co.

X: Lutonal IC/123-poly (isobutylene), Badische Anilin- und Soda Fabrik.

Y: Buna Huls CB 10-cis poly butadiene raw elastomer, Chemische Werke Huels.

Z: Versamid 930-polyamide, General Mills, Inc.

\bar{A} : Ester gum BL, Hercules Incorporated.

\bar{B} : Cymel 300-hexamethoxy melamine, American Cyanamid Co.

\bar{C} : Piccolyte S100-terpene resin, Pennsylvania Industrial Chemical Corp.

\bar{D} : Durez 14,383-furfuryl alcohol resin, Hooker Chemical Co.

\bar{E} : Piccopale[®]J 110-petroleum hydrocarbon resin, Pennsylvania Industrial Chemical Co

\bar{F} : Vipla KR-poly (vinyl chloride), K=50, Montecatini.

\bar{G} : Piccoumarone 450L-coumarone-indene resin, Pennsylvania Industrial Chemical Corp

\bar{L} : Milled wood lignin-Special sample from prof. A. Björkman.

Extracted from Hansen, C.M., 1967. *The Three Dimensional Solubility Parameter and Solvent Diffusion Coefficient*. Danish Technical Press, Copenhagen.

Table 3.4 Hansen solubility parameters of various solvents

Solvent	Dispersion	Polar	Hydrogen
1,2-Diethyl benzene	17.7	0.1	1
1,4-Dioxane	19	1.8	7.4
1-Butanol	16	5.7	15.8
1-Butene	13.2	1.3	3.9
1-Heptene	15	1.1	2.6
1-Hexene	14.7	1.1	0
1-Pentanol	15.9	4.5	13.9
1-Propanol	16	6.8	17.4
2,3-Dichlorobenzene	19.7	12.6	4.4
2,4-Dichlorobenzene	20.4	8.7	4.2
2-Butanol	15.8	5.7	14.5
2-Pentanol	15.6	6.4	13.3
2-Propanol	15.8	6.1	16.4
Acetic acid	14.5	8	13.5
Acetone	15.5	10.4	7
Acrylic acid	17.7	6.4	14.9
Benzene	18.4	0	2
Butane	14.1	0	0
Carbon tetrachloride	17.8	0	0.6
Chlorobenzene	19	4.3	2
Chloroform	17.8	3.1	5.7
Cyclohexane	16.8	0	0.2
Diethyl carbonate	16.6	3.1	6.1
Diethyl ether	14.5	2.9	5.1
Diethyl ketone	15.8	7.6	4.7
Diethylene glycol	16.6	12	20.7
Dimethyl carbonate	15.5	3.9	9.7
Ethanol	15.8	8.8	19.4
Ethyl acetate	15.8	5.3	7.2
Ethyl benzene	17.8	0.6	1.4
Ethylene dichloride	19	7.4	4.1
Ethylene glycol	17	11	26
Glycerol	17.4	12.1	29.3
Heptane	15.3	0	0
Hexane	14.9	0	0
m-Dichlorobenzene	19.7	5.1	2.7
Methanol	15.1	12.3	22.3
Methylacrylic acid	15.8	2.8	10.2
Methylene dichloride	18.2	6.3	6.1

Continued

Table 3.4 Hansen solubility parameters of various solvents —cont'd

Solvent	Dispersion	Polar	Hydrogen
<i>n</i> -Butyl acetate	15.8	3.7	6.3
Octane	15.5	0	0
Octanol	17	3.3	11.9
<i>o</i> -Dichlorobenzene	19.2	6.3	3.3
<i>o</i> -Xylene	17.8	1	3.1
<i>p</i> -Dichlorobenzene	19.7	5.6	2.7
<i>p</i> -Diethyl benzene	18	0	0.6
Phenol	18	5.9	14.9
Propionic acid	14.7	5.3	12.4
Tetrahydrofuran	16.8	5.7	8
Toluene	18	1.8	2
Trichloroethylene	18	3.1	5.3
Triethylene glycol	16	12.5	18.6
Water	15.5	16	42.3
Xylene	17.6	1	3.1

Extracted from Shao, P., Huang, R.Y.M., 2007. Polymeric membrane pervaporation. *J. Membr. Sci.* 287, 162–179.

equation that can easily determine the condition of solution or interaction between the solvent (subscript 1) and the polymer (subscript 0) can be written as:

$$R_A^2 = 4(\delta_{d1} - \delta_{d0})^2 + (\delta_{p1} - \delta_{p0})^2 + (\delta_{h1} - \delta_{h0})^2 \quad (3.40)$$

Being R_A the distance between a solute's center point (e.g., polymer) and the point representing the solvent. The relative energy difference (RED) of the system is defined as the ratio

$$RED = \frac{R_A}{R_0} \quad (3.41)$$

Thus it is possible to say that if:

RED < 1, the components are alike and will dissolve.

RED = 1 the system will partially dissolve (possible swelling).

RED > 1, the system will not dissolve.

The application of the Hansen solubility approach in pervaporation has received recent attention due to the ability of the model to explain coupling effects. Previously, interactions of pure solvents with a polymer have been indicated but the approach is of utmost interest when mixtures of solvents are involved. First, the distance between two solvents in the sphere may be an indicator of the dissimilarity of those two solvents, thus by proper selection of the membrane, the separation factor of the two components may be proportional to that characteristic distance

(Mulder and Smolders, 1984). The ideal polymer should present high chemical resistance (compatibility), sorption capacity, and good mechanical strength in the solution in addition to a good interaction preferably with one of the components of the mixture for effective separation. Thus it is worth doing some calculations before starting the experimental work so that we take advantage of the current literature and previous experiences in the selection of the membrane. And second, when two solvents are in a mixture, the position of this mixture in the sphere is different than that of the pure solvents. This means that the solubility of the mixture in the polymer will be different and a larger or smaller interaction may appear, explaining possible coupling effects. The Hansen solubility approach allows thus predicting somehow the behavior of the feed solution in contact with the membrane.

3.6.3 EXAMPLES OF APPLICATION

Some examples of application of the Hansen's solubility parameter and Flory-Huggins interaction parameter in pervaporation can be found in the literature. Ravindra et al. (2000) applied pervaporation for the separation of water-hydrazine and water-monomethylhydrazine mixtures at azeotropic compositions using ethylcellulose membranes, which were previously selected using the Hansen's solubility parameter and Flory-Huggins interaction parameter models (Sridhar et al., 2000). They found the highest value of the vectorial distance in the 3D diagram of the Hansen solubility parameters (being the polymer in the center of the sphere) for water, followed by hydrazine and finally monomethylhydrazine. Similarly, the Flory-Huggins interaction parameters were the highest for the pair water-polymer, followed by the pair polymer-hydrazine and polymer-monomethylhydrazine. Having water the lowest solubility in the polymer led to a lower sorption and an easier (faster) diffusion through the membrane compared to the other solvents. The interaction of water molecules with the polymer is weaker and they can flow more freely through the membrane barrier (Sridhar et al., 2000). The greater affinity between the ethylcellulose membranes and the monomethylhydrazine involved that the molecules of the latter would be held strongly within the polymer matrix as a result of which its diffusion could be retarded. This was corroborated by pervaporation experiments, which showed a maximum membrane resistance toward water when compared to pure hydrazine and monomethylhydrazine, which implies that the membrane has lower affinity for water, containing a lower quantity of water at any time. This fact together to a lower desorption resistance and a higher diffusion coefficient allowed water molecules to move faster into the membrane and to leave the membrane without much resistance at the permeate side. On the other hand, hydrazine and monomethylhydrazine almost doubled the sorption values but because of their lower diffusivity values, their transfer rates are not as high as water molecules. Thus excessive interaction with the polymer matrix and higher desorption resistance resulted in higher retention time for these molecules compared to water in the membrane. Higher permeation of water is then envisaged in the studied polymer (Ravindra et al., 2000).

Hydrophobic ceramic membranes have been studied by Kujawa et al. (2015). Various types of alumina and titania ceramic membranes were modified with 1H,1H,2H,2H-perfluorooctyltriethoxysilane (named C6) to achieve a hydrophobic character on the surface. Pure water and binary water-organic mixtures (methyl tertbutyl ether (MTBE)/water, ethyl acetate/water and butanol/water) were tested at low concentration of organics. The Hansen solubility parameters were determined for each compound and the highest distance parameter was found to be for water and C6, suggesting that water is the least compatible solvent with C6 grafting molecules. On the other hand, MTBE-C6 presented the lowest value, thus MTBE seems to have a better solubility in C6. The lowest distance parameter found for MTBE correlates well with the highest selective properties of titania membranes in contact with the studied mixtures (Kujawa et al., 2015).

Araki et al. (2016) plotted the relationship between the distance R_A calculated as $R_A = [4(\delta_{d1} - \delta_{d2}) + (\delta_{p1} - \delta_{p2}) + (\delta_{h1} - \delta_{h2})]$ and the experimental flux of different solvents through different membranes (Fig. 3.8). Clearly, higher solubility of the compound in the membrane (i.e., lower R_A) lead to higher fluxes. On the other hand, Bettens et al. (2005) studied the pervaporation mechanism of pure components (water, methanol, ethanol, 2-propanol, and n-propanol) through a commercial microporous silica membrane. They observed water fluxes much higher than the alcohol fluxes (100 times higher). The Hansen solubility parameters were calculated, and the

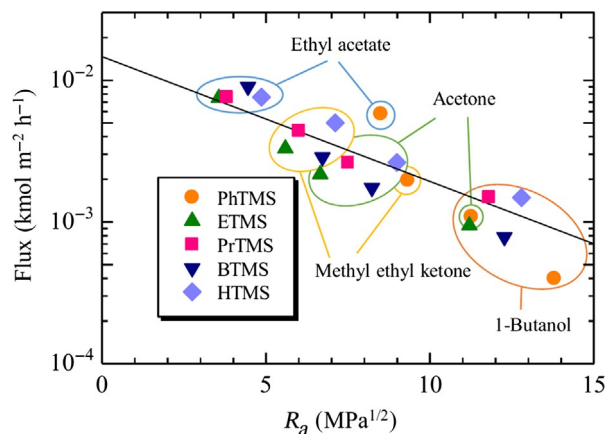


FIG. 3.8

Relationship between R_A and the experimental flux obtained for different solvents and membrane polymers. PhTMS: Phenyltrimethoxysilane; ETMS: ethyltrimethoxysilane; PrTMS: n-propyltrimethoxysilane; BTMS: isobutyltrimethoxysilane; HTMS: n-hexyltrimethoxysilane. Reproduced with permission from Araki, S., Gondo, D., Imasaka, S., Yamamoto, H., 2016. Permeation properties of organic compounds from aqueous solutions through hydrophobic silica membranes with different functional groups by pervaporation. *J. Membr. Sci.* 514, 458–466.

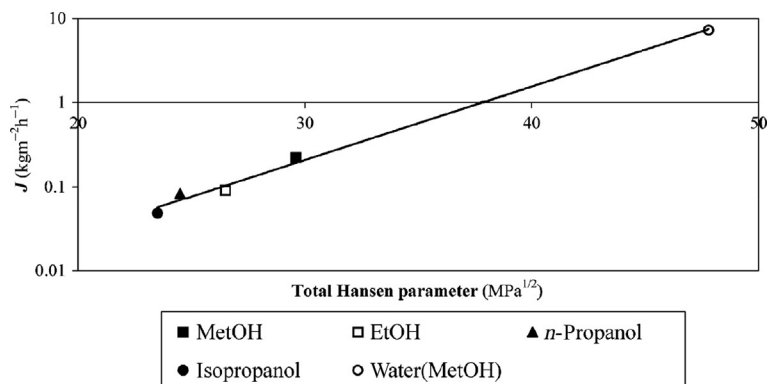


FIG. 3.9

Flux, J , as a function of total Hansen parameter (all values taken at 50°C).

Reproduced with permission from Bettens, B., Dekeyser, S., Van der Bruggen, B., Degève, J., Vandecasteele, C., 2005. Transport of pure components in Pervaporation through a microporous silica membrane. *J. Phys. Chem. B* 109, 5216–5222.

total value, expressed as $(\delta_d^2 + \delta_p^2 + \delta_h^2)^{1/2}$, was plotted versus the flux of pure compounds as shown in Fig. 3.9. They observed that especially the hydrogen bonding parameter showed a good exponential relation with the flux, but the polar parameter showed a fair correlation, while the disperse parameter had no correlation with the fluxes. This indicates that sorption on the silica layer is mainly due to hydrogen bond formation (Bettens et al., 2005) and water flux is favored due to its good sorption on the membrane, which is a key step in the pervaporation process.

The results presented previously are some examples of how Hansen solubility parameters or Flory-Hugging interaction parameters are being applied to determine the interactions between the components and the membrane. However, when interpreting the results obtained in pervaporation, one must always keep in mind the differences between the transmembrane flux, affected by the driving force, and the permeability, in which the effect of the driving force has been eliminated as explained in Section 3.4. If not, wrong interpretations can be done. Villegas et al. (2015) showed a clear case in which explaining the fluxes in terms of the Hansen solubility parameters is not enough. They evaluated poly(3-hydroxybutyrate) (PHB) membranes for methanol/water separation. The R_A distance calculated using Eq. (3.40) for both methanol and water is larger than R_0 for the polymer, but methanol is nearest, which suggest more affinity methanol-polymer than water-polymer. In addition, methanol fluxes were higher than those of water at all temperatures when pure feed solutions were studied. Larger interaction of methanol with the polymer could suggest lower fluxes as observed in the previous examples, but we cannot forget that the effect of the driving force is present and the methanol vapor pressure is approximately five times higher than that of water in the studied temperature

range, that is, a driving force five times higher for methanol than for water. Thus calculating permeabilities (or permeances) is essential to evaluate the real performance of the membrane (the real separation that the membrane is producing). Results of permeances showed that the permeance of methanol was lower than the permeance of water. Regarding the pervaporation results of mixtures methanol/water, water was also the preferred compound for permeation but its permeance was more than double than that as pure solvent. Methanol is enhancing water permeation due to its higher affinity toward the membrane, plasticizing the polymeric matrix and helping water to penetrate the membrane due to the formation of clusters water-alcohol (Villegas et al., 2015). Coupling effects were thus clearly observed and described using the indicated models.

3.7 CONCLUDING REMARKS

This chapter on pervaporation has aimed at showing the main differences between the analysis of the performance of the process and the performance of the membrane as well as the variables and parameters that are involved. The coupling effects that may appear due to the interaction among components and the membrane have been also evaluated. As a final summary, the following procedure is recommended to carry out a complete evaluation of pervaporation:

- (1) Evaluation of the driving force of the system and determination of target compounds for permeation so that the initial concept of applying pervaporation makes sense. Those compounds with the largest driving force should be targeted to permeate through the membrane. Driving force calculations and interpretation shown in Section 3.4 could be taken as reference to perform this evaluation.
- (2) Experimental evaluation of permeances (or permeabilities) and selectivities of the membranes for the pure components and the mixtures of study (i.e., evaluation of the membrane performance). The comparison among results for pure components and mixtures allows identifying coupling effects, which is important to understand the mass transfer through the membrane and the interactions that are taking place. The best situation is that the membrane would enhance the permeation of the target compounds selected in the previous point. Membrane development plays thus a key role in pervaporation.
- (3) Experimental evaluation of transmembrane fluxes and separation factors (i.e., evaluation of the process performance). This step is required to finally determine the total membrane area and the technical (and economic) viability of applying pervaporation.
- (4) Elaboration of McCabe-Thiele diagrams and comparison with distillation. As indicated in Section 3.5, McCabe-Thiele diagrams are useful to visualize easily the differences of applying pervaporation or distillation.

REFERENCES

- Araki, S., Gondo, D., Imasaka, S., Yamamoto, H., 2016. Permeation properties of organic compounds from aqueous solutions through hydrophobic silica membranes with different functional groups by pervaporation. *J. Membr. Sci.* 514, 458–466.
- Baker, R.W., Wijmans, J.G., Huang, Y., 2010. Permeability, permeance and selectivity: a preferred way of reporting pervaporation performance data. *J. Membr. Sci.* 348, 346–352.
- Berendsen, W.R., Radmer, P., Reuss, M., 2006. Pervaporative separation of ethanol from an alcohol—ester quaternary mixture. *J. Membr. Sci.* 280, 684–692.
- Bettens, B., Dekeyser, S., Van der Bruggen, B., Degève, J., Vandecasteele, C., 2005. Transport of pure components in Pervaporation through a microporous silica membrane. *J. Phys. Chem. B* 109, 5216–5222.
- Brun, J.P., Larchet, C., Melet, R., Bulvestre, G., 1985. Modeling of the pervaporation of binary mixtures through moderate swelling, non-reacting membranes. *J. Membr. Sci.* 23, 257.
- Cao, S., Shi, Y., Chen, G., 2000. Influence of acetylation degree of cellulose acetate on pervaporation properties for MeOH/MTBE mixture. *J. Membr. Sci.* 165, 89–97.
- Chapman, P.D., Oliveira, T., Livingston, A.G., Li, K., 2008. Membranes for the dehydration of solvents by pervaporation. *J. Membr. Sci.* 318, 5–37.
- Dondos, A., Rempp, P., Benoit, H., 1970. Effet des propriétés thermodynamiques des mélanges de solvants sur les dimensions de chaînes macromoléculaires. *J. Polym. Sci. C* 30, 9.
- Feng, X., Huang, R.Y.M., 1996. Estimation of activation energy for permeation in pervaporation processes. *J. Membr. Sci.* 118, 127–131.
- Flory, P.J., 1953. *Principles of Polymer Chemistry*. Cornell Univ. Press, Ithaca.
- George, S.C., Thomas, S., 2001. Transport phenomena through polymeric systems. *Progr. Polym. Sci.* 26, 985–1017.
- Hansen, C.M., 1967. *The Three Dimensional Solubility Parameter and Solvent Diffusion Coefficient*. Danish Technical Press, Copenhagen.
- Kashemekat J., Wiljmans J.G., Baker R.W. Removal of organic solvent containments from industrial effluent streams by Pervaporation, Ed. By R. Bakish, Proc. 4th Int. Conf. On Pervaporation, Process in Chemical Industry, Bakish Materials Corporation, Englewood, NJ, 321, 1981.
- Kober, P.A., 1917. Pervaporation, perstillation and percrystallization. *J. Am. Chem. Soc.* 39, 944–948.
- Kujawa, J., Cerneaux, S., Kujawski, W., 2015. Removal of hazardous volatile organic compounds from water by vacuum pervaporation with hydrophobic ceramic membranes. *J. Membr. Sci.* 474, 11–19.
- Kujawski, W., 2000. Application of Pervaporation and vapor permeation in environmental protection. *Pol. J. Environ. Stud.* 9 (1), 13–26.
- Lipnizki, F., Trägårdh, G., 2001. Modelling of pervaporation: Models to analyze and predict the mass transport in pervaporation. *Sep. Purif. Method* 30, 49–125.
- Lipski, C., Côté, P., 1990. The use of Pervaporation for the removal of organic contaminants from water. *Environ. Prog.* 9, 254–261.
- Lonsdale, H.K., Merten, U., Riley, R.L., 1965. Transport properties of cellulose acetate osmotic membranes. *J. Appl. Polym. Sci.* 9, 1341.
- Luis, P., Degève, J., Van der Bruggen, B., 2013. Separation of methanol-n-butyl acetate mixtures by pervaporation: potential of 10 commercial membranes. *J. Membr. Sci.* 429, 1–12.

- Luis, P., Van der Bruggen, B., 2015a. Pervaporation modeling: state of the art and future trends. In: Basile, A., Figoli, A., Khayet, M. (Eds.), *Pervaporation, Vapour Permeation and Membrane Distillation. Principles and Applications. A Volume in Woodhead Publishing Series in Energy*. ISBN 978-1-78242-246-4, pp. 87–106.
- Luis, P., Van der Bruggen, B., 2015b. The driving force as key element to evaluate the pervaporation performance of multicomponent mixtures. *Sep. Purif. Technol.* 148, 94–102.
- Merten, U., 1966. Transport properties of osmotic membranes. In: Merten, U. (Ed.), *Desalination by Reverse Osmosis*. The M.I.T. Press, Cambridge, MA, p. 15.
- Mulder, M.H.V., Smolders, C.A., 1984. On the mechanism of separation of ethanol/water mixtures by pervaporation I. Calculations of concentration profiles. *J. Membr. Sci.* 17, 289–307.
- Okada, T., Matsuura, T., 1991. A new transport model for pervaporation. *J. Membr. Sci.* 59, 133–149.
- Ravindra, R., Sridhar, S., Khan, A.A., Rao, A.K., 2000. Pervaporation of water, hydrazine and monomethylhydrazine using ethylcellulose membranes. *Polymer* 41, 2795–2806.
- Ray, S.K., Sawant, S.B., Joshi, J.B., Pangarkar, V.G., 1997. Development of new synthetic membranes for separation of benzene–cyclohexane mixtures by pervaporation: A solubility parameter approach. *Ind. Eng. Chem. Res.* 36, 5265–5276.
- Ray, S.K., Sawant, S.B., Joshi, J.B., Pangarkar, V.G., 1999. Methanol selective membranes for separation of methanol–ethylene glycol mixtures by pervaporation. *J. Membr. Sci.* 154, 1–13.
- Seader, J.D., Henley, E.J., Roper, D.K., 2013. *Separation Process Principles*, third ed. Wiley, Hoboken, NJ. (978-0-470-48183-7).
- Semenova, S.I., Ohya, H., Soontarapa, K., 1997. Hydrophilic membranes for pervaporation: an analytical review. *Desalination* 110, 251.
- Shao, P., Huang, R.Y.M., 2007. Polymeric membrane pervaporation. *J. Membr. Sci.* 287, 162–179.
- Sridhar, S., Ravindra, R., Khan, A.A., 2000. Recovery of Monomethylhydrazine liquid propellant by pervaporation technique. *Ind. Eng. Chem. Res.* 39, 2485–2490.
- Tang, J., Sirkar, K.K., Majumdar, S., 2013. Permeation and sorption of organic solvents and separation of their mixtures through an amorphous perfluoropolymer membrane in pervaporation. *J. Membr. Sci.* 447, 345–354.
- Villegas, M., Castro Vidaurre, E.F., Gottifredi, J.C., 2015. Sorption and pervaporation of methanol/water mixtures with poly(3-hydroxybutyrate) membranes. *Chem. Eng. Res. Des.* 94, 254–265.
- Vrentas, J.S., Duda, J.L., 1977a. Diffusion in polymer-solvent systems, I. Reexamination of the free-volume theory. *J. Polym. Sci.* 15, 403.
- Vrentas, J.S., Duda, J.L., 1977b. Diffusion in polymer-solvent systems, II. A predictive theory for the dependence of diffusion coefficients on temperature, concentration, and molecular weight. *J. Polym. Sci.* 15, 417–439.
- Vrentas, J.S., Duda, J.L., Huang, W.J., 1986. Regions of Fickian diffuse ion in polymer-solvent systems. *Macromolecules* 19, 1718.
- Wijmans, J.G., Baker, R.W., 1995. The solution-diffusion model: a review. *J. Membr. Sci.* 107, 1–21.

Gas permeation and supported liquid membranes

Patricia Luis

*Materials & Process Engineering (iMMC-IMAP), Catholic University of Louvain,
Louvain-la-Neuve, Belgium*

CHAPTER OUTLINE

4.1 Process Description	103
4.2 General Overview of Applications	109
4.2.1 Gas Permeation	109
4.2.2 Supported Liquid Membranes	111
4.3 Mass Transfer in Gas Permeation	114
4.3.1 Mass Transfer Through Porous Membranes	114
4.3.2 Mass Transfer Through Dense Membranes	116
4.4 Mass Transfer in SLMs	118
4.4.1 Gas Feed/Gas Permeate	120
4.4.2 Liquid Feed/Gas Permeate (Pervaporation)	121
4.4.3 Liquid Feed/Liquid Permeate (Liquid Pertraction)	121
4.5 Interpretation of Results	122
4.5.1 Gas Separation	123
4.5.2 Selective Separation of Liquids by Pervaporation Using SLMs	129
4.5.3 Selective Separation of Liquids by Liquid Pertraction Using SLMs	135
4.6 Concluding Remarks	145
References	146

4.1 PROCESS DESCRIPTION

The application of gas permeation membranes and supported liquid membranes has increased significantly due to the continuous development of more selective and permeable membranes. *Gas permeation* involves a thin membrane where the feed gas, at high pressure P_F contains some low-molecular-weight species ($MW < 50$) to be separated from higher-molecular-weight species (Seader et al., 2013). The other side of the membrane (permeate side) is kept at lower pressure P_P to provide the adequate

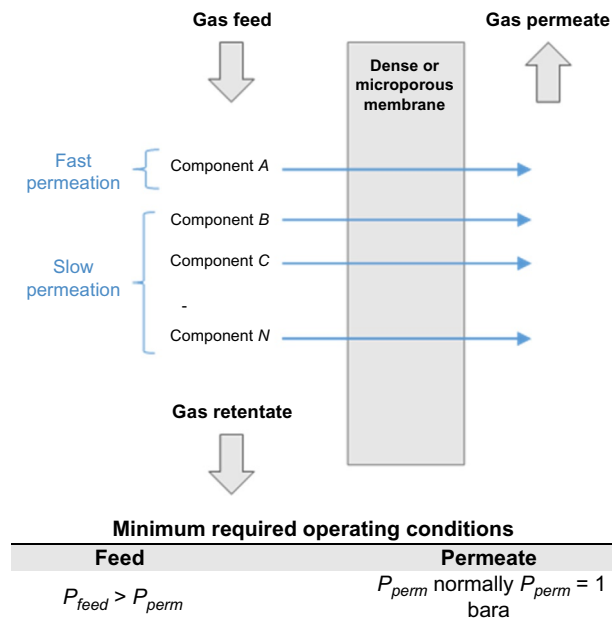


FIG. 4.1

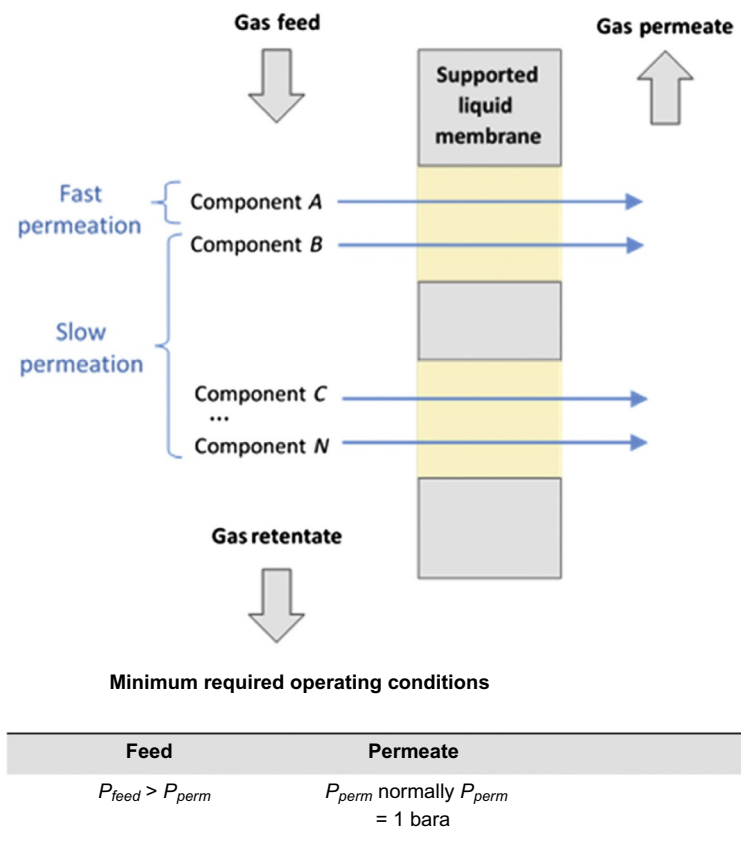
Gas permeation of a multicomponent mixture with N components. P_{feed} , feed pressure; P_{perm} , permeate pressure.

driving force. The membrane is commonly a dense membrane but microporous membranes may be found for this application. Fig. 4.1 shows the schema of mass transfer in gas permeation. A dense membrane involves the sorption of the species on the membrane surface, permeation through the membrane and finally, desorption at the permeate side. The mass transfer can be thus described in terms of the solution-diffusion model, and the degree of separation will depend on both phenomena, adsorption and diffusion. On the other hand, if the membrane is microporous, a sieving effect will determine which molecules cannot pass through the membrane due to the pore size of the membrane. In this case, the molecular weights of the target compound and the rest of species need to be very different to ensure an acceptable separation.

Supported liquid membranes (SLM) refer to porous membranes that contain a liquid inside the pores and it is kept there by capillary forces. They were investigated for the first time by Li (1969). The number of applications of this kind of membranes has grown significantly in the last years, related to three kinds of configurations: gas feed/gas permeate (e.g., applied in gas separation), liquid feed/liquid permeate (e.g., applied in liquid pertraction), and liquid feed/gas permeate (e.g., applied in pervaporation). When both sides of the membranes are a gas phase, the principle of functioning is very similar to that of gas permeation indicated previously. The feed stream

is a gas phase containing the target component to be separated by permeation through the membrane to the permeate side. Fig. 4.2A represents the schema of the separation. A difference of pressures in both sides of the membrane is required and a selective liquid for the target compound is used as the filler of the membrane pores. It is very common to find applications in which the permeate side is kept under vacuum to enhance the mass transfer by a large driving force. However, a nonvolatile liquid is required inside the membrane pores to avoid losses and instability of the membrane over time.

The application of SLMs for the extraction of a component from a liquid stream can be carried out by using another liquid phase at the permeate side, which can be



(A)

FIG. 4.2

Schema of a supported liquid membrane: (A) Separation of a multicomponent gas mixture with N components. P_{feed} , feed pressure; P_{perm} , permeate pressure;

(Continued)

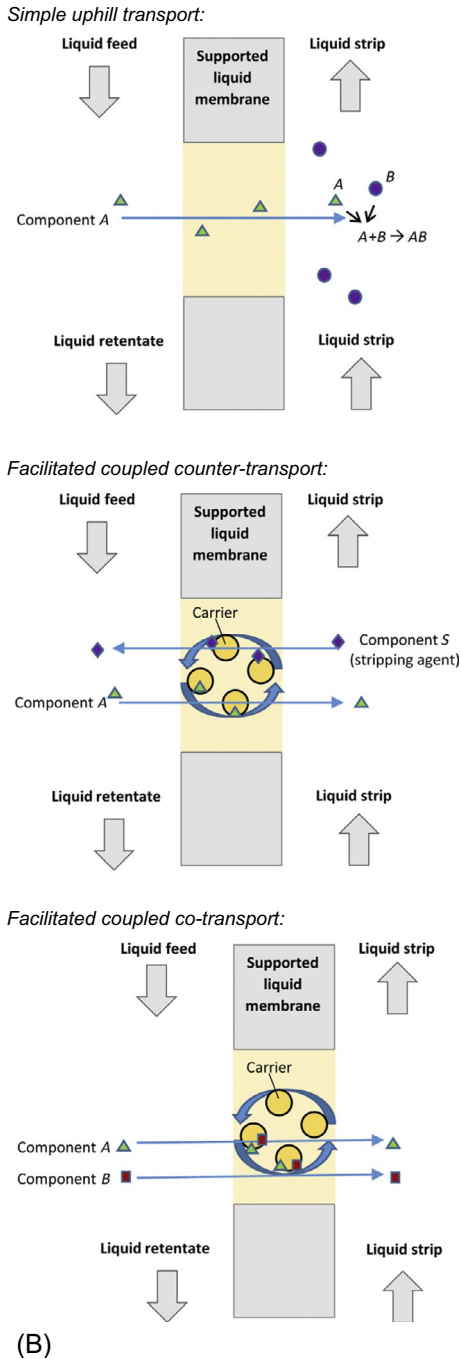
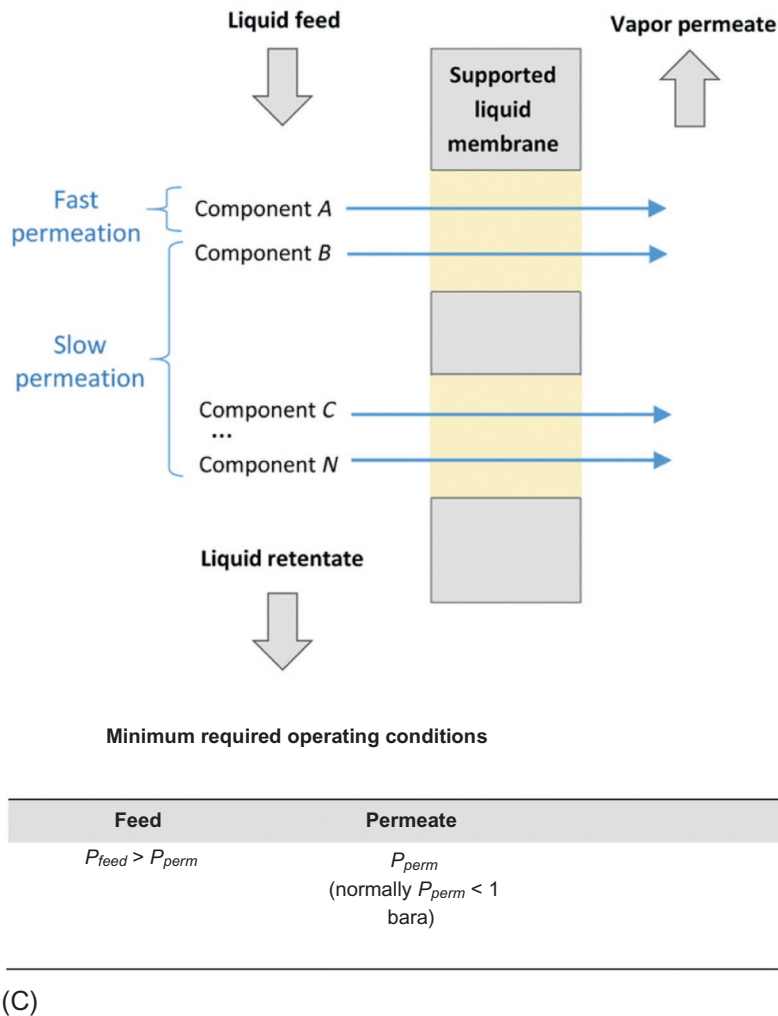


FIG. 4.2, CONT'D

(B) separation of a multicomponent liquid mixture with N components using a reextraction agent (liquid pertraction); and

(Continued)

**FIG. 4.2, CONT'D**

(C) separation of a multicomponent liquid mixture with N components using a gas or vacuum phase (pervaporation).

(B) Based on Kocherginsky, N.M., Yang, Q., Seelam, L., 2007. *Recent advances in supported liquid membrane technology. Sep. Purif. Technol.* 53, 171–177.

either aqueous or organic. A typical liquid membrane consists of a thin layer of organic phase immobilized onto a microporous support between two aqueous phases of different compositions (the feed and the stripping phases) (Parhi, 2013). The feed and stripping phases are miscible and are separated by the immiscible liquid within the membrane. The specified component(s) are extracted from the feed due to the favorable thermodynamic conditions set around the interface feed membrane, and

simultaneously stripped by the stripping phase because of the new equilibrium conditions at the interface membrane-stripping phase (Boyadzhiev, 1990). This technology is commonly known as liquid pertraction, from the latin “*per-traho*” and first introduced by Schlosser and Kossaczky (1975). Several systems can be developed. For example, if the liquid inside the membrane pores is an organic liquid immiscible with the aqueous feed and strip streams, SLM can be used to separate the two aqueous phases. It may also contain an extractant, a diluent which is generally an inert organic solvent to adjust viscosity and sometimes also a modifier to avoid so-called third phase formation (Kocherginsky et al., 2007). The opposite situation can be also considered in which an aqueous solution is inside the membrane and two organic phases conform the feed and the permeate sides. In principle, no transmembrane pressure or voltage is required but sometimes some overpressure is applied to ensure the stability of the membrane. The driving force is based on the difference of concentrations between the feed stream and the permeate. Three possible transfer mechanisms that control the removal and concentration of the transferred component may take place. The first case is known as “*simple uphill transport*” since the component A is pumped against the apparent concentration gradient because of the irreversible chemical reaction $A+B \rightarrow AB$ taking place in the stripping solution. The product AB or the ions existing after its dissociation are insoluble in the membrane liquid and for this reason, there is no backtransport of A across the membrane but there is an accumulation in the stripping phase (Boyadzhiev, 1990). A common application of this process is the extraction of weak acids or bases (e.g., phenols, amines, or antibiotics) from dilute solutions. A second kind of transport is used typically for the removal of ions from the feed solution. Since electrical neutrality has to be preserved in the entire process, the charged species A in the feed solution are extracted by the carrier and moves across the membrane as a complex and finally exchange A with the charged species C, which has the same charge as A and are transported by the carrier to the feed solution. This process is called “*facilitated coupled counter-transport*.” In other cases, the carrier (e.g., amines) is able to carry the positively charged species together with the negatively charged species from the feed solution to the permeate side (strip solution). This process is called “*facilitated coupled cotransport*” (Kocherginsky et al., 2007) and it is of interest for the removal of various metals like copper or zinc from diluted neutral or slightly acidic solutions by using suitable chelating agents as carriers (the metal ions are replaced in the feed by hydrogen ions from the stripping mineral acid) (Boyadzhiev, 1990). Fig. 4.2B shows the schema of mass transfer in those three scenarios.

Finally, SLMs are also used in systems like pervaporation, in which the components of a liquid solution have to be selectively separated by imposing a driving force based on the differences of partial pressure across the membrane and a gaseous phase or vacuum is found at the permeate side. The process description has been exposed in detail in Chapter 3. Fig. 4.2C presents the schema of the mass transfer in pervaporation using SLMs.

The main advantages of using SLMs are the relatively small volume of liquid that is required inside the pores of the membrane, the tunable character of the membrane by selecting the most appropriate filling liquid, the mass transfer is not governed by

the equilibrium and, in the case of liquid extraction, the possibility of having the extraction and reextraction steps in the same device. On the other hand, the main disadvantage observed when using SLMs is the problem of low stability of the liquid phase within the pores. The major mechanisms attributed to the displacement of the liquid membrane are a progressive wetting of the membrane pores by the aqueous phase, the pressure difference across the membrane, dissolution of the liquid membrane in the aqueous phase, the formation of an emulsion in the liquid membrane, and the blockage of membrane pores by precipitation of the carrier complex (Ong et al., 2014). This lack of stability has justified the rapid introduction of ionic liquids as the filling liquid due to their negligible vapor pressure and tuning properties that can adapt to the separation requirements (selectivity, viscosity, compatibility, etc.). Ionic liquids are salts with a melting point lower than 100°C. They show a very low vapor pressure, reducing the costs and environmental risks of air pollution, and they are thermally robust with liquid ranges of, for example, 300°C, compared to 100°C for water. Regarding their ecotoxicity to aquatic environments, special care should be taken when selecting the ionic liquid since their toxicity varies very largely depending on the kind of cation, anion, and the length of the carbon chains (Luis et al., 2007). When ionic liquids are used to impregnate the pores of a membrane, we refer to these SLMs as supported ionic liquid membranes (SILMs). Stability studies on SILMs have demonstrated high operational and structural stability in liquid/liquid and gas/gas separations, even at relatively high-temperature/high-pressure conditions (up to 300°C and 10 bar), which makes possible their industrial application (Lozano et al., 2011). Other options to increase the stability of SLMs are the use of two porous supports that separate the organic and aqueous phases; formation of barrier layers on a membrane surfaces, either by physical deposition or by interfacial polymerization; stabilization of the SLM by plasma polymerization surface coating; formation of polymer inclusion membranes by casting a viscous mixture solution composed of a liquid membrane, a plasticizer, and a base polymer; or gelation of the liquid membrane (Yang et al., 2000; Kocherginsky et al., 2007; Ong et al., 2014).

The application of gas permeation membranes or supported liquid membranes is thus directly connected with the development of novel materials, additives, and so on, in order to improve the separation and minimize the required membrane area. The next section will provide an introduction to the state of the art of applications of both systems in order to show the main research areas that are under study. The following sections will be focused on the mathematical description of these systems and the interpretation of results.

4.2 GENERAL OVERVIEW OF APPLICATIONS

4.2.1 GAS PERMEATION

Gas permeation presents several advantages, such as low capital investment, ease of installation and operation, absence of rotating parts, high process flexibility, low weight and space requirements, and low environmental impact, which make it a very

competitive technology with absorption, pressure swing adsorption, and cryogenic distillation in the separation of components in gas phase (Seader et al., 2013). The first application of gas permeation was oriented to the separation of air, reaching purities limited economically to a retentate of 95%–99.9% N₂ and a permeate of 30%–45% O₂. Other applications increased dramatically, such as the separation of hydrogen from methane, adjustment of H₂-to-CO ratio in synthesis gas, CO₂ removal, drying of natural gas and air, removal of helium, and removal of organic solvents from air. Separation of CO₂ from a gas stream has received special attention due to the environmental implications regarding climate change. As membrane configuration, spiral-wound and hollow fiber modules are the selected choice for polymeric membranes due to their high packing density. Inorganic membranes are limited to a tubular or capillary configuration due to the restrictions during the manufacture.

Typical membrane materials used in gas permeation are cellulose acetates and polysulfones, polyimides, polyamides, polycarbonates, polyetherimides, sulfonated polysulfones, Teflon, polystyrene, and silicone rubber for low temperatures (commonly <70°C). For high temperature, polymeric membranes may be critically damaged and membranes made of glass, carbon, or inorganic oxides should be used (Seader et al., 2013). Ionic liquids have also reached a large interest. The application of ionic liquids in gas separation has been mainly developed in three areas: (i) supported ionic liquid membranes (SILMs), (ii) polymerized ionic liquids, and (iii) polymer-IL blends and mixed-matrix membranes (Karaszova et al., 2014). The application of SILMs for gas separation is described in Section 4.2.2. Polymerized ionic liquid membranes were first synthesized by Bara et al. (2007) using styrene and acrylate polymerizable groups connected to imidazolium-based ionic liquids ([C_nmim][Tf₂N] with $n = 1, 4$ or 6). The mechanical stability of the membrane was improved by adding a cross-linking agent. The idea is that ionic liquids with appropriate structure can polymerize via the cation and/or anion, forming solid films, combining the unique properties of ionic liquids with the flexibility and properties of macromolecular architectures (Martínez-Palou et al., 2014). Thus novel structures with new properties can be developed. This kind of membranes has been deeply investigated in order to achieve competitive permeabilities and selectivities. One of the applications of polymerized ionic liquids is CO₂ separation from other gases (Martínez-Palou et al., 2014). Several ionic liquids have been polymerized but in general, the permeabilities are much lower than those obtained with SILMs (Bara et al., 2008a, b; Simons et al., 2010; Carlisle et al., 2010; Bara et al., 2008a, b; Li et al., 2012). For this reason, the formation of gelled structured liquid membranes (a gelator is added to the ionic liquid to form a stable gel) (Voss et al., 2009; LaFrates et al., 2010) is considered as a good approach to achieve the performance of classical SILMs with a good mechanical stability.

Polymer-IL blends and mixed-matrix membranes are formed when the ionic liquid is incorporated into a polymeric matrix. The ionic liquid content affects the permeability and the selectivity for various gases and vapors, showing a large affinity

to CO₂, which presented relevance for CO₂/H₂ separation (Friess et al., 2012). Gas transport properties of polymer-IL membranes were poorer than SILMs but still their potential is not fully explored. The large number of combinations of polymers-IL makes this field of research a challenge as well as an opportunity to find the best membrane for a specific separation.

4.2.2 SUPPORTED LIQUID MEMBRANES

Several applications of SLMs have been developed in the last years; they can be grouped into four main groups: (i) gas separation, (ii) separation of organic compounds, (iii) separation of ions, and (iv) pervaporation and vapor permeation.

Gas separation

The application of supported ionic liquid membranes (SILMs) in gas separation has been extensively studied in order to increase the selectivity while keeping high permeability in comparison with polymeric membranes, as well as promoting a longer stability than classical SLMs. CO₂ capture from flue gases is a main domain of research due to the current necessity of finding solutions to global warming. However, the high temperature and low partial pressure of CO₂ in flue gases makes its separation a real challenge. A review of several papers describing different applications of SILMs for CO₂ separation from other gases can be found in the literature (Martínez-Palou et al., 2014). The treatment of bio-methane from anaerobic digesters has also a growing interest (Park et al., 2009; Scovazzo et al., 2009). In addition, the presence of water vapor in the gas stream increases the gas permeability through the SILM but it may decrease the selectivity of the target compound. This effect has been observed by Neves et al. (2010a) when studied the separation of CO₂/N₂ and CO₂/CH₄ mixtures using imidazolium-based ionic liquids and it was endorsed to the formation of water clusters inside the membrane, mainly in the less hydrophobic ionic liquids. Nevertheless, the large potential of SILM for gas separation has been demonstrated by comparison with the performance of gas permeation membranes (Scovazzo et al., 2004; Scovazzo, 2009). The tunable character of ionic liquids makes them also a good membrane filler to prepare objective-oriented membranes, that is, membranes designed to separate a specific target compound. Two critical properties of the ionic liquid can have a significant influence on the SILM performance: molar volume and viscosity. According to Scovazzo (2009), the CO₂ selectivity is a function of the molar volume of the ionic liquid, while the CO₂ permeability depends mainly on the viscosity. SILMs are a promising alternative technology for separating mixtures of gases of great interest to the oil industry such as the separation of H₂S/CH₄, CO₂/CH₄, CH₄/H₂O, CO₂/N₂, CO₂/H₂, CO₂/CH₄, H₂/N₂, H₂/CH₄, CH₄/N₂, propane/propene, and mercaptans/hydrocarbons (Martínez-Palou et al., 2014).

Separation of organic compounds

Application of SLMs for the separation of organic compounds has been also a focus of attention as an alternative technology to conventional liquid/liquid extraction. Waste water treatment may involve the removal of phenols and ammonia due to the current environmental constraints (Parhi, 2013). Also, SLMs are applied for the selective separation of reagents and products of transesterification reactions, for example, those reactions oriented to the production of organic esters of interest in the perfumery and flavor industries (Lozano et al., 2011). The development of novel SLMs has also brought researchers to investigate in depth the use of ionic liquids as the filler liquid inside the membrane (SILMs) and relevant conclusions on the effect of the ionic liquid structure on the selectivity of the separation have been obtained. In general, membrane selectivity depends mainly on the kind of anion of the ionic liquid. In addition, a decrease in the chain length of the alkyl substituents of imidazolium-based ionic liquids led to an increase in the selectivity (Lozano et al., 2011).

Separation of ions

The application of supported liquid membranes for the extraction of species such as metals from an aqueous feed solution involves the selection of an organic phase as extractant that gives high selectivity to the separation. Separation and concentration of metal ions is a key point in the hydrometallurgical industry and here, the use of SLMs involves great advantages (e.g., modular systems, easy operation, low cost) in comparison with other extraction methods. Some examples are the recovery of copper, zinc, nickel, chromium (VI), mercury, cadmium, and uranium (Dehaan et al., 1989; Chiarizia et al., 1990; Breembroek et al., 1998; Parhi, 2013).

Transport of smaller ions such as sodium (Na^+) and chloride (Cl^-) using imidazolium-based ionic liquids has also been studied (Fortunato et al., 2004). The mass transport of these ions through the membrane was found to be mainly by transport through water microenvironments inside the membrane. Thus the presence of water inside the ionic liquid has a very significant effect on the mass transport of ions.

Pervaporation and vapor permeation

Over the past decade, most pervaporation processes have involved the use of solid membranes (polymeric, ceramic, or composed of both polymeric and inorganic membranes). Recently, the use of liquid membranes has taken a remarkable interest since the diffusion of components through a liquid is few orders of magnitude higher than that through a solid. SLMs acquire thus an interesting application in pervaporation processes. Common organic solvents used as the liquid membrane are hydrophobic ethers and esters, hydrocarbons, and long chain alcohols, and more recently, ionic liquids (Ong et al., 2014). Thus pervaporation using SLMs and SILMs has been suggested for several applications (Schäefer et al., 2001; Branco et al., 2002a, b; Izák et al., 2005, 2006a, b, 2008, 2009a, b; Plaza et al., 2013). Generally, S(I)LMs have been used in pervaporation for the separation of mixtures composed of

(Ong et al., 2014) butanol/water, ethanol/water, diacetyl/water, trichloroethylene/water, acetic acid/water, 1,3-propanediol/water, butanol/acetone/water, and acetone/butanol/ethanol/water. The effect of some operating conditions has been evaluated (Martínez-Palou et al., 2014). In general, it could be said that a low downstream pressure increases the driving force in the system, leading to an increase in the transmembrane flux, but also, it could result in the loss of immobilized liquid membrane from the support. Thus the pressure difference across the SLM should not exceed the minimum transmembrane pressure, P_c , which is defined as the minimum pressure required to push the immobilized liquid membrane out of the largest pores. This pressure is calculated based on the Laplace-Young equation:

$$P_c = \frac{2\gamma \cos\theta}{r} \quad (4.1)$$

where γ is the interfacial tension between the feed solution and the SLM, θ is the contact angle between the membrane pores and the immobilized liquid membrane, and r is the pore radius.

Regarding the temperature, it is common that higher temperature leads to a larger transmembrane flux due to the increased driving force for the pervaporation process (due to the increased difference between the equilibrium partial pressure on the feed side and the partial pressure on the permeate side). In addition, higher feed temperatures reduce the viscosity of the liquid membrane and the resistance to mass transport in the SLM, promoting greater diffusivity of the targeted component to pass through the SLM. The thermal stability of the porous support and the liquid membrane may be negatively affected, though. Thus degradation or loss of the liquid membrane could also occur and the appropriate operation conditions should be selected. The application of SILMs for industrial pervaporation is not a reality yet. Several issues have to be solved, such as the low separation flux, even though it may be enhanced by the presence of the ionic liquid, and poor separation properties (Karaszova et al., 2014).

Other applications

Analytical or electrochemical applications have been also reported to some extent in the literature (Lozano et al., 2011). For example, the trace determination of toxic compounds involves a preconcentration step prior to the analysis due to the low concentration of the toxic in the sample. Liquid/liquid extraction or solid-phase extraction is commonly used to perform this enrichment step. However, aiming at minimizing the amount of solvent required, other preconcentration techniques have been developed recently. Among them, two techniques can take advantage of the use of supported (ionic) liquid membranes: liquid-phase microextraction and solid-phase microextraction. The former has been used combined with high performance liquid chromatography (HPLC) for the determination of chlorophenols and sulfonamides in environmental water samples (Peng et al., 2007; Tao et al., 2009); and the later for the determination of polycyclic aromatic hydrocarbons (PAHs) in water by combination

with gas chromatography-mass spectrometry (GC-MS) (Hsieh et al., 2006). Electrochemical applications are justified by the similar electrical resistance values of SILMs in comparison with those of Nafion membranes (Lozano et al., 2011). Using ionic liquids allow developing tailor-made proton conducting membranes for fuel cell applications (Fortunato et al., 2006) or other applications in which stability at high temperature (100–200°C) is required (Neves et al., 2010b).

4.3 MASS TRANSFER IN GAS PERMEATION

Gas permeation normally involves the use of polymeric membranes (dense membranes). However, due to the limitation of polymer under harsh conditions, such as high temperatures, the use of inorganic materials (porous membranes) has been also developed. Thus the mass transfer in porous and dense membranes is presented. Fig. 4.3 shows schematically the concentration profiles present in both kinds of membranes.

4.3.1 MASS TRANSFER THROUGH POROUS MEMBRANES

The rate of diffusion of a component i through a membrane can be described in terms of Fick's law. In gas permeation, both sides of the membrane are gas phase. Fig. 4.3A shows the concentration profile of the target component. Thus assuming ideal gas behavior and equal pressure and temperature on either side of the membrane the rate of diffusion expressed in terms of partial pressure driving force is:

$$J_i = \frac{D_{e_i} c_M}{Pl_M} (p_{i0} - p_{iL}) = \frac{D_{e_i}}{RTl_M} (p_{i0} - p_{iL}) \quad (4.2)$$

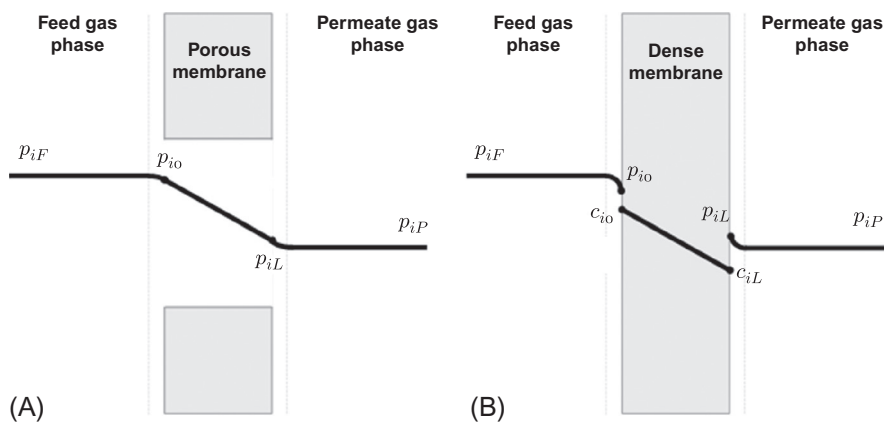


FIG. 4.3

Concentration profile of a component i in gas separation applications through: (A) a porous membrane; (B) a dense membrane.

where c_M is the total gas mixture concentration given as P/RT by the ideal-gas law. The permeance, $\left(\frac{P_i}{l_M}\right)$, of a species is defined as the flow rate of that species per unit cross-sectional area of membrane per unit driving force, being analogous to a mass transfer coefficient. Thus it can be calculated as

$$\left(\frac{P_i}{l_M}\right) = \frac{J_i}{(p_{i0} - p_{iL})} = \frac{D_{e_i}}{RT} \quad (4.3)$$

The permeance $\left(\frac{P_i}{l_M}\right)$ is the ratio of the permeability, P_i , to the membrane thickness, l_M .

The kind of diffusion that takes place through the membrane is ordinary diffusion and/or in series with Knudsen diffusion. Fig. 4.4 shows the main mechanisms for transport through a membrane. Fig. 4.4A refers to convective, bulk flow, existing by a difference of pressure, in which the pore diameter is large compared to the molecular diameter of species. Thus no selective separation occurs and it is not relevant for the typical membranes used for gas permeation. When the pressure is the same at both sides of the membrane so that there is not bulk flow but there exists a difference of fugacity, activity, chemical potential, concentration, or partial pressure, permselective diffusion of species through the membrane pores takes place according to the schema in Fig. 4.4B. If the pores are small enough so that they have a similar size than some of the species in the feed mixture, the separation will be enhanced due to a restricted diffusion, causing size exclusion or sieving of larger molecules (Fig. 4.4C). Concretely, for gas diffusion in which the pore size and/or pressure (typically a vacuum) is such that the mean free path of the molecules is greater than the pore diameter, the so-called Knudsen diffusion is considered and it is dependent on molecular weight (Seader et al., 2013). Thus considering that

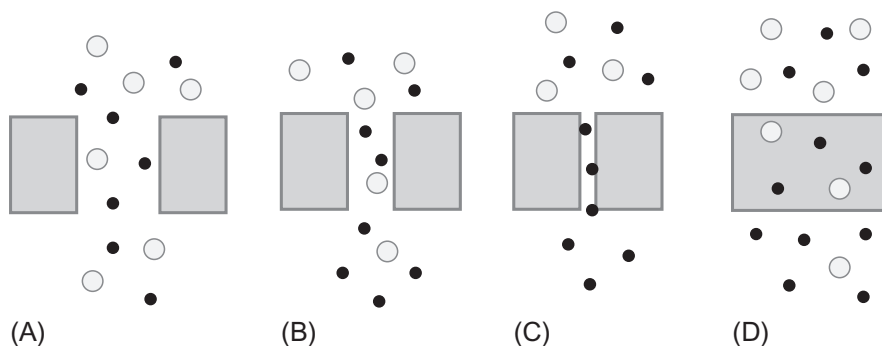


FIG. 4.4

Mechanisms of transport in membranes (Seader et al., 2013): (A) bulk flow through pores, (B) diffusion through pores, (C) restricted diffusion through pores, and (D) solution-diffusion through dense membrane.

ordinary diffusion and/or Knudsen diffusion take place and assuming absence of bulk and restrictive diffusion, the diffusion coefficient can be calculated as:

$$D_{e_i} = \frac{\epsilon}{\tau} \left[\frac{1}{(1/D_i) + (1/D_{K_i})} \right] \quad (4.4)$$

where D_i is the molecular diffusivity, and D_{K_i} is the Knudsen diffusivity, which from the kinetic theory of gases as applied to a straight, cylindrical pore of diameter d_p is

$$D_{K_i} = \frac{d_p \bar{v}_i}{3} \quad (4.5)$$

where \bar{v}_i is the average molecule velocity given by

$$\bar{v}_i = (8RT/\pi M_i)^{1/2} \quad (4.6)$$

where M is molecular weight. Combining Eqs. (4.5), (4.6):

$$D_{K_i} = 4850 d_p (T/M_i)^{1/2} \quad (4.7)$$

where D_K is cm^2/s , d_p is cm , and T is K .

Eq. (4.3) can be thus rewritten as follows to calculate the permeance $\left(\frac{P_i}{l_M}\right)$ of each species:

$$\left(\frac{P_i}{l_M}\right) = \frac{\epsilon}{RT\tau l_M} \left[\frac{1}{(1/D_i) + (1/D_{K_i})} \right] \quad (4.8)$$

When Knudsen flow predominates, as it often does for micropores, a selectivity based on the permeability ratio for species A and B is simply given by the ratio of the molecular weights of the species (Seader et al., 2013)

$$\frac{P_{M_A}}{P_{M_B}} = \left(\frac{M_B}{M_A}\right)^{1/2} \quad (4.9)$$

4.3.2 MASS TRANSFER THROUGH DENSE MEMBRANES

Gas permeation in dense membranes presents a mechanism of transport that can be described by the solution-diffusion model, which is a combination of the following three fundamental steps: (i) sorption of the targeted component from the feed gas to the membrane, (ii) diffusion of the targeted component within the membrane, and (iii) desorption of the targeted component to the gas phase at the permeate side of the membrane. Fig. 4.3B shows the concentration profile of the target component in a dense membrane, and Fig. 4.4D shows the mechanism of mass transfer through the membrane. The mass transfer can be described by applying Fick's first law of diffusion under conditions of steady state, that is, when the concentration does not vary with time (George and Thomas, 2001; Luis and Van der Bruggen, 2013):

$$J_i = -D_i \left(\frac{\partial c_i}{\partial x} \right) \quad (4.10)$$

where D_i is the diffusivity of the solute in the membrane. The integration of this equation gives:

$$J_i = \frac{D_i}{l_M} (c_{i_0} - c_{i_L}) \quad (4.11)$$

where l is the membrane thickness and c_{i_0} and c_{i_L} are the concentration of component i on the feed and permeate interfaces with the membrane. In addition, assuming thermodynamic equilibrium at the fluid-membrane interfaces, the concentrations can be related to partial pressures adjacent to the membrane faces by Henry's law as (Seader et al., 2013)

$$H_{i_0} = \frac{c_{i_0}}{p_{i_0}} \quad (4.12)$$

$$H_{i_L} = \frac{c_{i_L}}{p_{i_L}} \quad (4.13)$$

with H_i as the solubility coefficient. Normally, it is possible to assume that H_i is independent of the total pressure and that the temperature at both sides of the membranes is similar. Thus the simplification that $H_{i_0} = H_{i_L} = H_i$ is possible (Seader et al., 2013), and Eq. (4.11) can be written as

$$J_i = \frac{D_i H_i}{l_M} (p_{i_0} - p_{i_L}) \quad (4.14)$$

In addition, in gas separation, the external mass transfer resistances or concentration polarization effects are generally negligible ($p_{i_f} = p_{i_0}$ and $p_{i_L} = p_{i_p}$). The rate of membrane transport can thus be calculated as a function of the partial pressure driving force as follows (Seader et al., 2013):

$$J_i = \frac{H_i D_i}{l_M} (p_{i_f} - p_{i_p}) = \frac{P_{M_i}}{l_M} (p_{i_f} - p_{i_p}) \quad (4.15)$$

The product $P_{M_i} = H_i D_i$ is the *permeability* (with units for instance of $\text{mol m}^{-1} \text{s}^{-1} \text{Pa}^{-1}$) and depends on both the solubility of the gas i within the membrane, H_i , and its diffusivity through the membrane, D_i . The permeability P_{M_i} of a gas component i can be then obtained by dividing the partial flux J_i ($\text{mol m}^{-2} \text{s}^{-1}$) by the driving force using Eq. (4.15). The ratio $\frac{P_{M_i}}{l_M}$ is called *permeance* ($\text{mol m}^{-2} \text{s}^{-1} \text{Pa}^{-1}$) and it is widely used when the membrane thickness is unknown. It is defined as the flux per unit pressure difference between the two sides of the membrane. Other common units for gas permeability and permeance are barrer ($1 \text{ barrer} = 10^{-10} \text{ cm}^3(\text{STP}) \text{ cm cm}^{-2} \text{ s}^{-1} (\text{cmHg})^{-1}$) and GPU ($1 \text{ GPU} = 10^{-6} \text{ cm}^3(\text{STP}) \text{ cm}^{-2} \text{ s}^{-1} (\text{cmHg})^{-1}$), respectively. In general, diffusivity decreases and solubility increases with increasing molecular weight of the gas species (Seader et al., 2013).

The separation factor is commonly used to evaluate the degree of separation in the permeation process. Considering two components, A and B :

$$\beta_{AB} = \frac{y_A/x_A}{y_B/x_B} \quad (4.16)$$

where y_A and y_B are the mole fraction of component A and B , respectively, in the permeate; and x_A and x_B are the mole fraction of component A and B , respectively, in the retentate (feed) side of the membrane.

The selectivity, α_{AB} , is defined as the ratio of permeabilities, P_{M_i} , or permeances, P_{M_i}/l_M , between two species A and B :

$$\alpha_{AB} = \frac{P_{M_A}}{P_{M_B}} = \frac{P_{M_A}/l_M}{P_{M_B}/l_M} \quad (4.17)$$

The relationship between separation factor and selectivity can be found easily by introducing Eq. (4.15) in Eq. (4.17) (Luis and Van der Bruggen, 2013):

$$\alpha = \frac{y_{\text{CO}_2}/(1-y_{\text{CO}_2})}{\left(x_{\text{CO}_2} - \frac{P_{\text{perm}}}{P_{\text{feed}}} y_{\text{CO}_2}\right)} \bigg/ \frac{1}{\left(1-x_{\text{CO}_2} - \frac{P_{\text{perm}}}{P_{\text{feed}}}(1-y_{\text{CO}_2})\right)} \quad (4.18)$$

with p_F and p_P being the total pressure in the feed and permeate, respectively. If a negligible partial pressure of each compound in the permeated side (maximum driving force) is considered due to a very low total pressure in the permeate side or much smaller than the pressure in the feed side, that is, $p_p \approx 0$ or $p_p \ll p_F$, the selectivity becomes:

$$\alpha = \frac{y_{\text{CO}_2}/(1-y_{\text{CO}_2})}{x_{\text{CO}_2}/(1-x_{\text{CO}_2})} \quad (4.19)$$

which is the separation factor. Thus the selectivity and the separation factor are coincident when the pressure at the permeate side is negligible in comparison with the pressure at the feed side. The membrane performance of gas permeation can be evaluated via the calculation of permeability P (or permeance, P/l) of the target compound and the membrane selectivity.

4.4 MASS TRANSFER IN SLMs

As indicated in Section 4.2.2, supported liquid membranes are used in different applications that may involve both gas and liquid phases, for example, gas feed/gas permeate (e.g., gas separation, vapor permeation), liquid feed/gas permeate (e.g., pervaporation), and liquid feed/liquid permeate (e.g., liquid pertraction). The description of mass transfer through a supported liquid membrane for gas separation or vapor permeation can be done as described in Section 4.3 and following the schema of Fig. 4.5A. In case of pervaporation applications, the reader is invited to follow the mass transfer description developed in Chapter 3, taking into account the schema in Fig. 4.5B. The description of mass transfer in liquid pertraction, or liquid/liquid extraction using membranes, aiming at the separation of a multicomponent liquid mixture is shown in this section. Fig. 4.5C shows the concentration profile of the targeted component i through the SLM for this purpose.

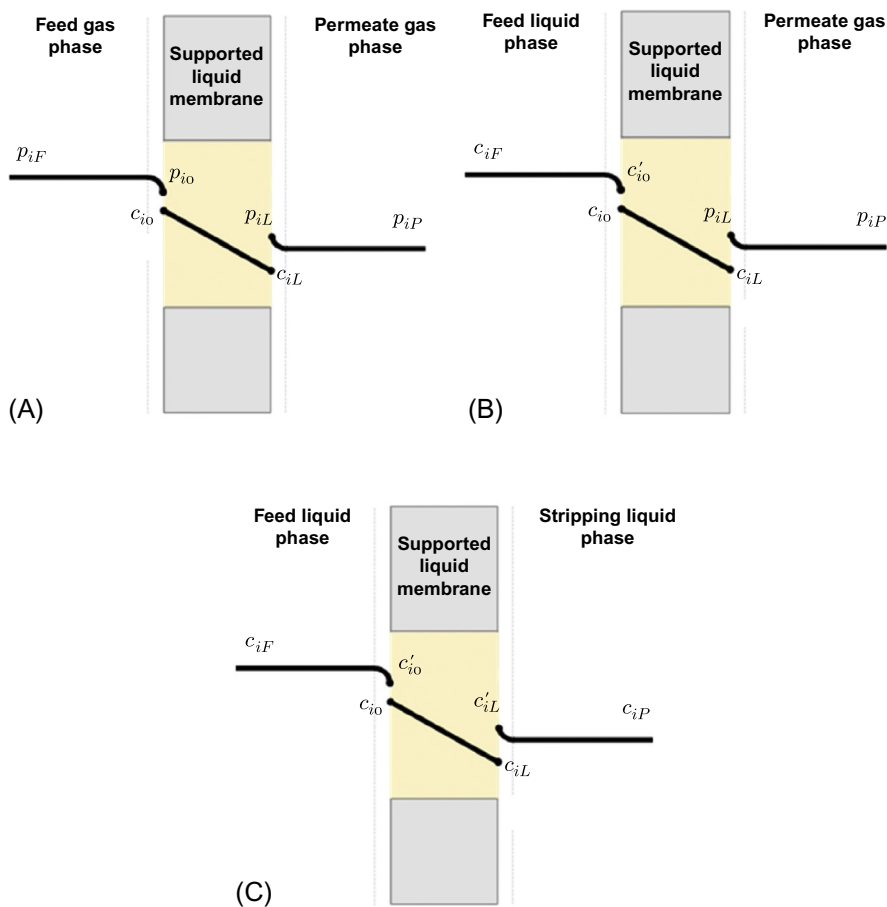


FIG. 4.5

Concentration profile of a component i in a supported liquid membrane for: (A) gas separation or vapor permeation, (B) pervaporation, and (C) liquid pertraction.

In liquid/liquid applications, the description of mass transfer of the solute from the feed phase to the receiving phase through the SLM involves several steps (Lozano et al., 2011): (i) Forced convection from the bulk of the feed solution to the feed-membrane interface, (ii) partition of the substrates between the feed phase (c'_{i0}) and the liquid immobilized in the organic membrane (c_{i0}), (iii) diffusion across the liquid membrane to the membrane-receiving interface under the action of the concentration gradient, (iv) partition of the substrates between the liquid immobilized in the organic membrane (c_{iL}) and the receiving phase (c'_{iL}), (v) forced convection from the membrane-receiving interface to the bulk of the receiving phase. The presence of the supported liquid breaks the continuity of the concentration profile and two thermodynamic equilibrium partition coefficients have to be considered, one for the feed liquid in contact with the supported liquid, K_{i_0} ,

$$K_{i_0} = \frac{c_{i0}}{c'_{i0}} \quad (4.20)$$

and another for the stripping liquid in contact with the supported liquid, K_{i_L} :

$$K_{i_L} = \frac{c_{iL}}{c'_{iL}} \quad (4.21)$$

Applying the Fick's law allows calculating the transmembrane flux:

$$J_i = \frac{D_i}{l_M} (c_{i0} - c_{iL}) \quad (4.22)$$

where D_i is the diffusivity of the solute in the membrane.

Combining Eqs. (4.20)–(4.22), and assuming that the partition coefficients do not depend on the concentration ($K_{i_0} = K_{i_L} = K_i$), then

$$J_i = \frac{K_i D_i}{l_M} (c'_{i0} - c'_{iL}) \quad (4.23)$$

or

$$J_i = \frac{K_i D_i}{l_M} (c_{iF} - c_{iP}) \quad (4.24)$$

if the resistances to mass transfer in the two boundary layers adjacent to the membrane surface are negligible ($c'_{i0} = c_{iF}$ and $c'_{iL} = c_{iP}$).

Similar to Eq. (4.15) for gas separation, the permeability P_{M_i} is defined as the product of the partition coefficient K_i , which accounts for the solubility of the compound i within the membrane, and the diffusion coefficient D_i , which accounts for the diffusion through the membrane (Seader et al., 2013):

$$P_{M_i} = K_i D_i \quad (4.25)$$

Thus by introducing Eq. (4.25) in Eq. (4.24):

$$J_i = \frac{P_{M_i}}{l_M} (c_{iF} - c_{iP}) \quad (4.26)$$

which allows the experimental calculation of the permeability P_{M_i} or the permeance $\frac{P_{M_i}}{l_M}$. The separation factor and selectivity can be calculated by Eqs. (4.16), (4.17), respectively.

For practical reasons related to the kind of experimental system used to perform the experiments, several expressions have been developed depending on the fluid phases at both sides of the membrane in order to obtain values of permeability in a straightforward way from the experimental data. These expressions are shown as follows.

4.4.1 GAS FEED/GAS PERMEATE

When supported liquid membranes are used for gas separation, it is common to calculate the permeability of a gas from the pressure data from the feed and permeate compartments of the experimental system (Cussler, 1997):

$$\frac{1}{b} \ln\left(\frac{\Delta p_0}{\Delta p}\right) = P \frac{t}{\delta} \quad (4.27)$$

$$\Delta p_0 = p_{feed,t=0} - p_{permeate,t=0} \quad (4.28)$$

$$\Delta p = p_{feed,t} - p_{permeate,t} \quad (4.29)$$

where p_{feed} and $p_{permeate}$ are the pressures in the feed and permeate compartments, respectively; P is the permeability; t is the time; and δ is the membrane thickness. The geometric parameter b is experimentally calculated from:

$$b = A_m \left(\frac{1}{V_{feed}} + \frac{1}{V_{permeate}} \right) \quad (4.30)$$

V_{feed} and $V_{permeate}$ are the volumes of the feed and permeate compartments, respectively, and A_m is the membrane area. The data can be plotted as $\frac{1}{b} \ln\left(\frac{\Delta p_0}{\Delta p}\right)$ versus $\frac{t}{\delta}$ and the permeability is obtained from the slope.

4.4.2 LIQUID FEED/GAS PERMEATE (PERVAPORATION)

Similar to solid pervaporation membranes, the transportation of the targeted component across the liquid membrane can be explained by the solution-diffusion model, which is a combination of the following three fundamental steps: (i) sorption of the targeted component from the feed liquid to the membrane, (ii) diffusion of the targeted component in the membrane, and (iii) desorption of the targeted component to the vapor phase on the downstream side of the membrane. The transport mechanism of the targeted component in the liquid within the membrane pores consists of either simple permeation or facilitated transport (Ong et al., 2014). In simple permeation, the targeted component passes through the membrane based on its solubility in the liquid without any reaction taking place during the transfer. In facilitated transport, a carrier is used in order to help components with lower solubility to pass through the membrane. The carrier forms a complex that is soluble in the liquid membrane (but not in the feed phase) by a reversible reaction that takes place at the feed-membrane interface. The target compound is released at the permeate-membrane interface. Both mechanisms obey Fick's law, where the solute is transported from high to low chemical potential, which is achieved by a difference of partial pressure of the targeted component between the feed and permeate phases.

Thus the specific description of mass transfer in pervaporation using SLM can be performed following the procedure indicated in Chapter 3.

4.4.3 LIQUID FEED/LIQUID PERMEATE (LIQUID PERTRACTION)

The flux can be alternatively expressed as the number of moles of solute i ($N_{p,i}$) transported through a specific area of membrane surface (A) per time unit. Thus Eq. (4.26) can be written as (Hernández-Fernández et al., 2007):

$$\frac{dN_{iP}}{dt} = \frac{P_{M_i} A}{l_M} (c_{iF} - c_{iP}) \quad (4.31)$$

N_{iP} can be expressed in terms of the concentration of solute as

$$N_{iP} = c_p V_p \quad (4.32)$$

where V_p is the volume of the receiving phase. If the volume of both receiving phase and feed phase are kept identical throughout the experiment ($V_p = V_f = V$), then Eq. (4.31) can be expressed as:

$$\frac{dC_{iP}}{dt} = \frac{P_{M_i} A}{l_M V} (c_{iF} - c_{iP}) \quad (4.33)$$

The concentration in the feed phase can be calculated as a function of the initial concentration of the solute in the feed phase, c_{iF0} , as:

$$c_{iF} = c_{iF0} - c_{iP} \quad (4.34)$$

Thus Eq. (4.33) becomes:

$$\frac{dC_{iP}}{dt} = \frac{P_{M_i} A}{l_M V} (c_{iF0} - 2c_{iP}) \quad (4.36)$$

After rearranging:

$$\frac{dC_{iP}}{(c_{iF0} - 2c_{iP})} = \frac{P_{M_i} A}{l_M V} dt \quad (4.37)$$

Eq. (4.37) can be analytically solved by using the following initial conditions:

$$t = 0 \quad c_{iP} = 0 \quad (4.38a)$$

$$t = t \quad c_{iP} = c_{iP} \quad (4.38b)$$

Integrating both terms in Eq. (4.37) leads to:

$$\ln \left[\frac{c_{iF0} - 2c_{iP}}{c_{iF0}} \right] = -2 \frac{P_{M_i} A}{l_M V} t \quad (4.39)$$

which shows that the term $\ln \left[\frac{c_{iF0} - 2c_{iP}}{c_{iF0}} \right]$ is a linear function of time. By representing $\ln \left[\frac{c_{iF0} - 2c_{iP}}{c_{iF0}} \right]$ versus t , the permeance $\frac{P_{M_i}}{l_M}$ can be directly calculated from the slope of the linear function.

4.5 INTERPRETATION OF RESULTS

The evaluation of results of transmembrane fluxes, permeances or permeabilities, separation factors, and selectivities gives essential information to determine the process performance and membrane performance. As already indicated in [Chapter 1](#), process performance is a measure of how efficient or effective a process is. The focus is then on the technical and economic availability of the process using membrane

technology. The final output would be the total membrane area that is required to achieve a specific separation objective, the optimal operation conditions (temperature, pressure, flowrate, etc.), and the overall cost. On the other hand, membrane performance focuses specifically on the membrane, that is, the membrane capacity to separate the mixture. Thus the evaluation of process performance should be done in terms of transmembrane fluxes and separation factors, while the evaluation of the membrane performance is based on permeabilities (or permeances) and selectivities. In this section, examples in gas separation (using dense or SLMs), pervaporation using SLMs, and liquid pertraction with SLMs will be developed.

4.5.1 GAS SEPARATION

In gas separation, it has been observed that the selectivity for gas pairs varies inversely with the permeability of the more permeable gas of the specific pair. This effect may be due to the fact that as the polymer molecular spacing becomes tighter the permeability decreases due to the decrease of diffusion coefficients, but the separation characteristics are enhanced (Robeson, 1991). Robeson (1991) performed an analysis of the literature data for binary mixtures containing He, H₂, O₂, N₂, CH₄, and CO₂ and represented a log-log plot of α_{ij} (separation factor = P_i/P_j) versus P_i (where P_i = permeability of the more permeable gas). Above the linear upper bound on the log-log plot, virtually no values exist. Thus an upper bound could be established to indicate the state of the art in gas separation and it is revisited by Robeson and other researchers frequently for polymeric dense membranes and SLMs with application in gas separation (Robeson, 1991, 2008; Freeman, 1999; Dal-Cin et al., 2008). This way of representing results is very useful to determine the membrane performance and allows a straightforward comparison with the separation achieved by novel membranes.

In order to overcome the trade-off between permeability and selectivity, the most intensive research has been focused on the development of novel materials and membranes that allow high permeation while keeping high selectivity. In addition to polymeric and ceramic membranes (Merkel et al., 2000; Lin and Freeman, 2004; Powell and Qiao, 2006; Minelli and Sarti, 2013; Anderson et al., 2012), carbon-based molecular sieves (Jiang and Chung, 2006; Husain and Koros, 2007; Czaperek et al., 2010; Smart et al., 2010), mixed-matrix membranes that combine polymers with ceramic materials, nanoparticles, and so on (Jiang and Chung, 2006; Husain and Koros, 2007) are a center of attention. An example is the fast development of new membranes for CO₂ capture. The need for a relevant solution that can decrease the emissions of this component to the atmosphere has motivated an extensive research in this area. The upper bound for the separation of CO₂/N₂ mixtures has been observed to be around 10^4 – 10^5 barrer of CO₂ permeability and selectivities lower than 10 (Robeson, 1991; Robeson, 2008). But recent developments have indicated an overcoming of this limit, as shown in Fig. 4.6 (Luis and Van der Bruggen, 2013). Polymerized ionic liquids have shown advantage over their respective ionic liquid in a traditional absorption system (Tang et al., 2005), capturing almost double the amount of CO₂ (Hasib-ur Rahman et al., 2010). In addition, research on SLMs has been performed to find the liquid that gives high permeability, high selectivity, and long-term stability. Ionic

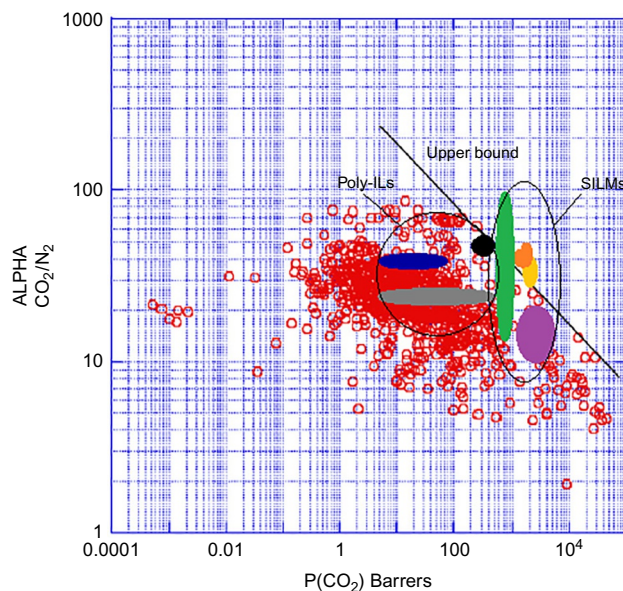


FIG. 4.6

CO₂/N₂ Selectivity versus CO₂ permeability of several polymerized ionic liquid membranes and supported ionic liquids membranes in relation to the 2008 Robeson upperbound (Robeson, 2008).

Reproduced with permission from Luis, P., Van der Bruggen, B., 2013. The role of membranes in postcombustion CO₂ capture. *Greenhouse Gas Sci. Technol.* 3, 1–20.

liquids forming SILMs have demonstrated to be good candidates for gas separation (i.e., separation of other gases from hydrocarbons mixtures of great interest for the oilfield such as sulfur dioxide, carbon monoxide, hydrogen, nitrogen, water (dehydration), and olefin/paraffin separation) (Martínez-Palou et al., 2014). Indeed, some supported ionic liquid membranes are showing higher CO₂ permeability and CO₂/N₂ selectivity than those included in the revisited upper bound by Robeson (2008). However, due to the large number of ionic liquids that can be candidates to form a SILM, a growing interest of the effect of the ionic liquid's properties on the permeability and selectivity has been observed in the literature. First sights of a general performance have been inferred (Neves et al., 2010a): (i) the gas diffusivity decreases for the more viscous ionic liquids, but still, a higher increase in solubility leads to an overall increase in permeability. Thus solubility effects play a more important role in the transport of gases. Therefore for strongly interacting gases, such as N₂ and CO₂, the resulting permeability is conditioned by the solubility and not by the diffusivity. (ii) Gas humidity leads to an increase of permeability and a decrease of selectivity. It is thought that the presence of water microdomains inside the ionic liquid provides an easier environment for diffusion due to a lower viscosity than that of the dry ionic liquid, although the effect of the presence of water will be more important in gases

that are more affected by diffusion in contrast with gases whose permeability is essentially controlled by solubility. In addition, more hydrophilic ionic liquids can absorb more water, leading to larger water clusters.

The effect of the temperature on the upper bound has been also evaluated. Rowe et al. (2010) proposed a model describing the influence of temperature on the permeability/selectivity trade-off of polymeric membranes. The model was used to predict the influence of temperature on upper bound behavior for several gas pairs including O_2/N_2 , H_2/N_2 , CO_2/CH_4 , CO_2/N_2 , H_2/CO_2 , and CO_2/H_2 . An example is shown in Fig. 4.7 for the separation of the mixture CO_2/N_2 . In general, the predicted upper bound shifts vertically with temperature (the higher the temperature, the lower the selectivity), and the direction and magnitude of the shift depend on the sizes and condensabilities of the gases considered (Rowe et al., 2010). For the mixture CO_2/N_2 , a decrease of $>50\%$ in selectivity is expected for a given permeability when the temperature increases $50^\circ C$.

The membrane stability is a point of attention that has to be evaluated carefully in order to ensure the long-term application of the technology (Kovvali and Sirkar, 2003). Several studies have shown that the interaction between the membrane and the supported liquid is critical to ensure a good stabilization. An example is shown in Fig. 4.8. Several ionic liquids are supported in two different membranes, one with a more hydrophilic character and a second one with more hydrophobic character (Neves et al., 2010a). It is observed that a better stability is achieved when using

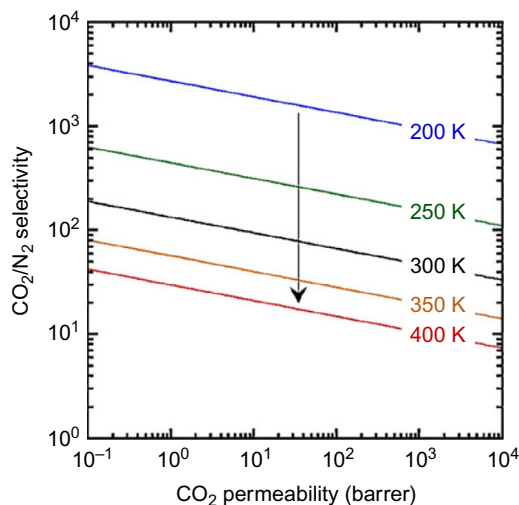


FIG. 4.7

Influence of temperature on the predicted upper bound behavior for CO_2/N_2 separation. Reproduced with permission from Rowe, B.W., Robeson, L.M., Freeman, B.D., Paul, D.R., 2010. Influence of temperature on the upper bound: theoretical considerations and comparison with experimental results. *J. Membr. Sci.* 360, 58–69.

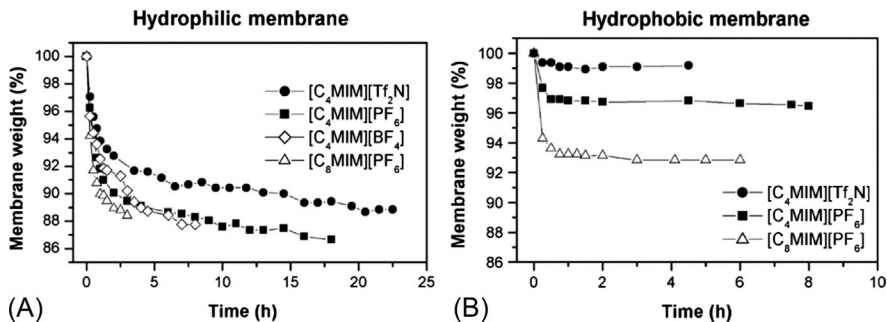


FIG. 4.8

Relative membrane weight in (A) hydrophilic, and (B) hydrophobic membranes immobilized with different room temperature ionic liquids as a function of time. Applied pressure difference: 1 bar.

Reproduced with permission from Neves, L.A., Crespo, J.G., Coelho, I.M., 2010a. Gas permeation studies in supported ionic liquid membranes. *J. Membr. Sci.* 357, 160–170. Neves, L.A., Benavente, J., Coelho, I.M., Crespo, J.G., 2010b. Design and characterisation of Nafion membranes with incorporated ionic liquids cations. *J. Membr. Sci.* 347, 42–52.

the hydrophobic membrane since it presents a lower value of weight loss and achieves a stable weight more rapidly. Because the studied ionic liquids were hydrophobic, it is assumed that the higher stability is due to a stronger interaction between the membrane and the ionic liquid.

After the evaluation of membrane performance by determining the permeability (or permeance) and selectivity of the membrane for the target compound, the next step is to determine if the proposed system presents economic viability. To do that, the performance of the process should be evaluated in terms of transmembrane flux and separation factor. The removal rate of the target compound, that is, the amount of that compound that has to be removed per year, divided by the transmembrane flux gives directly the overall membrane area that is required for the separation:

$$A = \frac{\text{removal rate of } i}{\Delta P_i \cdot \left(\frac{P}{l}\right)} \quad (4.40)$$

Luis and Van der Bruggen (2013) presented a simple calculation on the process performance for CO_2 removal considering a CO_2 removal rate of 10^5 tons of CO_2 per year ($1.61 \text{ m}^3 \text{ s}^{-1}$) and a membrane thickness of $l_M = 1 \text{ }\mu\text{m}$. The membrane area required as a function of a typical range of CO_2 permeability (100–1000 barrer) for different driving forces (partial pressure of CO_2 in the feed stream and considering negligible the value in the permeate side) is shown in Fig. 4.9. For a feed gas stream containing 15 vol% CO_2 at atmospheric pressure ($p_{CO_2} = 0.15 \text{ bar}$), about 10^4 – 10^5 m^2 of membrane area are needed.

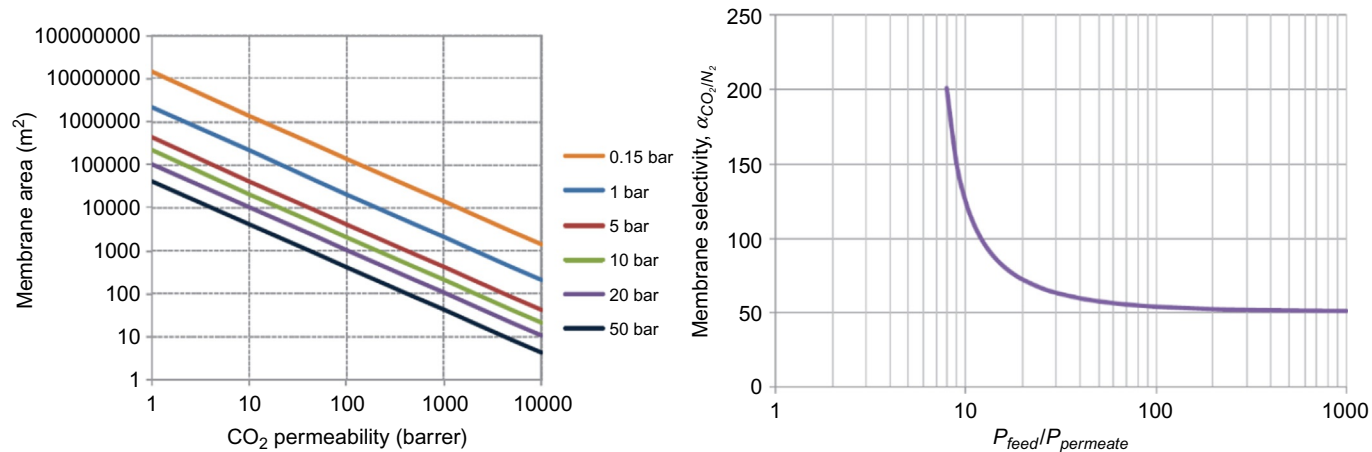


FIG. 4.9

(A) Membrane area versus CO₂ permeability calculated using Eq. (4.40). The pressure refers to the partial pressure of CO₂ in the feed gas; (B) required membrane selectivity to achieve 90 vol% CO₂ in the permeate stream as a function of the pressure ratio between the feed and the permeate sides (feed: 15 vol% CO₂/85 vol% N₂).

Reproduced with permission from Luis, P., Van der Bruggen, B., 2013. The role of membranes in postcombustion CO₂ capture. Greenhouse Gas Sci. Technol. 3, 1–20.

Regarding the degree of separation, Eq. (4.16) can be used to make an estimation of the required separation factor (or selectivity according to Eq. (4.17)) to achieve a specific permeate concentration in a situation of maximum driving force. For example, considering a feed stream with 15 vol% CO₂ and a permeate with 90 vol% CO₂, a membrane with selectivity higher than 50 is required. Luis and Van der Bruggen (2013) also represented the effect of the pressure ratio between the permeate and the feed (P_{feed}/P_{perm}) on the selectivity to achieve a permeate concentration of 90 vol% CO₂ ($y_{CO_2}=0.9$), according to Eq. (4.18). Fig. 4.9B shows the results of the study. As observed, if the pressure ratio is about 10, a membrane with selectivity above 100 is required, and the membrane selectivity reaches a plateau value as the pressure ratio increases since the role of membrane selectivity is less important as the pressure ratio increases (Belaïssaoui et al., 2012).

Thus it is possible to determine the technical viability of the separation by considering the partial pressure of the component in the feed stream and the separation objective (CO₂ purity and recovery ratio). For example, for CO₂ separation from flue gases, it has been inferred that only gas streams with concentration of CO₂ higher than 20 vol% allow using a stand-alone membrane process with lower energy demand than the standard MEA (monoethylamine)-based absorption process. Lower concentrations of CO₂ in the feed stream involve very selective membranes (selectivity higher than 100 as shown in Fig. 4.9B) or the application of multistage membrane processes (Belaïssaoui et al., 2012). Furthermore, recent studies have concluded that increasing the membrane permeance (or permeability) is more important than increasing the selectivity above a value of 30 to further reduce the cost of CO₂ capture from flue gas (Merkel et al., 2010).

The process performance is thus restricted by the pressure ratio across the membrane and cost and energy considerations limit the maximum pressure ratio attainable by feed compression and/or permeate vacuum to about 10 (Merkel et al., 2010). Thus when a single-stage membrane process cannot satisfy the required separation, a multistage membrane design is necessary to achieve the desired CO₂ recovery and purity such as those that use incoming combustion air as sweep gas to generate driving force. Different multistage process design can be formulated. An example of a two-step vacuum membrane process is shown in Fig. 4.10A. The obtained CO₂ presents the required purity to be directly sequestered. This process achieves 90% CO₂ capture and produce 95+% supercritical CO₂ ready for sequestration. Other configurations such as a two-step counter-flow/sweep design shown in Fig. 4.10B are more economical, using vacuum in the first module instead of compressing the feed gas to increase the driving force since the volume of the permeate gas passing through the vacuum pump is only a fraction of the volume of the flue gas (Merkel et al., 2010).

Thus the limitations of the membrane performance can be overcome by an appropriate design that leads to the required process performance. It is thus important to distinguish between the state of the art of membranes (upper bound as indicator of the membrane performance) and the process performance, which can be optimized by an appropriate process design.

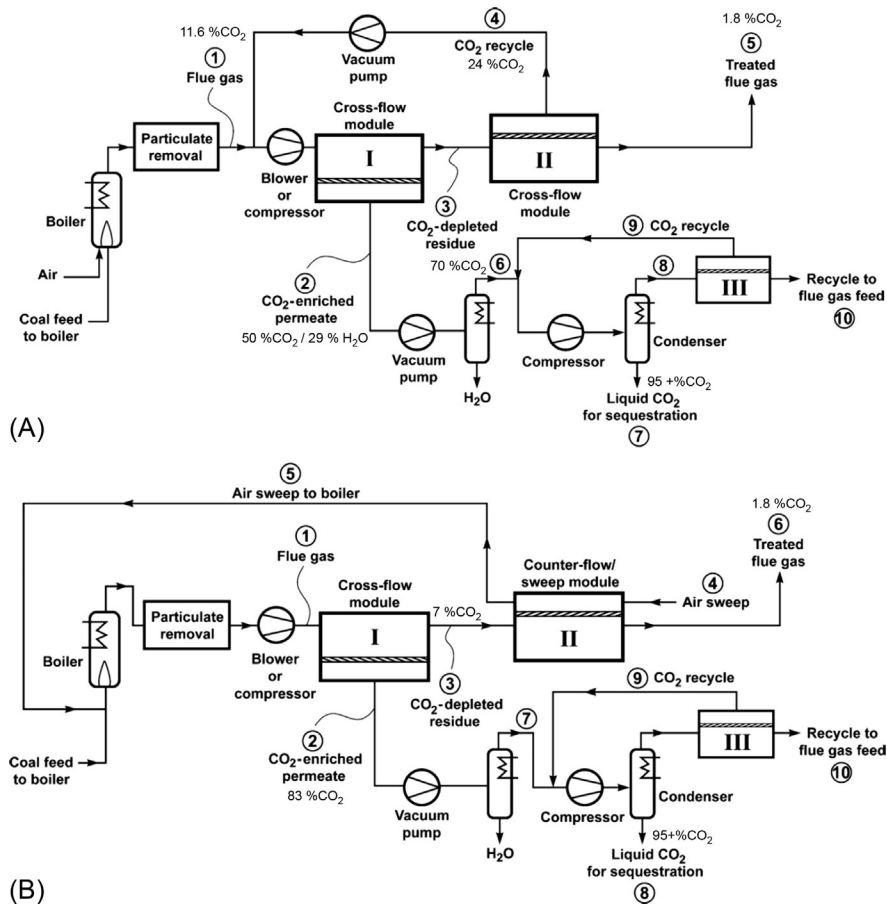


FIG. 4.10

Simplified flow diagram of (A) a two-step vacuum membrane process to capture and sequester CO₂ in flue gas from a coal-fired power plant; (B) a two-step counter-flow/sweep membrane process to capture and sequester CO₂ in flue gas from a coal-fired power plant. The base-case membrane with a CO₂ permeance of 1000 GPU and a CO₂/N₂ selectivity of 50 was considered.

Modified from Merkel et al. (2010).

4.5.2 SELECTIVE SEPARATION OF LIQUIDS BY PERVAPORATION USING SLMS

Application of SLMs in pervaporation has attracted the attention of many researchers in the last years, mainly due to the use of ionic liquids as the supported liquid. The interpretation of results and required discussion of this kind of systems should be done by following the procedure indicated in Chapter 3. Nevertheless, some specific examples for the application of S(I)LMs are included in this section.

Pervaporation is one of the most studied membrane separation processes due to its effectiveness in the separation of challenging liquid mixtures, such as those containing azeotropes, at low energy consumption. Dense solid membranes are the most common membranes used in pervaporation. However, the use of SLMs has attracted the attention of many researchers since the rate of molecular diffusion in liquid is much higher than that in a solid membrane (Ong et al., 2014). In addition, SLMs can be prepared with a small amount of liquid within the pores of the membrane, decreasing the capital cost of the overall process. The membrane area required for the separation will be determined by the transmembrane flux (the higher the flux, the lower the necessary membrane area), while the energy consumption will be conditioned by the selectivity of the membrane toward the target component (the higher the selectivity, the lower the energy consumption). Thus the evaluation of the membrane performance by determining the permeance and selectivity, and the process performance by the flux and separation factors, are essential to conclude on the technical and economic viability of pervaporation using a specific SLM for a specific application. A comparison between the pervaporation performance of SLMs with other solid membranes was summarized by Ong et al. (2014). SLMs showed a competitive permeation flux and selectivity in separating organic compounds from aqueous solutions, with a selectivity enhanced by the use of SLM. Several factors should be studied when evaluating pervaporation using SLMs: the effect of feed concentration, the effect of temperature, the effect of the downstream pressure (at the permeate side), and the membrane stability.

Effect of feed concentration

The concentration of the target compound in the feed solution will affect the driving force of the separation. According to Fick's laws of diffusion, solubility and diffusivity are concentration dependent and molecules tend to move from regions of high concentration to regions of low concentration (Ong et al., 2014). Higher concentration of the targeted component means a higher concentration gradient between the feed solution and the permeate side, enhancing the transmembrane flux of the target component through the membrane. An example can be observed in Fig. 4.11A, which shows the effect of concentration of the target compound (butanol) on the transmembrane flux using three different membranes, one membrane without supported liquid and two membranes with two different ionic liquids as supported liquids (Izák et al., 2009a, b). Fig. 4.11B shows the effect of feed concentration on the pervaporation of acetic acid through a membrane with trioctylamine (TOA) as the liquid membrane (Qin et al., 2003). As observed, the flux of acetic acid increases significantly with the feed concentration, which is due to the increase in driving force due to the larger concentration of acetic acid in the feed solution. Regarding the degree of separation, higher separation factors are expected when increasing the feed concentration. However, the performance of the membrane cannot be evaluated without removing the effect of the driving force in the separation. The permeability (or permeance) and selectivity should be calculated in order to remove the effect of the driving force and evaluate the real separation of the membrane. An example is shown in Fig. 4.11C. Cascon and Choudhari (2013) studied the separation of

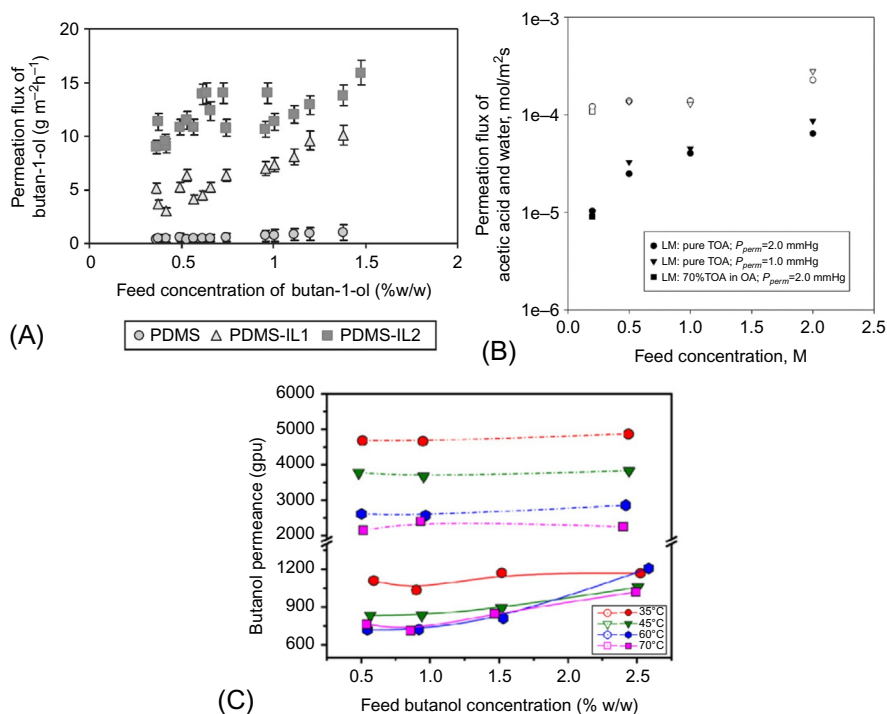


FIG. 4.11

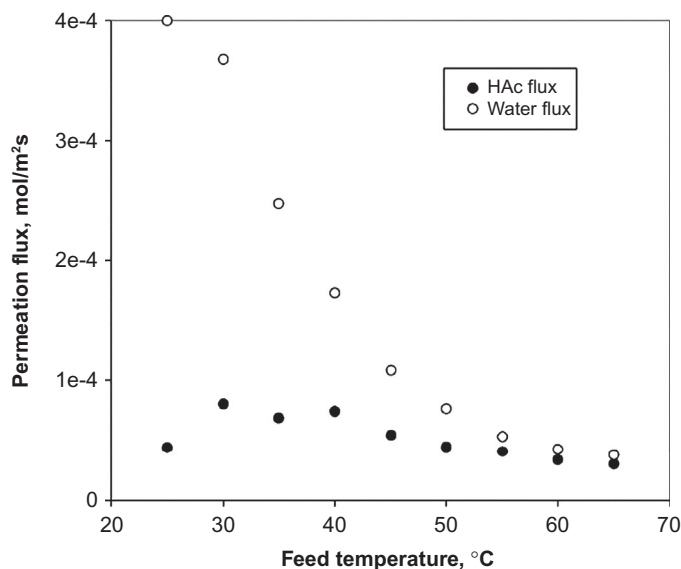
(A) Dependence of butan-1-ol permeation flux on feed concentration. \circ PDMS; \blacksquare PDMS + 1-ethenyl-3-ethyl-imidazolium hexafluorophosphate ionic liquid; \triangle PDMS + tetrapropylammonium tetracyano-borate ionic liquid, (B) permeation fluxes of acetic acid (filled symbols) and water (unfilled symbols) as a function of acetic acid concentration in the feed solution using trioctylamine (TOA) as the liquid membrane, (C) permeance of 1-butanol using SILMs based on $[\text{Ph}_3\text{t}][\text{INTf}_2]$ (solid lines) and $[\text{Ph}_3\text{t}][\text{DCN}]$ (dashed lines) ($1 \text{ GPU} = 1 \times 10^{-6} \text{ cm}^3(\text{STP}) \text{ cm}^{-2} \text{ s}^{-1} \text{ cm Hg}^{-1}$).

(A) Reproduced with permission from Izák, P., Friess, K., Hynek, V., Ruth, W., Fei, Z., Dyson, J.P., Kragl, U., 2009a. Separation properties of supported ionic liquid-polydimethylsiloxane membrane in pervaporation process. *Desalination* 241, 182–187; Izák, P., Friess, K., Hynek, V., Ruth, W., Fei, Z., Dyson, J.P., Kragl, U., 2009b. Separation properties of supported ionic liquid-polydimethylsiloxane membrane in pervaporation process. *Desalination* 241, 182–187. (B) Reproduced with permission from Qin, Y., Sheth, J.P., Sirkar, K.K., 2003. Pervaporation membranes that are highly selective for acetic acid over water. *Ind. Eng. Chem. Res.* 42, 582–595, and (C) Reproduced with permission from Cascon, H.R., Choudhari, S.K., 2013. 1-Butanol pervaporation performance and intrinsic stability of phosphonium and ammonium ionic liquid-based supported liquid membranes. *J. Membr. Sci.* 429, 214–224.

1-butanol from water using SILMs composed of trihexyl(tetradecyl)phosphonium bis(trifluoromethylsulfonyl)imide ($[\text{Ph}_3\text{t}][\text{NTf}_2]$) or trihexyl(tetradecyl)phosphonium dicyanamide ($[\text{Ph}_3\text{t}][\text{DCN}]$). They observed a clear increase of flux with the feed concentration but, as observed in Fig. 4.11C, the permeance was practically constant, which means that the driving force was only responsible for the increase of flux.

Effect of feed temperature

The feed temperature is a key variable in the pervaporation process using SLMs for two reasons: (i) the vapor pressure of the feed solution increases with temperature, leading to a larger driving force that will enhance the transmembrane flux; and, (ii) the viscosity of the liquid membrane decreases with temperature, which will increase the diffusivity of the target compound through the SLM. However, higher temperature does not always produce an enhancement of flux. For example, in the separation of acetic acid/water studied by [Qin et al. \(2003\)](#), it was observed that the higher the temperature, the higher the acetic acid concentration in the permeate, and the higher the acetic acid selectivity. However, the permeation fluxes of both components (acetic acid and water) decreased sharply with an increase of temperature. [Fig. 4.12](#) shows these results of transmembrane flux as a function of the temperature. Higher temperature increased the vapor pressures of acetic acid and water, which means higher driving forces for pervaporation, but it also reduced sharply the partition coefficient of acetic acid between the liquid membrane phase and the aqueous phase and the solubility of water in the liquid membrane phase. The solubility of water was more significantly influenced by the temperature increase than the acetic acid solubility; this explains why water permeation flux decreased more sharply than

**FIG. 4.12**

Effect of the temperature on the permeation fluxes of acetic acid and water using trioctylamine (TOA) as the liquid membrane.

Reproduced with permission from Qin, Y., Sheth, J.P., Sirkar, K.K., 2003. Pervaporation membranes that are highly selective for acetic acid over water. *Ind. Eng. Chem. Res.* 42, 582–595.

acetic acid. Nevertheless, the effect of the temperature should be also studied in terms of permeability, selectivity, and membrane stability.

Effect of the downstream pressure

Downstream pressure affects also the driving force for the separation and it may be a critical factor in the stability of the membrane. It is thought that a lower downstream pressure leads to a higher selectivity and flux since the driving force is also increased (Qin et al., 2003; Ong et al., 2014). An example can be observed in Fig. 4.13, following the separation of acetic acid-water (Qin et al., 2003). However, the magnitude of the changes in flux may not be proportional to the change of driving force, involving other phenomena related to the extraction mechanism (Qin et al., 2003). Thus calculating the permeability and selectivity is very relevant to remove the effect of the driving force in the calculations and determine the membrane behavior under different operation conditions.

In addition, a physical limit appears when the liquid is pushed out of the membrane due to the pressure difference between both sides of the membrane. The critical pressure at which that happens can be calculated by the Laplace equation, as indicated in Section 4.2 (Eq. 4.1). Thus the difference in pressure at both sides of the membrane should be such that the critical pressure is not overcome.

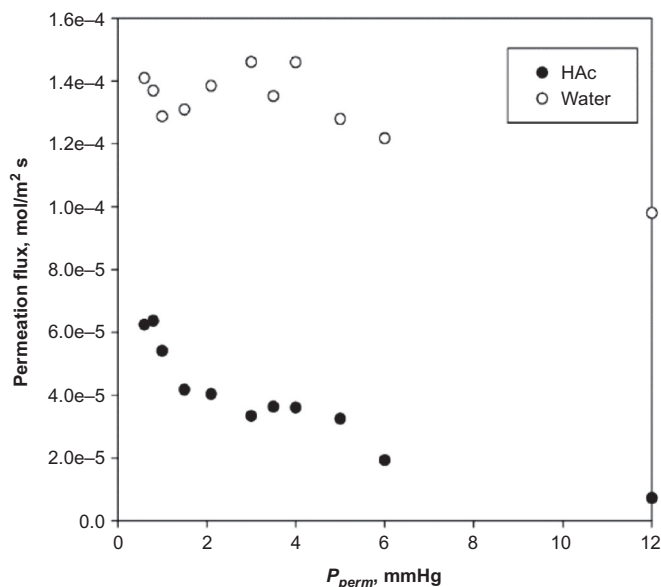


FIG. 4.13

Influence of permeate side pressure on the permeation flux of acetic acid and water using trioctylamine (TOA) as the liquid membrane.

Reproduced with permission from Qin, Y., Sheth, J.P., Sirkar, K.K., 2003. Pervaporation membranes that are highly selective for acetic acid over water. *Ind. Eng. Chem. Res.* 42, 582–595.

Stability of SLMs in pervaporation

Instability of SLMs in pervaporation may be produced by the displacement of the liquid membrane due to a progressive wetting of the pores in the membrane support by the feed phase, the pressure difference across the membrane (overcoming the critical transmembrane pressure), dissolution of the liquid membrane in the feed phase, the formation of an emulsion in the liquid membrane, the blockage of membrane pores by precipitation of the carrier complex, and the volatilization of the liquid membrane due to the vacuum existing in the permeate side (Ong et al., 2014). Several strategies have been applied to reduce the risk of loss of membrane stability, such as surface coating (Thongsukmak and Sirkar, 2007), using a polymer inclusion membrane (Kohoutová et al., 2009; Matsumoto et al., 2011), or gelation of the liquid membrane (Neplenbroek et al., 1992; Kemperman et al., 1997; Jansen et al., 2011; Voss et al., 2009). In addition, most of the SLMs that are currently developed include ionic liquids as the liquid membrane, leading to supporting ionic liquid membranes (SILMs). The fact that ionic liquids have a negligible vapor pressure and high viscosity are factors that make them good candidates as liquid membranes for pervaporation. Studies on stability of S(I)LMs are common in the literature. An example can be found in Fig. 4.14 for the separation of 1-butanol from water (Cascon and Choudhari (2013). Fig. 4.14A and B show the example of a potential stable membrane and an instable membrane, respectively (Cascon and Choudhari (2013). The stable membrane showed a constant performance for about 90h of experiment.

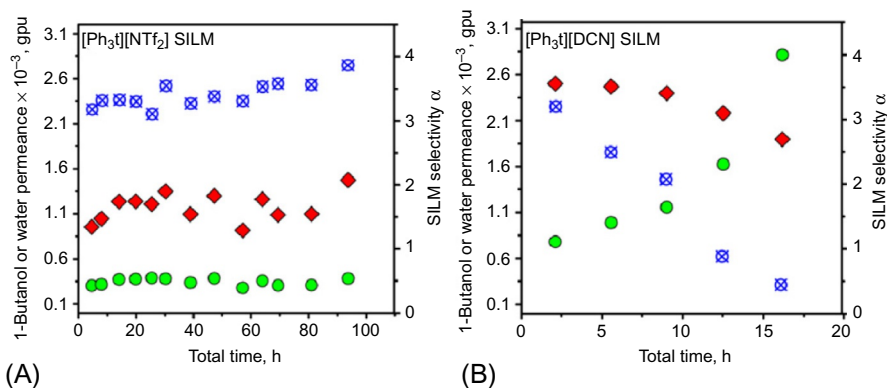


FIG. 4.14

Pervaporation performance of a SILM containing the ionic liquids: (A) trihexyl(tetradecyl) phosphonium bis (trifluoromethylsulfonyl)imide ($[\text{Ph}_3\text{t}][\text{NTf}_2]$) and (B) trihexyl(tetradecyl) phosphonium dicyanamide ($[\text{Ph}_3\text{t}][\text{DCN}]$), for the separation of 1-butanol from water. Diamonds refer to 1-butanol permeance; circles refer to water permeance; and crossed circles refer to the SILM selectivity.

Reproduced with permission from Cascon, H.R., Choudhari, S.K., 2013. 1-Butanol pervaporation performance and intrinsic stability of phosphonium and ammonium ionic liquid-based supported liquid membranes. *J. Membr. Sci.* 429, 214–224.

The instability of the membrane shown in Fig. 4.14B was due to the displacement of the ionic liquid from the support's pores to the feed solution, causing the monotonous increase of the water permeance and the decrease of 1-butanol permeance. After 16 h, the SILM had become more selective to water than to 1-butanol. The evaluation of the membrane stability is thus an essential factor to ensure the long-term stability of the SLM in pervaporation.

The cited operational factors have a direct influence on the driving force, thus calculating the permeance (or permeability) is critical to remove this influence from the calculations and be able to evaluate the real separation caused by the membrane and the mass transfer mechanisms that are involved. However, the attention of most researchers has been focused mainly on the determination of fluxes and separation factors, evaluating thus the performance of the process. A special consideration of both process and membrane performance, as well as the effect of the driving force, should be taken into account according to the guideline included in Chapter 3.

4.5.3 SELECTIVE SEPARATION OF LIQUIDS BY LIQUID PERTRACTION USING SLMs

Using SLMs leads to a very (theoretically) efficient technology since it does not use pressure or voltage and it is based on the difference of chemical energy as a driving factor of the process, for example, using simple H^+ concentration difference. Coupled co- or counter-ion transport allows to get an active transport of the targeted species from diluted solutions into more concentrated and to collect toxic or precious species in a small volume of the acceptor solution. Sometimes, it is even possible to reach saturation of the strip solutions and finally precipitation of the product (Kocherginsky et al., 2007). The application of SLMs for the selective separation of liquids or liquid pertraction has demonstrated that this technology indeed is able to reach levels of separation that are very competitive with the conventional processes. In addition, the use of ionic liquids has brought this technology to the top of current research in order to develop novel membranes that are more permeable, more selective to the target compound and more stable in the long run.

As indicated in Section 4.1 (Fig. 4.2B), three main mechanisms of transport may take place in liquid pertraction: uphill transport, facilitated coupled counter-transport, and facilitated coupled cotransport. Fig. 4.15 shows examples of different systems described by these mechanisms.

Many researchers have applied SLMs in processes for the separation of toxic (and valuable) metals from water, such as cadmium (Cd^{+2}) (He et al., 2000), vanadium (V^{+5}) (Chaudry et al., 2007), silver (Ag^{+1}) (Chaudry et al., 2008), or mercury (Hg^{+2}) (Chakrabarty et al., 2010), among others. Also, SILMs have been applied in the separation of liquid contaminants of hydrocarbons (sulfurated, nitrogenated, and aromatic compounds) in oil industry (Martínez-Palou et al., 2014).

Several variables are studied in order to determine their effect on the permeability and selectivity of the separation. Among them, it is worth mentioning the effect of the feed concentration, the effect of kind and concentration of the stripping (receiving)

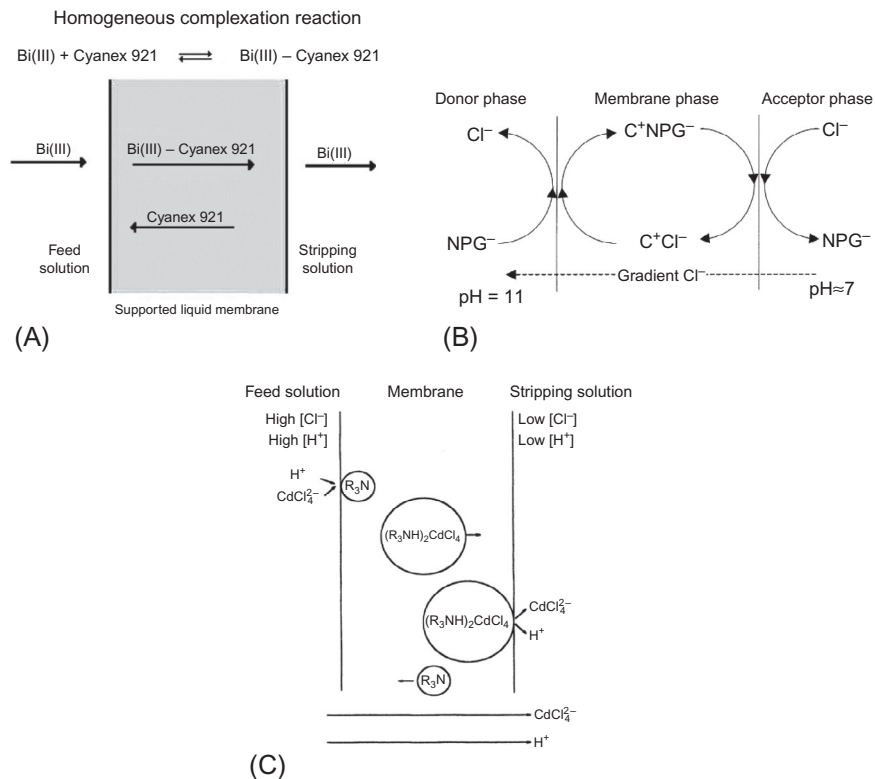


FIG. 4.15

Schematic diagram of: (A) Uphill mass transfer of Bi(III) through SLM using Cyanex 921 as extractant; (B) facilitated coupled counter-transport of glyphosate (NPG^-) through the SLM with Aliquat 336 as a carrier (C^+); and (C) facilitated coupled cotransport of Cd(II) through the SLM with tricapryl amine (N_{235} , $\text{N}(\text{C}_n\text{H}_{2n+1})_3$, $n=8-10$) and tri-*n*-octylamine ($\text{N}(\text{C}_8\text{H}_{17})_3$, TNOA) as the carriers (R_3N), which were diluted in carbon tetrachloride.

(A) Reproduced with permission from Reyes-Aguilera, J.A., Gonzalez, M.P., Navarro, R., Saucedo, T.I., Avila-Rodriguez, M., 2008. Supported liquid membranes (SLM) for recovery of bismuth from aqueous solutions. *J. Membr. Sci.* 310, 13–19. (B) Reproduced with permission from Dzygiel, P., Wieczorek, P., 2000. Extraction of glyphosate by a supported liquid membrane technique. *J. Chromatogr. A*, 889, 93–98. (C) Reproduced with permission from He, D., Ma, M., Zhao, Z., 2000. Transport of cadmium ions through a liquid membrane containing amine extractants as carriers. *J. Membr. Sci.* 169, 53–59.

agent, the effect of the carrier concentration, the kind of contactor, the membrane stability, and the kind of support.

Effect of feed concentration

A typical study in liquid pertraction is the evaluation of the feed concentration on the extraction of the species of interest. For example, Fig. 4.16 shows the variation of flux and permeability with the concentration of silver ions in the feed solution.

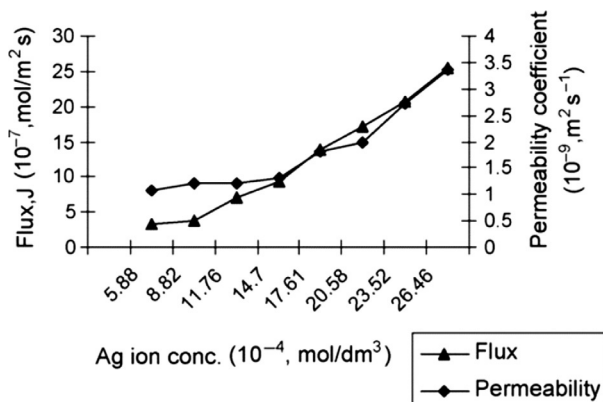


FIG. 4.16

Effect of silver ion concentration on permeation rate of Ag(I) ions.

Reproduced with permission from Chaudry, M.A., Bukhari, N., Mazhar, M., 2008. Coupled transport of Ag(I) ions through triethanolamine–cyclohexanone-based supported liquid membranes. *J. Membr. Sci.* 320, 93–100.

An increase of both flux and permeability is observed. It is expected that the flux increases since it is directly proportional to the feed concentration, c_{iF} , as indicated in Eq. (4.26), which happens if the carrier is not saturated with solute so that as the solute concentration increases, the chemical potential gradient across the membrane is also increased. This increase of flux should reach a limit for a given feed concentration depending on the equilibrium to be reached in the extraction and stripping reactions (Chaudry et al., 2008). Thus the removal of silver anions is faster at higher concentration of silver ions in the feed solution. Regarding the permeability coefficient, a constant value would be expected if the change in concentration in the receiving phase were negligible. For low concentrations of feed solution, this may be the situation since the flux is also small. However, higher feed concentrations lead to higher fluxes and higher concentration in the receiving phase, which affects the permeability as shown in Eq. (4.26). Keeping both the flux and permeability as high as possible is the way to achieve a good process and membrane performance, respectively. Thus it is evident that, in this kind of situations, the higher the feed concentration, the better.

This positive effect of a high feed concentration has been observed very commonly in the literature. For example, Di Luccio et al. (2002) also indicated that the flux increased with the feed concentration in the pertraction of fructose from mixtures of fructose and glucose; Chaudry et al. (2007) observed that the flux of vanadium (V) ion increased with the feed concentration; and Chakrabarty et al. (2010) studied the extraction of mercury from aqueous streams and observed the same effect. Zidi et al. (2010) also observed an increase of the initial flux with the increase of the initial phenol concentration in the feed phase and membrane saturation phenomenon was not perceived. However, a decrease in the extraction efficiency has

been also observed in the literature (Dzygiel and Wieczorek (2000)). Thus the study of the influence of the feed concentration should be performed for each application.

Other factors related to the feed concentration may have an important influence on the extraction process depending on the kind of mass transfer process (uphill, coupled cotransport or coupled counter-transport).

The pH of the feed solution may determine the degree of dissociation of the target species to be extracted. For example, the research performed by Zidi et al. (2010) required a pH lower than 2 in the feed solution in order to keep phenol (target compound) in its molecular form, which is the only one that can diffuse through the studied SLM by an uphill mechanism since it is soluble in the carrier. In this case, an increase of pH leads to a decrease in the transport efficiency of phenol.

In addition, the effect of the pH in the feed solution is an important factor when the species to be extracted is a multicharged compound. Glyphosate can present functional groups either positively (secondary amino group) or negatively (phosphonic and carboxylic group) charged in water solution, thus the extraction efficiency will be affected by the pH (Dzygiel and Wieczorek (2000)). The more transportable (active) form of glyphosate in the solution, the more molecules can interact with the carrier molecule at the feed/membrane interface. Thus as observed by Dzygiel and Wieczorek (2000), higher pH leads to higher extraction efficiency (more negatively charged molecules of glyphosate are in the solution). The mass transfer is also highly affected when it is driven by a concentration gradient of hydrogen ions. This is the case of transport of mercury using trioctylamine as carrier, which occurs due to a coupled cotransport mode in which the transport of the species, that is, hydrogen and mercury, occur in the same direction (Chakrabarty et al. 2010). HCl was used to adjust the pH and as provider of H^+ ions. Thus if the initial feed concentration of mercury is low, the excess of chloride ions is larger. An increase in chloride ions possibly inhibits the interfacial reaction at the feed/membrane interface which eventually lowers the percentage extraction of mercury at lower initial feed concentration. Therefore too high concentration of coupling coions (H^+ , Cl^-) may produce a significant reduction of performance. This effect was also observed by Chaudry et al. (2008), who varied the concentration of HNO_3 between 0.5 and 2.5 M in the extraction of silver (I), being H^+ and NO_3^- the coupled coions that travel in the same direction as silver ions (Fig. 4.17). He et al. (2000) observed the same trend in the extraction of cadmium ions using HCl as the coions provider. This shows the importance of the amount of protons in the feed phase. If there are too many protons in the feed phase, the reactions that take place on the feed-membrane interface may be shift backward and there will be difficulties in achieving the desired species to be transported (e.g., $CdCl_4^{2-}$, as shown in Fig. 4.15C).

The presence of HCl in the feed may be necessary to form the adequate species to be transported through the membrane. Reyes-Aguilera et al., 2008 performed the extraction of bismuth from aqueous solutions by using as carrier Cyanex 921 solved in kerosene. In this case, uphill mass transfer takes place and the neutral complex $BiCl_3$ is the species with the greatest possibility of being extracted by Cyanex 921. The species $BiCl_3$ does prevail and presents its highest molar fraction between

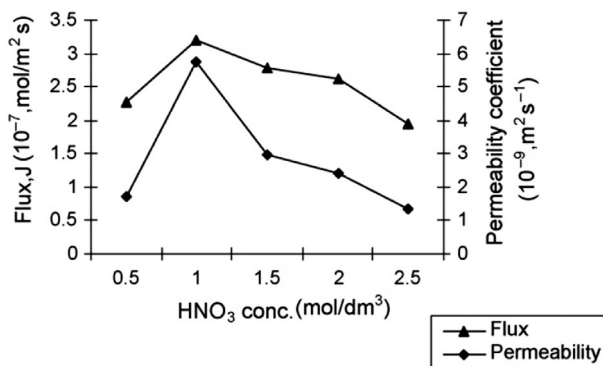


FIG. 4.17

Effect of HNO₃ concentration on permeation rate of Ag(I) ions.

Reproduced with permission from Chaudry, M.A., Bukhari, N., Mazhar, M., 2008. Coupled transport of Ag(I) ions through triethanolamine–cyclohexanone-based supported liquid membranes. *J. Membr. Sci.* 320, 93–100.

concentrations of 0.2 and 1 M HCl. Therefore it is possible to carry out Bi(III) extraction by means of SLM using that range of HCl concentration in the feed solution. Increasing the HCl concentration, Bi(III) extraction increases; but higher concentration involves the formation of a charged species (BiCl₄⁻) instead of the neutral BiCl₃, thus the extraction decreases significantly.

Effect of kind and concentration of the stripping (receiving) agent

The stripping reaction at the membrane/receiving phase interface plays a key role in the mass transfer through the membrane. If the transported species are not completely stripped, the membrane phase will gradually be saturated, limiting the mass transfer and decreasing the permeation rate. The kind of stripping agent used in liquid pertraction is a very important factor to ensure the extraction. An example of lack of extraction because of the stripping agent was shown by (Reyes-Aguilera et al., 2008). They used Cyanex-921 solutions in kerosene as the carrier within the membrane pores to extract bismuth (III) from aqueous streams. Bi(III) extracted into the SLM could not be recovered in the stripping phase when H₂O was employed as stripping solution but it accumulated in the SLM. This indicates that the H₂O medium is not strong enough to destabilize the Bi(III)-Cyanex 921 complex present in the membrane, to cause the release of the metal into the stripping solution. On the other hand, when using 0.2 M H₂SO₄ as stripping solution, the authors observed that the transferred Bi(III) was completely recovered in the stripping solution.

The concentration of the stripping agent is also a critical issue in liquid pertraction. In general, the higher the concentration of the stripping agent, the higher the flux of species through the membrane since the driving force is enhanced, but a plateau or maximum value of flux and permeability has been observed in which higher concentrations of stripper do not produce an increase in flux or permeability. The reasons of this behavior have to be explained by looking in detail to the studied

system. For example, Chakrabarty et al. (2010) showed that an increase of NaOH concentration (stripping phase) led to a sharp increase of mercury extraction, but this increase becomes marginal at concentrations higher than 0.1 M NaOH. At a higher concentration of NaOH, more number of OH⁻ ions are added to salt of mercury and it yields a precipitate of HgO or Hg. This precipitation was considered to be the responsible for the decrease of the extraction rate due to membrane clogging. Chaudry et al. (2008) observed an increase of flux and permeability with the increase of KCN concentration (stripping agent) in silver extraction, reaching a maximum value at 1.5 M KCN. Beyond that concentration, a decrease in flux and permeability was produced. In this case, the increase in concentration of KCN will help the decomposition of Ag (I)-carrier complex but beyond this concentration (1.5 M), the KCN dissociation to K⁺ and CN⁻ may be less to furnish cyanide anions and hence to slow the stripping action.

In processes governed by coupled counter-transport, the concentration of salt in the receiving or stripping phase is critical since the target compound in the feed solution will be transported through the membrane due to a driving force, which is a gradient of counter-ions from the receiving phase to the feed solution. The function of the carrier is to facilitate the transfer of the species from the feed to the receiving phase and the counter-ion from the receiving phase to the feed solution. As observed by Dzygiel and Wieczorek, 2000, at the interface between the feed phase and the membrane, the target species and the carrier form an ion-pair complex, which becomes neutral. Then, the complex diffuses through the membrane and at the interface between the membrane and the receiving phases, the carrier exchanges the target species by the counter-ion, which diffuses back to the feed solution. Hence, the overall mass transfer involves transport of the target compound from the feed phase to the receiving phase, and transport of the counter-ion from the receiving phase to the feed phase. If there is no driving force, the extraction process reaches equilibrium. By increasing the concentration of the salt in the receiving phase, the driving force is increased and higher extraction is achieved. However, this increase of extraction efficiency presents a limit, as indicated by Dzygiel and Wieczorek (2000).

Effect of the carrier concentration

He et al. (2000) studied the extraction of cadmium (II) from water by using a SLM with tricapryl amine and tri-*n*-octylamine as the carriers diluted in carbon tetrachloride. The flux was observed to increase with the concentration of the carrier until reaching a maximum, starting to decrease at higher concentrations. The interface between the feed phase and the membrane is not saturated by the carrier at low concentration, which may explain the larger flux. In addition, the authors also observed an increase in permeability with the increase of the carrier concentration but reaching a maximum (1.0 M carrier). Beyond that, a decrease in permeability was observed. The reason was attributed to an increase in the hindrance to diffusion as a result of an increase in membrane viscosity when the carrier concentrations are increased.

The same effect was observed by Chaudry et al. (2008) in the extraction of silver ions (Fig. 4.18). Both the flux and the permeability coefficient increase with the

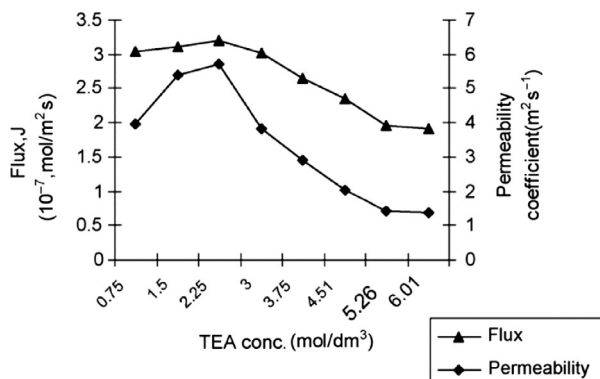


FIG. 4.18

Effect of triethanolamine (TEA) concentration on permeation rate of Ag(I) ions.

Reproduced with permission from Chaudry, M.A., Bukhari, N., Mazhar, M., 2008. Coupled transport of Ag(I) ions through triethanolamine–cyclohexanone-based supported liquid membranes. *J. Membr. Sci.* 320, 93–100.

concentration of triethanolamine (TEA, carrier) until reaching a maximum at 2.25 M carrier. Higher concentrations lead to a dramatic decrease of flux and permeability. The increase of flux and permeability is due to the fact that increasing TEA concentration involves larger amount of TEA molecules to associate with Ag ions. However, a concentration larger than 2.25 M increases the viscosity too much and opposite frictional forces appear, leading to a decrease in flux and permeability. As support of this discussion, the authors calculated the distribution coefficient for silver ion in the organic and aqueous phases as a function of the TEA concentration. The observed trend was similar than that of flux and permeability, that is, increase up to 2.25 M followed by a dramatic decrease. Thus silver ions remain in the feed solution at higher concentration of the carrier.

Increasing the concentration of the carrier presented a plateau value in the extraction efficiency of glyphosate from water (Dzygiel and Wieczorek (2000)). The authors attributed this phenomenon to a two competing factors: the concentration gradient of the glyphosate complex, and the viscosity of the organic phase in the liquid membrane. High fluxes can be obtained when a large chemical potential (concentration gradient) and diffusion coefficient are maintained. Thus increasing the concentration of the carrier leads to an increase in the concentration gradient because more amount of glyphosate could be extracted through the membrane, but it also leads to an increase in viscosity, which decreases the diffusion coefficient, producing a decrease in mass transfer of the carrier-analyte complex within the membrane phase.

Also the extraction of phenol from aqueous solutions has shown the same trend (Zidi et al., 2010): the initial flux is dependent on the carrier concentration in the membrane organic phase, increasing until reaching an optimal value at a carrier concentration around 20%. The flux increase can be explained because at low carrier

concentration, diffusion of the complex across the liquid membrane is the rate-determining step. An increase of the carrier concentration in the membrane phase would increase the extraction of phenol and hence, the transport of these species at higher speed. Above the optimal value, the phenol transport flux decreases. The increase of the carrier viscosity may be the reason, which would indicate that the effective diffusivity of these species decreases significantly while the reaction rate of their formation increases rather slowly as the carrier concentration increases above 20% (i.e., the increase of the carrier concentration at this point does not compensate for the increase in the solution viscosity) (Zidi et al., 2010).

Kind of contactor

SLMs can be configured as a flat sheet or a cylindrical configuration, typically as a hollow fiber membrane to obtain large surface area per unit volume. Flat sheet supported liquid membranes are the simplest form of the liquid membrane, which allows an easy manufacture. On the other hand, hollow fiber supported liquid membranes are packed within a housing, with the feed phase passing through one side of the membrane (lumen side or shell side) and the stripping or receiving phase through the other side (shell side or lumen side). Supporting the liquid within the pores of the membrane presents more complexity than with flat membranes but the larger surface area achieved compensates this issue.

Using flat or hollow fiber membranes has shown significant differences in liquid pertraction. The pertraction of fructose from mixtures of fructose and glucose has been applied using those two different configurations (Di Luccio et al., 2002). The flat sheet system produced fructose/glucose selectivities up to 14, while in the hollow fiber system fructose fluxes 20 times higher than glucose were obtained, using low carrier concentrations. This result was attributed to increased membrane stability. In the hollow fiber system the pore size of the support is smaller and the disturbance caused at the membrane surface by the flow is probably lower than in the flat sheet cell, preserving the membrane stability during the experiment. Thus the configuration and fluid dynamics of the system may affect significantly the membrane stability and, therefore the membrane performance.

Stability of the SLM

Supported liquid membranes consist of a porous support in which the membrane liquid is introduced within the membrane pores, remaining there by capillary forces. After long-term use, the membrane may deteriorate due to several phenomena, such as loss of membrane solvent and/or carrier, formation of emulsion, and so on (Zha et al., 1995). The stability of SLMs can be evaluated by means of different approaches: measuring physicochemical properties of the organic phases (interfacial tensions, viscosities, contact angles, and water solubilities); following the progressive wetting of SLMs by aqueous solutions or even using a noninvasive technique such as impedance spectroscopy runs (Hill et al., 1996). But three methods are receiving the largest attention in the recent literature, focused on the evaluation of (i) the amount of liquid within the membrane pores that is lost over time, (ii) the

decrease of the species permeability coefficient over time (e.g., simple linear relation between the logarithm of permeability and the number of runs), (iii) the concentration of species in the feed phase (stripping agent, carrier, H^+ , OH^-) that are present due to the leakage and direct channeling between the feed and the receiving phase. This procedure requires a complete understanding of the kind of mass transfer process (uphill, coupled counter-transport or coupled cotransport) that is taking place so that the observed changes are attributed to channeling between phases and not to the mass transfer process itself. For example, Fig. 4.19A shows the dramatic increase of pH in the feed solution due to the pass of the stripping phase (NaOH) to the feed phase by channeling for the coupled cotransport of mercury (Chakrabarty et al., 2010). On the other hand, an increase of pH in the feed phase may be the normal trend due to the decrease of H^+ ions produced in coupled cotransport under unsteady-state conditions, as shown in Fig. 4.19B (Chaudry et al., 2008).

Using organic solvents as supported liquid may bring many difficulties from the point of view, of membrane stability. The application of SLMs in industrial processes has been very questioned, limiting its use and interest. Therefore ionic liquids have been introduced to replace the volatile organic solvents and create a new perception of the potential use of these novel supported ionic liquid membranes (SILM) in separation processes.

The selective separation of substrates and products of transesterification reactions has been evaluated by used SILMs. For example, the ionic liquid based on 1-*n*-alkyl-3-methylimidazolium cation (*n*-butyl, *n*-octyl) and the hexafluorophosphate anion has been supported in several polymeric membranes (Fluoropore,

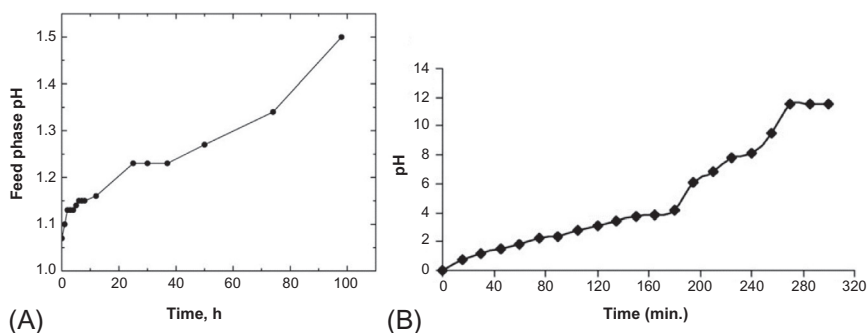


FIG. 4.19

(A) Stability of SLM on the basis of the variation of pH in the feed phase due to channeling in mercury extraction; (B) Variation of pH in the feed phase with time due to coupled co-transport in silver extraction.

(A) Reproduced with permission from Chakrabarty, K., Saha, P., Ghoshal, A.K., 2010. Separation of mercury from its aqueous solution through supported liquid membrane using environmentally benign diluent. *J. Membr. Sci.* 350, 395–401. (B) Reproduced with permission from Chaudry, M.A., Bukhari, N., Mazhar, M., 2008. Coupled transport of $Ag(I)$ ions through triethanolamine–cyclohexanone-based supported liquid membranes. *J. Membr. Sci.* 320, 93–100.

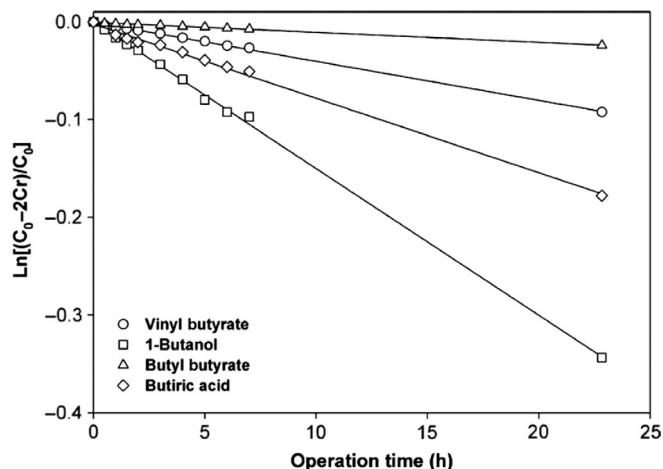


FIG. 4.20

Plots of $\ln \left[\frac{C_{iFO} - 2C_{iP}}{C_{iFO}} \right]$ vs operation time for the transport of vinyl butyrate, 1-butanol, butyl butyrate, and butyric acid through a Nylon membrane with supported [bmim][PF₆].

Reproduced with permission from Hernández-Fernández, F.J., de los Ríos, A.P., Rubio, M., Tomás-Alonso, F., Gómez, D., Villora, G., 2007. A novel application of supported liquid membranes based on ionic liquids to the selective simultaneous separation of the substrates and products of a transesterification reaction. *J. Membr. Sci.* 293, 73–80.

Durapore, Mitex, Isopore, and Nylon) in order to separate vinyl butyrate, 1-butanol, butyl butyrate, and butyric acid (Hernández-Fernández et al., 2007). Fig. 4.20 shows the experimental results using the linear representation of Eq. (4.39). The permeance values can be obtained from the slope. The slopes of the SILMs were significantly lower than those of the plain membranes (without supported ionic liquid) because the presence of the ionic liquid introduces an additional mass transfer resistance for the transport of the compounds. However, the plain membranes offered no selectivity for the separation of the compounds while the SILMs showed substantial differences in selectivity due to the fact that the ionic liquid offers different mass transfer resistance for each compound. The best results were found when using Nylon and Isopore as support, which are the hydrophilic organic membranes. Thus an interesting conclusion is that the higher the interactions between the cation and anion of the ionic liquid and the membrane, the more efficient the immobilization. Thus the selection of the ionic liquid-membrane pair should be done considering that the ionic liquid must *like* the membrane so that the maximum wettability is achieved. A second critical conclusion obtained from this work is related to the selection of the supported ionic liquid. It was observed that the increase in the values of the IL/hexane partition coefficient was in agreement with the increase of permeability values for the compounds, which indicates that the transport is mainly regulated by the IL's affinity toward each solute, as also observed between some isomeric amines (hexylamine, diisopropylamine, and trimethylamine) and the ionic liquid 1-*n*-butyl-3-methylimidazolium hexafluorophosphate or [BMIM][PF₆] (Branco et al., 2002a,

b). Thus the capability of a given SLM to separate the target compounds can be assessed simply by evaluating the partition coefficient of each compound between the receiving/feed phase and the liquid phase supported in the membrane (Hernández-Fernández et al., 2007).

However, this statement cannot be generalized. The literature shows other situations, too. For example, the study of phenol extraction from aqueous solutions using a solution of tributyl phosphate in kerosene supported within the pores of two different membranes made of polypropylene and PVDF with the same pore size (Zidi et al., 2010). The results showed better stability in the case of the PVDF support in spite of being generally a less hydrophobic material. Thus stability studies are mandatory in order to prove the long-term operation of the membranes since the polymeric support characteristics present an important effect on the SLM stability.

Effect of the kind of support

The solid support of SLMs is typically a hydrophobic or hydrophilic polymer that can be heterogeneous or homogeneous, with a symmetric or asymmetric structure, and may be neutral or may carry positive or negative charges or both (Parhi, 2013). Several materials may be used, for example, PTFE, polypropylene, and polysulfones. It is essential to select a support material that is thermally and chemically stable on exposure to the feed and the receiving phases and the impregnating solvents. In principle, a hydrophobic material would be preferred if an organic carrier is going to be supported within the membrane pores, and a hydrophilic material would be used for hydrophilic carriers. In this way, the interaction between the support and the carrier is enhanced and a more stable SLM is obtained. In addition, the chemical composition and physical properties of the support such as thickness, porosity, and tortuosity may have an important influence on the flux of chemical species (Zidi et al., 2010). Clear variations have been observed in the literature from the point of view of transmembrane flux and membrane stability (Reyes-Aguilera et al., 2008; Chakrabarty et al., 2010). Thus it is advisable to evaluate several supports that fit with the application before running a complete experimental study of liquid pertraction.

4.6 CONCLUDING REMARKS

In this chapter, the main applications and the mass transfer description of gas permeation and supported liquid membranes have been presented. *Gas permeation* technology is used for the separation of gas mixtures, aiming at the concentration of a target compound for economic or environmental reasons. Gas permeation normally involves the use of dense polymeric membranes but due to the harsh conditions of some gas streams, the use of inorganic porous membranes has been also researched. The mechanism of mass transport in dense membranes that can be described by the solution-diffusion model by applying Fick's first law of diffusion under conditions of steady state. Also, the rate of diffusion of a component through a porous membrane can be described in terms of Fick's law. The membrane performance of gas permeation is evaluated by means of the permeability P (or permeance, P/l) of the target

compound and the membrane selectivity, which is coincident with the separation factor when the pressure at the permeate side is negligible in comparison with the pressure at the feed side. Using the upper bound developed by Robeson is a straightforward way to determine the performance of novel membranes regarding the current state of the art. In general, it has been observed that increasing the membrane permeance (or permeability) is more important than increasing the selectivity. On the other hand, the process performance should be evaluated in terms of transmembrane flux and separation factor to determine its economic viability. The process performance is restricted by the pressure ratio across the membrane and cost and energy considerations limit the maximum pressure ratio attainable by feed compression and/or permeate vacuum to about 10.

Supported liquid membranes (SLM) refer to porous membranes that contain a liquid inside the pores and it is kept there by capillary forces. The number of applications of this kind of membranes can be related to three kinds of configurations: gas feed/gas permeate (e.g., applied in gas separation and vapor permeation), liquid feed/liquid permeate (e.g., applied in liquid pertraction), and liquid feed/gas permeate (e.g., applied in pervaporation). Each configuration requires a specific description of the mass transfer due to the different fluid phases present. The description of mass transfer through a supported liquid membrane for gas separation can be done as in gas permeation using dense membranes since both systems follow the same principle of separation. In case of pervaporation applications, the mass transfer can be described by following [Chapter 3](#). Finally, the description of mass transfer in liquid pertraction is shown in [Section 4.4](#). The main advantages of using SLM are the relatively small volume of liquid that is required inside the pores of the membrane, the tunable character of the membrane by selecting the most appropriate filling liquid and, the mass transfer is not governed by the equilibrium and, in the case of liquid extraction, the possibility of having the extraction and reextraction steps in the same device. On the other hand, the main disadvantage observed when using SLM is the problem of low stability of the liquid phase in the pores. Higher stability has been achieved by using ionic liquids to impregnate the pores of a membrane, leading to supported ionic liquid membranes (SILM). Several variables constitute the focus of most studies performed for S(I)LMs, such as the effect of feed concentration, the effect of temperature, the effect of the downstream pressure or the concentration of the stripping (receiving) agent, and the membrane stability. As for gas permeation, the evaluation of results of permeances (or permeabilities) and selectivities should be done to evaluate the membrane performance, while fluxes and separation factors will give essential information on the process performance.

REFERENCES

- Anderson, M., Wang, H., Lin, Y.S., 2012. Inorganic membranes for carbon dioxide and nitrogen separation. *Rev. Chem. Eng.* 28, 101–121.
- Bara, J.E., Lessmann, S., Gabriel, J., Hatakeyama, E.S., Noble, R.D., Gin, D.L., 2007. Synthesis and performance of polymerizable ionic liquids as gas separation membranes. *Ind. Eng. Chem. Res.* 46, 5397–5404.

- Bara, J.E., Hatakeyama, E.S., Gabriel, C.J., Zeng, X., Lessmann, S., Gin, D.L., Noble, R.D., 2008a. Synthesis and light gas separation in cross-linked gemini room temperature ionic liquid polymer membranes. *J. Membr. Sci.* 316, 186–191.
- Bara, J.E., Hatakeyama, E.S., Gin, D.L., Noble, R.D., 2008b. Improving CO₂ permeability in polymerized room-temperature ionic liquid gas separation membranes through the formation of a solid composite with a room-temperature ionic liquid. *Polym. Adv. Technol.* 19, 1415–1420.
- Belaïssaoui, B., Willson, D., Favre, E., 2012. Membrane gas separations and post-combustion carbon dioxide capture: parametric sensitivity and process integration strategies. *Chem. Eng. J.* 211–212, 122–132.
- Boydzhiev, L., 1990. Liquid pertraction or liquid membranes—state of the art. *Sep. Sci. Technol.* 25, 187–205.
- Branco, L.C., Crespo, J.G., Afonso, C.A.M., 2002a. High selective transport of organic compounds by using supported liquid membranes based on ionic liquids. *Angew. Chem. Int. Ed.* 41, 2771–2773.
- Branco, L.C., Crespo, J.G., Afonso, C.A.M., 2002b. Studies on the selective transport of organic compounds by using ionic liquids as novel supported liquid membranes. *Chem. Eur. J.* 8, 3865.
- Breembroek, G.R.M., van Straalen, A., Witkamp, G.J., van Rosmalen, G.M., 1998. Extraction of cadmium and copper using hollow fiber supported liquid membranes. *J. Membr. Sci.* 146, 185–195.
- Carlisle, T.K., Bara, J.E., Lafrate, A.L., Gin, D.L., Noble, R.D., 2010. Main-chain imidazolium polymer for CO₂ separations: an initial study of a new ionic liquid-inspired platform. *J. Membr. Sci.* 359, 37–43.
- Cascon, H.R., Choudhari, S.K., 2013. 1-Butanol pervaporation performance and intrinsic stability of phosphonium and ammonium ionic liquid-based supported liquid membranes. *J. Membr. Sci.* 429, 214–224.
- Chakrabarty, K., Saha, P., Ghoshal, A.K., 2010. Separation of mercury from its aqueous solution through supported liquid membrane using environmentally benign diluent. *J. Membr. Sci.* 350, 395–401.
- Chaudry, M.A., Bukhari, N., Mazhar, M., Tazeen, F., 2007. Vanadium(V) ions transport through tri-n-octyl amine cyclohexane supported liquid membranes. *Sep. Purif. Technol.* 54, 227–233.
- Chaudry, M.A., Bukhari, N., Mazhar, M., 2008. Coupled transport of Ag(I) ions through triethanolamine–cyclohexanone-based supported liquid membranes. *J. Membr. Sci.* 320, 93–100.
- Chiarizia, R., Horwitz, E.P., Rickert, P.G., Hodgson, K.M., 1990. Application of supported liquid membranes for removal of uranium from groundwater. *Sep. Sci. Technol.* 25, 1571–1586.
- Cussler, E.L., 1997. Diffusion. In: *Mass Transfer in Fluid Systems*. 2nd ed. Cambridge University Press, New York, NY.
- Czyperek, M., Zapp, P., Bouwmeester, H.J.M., Modigell, M., Ebert, K., Voigt, I., Meulenberga, W.A., Singheisera, L., Stöver, D., 2010. Gas separation membranes for zero-emission fossil power plants: MEM-BRAIN. *J. Membr. Sci.* 359, 149–159.
- Dal-Cin, M.M., Kumar, A., Layton, L., 2008. Revisiting the experimental and theoretical upper bounds of light pure gas selectivity–permeability for polymeric membranes. *J. Membr. Sci.* 323, 299–308.
- Dehaan, A.B., Bartels, P.V., Degraauw, J., 1989. Extraction of metal-ions from waste-water-modeling of the mass-transfer in a supported-liquid membrane process. *J. Membr. Sci.* 45, 281–297.

- Di Luccio, M., Smith, B.D., Kida, T., Alves, T.L.M., Borges, C.P., 2002. Evaluation of flat sheet and hollow fiber supported liquid membranes for fructose pertraction from a mixture of sugars. *Desalination* 148, 213–220.
- Dzygiel, P., Wiczorek, P., 2000. Extraction of glyphosate by a supported liquid membrane technique. *J. Chromatogr. A* 889, 93–98.
- Fortunato, R., Afonso, C.A.M., Reis, M.A.M., Crespo, J.G., 2004. Supported liquid membranes using ionic liquids: study of stability and transport mechanism. *J. Membr. Sci.* 242, 197–209.
- Fortunato, R., Branco, L.C., Afonso, C.A.M., Benavente, J., Crespo, J.G., 2006. Electrical impedance spectroscopy characterisation of supported ionic liquid membranes. *J. Membr. Sci.* 270, 42–49.
- Freeman, B., 1999. Basis of permeability/selectivity tradeoff relations in polymeric gas separation membranes. *Macromolecules* 32, 375–380.
- Friess, K., Jansen, J.C., Bazzareli, F., Izak, P., Jarmarova, V., Kačírková, M., 2012. High ionic liquid content polymeric gel membranes: Correlation of membrane structure with gas and vapor transport properties. *J. Membr. Sci.* 415, 801–809.
- George, S.C., Thomas, S., 2001. Transport phenomena through polymeric systems. *Prog. Polym. Sci.* 26, 985–1017.
- Hasib-ur Rahman, M., Siaj, M., Larachi, F., 2010. Ionic liquids for CO₂ capture—development and progress. *Chem. Eng. Process.* 49, 313–322.
- He, D., Ma, M., Zhao, Z., 2000. Transport of cadmium ions through a liquid membrane containing amine extractants as carriers. *J. Membr. Sci.* 169, 53–59.
- Hernández-Fernández, F.J., de los Ríos, A.P., Rubio, M., Tomás-Alonso, F., Gómez, D., Vllora, G., 2007. A novel application of supported liquid membranes based on ionic liquids to the selective simultaneous separation of the substrates and products of a transesterification reaction. *J. Membr. Sci.* 293, 73–80.
- Hill, C., Dozol, J.-F., Rouquette, H., Eymard, S., Tournois, B., 1996. Study of the stability of some supported liquid membranes. *J. Membr. Sci.* 114, 73–80.
- Hsieh, Y.-N., Huang, P.-C., Sun, I.-W., Whang, T.-J., Hsu, C.-Y., Huang, H.-H., Kuei, C.-H., 2006. Nafion membrane-supported ionic liquid-solid phase microextraction for analyzing ultra trace PAHs in water samples. *Anal. Chim. Acta* 557, 321–328.
- Husain, S., Koros, W., 2007. Mixed matrix hollow fiber membranes made with modified HSSZ-13 zeolite in polyetherimide polymer matrix for gas separation. *J. Membr. Sci.* 288, 195–207.
- Izák, P., Mateus, N.M.M., Afonso, C.A.M., Crespo, J.G., 2005. Enhanced esterification conversion in a room temperature ionic liquid by integrated water removal with pervaporation. *Sep. Purif. Technol.* 41, 141.
- Izák, P., Kockerling, M., Kragl, U., 2006a. Stability and selectivity of a multiphase membrane, consisting of dimethylpolysiloxane on an ionic liquid, used in the separation of solutes from aqueous mixtures by pervaporation. *Green Chem.* 8, 947–948.
- Izák, P., Kockerling, M., Kragl, U., 2006b. Solute transport from aqueous mixture through supported ionic liquid membrane by pervaporation. *Desalination* 199, 96–98.
- Izák, P., Ruth, W., Fei, Z., Dyson, P.J., Kragl, U., 2008. Selective removal of acetone and butan-1-ol from water with supported ionic liquid-polydimethylsiloxane membrane by pervaporation. *Chem. Eng. J.* 139, 318–321.
- Izák, P., Friess, K., Hynek, V., Ruth, W., Fei, Z., Dyson, J.P., Kragl, U., 2009a. Separation properties of supported ionic liquid-polydimethylsiloxane membrane in pervaporation process. *Desalination* 241, 182–187.

- Izák, P., Friess, K., Hynek, V., Ruth, W., Fei, Z., Dyson, J.P., Kragl, U., 2009b. Separation properties of supported ionic liquid-polydimethylsiloxane membrane in pervaporation process. *Desalination* 241, 182–187.
- Jansen, J.C., Friess, K., Clarizia, G., Schauer, J., Izák, P., 2011. High ionic liquid content polymeric gel membranes: Preparation and performance. *Macromolecules* 44, 39–45.
- Jiang, L.Y., Chung, T.S., 2006. Fabrication of mixed matrix hollow fibers with intimate polymer-zeolite interface for gas separation. *AIChE J.* 52, 2898–2908.
- Karaszova, M., Kacirkova, M., Friess, K., Izak, P., 2014. Progress in separation of gases by permeation and liquids by pervaporation using ionic liquids: a review. *Sep. Purif. Technol.* 132, 93–101.
- Kemperman, A.J.B., Damink, B., van den Boomgaard, T., Strathmann, H., 1997. Stabilization of supported liquid membranes by gelation with PVC. *J. Appl. Polym. Sci.* 65, 1205–1216.
- Kocherginsky, N.M., Yang, Q., Seelam, L., 2007. Recent advances in supported liquid membrane technology. *Sep. Purif. Technol.* 53, 171–177.
- Kohoutová, M., Sikora, A., Hovorka, S., Randová, A., Schauer, J., Tišma, M., Setnicková, K., Petrickovic, R., Guernik, S., Greenspoon, N., Izák, P., 2009. Influence of ionic liquid content on properties of dense polymer membranes. *Eur. Polym. J.* 45, 813–819.
- Kovvali, A.S., Sirkar, K.K., 2003. Stable liquid membranes—recent developments and future directions. In: Li, N.N. (Ed.), *In: Advanced Membrane Technology, Annals of the New York Academy of Sciences* Vol. 984. New York Acad. Sciences, New York, pp. 279–288.
- LaFrate, A.L., Gin, D.L., Noble, R.D., 2010. High water vapor flux membranes based on novel diol-imidazolium polymers. *Ind. Eng. Chem. Res.* 49, 11914–11919.
- Li, N.N., 1969. Permeation through liquid surfactant membranes. *AIChE J.* 17, 459–463.
- Li, P., Paul, D.R., Chung, T.S., 2012. High performance membranes based on ionic liquid polymers of CO₂ separation from flue gas. *Green Chem.* 14, 1052–1063.
- Lin, H., Freeman, B.D., 2004. Gas solubility, diffusivity and permeability in poly(ethylene oxide). *J. Membr. Sci.* 239, 105–117.
- Lozano, L.J., Godínez, C., de los Ríos, A.P., Hernandez-Fernandez, F.J., Sanchez-Segado, S., Alguacil, F.J., 2011. Recent advances in supported ionic liquid membrane technology. *J. Membr. Sci.* 376, 1–14.
- Luis, P., Van der Bruggen, B., 2013. The role of membranes in postcombustion CO₂ capture. *Greenhouse Gas Sci. Technol.* 3, 1–20.
- Luis, P., Ortiz, I., Aldaco, R., Irabien, A., 2007. A novel group contribution method in the development of a QSAR for predicting the toxicity (*Vibrio fischeri* EC50) of ionic liquids. *Ecotoxicol. Environ. Saf.* 67, 423–429.
- Martínez-Palou, R., Likhanova, N.V., Olivares-Xometl, O., 2014. Supported ionic liquid membranes for separations of gases and liquids: An overview. *Pet. Chem.* 54, 595–607.
- Matsumoto, M., Murakami, Y., Kondo, K., 2011. Separation of 1-butanol by pervaporation using polymer inclusion membranes containing ionic liquids. *Solvent Extr. Res. Dev. Jpn.* 18, 75–83.
- Merkel, T.C., Bondar, V.I., Nagai, K., Freeman, B.D., Pinnau, I., 2000. Gas sorption, diffusion, and permeation in poly(dimethylsiloxane). *J. Polym. Sci. Polym. Phys.* 38, 415–434.
- Merkel, T.C., Lin, H., Wei, X., Baker, R., 2010. Power plant post-combustion carbon dioxide capture: An opportunity for membranes. *J. Membr. Sci.* 359, 126–139.
- Minelli, M., Sarti, G.C., 2013. Permeability and diffusivity of CO₂ in glassy polymers with and without plasticization. *J. Membr. Sci.* 435, 176–185.
- Neplebroek, A.M., Bargeman, D., Smolders, C.A., 1992. Supported liquid membranes: Instability effects. *J. Membr. Sci.* 67, 121–132.

- Neves, L.A., Crespo, J.G., Coelhoso, I.M., 2010a. Gas permeation studies in supported ionic liquid membranes. *J. Membr. Sci.* 357, 160–170.
- Neves, L.A., Benavente, J., Coelhoso, I.M., Crespo, J.G., 2010b. Design and characterisation of Nafion membranes with incorporated ionic liquids cations. *J. Membr. Sci.* 347, 42–52.
- Ong, Y.T., Yee, K.F., Cheng, Y.K., Tan, S.H., 2014. A review on the use and stability of supported liquid membranes in the pervaporation process. *Sep. Purif. Rev.* 43, 62–88.
- Parhi, P.K., 2013. Supported liquid membrane principle and its practices: a short review. *J. Chem.* 2013, Article ID 618236. <https://doi.org/10.1155/2013/618236>.
- Park, Y.-I., Kim, B.-S., Byun, Y.-H., Lee, S.-H., Lee, E.-W., Lee, J.-M., 2009. Preparation of supported ionic liquid membranes (SILMs) for the removal of acidic gases from crude natural gas. *Desalination* 236, 342–348.
- Peng, J., Liu, J., Hu, X., Jiang, G., 2007. Direct determination of chlorophenols in environmental water samples by hollow fiber supported ionic liquid membrane extraction coupled with high-performance liquid chromatography. *J. Chromatogr. A* 1139, 165–170.
- Plaza, A., Merlet, G., Hasanoglu, A., Isaacs, M., Sanchez, J., Romero, J., 2013. Separation of butanol from ABE mixtures by sweep gas pervaporation using a supported gelled ionic liquid membrane: analysis of transport phenomena and selectivity. *J. Membr. Sci.* 444, 201–212.
- Powell, C.E., Qiao, G.G., 2006. Polymeric CO₂/N₂ gas separation membranes for the capture of carbon dioxide from power plant flue gases. *J. Membr. Sci.* 279, 1–49.
- Qin, Y., Sheth, J.P., Sirkar, K.K., 2003. Pervaporation membranes that are highly selective for acetic acid over water. *Ind. Eng. Chem. Res.* 42, 582–595.
- Reyes-Aguilera, J.A., Gonzalez, M.P., Navarro, R., Saucedo, T.I., Avila-Rodriguez, M., 2008. Supported liquid membranes (SLM) for recovery of bismuth from aqueous solutions. *J. Membr. Sci.* 310, 13–19.
- Robeson, L.M., 1991. Correlation of separation factor versus permeability for polymeric membranes. *J. Membr. Sci.* 62, 165–185.
- Robeson, L.M., 2008. The upper bound revisited. *J. Membr. Sci.* 320, 390–400.
- Rowe, B.W., Robeson, L.M., Freeman, B.D., Paul, D.R., 2010. Influence of temperature on the upper bound: Theoretical considerations and comparison with experimental results. *J. Membr. Sci.* 360, 58–69.
- Schäfer, T., Rodríguez, C.M., Afonso, C.A.M., Crespo, J.G., 2001. Selective recovery of solutes from ionic liquids by pervaporation—a novel approach for purification and green processing. *Chem. Commun.* 1622.
- Schlosser, S., Kossaczky, E., 1975. In: Pertraction through liquid membrane. Proc. 5th Int. Congress CHISA, Prague.
- Scovazzo, P., 2009. Determination of the upper limits, benchmarks, and critical properties for gas separations using stabilized room temperature ionic liquid membranes (SILMs) for the purpose of guiding future research. *J. Membr. Sci.* 343, 199–211.
- Scovazzo, P., Kieft, J., Finan, D.A., Koval, C., DuBois, D., Noble, R., 2004. Gas separations using non-hexafluorophosphate anion supported ionic liquid membranes. *J. Membr. Sci.* 238, 57–63.
- Scovazzo, P., Havard, D., McShea, M., Mixon, S., Morgan, D., 2009. Long-term, continuous mixed-gas dry fed CO₂/CH₄ and CO₂/N₂ separation performance and selectivities for room temperature ionic liquid membranes. *J. Membr. Sci.* 327, 41–48.
- Seader, J.D., Henley, E.J., Roper, D.K., 2013. *Separation Process Principles*, 3rd ed. (978-0-470-48183-7).

- Simons, K., Nijmeijer, K., Bara, J.E., Noble, R.D., Wessling, M., 2010. How do polymerized room-temperature ionic liquid membranes plasticize during high pressure CO₂ permeation? *J. Membr. Sci.* 360, 202–209.
- Smart, S., Lin, C.X.C., Ding, L., Thambimuthu, K., Diniz da Costa, J.C., 2010. Ceramic membranes for gas processing in coal gasification. *Energy Environ. Sci.* 3, 268–278.
- Tang, J., Tang, H., Sun, W., Radosz, M., Shen, Y., 2005. Poly(ionic liquid)s as new materials for CO₂ absorption. *J. Polym. Sci. Polym. Chem.* 43, 5477–5489.
- Tao, Y., Liu, J., Hu, X., Li, H., Wang, T., Jiang, G., 2009. Hollow fiber supported ionic liquid membrane microextraction for determination of sulfonamides in environmental water samples by high-performance liquid chromatography. *J. Chromatogr. A* 1216, 6259–6266.
- Thongsukmak, A., Sirkar, K.K., 2007. Pervaporation membranes highly selective for solvents present in fermentation broths. *J. Membr. Sci.* 302, 45–58.
- Voss, B.A., Bara, J.E., Gin, D.L., Noble, R.D., 2009. Physically gelled ionic liquids: Solid membrane materials with liquid like CO₂ gas transport. *Chem. Mater.* 21, 3027–3029.
- Yang, X.J., Fane, A.G., Bi, J., Griesser, H.J., 2000. Stabilization of supported liquid membranes by plasma polymerization surface coating. *J. Membr. Sci.* 168, 29–37.
- Zha, F.F., Fane, A.G., Fell, C.J.D., 1995. Instability mechanism of supported liquid membranes in phenol transport process. *J. Membr. Sci.* 107, 59–74.
- Zidi, C., Tayeb, R., Ali, M.B.S., Dhahbi, M., 2010. Liquid–liquid extraction and transport across supported liquid membrane of phenol using tributyl phosphate. *J. Membr. Sci.* 360, 334–340.

Membrane contactors

Patricia Luis

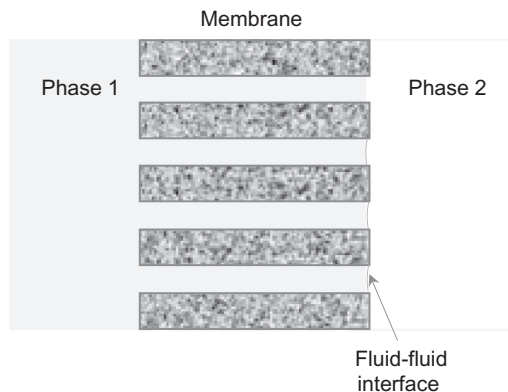
*Materials & Process Engineering (iMMC-IMAP), Catholic University of Louvain,
Louvain-la-Neuve, Belgium*

CHAPTER OUTLINE

5.1 Process Description	153
5.2 Mathematical Description of Mass Transfer in a Membrane Contactor	158
5.2.1 Film Theory and Resistance-in-Series Model	158
5.2.2 Modeling Based on Differential Equations	160
5.3 Membrane-Based Absorption	165
5.3.1 Comments on Membrane Wetting in the Resistance-in-Series Model ..	171
5.3.2 Comments on Membrane Wetting in the Model Based on Differential Equations	172
5.4 Membrane-Based Solvent Extraction	174
5.5 Membrane Distillation-Crystallization	179
5.6 Membrane Emulsification	186
5.7 Contactor Membrane Reactors	196
5.7.1 Interfacial Membrane Contactor	196
5.7.2 Forced Flow Through	199
References	204
Further Reading	208

5.1 PROCESS DESCRIPTION

A membrane contactor is a device containing a ceramic or polymeric porous membrane in which the objective is to promote the contact between two phases. The membrane does not give selectivity to the separation since it is only a physical barrier that separates the two phases. Thus the kind of membrane considered in this Chapter relates to the *Approach ii* according to the classification indicated in [Chapter 1](#). This involves that all compounds could permeate through the membrane without any selective separation. The selectivity of the separation is normally

**FIG. 5.1**

General working principle of a membrane contactor.

obtained by using a separation fluid at the other side of the membrane. Thus the feed stream and the separation fluid will be in contact only through the membrane pores. A schematic diagram can be observed in Fig. 5.1. A membrane contactor is thus a device that achieves gas-liquid or liquid-liquid mass transfer without dispersion of one phase within another. This is accomplished by passing the fluids on opposite sides of a microporous membrane and controlling carefully the pressure difference between both fluids so that one of them is immobilized in the pores of the membrane and the fluid-fluid interface is located at the mouth of each pore. Gabelman and Hwang (1999) elaborated an inspiring review that has become a basic starting point for those that are interesting in this technology. The main role of the membrane is to act as a barrier and to increase the surface for mass transfer exchange between both phases. The main challenge of designing and operating conventional devices is to maximize the mass transfer rate by producing as much interfacial area as possible, and a major disadvantage is the interdependence of the two fluid phases to be contacted, which may lead to the formation of emulsions, foaming, unloading, and flooding. Thus nondispersive contact via a microporous membrane offered by the membrane contactor is a technological alternative to many conventional processes in the industry that overcomes those disadvantages while giving more interfacial area (Gabelman and Hwang, 1999). Table 5.1 presents several conventional processes that can be substituted by membrane contactors. Recognized advantages of using membrane contactors in comparison with a conventional process are more operational flexibility (independent control of fluid flow rates, no emulsions, no flooding at high flow rates, no unloading at low flow rates, no density difference between liquids required, no drop dragging of liquid phase), controlled and known high interfacial area, linear scale-up (modular equipment), compact, and less energy consuming. Membrane contactors typically offer 30 times more area than what is achievable in gas absorbers and 500 times what is obtainable in liquid-liquid extraction columns (Gabelman and Hwang, 1999).

Table 5.1 Conventional unit operations that can be substituted by membrane contactors

Conventional unit operations	Membrane contactors
Scrubbers/Strippers (absorption/desorption)	Membrane strippers/scrubbers
Packed columns, mixer-settler, centrifugal devices (liquid-liquid extraction)	Membrane extractors
Distillation columns, evaporators	Membrane distillation and osmotic distillation
Crystallizers	Membrane crystallizers
High pressure homogenizers	Membrane emulsifiers
Chemical reactors	Contact membrane reactors

Several configurations are proposed when working with membrane contactors, such as flat sheets, capillary membranes, or hollow fiber membranes. However, hollow fiber membranes are the main applied configuration in current research due to the large contact surface that can provide. Sometimes, the membrane contactors found in the market are designed for pressure-driven filtration processes such as microfiltration or ultrafiltration, but they are proposed by researchers to fulfill other applications such as gas absorption or liquid-liquid extraction.

The mass transfer in membrane contactors takes place through the membrane pores thanks to a driving force generated by a difference of concentration (or partial pressure) and/or a difference of temperature. The kind of contacting phases (gas-liquid, liquid-liquid, liquid-solid) and the objective of the separation will determine the basic mechanisms of the driving force. Fig. 5.2 shows a summary of the different applications of membrane contactors as well as the phases involved, the profiles of driving forces, and the main kind of polarization that may occur (Drioli and Curcio, 2004; Curcio and Drioli, 2005).

Membrane distillation and osmotic membrane distillation use distillation process to remove water from a liquid stream in the form of vapor through the membrane pores. Microporous hydrophobic membranes are used, which will prevent membrane wetting, and volatile compounds of the feed solution may be transported through the membrane pores in gas phase due to a temperature and a concentration gradient (partial pressure difference) that acts as the driving force at both sides of the membrane, which depends on the temperature and composition in the layers adjacent to the membrane surface (Curcio and Drioli, 2005; Gryta, 2005). In the case of osmotic distillation, the transport of molecules through the membrane is due to a difference in vapor pressure provided by a low-vapor-pressure solution (normally a very concentrated osmotic solution) on the permeate side of the membrane. Thus the mass transfer will take place from the feed solution to the osmotic solution.

Membrane crystallization is an extension of membrane distillation with the objective of concentrating the salts present in the liquid stream until reaching supersaturation. Then, the concentrated liquid stream is passed through a crystallizer to

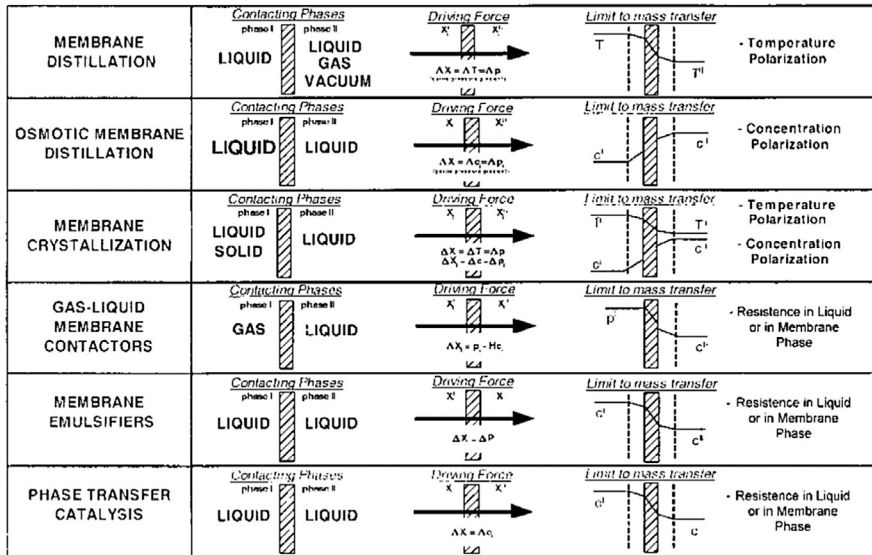


FIG. 5.2

Overview of membrane contactors.

Reprinted with permission from Curcio, E., Enrico, D., 2005. Membrane distillation and related operations—a review. *Sep. Purif. Rev.* 34, 35–86.

produce salt crystals. The presence of the membrane enhances heterogeneous nucleation, although crystals growing should take always place outside the contactor in order to prevent membrane blockage.

Gas-liquid membrane contactors allow the mass transfer from a gas phase stream to a liquid phase (e.g., absorption of CO_2 , SO_2 , NO , H_2S , NH_3 , oxygen removal in semiconductor industry for the production of ultrapure water, carbonation of beverages, nitrogenation of beer to provide a dense foam head, ozonation for water treatment) or from a liquid stream to the gas phase (e.g., removal of trace of oxygen at levels of <10 ppb from water for ultrapure water preparation for the electronics industry, the removal of CO_2 from fermentation broth) (Sengupta et al., 1998; Sirkar, 1995; Curcio and Drioli, 2005). The driving force is difference of concentrations or partial pressures at both sides of the membrane. The membrane pores are expected to be filled by gas so that the mass transfer resistance is lower, which will be determined by the transmembrane pressure.

Uniform emulsions can be produced by using membrane contactors since high-stable droplets are created by forcing the dispersed phase through the pores of the membrane, reducing energy input and wall shear stress with respect to high-pressure homogenizers and rotor-stator systems (Curcio and Drioli, 2005). In this case, the dispersed phase has to pass through the membrane pores to the dispersing phase. Thus considerations on how important is to avoid or at least minimize membrane

wetting, which are critical for the other systems based on membrane contactors, are not relevant in membrane emulsifiers. Membrane emulsification increases the stability of the emulsion and decreases coalescence phenomena. In addition, the droplet size can be easily controlled since it is directly related to the size of the membrane pores. Applications of membrane emulsification are mainly found in the preparation of food emulsions.

Finally, membrane contactors are also used to perform chemical reactions. Contactor membrane reactors are used to intensify the contact between reactants. The system may have a membrane which can be used as a barrier to separate two fluid phases, for example, two reactants or the reactants from an extracting agent, with the catalyst in solution or within the membrane pores (interfacial contactor); or it can work with the mixed reactants being pushed through the membrane pores, where the reaction will take place (forced flow-through contactor). The product will hence be collected at the other side of the membrane. A typical application of contactor membrane reactors is in phase transfer catalysis operations. The catalytically active phase deposited on the surface of inorganic membrane layers promotes the reaction between absorbed reactant species. A phase transfer catalyst is used to transfer a reactant from one phase into the other, allowing the reaction to occur (Drioli and Romano, 2001; Curcio and Drioli, 2005).

In membrane contactors, the membrane pores are typically filled by one of the two fluid phases. The fluid phase that will fill the membrane pores will be determined by the breakthrough pressure. The breakthrough pressure is the minimum pressure required for one phase to go through the membrane pores to the other side of the membrane. This pressure is calculated assuming that the pores are ideal cylinders (Charcosset et al., 2004):

$$P_c = \frac{4\gamma \cos\theta}{\bar{d}_p} \quad (5.1)$$

where P_c is the breakthrough pressure, γ the interfacial tension, θ the contact angle of the liquid to wet the membrane, and \bar{d}_p the average pore diameter. If the transmembrane pressure is greater than the breakthrough pressure, the liquid will go through the membrane pores. Eq. (5.1) is not considering tortuosities in the pores, irregularities in the pore openings at the membrane surface, or effects of surface wettability. Thus the value predicted by Eq. (5.1) may be lower than the real one. The pressure difference has to be always lower than the breakthrough pressure unless the intention is to have the fluid going through the membrane as happens in membrane emulsification or in forced flow-through contactors. In membrane-based absorption, for example, membrane wetting is a nuisance and the gas phase is desired to be inside the pores of the membrane so that diffusion through the membrane pores is easier. Thus a good control of pressures is an important aspect in membrane contactors to ensure the stability of the phases in the system.

Membrane contactors are becoming a powerful technology with a large number of applications that includes gas-liquid, liquid-liquid, and liquid-liquid-solid systems. The main reason is the flexibility found in the kind of membranes that can

be used. The membrane acts merely as a barrier. No selectivity or separation is expected from the membrane, which means that only mechanical and chemical resistance is demanded. The driving force is achieved by using selective solvents, vacuum, sweep gas, osmotic solutions, and so on, depending on the system. Thus the membrane is never a limitation in terms of performance (although wetting and other operation issues may appear) and the researcher/user faces a tremendous freedom to develop new systems and applications. In the following subsections, specific aspects related to the general mathematical description of mass transfer in hollow fiber membrane contactors as well as specific aspects to consider in membrane-based absorption, membrane-based extraction, membrane distillation-crystallization, membrane emulsification, and contactor membrane reactors are presented.

5.2 MATHEMATICAL DESCRIPTION OF MASS TRANSFER IN A MEMBRANE CONTACTOR

The description of the mass transfer in a hollow fiber membrane contactor can be done by following different approaches. Assuming that the resistance to mass transfer is occurring only in films of fluid close to the membrane interface as well as in the membrane itself leads to a very simple model called the resistance-in-series model. Each resistance, that is, the resistances in the feed phase, the membrane, and the receptive phase, is represented by the inverse of a mass transfer coefficient, and the overall resistance by the inverse of an overall mass transfer coefficient. This model assumes linear profiles of concentration and thermodynamic equilibrium at the fluid-fluid interfaces within the membrane pores. More complex models can be developed if the concentration profiles are described by a differential mass balance in portion of fluids or even within the membrane. The following lines show a brief description of those possibilities.

5.2.1 FILM THEORY AND RESISTANCE-IN-SERIES MODEL

The film theory has been extensively applied to describe the mass transfer in systems in which fluid phases are present. The theory considers that the resistance to mass transfer in a given turbulent fluid phase is present in a thin layer adjacent to the interface that is called a film (Seader et al., 2011). In gas-liquid and liquid-liquid separation processes, the mass transfer resistance in both phases has to be considered, and the presence of a membrane introduces a third phase to be also evaluated. An example is shown in Fig. 5.3A for a gas-liquid interface where the component in fluid A diffuses into fluid B. If two films are considered (one for each fluid phase), one speaks about the double-film theory (Fig. 5.3B). When a porous membrane is present in between the two fluid phases, as happens in a membrane contactor, the same approach can be considered. In this case, the film is adjacent to the fluid-membrane interface, as represented in Fig. 5.3C.

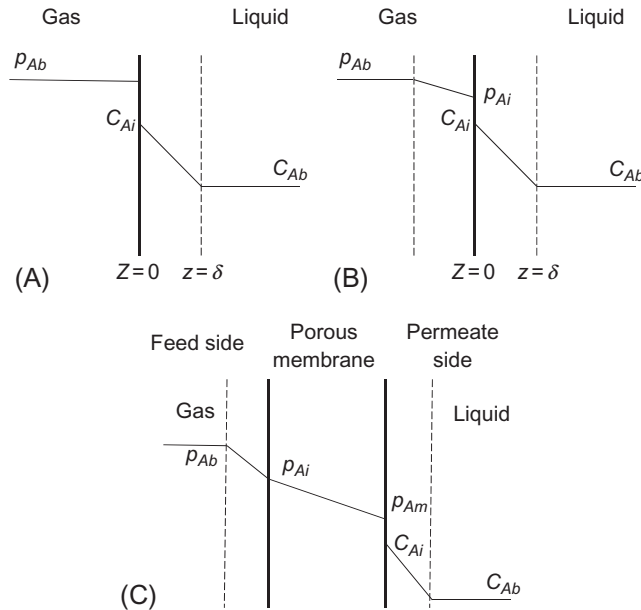


FIG. 5.3

Concentration and partial pressure profiles for solute transport through membranes: (A) film theory; (B) double-film theory; (C) double-film theory with a membrane in between the fluid phases.

At the interface, phase equilibrium is assumed. Thus a solubility relationship like Henry's law for gas-liquid systems ($H_A = c_A/p_A$), or a partition coefficient for liquid-liquid systems ($P = c_A/c_A'$), can be considered. Molecular diffusion occurs through the film of thickness δ with a driving force $c_{Ai} - c_{Ab}$, where c_{Ab} is the bulk average concentration of A in the receiving fluid phase in Fig. 5.3A. Thus applying and integrating the Fick's first law gives:

$$J_A = \frac{D_{AB}}{\delta} (c_{Ai} - c_{Ab}) = \frac{c \cdot D_{AB}}{\delta} (x_{Ai} - x_{Ab}) \quad (5.2)$$

If the film theory is extended to two films in series, each film presents a resistance to mass transfer but the concentrations in the two fluids at the interface are assumed to be in phase equilibrium. Considering steady-state mass transfer of A from a gas, across the gas-liquid interface, and into a liquid, the mass transfer can be written in the same way as Eq. (5.2). Normally, the ratio $\frac{D_{AB}}{\delta}$ is unknown since the thickness of the films depends on the flow conditions, and is replaced by a mass transfer coefficient for each film, which considers the mass transfer resistance of each film. This approach is the basis of the resistance-in-series model since each film of fluid and the membrane produces a specific resistance, represented by the inverse of the individual mass transfer coefficients. Thus

$$J_A = k_g(p_{Ab} - p_{Ai}) \quad (5.3a)$$

$$J_A = k_l(c_{Ai} - c_{Ab}) \quad (5.3b)$$

c_{Ai} and p_{Ai} are the concentration of the component A at the interface, in the liquid and gas side, respectively. They are related by the Henry's law since it is considered that they are in equilibrium: $c_{Ai} = H_A p_{Ai}$. Substituting the Henry's law relationship in Eq. (5.3b) to eliminate c_{Ai} , and introducing the resulting expression in Eq. (5.3a), gives:

$$J_A = \frac{p_{Ab}H_A - c_{Ab}}{(H_A/k_g) + (1/k_l)} \quad (5.4)$$

If a membrane is separating the two fluid phases as in Fig. 5.3C, Eqs. (5.3a), (5.3b) should be completed with a third equation that describes the mass transfer through the membrane (assuming gas in the pores):

$$J_A = k_m(p_{Ai} - p_{Am}) \quad (5.3c)$$

The equilibrium at the gas-liquid interface is given by $c_{Ai} = H_A p_{Am}$. Thus following the same substitution procedure, Eq. (5.4) would become:

$$J_A = \frac{p_{Ab}H_A - c_{Ab}}{(H_A/k_g) + (1/k_m) + (1/k_l)} \quad (5.5)$$

The overall mass transfer coefficient, $K_{overall}$, can be thus defined as

$$\frac{1}{K_{overall}} = \frac{H_A}{k_g} + \frac{1}{k_m} + \frac{1}{k_l} \quad (5.6)$$

Eq. (5.5) can be written as

$$J_A = K_{overall}(p_{Ab}H_A - c_{Ab}) \quad (5.7)$$

which is a very practical way to evaluate the mass transfer through the membrane since the bulk concentrations, p_{Ab} and c_{Ab} , are known. Eq. (5.6) is the basis of the resistance-in-series model. Each term of the equation represents one resistance to mass transfer, thus the overall resistance, $\frac{1}{K_{overall}}$, is the result of the sum of the resistances given by the gas phase (R_g), the membrane (R_m), and the liquid phase (R_l):

$$R_{overall} = R_g + R_m + R_l \quad (5.8)$$

The mathematical description shown previously is an example of mass transfer in a gas-liquid system with pores filled with gas. A more detailed explanation is included in the specific sections of this chapter.

5.2.2 MODELING BASED ON DIFFERENTIAL EQUATIONS

The mass transfer takes place through the membrane pores and no mixing between phases occurs. The fluid flow in the membrane contactor can be described using the laminar flow model in the tube side and the Happel's free surface model (Happel, 1959) in the shell side. The Happel's free surface model assumes that the fibers

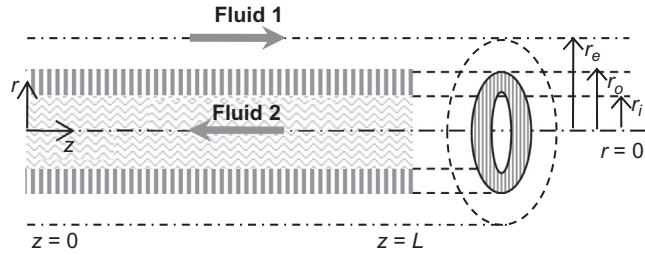


FIG. 5.4

Axial and radial coordinates of a fiber.

Reproduced with permission from Luis, P., Garea, A., Irbaien, A., 2010. Modelling of a hollow fiber ceramic contactor for SO₂ absorption. *Sep. Purif. Technol.* 72, 174–179.

are distributed evenly through the shell space, which allows the results obtained with a single fiber to be generalized to the entire module (Gabelman and Hwang, 1999). The coordinates of a fiber are shown in Fig. 5.4. The radial position of $r=0$ is the center of a fiber and the radial distances r_i , r_o , and r_e are the inner radius, outer radius, and Happel's free distance of the fiber. The axial distance of $z=0$ means the inlet position of a fiber and the axial distance of $z=L$ represents the outlet position of a fiber. One fluid phase is fed to the shell side at $z=0$ and the other fluid phase is passed through the tube side at $z=L$. It is assumed that local equilibrium at the fluid-fluid interface takes place and mass transfer is only produced by diffusion.

Shell side

In order to describe the mass transfer in the shell side of the fiber, the following assumptions can be considered: (1) steady state and isothermal condition, (2) no axial diffusion, (3) using Happel's free surface model (Happel, 1959) to characterize the velocity profile at the shell side, (4) the physical properties of the fluid were constant, (5) constant shell side pressures. Based on the Happel's free surface model (Happel, 1959), only a portion of the fluid surrounding the fiber is considered, which may be approximated as a circular cross section.

The partial differential equation of the mass balance for cylindrical coordinates is obtained using Fick's law of diffusion and it is given as follows:

$$u_{z,g} \frac{\partial C_{A,feed}}{\partial z} = D_{A,feed} \left[\frac{1}{r} \frac{\partial}{\partial r} \left(r \frac{\partial C_{A,feed}}{\partial r} \right) \right] \quad (5.9)$$

The velocity profile in the shell side may be deduced from the Happel's free surface model (Happel, 1959):

$$u_{z,g} = u_{\max,g} \cdot f(r) = 2u_{m,g} \cdot f(r) \quad (5.10)$$

$$f(r) = \left[1 - \left(\frac{r_o}{r_e} \right)^2 \right] \cdot \left[\frac{\left(\frac{r}{r_e} \right)^2 - \left(\frac{r_o}{r_e} \right)^2 + 2 \cdot \ln \left(\frac{r_o}{r} \right)}{3 + \left(\frac{r_o}{r_e} \right)^4 - 4 \cdot \left(\frac{r_o}{r_e} \right)^2 + 4 \cdot \ln \left(\frac{r_o}{r_e} \right)} \right] \quad (5.11)$$

where r_e is the free surface radius defined as:

$$r_e = \left(\frac{1}{\varphi}\right)^{0.5} \cdot r_o \quad (5.12)$$

and φ is the fiber packing density, calculated as:

$$\varphi = \frac{n \cdot r_o^2}{r_{cont}^2} \quad (5.13)$$

where n is the number of fibers and r_{cont} is the radius of the hollow fiber contactor. The boundary conditions are the following.

$$r = r_e, \quad \frac{\partial C_{A,feed}}{\partial r} = 0; \quad (\text{symmetry condition}) \quad (5.14a)$$

$$r = r_o, \quad D_{A,feed} \frac{\partial C_{A,feed}}{\partial r} = k_m \cdot S \cdot (C_{A,feed} - C_A^*); \quad (5.14b)$$

$$z = 0, \quad C_{A,feed} = C_{A,in} \quad (5.14c)$$

where $D_{A,feed}$ is the diffusion coefficient of component A in the feed phase, S is a geometric factor based on the outer radius, and C_A^* is the concentration of component A in the feed phase in equilibrium with the receiving phase at the membrane-liquid interface.

According to Eq. (5.14b), the mass transfer through the membrane is described in terms of a mass transfer coefficient (k_m) which involves the assumption of a single resistance of the membrane and linear profile of concentration through the thickness of the membrane.

The differential mass balance in Eq. (5.9) can be converted to dimensionless by introducing the following dimensionless variables (Luis et al., 2010):

$$\theta = \frac{r}{r_o}, \quad \bar{z} = \frac{z}{L}, \quad \bar{C}_A = \frac{C_{A,feed}}{C_{A,in}} \quad (5.15a)$$

$$Sh_m = \frac{k_m \cdot S \cdot r_o}{D_{A,feed}} \quad (\text{Sherwood number}) \quad (5.15b)$$

$$Gz_{ext} = \frac{u_{m,g} d_o^2}{D_{A,feed} L} \quad (\text{Graetz number in the shell side, with } d_o = 2r_o) \quad (5.15c)$$

The resulting dimensionless mass balance and boundary conditions are:

$$\frac{Gz_{ext}}{2} \cdot f(\bar{r}) \cdot \frac{\partial \bar{C}_A}{\partial \bar{z}} = \frac{1}{\theta} \frac{\partial}{\partial \theta} \left(\theta \frac{\partial \bar{C}_A}{\partial \theta} \right) \quad (5.16)$$

$$f(\bar{r}) = \left[1 - \left(\frac{r_o}{r_e} \right)^2 \right] \cdot \left[\frac{\left(\frac{\bar{r} \cdot r_o}{r_e} \right)^2 - \left(\frac{r_o}{r_e} \right)^2 + 2 \cdot \ln \left(\frac{1}{\bar{r}} \right)}{3 + \left(\frac{r_o}{r_e} \right)^4 - 4 \cdot \left(\frac{r_o}{r_e} \right)^2 + 4 \cdot \ln \left(\frac{r_o}{r_e} \right)} \right] \quad (5.17)$$

$$\theta = \frac{r_e}{r_o}, \quad \frac{\partial \bar{C}_A}{\partial \theta} = 0 \quad (5.18a)$$

$$\theta = 1, \quad \frac{\partial \bar{C}_A}{\partial \theta} = Sh_m \cdot (\bar{C}_A - \bar{C}_{A,rec}) \quad (5.18b)$$

$$\bar{z} = 0, \quad \bar{C}_A = 1 \quad (5.18c)$$

Inside the fiber

Inside the fiber or lumen side, the following assumptions can be considered: (1) Steady state and isothermal condition, (2) no axial diffusion, (3) fully developed parabolic velocity profile in the hollow fiber, (4) the physical properties of the fluid were constant, and (5) constant tube side pressure. Considering these assumptions, the mass conservation equation inside hollow fibers is given as (Bird et al., 2002):

$$u_{z,l} \frac{\partial C_{A,rec}}{\partial z} = D_{A,rec} \left[\frac{1}{r} \frac{\partial}{\partial r} \left(r \frac{\partial C_{A,rec}}{\partial r} \right) \right] \quad (5.19)$$

When the velocity is fully developed in a laminar flow, the axial velocity can be written as.

$$u_{z,l} = u_{\max,l} \left[1 - \left(\frac{r}{r_i} \right)^2 \right] = 2u_{m,l} \left[1 - \left(\frac{r}{r_i} \right)^2 \right] \quad (5.20)$$

Eq. (5.19) can be rewritten as:

$$2u_{m,l} \left[1 - \left(\frac{r}{r_i} \right)^2 \right] \frac{\partial C_{A,rec}}{\partial z} = D_{SO_2,l} \left[\frac{1}{r} \frac{\partial}{\partial r} \left(r \frac{\partial C_{A,rec}}{\partial r} \right) \right] \quad (5.21)$$

The boundary conditions are the following.

$$r = 0, \quad \frac{\partial C_{A,rec}}{\partial r} = 0 \quad (\text{symmetry condition}) \quad (5.22a)$$

$$r = r_i, \quad D_{SO_2,l} \frac{\partial C_{A,rec}}{\partial r} = D_{SO_2,g} \frac{\partial C_{A,rec}}{\partial r} \quad (5.22b)$$

$$z = L, \quad C_{A,rec} = 0 \quad (5.22c)$$

where $D_{A,rec}$ is the diffusion coefficient of the component A in the receiving phase. It is assumed that the receiving phase does not have or have a negligible quantity of component A at the inlet of the contactor ($z=L$).

The bulk average or “mixing cup” values of component A concentration in the receiving phase at $z=0$ (contactor outlet) is defined as.

$$C_{A,z=0} = \frac{\int_0^{r_i} C_{A,rec} u_{z,l} 2\pi r dr}{\int_0^{r_i} u_{z,l} 2\pi r dr} = \frac{4}{r_i^2} \int_0^{r_i} C_{A,rec} \left[1 - \left(\frac{r}{r_i} \right)^2 \right] r dr \quad (5.23)$$

The previous model equations can be rewritten in the dimensionless form as.

$$\frac{Gz_{int}}{2} [1 - \bar{r}^2] \frac{\partial \bar{C}_{A,rec}}{\partial \bar{z}} = \frac{1}{\bar{r}} \frac{\partial}{\partial \bar{r}} \left(\bar{r} \frac{\partial \bar{C}_{A,rec}}{\partial \bar{r}} \right) \quad (5.24)$$

with the boundary conditions.

$$\bar{r} = 0, \quad \frac{\partial \bar{C}_{A,rec}}{\partial \bar{r}} = 0 \quad (5.25a)$$

$$\bar{r} = 1, \quad \frac{\partial \bar{C}_{A,rec}}{\partial \bar{r}} = \frac{\partial \bar{C}_A}{\partial \bar{r}} \cdot \frac{D_{A,feed}}{D_{A,rec}} \cdot H \quad (5.25b)$$

$$\bar{z} = 1, \quad \bar{C}_{A,rec} = 0 \quad (5.25c)$$

where the dimensionless variables are defined as.

$$\bar{r} = \frac{r}{r_i}, \quad \bar{z} = \frac{z}{L}, \quad \bar{C}_A = \frac{C_A}{C_{A,sat}} \quad (5.26a)$$

$$Gz_{int} = \frac{u_{m,l} d_i^2}{D_{A,rec} L} \quad (\text{Graetz number in the tube side, with } d_i = 2r_i) \quad (26b)$$

The dimensionless mixing cup may be also rewritten as.

$$\bar{C}_{A,rec, \bar{z}=0} = 4 \int_0^1 \bar{C}_{A,rec} [1 - \bar{r}^2] \bar{r} d\bar{r} \quad (5.27)$$

Membrane

The following equation can be used to describe the mass transport through the membrane, which considers that diffusion is the only mechanism for mass transport (Faiz and Al-Marzouqi, 2009):

$$D_{i,membrane} \left[\frac{\partial^2 C_{i,membrane}}{\partial r^2} + \frac{1}{r} \frac{\partial C_{i,membrane}}{\partial r} + \frac{\partial^2 C_{i,membrane}}{\partial z^2} \right] = 0 \quad (5.28)$$

The diffusion coefficient inside the membrane pores, $D_{i,membrane}$, is defined as an effective diffusion in order to account for the membrane's porosity, ε , and tortuosity, τ :

$$D_{i,membrane} = \frac{D_i \cdot \varepsilon}{\tau} \quad (5.29)$$

The boundary conditions are given as.

$$\text{At } r = R_1, C_{i, \text{membrane}} = \frac{C_{i, \text{lumen}}}{m_i} \quad (5.30a)$$

$$\text{At } r = R_2, C_{i, \text{membrane}} = C_{i, \text{shell}} \quad (5.30b)$$

where m_i is the solubility of the component i in the receiving phase.

The mathematical description included in this section is a general way to account for the mass transfer that take place from the feed phase to the receiving phase through a porous membrane. Nevertheless, the kind of fluid (gas or liquid) and the kind of species to be transported generate specificity in the system. The next sections include particular aspects to consider for each kind of application in a membrane contactor.

5.3 MEMBRANE-BASED ABSORPTION

Using a membrane contactor to separate a gas-liquid interface is considered as a clean technology since dragging of drops of solvent is avoided. Solvent losses are thus reduced, gas and liquid flow rates can be independently controlled and a determined interfacial area is obtained. Normally, a hollow fiber contactor is used with gas and liquid flowing on opposite sides of the membrane. The fluid-fluid interface is formed at the mouth of the membrane pores. In order to keep that interface immobilized and stable and to work under conditions of no membrane wetting, a very small pressure drop across the membrane is required. A small overpressure may be needed at the gas phase so that membrane wetting is minimized, or at the liquid phase in order to avoid bubbling of gas into the liquid. The breakthrough pressure given by Eq. (5.1) should be taken into account. The membrane material and kind of solvent will determine the best operating conditions. In order to fill the pores with gas, hydrophobic membranes should be used when the absorption solvent is hydrophilic (e.g., a hydrophobic polymeric contactor for CO₂ capture using aqueous solutions) (El-Naas et al., 2010) and hydrophilic membranes with hydrophobic solvents (e.g., a hydrophilic ceramic contactor for SO₂ capture using *N,N*-dimethylaniline) (Luis et al., 2008). The liquid gives selectivity to the separation and it should have good chemical compatibility with the exposed materials and avoid membrane wettability in order to ensure a long-term application. Toxicity and volatility are also key aspects to be considered when selecting the solvent since if the solvent is very volatile, it will tend to go to the gas phase even if the liquid-gas contact takes place within the pores of the membrane. Ideal solvents are thus those with high affinity for the target compound, low volatility, and low (or none) toxicity. The desorption or recovery step that follows the absorption is also a critical point in the design of the overall process. If thermal absorption is considered, the solvent should have low heat of absorption to decrease the energy during regeneration. If a solid product is envisaged, such as

carbonates or bicarbonates, posttreatment of the precipitated solid should be considered. An integrated approach using membrane contactors has been proposed in the literature in order to capture carbon dioxide and produce pure crystals of sodium carbonate. Membrane-based absorption and membrane distillation-crystallization have been integrated to achieve this purpose (Ye et al., 2013, 2016; Li et al., 2016; Ruiz-Salmón et al., 2017; Ruiz-Salmón and Luis, 2018). Indeed, one application of membrane contactors in gas-liquid systems that is currently leading the research on this technology is capture of carbon dioxide, mainly for postcombustion capture (i.e., CO₂/N₂ separation). CO₂ is transferred from the gas phase through the porous membrane to the liquid phase due to a driving force based on differences in concentration. Examples of absorption solvents used for CO₂ capture in membrane contactors are diethylamine (DEA), monoethylamine (MEA), aqueous solutions of alkaline salts, amino acids, or enzymes. Other applications are removal of other acid gases from gas streams (e.g., SO₂, H₂S) or volatile organic compounds.

The core of the experimental system to perform membrane-based absorption is the membrane contactor. Fig. 5.5 shows a typical experimental setup. The gas and liquid streams are introduced (normally) in countercurrent. Mass flow controllers can be used to control accurately the flow rate of the gas phase. The gas may flow inside the pores and the liquid outside or vice versa. The liquid phase can be recycled, taking into account that a pseudo steady state can be achieved. The gas phase is analyzed at the outlet of the contactor as well as the liquid phase, if required to check the mass balance. Some pretreatment of the gas phase may be required prior to be sent to the analyzer in order to eliminate interferences in the measurements, mainly if a volatile solvent is used.

The transmembrane flux can be calculated for the gas and the liquid phases according to these equations:

$$J_{A,g} = \frac{Q_g}{A} (C_{A,g}^{IN} - C_{A,g}^{OUT}) \quad (5.31a)$$

$$J_{A,l} = \frac{V_L}{A \cdot \Delta t} (C_{A,l,t+\Delta t} - C_{A,l,t}) \quad (5.31b)$$

where Q_g is the gas flow rate, A is the membrane area, and V_L is the total volume of absorption liquid in the system. Since the liquid is recycled into the process, $J_{A,l}$ is calculated considering the experimental concentration in a period of time Δt . At steady state, both gas and liquid fluxes should be equal. The mass transfer takes place by diffusion across the interface and the driving force for separation is a concentration gradient based on the solubility of the gas component into the liquid phase. As indicated in Section 5.2, the mass transfer through the membrane can be described by definition of an overall mass transfer coefficient, $K_{overall}$. This coefficient can be experimentally evaluated from the flux through the membrane calculated from Eqs. (5.31a) or (5.31b). Since $J_{A,g} = J_{A,l} = J_A$:

$$K_{overall} = \frac{J_A}{\Delta y_{lm} (P_T / RT)} \quad (5.32)$$

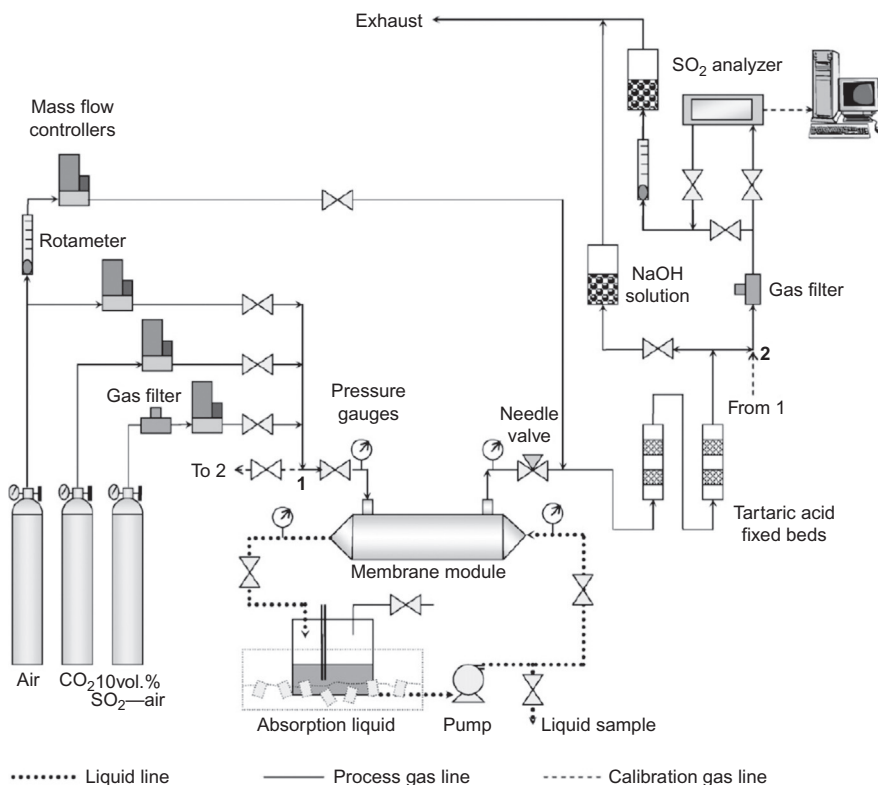


FIG. 5.5

Experimental setup for membrane-based gas absorption. Example of removal of SO_2 from a gas stream using dimethylaniline. Beds of tartaric acid are used to remove traces of solvent found in the gas stream before analysis.

Reproduced with permission from Luis, P., Gara, A., Irbien, A., 2009. Zero solvent emission process for sulfur dioxide recovery using a membrane contactor and ionic liquids. *J. Membr. Sci.* 330, 80–89.

P_T is the total pressure in the gas phase and Δy_{lm} is the logarithmic mean of the driving force based on gas phase molar fractions and taking into account the concentration of i at the inlet ($y_{i(g),in}$) and the outlet ($y_{i(g),out}$) of the contactor:

$$\Delta y_{lm} = \frac{(y_{i(g),in} - y_{in}^*) - (y_{i(g),out} - y_{out}^*)}{\ln \left(\frac{y_{i(g),in} - y_{in}^*}{y_{i(g),out} - y_{out}^*} \right)} \quad (5.33)$$

If the concentration of i in the liquid phase is very far from the saturation value, y_{in}^* and y_{out}^* in Eq. (5.33) can be considered negligible since the influence of the gas-liquid equilibrium is insignificant.

The removal efficiency of the target compound i (%) is defined by the following equation:

$$\text{Removal efficiency} = \left(1 - \frac{C_{A,g}^{OUT}}{C_{A,g}^{IN}} \right) \quad (5.34)$$

The removal efficiency together with the transmembrane flux gives information on the process performance. On the other hand, the overall mass transfer coefficient allows evaluating the membrane performance. Thus evaluating the overall mass transfer coefficient is of utmost interest to determine the degree of application of this technology and to compare with conventional absorption systems (absorption columns). In addition, the overall mass transfer coefficient will have a direct impact on the membrane area required for the separation. Fig. 5.6 shows an example for CO₂ capture. The higher the mass transfer coefficient, the lower the area. Overall mass transfer coefficients ranging between 10⁻⁵ and 10⁻³ m s⁻¹ are common in this technology, involving contactors with a membrane area of around 10⁵–10⁷ m² to capture 10⁵ t CO₂ per year and reaching an outlet gas stream with <0.1 vol% CO₂ (Luis and Van der Bruggen, 2013).

According to Eq. (5.32), if a plot of the transmembrane flux versus the driving force is done, a straight line should be obtained, whose slope is the overall mass transfer coefficient, as shown in Fig. 5.7. If a linear relationship is not obtained, the overall mass transfer coefficient varies with the driving force, which may be due to phenomena of concentration polarization. Physically, it means that a higher

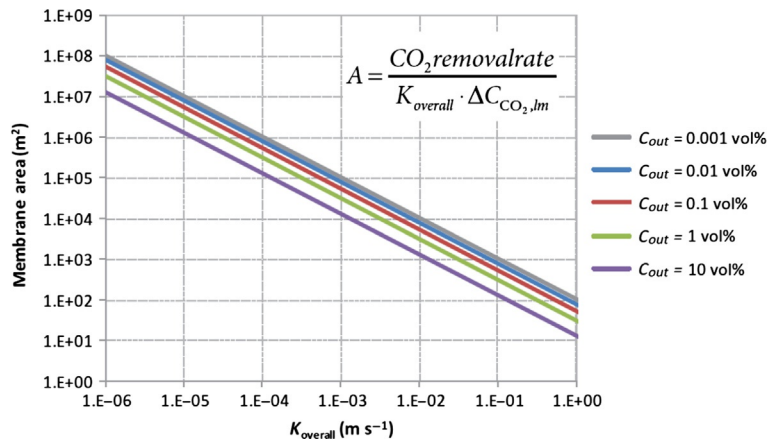
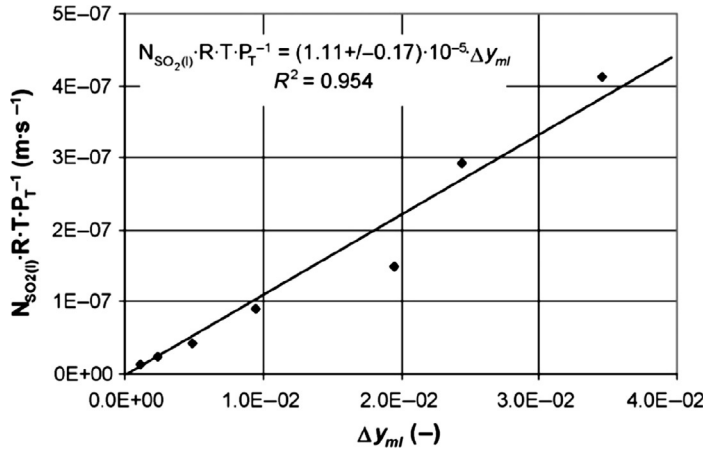


FIG. 5.6

Membrane area versus the overall mass transfer coefficient of a membrane contactor.

C_{out} refers to the concentration (vol%) of CO₂ in the gas product. CO₂ removal rate = 1.105 tons of CO₂ per year (1.61 m³ s⁻¹); feed concentration = 15 vol% CO₂.

Reproduced with permission from Luis, P., Van der Bruggen, B., 2013. The role of membranes in postcombustion CO₂ capture. *Greenhouse Gas Sci. Technol.* 3, 1–20. <https://doi.org/10.1002/ghg>.


FIG. 5.7

Absorption flux ($N_{SO_2(l)}$) versus sulfur dioxide logarithmic mean molar fraction (Δy_{mf}) in a membrane contactor to capture SO_2 using *N,N*-dimethylaniline is used as absorption liquid. Reproduced with permission from Luis, P., Garea, A., Irbien, A., 2009. Zero solvent emission process for sulfur dioxide recovery using a membrane contactor and ionic liquids. *J. Membr. Sci.* 330, 80–89.

driving force does not produce a higher transmembrane flux. Nevertheless, in gas-liquid systems, concentration polarization is less common.

The experimental overall mass transfer coefficient obtained from Eq. (5.32) or graphically as indicated in Fig. 5.7 can be compared with that obtained by applying the resistance-in-series model explained in Section 5.2. In a gas-liquid system, the membrane pores should be filled with gas in order to minimize the mass transfer resistance within the membrane pores. However, membrane wetting may take place, leading to a significant increase of the membrane resistance. The resistance-in-series model splits the overall mass transfer coefficient, $K_{overall}$, as a combination of the membrane mass transfer coefficient, k_{mg} for gas filled pores (nonwetted mode) or k_{ml} for liquid filled pores (wetted mode), and the liquid side, k_l , and gas side, k_g , mass transfer coefficients, according to Fig. 5.8A. Eq. (5.6) in Section 5.2 can be completed by adding the enhancement factor, E , since a chemical reaction in the liquid side takes place ($E = 1$ for physical absorption), and the inner, outer, and mean-logarithmic diameters of the hollow fiber in order to take into account the system geometry (Yang et al., 2006; Luis et al., 2009):

$$\frac{1}{K_{overall}} = \frac{1}{k_g} + \frac{d_o}{k_{mg} \cdot d_{lm}} + \frac{H \cdot d_o}{k_l \cdot d_i \cdot E} \quad \text{Non-wetted mode} \quad (5.35a)$$

or

$$R_{overall,g} = R_g + R_{mg} + R_l \quad (5.35b)$$

The individual mass transfer coefficient for the membrane, k_m , can be calculated as the ratio of an effective diffusivity and the membrane thickness using Eq. (5.36):

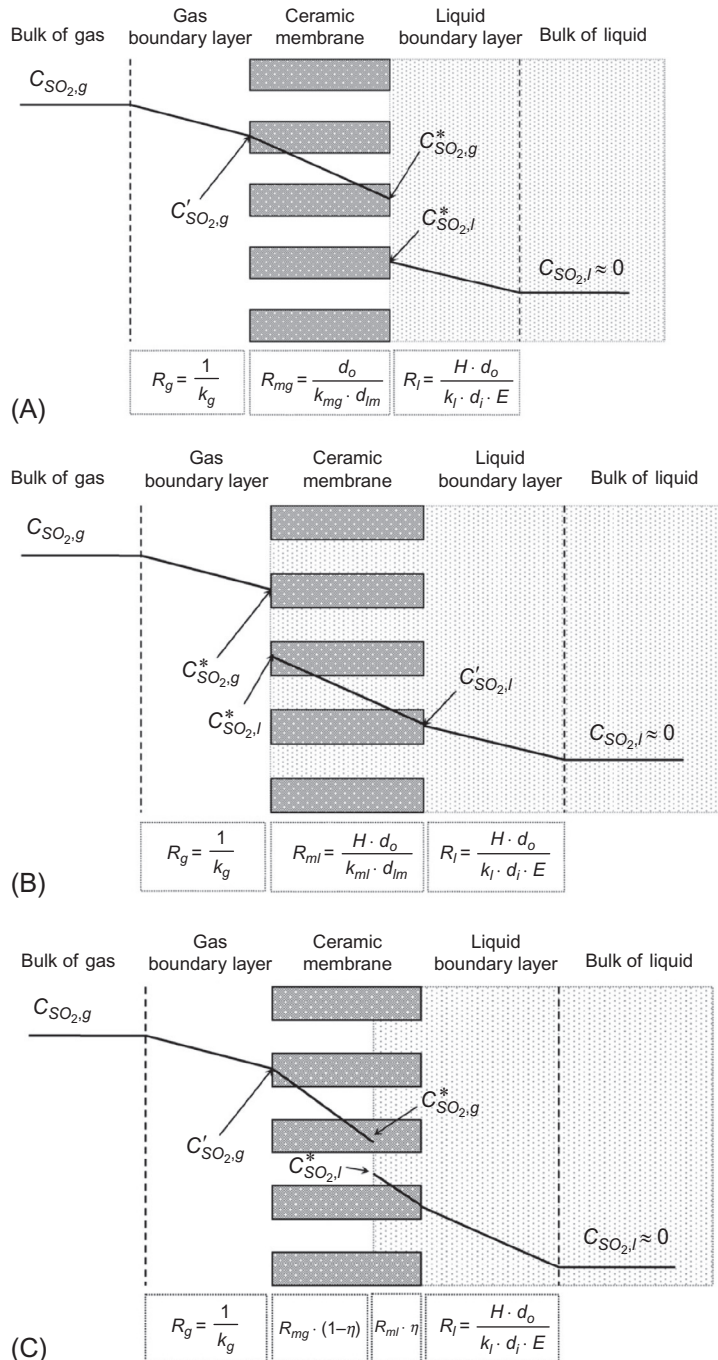


FIG. 5.8

Schematic diagram of mass transfer. Mass transfer through the porous membrane and local concentrations in membrane-based gas absorption of SO₂: (A) nonwetted mode; (B) wetted mode; (C) partially wetted mode.

Reproduced with permission from Luis, P., Garea, A., Irabien, A., 2009. Zero solvent emission process for sulfur dioxide recovery using a membrane contactor and ionic liquids. *J. Membr. Sci.* 330, 80–89.

$$k_{mg} = \frac{D_{eff,g}}{\delta} = \frac{D_{A,g} \cdot \varepsilon}{\tau \cdot \delta} \quad (5.36)$$

Nonwetting is a theoretical situation, thus it is possible to consider that the overall mass transfer coefficient obtained with Eq. (5.35a) is the maximum value. If wetting occurs, the experimental value will be smaller.

For gas flowing outside parallel to the hollow fiber, the mass transfer coefficient in the gas phase can be estimated from (Cussler, 1997)

$$\frac{k_g \cdot d_h}{D_{A,g}} = 1.25 \cdot \left(\frac{d_h^2 \cdot \nu_g}{L \cdot \nu} \right)^{0.93} \cdot \left(\frac{\nu}{D_{A,g}} \right)^{1/3} \quad (5.37)$$

$$d_h = \frac{d_{cont}^2 - n \cdot d_o^2}{n \cdot d_o} \quad (5.38)$$

where d_h is the hydraulic diameter, $D_{A,g}$ is diffusion coefficient in the gas phase, L is the fiber length, and ν is the kinematic viscosity. When the flow inside the hollow fiber is laminar, the mass transfer coefficient in the tube (liquid phase) is given by the L ev equation (Cussler, 1997):

$$\frac{k_l \cdot d_i}{D_{A,l}} = 1.62 \cdot \left(\frac{d_i^2 \cdot \nu_l}{L \cdot D_{A,l}} \right)^{1/3} \quad (5.39)$$

where d_i is the internal fiber diameter, and $D_{A,l}$ is the diffusion coefficient in the liquid phase.

The description of mass transfer by means of differential equations instead of resistance-in-series can be done as indicated in Section 5.2. Some considerations on membrane wetting are included later for both methods.

5.3.1 COMMENTS ON MEMBRANE WETTING IN THE RESISTANCE-IN-SERIES MODEL

The use of membrane contactors has shown typically membrane wetting after some time of operation. Mathematically, one could calculate an individual mass transfer coefficient for the membrane considering that the membrane pores are filled with liquid (Fig. 5.8B). This calculation would lead to the minimum overall mass transfer coefficient. Thus for the wetted mode, the overall mass transfer coefficient is calculated from:

$$\frac{1}{K_{overall}} = \frac{1}{k_g} + \frac{H \cdot d_o}{k_{ml} \cdot d_{lm}} + \frac{H \cdot d_o}{k_l \cdot d_i \cdot E} \quad \text{Wetted mode} \quad (5.40a)$$

or

$$R_{overall,l} = R_g + R_{ml} + R_l \quad (5.40b)$$

where d_o , d_i , and d_{lm} are the outside, inside, and log mean diameters of the hollow fiber. For a porous membrane wetted by the membrane, the mass transfer through the membrane is calculated as the effective diffusion coefficient, D_{eff} , of the absorbing

gas divided by the membrane thickness (Cussler, 1997; Gabelman and Hwang, 1999):

$$k_m = k_{ml} = \frac{D_{eff,l}}{\delta} = \frac{D_{SO_2,l} \cdot \varepsilon}{\tau \cdot \delta} \quad (5.41)$$

However, the real situation may be a partially wetted membrane. In this case, the overall mass transfer coefficient will be a value between the $K_{overall}$ obtained under nonwetted conditions and totally wetted conditions. The mechanism of partial wetting can be used to explain the results according to the method proposed in recent studies (Lu et al., 2005; Lu et al., 2008). It is based on considering that the membrane resistance is a function of the resistance of pores filled with gas and pores filled with liquid. The membrane resistance can be separated in two new resistances according to Eq. (5.38) and Fig. 5.8C:

$$\frac{1}{K_{overall}} = \frac{1}{k_g} + \frac{1}{k_{mg}} \cdot \frac{d_o}{d_{lm}} \cdot (1 - \eta) + \frac{H}{k_{ml}} \cdot \frac{d_o}{d_{lm}} \cdot \eta + \frac{H \cdot d_o}{k_l \cdot d_i \cdot E} \quad \text{Partial wetting} \quad (5.42a)$$

or

$$R_{overall} = R_g + R_{mg} \cdot (1 - \eta) + R_{ml} \cdot \eta + R_l \quad (5.42b)$$

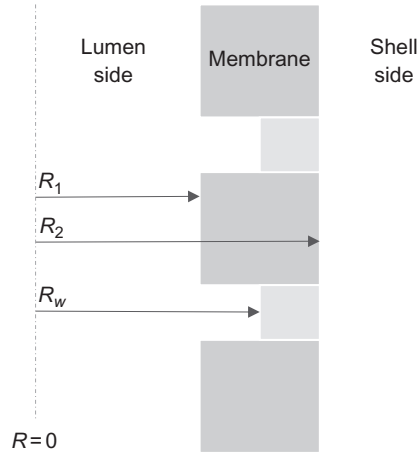
where η is the wetting ratio defined as a ratio of the pore length wetted by liquid to the total length.

An example of this methodology can be found in Luis et al. (2009) for absorption of SO_2 using a ceramic membrane contactor and N,N -dimethylaniline or the ionic liquid 1-ethyl-3-methylimidazolium ethylsulfate ([EMIM][EtSO₄]) as the absorption liquids. The authors found a significant difference between the estimated mass transfer coefficients when pores are filled with gas and the experimental overall mass transfer coefficients when using both solvents. The discussion was focused on partial wetting of the membrane. The wetting fraction η took a value of around 74% and 4% when N,N -dimethylaniline and [EMIM][EtSO₄] were used, respectively. This large difference of wetting depending of the used solvent was explained in terms of difference of viscosity. The ionic liquid has a viscosity of 97.6×10^{-3} Pas (Gómez et al., 2006; Ranke et al., 2007) compared to the viscosity of N,N -dimethylaniline (1.20×10^{-3} Pas), which would make more difficult the wetting of the membrane. In addition, capillary condensation of N,N -dimethylaniline into the pores could increase the wetting phenomenon.

5.3.2 COMMENTS ON MEMBRANE WETTING IN THE MODEL BASED ON DIFFERENTIAL EQUATIONS

If the absorption liquid penetrates into the membrane pores, a mathematical model that considers gas inside the pores will lead to a poor interpretation of the reality. Partial wetting can be considered by dividing the membrane in two sections: a gas-filled section and a liquid-filled section.

Gas-filled section. The material balance for this section can be considered to be due to diffusion in the gas phase (Fig. 5.9):


FIG. 5.9

Schematic diagram of membrane wetting and radial coordinates.

$$D_{i,g-membrane} \left[\frac{\partial^2 C_{i,g-membrane}}{\partial r^2} + \frac{1}{r} \frac{\partial C_{i,g-membrane}}{\partial r} + \frac{\partial^2 C_{i,g-membrane}}{\partial z^2} \right] = 0 \quad (5.43)$$

With the boundary conditions:

$$\text{At } r = R_w, C_{i,g-membrane} = \frac{C_{i,l-membrane}}{m_i} \quad (5.44a)$$

$$\text{At } r = R_2, C_{i,g-membrane} = C_{i,shell} \quad (5.44b)$$

Liquid-filled section. The portion of the membrane wetted by the liquid can be described by considering diffusion and reaction in the liquid phase:

$$D_{i,l-membrane} \left[\frac{\partial^2 C_{i,l-membrane}}{\partial r^2} + \frac{1}{r} \frac{\partial C_{i,l-membrane}}{\partial r} + \frac{\partial^2 C_{i,l-membrane}}{\partial z^2} \right] + R_{i,membrane} = 0 \quad (5.45)$$

The reaction takes place inside the membrane pores. Therefore the porosity should be considered in the reaction term:

$$R_{i,membrane} = R_i \cdot \varepsilon \quad (5.46)$$

The boundary conditions are:

$$\text{At } r = R_1, C_{i,l-membrane} = C_{i,lumen} \quad (5.47a)$$

$$\text{At } r = R_w, C_{i,l-membrane} = C_{i,g-membrane} \cdot m_i \text{ for the absorbed species} \quad (5.47b)$$

$$\frac{\partial C_{i,membrane}}{\partial r} = 0 \text{ for the nonabsorbed species} \quad (5.47c)$$

Alternatively, a mass transfer coefficient k_m whose inverse represents the resistance to mass transfer caused by the membrane can be defined, as indicated in the resistance-in-series model. If membrane pores are assumed to be filled with gas, a theoretical value k_{mg} could be calculated according to Eq. (5.36). The dimensionless equation containing the mass transfer coefficient in the membrane is then represented by the Sherwood number Sh_{mg} :

$$Sh = \frac{k_{mg} S r_o}{D_{A,g}} \quad (5.48)$$

where k_{mg} is the theoretical mass transfer coefficient of the nonwetted membrane. When membrane wetting takes place, the Henry's law coefficient, H , and the fraction of wetting would have to be considered in the calculations. However, there is a lack of certainty in those parameters. A strategy could be to define an "effective" Sherwood number that includes the uncertainty: $Sh_{eff} = Sh/H$.

5.4 MEMBRANE-BASED SOLVENT EXTRACTION

Membrane-based solvent extraction or nondispersive solvent extraction is an alternative of classical solvent extraction where mass transfer between immiscible liquids occurs at the immobilized L-L interface at the mouth of pores of a microporous wall (Schlosser et al., 2005). This technology has been considered as a useful modern technique for metals extraction, recovery and separation of organic acids and isomers, and more generally, in chemical and pharmaceutical technology, biotechnology, food processing, and environmental engineering (Younas et al., 2011; Raynie, 2006; Schlosser et al., 2005; San Román et al., 2010). The solvent has to be regenerated in order to reuse it and recover the solute. The extraction can be done using also membrane contactors and a stripping solution or by other methods such as distillation. Fig. 5.10A shows the principle of membrane-based extraction. The membrane, filled with the solvent, separates effectively the feed solution and the solvent, occurring the transfer of solute through the membrane from the feed to the solvent phase.

Another process that is based on the same principles that membrane-based extraction is pertraction through a liquid membrane where both extraction and stripping of the solute take place in the same equipment (Schlosser et al., 2001, 2005). The liquid membrane can be in the configuration of a supported liquid membrane (the solvent is kept within the membrane pores) (Fig. 5.10B), or as a bulk liquid membrane (Fig. 5.10C), in which the membrane stability is not a problem like when using supported liquid membranes but a higher mass transfer resistance is expected due to a thicker liquid membrane layer between walls (Schlosser et al., 2001).

The mass transfer through the membrane is produced due to several mechanisms: physical solubility of the solutes into the solvent, or chemical or biochemical reactions. To find the appropriate extractant is a difficult task. Several aspects should be fulfilled. First, the complex formed by the solute and extractant has to be soluble in

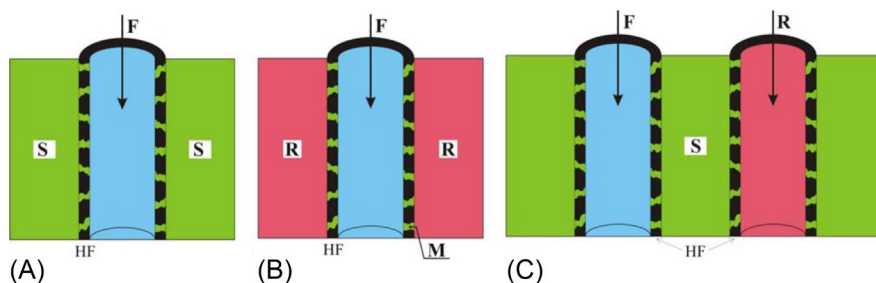


FIG. 5.10

Processes with immobilized L-L interface(s). (A) Membrane-based solvent extraction; (B) pertraction through supported liquid membrane; (C) pertraction through bulk liquid membrane with two immobilized L-L interfaces in a hollow fiber contactor. *F*, feed (donor) phase; *HF*, hollow fiber (microporous, hydrophobic); *M*, membrane phase; *R*, stripping (acceptor) solution; *S*, solvent.

Reproduced with permission from Schlosser, S., Kertész, R., Marták, J., 2005. Recovery and separation of organic acids by membrane-based solvent extraction and pertraction. An overview with a case study on recovery of MPCA. Sep. Purif. Technol. 41, 237–266.

the diluent that forms with the extractant a solvent. The selection of an adequate diluent or addition of a modifier to the solvent could be necessary. The diluent type may have a great influence on the solvent performance. Furthermore, the composition of the feed and its pH can have a significant influence in the transport rate in extraction. If there are components that compete with the target solute(s), the transport rate will decrease. Thus the presence of those compounds should be avoided or kept at minimum concentration. The transport rate will be also decreased by the adsorption of surfactants on the liquid-membrane interface. The kind of the stripping reagent and its concentration in the stripping solution may also affect the process performance. The most important is to have an excess of reagent and to avoid the formation of a boundary layer depleted in the reagent (Schlosser et al., 2005).

A typical experimental setup used in membrane-based liquid extraction is shown in Fig. 5.11. It consists basically of two reservoirs for the feed and extractant solutions and the membrane contactor. Control of the flow rates and pressures is required to evaluate correctly the process performance. Commonly, periodic samples are taken from the feed tank in order to evaluate the variation of concentration over time, which allows calculating the amount of component that is extracted.

The mass transfer analysis in the hollow fiber contactor is based on the Fick's law of diffusion and film theory as explained in Section 5.2. The overall mass transfer coefficient, K_{aq} , is thus the main parameter to be determined:

$$J = K_{aq}A(C_{aq} - C_{aq}^*) \quad (5.49)$$

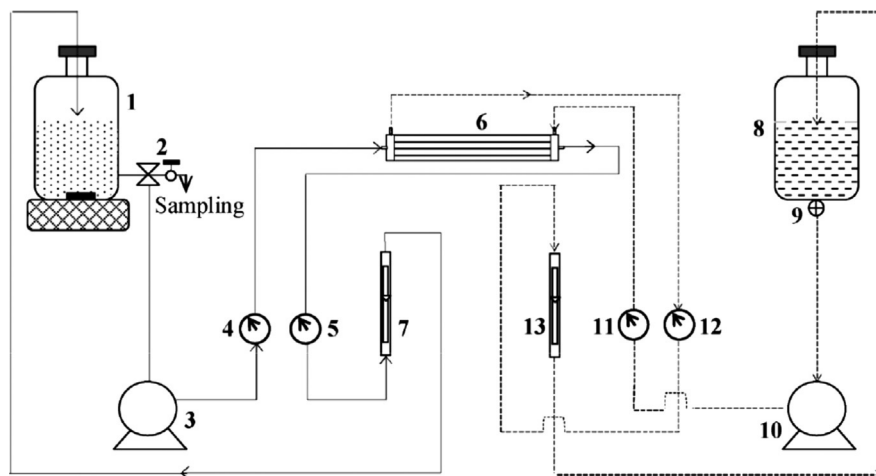


FIG. 5.11

Scheme of a typical experimental setup for membrane-based extraction using a hollow fiber membrane module. (1) SA-water tank with stirrer. (2) Valve and sampling port. (3) Gear pump (lumen side). (4) Pressure gauge (lumen side inlet). (5) Pressure gauge (lumen side outlet). (6) HFMC module. (7) Flowmeter (lumen side). (8) Extractant tank. (9) Flow control valve (extractant tank). (10) Gear pump (shell side). (11) Pressure gauge (shell side inlet). (12) Pressure gauge (shell side outlet). (13) Flowmeter (shell side).

Reproduced with permission from Agrahari, G.K., Pandey, N., Verma, N., Bhattacharya, P.K., 2014. Membrane contactor for reactive extraction of succinic acid from aqueous solution by tertiary amine. *Chem. Eng. Res. Des.* 92, 2705–2714.

where J is the mass flow rate of solute from aqueous phase to organic phase, A is the surface area of the membrane, C_{aq} is the concentration of solute in the aqueous phase at time “ t ,” and C_{aq}^* is the hypothetical concentration of the solute in aqueous phase in equilibrium with organic phase at the same time. In this case, K_{aq} is based on the aqueous phase side but it could be defined similarly for the organic phase.

Evaluation of mass transfer coefficients is of most importance since they determine the rate at which equilibrium is approached, control the time required for a given separation and therefore the size and cost of the equipment to be used (Viegas et al., 1998). The overall mass transfer coefficient can be related to individual mass transfer coefficients at the aqueous phase side (k_{aq}), within the membrane (k_m), and at the organic phase side (k_{org}), following the resistance-in-series model described in Section 5.2. For aqueous phase flowing in flow-cell (outside the fiber) without chemical reaction or with instantaneous chemical reaction at the interface (Younas et al., 2011):

$$\frac{1}{K_{aq}} = \frac{1}{k_{aq}} + \frac{d_{ext}}{Pk_m d_{lm}} + \frac{d_{ext}}{Pk_{org} d_{int}} \quad (5.50)$$

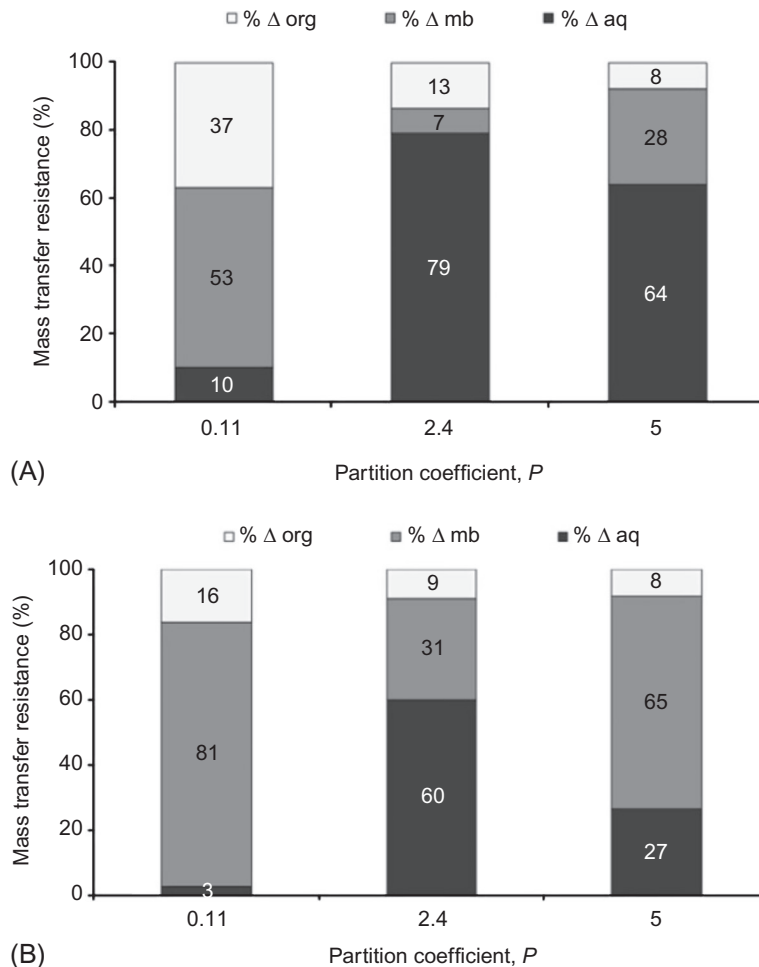
and for aqueous phase flowing inside the fiber of a hydrophobic membrane, based on aqueous phase side concentration and without chemical reaction or with instantaneous chemical reaction at the interface,

$$\frac{1}{K_{aq}} = \frac{1}{k_{aq}} + \frac{d_{int}}{Pk_m d_{lm}} + \frac{d_{int}}{Pk_{org} d_{ext}} \quad (5.51)$$

P is the partition coefficient defined as the ratio of solute concentration in organic phase to that in aqueous phase at equilibrium; d_{int} and d_{ext} are the inner and outer diameter of the fiber, respectively; d_{lm} is the logarithmic mean diameter. The calculation of the local mass transfer coefficients (k_{aq} , k_m , and k_{org}) can be done by using correlations similar to those shown in Eqs. (5.36), (5.37), and (5.39).

The first term of the right side in Eqs. (5.50) and (5.51) is the resistance produced by the aqueous phase; the second term is the resistance produced by the membrane; and the third term, the resistance produced by the extractant. In this way, the analysis of the importance of each resistance when varying the operating conditions can be performed. For example, Younas et al. (2011) determined the effect of flow rates and value of the partition coefficient on the mass transfer resistances for the extraction of copper (II) from aqueous solutions. Fig. 5.12A and B shows the results for a flow rate of 1.67×10^{-6} and $16.67 \times 10^{-6} \text{ m}^3 \text{ s}^{-1}$ (for both the organic and the aqueous phase), respectively. As general conclusions, they observed that the partition coefficient, which changes with the type of diluents, is the foremost parameter for mass transfer resistance analysis. As the partition coefficient decreases, the mass transfer resistance offered by the membrane increases, although the viscosity of the extractive phase will have a significant effect as well, which could explain the variation to this general conclusion. Increasing the flow rate produces a significant decrease of the resistances produced by the fluid phases. Therefore the membrane contributes more to the total resistance. This is a clear indication of mass transfer limitations in the fluid phases which can be improved by increasing the turbulence, that is, increasing the flow rate.

The overall resistance of mass transfer (the inverse of the overall mass transfer coefficient) can be plotted as a function of the inverse of the fluid velocity, which is the typically used Wilson plot method. This method allows the determination of the addition of other resistances as well as its dependence with the fluid velocity. This method has some limitations since it only accepts one variable (the fluid velocity). However, its usefulness and interest has been demonstrated in the literature (Viegas et al., 1998; Coelho et al., 2000). Fig. 5.13 shows the Wilson plot method elaborated by Viegas et al. (1998) when the tube side Reynolds number is varied (Fig. 5.13A) and when the shell side Reynolds number is varied (Fig. 5.13B) in the removal of valeric acid from an aqueous phase. The intercepts are the complementary resistances of each side (the other side resistance plus the resistance of the membrane itself). This is a very simple way to evaluate the variation of mass transfer coefficients with the fluid velocity. However, this methodology involves large errors. Viegas et al. (1998) developed a new methodology that considers the

**FIG. 5.12**

Mass transfer resistance analysis for copper (II) extraction with TFA: (A) $Q_{aq} = Q_{org} = 1.67 \times 10^{-6} \text{ m}^3 \text{ s}^{-1}$; (B) $Q_{aq} = Q_{org} = 16.67 \times 10^{-6} \text{ m}^3 \text{ s}^{-1}$.

partition coefficient as a function of time and concentration, achieving a single analytical expression. The Wilson plot methodology can be thus used acceptably to develop mass transfer correlations in systems operating in steady-state conditions and when the only variable is the fluid velocity. In systems where a parameter is a function of another variable or when operating in a transient state, the methodology proposed by Viegas et al. (1998) should be considered for a more accurate evaluation.

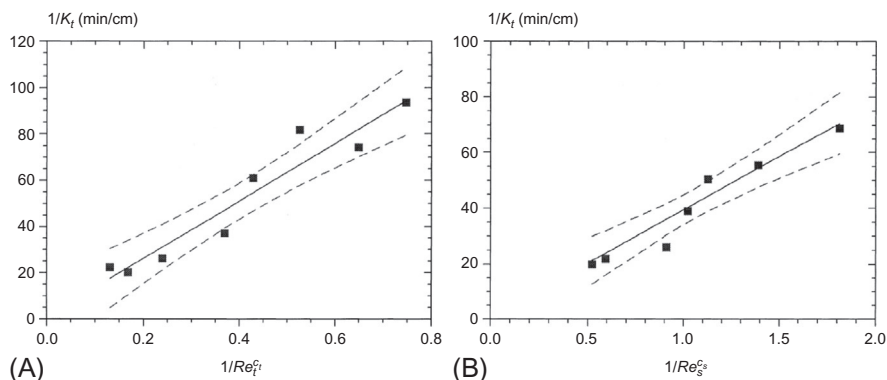


FIG. 5.13

Wilson plot representation considering a constant partition coefficient: (A) tube side and (B) shell side. Squares: experimental data; continuous line: model fitting; discontinuous line: 95% confidence limits.

Reproduced with permission from Viegas, R.M.C., Rodríguez, M., Luque, S., Alvarez, J.R., Coelho, I.M., Crespo, J.P.S.G., 1998. Mass transfer correlations in membrane extraction: analysis of Wilson-plot methodology. *J. Membr. Sci.* 145, 129–142.

5.5 MEMBRANE DISTILLATION-CRYSTALLIZATION

Membrane distillation is a novel alternative to separate mixtures containing volatile components. Like in distillation, vaporization of the feed solution is produced. However, the presence of the membrane generates a driving force based on a difference of concentration in addition to temperature. This driving force allows working at lower temperatures than conventional distillation without requiring reaching the boiling point of the feed mixture.

In membrane distillation, a microporous hydrophobic membrane is used since normally, the target separation is an aqueous solution and membrane wetting should be prevented. The feed aqueous solution is normally heated, although it is possible to work at room temperature if a concentration gradient is provided, for example, by using an osmotic solution (high concentrated solution of salts) at the permeate side. Typical feed temperatures vary in the range of 30–60°C. The volatile compounds in the feed solution evaporate and a vapor-liquid interface is created at the mouth of the pore. Those components diffuse and/or convect across the membrane pores, being condensed and/or removed on the opposite side of the membrane (permeate or distillate) (Curcio and Drioli, 2005). The hydrophobic character of the membrane prevents the inclusion of liquid inside the pores of the membrane in order to minimize its resistance to mass transfer. In addition, nonvolatile solutes are rejected and kept in the feed side.

Several configurations have been developed in membrane distillation depending on how the driving force is generated:

- Direct contact membrane distillation (DCMD): the permeate side of the membrane is a condensing fluid (commonly pure water) that is directly in contact with the membrane. The driving force is generated by the difference of temperature between the feed solution and the condensing fluid.
- Osmotic membrane distillation (OMD): an osmotic (high concentrated) solution is used at the permeate side to create a concentration-based driving force (vapor pressure difference between both membrane sides related to the water activities in the feed and osmotic solutions) to transfer water from the feed solution to the osmotic solution. The salts selected as osmotic pressure agents are normally NaCl (because of its low cost), MgCl₂, CaCl₂, and MgSO₄ (65). The temperature in the feed solution can be increased while keeping the osmotic solution at room (or lower) temperature to take advantage of the temperature gradient that is generated. As reference, when the osmotic evaporation is carried out at room temperature, transmembrane fluxes generally range between 0.2 and 0.4 L/m²h are obtained (66). (Curcio and Drioli, 2005).
- Air gap membrane distillation (AGMD): the vaporized solvent is recovered on a condensing surface separated from the membrane by an air gap. The driving force is a concentration and/or temperature gradient across the membrane.
- Vacuum membrane distillation (VMD): vacuum is applied at the permeate side of the membrane. A large difference in partial pressure is produced thanks to the applied vacuum.
- Sweep gas membrane distillation (SGMD): a sweep gas is used at the other side of the membrane to recover the vaporized compound, establishing a difference in partial pressure across the membrane.

Membrane crystallization appears as an extension of the working principle of membrane distillation. As in membrane distillation, volatile solvents in the feed solution are evaporated and transfer through the membrane pores to the permeate side at the other side of the membrane. The objective is to concentrate the feed solution above their saturation limit, reaching a supersaturation that allows crystals to nucleate and grow. The role of the membrane in membrane crystallization is twofold. On one hand, it is the barrier that separates the feed phase from the permeate side, according to the characteristics of membrane contactors. On the other hand, the membrane acts as a solid support on which the solute molecules can converge forming clusters (nuclei) or growth units, leading to a heterogeneous nucleation. This is due to the decrease in the energetic barrier of nucleation, ΔG^* , that must be reached to induce the formation of stable nuclei. This energetic barrier is related to the minimum size of cluster (the critical nucleus, r^*) that have to be achieved to be likely to grow spontaneously. The nucleation barrier is calculated as (Curcio and Drioli, 2005):

$$\Delta G^* = \frac{16\pi v^2 \gamma^3}{3[kT \ln S]^2} \quad (5.52)$$

where v is the molar volume occupied by a growth unit, γ the surface energy, and S the supersaturation. When the supersaturation S tends to 1, the energy barrier tends to infinite. Thus it is necessary to exceed the supersaturation value to observe spontaneous homogeneous precipitation. In addition, if a membrane is in contact with the crystallizing solution, the energy of nucleation decreases and heterogeneous nucleation may take place. The literature gives an equation to estimate the reduction of the energy produced when a substrate is present as a function of the contact angle θ formed between the solute and the substrate (membrane) (Curcio and Drioli, 2005):

$$\Delta G^{het} = \Delta G^{hom} \left[\frac{1}{2} - \frac{3}{4} \cos\theta + \frac{1}{4} \cos^3\theta \right] \quad (5.53)$$

Three situations can be highlighted:

- $\theta = 180^\circ$: the solution wets the substrate completely. In this case, both energies are coincident, $\Delta G^{het} = \Delta G^{hom}$;
- $\theta = 90^\circ$: hydrophilic-hydrophobic limit. The energy of nucleation barrier for heterogeneous nucleation is half the value for homogeneous nucleation, $\Delta G^{het} = \frac{1}{2} \Delta G^{hom}$;
- $\theta < 90^\circ$: hydrophobic membrane. The energy of nucleation barrier for heterogeneous nucleation is lower than the half of the value for homogeneous nucleation, $\Delta G^{het} < \frac{1}{2} \Delta G^{hom}$.

As consequence, the hydrophobic character of the membrane has an important relevance in the crystallization process. Fig. 5.14 shows the reduction in the energy barrier for several common membrane materials (Curcio and Drioli, 2005).

The transmembrane flux (J , $\text{m}^3 \text{m}^{-2} \text{s}^{-1}$) of water through the membrane can be experimentally calculated by weighing the feed reservoir over time since a decrease of water is produced, concentrating the feed solution:

$$J(t_i) = -\frac{1}{A} \frac{dV_p}{dt} \approx -\frac{1}{A\rho_{water}} \frac{dw_f}{dt} = -\frac{1}{A\rho_{water}} \frac{w_f(t_{i+1}) - w_f(t_i)}{t_{i+1} - t_i} \quad (5.54)$$

where V_p (m^3) is the volume of water permeated from the feed solution to the permeate side, A (m^2) is the membrane area, ρ_{water} (kg m^{-3}) is the density of water, w_f (kg) is the weight of the reservoir containing the feed solution at time t_i (s).

If a concentration profile exists, as happens in osmotic membrane crystallization, the mass transfer from the feed to the osmotic solution is determined as the difference of water activity at both sides of the membrane. The overall mass transfer coefficient, K_{ov} ($\text{m Pa}^{-1} \text{s}^{-1}$), relates thus the transmembrane flux and the driving force (Ye et al., 2013; Li et al., 2014):

$$J = K_{ov} (p_f^* a_f - p_p^* a_p) \quad (5.55)$$

where J is the water flux calculated in Eq. (5.1); a is the water activity of the feed (f) and osmotic (p) side; and p_f^* and p_p^* are the water vapor pressures (Pa) of the feed and the osmotic solution, respectively. The water activity of a pure solution can be

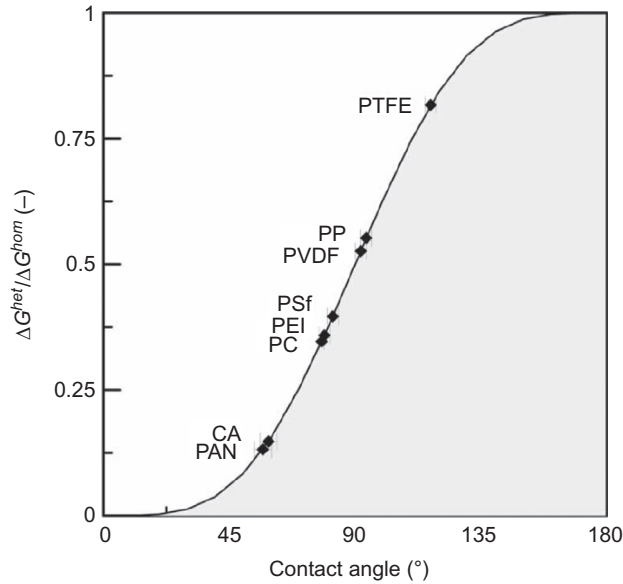


FIG. 5.14

Reduction in the free energy of the nucleation barrier due to heterogeneous nucleation as a function of the water contact angle with the polymeric surface (CA, cellulose acetate; PAN, polyacrylonitrile; PC, polycarbonate; PET, polyetherimide; PES, polyethersulfone; PP, polypropylene; PSf, polysulfone; PTFE, polytetrafluoroethylene; PVDF, polyvinylidene fluoride).

Reproduced with permission from Curcio, E., Enrico, D., 2005. Membrane distillation and related operations—a review. *Sep. Purif. Rev.* 34, 35–86.

calculated by Eqs. (5.3a), (5.3b) if the values of the osmotic coefficients are available in the literature, or by using the procedure described by Sandler (2006):

$$\varphi = \frac{-1000}{vmM} \ln a_w \quad (5.56)$$

where φ is the osmotic coefficient, v is the number of ions that the solute molecule dissociates in the solution, m is the molality (mol kg^{-1}), M is the molar mass of the solvent, and a_w is the water activity. The vapor pressure of water (p^*) depends on the temperature (T) of the solution and it can be calculated by the Antoine equation (pressure in mm Hg and temperature in °C) (Luis et al., 2013):

$$p^*(T) = 10^{8.07131 - \frac{1730.63}{233.426 + T}} \quad (5.57)$$

Regarding the temperature gradient, an experimental heat transfer coefficient (U_{exp} , $\text{W m}^{-2} \text{K}^{-1}$) can be calculated following a semiempirical procedure in which the heat by convection (Q_{conv} , W m^{-2}) and conduction (Q_{cond} , W m^{-2}) are involved (based on the equation described by Gryta et al. (1997)):

$$U_{exp} = \frac{Q_{conv} + Q_{cond}}{\Delta T \ln} = \frac{J_w c_p \Delta T_b + \frac{k_{mem}}{\delta} \Delta T_w}{\Delta T \ln} \quad (5.58)$$

where J_w is the permeate flux ($\text{Kg m}^{-2} \text{s}^{-1}$), c_p is the heat capacity ($\text{J kg}^{-1} \text{K}^{-1}$), k_m is the thermal conductivity of the membrane ($\text{W m}^{-1} \text{K}^{-1}$), and δ is the membrane thickness (m); $\Delta T \ln$, ΔT_b , ΔT_w are the logarithm mean temperature, the difference of temperature among the feed and the osmotic side in the bulk and in the membrane surface, respectively.

The resistance-in-series model is typically applied in membrane distillation-crystallization. Fig. 5.15 shows a scheme of the concentration and temperature profiles and the resistances in osmotic membrane distillation (Ruiz-Salmón and Luis, 2018).

The mass transfer coefficient inside the fibers (feed side) can be calculated from (Gabelman and Hwang, 1999):

$$k_f = \frac{Sh D_{Na_2CO_3, water}}{d_i} \quad (5.59)$$

$$Sh = 0.664 Re^{0.5} Sc^{0.33} \left(\frac{d_i}{l} \right)^{0.33} \quad (5.60)$$

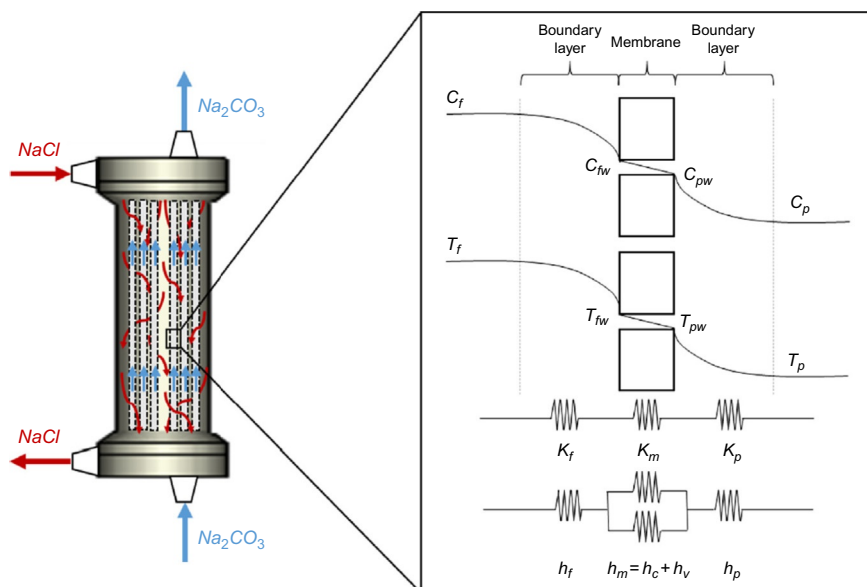


FIG. 5.15

Counter-current mode in osmotic membrane distillation (left) and mass and heat transfer resistances (right).

Reproduced with permission from Ruiz-Salmón, I., Luis, P., 2018. Membrane crystallization via membrane distillation. *Chem. Eng. Process. Process Intensif.* 123, 258–271.

$$Re = \frac{\rho_f v_f d_i}{\eta_f} \quad (5.61)$$

$$Sc = \frac{\eta_f}{\rho_f D_{Na_2CO_3, water}} \quad (5.62)$$

where Sh , Re , and Sc are the Sherwood, Reynolds, and Schmidt numbers, respectively; d_i (m) is the inside diameter of the fibers; ρ (kg m^{-3}) and η (Pa s), the density and the viscosity of the solution, respectively; v (m s^{-1}), the velocity of the fluid through the fibers and $D_{Na_2CO_3, water}$ ($\text{m}^2 \text{s}^{-1}$) is the diffusivity of Na_2CO_3 in water.

The mass transfer coefficient at the shell side (osmotic solution) is calculated from (Gabelman and Hwang, 1999):

$$k_p = \frac{Sh D_{NaCl, water}}{d_h} \quad (5.63)$$

$$Sh = 5.8 \left(\frac{d_h(1-\phi)}{l} \right) Re^{0.6} Sc^{0.33} \quad (5.64)$$

$$Re = \frac{\rho_p v_p d_h}{\mu} \quad (5.65)$$

$$Sc = \frac{\mu_p}{\rho_p D_{NaCl, water}} \quad (5.66)$$

where l (m) is the length; d_h (m), the hydraulic diameter; and ϕ is the packing fraction of the fibers in the shell.

The mass transfer coefficient in the membrane is calculated from (Gabelman and Hwang, 1999):

$$k_m = \frac{1}{RT} \left(\frac{D_w^k D_{w-a}^\circ}{D_{w-a}^\circ + p_a D_w^k} \right) \left(\frac{M}{\delta} \right) \quad (5.67)$$

$$D_w^k = \frac{2\epsilon r_p}{3\tau} \sqrt{\frac{8RT_{avg}}{\pi M}} \quad (5.68)$$

$$D_w^\circ(T) = -2.775 \cdot 10^{-6} + 4.479 \cdot 10^{-8} T + 1.656 \cdot 10^{-10} T^2 \quad (5.69)$$

where D_w^k is the water Knudsen diffusion; D_w° , the water air diffusion; T , the temperature along the membrane; p_a is the partial pressure of air in the pore (it is assumed $p_a = 101,325$ Pa); τ , the tortuosity of the membrane; ϵ , the porosity of the membrane; δ , the thickness of the membrane; and r_p , the radius of the pores.

In membrane distillation, a temperature gradient is part of the driving force of the system. Thus the heat transfer coefficients in the feed (h_f) and permeate (h_p) ($\text{W m}^{-2} \text{K}^{-1}$) and the temperature polarization coefficient (TPC) can be calculated

from correlations (Gryta et al., 1997; Tun et al., 2005; Alkudhiri et al., 2012; Lawson and Lloyd, 1997):

$$h = \frac{Nu k_{fluid}}{d} \quad (5.70)$$

$$Nu = 1.86 \left(Re Pr \frac{d}{l} \right)^{0.33} \left(\frac{\eta}{\eta_w} \right)^{0.14} \quad (5.71)$$

$$Pr = \frac{C_p \eta}{k_{fluid}} \quad (5.72)$$

where Nu and Pr are the Nusselt and Prandtl numbers, respectively; k_{fluid} is the thermal conductivity of the fluid ($\text{W m}^{-1} \text{K}^{-1}$); d (m) is d_i and d_h for the feed and the osmotic side, respectively; η and η_w are the viscosity of the solution (feed or osmotic solution) and the water, respectively; C_p is the heat capacity ($\text{J kg}^{-1} \text{K}^{-1}$); and k_{fluid} is the thermal conductivity of the fluid ($\text{W m}^{-1} \text{K}^{-1}$).

The heat transfer through the membrane by conduction (h_c) and vapor movement (h_v), and the temperature polarization coefficient (TPC) are given by:

$$h_c = \frac{k_{mem}}{\delta} = \frac{\epsilon k_g + (1 - \epsilon) k_s}{\delta} \quad (5.73)$$

$$h_v = \frac{J_w \Delta H_v}{\Delta T_w} \quad (5.74)$$

$$\Delta T_w = T_{fw} - T_{pw} \quad (5.75)$$

$$T_{fw} = T_f - (T_f - T_p) \left(\frac{\frac{1}{h_f}}{\frac{1}{h_c + h_v} + \frac{1}{h_f} + \frac{1}{h_p}} \right) \quad (5.76)$$

$$T_{pw} = T_p + (T_f - T_p) \left(\frac{\frac{1}{h_p}}{\frac{1}{h_c + h_v} + \frac{1}{h_f} + \frac{1}{h_p}} \right) \quad (5.77)$$

$$TPC = \frac{\Delta T_w}{T_f - T_p} \quad (5.78)$$

where k_{mem} , k_g , k_s are the thermal conductivity of the membrane, the air and the solid phase of the membrane, respectively; ΔH_v is the latent heat of vaporization (J kg^{-1}); ΔT_w is the temperature difference (K) among the temperature near the membrane wall in the feed (T_{fw}) and the permeate side (T_{pw}).

The effect of the operating conditions such as the concentration of the osmotic solution, the feed concentration, and the temperature on the overall mass transfer coefficient gives very valuable information on possible effects of concentration or temperature polarization. On the other hand, studying the effect of the flow rates of the feed and osmotic solutions allows determining the degree of turbulence needed in the fluid phases to minimize their mass transfer resistance. Fig. 5.16 is an example of this kind of studies for the concentration and further crystallization of Na_2CO_3 using an osmotic solution of NaCl (Ruiz-Salmón and Luis, 2018). Flow rates under 50 mL min^{-1} showed low turbulence, leading to concentration polarization. High concentration in the osmotic solution led to higher fluxes but the overall membrane coefficient did not increase as expected. A possible phenomenon of concentration polarization and/or membrane wetting could explain this loss of performance. In addition, increasing the temperature did not produce a significant increase of the overall mass transfer coefficient in spite of increasing the flux. Thus temperature polarization was observed. Regarding the heat transfer coefficient (Fig. 5.17), high concentration of the NaCl solution influences slightly the heat transfer but this effect disappears as soon as the feed temperature was increased above 35°C .

5.6 MEMBRANE EMULSIFICATION

Emulsions are mixtures consisting of a dispersed phase uniformly distributed in a continuous phase. Oil-in-water (o/w) emulsions have oil droplets uniformly dispersed in water. On the other hand, water-in-oil (w/o) emulsions present water droplets uniformly dispersed in oil. Systems with an emulsion as the dispersed phase are called multiple emulsions, like water-in-oil-in-water (w/o/w) emulsions. Emulsions play a critical role in the formulation of pharmaceutical compounds, cosmetics, food, pigment dispersions, and synthesis of latex. They are present in our daily life as creams, mayonnaise, butter, margarine, sauces, and so on. The conventional equipment used to prepare emulsions is typically based on colloid mills, high-speed rotor-stator systems, and high-pressure dispersing homogenizers. These methods achieve the desired size distribution of the droplets by the generation of turbulent breakup, where high shear stress is applied to deform and disrupt larger droplets in order to keep the stability of the emulsion and avoid coalescence. Energy consumption is generally elevated because only a fraction of the energy input is used for droplet breakup. In a high-pressure homogenizer about 99.8% of the energy supplied is lost and converted into heat (Drioli et al., 2005). Using a membrane contactor offers the advantage of decreasing energy consumption and achieving a homogenous size distribution of droplets. The working principle is different than with other systems using membrane contactors since in membrane emulsification, the dispersed phase is pressed through the membrane pores to the other side of the membrane. If a crossflow configuration is used, the droplets formed at the pore mouth are detached by the action of the drag force given by the tangential flow of the continuous phase flowing along the membrane surface (Giorno et al., 2005). Fig. 5.18 shows the working

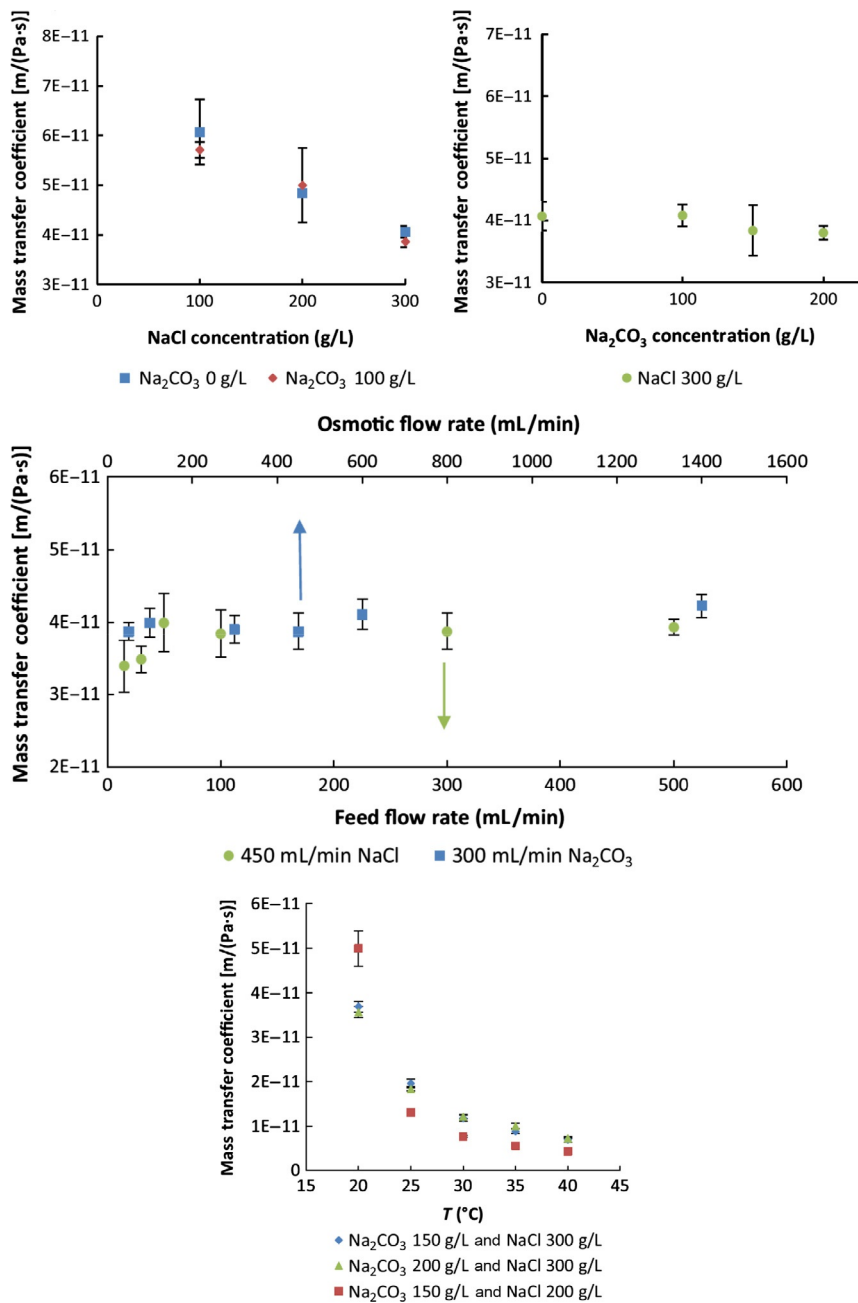


FIG. 5.16

Mass transfer coefficient as a function of (A) the concentration of Na₂CO₃ (feed solution); (B) the concentration of NaCl (osmotic solution); (C) the feed and osmotic flow rates (Na₂CO₃ and NaCl concentration are 150 and 300 gL⁻¹, respectively); (D) feed temperature.

Reproduced with permission from Ruiz-Salmón, I., Luis, P., 2018. Membrane crystallization via membrane distillation. Chem. Eng. Process. Process Intensif. 123, 258–271.

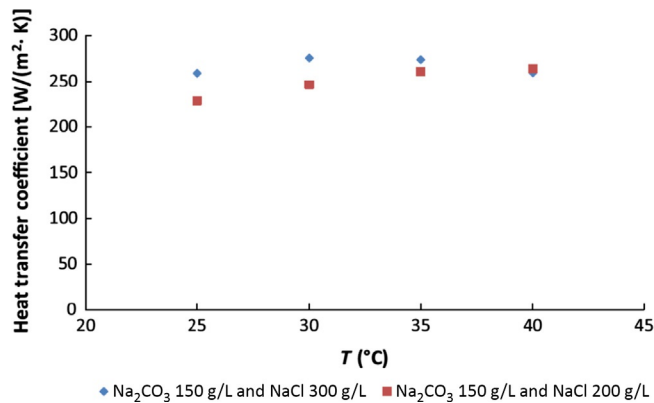


FIG. 5.17

Heat transfer coefficient as a function of the temperature.

Reproduced with permission from Ruiz-Salmón, I., Luis, P., 2018. Membrane crystallization via membrane distillation. *Chem. Eng. Process. Process Intensif.* 123, 258–271.

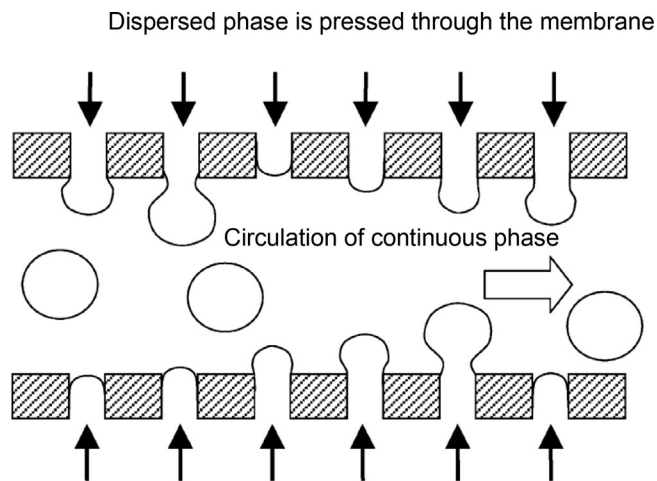


FIG. 5.18

Principle of membrane emulsification.

Reproduced with permission from Rayner, M., Tragardh, G., Tragardh, C., 2005. The impact of mass transfer and interfacial expansion rate on droplet size in membrane emulsification processes. *Colloids Surf. A: Physicochem. Eng. Asp.* 266, 1–17.

principle of membrane emulsification and Fig. 5.19 presents an example of emulsions created by using this technology.

A typical lab-scale system to perform experimental tests of membrane emulsification is shown in Fig. 5.20. The membrane contactor is the core of the experimental plant. A careful control of pressure and temperature is required. The permeate flux

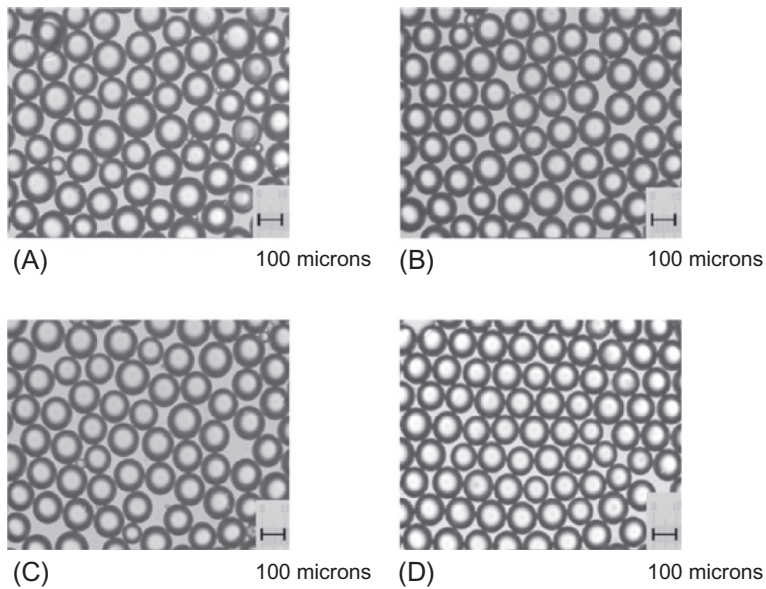


FIG. 5.19

Optical microscope images of drops formed using membranes with 80- μm pore spacing under different conditions: (A) 2V agitation (3.5 Hz (210 rpm))—0.5 Pa peak shear at membrane; (B) 3V agitation (5.6 Hz (340 rpm))—1.2 Pa peak shear at membrane; (C) 4V agitation (6.833 Hz (410 rpm))—1.7 Pa peak shear at membrane; (D) 6V agitation (10.833 Hz (650 rpm))—3.6 Pa peak shear at membrane.

Reproduced with permission from Egidì, E., Gasparini, G., Holdich, R.G., Vladisavljević, G.T., Kosvintsev, S.R., 2008. Membrane emulsification using membranes of regular pore spacing: droplet size and uniformity in the presence of surface shear. *J. Membr. Sci.* 323, 414–420.

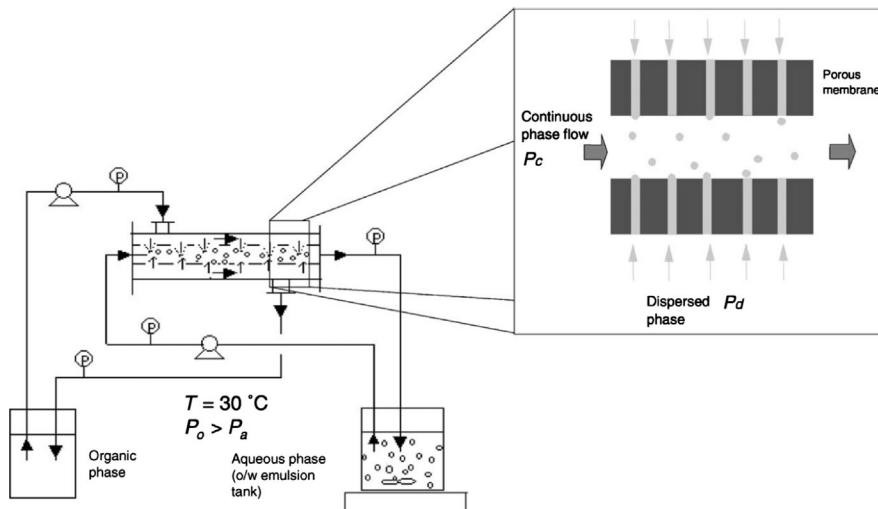


FIG. 5.20

Schematic representation of the membrane emulsification system.

Reproduced with permission from Giorno, L., Li, N., Drioli, E., 2003a. Preparation of oil-in-water emulsions using polyamide 10 kDa hollow fiber membrane. *J. Membr. Sci.* 217, 173–180, Giorno, L., Li, N., Drioli, E., 2003b. Use of stable emulsion to improve stability, activity, and enantioselectivity of lipase immobilized in a membrane reactor. *Biotechnol. Bioeng.* 84, 677–685.

(flux of the dispersed phase), J_d , can be calculated indirectly by measuring the weight decrease of the dispersed phase (Δw) as a function of time:

$$J_d = \frac{\Delta w}{\Delta t \cdot A} \quad (5.79)$$

where A is the membrane area.

The driving force is given by the transmembrane pressure, that is, the pressure difference between the dispersion phase and the continuous phase. Taking into account the pressure drop of the membrane contactor, the transmembrane pressure, ΔP_{TM} , can be calculated considering an average pressure between the inlet and the outlet of the contactor (Giorno et al., 2003a, b):

$$\Delta P_{TM} = \frac{1}{2}(P_{d,in} + P_{d,out}) - \frac{1}{2}(P_{c,in} + P_{c,out}) \quad (5.80)$$

where $P_{d,in}$ and $P_{d,out}$ are the pressure of the dispersion phase at the inlet and outlet, respectively, and $P_{c,in}$ and $P_{c,out}$ are the pressure of the continuous phase at the inlet and outlet, respectively. This transmembrane pressure should be higher than the breakthrough pressure indicated in Eq. (5.1) in order to press the dispersed fluid through the pores of the membrane.

The stability of the emulsions depends on several factors, such as the droplet size, the emulsifying agent, net charge, and mechanical and physical properties of the adsorbed film. Among these factors, the droplet size is the most important parameter. Microemulsions, or emulsions with droplet size in the range 20–80 nm, are thermodynamically stable mixtures of oil in water or water in oil. When droplets are larger, the interface between the oil and the water phase must be stabilized by surfactant molecules, which prevent immediate aggregation or coalescence and whose properties largely determine the behavior of the emulsion (Giorno et al., 2005). The final droplet size and size distribution are determined by the membrane material, pore size and porosity, as well as process parameters such as the crossflow velocity of the continuous phase and the transmembrane pressure.

The membrane material should be selected so that the membrane is not wetted with the dispersed phase. The reason behind this is that using hydrophobic membranes for making an o/w emulsion resulted in polydispersed emulsions with a larger average droplet size than when using a hydrophilic membrane (Nakashima et al., 1991). Making w/o emulsions using hydrophilic membranes has resulted in droplets smaller than the pore size and dependent on the structure of the pore and not only on the diameter (Kandori et al., 1991). Thus in oil-in-water emulsions (oil: dispersed phase; water: continuous phase), the membrane will be hydrophilic, whereas in water-in-oil emulsions (water: dispersed phase; oil: continuous phase), the membrane will be hydrophobic (Drioli et al., 2005). A typical membrane material in membrane emulsification is porous glass due to the widely used Shirasu porous glass (SPG) membrane (Ise Chemical Co, Japan) synthesized from $\text{CaO-Al}_2\text{O}_3\text{-B}_2\text{O}_3\text{-SiO}_2$ -type glass made from “Shirasu,” a Japanese volcanic ash (Nakashima et al., 1991). Other membranes have been used to prepare oil-in-water emulsions (commercial microfiltration membranes of ceramic α -alumina from Membrflow, Germany; α -alumina- and zirconia coated membranes from SCT, France;

polytetrafluoroethylene membranes from Advantec Tokyo Ltd. and Goretex, Japan) (Suzuki et al., 1998; Schröder and Schubert, 1999a,b; Joscelyne and Trägårdh, 1999; Kanichi et al., 2002; Yamazaki et al., 2002) or water-in-oil emulsions (microporous polypropylene hollow fibers from Microdyn, Germany; polytetrafluoroethylene membranes from Advantec, Japan) (Suzuki et al., 1998; Vladislavljevic et al., 2002). In order to achieve permeation of the organic phase when using hydrophilic membranes, or permeation of the aqueous phase through the hydrophobic membrane, a pretreatment of the membrane is thus necessary. This pretreatment normally consists on removing the internal liquid phase and substituting it by the phase to be dispersed. It may affect the pore size of the membranes, thus it is important to apply an appropriate pretreatment method in order to obtain the desired size of the droplets. [Giorno et al. \(2005\)](#) evaluated the effect of four different procedures on the final size of the droplets. Basically, the pretreatment consisted in washing the membrane with a gradient of miscible solvents and solvent solutions of decreasing polarity, to shift the internal phase from polar to nonpolar and to allow the permeation of the organic phase ([Giorno et al., 2003a,b, 2005](#)). [Fig. 5.21](#) clearly shows the significant variation of the final droplet size depending on the pretreatment used due to the modification

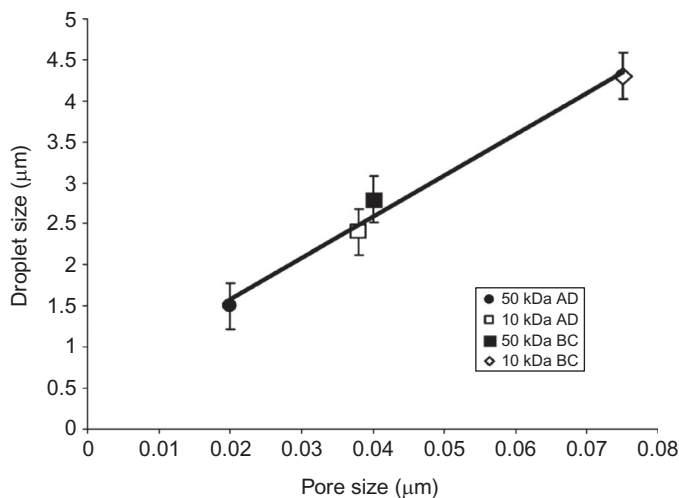


FIG. 5.21

Relationship between pore size and droplet size obtained by [Giorno et al. \(2005\)](#) using two membranes (polyamide capillary membranes with nominal molecular weight cutoff of 10 and 50 kDa) after pretreatment following four different procedures (A: subsequent permeation of pure water, water-isopropanol (50:50), and pure isooctane; B and C: pure water, water-isopropanol (80:20), isopropanol-isooctane (50:50 and 20:80), and then pure isooctane; the difference between B and C is the different contact time of membranes with the solutions; D: water, isopropanol-isooctane (50:50), and then pure isooctane).

Reproduced with permission from [Giorno, L., Mazzei, R., Oriolo, M., De Luca, G., Davoli, M., Drioli, E., 2005. Effects of organic solvents on ultrafiltration polyamide membranes for the preparation of oil-in-water emulsions.](#)

J. Colloid Interface Sci. 287, 612–623.

of the membrane pore size. The effect of solvents on the thin layer of asymmetric polyamide membranes showed a clear change in the membrane morphology and pore structure.

Regarding the pore size, a linear correlation ($y = m \cdot x$) between membrane pore size (y) and droplet size (x) has been generally observed where the value of m may range from 2 to 10 depending on the properties of the organic, water, and membrane (Rayner and Tragardh, 2002). This effect can be also observed in Fig. 5.21. For SPG membranes, values of m range typically from 2 to 10. For membranes other than SPG, the values reported for m are higher, typically 3–50 (Charcosset et al., 2004).

Finally, the porosity of the membrane surface also plays an important role in the droplet size since it determines the distance between two adjacent pores, which is critical to ensure that two adjacent droplets do not come too close, leading to coalescence (Charcosset et al., 2004). As a reference, a maximum membrane porosity to prevent coalescence of droplets growing on neighboring pores of 5 μm diameter has found to be 1.5% (Abrahamse et al., 2001).

Process parameters influence the final size and distribution of droplets in the emulsion as well. The crossflow velocity will cause the detachment of droplets formed at the membrane surface. The droplet size becomes smaller as the wall shear stress (caused by the crossflow of the continuous phase) increases (Charcosset et al., 2004). Fig. 5.22 shows the variation of droplet diameter observed by Rayner and Tragardh (2002) as a function of the wall shear stress. An appropriate control of the flow rate of the continuous phase is thus essential.

Another process parameter is the transmembrane pressure. Increasing the transmembrane pressure will increase the flux of the dispersed phase through the

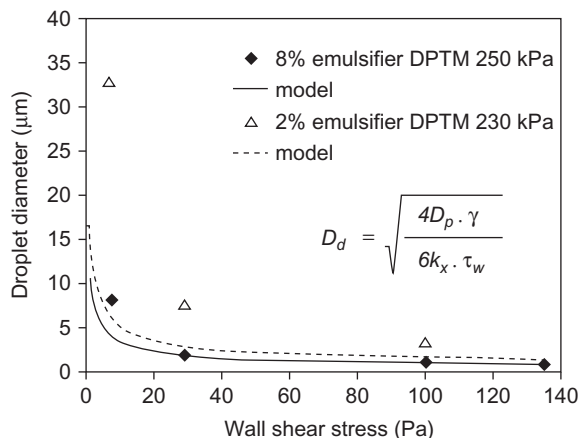


FIG. 5.22

Variation of droplet diameter with the wall shear stress.

Reproduced with permission from Rayner, M., Tragardh, G., 2002. Membrane emulsification modelling: how can we get from characterization to design? *Desalination* 145, 165–172.

membrane according to the Darcy's law, but it will also increase the average droplet pore size and the size distribution because of droplet coalescence at the membrane surface. Fig. 5.23 shows an example of the effect of the transmembrane pressure on the flux of the dispersed phase. Adding surfactants may become a need to have high transmembrane flux while keeping the formation of small droplets.

The mathematical description of the mass transfer in membrane emulsification begins with the application of Darcy's law, which relates the dispersed phase flux, J_d , to the transmembrane pressure, ΔP_{TM} :

$$J_d = \frac{\beta \cdot \Delta P_{TM}}{\mu \delta} \quad (5.81)$$

where β is a factor, which can be called permeability, that depends on the membrane structure, δ is the membrane thickness, and μ is the viscosity of the dispersed phase (Rayner and Tragardh, 2002; Charcosset et al., 2004). If the membrane is assumed to have n uniform cylindrical pores of radius r , the permeability β can be calculated from the Hagen-Poiseuille equation (Charcosset et al., 2004):

$$\beta = \frac{nr^2}{8\pi} \quad (5.82)$$

Using an overall mass transfer coefficient, $K_{overall}$, defined as $K_{overall} = \frac{\beta}{\mu \delta}$ is also useful when studying membrane emulsification, and the application of the resistance-in-series model could be of interest to determine the main mass transfer limitations.

A limiting factor for emulsion production on a commercial scale is the low flux of the disperse phase through the membrane. Thus achieving a good mass transfer

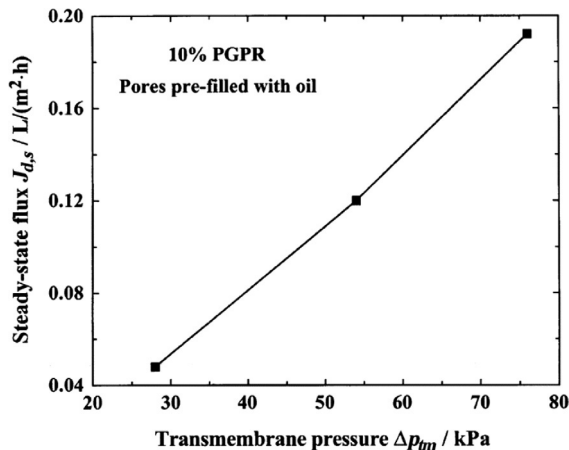


FIG. 5.23

Steady-state dispersed phase flux versus transmembrane pressure through the pores. Reproduced with permission from Vladislavljevic, G.T., Tesch, S., Schubert, H., 2002. Preparation of water-in-oil emulsions using microporous polypropylene hollow fibers: influence of some operating parameters on droplet size distribution. *Chem. Eng. Process.* 41, 231–238.

through the membrane is a key objective in current research. The porosity and pore size of the membrane will influence the mass transport as well as the mass transfer resistance produced by the liquid phases. In order to decrease the mass transfer resistance produced by the liquid phases, an appropriate control of the fluid dynamics is required (Joscelyne and Trägårdh, 2000). Controlling the droplet size is also crucial in the emulsification process. It involves having a deep knowledge about the process of droplet formation and detachment at the membrane surface, the behavior of the dispersed phase through the membrane itself, and other phenomena that may occur within the process (Vladisavljević and Schubert, 2003). Research on modeling of membrane emulsification is thus oriented to develop mathematical models that predict the effect of input parameters (e.g., transmembrane pressure, shear rate, membrane pore size) on process output (e.g., droplet size, production rate) (Spyropoulos et al., 2014). In this way, a good control over the final properties of the emulsion can be achieved.

If emulsifiers (substances that confer long-term stability) or surfactants (surface active agents that reduce interfacial tension) are added into the emulsion, the droplet size will be modified due to their coupled transport to the expansion rate of the oil-water interface. The type of surfactant used influences significantly the droplet size (Schröder et al., 1998; Schröder and Schubert, 1999a, b). The viscosity of the dispersed phase has an important effect on the transmembrane flux and the droplet size. If the viscosity of the dispersed phase is high, the flux through the membrane will be low (see equation X-Darcy), and as a consequence, the droplet diameter will be large compared with the mean pore diameter (Charcosset et al., 2004).

Droplet expansion and adsorption at the interface are coupled, thus the rates of droplet expansion and droplet detachment as well as the adsorption rate of the emulsifier/surfactant to the growing interfacial area become relevant over the involved time scales (Rayner et al., 2005). When a new droplet begins to grow from a pore, some surfactant is already present at the interface. However, the surfactant surface coverage decreases over time because the area of the droplet is increasing. The consequence is that additional surfactant molecules can be adsorbed, which leads to the transport of the surfactant to the surface droplet. In order to obtain the surface coverage of the emulsifier/surfactant over time, the mass transfer coefficient in the continuous phase, k_{cts} , should be analyzed. Two cases can be considered (Rayner et al., 2005):

Case i: low wall shear rates where the process is dominated by molecular diffusion through an “infinite” boundary layer. In this case, it is observed that

$$\pi \leq \frac{\delta^2}{Dt} < \infty \quad (5.83)$$

where D is the diffusion coefficient of the surfactant, δ is the boundary layer height, and t is the droplet formation time.

The penetration theory is then applied to calculate the point value of the mass transfer coefficient in the continuous phase:

$$k_{cts} = \sqrt{\frac{D}{\pi t}} \quad (5.84)$$

The penetration theory (Higbie, 1935) considers that the depth of penetration is less than the total depth of the liquid boundary layer, thus the total depth is assumed to be infinite. Velocity gradients within the fluids are ignored since mass transport takes place mainly by molecular diffusion and a balance for the surfactant in the continuous phase is governed by Fick's second law.

Case ii: moderate wall shear rates where both diffusion and flow convection are taken into account. In this case:

$$\frac{\partial^2}{Dt} < \pi \quad (5.85)$$

The Reynolds analogy is applied to calculate the mass transfer coefficient:

$$k_{cts} = \frac{\tau_{wall}}{\rho U} \frac{1}{1 + \alpha(Sc - 1)} \quad (5.86)$$

where U is the average velocity in the continuous phase; ρ is the density; τ_{wall} is the wall shear stress; α is the ratio of the velocity at the edge of the viscous sublayer to the average velocity (equal to $2.0 Re^{-1/8}$ for pipe flow); and the Schmidt number, Sc , gives the dimensionless relationship. The Reynolds analogy relates the heat and mass transfer rates to momentum transfer through shear stress. It assumes that elements of fluid are brought from remote regions in the bulk to the surface by the action of turbulent eddies without mixing with the intermediate fluid along the way, and instantaneously reach equilibrium upon contact with the interfacial layers (Coulson and Richardson, 1999). This theory has been extended for viscous sublayers by Taylor and Prandtl (Taylor, 1916; Prandtl, 1910, 1928).

The diffusion coefficient of the polymeric surfactant, D , can be calculated by the Stokes-Einstein equation:

$$D = \frac{kT}{a\mu} \quad (5.87)$$

where k is the Boltzmann constant, T is temperature, μ is viscosity of the continuous phase, and a is the length of the molecule which is assumed to be two times the radius of gyration of a polymer in solution ($R_g \approx M_W^{0.6} \times 10^{-9}$ nm).

The reader is addressed to Rayner et al. (2005) for a complete mathematical description of the transport process indicated in cases *i* and *ii*.

Modeling the droplet size as a function of the kind of mechanism that will cause the detachment of the droplets from the membrane surface (produced spontaneously or due to shear stress) has been performed intensively in the literature (Yasuno et al., 2002; Kobayashi et al., 2003; Christov et al., 2002; Sugiura et al., 2001; Rayner et al., 2004; Schröder and Schubert, 1999a, b; Joscelyne and Trägårdh, 1999). Droplet formation spontaneously occurs when the droplet break off occurs due to the minimization of free energy (a crossflow is not applied) (Sugiura et al., 2001; Rayner et al., 2004). On the other hand, shear-induced droplet formation happens when the flow of a continuous phase produces a shear stress on the emerging droplets, causing their detachment from the surface. The continuous phase produces thus an effect on

the size and distribution of the droplets. In this case, the droplet diameter can be predicted based on a force balance, in which the capillary force and the opposing drag force seem to be the most important. Works performed by [Rayner et al. \(2004\)](#), [Peng and Williams \(1998\)](#), and [Schröder et al. \(1998\)](#) can be taken as an starting point for interested readers.

5.7 CONTACTOR MEMBRANE REACTORS

Membrane reactors combine reaction and a membrane process in the same single unit creating synergies. In general terms, there are three main systems that fit within the category of a membrane reactor: “extractor,” “distributor,” and “contactor” ([Westermann and Melin, 2009](#)). The “extractor” selectively removes the products from the reaction mixture; the “distributor” controls the addition of reactants to the reaction mixture; and the “contactor” intensifies the contact between reactants. In this chapter, the contactor concept will be considered.

In a contactor membrane reactor, the membrane can be used in two main ways ([Fig. 5.24](#)): (i) the membrane is a barrier between two fluid phases (gas-liquid or liquid-liquid phases) that will contact each other inside the pores of the membrane (interfacial contactor). The reaction takes place inside the pores and the reaction product will have preference by one or both phases. The membrane can be catalytically active or the catalyst can be in the feed solution. In the latter case, an extractant is required at the other side of the membrane with high selectivity for the reaction product; or (ii) the fluid phase containing the reagents is pushed through the membrane pores. In contact with catalyst, the reaction will take place and the reaction product will be collected at the other side of the membrane. In this case, the membrane is always catalytically active, thus the reaction will take place on the catalytic sites within the membrane structure.

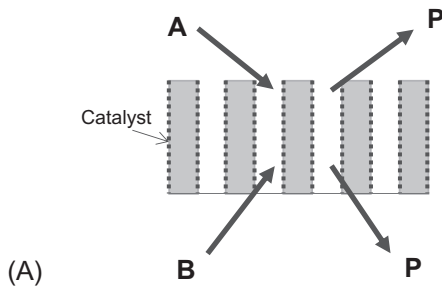
- (a) Interfacial contactor that separates two immiscible reagents. The catalyst is within the membrane pores:
- (b) Interfacial contactor that uses an extractant to extract selectively the reaction product. The catalyst is within the membrane pores or in the feed fluid phase:
- (c) Forced flow-through contactor in which the feed fluid phase goes through the membrane pores. The catalyst is within the membrane pores:

5.7.1 INTERFACIAL MEMBRANE CONTACTOR

In a gas-liquid configuration based on the interfacial contactor ([Fig. 5.24A](#)), the catalytically active layer faces the liquid side. The gas diffuses through the membrane support layer and dissolves in the liquid at the gas-liquid interface. This gas-liquid interface will be placed somewhere within the membrane pores depending on the transmembrane pressure. The reaction zone is located inside the catalytically active membrane, preferentially with partially wetted active sites, which consequently

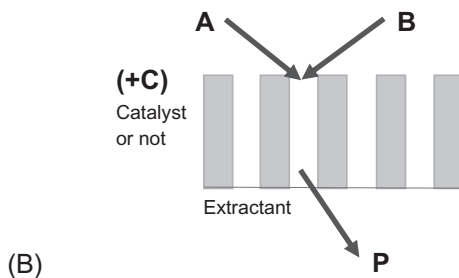
Interfacial contactor that separates two immiscible reagents.

The catalyst is within the membrane pores:



Interfacial contactor that uses an extractant to extract selectively the reaction product.

The catalyst is within the membrane pores or in the feed fluid phase:



Forced-flow through contactor in which the feed fluid phase goes through the membrane pores.

The catalyst is within the membrane pores:

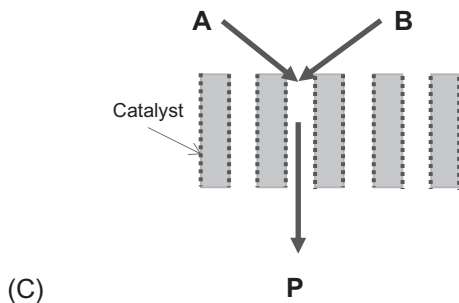


FIG. 5.24

Principles of contactor membrane reactors for the reaction $A + B \rightarrow P$: (A) interfacial contactor separating two immiscible reagents; (B) interfacial contactor using an extracting agent, and (C) forced flow-through contactor.

increases the concentration of gaseous reactant on these sites and enhances the overall reaction rate (Vospernik et al., 2003). The solute further diffuses through the liquid-filled pores and reacts at the catalytically active sites that are located at the pore walls. The reaction products normally tend to diffuse in the direction of the liquid side due to the pressure gradient (Westermann and Melin, 2009). This kind of configuration allows a lot of operational freedom: the gas and liquid flow rates can be varied independently, the transmembrane pressure can be adapted to control the location of the gas-liquid interface, additional substances can be targeted to the catalytic region without mass transfer resistances, and low pressures can be applied since the gas is supplied directly where it is consumed. Some examples of this configuration can be found in the recent literature (Sanchez Marcano and Tsotsis, 2002).

In aqueous-organic contactor, the membrane contactor separates two immiscible phases (Fig. 5.24A and B). The porous membrane is not permselective, but it simply assures well-defined separation and contact between the two liquid phases flowing from opposite sides of the membrane. The membrane can be inert with the catalyst being dissolved in one of the fluid phases, or it can be catalytically active if the catalyst is deposited on the surface of the membrane in order to promote the reaction between adsorbed reactant species. The membrane defines the reaction volume by providing a contacting zone for two immiscible phases. As in the gas-liquid system, the use of membrane contactors introduces a large flexibility in the operation since the flow rates of the two phases involved can be changed independently, as well as the reactant concentration and pressures. A typical application is in phase transfer catalysis, where two immiscible phases containing a water soluble nucleophilic reagent and an organic soluble electrophilic reagent (e.g., anions and organic substrates) are contacted, and a phase transfer catalyst (usually salts like tetraalkylammonium and tetraalkylphosphonium) is used to transfer a reactant from one of these phases into the other, allowing the reaction to occur (Drioli et al., 2005). The separation of the product and the phase transfer catalyst is a main technical challenge where membrane technology (nanofiltration and membrane contactors) offers the possibility of a nondestructive separation that allows reusing the catalyst (DeSmet et al., 2001; Scarpello et al., 2002; Bono et al., 1997; Lopez and Matson, 1997; Noworyta, 2001; Trusek-Holownia and Noworyta, 2002; Giorno et al., 2003b). The microporous membrane used in membrane contactors contributes to increasing the extraction flux due to its large surface. The transfer of the reaction product from the aqueous media to the organic phase enables equilibrium-limited reactions to be carried out to completion due to the combination of catalytic and separation processes, such as in transesterification reactions (Maia Filho et al., 2016). The membrane material may have a hydrophobic or hydrophilic character, thus the membrane will belong to the organic or aqueous phase, respectively (Drioli et al., 2005). Fig. 5.25 shows the typical mechanism in phase transfer catalysis. There is ions partition between the two phases, and the reaction rate is determined by intrinsic kinetics and transport rate (Jia et al., 2014). In case of the presence of the extraction phase, the membrane allows for contact of the reaction medium with the extraction phase without emulsion formation or typical phase separation problems (Sirkar, 2008).

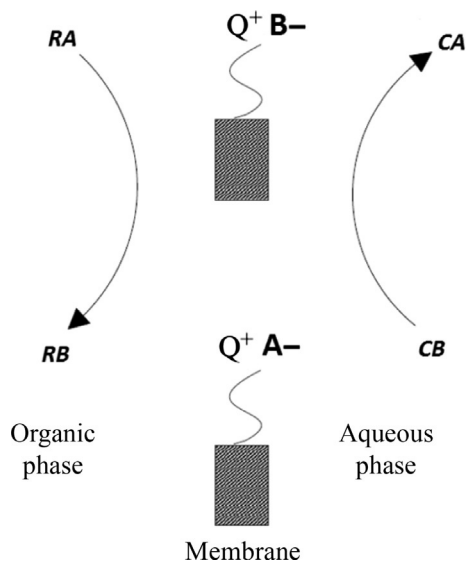


FIG. 5.25

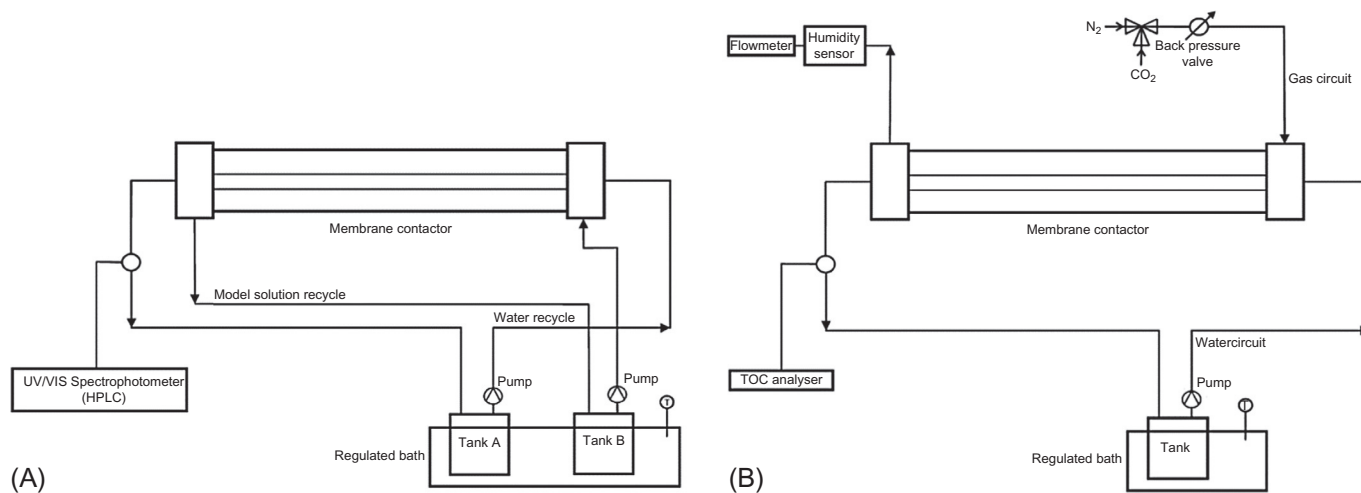
Diagram of phase transfer catalysis mechanism.

Modified from Jia, Z., Zhen, T., Zhang, X., 2014. Application of phase-transfer catalytic membrane reactor in liquid-liquid nucleophilic substitution reaction: effects of operating parameters. *J. Membr. Sci.* 454, 316–321.

A typical experimental system using a contactor membrane reactor as an interfacial contactor is shown in Fig. 5.26 for liquid-liquid systems and gas-liquid systems. Hollow fiber membrane contactors are very common in this application due to their high membrane surface per unit of volume. However, other configurations based on flat membranes can be found in the literature (Maia Filho et al., 2016).

5.7.2 FORCED FLOW THROUGH

In interfacial membrane contactors, mass transport limitation by pore diffusion can occur if the reaction is very fast. A way to minimize the pore diffusion is to pump the whole reaction solution through an asymmetric (ceramic) membrane or a support coated with catalytically active metals (Reif and Dittmeyer, 2003). This configuration is called forced flow-through mode (Fig. 5.24C), where the reactants are premixed and supplied from the same side. The membrane is providing the reaction space with short controlled residence time and high catalytic activity. The objective is to reach complete conversion in minimum time or space, taking advantage of the high catalytic efficiency, or to reach maximum selectivity for a given reaction due to the narrow contact time distribution (Westermann and Melin, 2009). If the reaction solution is pumped through the membrane fast enough, there will not be concentration gradients in the pore system of the catalytic layer and pore diffusion can be totally eliminated. However, if the reaction is not fast enough to achieve a total

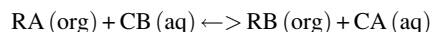
**FIG. 5.26**

Schematic drawing of a ceramic membrane contactor for (A) L-L and (B) G-L mass transfer studies.

Reproduced with permission from Vospernik, M., Pintar, A., Bercic, G., Levec, J., 2003. Mass transfer studies in gas-liquid-solid membrane contactors. Catal. Today 79-80, 169-179.

conversion with one pass through the membrane, a product recycle is necessary (Reif and Dittmeyer, 2003). In this configuration, gas-phase reaction (e.g., isomerization of 1-butene, CO oxidation, decomposition of VOCs) or liquid-phase reactions (e.g., water denitrification, sunflower oil partial hydrogenation) can take place.

In contactor membrane reactors, the study is normally focused on the reactor rate and the product yield and conversion. For example, considering the overall reaction:



the apparent reaction rate can be calculated as (Jia et al., 2014):

$$-\frac{dC_{RA}}{dt} = k_{obs} C_{RA} C_{CB} \quad (5.88)$$

With k_{obs} the observed reaction rate constant, including the effects of intrinsic kinetics and mass transfer; C_{RBr} and C_{KI} are the concentration of RA and CB calculated using the whole volume (volume organic phase plus the volume of the aqueous phase) of the system. Solving the integral with $C_{CB}/C_{RA} = M$, and x as the conversion of RA at time t , leads to the following equation (Jia et al., 2014):

$$\frac{\ln(M-x)}{C_{CB,0} - C_{RA,0}} = W = k_{obs} t \quad (5.89)$$

Thus plotting W versus t leads to a slope of value k_{obs} .

Several variables may affect the observed reaction rate constant, such as the concentrations and flow rates of the organic phase and the aqueous phase. Fig. 5.27 shows the effect of those variables on the reaction rate constant (slope) in an interface membrane reactor used for liquid-liquid nucleophilic reactions between n -bromooctane and KI aqueous solution, the overall reaction being $\text{RBr (org)} + \text{KI (aq)} \leftrightarrow \text{RI (org)} + \text{KBr (aq)}$ (Jia et al., 2014).

From those results, it is clear that mass transfer cannot be neglected in the interfacial membrane contactor. Varying the flow rate of the solutions has a large effect in the observed reaction rate constant, which is an indication of mass transfer resistance in the liquid phase. Diffusion is governing the mass transfer and limiting the reaction rate. In order to elevate the reaction rate, the flow rate of both phases should be increased. Increasing the concentration of the reagents lead also to an increase of the observed reaction rate constant, attributed to the increased diffusion rate of the ions Br^- and I^- from the organic phase and the aqueous phase, respectively, to the L-L interface. The structure and catalytic composition of the membranes presents also a relevant importance in the observed reaction rate constant (Jia et al., 2014). The selection of the appropriate pore dimensions strongly depends on the intended application and the allowable pressure drop (Westermann and Melin, 2009). Thus general guidelines or optimal work conditions are difficult to be established for the moment.

Due to the mass transfer limitations in interfacial membrane contactors, the forced-flow through contactor offers an interesting alternative that minimize diffusional problems. Reif and Dittmeyer (2003) presented the comparison of both

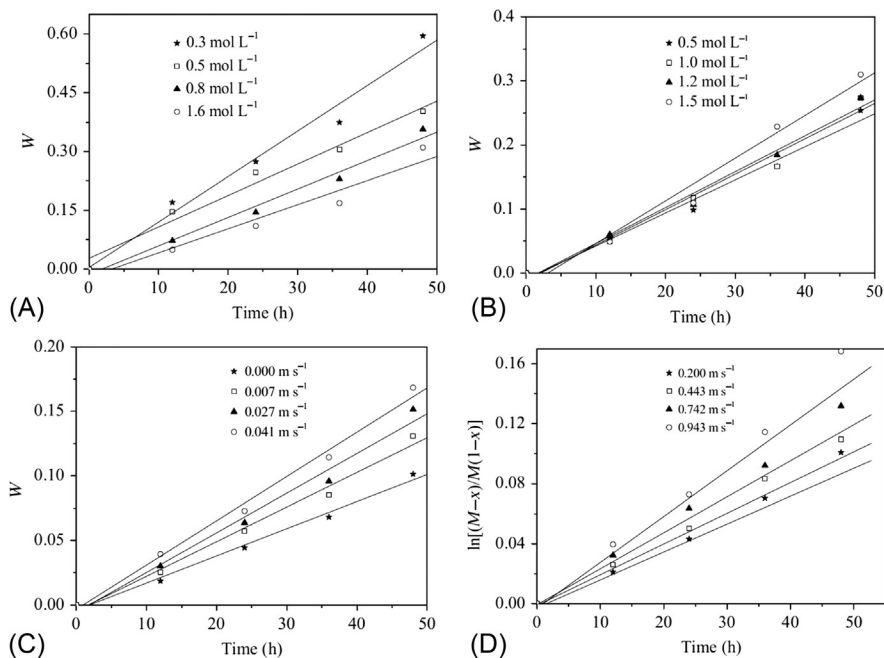


FIG. 5.27

Effects of (A) *n*-bromooctane concentration; (B) KI concentration; (C) KI flow rate; and (D) organic solution flow rate, on the observed reaction rate (slope) according to Eq. (5.89).

Reproduced with permission from Jia, Z., Zhen, T., Zhang, X., 2014. Application of phase-transfer catalytic membrane reactor in liquid–liquid nucleophilic substitution reaction: effects of operating parameters. *J. Membr. Sci.* 454, 316–321.

configurations to perform the catalytic nitrate/nitrite reduction in water. The reactions involved were as follows:

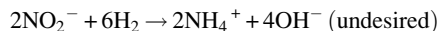
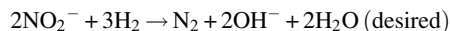
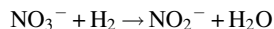


Fig. 5.28 shows the forced-flow through performance at different flow rates through the membrane in comparison with the interfacial contactor (catalytic diffuser) for catalytic nitrite reduction. The catalyst activity is not high when low flow rates are applied in the forced-flow contactor. The higher the flow rate through the membrane, the higher the catalyst activity until reaching a plateau value. The ammonium formation, which is the product of the undesired reaction, is also affected by the flow rate. The shorter the contact time in the porous support, the less ammonium is

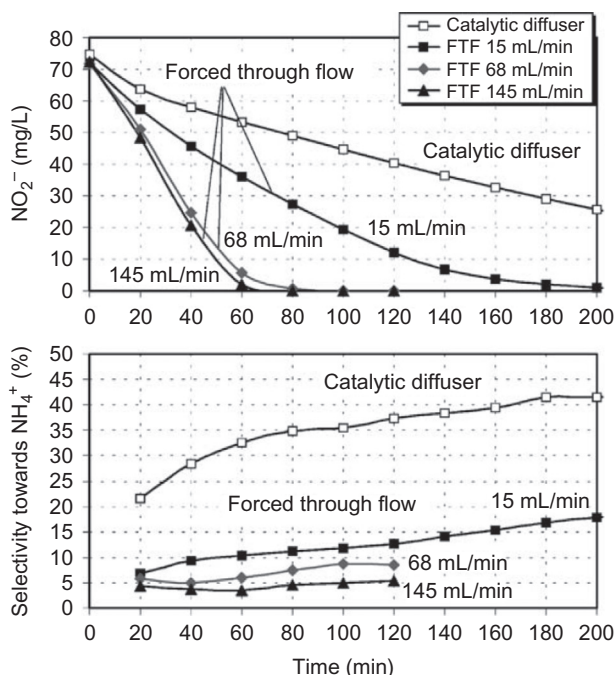


FIG. 5.28

Comparison between forced-flow through contactor at several flow rates through the membrane and interfacial contactor (catalytic diffuser). For the forced flow-through experiment: ceramic support ($\alpha\text{-Al}_2\text{O}_3$); average pore diameter of $3\mu\text{m}$ coated with 18.6 mg Pd. Water was externally saturated with gas ($\text{H}_2:\text{CO}_2$ -ratio = 3:2) at atmospheric pressure. For the catalytic diffuser: asymmetric, tubular, ceramic membrane with a ZrO_2 -top membrane layer with 18.6 mg Pd; 5 bar overpressure in membrane. $\text{H}_2:\text{CO}_2$ -ratio = 3:2. Temperature: 20°C . Reaction volume in both experiments: 750 mL.

Reproduced with permission from Reif, M., Dittmeyer, R., 2003. Porous, catalytically active ceramic membranes for gas-liquid reactions: a comparison between catalytic diffuser and forced through flow concept. *Catal. Today* 82, 3-14.

produced. The interfacial contactor (catalytic diffuser) is presented as a less interesting option in terms of catalytic activity (Reif and Dittmeyer, 2003). The forced-flow contactor decreases the mass transport limitations and intensifies the contact between reactants and the catalytic material. However, membrane blocking and a higher energy consumption to push the fluid through the membrane are weak points of this configuration. Depending on the application, the interfacial contactor may be more advantageous. Conversion, mass transfer limitations, energy consumption, and blocking of the membrane are aspects that will affect directly the overall cost of the process and should be considered for a specific application.

REFERENCES

- Abrahamse, A.J., van der Padt, A., Boom, R.M., Heij, W.B.C., 2001. Process fundamentals of membrane emulsification: simulation with CFD. *AICHE J.* 47, 1285–1291.
- Alkhdhiri, A., Darwish, N., Hilal, N., 2012. Membrane distillation: a comprehensive review. *Desalination* 287, 2–18.
- Bird, R.B., Stewart, W.E., Lightfoot, E.N., 2002. *Transport Phenomena*, second ed. John Wiley & Sons, Inc., New York.
- Bono, Y., Fukushima, K., Araya, G., Nabetani, H., Nakajima, M., 1997. Performance of perstractive enzyme reactor for synthesis of aspartame precursor. *J. Chem. Technol. Biotechnol.* 70, 171–178.
- Charcosset, C., Limayem, I., Fessi, H., 2004. The membrane emulsification process—a review. *J. Chem. Technol. Biotechnol.* 79, 209–218.
- Christov, N.C., Ganchev, D.N., Vassileva, N.D., Denkov, N.D., Danov, K.D., Krachevsky, P.A., 2002. *Colloids Surf. A Physicochem. Eng. Asp.* 209, 83.
- Coelhoso, I.M., Cardoso, M.M., Viegas, R.M.C., Crespo, J.P.S.G., 2000. Transport mechanisms and modelling in liquid membrane contactors. *Sep. Purif. Technol.* 19, 183–197.
- Coulson, J.M., Richardson, J.F., 1999. *Chemical Engineering*, sixth ed. vol. 1. Butterworth Heinemann, Oxford.
- Curcio, E., Drioli, E., 2005. Membrane distillation and related operations—a review. *Sep. Purif. Rev.* 34, 35–86.
- Cussler, E.L., 1997. *Diffusion*. In: *Mass Transfer in Fluid Systems*, second ed. Cambridge University Press, United States of America.
- DeSmet, K., Aerts, S., Ceulemans, E., Vankelecom, I.F.J., Jacobs, P.A., 2001. Nanofiltration-coupled catalysis to combine the advantages of homogeneous and heterogeneous catalysis. *Chem. Commun.* 597–598.
- Drioli, E., Romano, M., 2001. Progress and new perspectives on integrated membrane operations for sustainable industrial growth. *Ind. Eng. Chem. Res.* 40, 1277–1300.
- Drioli, E., Curcio, E., 2004. Perspectives for membrane contactors application in water treatment. *J. Ind. Eng. Chem.* 10 (1), 24–32.
- Drioli, E., Curcio, E., Di Profio, G., 2005. State of the art and recent progresses in membrane contactors. *Chem. Eng. Res. Des. J.* 83, 223–233.
- El-Naas, M.H., Al-Marzouqi, M., Marzouk, S.A., Abdullatif, N., 2010. Evaluation of the removal of CO₂ using membrane contactors: membrane wettability. *J. Membr. Sci.* 350, 410–416.
- Faiz, R., Al-Marzouqi, M., 2009. Mathematical modeling for the simultaneous absorption of CO₂ and H₂S using MEA in hollow fiber membrane contactors. *J. Membr. Sci.* 342, 269–278.
- Gabelman, A., Hwang, S., 1999. Hollow fiber membrane contactors. *J. Membr. Sci.* 159, 61–106.
- Giorno, L., Na, L., Drioli, E., 2003a. Preparation of oil-in-water emulsions using polyamide 10kDa hollow fiber membrane. *J. Membr. Sci.* 217, 173–180.
- Giorno, L., Li, N., Drioli, E., 2003b. Use of stable emulsion to improve stability, activity, and enantioselectivity of lipase immobilized in a membrane reactor. *Biotechnol. Bioeng.* 84, 677–685.
- Giorno, L., Mazzei, R., Oriolo, M., De Luca, G., Davoli, M., Drioli, E., 2005. Effects of organic solvents on ultrafiltration polyamide membranes for the preparation of oil-in-water emulsions. *J. Colloid Interface Sci.* 287, 612–623.

- Gómez, E., González, B., Calvar, N., Tojo, E., Domínguez, A., 2006. Physical properties of pure 1-ethyl-3-methylimidazolium ethylsulfate and its binary mixtures with ethanol and water at several temperatures. *J. Chem. Eng. Data* 51, 2096–2102.
- Gryta, M., 2005. Osmotic MD and other membrane distillation variants. *J. Membr. Sci.* 246, 145–156.
- Gryta, M., Tomaszewska, M., Morawski, A.W., 1997. Membrane distillation with laminar flow. *Sep. Purif. Technol.* 11, 93–101.
- Happel, J., 1959. Viscous flow relative to arrays of cylinders. *AIChE J.* 5, 174–177.
- Higbie, R., 1935. The rate of absorption of a pure gas into a still liquid during short periods of exposure. *Trans. Am. Inst. Chem. Eng.* 31, 365–389.
- Jia, Z., Zhen, T., Zhang, X., 2014. Application of phase-transfer catalytic membrane reactor in liquid–liquid nucleophilic substitution reaction: effects of operating parameters. *J. Membr. Sci.* 454, 316–321.
- Joscelyne, S.M., Trägårdh, G., 2000. Membrane emulsification—a literature review. *J. Membr. Sci.* 169, 107–117.
- Joscelyne, S.M., Trägårdh, G., 1999. Food emulsions using membrane emulsification: conditions for producing small droplets. *J. Food Eng.* 39, 59–64.
- Kandori, K., Kishi, K., Ishikawa, T., 1991. Formation mechanisms of monodispersed W/O emulsions by SPG filter emulsification method. *Colloids Surf.* 61, 269–279.
- Kanichi, S., Yuko, O., Yoshio, H., 2002. Properties of Solid Fat O/W Emulsions Prepared by Membrane Emulsification Method Combined with Pre-Emulsification. *3^e i^eme Congr^es Mondial de l'Emulsion*, 24–27 September 2002, Lyon, France, p. 215.
- Kobayashi, I., Nakajima, M., Mukataka, S., 2003. *Colloids Surf. A Physicochem. Eng. Asp.* 229, 33.
- Lawson, K.W., Lloyd, D.R., 1997. Membrane distillation. *J. Membr. Sci.* 124, 1–25.
- Li, W., Van der Bruggen, B., Luis, P., 2014. Integration of reverse osmosis and membrane crystallization for sodium sulphate recovery. *Chem. Eng. Process. Process Intensif.* 85, 57–68.
- Li, W., Van der Bruggen, B., Luis, P., 2016. Recovery of Na₂CO₃ and Na₂SO₄ from mixed solutions by membrane crystallization. *Chem. Eng. Res. Des.* 106, 315–326.
- Lopez, J., Matson, S., 1997. A multiphase/extractive enzyme membrane reactor for production of diltiazem chiral intermediate. *J. Membr. Sci.* 125, 189–211.
- Lu, J., Wang, L., Sun, X., Li, J., Liu, X., 2005. Absorption of CO₂ into aqueous solutions of methyl-diethanolamine and activated methyl-diethanolamine from a gas mixture in a hollow fiber contactor. *Ind. Eng. Chem. Res.* 44, 9230–9238.
- Lu, J., Zheng, Y.F., Cheng, M.D., 2008. Wetting mechanism in mass transfer process of hydrophobic membrane gas absorption. *J. Membr. Sci.* 308, 180–190.
- Luis, P., Van der Bruggen, B., 2013. The role of membranes in postcombustion CO₂ capture. *Greenhouse Gas Sci. Technol.* 3, 1–20. <https://doi.org/10.1002/ghg>.
- Luis, P., Garea, A., Irabien, A., 2010. Modelling of a hollow fiber ceramic contactor for SO₂ absorption. *Sep. Purif. Technol.* 72, 174–179.
- Luis, P., Garea, A., Irabien, A., 2008. Sulfur dioxide non-dispersive absorption in N,N-dimethylaniline using a ceramic membrane contactor. *J. Chem. Technol. Biotechnol.* 83, 1570–1577.
- Luis, P., Garea, A., Irabien, A., 2009. Zero solvent emission process for sulfur dioxide recovery using a membrane contactor and ionic liquids. *J. Membr. Sci.* 330, 80–89.
- Luis, P., Van Aabel, D., Van der Bruggen, B., 2013. Technical viability and exergy analysis of membrane crystallization: closing the loop of CO₂ sequestration. *Int. J. Greenhouse Gas Control* 12, 450–459.

- Maia Filho, D.C., Salim, V.M.M., Borges, C.P., 2016. Membrane contactor reactor for transesterification of triglycerides heterogeneously catalyzed. *Chem. Eng. Process.* 108, 220–225.
- Nakashima, T., Shimizu, M., Kukizaki, M., 1991. Membrane emulsification by microporous glass. *Key Eng. Mater.* 61–62, 513–516.
- Noworyta, A., 2001. Membrane reactors. In: Noworyta, A., Trusek-Holownia, A. (Eds.), *Membrane Separations*. Argi, Wroclaw, pp. 97–119.
- Peng, S.J., Williams, R.A., 1998. Controlled production of emulsions using a crossflow membrane—Part I: droplet formation from a single pore. *Trans. IChemE* 76A, 894–901.
- Prandtl, L., 1910. Eine Beziehung zwischen Wärmeaustausch und Strömungswiderstand der Flüssigkeiten. *Physik Z.* 11, 1027.
- Prandtl, L., 1928. Bemerkung über den Wärmeübergang im Röhr. *Physik Z.* 29, 487.
- Ranke, J., Stolte, S., Störmann, R., Aming, J., Jastorff, B., 2007. Design of sustainable chemical products—the example of ionic liquids. *Chem. Rev.* 107, 2183–2206.
- Rayner, M., Trägårdh, G., Trägårdh, C., Dejmek, P., 2004. Using the surface evolver to model droplet formation processes in membrane emulsification. *J. Colloid Interface Sci.* 279, 175–185.
- Rayner, M., Tragardh, G., Tragardh, C., 2005. The impact of mass transfer and interfacial expansion rate on droplet size in membrane emulsification processes. *Colloids Surf. A: Physicochem. Eng. Asp.* 266, 1–17.
- Rayner, M., Tragardh, G., 2002. Membrane emulsification modelling: how can we get from characterization to design? *Desalination* 145, 165–172.
- Raynie, D.E., 2006. Modern extraction techniques. *Anal. Chem.* 78, 3997–4003.
- Reif, M., Dittmeyer, R., 2003. Porous, catalytically active ceramic membranes for gas–liquid reactions: a comparison between catalytic diffuser and forced through flow concept. *Catal. Today* 82, 3–14.
- Ruiz-Salmón, I., Janssens, R., Luis, P., 2017. Mass and heat transfer study in osmotic membrane distillation-crystallization for CO₂ valorization as sodium carbonate. *Sep. Purif. Technol.* 176, 173–183.
- Ruiz-Salmón, I., Luis, P., 2018. Membrane crystallization via membrane distillation. *Chem. Eng. Process. Process Intensif.* 123, 258–271.
- Sandler, S.I., 2006. *Chemical, Biochemical, and Engineering Thermodynamics*, fourth ed. John Wiley & Sons, USA.
- Sanchez Marcano, J.G., Tsotsis, T.T., 2002. *Catalytic membranes and membrane reactors*. Wiley-VCH, Weinheim.
- San Román, M.F., Bringas, E., Ibañez, R., Ortiz, I., 2010. Liquid membrane technology: fundamentals and review of its applications. *J. Chem. Technol. Biotechnol.* 85, 2–10.
- Scarpello, J.T., Nair, D., Freitas dos Santos, L.M., White, L.S., Livingston, A.G., 2002. The separation of organometallic catalysts using solvent resistant nanofiltration. *J. Membr. Sci.* 180, 1–15.
- Schlosser, S., Sabolová, E., Kertész, R., Kubisová, L., 2001. Factors influencing transport through liquid membranes and membrane-based solvent-extraction. *J. Sep. Sci.* 24, 509.
- Schlosser, S., Kertész, R., Marták, J., 2005. Recovery and separation of organic acids by membrane-based solvent extraction and pertraction. An overview with a case study on recovery of MPCA. *Sep. Purif. Technol.* 41, 237–266.
- Schröder, V., Behrend, O., Schubert, H., 1998. Effect of dynamic interfacial tension on the emulsification process using microporous, ceramic membranes. *J. Colloid Interface Sci.* 202, 334–340.

- Schröder, V., Schubert, H., 1999a. Influence of emulsifier and pore size on membrane emulsification. *Spec. Publ. R. Soc. Chem.* 227, 70–80.
- Schröder, V., Schubert, H., 1999b. Production of emulsions using microporous, ceramic membranes. *Colloids Surf. A Physicochem. Eng. Asp.* 152, 103–109.
- Seader, J.D., Henley, E.J., Roper, K., 2011. *Separation Process Principles: Chemical and Biochemical Operations*, 3rd ed. Wiley, Hoboken, NJ.
- Sengupta, A.; Peterson, P. A.; Miller, B. D.; Schneider, J.; Fulk, C. W., Jr. Large-scale application of membrane contactors for gas transfer from or to ultrapure water. *Sep. Purif. Technol.* 1998, 14, 189–200.
- Sirkar, K.K., 2008. Membranes, phase interfaces, and separations: Novel techniques and membranes—an overview. *Ind. Eng. Chem. Res.* 47 (15), 5250–5266.
- Sirkar, K.K., 1995. Membrane separations: newer concepts and applications for the food industry. In: Singh, R.K., Rizvi, S.S.H. (Eds.), *Bioseparation Processes in Foods*. Marcel Dekker, New York (Chapter 10).
- Spyropoulos, F., Lloyd, D.M., Hancocks, R.D., Pawlik, A.K., 2014. Advances in membrane emulsification. Part B: recent developments in modelling and scale-up approaches. *J. Sci. Food Agric.* 94, 628–638.
- Sugiura, S., Nakajima, M., Iwamoto, M., Seki, M., 2001. Interfacial tension driven monodispersed droplet formation from microfabricated channel array. *Langmuir* 17, 5562.
- Suzuki, K., Fujiki, I., Hagura, Y., 1998. Preparation of corn oil/water and water/corn oil emulsions using PTFE membranes. *Food Sci. Technol.* 4, 164–167.
- Taylor, G.I., 1916. Conditions at the Surface of a Body Exposed to the Wind. *Brit. Adv. Com. Aero. Rep. Mem. No. 272*, 423–429.
- Trusek-Holownia, A., Noworyta, A., 2002. Catalytic membrane preparation for enzymatic hydrolysis reactions carried out in the membrane phase contactor. *Desalination* 144, 427–432.
- Tun, C.M., Fane, A.G., Matheickal, J.T., Sheikholeslami, R., 2005. Membrane distillation crystallization of concentrated salts—flux and crystal formation. *J. Membr. Sci.* 257, 144–155.
- Viegas, R.M.C., Rodríguez, M., Luque, S., Alvarez, J.R., Coelho, I.M., Crespo, J.P.S.G., 1998. Mass transfer correlations in membrane extraction: analysis of Wilson-plot methodology. *J. Membr. Sci.* 145, 129–142.
- Vladislavljević, G.T., Schubert, H., 2003. Influence of process parameters on droplet size distribution in SPG membrane emulsification and stability of prepared emulsion droplets. *J. Membr. Sci.* 225, 15–23.
- Vladislavljević, G.T., Tesch, S., Schubert, H., 2002. Preparation of water-in-oil emulsions using microporous polypropylene hollow fibers: influence of some operating parameters on droplet size distribution. *Chem. Eng. Process.* 41, 231–238.
- Vospersnik, M., Pintar, A., Bercic, G., Levec, J., 2003. Mass transfer studies in gas–liquid–solid membrane contactors. *Catal. Today* 79–80, 169–179.
- Westermann, T., Melin, T., 2009. Flow-through catalytic membrane reactors—principles and applications. *Chem. Eng. Process.* 48, 17–28.
- Yamazaki, N., Yuyama, H., Nagai, M., Ma, G.H., Omi, S., 2002. A comparison of membrane emulsification obtained using SPG (Shirasu porous glass) and PTFE [poly(tetrafluoroethylene)] membranes. *J. Dispers. Sci. Technol.* 23, 279–292.
- Yang, D., Barbero, R.S., Devlin, D.J., Cussler, E.L., Colling, C.W., Carrera, M.E., 2006. Hollow fibers as structured packing for olefin/paraffin separations. *J. Membr. Sci.* 279, 61–69.

- Yasuno, M., Nakajima, M., Iwamoto, S., Maruyama, T., Sugiura, S., Kobayashi, I., Shono, A., Satoh, K., 2002. Visualisation and characterization of SPG membrane emulsification. *J. Membr. Sci.* 210, 29.
- Ye, W., Lin, J., Shen, J., Luis, P., Van der Bruggen, B., 2013. Membrane crystallization of sodium carbonate for carbon dioxide recovery: effect of impurities on the crystal morphology. *Cryst. Growth Des.* 13, 2362–2372.
- Ye, W., Lin, J., Tækker Madsen, H., Gydesen Sjøgaard, E., Hélix-Nielsen, C., Luis, P., Van der Bruggen, B., 2016. Enhanced performance of a biomimetic membrane for Na_2CO_3 crystallization in the scenario of CO_2 capture. *J. Membr. Sci.* 498, 75–85.
- Younas, M., Druon-Bocquet, S., Sanchez, J., 2011. Experimental and theoretical mass transfer transient analysis of copper extraction using hollow fiber membrane contactors. *J. Membr. Sci.* 382, 70–81.

FURTHER READING

- Karoor, S., Sirkar, K., 1993. Gas absorption studies in microporous hollow fiber membrane modules. *Ind. Eng. Chem. Res.* 32, 674–684.
- Zheng, J.M., Xu, Y.Y., Xu, Z.K., 2003. Shell side mass transfer characteristics in a parallel flow hollow fiber membrane module. *Sep. Sci. Technol.* 38, 1247–1267.

Membrane bioreactors

Cláudia F. Galinha*, Sandra Sanches[†], João G. Crespo*

LAQV - REQUIMTE, Department of Chemistry, Faculty of Sciences and Technology, NOVA University of Lisbon, Caparica, Portugal* iBET, Institute of Experimental Biology and Technology, Oeiras, Portugal[†]

CHAPTER OUTLINE

6.1 Process Description	209
6.2 General Overview of Applications	211
6.3 Design of Membrane Bioreactors	212
6.3.1 Enzymatic Membrane Bioreactors	212
6.3.2 Microbial Membrane Bioreactors	215
6.3.3 Animal and Plant Cell Bioreactors	224
6.4 Monitoring and Control of Membrane Bioreactors	225
6.4.1 Off-Line Monitoring	226
6.4.2 Online, Real-Time Monitoring of Membrane Bioreactors	230
6.5 Modeling of Membrane Bioreactors	232
6.5.1 Mechanistic Modeling Approaches	232
6.5.2 Multivariate Statistical Analysis Methods	237
6.5.3 Hybrid Modeling	241
6.6 Conclusions and Outlook	242
References	243

6.1 PROCESS DESCRIPTION

Membrane bioreactors offer a unique opportunity to restrict the physical space of a biocatalyst, which can be an enzyme, a microorganism, or a plant/animal cell. By restricting the physical space of a catalyst its continuous use, or reuse, becomes possible avoiding loss by washing out from the reactor. This feature represents a huge advantage considering the cost of the biocatalyst (or the time and work necessary to reload a reactor) and the fact that the outlet stream will be free of biocatalyst, making the process of product recovery significantly easier.

By restricting the physical space of the biocatalyst, it becomes possible to operate the bioreactor uncoupling the biocatalyst residence time from the hydraulic residence time. This is particularly important when using microorganism or cells that have a relatively slow growth kinetics. When dealing with microbial or cell bioreactors, the adjustment of the biocatalyst residence time (commonly designated as solids residence time, SRT) makes possible to increase its concentration and control it at a desirable level. This control can be easily implemented by establishing a microbial/cell purge.

There are several ways to restrict the physical space of a biocatalyst. When dealing with enzymes (biocatalyst that does not duplicate) it is common to immobilize it to a membrane. This immobilization may be achieved by covalent or ionic bonding to the membrane surface, but it may also be immobilized by entrapment within the membrane. Covalent and ionic bonding are techniques that usually lead to a very effective linking of the biocatalyst to the membrane but, on the other hand, it may induce changes on the enzyme conformation which may impact its activity and selectivity. Therefore it is common to observe situations where the enzymatic stability improves at the cost of a decrease of activity and selectivity.

The restriction of the physical space of a biocatalyst may also be achieved by entrapment within the porous structure of a supporting membrane. In this case, the biocatalyst is forced through the pores and imprisoned within the void free space of the membrane. If asymmetric ultrafiltration membranes are used, this physical confinement may be rather effective and long operation periods may be attained without a significant biocatalyst loss to the contacting fluid phase(s).

Alternatively, the biocatalyst may be allowed to move freely in suspension—mass transfer limitations may be easily overcome—and a micro-/ultra-filtration membrane is used just to avoid its permeation and loss from the reactor. The membrane acts as a permselective barrier that allows products to permeate but retains the biocatalyst in a reduced physical space. In this case, the biocatalyst may be an enzyme, a microorganism, or a eukaryotic cell, active and able to duplicate. This type of membrane bioreactor assumes usually two possible configurations: 1—an external loop recycle reactor, or 2—a submerged membrane reactor.

In the external loop recycle reactor (Judd, 2006) the membrane unit (usually a micro- or ultrafiltration membrane) is external to reaction vessel (also known as “side-stream MBR”); the retentate containing the biocatalyst is recycled to the reactor, while the permeate is recovered free of biocatalyst. As mentioned previously, the hydraulic residence time (total volume of the reactive system /permeate flow rate) can be adjusted independently from the biocatalyst residence time (total volume of the reactive system/biocatalyst purge flow rate), which is quite advantageous. In this type of configuration, the operating conditions in the reaction vessel and in the membrane module can be adjusted independently, which gives a large degree of freedom for design and operation of these systems.

The submerged membrane bioreactors were first proposed in 1988 by Yamamoto and coworkers (Yamamoto et al., 1988). This concept involves the direct immersion of the membrane in the medium of the bioreactor. The permeate is sucked through

the membrane—both flat-sheet and hollow fiber configurations are commercially available—and removed from the reactor, which is fed continuously and operated at constant volume. This configuration is particularly successful for aerobic treatment of domestic wastewaters, because aeration assures simultaneously several tasks: provides oxygen to the microbial culture, keeps solids in suspension, improves external mass transfer conditions, and scours the membrane surface minimizing fouling. One of the most interesting aspects of submerged membrane bioreactors is the fact that the membrane is operated under very gentle transmembrane pressure, imposing a controlled and constant permeate flux, in order to adjust the convective transport of solutes and particulates to the membrane surface. Typically, these systems are operated under subcritical or sustainable permeate flux conditions, allowing for prolonged operation without the need for membrane cleaning.

The use of membrane bioreactors with eukaryotic cells is less generalized and implemented in large scale. In this case, the most common configurations are the ones described for microbial cells and, in particular, the use of submerged membrane bioreactors has been strongly suggested due to the possibility of operating under extremely gentle conditions, with minimal shear stress at the membrane surface. The possibility of using membranes to deliver oxygen in a nondispersive mode while simultaneously removing carbon dioxide has been also described in a number of exploratory works.

Finally, it is worth mentioning the research work developed with photocatalytic membrane bioreactors, namely, involving microalgae, and the use of dense, nonporous membranes for the transport of specific target compounds: the concept of Extractive Membrane Bioreactor (EMB) (Santos et al., 1995), Ion-Exchange Membrane Bioreactor (IEMB) (Fonseca et al., 2000), and Pervaporative Membrane Bioreactor (PMB) (Izák et al., 2005). None of these are applied at large scale but they represent very interesting approaches for the specific transport of a class of compounds (respectively, hydrophobic compounds (EMB), ionic compounds (IEMB), and volatile compounds (PMB)).

6.2 GENERAL OVERVIEW OF APPLICATIONS

For many researchers and engineers, the term “Membrane Bioreactor” applies exclusively to membrane bioreactors for wastewater treatment. This is by far the largest application of membrane bioreactors, with several large-scale plants running in Europe, Asia, and North America. This type of application involves the use of suspended mixed microbial cultures and the dominant configuration is the so-called submerged membrane bioreactor, due to the possibility to operate under controlled permeate flux, which renders low transmembrane pressures and allows for long operating periods without the need for plant maintenance for cleaning of the membranes. This type of application will be discussed in detail further in this chapter.

In terms of industrial applications is still worth mentioning the use of enzymatic membrane bioreactors using different types of configurations, namely, making use of

covalent/electrostatic binding and using physical entrapment within the membrane porous structure. The diversity of reported applications is huge but this number is not followed by a significant industrial use. Medical and pharmaceutical applications have been largely reported, as well as agro-food applications and wastewater treatment applications. Examples of industrial scale enzymatic membrane bioreactors in the pharmaceutical field include the production of amino acids with simultaneous regeneration of NADH by Evonik in Germany (Wandrey, 2004) and the hydrolysis of triglycerides by Kao Corporation in Japan (Nam and Furusaki, 1991). It is expected that application to lignocellulosic enzymatic process will be growing in the near future, as well as the use of specific enzymatic cocktails for treatment of extremely resilient effluents (some of them with limited volumes to be processed but without sustainable proved alternatives).

The generalized use of eukaryotic membrane bioreactors seems more distant, although a growing interest seems clear involving the use of microalgae membrane bioreactors.

A list of membrane bioreactors in industrial processes can be found elsewhere (Giorno et al., 2009).

6.3 DESIGN OF MEMBRANE BIOREACTORS

6.3.1 ENZYMATIC MEMBRANE BIOREACTORS

The purpose of this section is not to enumerate and describe the large number of scientific works about enzymatic membrane bioreactors published in the literature during the last 30 years but, otherwise to identify main achievements and relevant constraints and opportunities.

The first issue that should be examined critically is the way enzymes are immobilized. As discussed previously, covalent bonding and electrostatic interactions may be used to immobilize enzymes on membranes, in a rather stable and permanent mode. As a consequence, it is common to observe a high stability of the immobilized enzymes upon immobilization. However, due to potential changes of enzyme conformation induced by the immobilization process, it is also common to observe a significant decrease of the enzymatic activity—which may be lowered by 2–3 orders of magnitude—together with a loss of selectivity. This impact in activity and selectivity results from changes of conformation of the immobilized enzyme, which can be easily observed by well-established techniques such as natural steady-state fluorescence spectroscopy and fluorescence anisotropy (Portugal et al., 2006). When using these techniques, amino acids with a fluorescence response and a high quantum yield—such as tryptophan—will exhibit a fluorescence emission that changes with their local microenvironment. If a protein unfolds due to chemical bonding or interaction with a supporting membrane material, the local environment of these amino acids within the enzyme will also change.

As a consequence, shifts in their fluorescence emission are clearly observed: 1—a so-called red shift, with the emission maximum moving to higher wavelengths, when a protein amino acid such as tryptophan becomes more exposed to a polar microenvironment, which may happen when protein unfolding exposes these amino acids to the external solvent water; 2—a so-called blue shift may also be observed when the interaction of the enzyme with the immobilizing matrix induces a more compact folding that restricts the exposure of these amino acids to the solvent. Other fluorescence changes may also be observed, such as changes in the maximum fluorescence intensity and band broadening, which can be easily related with conformation changes and/or protein aggregation phenomena.

Fluorescence anisotropy may also provide extremely useful information: a lower anisotropy means that the natural fluorophores in a protein (such as tryptophan) move more freely, which is usually related with unfolding phenomena that lead to a less restricted microenvironment near those fluorophores. Fig. 6.1 shows how steady-state fluorescence spectroscopy and fluorescence anisotropy respond when changes in a protein conformation are induced.

The previous discussion is necessary if one wants to understand how important is to select and use immobilization techniques that induce the minimum change in the enzyme conformation, in order to keep its function, translated here by its activity and selectivity.

Modeling of these types of enzymatic membrane bioreactors, operated in a continuous mode with a full retention of the enzyme, is rather simple and reported

Protein: β -lactoglobulin

Fluorescence reporter: tryptophan

Chemical denaturant agent: Guanidine hydrochloride (GndHCl)

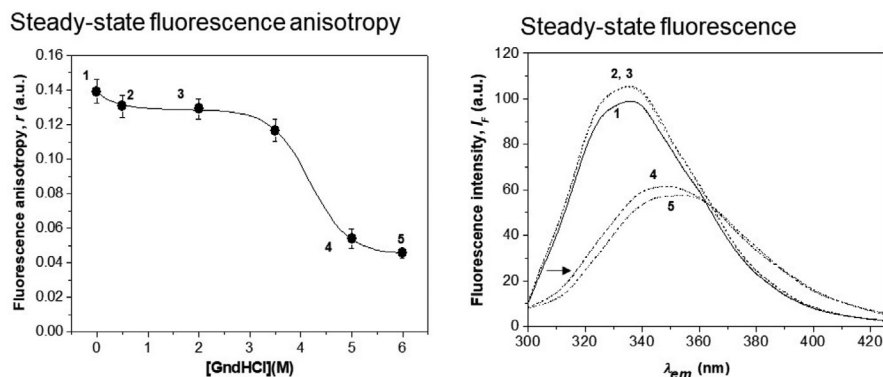


FIG. 6.1

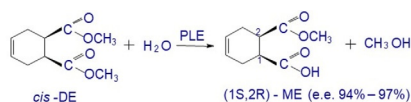
Protein-induced denaturation by addition of Guanidine Hydrochloride (GndHCl) monitored by steady-state fluorescence anisotropy (left) and steady-state fluorescence (right). Numbers 1–6 refer to increasing GndHCl concentrations.

previously in the literature. Simple mass balances to substrate(s) (S) and product(s) (P), integrated with the enzyme kinetics obtained in independent kinetic studies, allow to derive $S(t)$ and $P(t)$ equations that depend on the enzymatic kinetic parameters and the fluid residence time. If required, a term accounting for enzymatic deactivation/denaturation may also be included (Iorio et al., 1994).

Entrapment is a totally different approach for enzyme immobilization. The entrapment method of immobilization is based on the localization of the enzyme within the membrane matrix, restricting its physical domain. A very simple and effective way to assure immobilization by entrapment in membranes involves the use of asymmetric membranes. In this case, a solution with the enzyme is pumped from the open-pore side of the membrane to the tight-pore side. If a membrane with a molecular weight cutoff lower than the enzyme molecular mass is used, then the enzyme becomes imprisoned within the membrane porous structure. The advantage of this technique is that the impact on the enzyme conformation is significantly lower, especially if hydrophilic membranes are used, and the mass transfer conditions are rather good when comparing with enzyme immobilization techniques such as occlusion. Still, it is necessary to assure a good enzyme load and distribution of the enzyme within the membrane. Also, it is important to monitor possible enzyme losses during operation, from the membrane to the contacting fluid phases.

Immobilization by entrapment is particularly a well-suited technique if the enzymatic membrane bioreactor is operated as a membrane biphasic contactor. In this case, after immobilization of the selected enzyme within the asymmetric ultrafiltration membrane porous structure, the feed phase containing the substrate is brought into contact in one side of membrane, while a receiving phase for collecting the product of reaction is brought to contact on the opposite side. If the two phases, feed and receiving, have a different character, that is, an organic and an aqueous phase, then the membrane module works as a membrane contactor: if a hydrophilic membrane is selected, the pores of the membrane are wetted by the aqueous phase while the organic phase stays on the opposite side, contacting with the aqueous phase at the pores' mouth. If the two phases are equilibrated by a judicious selection of the pressure difference between them, then their interface remains stable during the operation process.

This type of enzymatic membrane bioreactor/biphasic membrane contactor represents an extremely interesting solution when substrate and product are not mutually soluble in the same type of solvent. Take, for example, the case of the enantiomeric conversion of the meso-diester dimethyl *cis*-cyclohex-4-ene-1,2-dicarboxylate to the enantiomerically pure (1*S*,2*R*)-cyclohex-4-ene-1,2-dicarboxylic acid monomethyl ester by a pig liver esterase (PLE), where the substrate is soluble in organic solvents such as hexane or heptane (allowed in food and pharma applications) but not soluble in water, and the product is soluble in water but not soluble in hexane or heptane (Sousa et al., 2005). In this case, an enzymatic membrane contactor can be designed where the organic feed phase containing the substrate contacts a membrane with PLE previously immobilized by entrapment, without penetrating its pores. On the receiving side an aqueous solution collects the product of reaction, which takes place at the



Physical entrapment of Pig Liver Esterase (PLE) inside the microporous structure of a polysulfone asymmetric hydrophilic ultrafiltration membrane

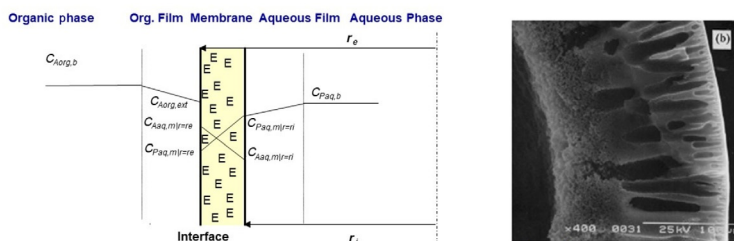


FIG. 6.2

Enzymatic enantioselective conversion of the meso-diester dimethyl *cis*-cyclohex-4-ene-1,2-dicarboxylate to the enantiomerically pure (1*S*,2*R*)-cyclohex-4-ene-1,2-dicarboxylic acid monomethyl ester, using Pig Liver Esterase immobilized by entrapment in the asymmetric porous structure of an ultrafiltration polysulfone membrane.

organic/aqueous interface, free of substrate. This type of system is particularly elegant because it allows for simultaneously accomplishing the target enzymatic reaction and assures a complete separation between substrate and product, with the recovery of a pure target product (see Fig. 6.2).

The mathematical modeling of this type of system is not particularly complex requiring the knowledge about the enzymatic kinetics and appropriate mass balances to the membrane contactor. This process modeling, for the reaction discussed previously performed in a hollow fiber membrane contactor is presented in Sousa et al. (2005).

6.3.2 MICROBIAL MEMBRANE BIOREACTORS

Membrane bioreactors for wastewater treatment

The major application of membrane bioreactor (MBR) systems, and the most studied, is in biological treatment of wastewaters. Biological treatment of wastewaters is done by a consortium of microorganisms (mainly bacteria and protozoa), the so-called activated sludge, that together can degrade and consume the organic and inorganic nutrients present in wastewaters. In conventional activated sludge (CAS) systems, the liquid effluent is obtained through sedimentation of solids, which depends on the settle ability of the biomass. However, by using membranes to retain suspended solids in MBRs, all solids have the same residence time (solids retention time, *SRT*), which is independent of the hydraulic retention time (*HRT*). Therefore MBRs can be operated at high biomass concentration, and, unlike the conventional

activated sludge systems, can easily retain slow growing organisms with poor settle ability, like nitrifying bacteria (Seviour and Nielsen, 2010).

Besides the biological advantages associated with the use of a membrane, the quality of the treated effluent is higher in MBRs than in CAS systems. Permeate high quality allows the direct application of the MBR technology when advanced treatments are required, such as for bathing water, sensitive discharge bodies of water, or water reuse. Additionally, due to high biomass concentration and the elimination of settlers, MBRs have smaller footprints than CAS, which can be valuable when a compact system is needed, such as in areas with high population density.

The MBR features are also advantageous in the treatment of industrial wastewaters, where the influent may have lower biodegradability and/or comprise toxic compounds, meaning that the microorganisms require more time for adaptation and have lower kinetic rates.

Generally, MBRs can be operated as side-stream or submerged (Fig. 6.3), according with the membranes placement and operation. In side-stream MBRs, membranes are placed externally to the biological reactor and the mixed liquor is pumped into the membrane module. In the membrane module, a permeate stream is generated and the concentrated sludge is recycled to the bioreactor. In the side-stream configuration, membrane filtration occurs as a typical cross-flow process.

In submerged MBRs, the membrane module is directly immersed in the mixed liquor, in the aerated bioreactor. This operating strategy was first introduced by Yamamoto et al. (1988) with the objective of reducing energy consumption associated with the recirculation pump in the side-stream configuration. The submerged MBR configuration corresponds to a dead-end filtration, with shear stress generated by the air bubble flow.

Besides the membrane module placement, the biological compartment of an MBR, like in CAS systems, can be operated in a wide range of bioreactor configurations to achieve specific nutrient removal (e.g., pre- or postdenitrification).

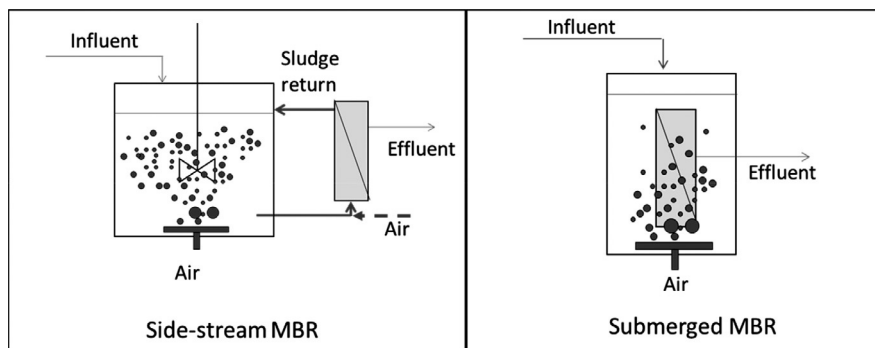


FIG. 6.3

Side-stream and submerged MBR configurations.

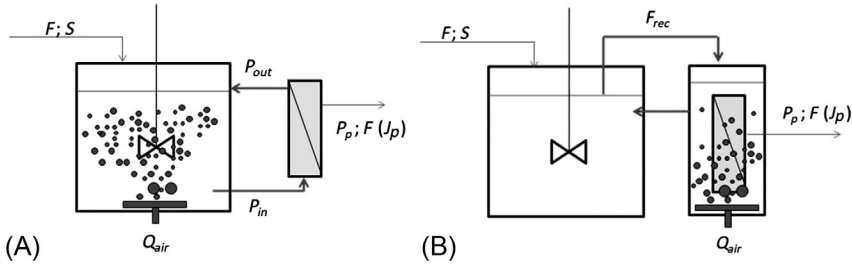


FIG. 6.4

Operating parameters in side-stream (A) and submerged (B) MBRs for wastewater treatment.

Fig. 6.4B shows an example of a submerged MBR with two compartments, the first under anoxic conditions (no oxygen supply) and the second (where the membrane module is submerged) under aerobic conditions.

The usual operating parameters associated with MBRs are permeate flux (J_p), hydraulic retention time (HRT), solids retention time (SRT), transmembrane pressure (TMP), recirculation ratio, cross-flow velocity, and aeration flow.

According to the configurations shown in Fig. 6.4, the following parameters can be defined: F is the volumetric flow of influent and effluent, J_p is the permeate flux, S is the substrate concentration, F_{rec} is the recirculation flow, Q_{air} is the air flow, P_p is the pressure in the permeate line, P_{in} is the pressure on feed side, P_{out} is the pressure on retentate side, V is the volume of the biological reactor, and X is the biomass concentration.

The permeate flux (defined as for other filtration processes) is the permeate flow per membrane area.

$$J_p = \frac{F}{\text{Membrane area}}$$

Since MBRs are usually operated in continuous mode, at constant volume, the permeate flow is also equal to the influent flow.

The HRT and SRT are, respectively, the residence time of liquid and solids inside the MBR.

$$HRT = \frac{V}{F}$$

$$SRT = \frac{V}{\text{Purge/time}}$$

While the HRT is dependent on flow, the SRT depends on regular purges of the reactor (including solids and liquid) and, thus the later can be infinite if no purges are made. However, longer SRT times, tending to infinite, result in older sludges, with high death rates and lower growth rates, leading to a decline in the biologic performance.

MBRs for wastewater treatment are usually operated at constant permeate flux (Drews, 2010), and thus the transmembrane pressure (*TMP*) is used as a fouling indicator parameter.

$$TMP = \frac{P_{in} + P_{out}}{2} - P_p$$

When calculating the *TMP* for submerged MBRs the pressure on the feed and retentate sides of the membrane is the same, and usually equal to atmospheric pressure (P_{atm}), and thus *TMP* can be simplified as $TMP = P_{atm} - P_p$.

Associated with the recirculation of media to the membrane module, in the side-stream configuration, and to the recirculation of media between two reactors in submerged configuration, the Recirculation ratio can be defined as:

$$\text{Recirculation ratio} = \frac{F_{rec}}{F}$$

Additionally, in side-stream MBRs, the velocity of flow can be calculated based on the recirculation flow and on the cross-flow section area.

$$\text{Flow velocity} = \frac{F_{rec}}{\text{Cross-flow section area}}$$

The operating conditions associated with the biological performance of MBRs for wastewater treatment are the substrate concentration in influent, usually calculated as food-to-microorganism ratio ($F:M$), the suspended solids (indicator of biomass concentration), and the aeration flow rate.

$$F : M = \frac{S \cdot F}{V \cdot X}$$

where the substrate (S) is organic carbon concentration, V is the total volume of liquid in the MBR, and X is the suspended solids or volatile suspended solids concentration.

Regarding the MBR operating conditions, the imposed permeate flux is probably the most important parameter in fouling control. Thus membrane bioreactors are usually operated at a low permeate flux (below critical flux) to avoid the deposition of particles on the membrane surface and keep permeability for a long operating time. The concept of critical flux was introduced by Field et al. (1995) and it is defined as the flux where the forces linked to filtration pressure and shearing forces are balanced. In MBR systems, the critical flux value depends on the characteristics of the membrane (e.g., pore diameter and material), characteristics of the mixed liquor, shear forces at the membrane surface, and temperature. The application of shear forces at the surface of the membranes is a current operational strategy to hamper fouling formation, either through the use of coarse air bubbles in submerged configurations or through increased cross-flow velocity (with or without addition of air) in side-stream configurations (Judd, 2006).

Despite clearly defined, there is no standard methodology to assess the exact value of the critical flux. Therefore the critical flux is often measured by the flux-step method from short-term experiments, where the permeate flux is imposed for

a specific duration of time, in incremental steps, while the TMP is recorded. The critical flux is then assumed to be near or below the flux at which the permeability decreases to below 90% of the permeability obtained in the first filtration step (when TMP is still constant) (Le Clech et al., 2003). However, even at very low fluxes TMP may increase with time, thus the concept of sustainable flux was introduced as the permeate flux at which the decrease in permeability is operationally acceptable (Bacchin et al., 2006).

In addition to the reactors configuration and operating conditions, different membrane types can be used in MBRs. For wastewater treatment, either tight microfiltration or loose ultrafiltration membranes are typically used. Since the filtration process determines which components of the mixed liquor can be permeated, the quality of an MBR effluent is also dependent on the membrane used. In fact, polysaccharides, proteins and peptides, colloids, bacteria, and virus will cross or be retained by the membrane in accordance with their sizes and the membrane properties. Other membrane characteristics that impact the performance of an MBR are the membrane material (usually polymeric, with a negative surface charge and hydrophilic) and the module configuration (normally composed by either flat-sheet membranes or hollow fiber membranes). Furthermore, in hollow fiber modules, packing density can impact permeate flux profile along the membrane fibers. A compromise between a sufficient space between fibers (low density bundle) and a large surface of filtration (high density bundle) should be obtained, avoiding problems such as prevention of dead zones or aeration homogeneity. In such cases, the use of computational fluid dynamics (CFD) enables the optimization of modules configuration.

Despite the reactor configuration, membrane module or operating conditions used (all affecting both the biological activity and filtration process), in MBRs for wastewater treatment the biological media is comprised by a broad variety of organic compounds with origin either in the incoming wastewater or as a result of microbial activity (e.g., humic compounds, polysaccharides, and proteins). These extracellular compounds can be either colloidal or soluble and are generally assumed to be the major cause of fouling in MBRs (Meng et al., 2009). Therefore tight monitoring of MBR performance is required in order to minimize extreme fouling events, reduce the requirements for membrane cleaning (increasing membranes' life span), and the development of effective strategies that minimize fouling.

MBRs as integrated processes of bio-production and separation

Besides wastewater treatment, MBRs are also used as an integrated process of bio-production and separation. Such application is extremely advantageous when the biological production is inhibited by the products formed and/or when high cell density is required.

The continuous feeding and permeation in an MBR, without changing the solids retention time, allows (i) the continuous feed of substrates and permeation of products, (ii) the maintenance of the concentration of products inside the MBR at constant

low levels (and thus avoiding inhibition by products), (iii) the maintenance of high feed that results in high biomass concentration (through high growth rates) and improved productivity.

Such as for wastewater treatment MBRs, the quality of the permeate effluent is also an advantage, facilitating the downstream processing of the desired products (Schiraldi et al., 2012).

The design of MBRs for bio-production is similar to the one for wastewater treatment; however, the configuration and membranes (material, type, configuration of modules) may be adjusted to the specificities of the microorganisms, substrates, and products for each process. For example, membrane pore size and material will depend on the size and characteristics (hydrophobicity) of the compounds (substrates and products) involved in the process. The requirements for sterilization, usually in processes involving pure cultures, will also affect the selection of the MBR configuration (e.g., allowing in situ sterilization) and the membrane material (resistance to temperature or disinfection solutions). Additionally, high cross-flow velocities or intense air bubbles may not be used with microorganisms that are sensible to shear stress.

Aerobic vs anaerobic MBRs

In MBRs with aerobic biological processes, the introduction of air is used not only to supply O₂ to biomass but also to score the membrane surface. This is more significant when a submerged configuration is used. However, in side cross configurations, the sparging of coarse air bubbles at the entrance of the membrane is also commonly used with the same function.

In anaerobic processes, alternatives to this air sparging should be used. Therefore depending on the process, other gases may be used (N₂, argon). However, the use of such gases increases the operating costs and may not be an option only in the production of high value products. Other strategies, such as recovery of gases (e.g., methane) and their recirculation inside the bioreactor can also be used.

Membrane photobioreactors

Photobioreactors (PBR) have emerged in the last decades as a potential sustainable technology to combine wastewater bioremediation by nutrient removal with the production of microalgal biomass. Although the use of microalgae in tertiary wastewater treatment has been suggested as a prospective method for advanced wastewater treatment, challenges are posed to this technology such as poor settle ability, biomass washout, and harvesting limitations. To overcome these issues, the recent introduction of membrane technology in photobioreactors gave rise to the membrane photobioreactor (MPBR) concept. This technology combines a conventional photobioreactor with a membrane process for the growth of photosynthetic microorganisms such as microalgae and/or bacteria. Different types of membrane processes (ultrafiltration, microfiltration, forward osmosis, ion exchange, gas exchange) and membrane configurations (hollow fiber, flat sheet) have been evaluated in membrane photobioreactors, where the membrane is applied as a key design feature for liquid or gas separation as a means to simultaneously treat wastewater and produce microalgae.

This new design concept of membrane photobioreactors with lower footprint area has demonstrated several advantages, whose nature and extent may depend on the MPBR configuration, which is selected based on the requirements for a given application. Generally, MPBRs offer enhanced rate of biomass production, and consequently improved removal efficiency and CO₂ fixation, compared with conventional photobioreactors, due to more efficient light penetration. Increasing microalgae production may also be achieved by the elimination of the negative impact of pollutants in the liquid influent on microalgae growth through the separation of microalgae cells and wastewater in two different chambers, which may be accomplished by using an annular ion-exchange membrane that also ensures the permeation of nutrients to the microalgae cultures (Chang et al., 2016). Another important advantage of the integration of the membrane in photobioreactors is the complete retention of microalgae cells, preventing biomass washout, eliminating further harvesting requirements and related costs, as well as enabling separate control of solids retention time and hydraulic retention time (Honda et al., 2012; Marbelia et al., 2014). The possibility to overcome the limitations of coculture photosynthetic oxygenation is offered by hollow fiber gas exchange membrane photobioreactors that enable to physically separate microalgae and bacteria cultures while ensuring their symbiotic relationship by facilitating the exchange of CO₂ and O₂ through a concentration gradient as the driving force. As a result, microalgal biomass is free of contaminants and thus can be easily harvested for several purposes. Furthermore, higher CO₂ and O₂ mass transfer efficiencies can be achieved and the loss of these gases to the atmosphere can be minimized. Besides these benefits, microalgal-bacterial symbiosis may bring many other advantages to this technology: (i) cost-effective aeration, given that microalgae provide heterotrophic bacteria with sufficient O₂ to degrade the organic pollutants, decreasing the energy requirements of intense mechanical aeration associated with conventional MBRs to achieve high removal rates (typically 45%–75% of the energy consumption (Rosso et al., 2008)); (ii) reduced risk of pollutants volatilization; and (iii) capture of the greenhouse gas CO₂ for microalgal biomass production (global warming mitigation).

Another noteworthy benefit of applying microalgae membrane photobioreactors is the potential to add value to the biomass produced through its processing toward the production of biofuels and bioenergy, lipids, pharmaceuticals, cosmetics, and feedstock (Najm et al., 2017).

As in conventional membrane bioreactors, membrane fouling is also considered an operational challenge in membrane photobioreactors. In these reactors, fouling is influenced by relationships between microalgae characteristics, matrix characteristics, operating conditions, and membrane properties, where the main foulant is algal-derived organic matter (AOM) that comprises carbohydrates, nitrogen-bearing compounds (e.g., amino acids, peptides, proteins, and nucleic acids), lipids, and organic acids (Pivokonsky et al., 2016). Fouling resulting from the deposition of microalgae on the membrane surface is usually reversible and can be alleviated by different aeration strategies. However, the economic viability of using different aeration types and rates is recommended for further analysis to support the design of membrane photobioreactors.

The main design features of photobioreactors include light utilization efficiency, gas transfer, mixing patterns, geometrical configuration, and building material (Carvalho et al., 2006). Light and CO₂ transfer are key processing parameters to meet optimum efficiency owing to the difficulties in controlling their stability throughout time and uniformity throughout space. The challenge in the design of photobioreactors is to overcome the constraints associated with the control of these parameters.

A typical photobioreactor is a three-phase system comprising the liquid phase (medium), the solid phase (cells), and the gas phase. Light, which is the unique feature of photoreactors and is often addressed as the fourth phase, is the main parameter affecting reactor design as it determines microalgal growth and, thus, photosynthetic efficiency (Posten, 2009). Light should therefore be provided at the appropriate intensity, duration, and wavelength (Carvalho et al., 2011). Light intensity decreases exponentially with the distance from the reactor wall due to light shading effects that result from the increase in the concentration of cells and products (increasing turbidity) or the formation of biofilm on the surface of reactor vessels (Chen et al., 2011, Chen et al., 2008). The following equation needs to be therefore considered in reactors' design:

$$\frac{I_L}{I_0} = e^{-\gamma L}$$

where I_L is the light intensity at depth L , I_0 is the original incident light intensity, and γ is the turbidity.

Although a short light path is theoretically favorable for achieving high light efficiency, conventional light sources cannot be in close contact with the microalgae culture because of heat generation. While excessive intensity may result in photooxidation and photoinhibition, low intensity may result in growth limitation. Consequently, the design of photobioreactors with an adequate illumination strategy is needed to achieve optimum light conversion efficiency for microalgae biomass production.

Microalgae are irradiated with only a small fraction of the incident radiation and grow in the nonlimited region. Therefore the surface-to-ground area ratio should be approximately 10 or higher, depending on the microalgae strain and the region where the reactor is operating. To estimate the photosynthetic efficiency for a selected species in a given photobioreactor, the illuminated surface area per unit volume of the culture should be determined. Thus the increase of the surface-to-ground area ratio should be carefully counterbalanced with reducing volume per ground area on the basis of the kinetics to provide no more light distribution than required and to save volume for high biomass concentration and reduce energy (Carvalho et al., 2011; Posten, 2009).

Michaelis-Menten equation is often used to describe saturation phenomena and can be applied as light-limited growth kinetic model to determine microalgae-specific growth rate, μ :

$$\mu = \mu_{max} \frac{I}{I + K_I}$$

where μ_{max} is the maximum specific growth rate, K_I is the saturation constant for light intensity, and I is the light intensity.

A reliable prediction of CO_2 transfer rates is required since a concentration gradient is observed as CO_2 is consumed by cells and/or lost to the atmosphere. According to the two-film theory, mass transfer of CO_2 from the gas to the cell phase comprises the following sequential stages: (i) transport from the bulk of the gas to the thin gaseous film at the interface, (ii) diffusion through the gas film, (iii) transport across the gas/liquid interface, (iv) diffusion through the adjacent liquid film, (v) transport from the thin liquid film to the liquid bulk, (vi) transport from the liquid bulk to the thin liquid film at the cell wall, (vii) diffusion through the outer cell liquid film, and (viii) metabolic uptake by the cell. At steady state, the rate of CO_2 transfer to the medium depends on the CO_2 uptake rate (Carvalho et al., 2006). The rate of mass transfer (N_{CO_2}) is, in general, proportional to the driving force and the area available for transfer is given by the following equation:

$$N_{\text{CO}_2} = k_L a (C_{\text{CO}_2 L}^* - C_{\text{CO}_2 L})$$

where k_L is the liquid-phase mass transfer coefficient, a is the specific area available for mass transfer, $C_{\text{CO}_2 L}^*$ is the concentration of CO_2 in the culture medium, and $C_{\text{CO}_2 L}$ is the concentration of CO_2 in the bulk of the culture medium. The parameter $k_L a$ characterizes the CO_2 mass transfer capability of the reactor and determines the cell growth rate. This parameter is therefore extremely important in design, scale-up, and operation of a photobioreactor (Carvalho et al., 2006; Talbot et al., 1991). Another important consideration is the delivery system implemented for CO_2 transfer as it determines the interface area between the gas and the liquid phases. CO_2 may be injected or sprayed into the medium as well as diffused through a membrane. The following features must be considered if CO_2 transfer is accomplished by membranes: (i) a significant membrane area is required as transfer rate is proportional to the membrane area; (ii) thick membrane walls should be employed to withstand the high pressures required to balance the transfer rates produced by bubbling; and (iii) pressurization of the membrane may originate microspacing within the polymer network of the membrane, to which bacteria may adhere, thus reducing the contact area and decreasing the transfer rate throughout time (Carvalho et al., 2006).

Although studies at lab scale point out membrane photobioreactors as a promising technology, concerns of increased costs and membrane fouling limit their full-scale application. Further research is, therefore, needed to attain adequate reactor geometries that ensure adequate light penetration and distribution as well as sufficient aeration/mixing of highly concentrated biomass. The complex interrelationships between operating conditions and process performance—biomass production, treatment effectiveness, and membrane fouling—is often overlooked and should be disclosed to provide improved designs and develop effective strategies that minimize fouling. The application of immobilized microalgal technology should be also further investigated given its potential to reduce membrane fouling (Luo et al., 2015), besides being able to improve microalgae biomass production and removal performance.

6.3.3 ANIMAL AND PLANT CELL BIOREACTORS

Recently, membrane bioreactors have become very attractive for the culture of animal and plant cells. The application of the membrane bioreactor concept in tissue engineering enables the design of *in vitro* physiological models (e.g., liver, pancreas, brain, skin, kidney) for the study of diseases and the development of molecular therapeutics. MBR technology is also interesting for the production of heterologous human and/or animal therapeutic proteins by transgenic plant cell cultures.

The interest of MBRs for animal cell culture relies on the possibility of culturing cells at high density, high volumetric productivity, and under closely monitored high perfusion in a similar *in vivo* microenvironment. The use of polymeric semipermeable membranes with different physicochemical and transport properties is appealing in tissue engineering and bioartificial organs since these membranes and biomembranes share similarities: (i) the selective transport of metabolites and nutrients to cells and the removal of catabolites/specific products from cells; (ii) resistance; and (iii) protection from shear stress, which is often achieved by operating at laminar flow regime. Furthermore, semipermeable membranes exhibit other important functions for the maintenance of cell viability and specific functions such as the ability to act as immunoselective barriers, as means for cell oxygenation, and to provide a large area for cell attachment (Curcio et al., 2005; Dionne et al., 1996; Drioli and De Bartolo, 2006; Wickramasinghe et al., 1992). Besides these advantages, the use of MBRs for plant cell culture brings other important benefits related to the reuse of the plant biomass for long-term production and the easier product recovery/purification (McDonald et al., 2005).

Membranes, which are a key design feature in the MBR, should combine properties of polymers such as biocompatibility, thermal/mechanical resistance, and elasticity with properties of membranes such as permeability, selectivity, and well-defined geometry. Hollow fiber membrane bioreactors have been designed and widely applied to overcome the nutrient diffusion limitations in tissue/organ engineering applications (Eghbali et al., 2016; Pörtner et al., 2005). Its geometry comprises several advantages related to compactness, large mass exchange surface area-to-bioreactor volume ratio (excellent mass transfer properties), cell protection from mechanical stress, and prevention from cell washout (De Napoli et al., 2014; Wung et al., 2014). Cylindrical hollow fiber bioreactors are composed of a bundle of parallel, semipermeable, hollow fibers assembled in a cylindrical housing/cartridge. These bioreactors are versatile since multiple possible paths are possible for the medium flow (through hollow fibers and/or through the extra capillary space) and cell location. The cells can be directly seeded on the outer surface or in the internal lumen of the fibers, while the medium flows in the internal fiber lumen. Rectangular hollow fiber reactors are composed of a hollow fiber membrane embedded within a scaffold with a rectangular shape, where the medium flows through the hollow fibers internal lumen and one or more cell sheets can be cultured on the top of the polymeric hollow fiber membrane scaffold (Eghbali et al., 2016). In both configurations, the size, number, fiber interdistance, and arrangement may be tuned according to the

application. In order to adequately recreate the *in vivo* environment, the following operating parameters should be designed and optimized: membrane bioreactor geometry (inner and outer fiber radii, the space between fibers, the bioreactor radius and length), medium culture flow parameters (flow regime, perfusion rate, and fluid properties), porous membrane parameters (porosity, pore size, hindrance factor, molecular weight cutoff, permeability, and membrane physicochemical properties), mass transport parameters relevant to oxygen, nutrients and waste species, as well as culture conditions (cell type, cell passage, and cell seeding density). The pore size of the membranes must be small enough to isolate the cells but sufficiently large to allow the appropriate mass transfer of nutrients to cells and the removal of waste metabolites (Buffington et al., 2014; Diban and Stamatialis, 2014; Iacovacci et al., 2016; Jansen et al., 2014). To attain optimum reactor designs, studies have focused on the development of 2D and 3D computational fluid dynamics (CFD) based on Navier-Stokes equations coupled to the Maxwell-Stefan convection-diffusion-reaction equation to predict nutrient or catabolite concentrations. However, to attain improved designs, more insights regarding the effects of design parameters in cell viability and functionality are still needed.

The application of MBR technology in animal and plant cell culture is mainly limited to small-to-medium scales since operating issues related with poor cell viability, poor process stability, product heterogeneity, and diffusion gradients need further improvement.

6.4 MONITORING AND CONTROL OF MEMBRANE BIOREACTORS

Despite its advantages, the application of MBR technology for wastewater treatment is still conditioned by the inevitable membrane fouling, by the operational high costs (mostly associated to the aeration of the membrane) (Judd, 2008) and by the complex control systems required (Lesjean et al., 2011). Therefore different characterization and monitoring tools were developed and studied in the last years to increase the monitoring ability, reduce fouling, and minimize costs (both due to fouling and operation).

Monitoring (and control) of MBRs require the monitoring of the two processes involved: biological reaction and membrane separation. Both processes are tightly related, and their specific performances affect each other. Membranes' selectivity affects the composition of biological media, while the biological performance affects the membrane, mainly due to fouling formation. In fact, in MBRs, the biological process can comprise different microorganisms and/or a broad variety of organic compounds involved in biological reactions, making MBRs particularly vulnerable to membrane fouling. Such diversity and complexity of reactions and compounds (including substrates, products, and intermediate metabolites) are tightly related with

membrane fouling development, meaning that several variables require simultaneous monitoring during process operation. This complexity increases greatly the challenge of process monitoring and control.

Monitoring of MBR systems for wastewater treatment is essential to produce high-quality effluents and meet legal requirements. As any biological process, MBRs require monitoring of both influent and effluent composition as well as the assessment of biological activity. Nevertheless, the use of membranes in wastewater biological treatment brings additional monitoring requirements related with activated sludge filterability, cake layer formation, and membrane fouling in order to define strategies and operating conditions that avoid major process upsets and maximize its performance.

When monitoring fouling, and despite the analytical methods used, the development of mathematical models is essential to correlate the experimental measurements with the fouling potential and fouling evolution/prediction (as described in the next sections). Such models are also required for the development of effective control tools.

6.4.1 OFF-LINE MONITORING

A set of analytical tools are used to characterize influents and effluents in wastewater treatment systems, including sum parameters (5-day biochemical oxygen demand, chemical oxygen demand, and total organic carbon), biosolids, ionic species, and other environmentally relevant molecules.

Sum parameters

Biological oxygen demand (BOD₅), chemical oxygen demand (COD), and total organic carbon (TOC) are routinely used to assess the global organic content of influents as well as the removal efficiency of the process. Biochemical oxygen demand is a measure of the microbial consumption of molecular oxygen during a five-day incubation period for the biochemical degradation of organic material (carbonaceous demand) as well as for the oxidation of inorganic material such as sulfides and ferrous iron. It may also be a measure of the amount of oxygen used to oxidize reduced forms of nitrogen (nitrogenous demand) (APHA, 2005). Although BOD₅ has been in use for a long time as a standard indicator of the potential biodegradability of a sample and thus of the process removal efficiency, its application is very time consuming, given the long incubation period (Scholes et al., 2016), and may result in underreporting values if samples comprise complex toxic components that cannot be degraded due to the absence of suitable microbial metabolic ability (Jordan et al., 2014).

Chemical oxygen demand (COD) is a measure of the concentration of organic compounds able to be oxidized that can be obtained by Open reflux (SM 5220 B), titrimetric (SM 5220 C), and colorimetric (SM 5220 D) methods (APHA, 2005). Despite the known interferences of colored samples in COD determination, the simple nature of the analytical procedures leads to the use of COD determination

as the most commonly used method for oxidation demand assessment (da Silva et al., 2011). Furthermore, while only biodegradable organic compounds are accounted in BOD₅ determination, COD assesses all organic compounds that can be oxidized. Monitoring COD:BOD₅ ratios in the effluent over time has been useful as an indicator of potential changes in the influent treatability and/or toxicity (Scholes et al., 2016). As both BOD₅ and COD determinations have drawbacks, there is a growing interest in the measurement of total organic carbon. Although TOC determination is a simple, rapid, and reliable determination that can be performed with little operator intervention, it does not provide information on the oxidation state. Moreover, capital costs are the most critical factor (Scholes et al., 2016). Given the time and operation complexity constraints associated with BOD₅ determination, COD and TOC are often preferred when frequent characterization of organic matter is required.

Biosolids

Total suspended solids (TSS) and volatile suspended solids (VSS) measurements (SM 2540 D, E, respectively; APHA, 2005) have been recognized as the most valuable data for MBR daily monitoring, providing information about nutrient removal efficiency and potential fouling (cake layer formation and filterability) (Scholes et al., 2016). Furthermore, the mass of volatile suspended solids, often referred as mixed liquor suspended solids (MLSS) is taken as total microbial biomass. It is used to assess the food-to-microorganism ratio and to ensure a balanced biomass production, providing important information for MBR operation and control. Despite widely accepted and used to monitor microbial biomass during the treatment, it is assumed that all volatile material is microbial biomass, which is not true. Furthermore, it does not provide any information regarding the viability and metabolic activity of the microorganisms as well as the composition of the microbial community. To further address microorganisms' status, several analyses may be carried out based on (i) respiration, through oxygen uptake rate determination; (ii) cell membrane integrity, through flow cytometry; (iii) enzyme levels detection, which may include the activity of several dehydrogenases and/or pyruvate kinases; and (iv) determination of adenosine-5'-triphosphate, which may indicate not only microbial viability but also potential toxicity and process changes. The identification of microbial members has been successfully carried out by fluorescence in situ hybridization (e.g., (Silva et al., 2012a)) and high throughput sequencing (e.g., (Silva et al., 2016)). Nevertheless, these methods have not been widely in use due to their complexity, the high level of scientific training required, and the difficulty in their application on-site.

Ionic species

The influent and effluent composition and process efficiency also include monitoring of the removal of several ionic species, in particular nitrogen (as ammonia, total nitrogen, organic nitrogen, nitrate, and nitrite) and phosphorus (as orthophosphate and total phosphorus). The determination of these two key regulated parameters may be achieved by colorimetric analysis, usually using commercial test kits, or by ion chromatography.

Ion chromatography analysis requires less operators' intervention and overcomes analytical constraints of colorimetric methods related with interferences in colored or sulfide-containing samples (APHA, 2005). Furthermore, many other ionic components that may be important for process monitoring, given the influent composition and/or the effluent requirements, may be quantified by ion chromatography such as chloride, chlorate, and bromide.

Other environmentally relevant molecules

In the last decades, due to higher environmental requirements and increased knowledge on the chemistry and microbiology of wastewater treatment, more specific monitoring analyses are being claimed. Within this scope, given the relevant concentrations and/or toxicological properties of some molecules in MBR influents, their specific monitoring is required to assess the treatment performance regarding their removal efficiency as well as their impact on the microbial community. Liquid and gas chromatography have been useful for this purpose, enabling the monitoring of emerging micropollutants such as pharmaceuticals and polycyclic aromatic hydrocarbons.

Fouling monitoring

Fouling monitoring and control is crucial to ensure high membrane permeability and, therefore, process performance with minimum operation costs associated with energy requirements and membrane lifetime. MBRs for wastewater treatment are usually operated at constant permeate flux (Drews, 2010) and transmembrane pressure (TMP) is used as a standard fouling indicator parameter. However, TMP increase does not provide insights on fouling mechanisms, the nature of the foulants, or the upcoming of extreme fouling (observed as a TMP jump). A set of methods was, thus, developed for this purpose, in order to optimize operating parameters and develop flux maintenance strategies that minimize/alleviate fouling and/or reduce the production of biological foulants. Such methods can be based on TMP, membrane permeability, and/or on the monitoring of fouling agents or physical properties of reactor samples.

To assess the physical properties of fouling and potential foulants, some authors developed filtration tests to determine the filtration resistances of fouling (Chu and Li, 2005) and of suspended solids, solutes, and colloids in the mixed liquor (Bouhabila et al., 2001). Additionally, filtration devices have also been used to characterize the fouling potential of mixed liquor as reversible or irreversible (Huyskens et al., 2008). Capillary suction time (CST), initially developed to predict sludge dewaterability (Gale and Baskerville, 1967), is a simple and inexpensive chromatography-based method that has been in use for a long time to obtain a good correlation of mixed liquor suspended solids with specific resistance to filtration, thus, fouling potential (e.g., Jorgensen et al., 2017). CST and sludge volume index (SVI), developed to assess the settling characteristics of biological suspensions, were used to assess sludge characteristics that would be directly linked to its fouling

potential. The physical properties of fouling and mechanisms have been addressed through the determination of fouling filtration resistance (Chen et al., 2016; Hong et al., 2014; Poorasgari et al., 2015) and the characterization of fouling (ir)reversibility (Jorgensen et al., 2014; Xiao et al., 2014). Although several empirical mathematical expressions describing membrane flux or fouling rate comprising mixed liquor suspended solids have been developed, findings on the effect of these parameters on membrane filtration are contradictory (Le-Clech et al., 2006; Meng et al., 2009). The chemical characterization of foulants has received much attention, with a particular emphasis on the nature of microbial organic solutes, known as extracellular polymeric substances (EPS) or soluble microbial products (SMP), which have been recognized as primarily responsible for fouling in MBRs (Judd, 2008). Monitoring EPS is, therefore, of the utmost importance to elucidate which MBR conditions correlate with EPS production. EPS are extremely heterogeneous and comprise carbohydrates, proteins, nucleic acids, (phospho)lipids, and other polymeric compounds found at or outside the cell surface and in the intercellular space of microbial aggregates (Judd, 2008). Among these components, proteins and polysaccharides are often considered the major contributors for fouling, thus, EPS concentration relies often on their analysis. Proteins determination has been achieved by a method described by Frolund et al. (1995), a modification of the classic method developed by Lowry et al. (1951), while polysaccharides have been traditionally determined by the method developed by Dubois et al. (1956). Given the time-consuming nature of these procedures that comprise extraction and analytical characterization, organic carbon and COD quantifications of EPS may be alternatively conducted despite the fact that EPS constituents cannot be distinguished (Lyko et al., 2008). Other techniques have been used to address EPS: size exclusion chromatography enables separation and characterization of EPS components based on their molecular size (Dominguez et al., 2010; Menniti et al., 2009) while the identification of the functional groups of the molecules described as foulants may be accomplished by excitation-emission matrix fluorescence spectroscopy (Kimura et al., 2009; Meng et al., 2011), Fourier transform infrared spectroscopy (Coburn et al., 2016), and ^{13}C -nuclear magnetic resonance spectroscopy (Meng et al., 2011). Proteins from soluble and bound EPS extracted from activated sludge may be identified by mass spectrometry analysis following gel electrophoresis (Silva et al., 2012b). Although confocal laser scanning microscopy and scanning electron microscopy (Fortunato et al., 2016; Jorgensen et al., 2017) are of much interest to attain microscopic structural properties of membrane fouling, their use is time consuming and requires specialized training.

Even though many studies have been conducted on the impact of specific EPS components on fouling since the mid-1990s, often contradictory trends have been reported, which is likely to be related with differences in the analytical methods for which there is no agreement, differences in system configurations, and the fact that these studies are usually limited to a narrow range of operating conditions (e.g., operating flux, hydraulic retention time, and sludge retention time) and influent quality (Drews, 2010; Judd, 2008).

Other parameters

Depending on the MBR process in study, several other parameters can be assessed to monitor and characterize the system. When using mixed microbial cultures, the assessment of the microbial community composition, based on DNA, is being increasingly employed to analyze shifts on the microbial community due to operational changes.

For other MBR processes not involving wastewaters neither mixed microbial cultures, several of the analysis mentioned before are not relevant. However, the monitoring of the specific compounds taking part on the biological process (substrates, products, by-products, or enzymes) usually requires specific analytical techniques according with the parameter to be assessed. In simple systems, monitoring of filtration performance and fouling formation may be required, which may be accomplished through mass balances as well as through the assessment of permeability and compounds rejections.

6.4.2 ONLINE, REAL-TIME MONITORING OF MEMBRANE BIOREACTORS

Although the off-line characterization techniques are reliable and provide detailed information concerning the specific compounds in an MBR, the implementation of real-time monitoring techniques able to assess simultaneously different parameters of biological and membrane performance greatly simplifies the operation of MBRs. They can reduce the effort spent on time-consuming analysis, might be used to anticipate the upcoming of process anomalies, and may be useful decision instruments in process control.

Among the parameters commonly monitored in MBR systems, some are measured online (such as TMP and dissolved oxygen) or can, nowadays, be measured online or at-line due to the development of new commercial sensors (e.g., MLSS, COD, TOC, NO_x). However, as the number of parameters to monitor increases, the use of specific sensors also increases the monitoring costs.

Due to their nondestructive characteristics, spectroscopic methods are being increasingly employed for the online monitoring of complex samples aiming to detect simultaneously several components. In fact, ultraviolet-visible, infrared, fluorescence, and Raman spectroscopy are gaining relevance within the biotechnology field, as online monitoring tools. Each spectral technique assesses different molecule types based on molecule properties. UV/Vis, NIR, and MIR spectroscopy primarily provide measurement of the light absorption of molecules, as well as their light scattering. Fluorescence spectroscopy uses the light emitted from excited fluorophores while Raman spectroscopy uses rare inelastic scattering effects. Thus by using the different spectral analysis nearly all important physical, biological, and chemical variables of a bioprocess are accessible by spectroscopy (Claßen et al., 2017). Actually, UV-Vis absorbance and fluorescence spectroscopy are extremely useful to monitor biological systems mainly composed (or affected) by proteins. This is the case of enzymatic bioreactors, as discussed earlier in this chapter. Additionally,

the use of excitation-emission fluorescence spectroscopy (also called two-dimensional fluorescence spectroscopy) is also useful in wastewater treatment MBR systems, since two of the major fouling agents recognized are proteins and humic compounds, which are easily identified by this scanning fluorescence technique. In Fig. 6.5, two fluorescence spectra acquired from an MBR for wastewater treatment show the two main fluorescence peaks, related with amino acids (at 280 nm of excitation) and with humic-like compounds (near 350 nm of excitation).

Spectroscopic methods can be used directly without using reagents, are nondestructive, fast, and with possible application in situ (through optical probes). They provide series of spectra, (corresponding to large sets of data) through the assessment of absorption, reflectance, transmission, or vibrational properties of chemical species. However, such sets of data, when acquired from complex biological systems, require the use of multivariate statistical analysis tools to extract meaningful quantitative information.

So far, spectroscopic techniques, applied to the detection of parameters in biological processes for wastewater treatment, were successfully correlated with parameters such as BOD, COD, TOC, EPS, MLSS, nitrate, ammonia, and nitrogen, among others (Mesquita et al., 2017). Additionally, the range of applicability of such techniques is increasing, either for the assessment of specific compounds or as a fingerprint of the biological status, when the complexity of the media makes the identification of compounds difficult (spectroscopic scanning techniques, covering broad ranges of wavelengths, do not focus on a single component).

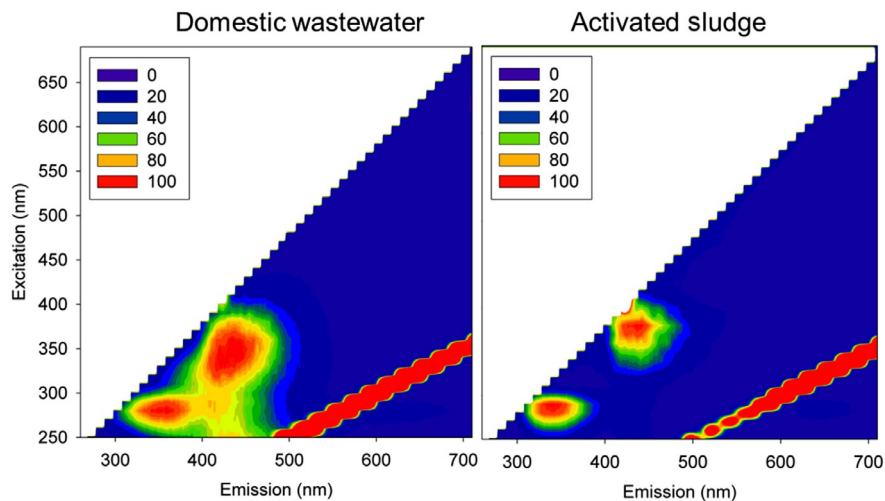


FIG. 6.5

Fluorescence spectra of an influent domestic wastewater and of activated sludge inside a pilot MBR for wastewater treatment.

Online monitoring of fouling is usually based on the monitoring of TMP or permeability. Although some methodologies are used off-line to assess fouling ability of specific MBR systems (such as flux-step methodology and filterability tests), some authors suggest the use of fouling rate (defined as $FR = dTMP/dt$) as an online monitoring method for early detection of significant fouling development, instead of using TMP or permeability alone (Monclús et al., 2011).

6.5 MODELING OF MEMBRANE BIOREACTORS

In view of the complexity of MBR systems and the wide range of monitoring techniques available, the development of mathematical methods to integrate and correlate different (and disperse) types of information can support the comprehension and monitoring of these systems. Therefore several modeling strategies have been developed and used with different objectives: to monitor, to simulate, to optimize, to control, to study and design.

Mathematical modeling of the MBR process usually includes the modeling of the biological reactions and of membrane performance, as well as their integration, resulting in complex modeling systems.

Modeling of biological reactions includes biological growth, consumption of substrates, and formation of products and by-products. Modeling of membrane filterability performance includes not only the modeling of membrane permeability, rejections, and diffusivities, but also fouling formation. Although biological and membrane performances can be modeled by independent models, they are tightly bound due to the role played by feed compounds, products, by-products, and biomass in membrane and due to the impact of the selective behavior of the membrane in the biological activity (Fig. 6.6).

6.5.1 MECHANISTIC MODELING APPROACHES

Biological models

Microbial mixed cultures

When modeling biological reactions in MBRs, activated sludge processes for wastewater treatment are the most studied systems. To model the biological wastewater treatment process, a high number of state variables and process descriptions, mostly based on Monod type kinetics, have been used and combined in modeling structures.

The Monod equation is an empirical mathematical model for the growth of microorganisms:

$$\mu = \frac{\mu_{max}S}{K_S + S}$$

where μ is the specific growth rate of the microorganisms (defined as $\mu = \frac{dX}{dt} \frac{1}{X}$), μ_{max} is the maximum specific growth rate of the microorganisms, S is the substrate concentration, X is the biomass concentration and K_S is the half-saturation or

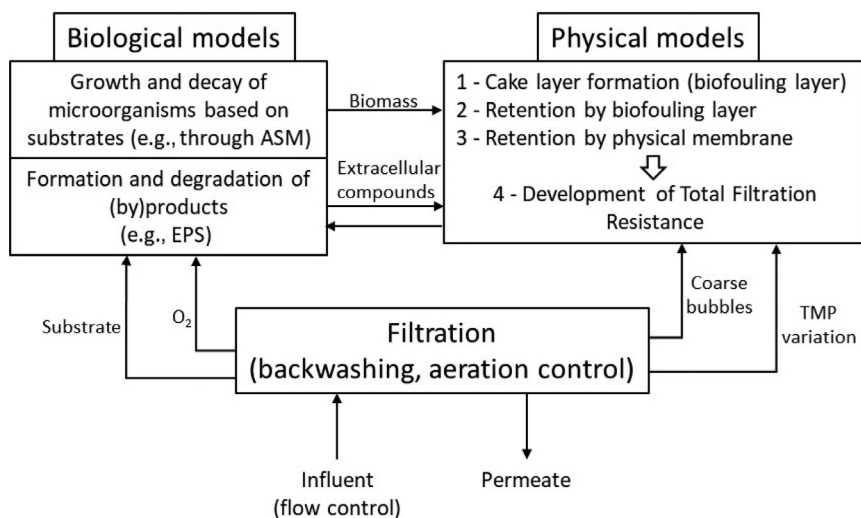


FIG. 6.6

Conceptual schematic of an integrated MBR model.

Adapted from Mannina, G., Di Bella, G., Viviani, G., 2011. An integrated model for biological and physical process simulation in membrane bioreactors (MBRs). J. Membr. Sci. 376, 56–69.

half-velocity constant (also known as substrate affinity constant). Monod kinetics may be applied to monitor one type of microorganism (pure cultures) or to a consortium of microorganisms (mixed microbial cultures), as well as to monitor the growth of one microbial culture microorganisms based on different substrates.

Activated sludge systems (which are microbial mixed cultures) have been widely studied, resulting in the deep understanding of the kinetics of the main heterotrophic and autotrophic biological processes, which sets the basis for the development of mechanistic models. These kinetic models have been summarized in four activated sludge models (ASM) by the International Water Association (IWA) Task Group on Mathematical Modeling for Design and Operation of Biological Wastewater Treatment (Henze et al., 2000). The first activated sludge model published, ASM1, was developed to model the biological treatment for organic carbon removal, nitrification, and denitrification. This model can predict oxygen demand and biomass production in activated sludge systems. ASM2 was developed later to incorporate phosphorus removal from wastewater, and ASM2d to account for the ability of phosphorus-accumulating organisms to use cell internal substrates for denitrification. ASM3 does not include phosphorus removal, but it was established to address problems found in the first model ASM1, such as the inclusion of internal cell storage compounds in heterotrophs (shifting the focus from hydrolysis to the storage of organic substrates) and the replacement of the death-regeneration concept by the growth-endogenous respiration model.

ASM were developed to describe conventional activated sludge (CAS) processes under correspondingly typical operating conditions. However, due to the similarity between the biological processes occurring in conventional activated sludge systems and in MBRs for wastewater treatment, ASM have been widely used to model the biological removal of nutrients in MBRs. Nevertheless, the specificities of the MBRs must be taken into account when applying an ASM to model their biological performance, for instance, the higher solids retention time, higher solids concentration and higher viscosity, selective accumulation of microbial products retained by the membrane, high aeration rates and large air bubbles for scouring (particularly in submerged MBRs), as well as good nitrification performance (due to the retention of slow-growing microorganisms).

According to [Fenu et al. \(2010\)](#), the application of the ASM to the MBR processes can be divided into unmodified and modified ASM in view of the adaptations made to the ASM to fit an MBR. The expression unmodified (or plain) encloses ASM applications similar to those originally specified for the CAS systems (process design, effluent characterization, oxygen demand, and biomass production) and without modification of the ASM model structure. However, it includes slight modifications to the biokinetic processes/parameters, to account for changes associated with the inclusion of membranes in activated sludge systems. Indeed, in systems with low organic loads (such as MBRs), the retained molecules may have a significant impact on the metabolic path, allowing further use of carbon-based metabolites. Additionally, the assessment of the active heterotrophic biomass in the influent wastewater (usually neglected in CAS modeling) also needs to be better addressed when modeling membrane bioreactors.

Despite the applicability of plain ASM to model the MBR biological performance, such models do not link the biological process of an MBR with membrane fouling. Therefore modifications to the ASM were developed to include models for the description of extracellular polymeric substances (EPS) and soluble microbial products (SMP) ([Jiang et al., 2008](#); [Lapidou and Rittmann, 2002](#)). In order to distinguish among different fractions of soluble microbial products that play different roles and have different fates in MBRs, SMP were subdivided by [Namkung and Rittmann \(1986\)](#) into utilization-associated products (UAP) and biomass-associated products (BAP). UAP are produced from the substrate degradation, whereas BAP are assumed to be produced by the decay of the active biomass, by the hydrolysis of bound extracellular polymeric substances or by the combination of both. These subdivisions of SMP are widely accepted and used in ASM modifications for MBRs modeling. Additionally, by expanding the models with EPS/SMP, it is also possible to account for specific types of molecules, as proteins and polysaccharides, or, for shifts in the molecular weight distribution. EPS and SMP submodels were developed either as integrating concepts in ASM type of models or developed as stand-alone descriptions of the concepts of production and degradation of EPS and SMP.

However, in ASM modified models including SMP/EPS description, the kinetic parameters are not easily determinable experimentally (e.g., associated with UAP and BAP) and the models are usually over parameterized. Therefore such models

are usually applicable only when the modeling objectives are linking biology with fouling, to predict soluble COD, and/or model high SRT processes (Fenu et al., 2010).

In general, ASM type of models are well accepted and extensively used when modeling the biological process in MBRs for wastewater treatment. However, despite the good predictions that may be achieved using ASM, these models are complex, involve the calibration of several model parameters, and require frequent input data related to the feed characteristics, which can fluctuate significantly throughout time. Therefore their use is dependent on the objective of the modeling system, since they may not be practical for monitoring and control.

Production with pure cultures

When modeling the MBR process for bio-production (usually with well-characterized microorganisms, substrates, and products), the equations and parameters used for cellular growth, production, and consumption can be simplified for one microorganism growth and be specific for the production kinetics. It may also include metabolic fluxes (when the metabolic pathways are known) and mass balances to estimate accurately the concentration of specific compounds. Stoichiometric, kinetic, and performance parameters of the biological process can, then, be estimated/calculated more accurately. Nevertheless, the selective behavior of the membrane, as well as the interaction between biological compounds and the membrane, may also have an impact on the system and may increase modeling complexity.

Physical models

Modeling the physical reactions at membrane level consists of four steps, tightly correlated with each other (Fig. 6.6): (1) cake layer formation during the membrane filtration, (2) retention of biological compounds by the biofouling layer, (3) retention of biological compounds by the physical membrane, and (4) modeling of the membrane resistances (to correlate them with TMP and permeability parameters).

For MBRs modeling purposes, the equations used for the description of the membrane separation step and fouling development are the same used for other membrane filtration systems, accordingly with the respective type of membrane used: usually microfiltration or ultrafiltration for cell MBRs and ultrafiltration or nanofiltration for enzymatic MBRs. However, the production and/or consumption of species due to the biological reaction as well as the specificities of the biofouling formed at membrane surface (which alters significantly the environment at membrane surface) affect and increase the complexity of the models' parameters/variables.

Consequently, the deposition of active cells at membrane surface may change locally the composition of the liquid media to be filtered. The compounds rejected by the membrane, and accumulated at membrane surface, may lead to the accumulation of active microorganisms that feed in such compounds and form products (and by-products) at membrane surface. Such events affect the concentration of soluble products at membrane surface and increase the complexity of diffusion models in

membrane and fouling layers. The complexity and mutability characteristics of biofouling in MBRs are the main reason for the difficulty to monitor, predict, and control the development of fouling and the upcoming of extreme fouling (observed as a TMP jump).

Resistances in series

Despite the complexity, modeling the filtration process is being mostly performed by a mechanistic approach, using Darcy's law as the theoretical starting point for the model equations and the resistances in series concept (Naessens et al., 2012).

Darcy's law directly relates membrane flux (usually constant in MBRs) to the measured transmembrane pressure, using a constant for the sludge viscosity, temperature, or total solids dependent parameter.

$$J_p = \frac{TMP}{\mu \cdot R_T}$$

where J_p is the permeate flux, TMP is the transmembrane pressure, μ is the viscosity of the permeate, and R_T is the total membrane resistances.

Using Darcy's law, it is possible to calculate the membrane resistance R_T , which is generally assumed to be the combined effect of the clean membrane resistance R_m and fouling mechanisms affecting the filtration process.

$$R_T = R_m + R_c + R_{irr}$$

In this example, the total resistance is calculated as the sum of the clean membrane resistance R_m , cake layer resistance R_c , and resistance by irreversible fouling R_{irr} . However, other fouling mechanisms are usually added, such as standard pore blocking resistance, complete pore blocking resistance, intermediate blocking resistance, pore blocking resistance, dynamic sludge film resistance, stable sludge cake resistance, fouling resistance, biofilm resistance (Naessens et al., 2012). Although the decomposition of total resistance can be done in numerous ways, a distinction between cake layer and pore blocking resistance is generally carried out.

The clean membrane resistance is an intrinsic characteristic of the membrane and can be determined using Darcy's law in ultrapure water filtration or it may be provided by the membrane manufacturer. The resistance components associated with fouling require the use of separate models for each one and are time dependent (due to biofouling accumulation or composition variation during operation time). These models are usually based on the exact mechanism taking place near the membrane surface or on a semiempirical calibration basis. Additionally, the resistances due to scaling and concentration polarization are commonly considered negligible in MBRs due to the strong effect of biofouling.

To model the resistance of a fouling component, the resistance can be decomposed as the product of the specific resistance with the mass of the respective layer.

$$R_c = r_c \cdot M_c$$

where r_c is the specific filtration resistance of the cake layer and M_c is the accumulated mass of the sludge attached in the cake. Using this approach, the accumulated

mass parameter is dependent on biological formation and degradation and the specific resistance may be assumed constant (calibrated at specific operating conditions) or assessed as a function of TMP, sludge concentration, floc sizes, sludge viscosity, and bound EPS concentration (Mannina et al., 2011; Li and Wang, 2006; Cho et al., 2005; Busch et al., 2007).

The information regarding mass profiles of biofouling agents (feed compounds, products, and by-products of biological activity, as well as the biomass itself) can be obtained from the biological models (such as ASM and their extensions) and, thus, integrating the modeling of membrane fouling with the biological modeling. Despite the descriptive ability of such integrated models, some of the biological parameters required are not measurable experimentally (e.g., UAP and BAP), which increases the modeling complexity, requiring calibration using experimental data to fit the measurable parameters (usually by iteratively changing the parameters that cannot be measured experimentally).

Other approaches used for fouling development include the use of models based on the probability of a particle to adhere to the membrane pore wall while passing through it, together with the probability of the particle landing in a specific pore (Griffiths et al., 2014). Although this model described the phenomenon associated to different fouling steps, it could not predict values of TMP or permeate flux at a given time, and did not consider either the biological media characteristics or the operating conditions.

For prediction of membrane fouling, computational fluid dynamics (CFD) tools can also be used (e.g., Yang et al., 2017). In such modeling systems, several equations are used to describe membrane fouling in a given MBR configuration. Although CFD tools application can be valuable in the dynamic prediction of cake layer formation, they require the use of simple system geometries and basic assumptions to simplify the numerical resolution.

Contrasting with the modeling of the biological process in MBRs, where ASM are well accepted, several modeling strategies have been proposed so far to model membrane fouling in complex biological systems. However, there is no consensus about the best modeling approach to be used to model fouling evolution in MBRs.

6.5.2 MULTIVARIATE STATISTICAL ANALYSIS METHODS

Although mechanistic modeling of biological processes has been largely studied and described, the integration of biological submodels with fouling (or filtration) models in complex MBR systems (such as for wastewater treatment) is still under discussion. The complexity of fouling mechanisms and the factors affecting its development, as well as the reciprocal dependence with the biological activity, increase greatly the number of parameters and equations required to model an MBR. Many of the parameters required for those models are difficult or impossible to assess experimentally, and the resulting models are too complex for monitoring and control purposes. In fact, for control purposes the models used should have less parameters, which must be based on online measurements and known operating conditions.

Therefore an alternative modeling approach to monitor and control complex MBR systems is multivariate statistical modeling, which is a powerful tool to study systems with several parameters and high complexity. Multivariate mathematical modeling, based on statistical analysis, relies on experimental and operating data, can deal with large data sets and allows the use of unconventional data, such as fingerprinting monitoring techniques. Due to the complexity of fouling formation in MBRs using mixed cultures and complex feeds, such nonmechanistic statistical modeling is usually applied to model the fouling and filtration performance, or to model the overall performance of an MBR.

Facing the difficulty to develop accurate mechanistic models that are not too complex or over parameterized, multivariate statistical modeling represents a good compromise to evaluate membrane fouling in MBRs, reducing the complex membrane fouling phenomenon to a black box, and considering only input parameters linked to the MBR and the wastewater characteristics. Multivariate statistical modeling is based on the principle that process phenomena and dynamics are inherently contained in the experimental data, thus, it does not require a priori knowledge on system mechanics. For this reason, these modeling methodologies (also called data-driven modeling) are usually seen as black boxes, or gray boxes, depending on the degree of mechanistic information that can be retrieved from the modeling system.

Artificial neural networks (ANN) are a type of black box model that is commonly used to simulate numerous physical systems. ANN can be seen as a mathematical representation of the brain, where neurons are represented by nodes, each containing a mathematical function, and organized in an input, output, and multiple hidden layers. The nodes in input layer, hidden layer(s), and output layer are interconnected, as in synapses in brain. ANN modeling is based on patterns, instead of equations, and can infer complex nonlinear relationships between target variables to be predicted (the outputs) and the input variables. Based on a sufficiently large experimental data set (containing both input and output measurements), a model can be created (calibrated or trained) for a specific process in the experimental range assessed. The quality of the model calibration (or neural network training) depends on the network architecture, such as the number of nodes per layer and the number of hidden layers, and on the data set used for calibration. A small data set will typically result in a low reliability of the network, whereas a too complex architecture and large training data set will result in model overfitting.

Due to its data-driven and black box characteristics, ANN models have limited extrapolation capacity and result in lower level of physical understanding of the system, when compared with mechanistic models. Nevertheless, some mechanistic insights can be obtained from the weights of the trained neural network. However, ANN models are most useful for system monitoring and control of complex systems, due to the low number of parameters required, in contrast with mechanistic models.

Despite their proved potential, the application of ANN to the filtration process within membrane bioreactors is scarce (Naessens et al., 2012). In fact, some studies focused on the prediction of overall MBR performance, as Pendashteh et al. (2011)

that modeled effluent COD, TOC, and oil & grease in the treatment of hypersaline oil wastewater, or Çinar et al. (2006) that modeled effluent COD, ammonia, nitrate, and total phosphate in an MBR fed with cheese whey. While other studies, focused on the prediction of the filtration performance alone through the use of ANN to model permeate flux evolution (Geissler et al., 2005), TMP, and the membrane permeability over time (Mirbagheri et al., 2015).

Principal component analysis (PCA) consists of a data transformation in which all variables are recombined into linearly independent combinations, called principal components (PC). PCA results in a new coordinate system with reduced noise and lower dimensionality through decomposition of a data matrix, X , into a “structure” part plus a “noise” part.

$$X = C \cdot P^T + \varepsilon$$

C are the scores matrix and have as many rows as the original data matrix and P^T are the loadings matrix and have as many columns as the original data matrix. The scores matrix can be seen as the representation of the initial data in the new and reduced coordinate system, composed by the new components, PC, while the loadings describe the “distance” between the initial coordinate system and the PC system. The ε matrix contains unexplained data variance, such as colinearity and noise.

Principal component analysis can be used either as a qualitative data analysis tool, through the analysis of loadings and scores plots, or for reduction of the number of parameters needed to describe spectroscopic data. PARAFAC (parallel factor analysis) is a decomposition method of multiway data that can be considered a generalization of the PCA to higher order arrays (Bro, 1997). It is particularly useful to find the scores matrices for fluorescence excitation-emission matrixes (EEM) resulting from two-dimensional (2D) fluorescence spectroscopy but with reduced dimension.

The so-called gray box models are usually based on multivariate regressions, from which result numerical equations, where the relationships between inputs and the output can be interpreted in a mechanistic way based on the regression coefficients. Projection to latent structures (PLS) is a multilinear regression technique related with PCA, in which the variable space is also subject to a data reduction, but the main goal is to use the reduced space to predict output variables. PLS is a nonparametric model that reveals linear relations between the data, by maximizing the covariance between the input matrix X , and the output Y . This technique combines features from the principal component analysis and multiple linear regression, and aims at the prediction of dependent variables (outputs) by decomposing iteratively both the X and Y matrices into reduced orthogonal factors, termed latent variables. Therefore PLS regression differs from traditional multivariate linear regression (MLR) due to elimination of redundancy in the input and output data. PLS is considered a simple but powerful predictive modeling technique due to its ability to handle colinearity between variables, data noise, and missing data. Furthermore, since the linear PLS model finds a new data arrangement, it is possible to determine and interpret the contribution of the input parameters to the model. A large

numerical value of the regression coefficients is highly correlated with the output, and similar profiles of regression coefficients provide the same contribution to the prediction.

When multilinear regression tools are not sufficient to predict an output, interaction and quadratic terms of the input parameters may be introduced as inputs in the models. Thus the resulting equations are able to describe nonlinear interactions:

$$y = a \cdot x_1 + b \cdot x_2 + c \cdot x_3 + \dots + d \cdot x_1^2 + e \cdot x_1 \cdot x_2 + f \cdot x_1 \cdot x_3 + \dots$$

where y is an output; x_n are the inputs; and a, b, c, \dots are the regression coefficients.

As for ANN, only a few studies focused on the use of multivariate regression tools, such as PLS, for MBR modeling, and most work is performed within general filtration applications (Naessens et al., 2012). Nevertheless, PLS modeling was successfully used to infer a correlation between sludge filterability and sludge characteristics (biomass concentration, relative hydrophobicity, sludge morphology, EPS, sludge dissociation constant, TOC, and surface charge) in municipal and industrial MBRs (Van den Broeck et al., 2011). A correlation was also found between TMP and suspended solids in influent wastewater, permeate flux, temperature, COD in the permeate and MLSS, using PLS modeling applied to a pilot MBR for domestic wastewater treatment (Galinha et al., 2012). Furthermore, this PLS model revealed to be sensitive to extreme fouling buildup (through comparison between predicted and measured TMP values). PLS modeling was also used in combination with ANN to select useful variables (among 21 variables related with influent and effluent characteristics, and operating conditions) and predict membrane permeability in an MBR for wastewater treatment (Han et al., 2018).

Besides the establishment of models to correlate operating conditions with performance parameters, in MBR modeling, multivariate statistical modeling can be also useful to analyze the large analytical amount of data that can be generated from such systems, including simultaneous acquisition of different measurements in influent, effluent and bulk streams, microbiologic and genetic data, and 3D spectra. Indeed, information from fingerprinting monitoring techniques, such as 2D fluorescence spectroscopy, FTIR/NIR or mass spectroscopy, can be extracted using first PCA or PARAFAC functions, to reduce spectra dimension, and then correlate them with performance parameters through multilinear regression techniques (such as PLS modeling) or ANN to obtain quantitative information (Galinha et al., 2013; Pons et al., 2004). Alternatively, spectra can be used directly (without dimension reduction) in the multivariate model, to predict the outputs (Galinha et al., 2011b; Pons et al., 2004; Wolf et al., 2001). However, without previous reduction, the spectral data set contain several colinear inputs (as well as noise), which increases the computational effort and may prevent model calibration (e.g., by overfitting due to high number of inputs). As for ANN, multilinear regression tools also require calibration, based on a statistically representative set of data, obtained with an intensive process characterization performed simultaneously to spectra acquisition.

When the objective of MBR modeling is process monitoring (as mentioned in the online monitoring section of this chapter) the use of spectroscopic data combined with multivariate data analysis can be applied either to predict quantitative biological parameters in the stream analyzed (such as BOD and COD in influent or influent streams, or MLSS in biological media), or as an additional information about biological status (usually in combination with other parameters) to predict filtration performance (such as TMP) or overall MBR performance. These two approaches were previously studied to monitor a pilot MBR for wastewater treatment, using 2D fluorescence spectroscopy combined with PLS modeling, both as a monitoring tool for system characterization (COD, nitrogen, phosphorus, and MLSS), and as system fingerprint for TMP prediction (Galinha et al., 2011a,b, 2012).

6.5.3 HYBRID MODELING

Hybrid modeling is defined as the integration of both mechanistic and nonmechanistic models in order to describe or predict the output variables. In MBRs, this combined approach is particularly important since several submodels are required to model their performance. Therefore, to avoid over parameterization, maintain accurate prediction, and integrate data assessed online, the use of submodels based on multivariate statistical analysis (mainly related with fouling prediction), integrated in a mechanistic model, can be highly useful.

Even when the modeling of both biological and filtration processes is performed mainly by a mechanistic approach, some parameters are particularly difficult to assess, such as influent characteristics in wastewater treatment processes (due to their high variability) or some components of filtration resistance associated with fouling (due to the complexity and mutability of fouling mechanisms). So, both mechanistic and data-driven approaches can provide process knowledge and support each other, in hybrid models, in which the disadvantages of the two approaches are eliminated as much as possible.

Therefore using hybrid modeling, it is possible to add extra information to mechanistic models when in conditions they are not able to accurately estimate the output variables, as shown in Fig. 6.7. Such additional information can be obtained through operating data, analytical data, or assessed online (e.g., as spectral data) and used to improve the prediction ability of the model (e.g., by modeling the residuals from the mechanistic model) (Galinha et al., 2013).

Additionally, even when the submodels of an MBR modeling system are well defined, changes in the range of operating conditions may affect the models' performance. If the shift in operating conditions affects the fouling mechanisms, the use of a specific mechanistic model for fouling resistance may not be possible in such conditions. Therefore if a data-driven model can be calibrated in that range, the combination of both models in a hybrid model, shifting between submodels based on the operating conditions, allows prediction of performance in all operating range (Dalmau et al., 2015).

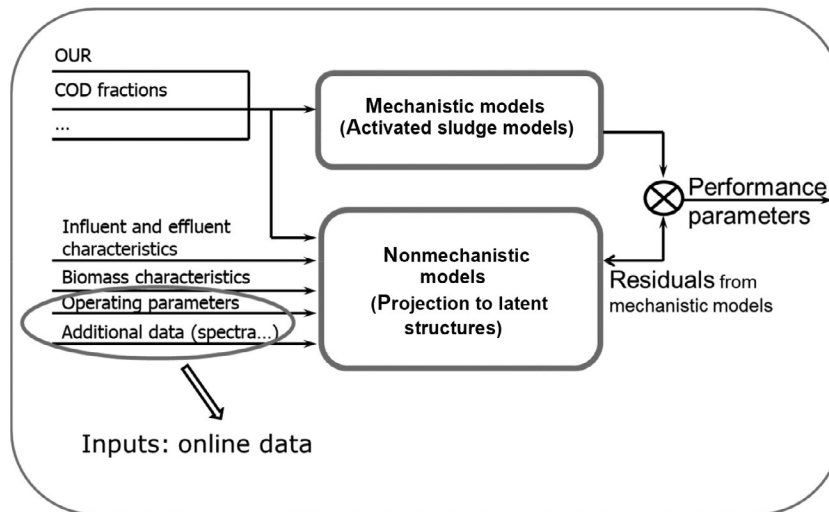


FIG. 6.7

Hybrid modeling approach for an MBR for wastewater treatment, aiming at integrating online data with a mechanistic model, to improve its prediction.

6.6 CONCLUSIONS AND OUTLOOK

From the information and discussion provided in this chapter it can be concluded that modeling of membrane bioreactors can be accomplished in many situations by using relatively simple mechanistic models. This is the case of enzymatic membrane bioreactors, where the enzymatic kinetics can be previously established and relatively simple models may be obtained by integrating the reaction contribution in the system's mass balances. The most complex situation may arise from cases where mass transfer limitations are prone to occur. Even though, the degree of complexity can be handled correctly without the need of using other type of mathematical approaches.

However, when dealing with situations where the composition of the media is complex and may originate metabolic pathways and fouling phenomena that depend from a large diversity of conditions that are interrelated, then mechanistic approaches may become too complex by requiring several submodels to model overall MBR performance. This is very much the situation of membrane bioreactors involving mixed microbial cultures. In this case, the complexity of the media composition, the microbial diversity, and the variety of interactions that may be established between the feed components and the membrane material make extremely difficult to be fully captured and described by mechanistic models without overparameterization. It is true that a number of reasonable assumptions and simplifications may be considered, but the final result is exactly that—a simplification—of the complex reality.

As discussed in this chapter, under those circumstances, multivariate statistical modeling may represent a valid and powerful alternative and no intellectual bias

should keep us away from this approach. Multivariate statistical analysis using tools such as Artificial Neural Networks (ANN) or Projection to Latent Structures (PLS) may be used when dealing with such complex situations. A number of examples were presented and discussed in the chapter and they prove how this approach may be valid and, more important, useful for process monitoring, modeling, and control.

A final word for the use of Hybrid Modeling, which can combine in a very powerful way a large diversity of information from different sources. Starting with what is known and partially described by mechanistic modeling and refining it with incorporation of other sources of information that may help us to polish the final model.

Considering the bright future of membrane bioreactors, that more and more will open to different type of biocatalysts and will use more sophisticated and target-specific membranes, modeling requirements will be challenging and will require open-minded approaches.

REFERENCES

- APHA, 2005. *Standard Methods for the Examination of Water and Wastewater*. Washington, DC, USA.
- Bacchin, P., Aimar, P., Field, R.W., 2006. Critical and sustainable fluxes: theory, experiments and applications. *J. Membrane Sci.* 281, 42–69.
- Bouhabila, E., Ben Aim, R., Buisson, H., 2001. Fouling characterisation in membrane bioreactors. *Sep. Purif. Technol.* 22 (3), 123–132.
- Bro, R., 1997. PARAFAC. Tutorial and applications. *Chemom. Intell. Lab. Syst.* 38, 149–171.
- Buffington, D.A., Westover, A.J., Johnston, K.A., Humes, H.D., 2014. The bioartificial kidney. *Transl. Res.* 163 (4), 342–351.
- Busch, J., Cruse, A., Marquardt, W., 2007. Modeling submerged hollow-fiber membrane filtration for wastewater treatment. *J. Membr. Sci.* 288, 94–111.
- Carvalho, A.P., Meireles, L.A., Malcata, F.X., 2006. Microalgal reactors: a review of enclosed system designs and performances. *Biotechnol. Prog.* 22 (6), 1490–1506.
- Carvalho, A.P., Silva, S.O., Baptista, J.M., Malcata, F.X., 2011. Light requirements in microalgal photobioreactors: an overview of biophotonic aspects. *Appl. Microbiol. Biotechnol.* 89 (5), 1275–1288.
- Chang, H.X., Fu, Q., Huang, Y., Xia, A., Liao, Q., Zhu, X., Zheng, Y.P., Sun, C.H., 2016. An annular photobioreactor with ion-exchange-membrane for non-touch microalgae cultivation with wastewater. *Bioresour. Technol.* 219, 668–676.
- Chen, C.Y., Saratale, G.D., Lee, C.M., Chen, P.C., Chang, J.S., 2008. Phototrophic hydrogen production in photobioreactors coupled with solar-energy-excited optical fibers. *Int. J. Hydrog. Energy* 33 (23), 6886–6895.
- Chen, C.Y., Yeh, K.L., Aisyah, R., Lee, D.J., Chang, J.S., 2011. Cultivation, photobioreactor design and harvesting of microalgae for biodiesel production: A critical review. *Bioresour. Technol.* 102 (1), 71–81.
- Chen, J., Zhang, M., Li, F., Qian, L., Lin, H., Yang, L., Wu, X., Zhou, X., He, Y., Liao, B.Q., 2016. Membrane fouling in a membrane bioreactor: high filtration resistance of gel layer and its underlying mechanism. *Water Res.* 102, 82–89.

- Cho, J., Song, K.G., Ahn, K.H., 2005. The activated sludge and microbial substances influences on membrane fouling in submerged membrane bioreactor: Unstirred batch cell test. *Desalination* 183, 425–429.
- Chu, H.P., Li, X.Y., 2005. Membrane fouling in a membrane bioreactor (MBR): sludge cake formation and fouling characteristics. *Biotechnol. Bioeng.* 90, 323–331.
- Çinar, Ö., Hasar, H., Kinaci, C., 2006. Modeling of submerged membrane bioreactor treating cheese whey wastewater by artificial neural network. *J. Biotechnol.* 123, 204–209.
- Claßen, J., Aupert, F., Reardon, K.F., Solle, D., Scheper, T., 2017. Spectroscopic sensors for in-line bioprocess monitoring in research and pharmaceutical industrial application. *Anal. Bioanal. Chem.* 409, 651–666.
- Coburn, K.M., Wang, Q.Z., Rediske, D., Viola, R.E., Hanson, B.L., Xue, Z., Seo, Y., 2016. Effects of extracellular polymeric substance composition on Bacteria disinfection by monochloramine: application of MALDI-TOF/TOE-MS and multivariate analysis. *Environ. Sci. Technol.* 50 (17), 9197–9205.
- Curcio, E., De Bartolo, L., Barbieri, G., et al., 2005. Diffusive and convective transport through hollow fiber membranes for liver cell culture. *J. Biotechnol.* 117, 309–321.
- da Silva, A., da Silva, R., Camoes, M., 2011. Optimization of the determination of chemical oxygen demand in wastewaters. *Anal. Chim. Acta* 699 (2), 161–169.
- Dalmau, M., Atanasova, N., Gabarrón, S., Rodriguez-Roda, I., Comas, J., 2015. Comparison of a deterministic and a data driven model to describe MBR fouling. *Chem. Eng. J.* 260, 300–308.
- De Napoli, I.E., Zanetti, E.M., Fragomeni, G., Giuzio, E., Audenino, A.L., Catapano, G., 2014. Transport modeling of convection-enhanced hollow fiber membrane bioreactors for therapeutic applications. *J. Membr. Sci.* 471, 347–361.
- Diban, N., Stamatialis, D., 2014. Polymeric hollow fiber membranes for bioartificial organs and tissue engineering applications. *J. Chem. Technol. Biotechnol.* 89 (5), 633–643.
- Dionne, K.E., Cain, B.M., Li, R.H., et al., 1996. Transport characterization of membranes for immunisolation. *Biomaterials* 17, 257–266.
- Dominguez, L., Rodriguez, M., Prats, D., 2010. Effect of different extraction methods on bound EPS from MBR sludges part II: influence of extraction methods over molecular weight distribution. *Desalination* 262 (1–3), 106–109.
- Drews, A., 2010. Membrane fouling in membrane bioreactors-characterisation, contradictions, cause and cures. *J. Membr. Sci.* 363, 1–28.
- Drioli, E., De Bartolo, L., 2006. Membrane bioreactor for cell tissues and organoids. *Artif. Organs* 30 (10), 793–802.
- Dubois, M., Gilles, K.A., Hamilton, J.K., Rebers, P.A., Smith, F., 1956. Colorimetric method for determination of sugars and related substances. *Anal. Chem.* 28 (3), 350–356.
- Eghbali, H., Nava, M.M., Mohebbi-Kalhor, D., Raimondi, M.T., 2016. Hollow fiber bioreactor technology for tissue engineering applications. *Int. J. Artif. Organs* 39 (1), 1–15.
- Fenu, A., Guglielmi, G., Jimenez, J., Sperandio, M., Saroj, D., Lesjean, B., Brepols, C., Thoeys, C., Nopens, I., 2010. Activated sludge model (ASM) based modelling of membrane bioreactor (MBR) processes: a critical review with special regard to MBR specificities. *Water Res.* 44, 4272–4294.
- Field, R.W., Wu, D., Howell, J.A., Gupta, B.B., 1995. Critical flux concept for microfiltration fouling. *J. Membr. Sci.* 100, 259–272.
- Fonseca, A.D., Crespo, J.G., Almeida, J.S., Reis, M.A., 2000. Drinking water denitrification using a novel ion-exchange membrane bioreactor. *Environ. Sci. Technol.* 34 (8), 1557–1562.

- Fortunato, L., Jeong, S., Wang, Y.R., Behzad, A.R., Leiknes, T., 2016. Integrated approach to characterize fouling on a flat sheet membrane gravity driven submerged membrane bioreactor. *Bioresour. Technol.* 222, 335–343.
- Frolund, B., Griebe, T., Nielsen, P.H., 1995. Enzymatic-activity in the activated-sludge floc matrix. *Appl. Microbiol. Biotechnol.* 43 (4), 755–761.
- Gale, R.S., Baskerville, R.C., 1967. Capillary suction method for determination of filtration properties of a solid/liquid suspension. *Chem. Ind.* 9, 355–356.
- Galinha, C.F., Carvalho, G., Portugal, C.a.M., Guglielmi, G., Reis, M.a.M., Crespo, J.G., 2011a. Two-dimensional fluorescence as a fingerprinting tool for monitoring wastewater treatment systems. *J. Chem. Technol. Biotechnol.* 86 (7), 985–992.
- Galinha, C.F., Carvalho, G., Portugal, C.a.M., Guglielmi, G., Oliveira, R., Crespo, J.G., Reis, M.a.M., 2011b. Real-time monitoring of membrane bioreactors with 2D-fluorescence data and statistically based models. *Water Sci. Technol.* 63 (7), 1381–1388.
- Galinha, C.F., Carvalho, G., Portugal, C.a.M., Guglielmi, G., Reis, M.a.M., Crespo, J.G., 2012. Multivariate statistically-based modelling of a membrane bioreactor for wastewater treatment using 2D fluorescence monitoring data. *Water Res.* 46 (11), 3623–3636.
- Galinha, C.F., Guglielmi, G., Carvalho, G., Portugal, C.a.M., Crespo, J.G., Reis, M.a.M., 2013. Development of a hybrid model strategy for monitoring membrane bioreactors. *J. Biotechnol.* 164 (3), 386–395.
- Geissler, S., Wintgens, T., Melin, T., Vossenkaul, K., Kullmann, C., 2005. Modelling approaches for filtration processes with novel submerged capillary modules in membrane bioreactors for wastewater treatment. *Desalination* 178, 125–134.
- Giorno, L., Mazzei, R., Drioli, E., 2009. Biochemical membrane reactors in industrial processes. In: Drioli, E., Giorno, L. (Eds.), *Membrane Operations: Innovative Separations and Transformations*. Wiley-VCH, Weinheim, pp. 397–409.
- Griffiths, I.M., Kumar, A., Stewart, P.S., 2014. A combined network model for membrane fouling. *J. Colloid Interface Sci.* 432, 10–18.
- Han, H., Zhang, S., Qiao, J., Wang, X., 2018. An intelligent detecting system for permeability prediction of MBR. *Water Sci. Technol.* 77, 467–478.
- Henze, M., Gujer, W., Mino, T., van Loosdrecht, M., 2000. *Activated Sludge Models: ASM1, ASM2, ASM2d and ASM3*. Scientific and Technical Report no 9, IWA publishing, London.
- Honda, R., Boonnorat, J., Chiemchaisri, C., Chiemchaisri, W., Yamamoto, K., 2012. Carbon dioxide capture and nutrients removal utilizing treated sewage by concentrated microalgae cultivation in a membrane photobioreactor. *Bioresour. Technol.* 125, 59–64.
- Hong, H., Zhang, M., He, Y., Chen, J., Lin, H., 2014. Fouling mechanisms of gel layer in a submerged membrane bioreactor. *Bioresour. Technol.* 166, 295–302.
- Huyskens, C., Brauns, E., Van Hoof, E., De Wever, H., 2008. A new method for the evaluation of the reversible and irreversible fouling propensity of MBR mixed liquor. *J. Membr. Sci.* 323, 185–192.
- Iacovacci, V., Ricotti, L., Menciasci, A., Dario, P., 2016. The bioartificial pancreas (BAP): biological, chemical and engineering challenges. *Biochem. Pharmacol.* 100, 12–27.
- Iorio, G., Calabro, V., Todisco, S., 1994. Enzyme membrane reactors. In: Crespo, J.G., Bøddeker, K.-W. (Eds.), *Membrane Processes in Separation and Purification*. Kluwer Academic Publishers, Dordrecht, pp. 149–167.
- Izák, P., Mateus, N.M.M., Afonso, C.A.M., Crespo, J.G., 2005. Enhanced esterification conversion in a room temperature ionic liquid by integrated water removal with pervaporation. *Sep. Purif. Technol.* 41 (2), 141–145.

- Jansen, J., Fedecostante, M., Wilmer, M.J., van den Heuvel, L.P., Hoenderop, J.G., Masereeuw, R., 2014. Biotechnological challenges of bioartificial kidney engineering. *Biotechnol. Adv.* 32 (7), 1317–1327.
- Jiang, T., Myngheer, S., De Pauw, D.J.W., Spanjers, H., Nopens, I., Kennedy, M.D., Amy, G., Vanrolleghem, P.A., 2008. Modelling the production and degradation of soluble microbial products (SMP) in membrane bioreactors (MBR). *Water Res.* 42, 4955–4964.
- Jordan, M.A., Welsh, D.T., Teasdale, P.R., 2014. Ubiquity of activated sludge ferricyanide-mediated BOD methods: a comparison of sludge seeds across wastewater treatment plants. *Talanta* 125, 293–300.
- Jorgensen, M.K., Keiding, K., Christensen, M.L., 2014. On the reversibility of cake buildup and compression in a membrane bioreactor. *J. Membr. Sci.* 455, 152–161.
- Jorgensen, M.K., Nierychlo, M., Nielsen, A.H., Larsen, P., Christensen, M.L., Nielsen, P.H., 2017. Unified understanding of physico-chemical properties of activated sludge and fouling propensity. *Water Res.* 120, 117–132.
- Judd, S., 2006. *The MBR Book, Principles and Applications of Membrane Bioreactors for Water and Wastewater Treatment*, second ed. Elsevier. ISBN 978-0-08-096682-3.
- Judd, S., 2008. The status of membrane bioreactor technology. *Trends Biotechnol.* 26 (2), 109–116.
- Kimura, K., Naruse, T., Watanabe, Y., 2009. Changes in characteristics of soluble microbial products in membrane bioreactors associated with different solid retention times: Relation to membrane fouling. *Water Res.* 43 (4), 1033–1039.
- Lapidou, C.S., Rittmann, B.E., 2002. Non-steady state modeling of extracellular polymeric substances, soluble microbial products, and active and inert biomass. *Water Res.* 36, 1983–1992.
- Le Clech, P., Jefferson, B., Chang, I.S., Judd, S.J., 2003. Critical flux determination by the flux-step method in a submerged membrane bioreactor. *J. Membr. Sci.* 227, 81–93.
- Le-Clech, P., Chen, V., Fane, T.A.G., 2006. Fouling in membrane bioreactors used in wastewater treatment. *J. Membr. Sci.* 284 (1–2), 17–53.
- Lesjean, B., Tazi-Pain, A., Thaire, D., Moeslang, H., Buisson, H., 2011. Ten persistent myths and the realities of membrane bioreactor technology for municipal applications. *Water Sci. Technol.* 63, 32–39.
- Li, X.y., Wang, X.m., 2006. Modelling of membrane fouling in a submerged membrane bioreactor. *J. Membr. Sci.* 278, 151–161.
- Lowry, O.H., Rosebrough, N.J., Farr, A.L., Randall, R.J., 1951. Protein measurement with the FOLIN phenol reagent. *J. Biol. Chem.* 193 (1), 265–275.
- Luo, Y.L., Jiang, Q., Ngo, H.H., Nghiem, L.D., Hai, F.I., Price, W.E., Wang, J., Guo, W.S., 2015. Evaluation of micropollutant removal and fouling reduction in a hybrid moving bed biofilm reactor-membrane bioreactor system. *Bioresour. Technol.* 191, 355–359.
- Lyko, S., Wintgens, T., Al-Halbouni, D., Baumgarten, S., Tacke, D., Drensla, K., Janot, A., Dott, W., Pinnekamp, J., Melin, T., 2008. Long-term monitoring of a full-scale municipal membrane bioreactor—characterisation of foulants and operational performance. *J. Membr. Sci.* 317 (1–2), 78–87.
- Mannina, G., Di Bella, G., Viviani, G., 2011. An integrated model for biological and physical process simulation in membrane bioreactors (MBRs). *J. Membr. Sci.* 376, 56–69.
- Marbelia, L., Bilad, M.R., Passaris, I., Discart, V., Vandamme, D., Beuckels, A., Muylaert, K., Vankelecom, I.F.J., 2014. Membrane photobioreactors for integrated microalgae cultivation and nutrient remediation of membrane bioreactors effluent. *Bioresour. Technol.* 163, 228–235.

- McDonald, K.A., Hong, L.M., Trombly, D.M., Xie, Q., Jackman, A.P., 2005. Production of human alpha-1-antitrypsin from transgenic rice cell culture in a membrane bioreactor. *Biotechnol. Progress* 21 (3), 728–734.
- Meng, F.G., Chae, S.R., Drews, A., Kraume, M., Shin, H.S., Yang, F.L., 2009. Recent advances in membrane bioreactors (MBRs): membrane fouling and membrane material. *Water Res.* 43 (6), 1489–1512.
- Meng, F.G., Zhou, Z.B., Ni, B.J., Zheng, X., Huang, G.C., Jia, X.S., Li, S.Y., Xiong, Y., Kraume, M., 2011. Characterization of the size-fractionated biomacromolecules: tracking their role and fate in a membrane bioreactor. *Water Res.* 45 (15), 4661–4671.
- Menniti, A., Kang, S., Elimelech, M., Morgenroth, E., 2009. Influence of shear on the production of extracellular polymeric substances in membrane bioreactors. *Water Res.* 43 (17), 4305–4315.
- Mesquita, D.P., Quintelas, C., Amaral, A.L., Ferreira, E.C., 2017. Monitoring biological wastewater treatment processes: recent advances in spectroscopy applications. *Rev. Environ. Sci. Biotechnol.* 16, 395–424.
- Mirbagheri, S.A., Bagheri, M., Bagheri, Z., Kamarkhani, A.M., 2015. Evaluation and prediction of membrane fouling in a submerged membrane bioreactor with simultaneous upward and downward aeration using artificial neural network-genetic algorithm. *Process. Saf. Environ. Prot.* 96, 111–124.
- Monclús, H., Ferrero, G., Buttiglieri, G., Comas, J., Rodriguez-Roda, I., 2011. Online monitoring of membrane fouling in submerged MBRs. *Desalination* 277, 414–419.
- Naessens, W., Maere, T., Nopens, I., 2012. Critical review of membrane bioreactor models—part I: Biokinetic and filtration models. *Bioresour. Technol.* 122, 95–106.
- Najm, Y., Jeong, S., Leiknes, T., 2017. Nutrient utilization and oxygen production by *Chlorella vulgaris* in a hybrid membrane bioreactor and algal membrane photobioreactor system. *Bioresour. Technol.* 237, 64–71.
- Nam, C.H., Furusaki, S., 1991. Membrane bioreactors: present and prospects. *Adv. Biochem. Eng. Biotechnol.* 44, 27–64.
- Namkung, E., Rittmann, B.E., 1986. Soluble microbial products (SMP) formation kinetics by biofilms. *Water Res.* 20, 795–806.
- Pendashteh, A.R., et al., 2011. Modeling of membrane bioreactor treating hypersaline oily wastewater by artificial neural network. *J. Hazard. Mater.* 192, 568–575.
- Pivokonsky, M., Naceradska, J., Kopecka, I., Baresova, M., Jefferson, B., Li, X., Henderson, R.K., 2016. The impact of algogenic organic matter on water treatment plant operation and water quality: a review. *Crit. Rev. Environ. Sci. Technol.* 46 (4), 291–335.
- Pons, M.N., Le Bonte, S., Potier, O., 2004. Spectral analysis and fingerprinting for biomedica characterisation. *J. Biotechnol.* 113, 211–230.
- Poorasgari, E., Vistisen Bugge, T., Lykkegaard Christensen, M., Koustrup Jørgensen, M., 2015. Compressibility of fouling layers in membrane bioreactors. *J. Membr. Sci.* 475, 65–70.
- Pörtner, R., Nagel-Heyer, S., Goepfert, C., Adamietz, P., Meenen, N.M., 2005. Bioreactor design for tissue engineering. *J. Biosci. Bioeng.* 100 (3), 235–245.
- Portugal, C.A.M., Lima, J.C., Crespo, J.G., 2006. Probing the change of enzymatic activity of horseradish peroxidase induced by membrane permeation using tryptophan fluorescence. *J. Membr. Sci.* 284 (1–2), 180–192.
- Posten, C., 2009. Design principles of photo-bioreactors for cultivation of microalgae. *Eng. Life Sci.* 9 (3), 165–177.

- Rosso, D., Larson, L.E., Stenstrom, M.K., 2008. Aeration of large-scale municipal wastewater treatment plants: state of the art. *Water Sci. Technol.* 57 (7), 973–978.
- Santos, L.M.F., Hömmerich, U., Livingston, A.G., 1995. Dichloroethane removal from gas streams by an extractive membrane bioreactor. *Biotechnol. Prog.* 11 (2), 194–201.
- Schiraldi, C., Alfano, A., Cimini, D., De Rosa, M., Panariello, A., Restaino OF, 2012. Application of a 22L scale membrane bioreactor and cross-flow ultrafiltration to obtain purified chondroitin. *Biotechnol. Prog.* 28 (4), 1012.
- Scholes, E., Verheyen, V., Brook-Carter, P., 2016. A review of practical tools for rapid monitoring of membrane bioreactors. *Water Res.* 102, 252–262.
- Seviour, R., Nielsen, P.H., 2010. *Micobial Ecology of Activated Sludge*. IWA Publishing, New York.
- Silva, A.F., Carvalho, G., Oehmen, A., Lousada-Ferreira, M., van Nieuwenhuijzen, A., Reis, M.A.M., Barreto Crespo, M.T., 2012a. Microbial population analysis of nutrient removal-related organisms in membrane bioreactors. *Appl. Microbiol. Biotechnol.* 93 (5), 2171–2180.
- Silva, A.F., Carvalho, G., Soares, R., Coelho, A.V., Crespo, M.T.B., 2012b. Step-by-step strategy for protein enrichment and proteome characterisation of extracellular polymeric substances in wastewater treatment systems. *Appl. Microbiol. Biotechnol.* 95 (3), 767–776.
- Silva, A.F., Antunes, S., Saunders, A., Freitas, F., Vieira, A., Galinha, C.F., Nielsen, P.H., Crespo, M.T.B., Carvalho, G., 2016. Impact of sludge retention time on the fine composition of the microbial community and extracellular polymeric substances in a membrane bioreactor. *Appl. Microbiol. Biotechnol.* 100 (19), 8507–8521.
- Sousa, H.A., Afonso, C.A.M., Mota, J.P.B., Crespo, J.G., 2005. Modelling the enantioselective hydrolysis of a meso-diester using pig liver esterase in a two-phase hollow fibre reactor. *Chem. Eng. Res. Des.* 83 (A3), 285–294.
- Talbot, P., Gortares, M.P., Lencki, R.W., Delanoue, J., 1991. Absorption of CO₂ in algal mass-culture systems—a different characterization approach. *Biotechnol. Bioeng.* 37 (9), 834–842.
- Van den Broeck, R., Krzeminski, P., Van Dierdonck, J., Gins, G., Lousada-Ferreira, M., Van Impe, J.F.M., van der Graaf, J.H.J.M., Smets, I.Y., van Lier, J.B., 2011. Activated sludge characteristics affecting sludge filterability in municipal and industrial MBRs: unraveling correlations using multi-component regression analysis. *J. Membr. Sci.* 378, 330–338.
- Wandrey, C., 2004. Biochemical reaction engineering for redox reactions. *Chem. Rec.* 4, 254–265.
- Wickramasinghe, S.R., Semmens, M.J., Cussler, E.L., 1992. Mass-transfer in various hollow fiber geometries. *J. Membr. Sci.* 69 (3), 235–250.
- Wolf, G., Almeida, J.S., Pinheiro, C., Correia, V., Rodrigues, C., Reis, M.A., Crespo, J.G., 2001. Two-dimensional fluorometry coupled with artificial neural networks: a novel method for on-line monitoring of complex biological processes. *Biotechnol. Bioeng.* 72, 297–306.
- Wung, N., Acott, S.M., Tosh, D., Ellis, M.J., 2014. Hollow fibre membrane bioreactors for tissue engineering applications. *Biotechnol. Lett.* 36 (12), 2357–2366.
- Xiao, K., Shen, Y.-x., Liang, S., Liang, P., Wang, X.-m., Huang, X., 2014. A systematic analysis of fouling evolution and irreversibility behaviors of MBR supernatant hydrophilic/hydrophobic fractions during microfiltration. *J. Membr. Sci.* 467, 206–216.

- Yamamoto, K., Hiasa, M., Mahmood, T., Matsuo, T., 1988. Direct Solid-Liquid Separation Using Hollow Fiber Membrane in an Activated Sludge Aeration Tank. In: Water Pollution Research and Control Brighton. Proceedings of the Fourteenth Biennial Conference of the International Association on Water Pollution Research and Control, Held in Brighton, UK, 18–21 July pp. 43–54.
- Yang, M., Yu, D., Liu, M., Zheng, L., Zheng, X., Wei, Y., Wang, F., Fan, Y., 2017. Optimization of MBR hydrodynamics for cake layer fouling control through CFD simulation and RSM design. *Bioresour. Technol.* 227, 102–111.

Ion-exchange membrane systems—Electrodialysis and other electromembrane processes

Bart Van der Bruggen*†

Department of Chemical Engineering, KU Leuven, Leuven, Belgium Faculty of Engineering and the Built Environment, Tshwane University of Technology, Pretoria, South Africa†*

CHAPTER OUTLINE

7.1 Introduction	251
7.2 Process Description	252
7.3 General Overview of Applications	260
7.4 Calculation of Selectivity in Electrodialysis	266
7.5 Ion Transport Through Ion-Exchange Membranes	270
7.6 Other Configurations of Electrodriven Membrane Processes	275
7.6.1 Diffusion Dialysis	275
7.6.2 Electro-Electrodialysis	276
7.6.3 Continuous Electrodeionization	278
7.6.4 Donnan Dialysis	281
7.6.5 Membrane Electrolysis	282
7.6.6 Fuel Cells	284
7.6.7 Capacitive Deionization	286
7.6.8 Electrodialysis With Bipolar Membranes	289
7.6.9 Reverse Electrodialysis	292
7.7 Conclusions	294
References	294
Further Reading	299

7.1 INTRODUCTION

Electrodialysis is a separation process using ion-exchange membranes and an electrical potential as a driving force (Strathmann, 2004a). Ion-exchange membranes contain charged functional groups and may be synthesized as homogenous or heterogeneous

membranes. In these structures, the charged groups are either chemically bonded to or physically mixed with a polymer matrix (Xu, 2005). The backbone provides the necessary strength and dimensional stability of the membrane (Kariduraganavar et al., 2006). Furthermore, monopolar ion-exchange membranes can be classified in two types, that is, anion-exchange membranes and cation-exchange membranes. Anion-exchange membranes contain positively charged groups. Ion-exchange membranes are able to retain ions with an equal charge while being permeable for ions with an opposite charge. Therefore anions can permeate through anion-exchange membranes while cations are retained. Similarly, cation-exchange membranes with negatively charged groups retain anions and are permeable for cations (Xu, 2005). In practice, sulfonic and carboxyl groups are predominantly used in cation-exchange membranes. Meanwhile, quaternary ammonium groups are preferred in anion-exchange membranes (Sata, 2004). A recent overview of new developments in the synthesis of ion-exchange membranes is given by Ran et al. (2017).

Today, electro dialysis is a well understood process. However, it is remarkable that it is one of the first membrane processes to be applied on large scale, already in the 1950s. The first description of electrodriven transport through a membrane was by Maigrot and Sabates (to demineralize sugar syrup) in 1890; patents were taken in Germany by Schollmeyer in 1900, and by Kollrepp and Wolf in 1902 (Van der Bruggen, 2017). The first publication appeared in 1903, while the first system for electro dialysis, consisting of permselective anion- and cation-exchange membranes in a three-compartment electro dialysis apparatus, was developed in 1939 by Mane-gold and Kalauch. A large-scale application for brackish water desalination was operated in the United States since 1955 (Van der Bruggen, 2017). Thus electro dialysis is one the most established membrane processes, which may come as a surprise.

In the second half of the 20th century, the process did not evolve much; the standard application for brackish water desalination had a stable, but small market. In the first decade of the 21st century this changed rapidly, due to a number of factors: the emergence of bipolar membranes, which allow for new and different applications where pH differences play a role (production and separation of acids and bases); the growing importance of resource recovery and related selective recovery of anions and metals; and the design of alternative electro dialysis stack configurations, which are intended for selective separation in a series of applications. As a consequence, electrodriven membrane processes are now among the most dynamic and innovative processes. They are often denoted as “green processes,” which is related to the method of producing the electrical power required in the process. Many examples of solar-driven electromembrane separation are known, which is a logical combination and indeed suggests a sustainable application. However, this may not be the case for all applications of electro dialysis or related processes.

7.2 PROCESS DESCRIPTION

The classical application of electro dialysis is based on a stack of alternating anion-exchange membranes and cation-exchange membranes. This is shown in Fig. 7.1 (Khan et al., 2016). An electrical potential is applied between a cathode and an

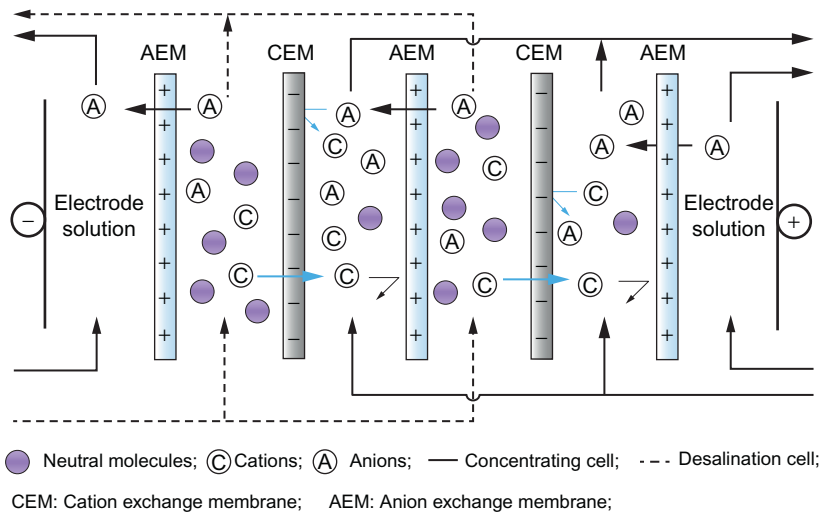


FIG. 7.1

Configuration of a classical electrodiagnosis stack (Khan et al., 2016).

anode; the membrane stack is positioned between cathode and anode as shown in Fig. 7.1. A feed flow containing ions is applied in between the cation-exchange membranes and the anion-exchange membranes. Cations migrate toward the cathode, through a cation-exchange membrane (CEM), but they are blocked in this compartment by the subsequent anion-exchange membrane. The cations are combined with anions coming from the opposite direction: these are migrating to the anode, through one anion-exchange membrane, but they are blocked by the subsequent cation-exchange membrane. In this way they remain in the same compartment as the cations, which is denoted as the ‘concentrate’ compartment. The compartments to the left and to the right are becoming depleted of cations as well as anions; this is denoted as the ‘diluate’ compartment. Transport of ions to the concentrate is remarkable, as it occurs against the concentration gradient. It has two limiting factors:

- Back diffusion due to the concentration gradient that is built up. This follows Fick’s law:

$$N_i = D_i \frac{dc_i}{dx} \quad (7.1)$$

in which c_i is the concentration of ion i , D_i is the diffusion coefficient of this ion through the membrane, and N_i is the flux of i through the membrane.

As the concentration in the concentrate increases during electrodiagnosis operation, the back diffusion flux increases as well. This continues until the electrical flux against the concentration gradient equals the back diffusion flux; this is the maximum effect that can be obtained.

- Ion depletion in the diluate. When ions are completely depleted from this compartment, the electrical resistance drastically increases. Thus the further

removal of ions becomes difficult, once a low concentration is reached, because not sufficient ions are available anymore to transfer the electrical charge. The (electrical) energy in the system is then used for water splitting:



So that further transport is limited to OH^- and H^+ , which is not a useful effect and decreases the efficiency of the system.

As a consequence, electrodialysis is typically operated in once-through mode for the diluate, although with some ion concentration remaining at the outlet, and with recycle of the concentrate in order to minimize the loss of water in the concentrate; this can be done until a concentration factor in the order of 200 is reached.

Apart from the membrane stack, a classical electrodialysis system consists of three separated circuits with three vessels for the diluate, the concentrate and the electrolyte rinsing solution. The flow rates and pressure are monitored by flow meters and pressure gauges, respectively. A schematic diagram of a typical batch electrodialysis system is shown in Fig. 7.2. An adjustable DC power source is used

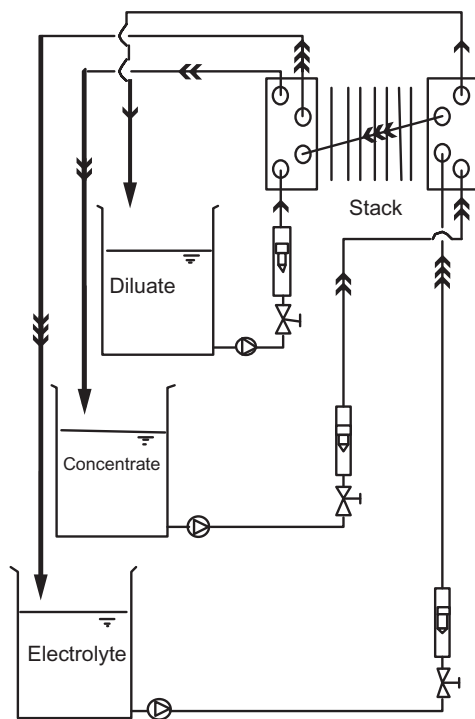


FIG. 7.2

Schematic diagram of the configuration of a basic electrodialysis system.

for electricity supply. Either constant current (CC) mode or constant voltage (CV) mode can be applied.

With a different stack configuration, other applications based on electrodriven membrane separation are possible. This is mainly the case for the use of bipolar membranes. A bipolar membrane is a combination of an anion-exchange membrane and a cation-exchange membrane, which would transport cations nor anions, but split water available in the thin layer between the cation-exchange membrane and the anion-exchange membrane into H^+ and OH^- . This is shown in Fig. 7.3. Since these ions are transported to opposite sides of the bipolar membrane, a different pH on both sides of the membrane is obtained, which is the basis for an interesting series of separations or combined reactions and separations.

A typical stack with bipolar membranes would thus have one additional compartment; this is shown in Fig. 7.4.

Other stack configurations with additional compartments have been developed as well; a key example of this is the ‘selectrodialysis’ stack shown in Fig. 7.5 (Zhang et al., 2012). In this stack, a sequence of a nonselective anion-exchange membrane and a monovalent selective anion-exchange membrane produces two compartments, one in which the multivalent ions remain (the ‘product’ compartment) and a second compartment where the monovalent ions are removed.

Some other configurations may make sense. One modification is the addition of an additional membrane in order to prevent leakage of ions due to back diffusion and nonselective transport. Some ions, and in particular H^+ , are very sensitive to this: they can leak through anion-exchange membranes because of their small size, and may thus contaminate the product compartment. An example of this is shown in Fig. 7.6; many variations on this approach can be found.

The flux of ions, and the resulting concentration profile in the compartment in the vicinity of the surface of the ion-exchange membrane under steady-state conditions

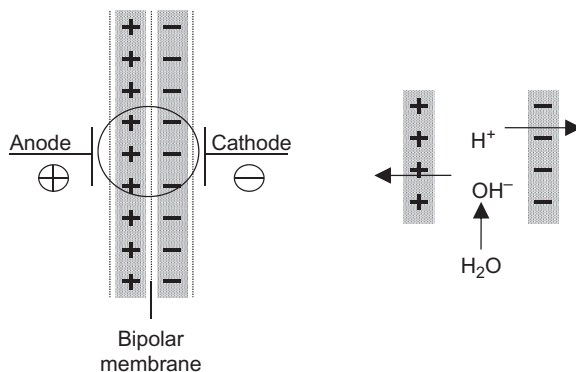


FIG. 7.3

The use of a bipolar membrane in electromembrane separations.

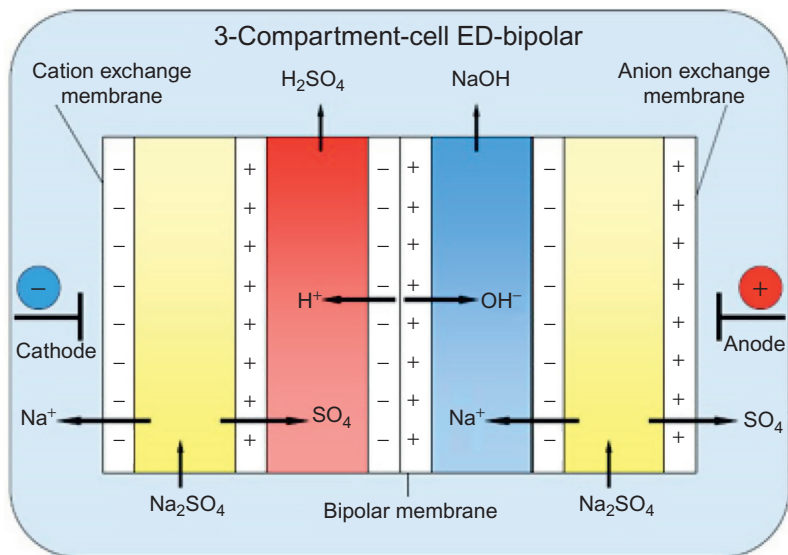


FIG. 7.4

Three-compartment electrodiolysis cell with a bipolar membrane (Fumatech, n.d.).

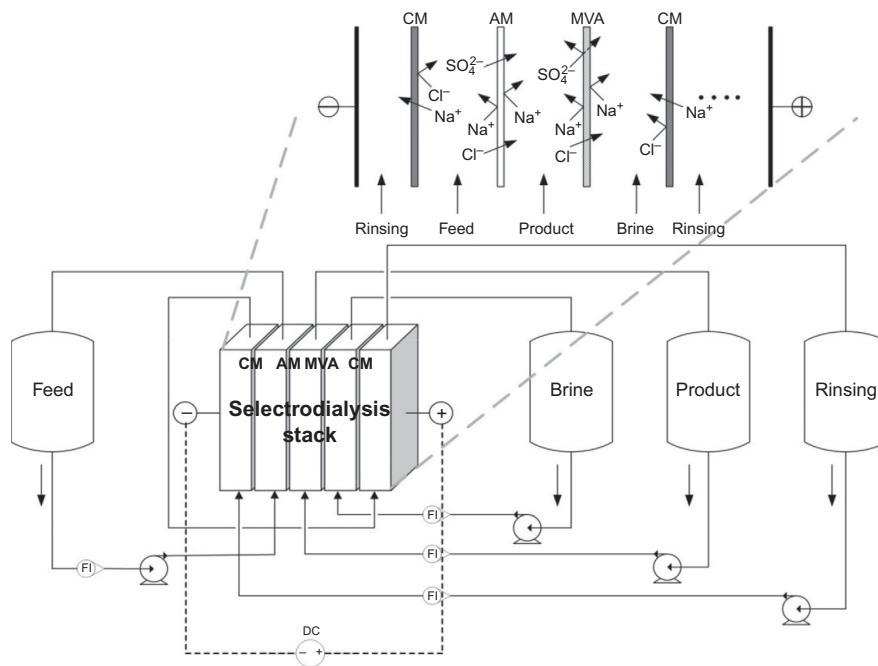


FIG. 7.5

Configuration of a selectrodialysis stack for selective separation of multivalent anions. CM is a cation-exchange membrane, AM is a nonselective anion-exchange membrane, and MVA is a selective anion-exchange membrane (Zhang et al., 2012).

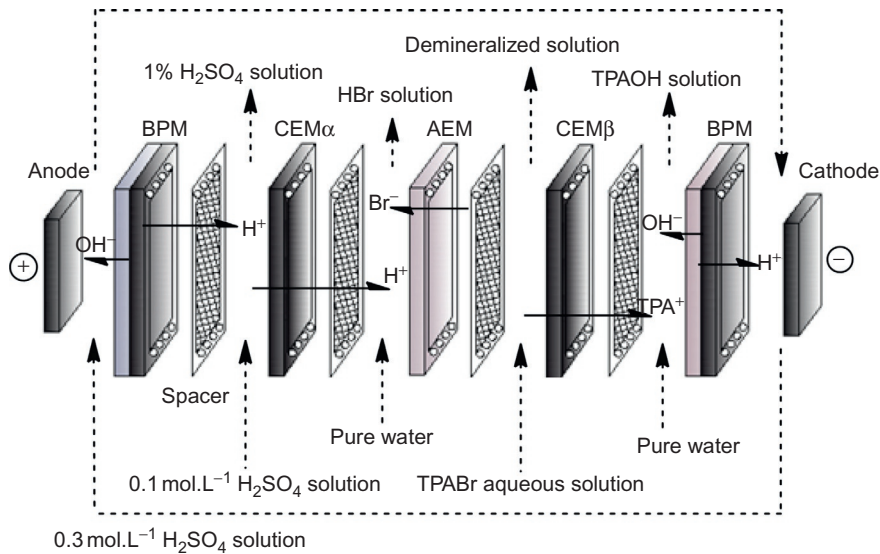


FIG. 7.6

Alternative stack with additional cation-exchange membrane to prevent leakage.

are shown in Fig. 7.7 for an anion-exchange membrane and transport of anions (a similar drawing can be made for a cation-exchange membrane).

In Fig. 7.7, the anions are mainly transported by electromigration; the related flux is J_a^E . In the boundary layers near the membrane surface, the anions are also migrated by diffusion, which is due to a concentration gradient in the boundary layers. Furthermore, because of the concentration difference of the diluate and the concentrate, anions diffuse back to the bulk. This flux is indicated by J_a^D . In steady state, the concentration of the anion in the diluate and the concentrate bulk can be expressed by b_c^D and b_c^C , respectively; in the diluate and the concentrate near the membrane surface, the anion concentration can be denoted by m_c^D and m_c^C , respectively.

Due to concentration polarization, the salt concentration at the membrane surface in the diluate compartment is reduced to zero, and no more ions are available to carry the electric current and the electrical resistance: the limiting current density (LCD) is reached. Thus the voltage drop across the boundary layer increases dramatically resulting in a much higher energy consumption and in severe water dissociation. Running the ED above the LCD leads to a substantially higher cost.

The limiting current density can be determined by measuring the current as a function of the applied voltage across a membrane. Cowan and Brown (Cowan and Brown, 1959) developed a procedure for determining the limiting current density in 1959, by plotting the overall resistance (Ohm) versus the reciprocal current density (m^2A^{-1}) as shown schematically in Fig. 7.8. The curve shows a sharp change in the resistance when the limiting current density is reached.

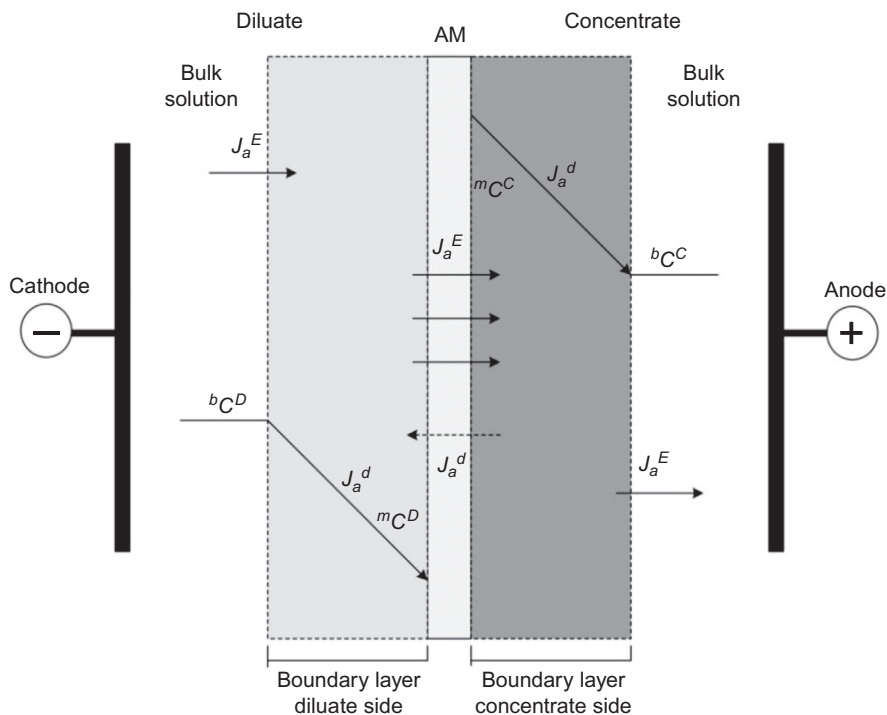


FIG. 7.7

Concentration polarization on an anion-exchange membrane during electro dialysis (shown for an anion-exchange membrane). J and c denote the flux and the concentration; the subscript a refers to anion, E and d refer to electromigration and diffusion, D and c refer to the diluate and concentrate solution, b and m refer to the bulk phase and membrane surface, respectively (Zhang, 2011).

The limiting current density can be approximated by the Lévêque equation (Volodina et al., 2005):

$$i_{\text{lim,model}} = 1.47 \frac{FDc_0}{h(T_1 - t_1)} \left(\frac{h^2 V}{LD} \right)^{1/3} \quad (7.2)$$

where D is the salt diffusion coefficient, c_0 the inlet concentration, h the distance between the membranes, V the average linear solution velocity, L the length of the membrane active area, T_1 and t_1 the salt counterion effective transport number in the membrane and the transport number in the solution, respectively, and F the Faraday constant.

Since $i_{\text{lim,model}}$ can also be written as

$$i_{\text{lim,model}} = \frac{FDc_0}{\delta(T_1 - t_1)} \quad (7.3)$$

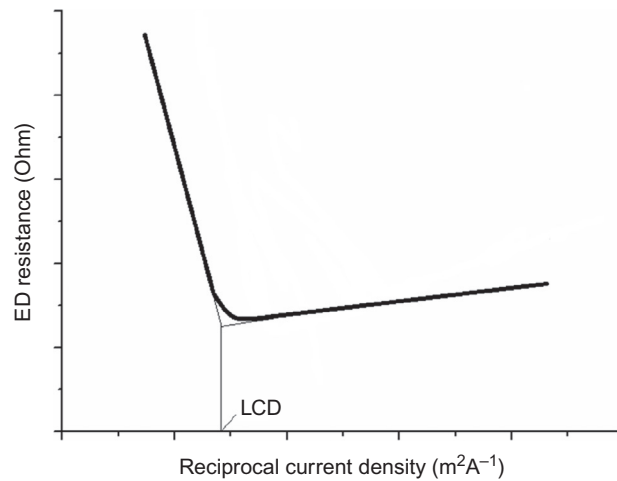


FIG. 7.8

Determination of limiting current density (LCD) (Zhang, 2011).

with δ the length-averaged thickness of the diffusion layer, δ can be calculated by comparing both equations.

In theory, a current larger than limiting current density cannot be reached. In practice, overlimiting currents can be reached. Fig. 7.9 shows a typical current-voltage curve with three main regions (Ghalloussi et al., 2014). The first region, where a linear relationship between current and voltage can be observed, is called the Ohmic region, since Ohm's Law is valid. As the current increases, concentration polarization shows its effect and due to the absence of ions near the boundary layer of

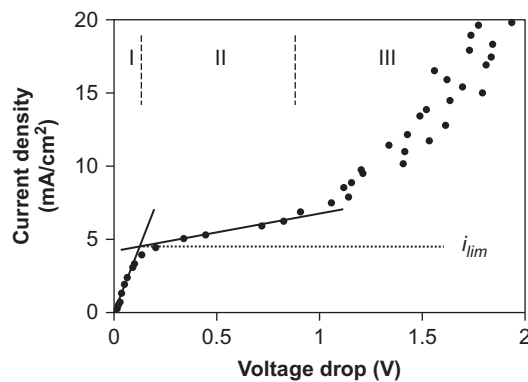


FIG. 7.9

Typical current-voltage curve, showing the Ohmic region, the limiting current density and the overlimiting region (Ghalloussi et al., 2014).

the membrane in the diluate compartment, the resistance increases and current cannot pass and despite the increasing voltage it stays constant. In this region, the limiting current density is reached. The third part, where the linear relation between current and voltage can be observed again, is called the overlimiting region.

In order to assess diffusive transport, the electrical potential is set to zero; this process is called diffusion dialysis and is applied when no electrical driving force can or should be applied. This process has a strong basis in medical applications, where it is known as hemodialysis and is applied for purification of blood in case of kidney failure. In diffusion dialysis, the potential of a concentration difference is also instrumental for mass transfer but pore-free ion-exchange membranes are used in this case, so that diffusive transport of ions in the absence of an electrical potential occurs. In diffusion dialysis, however, a stacked system is not used but rather only one type of membranes. When anion-exchange membranes are applied, anions such as chlorides, sulfates, or nitrates can be transported under their concentration gradient through an anion-exchange membrane, for the recovery of acids. The counterion is then H^+ which can permeate, since it has a high mobility and is a very small ion. In diffusion dialysis there is no production of electrical current, and electroneutrality is maintained by the combination of anion transport and diffusion of H^+ . The product stream would then contain purified acids.

7.3 GENERAL OVERVIEW OF APPLICATIONS

The classical application of electrodialysis is in nonselective removal of salt from brackish water. This has been the case for half a century, and is still valid today, although with a current focus mostly on the use of renewable energy, which is indeed a logical option for electrodialysis. An example is a directly coupled wind-electrodialysis system with no energy storage for drinking water production (Malek and Schulte-Herbruggen, 2016). Such system produces drinking water with sufficiently low salinity (<600 mg/L). Challenges are in coping with fluctuations; however, the specific energy consumption of the hybrid system remained relatively unaffected by the fluctuations, suggesting the system to be an electrically robust and reliable off-grid desalination technique for remote water stressed locations (Malek and Schulte-Herbruggen, 2016). Coupling electrodialysis for desalination of brackish water to solar energy is another logical option, especially for off-grid applications. In one example, brackish water with a salt concentration of 5482 mg/L (and a high concentration of arsenic, of 2.04 mg/L) was purified with electrodialysis powered by solar energy, including an electrical energy storage system composed of lithium ion batteries (Gonzalez et al., 2017). In the overall purification process, electrodialysis may be complemented by other technologies such as ion exchange and adsorption. Comparing different configurations or process sequences, it was concluded that a system that combines all technologies is more efficient than a single step electrodialysis for the removal of arsenic and salts. The ion-exchange step removes the divalent cations, whereas most of the arsenic is adsorbed in the

adsorption column system increasing the removal efficiency in the electro dialysis stage (Gonzalez et al., 2017). A salt removal of at least 95% is possible, in this specific example the arsenic removal was also good (over 99.9%). Thus one should consider the entire treatment train, in which electro dialysis may be complemented by other separation methods.

Other configurations of hybrid membrane systems based on electro dialysis have been suggested; a hybrid method of electro dialysis with forward osmosis driven by solar energy (EDFORD or ED-FO Renewable energy Desalination) can be used to produce high-quality water (potable) from secondary wastewater effluent or brackish water (Zhang et al., 2013). This system is shown in Fig. 7.10. Feedwater, which is either secondary effluent or brackish water, is drawn to the forward osmosis draw solution, while the organic and inorganic substances (ions, compounds, colloids, and particles) are rejected by the forward osmosis membrane. The diluted draw solution is then regenerated by the solar energy-driven electro dialysis. In this way, a nearly complete removal of all pollutants is obtained, so that the forward osmosis unit may replace a sequence of various processes, in a cost-effective way. Electro dialysis is then applied for a well-known (synthetic) solution, under ideal circumstances.

Such renewable energy powered membrane systems seem ideal for application in remote locations, as they can be operated without any external input; it is remarked,

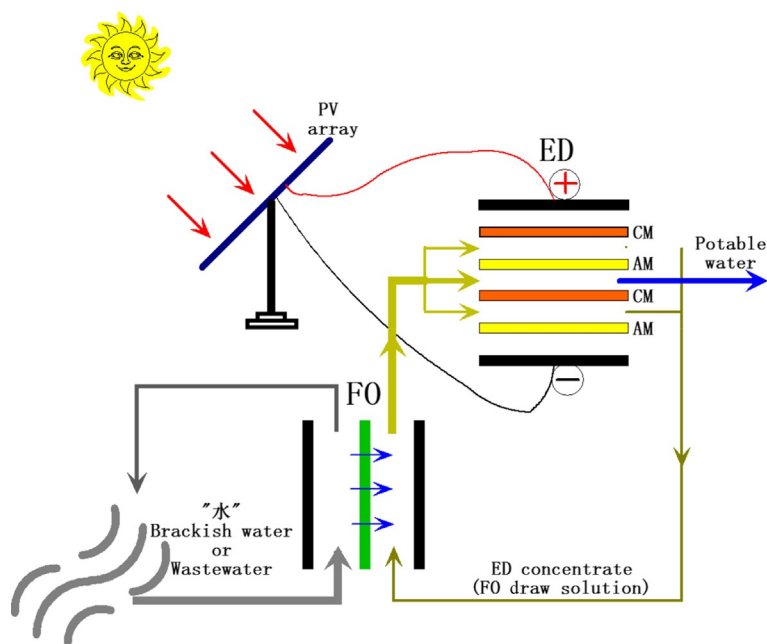


FIG. 7.10

Renewable energy powered electro dialysis and forward osmosis hybrid system (Zhang et al., 2013).

however, that the biggest hurdle to adoption of membrane technology powered by renewable energy in a remote location may not be cost, but rather sustainability issues such as the lack of skilled personnel for operation and maintenance, service networks, availability of spare parts, socioeconomic integration, and adaptive capacity of communities to transfer and develop technology appropriate to local needs and circumstances (Schäfer et al., 2014).

Following the same idea of electrodriven membrane separation as a sustainable technology, there is much attention to reversing the input and output so that the mixing energy of freshwater and brine is used for producing “green” energy. This is suggested to have a large potential based on theoretical calculations taking the flow of rivers into account. In theory, approximately 0.8 kWh can be obtained when 1 m³ of fresh water is mixed with seawater; thus nearly 2 TW of salinity gradient power can theoretically be generated on the basis of the total freshwater flow of the major rivers worldwide (Mei and Tang, 2018). Which fraction of this would be realistic is evidently an open question; so far, no full-scale plants have been commissioned, in spite of several pilot-scale investigations.

Fig. 7.11 gives an overview of the electrical current and energy production in electromembrane processes. In electrodialysis, electrical energy is consumed to drive ionic transport against the concentration gradient. In reverse electrodialysis, electricity is generated from the ionic current along the concentration gradient. When the electrical voltage output is zero, that is, a close-circuit condition, there is no electricity production or consumption. Ions can diffuse under their respective concentration gradients at rates faster than in reverse electrodialysis; this process is denoted as short circuit reverse electrodialysis (Mei and Tang, 2018). To further enhance the rates of transport of ions, an external voltage can be applied in the same direction to the ionic current. This configuration is voltage-assisted reverse electrodialysis and accelerates the ion removal from the high concentration stream at the expense of additional energy consumption. Both short circuit reverse electrodialysis and voltage-assisted reverse electrodialysis can have potential applications in desalination by removing salts from the high concentration solution at accelerated rates.

In order to make reverse electrodialysis economically viable, membranes with low resistance and high permselectivity are needed (Mei and Tang, 2018). Furthermore, an optimized spacer design is required in order to obtain a uniform flow distribution. This is related to the so-called shielding effect: a typical lab-scale stack for reverse electrodialysis using nonconductive spacers may have a 50% higher internal resistance (Veerman et al., 2009). Thus optimized (conductive) spacers are to be developed. These spacers should additionally minimize pressure drop and fouling. At present, not all these requirements seem to be already sufficiently fulfilled.

Other (emerging) applications of electrodriven membrane technology are related to either selective membranes, or to the use of bipolar membranes.

Applications of selective membranes (or hybrids) include the following:

- separating and purifying lithium from brines by using electrodialysis with monovalent selective ion-exchange membranes (Chen et al., 2018), which can be

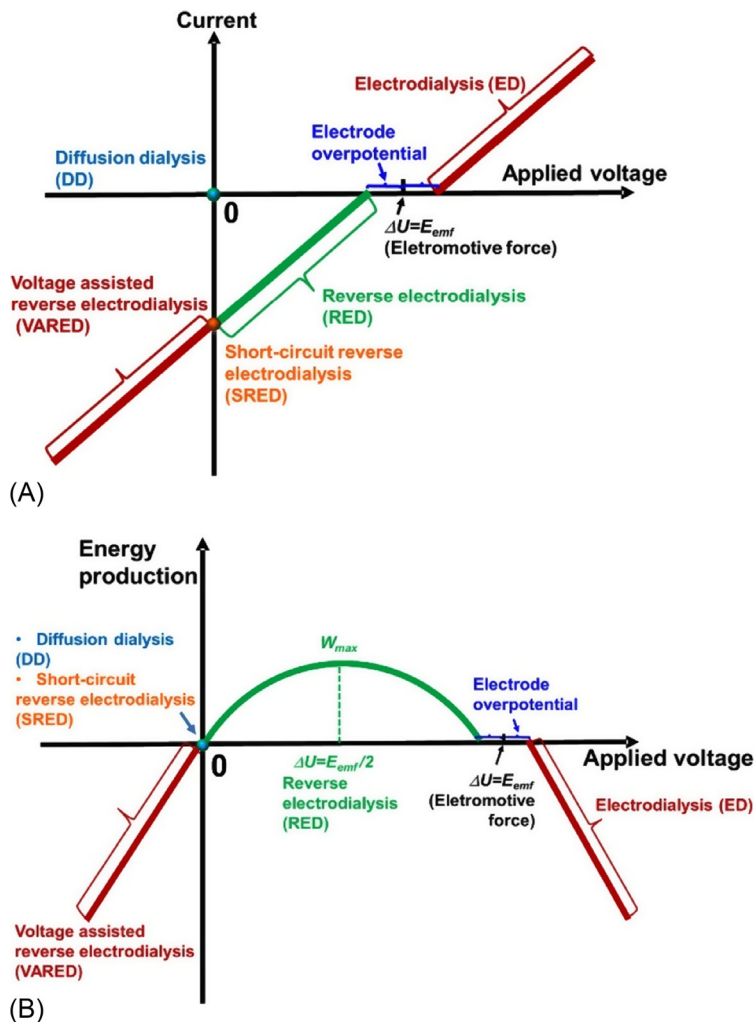


FIG. 7.11

(A) Current as a function of applied voltage in electro-dialysis (ED), reverse electro-dialysis (RED), short circuit reverse electro-dialysis (SRED), voltage-assisted reverse electro-dialysis (VARED), and diffusion dialysis (DD); (B) energy output as a function of applied voltage in ED, RED, SRED, VARED, and DD (Mei and Tang, 2018).

used to extract lithium from seawater rich in lithium such as the salt lakes located in West China, and the Dead Sea;

- heterogeneous nitrate selective membranes based on ion-exchange resins with nitrate affinity, in view of nitrate removal in drinking water production (Kikhavani et al., 2014);

- selective recovery and concentration of metallic cations with different or similar valences (such as Ag, Zn, Cu, and Cd), which are nearly impossible to separate in a classical electrodialysis system, by a combination with an in situ complexation reaction (Frioui et al., 2017);
- hardness removal from water sources (calcium and magnesium) with cation-exchange membranes selective for divalent ions (Farrokhzad et al., 2015);
- separation of peptides in electrodialysis with ultrafiltration membranes, based on charge and size effects, and with the pH as steering parameter for the process (Roblet et al., 2013);
- metathesis applications, such as the conversion of magnesium chloride and sodium sulfate to magnesium sulfate and sodium chloride (Alheritiere et al., 1998), the production of choline dihydrogen phosphate (Rottiers et al., 2017), and potassium nitrate synthesis from NaNO_3 and K_2SO_4 (Jaroszek et al., 2016);
- defluoridation of industrial effluents by electrodialysis in order control the fluoride concentration in ground water (Arfaoui et al., 2018);
- applications in the food industry, such as the deacidification of cranberry juice, with simultaneous production of pure acids (Serre et al., 2016);
- decreasing the conductivity of industrial wastewater (down to a conductivity in the diluate of 0.5 mS/cm) (Valero et al., 2015).

Bipolar membranes are used in a variety of different applications, related to the effect of pH changes; typical applications are in the production of acids and bases from the corresponding salt solutions. The principle of electrodialysis with bipolar membranes (referred to as either EDBM or BMED) for the production of organic acids is shown in Fig. 7.12 (Xu, 2002). The role of BMED is in removing the product acid, and simultaneously providing an equivalent amount of base for recycling to the

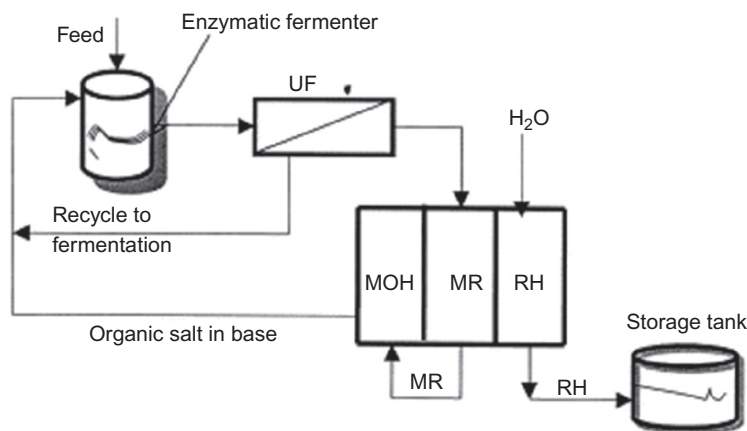


FIG. 7.12

Electrodialysis with bipolar membranes used in the production of organic acids (Xu, 2002).

fermenter, in order to adjust the pH; this is because the pH in the reactor should be nearly neutral. The fermenter can then be operated at relatively low product concentrations to assure a high productivity. The recovered acid is obtained at a significantly high concentration (in the order of 4–6 mol/L), which makes the subsequent purification via crystallization or other techniques relatively inexpensive.

Some reported applications of electrodialysis with bipolar membranes include the following:

- the separation of succinic acid from the postfermentation broth after bioconversion of raw glycerol (which is generated in a large amount as a by-product during the production of biodiesel); in addition to the pretreatment by ultrafiltration already suggested in Fig. 7.12, this was followed by extraction of the acid; the challenge in this study was in the selective extraction of succinic acid over acetic, lactic acids, and glycerol, rather than in operation of BMED (Prochaska et al., 2018);
- the production of lactobionic acid, a high value-added oxidation product of lactose with numerous potential applications in the food, pharmaceutical, and chemical industries; this is carried out from a sodium lactobionate solution obtained by the aerobic oxidation of lactose over gold nanoparticles supported on mesoporous silica, using a three-compartment bipolar membrane electrodialysis stack in which lactobionic acid is obtained as the product, and NaOH as the by-product (Gutierrez et al., 2013);
- the production of lactic acid, which has been historically one of the first applications of BMED (Siebold et al., 1995).

Other applications of EDBM often relate to the production of acids and bases from brines (Ghyselbrecht et al., 2014). This is of interest for industrial brines, where economical profits can be obtained when the acid concentration and the base concentration are above 2 M. Challenges in this process are the Fickian back diffusion, limiting the purity of the acid (and to a lower extent, also the base). Furthermore, membrane scaling by Mg, Ca, Ni, and so on, can be expected. This can be avoided by using a pretreatment or hybrid approach with pellet crystallization (Tran et al., 2015). The approach can be extended to desalination brines obtained in reverse osmosis. In that case, the total process cost for acid/base production was estimated at \$0.50/kg at a current density of 10 mA/cm², which is competitive for industrial application (Zhang et al., 2017).

The performance of an EDBM system is controlled by the permselectivity of the membranes and by diffusive transport. Due to the leakage of small ions through the membranes, caused by undesired diffusion of cations through anion membranes and of anions through cation membranes, the current efficiency is reduced. Mainly for small ions this can be a limitation; for this reason, producing base is easier than producing acid in EDBM, because the small H⁺ ion permeates relatively easily back through an anion-exchange membrane. Consideration must also be paid to water transport through membranes, which in general limits the concentration level of the acid and base produced. Furthermore, EDBM normally also requires a careful

pretreatment; the ultrafiltration process shown in Fig. 7.12 is an example. Lastly, it is necessary to remove multivalent cations and organic pollutants in case of membrane swelling and metallic hydroxides precipitation, which can be done by the fluidized bed reactor (pellet reactor) mentioned previously.

In addition to EDBM and different stack configurations, several variations of electromembrane processes are reported in this area: apart from conventional electrodialysis, electrometathesis, electro-ion substitution, electro-electrodialysis, electrohydrolysis with bipolar membranes, electrodeionization, and two-phase electro-dialysis (Huang et al., 2007).

7.4 CALCULATION OF SELECTIVITY IN ELECTRODIALYSIS

The selectivity in electrodialysis is in the first place related to the selectivity between cations and anions. Cation-exchange membranes should transport cations, while impeding the transport of anions; anion-exchange membranes should only transport anions and block all cations. This is the permselectivity of an ion-exchange membrane. Transport of ions through membranes is defined in terms of the transport number for a particular ion. The transport number T_i indicates the fraction of the total current that is carried by the ion i (Strathmann, 2009):

$$T_i = \frac{z_i J_i}{\sum_i z_i J_i} \quad (7.4)$$

The sum of the transport number of all ions in a solution should be 1; a transport number for all ions of the same charge of <1 means that a proportion of the current is carried by ions of the opposite charge in the wrong direction. The transport number can be as high as 0.98 for some anion-exchange membranes and should be higher than 0.9 for cation-exchange membranes.

The permselectivity can then be determined based on the transport numbers of cations and anions. It is defined as:

$$\Psi = \frac{t_Y^m - t_Y^s}{t_X^s} \quad (7.5)$$

where t is the transport number of an ion, Y refers to counterions and X refers to coions, m refers to the membrane phase, and s refers to the solution phase. When $t_Y^m = 1$ in Eq. (7.3), all ion transport through the membrane occurs via counterion transport, and the membrane is perfectly permselective. Alternatively, when $t_Y^m = t_Y^s$, ion transport through the membrane occurs in the same way as that in solution, and the permselectivity is equal to zero.

The transport number of a given membrane may be either the “static transport number,” which is calculated from the membrane potential, or the “dynamic transport number,” which is determined from measurement of the actual ion migration. In most cases, it is the static transport number which is given as a membrane

characteristic. Static transport numbers can be derived from membrane potential measurements across membranes that separate solutions of high and low electrolyte concentration. For many monovalent binary electrolytes, the membrane potential, E_m , can be used to determine the counterion transport number in a membrane, provided that the transport number can be assumed constant throughout the membrane (Geise et al., 2014).

$$t_Y^m = \frac{\left[E_m / \left(\frac{RT}{F} \ln \frac{a_{\pm}^{s0}}{a_{\pm}^{sL}} \right) \right] + 1}{2} \quad (7.6)$$

where R is the ideal gas constant, T is the absolute temperature, F is Faraday's constant, and a_{\pm}^{sk} is the average electrolyte activity (i.e., $a_{\pm}^{sk} = \sqrt{a_X^{sk} a_Y^{sk}}$) in solution at either the high concentration solution side of the membrane ($k=0$) or the low concentration solution side of the membrane ($k=L$).

It should be noted that Eq. (7.6) is not always valid; one constraint is that osmotic transport of water is neglected, which is not always possible.

The solution phase transport number is defined as:

$$t_i^s = \frac{|z_i| c_i^s D_i^s}{\sum_j |z_j| c_j^s D_j^s} \quad (7.7)$$

where z_i is the charge, c_i^s is the concentration in solution, and D_i^s is the self-diffusion coefficient of ion i . An example of how to calculate transport numbers in solution can be found in the literature (Strathmann, 2009), using the OLI Analyzer 9.0 (MSE database) electrolyte software package.

The determination of selectivity between ions of the same sign in electromembrane processes has not received much attention until recently. The obvious reason is that conventional ion-exchange membranes are not selective, and no selectivity between different ions is required for the dominant application, that is, desalination of brackish water.

The "membrane selective permeability" T_B^A was developed in order to express the difference in permeation between ions A and B (Itoh et al., 1986). It is defined as:

$$T_B^A = \left(\frac{z_A \bar{u}_A}{z_B \bar{u}_B} \right) K_B^A \quad (7.8)$$

with

$$K_B^A = \frac{c_A^m / c_B^m}{c_A^w / c_B^w} \quad (7.9)$$

where $z_A, z_B, \bar{u}_A, \bar{u}_B, c_A^m, c_B^m, c_A^w, c_B^w$ refer to charge, electrochemical mobility, ion concentration in the membrane, and ion concentration in water, respectively.

When the concentration of coions in the solution increases, the selectivity should thus decrease; it is assumed that the selectivity is equal to one when the concentration of coions in the solution is equal to the concentration of fixed charges on the membrane.

The mobility of different ions in an ion-exchange membrane is typically rather similar; the only exceptions to this are H^+ and OH^- , which have a mobility that is 5–8 times higher than that of other ions. This is the result of the interactions of molecular interactions of water dipoles with electrical charges. Protons form hydronium ions and are transported via a tunnel mechanism from one hydronium ion to the next water molecule. Cations, however, are transported by diffusion as ions with a hydrated shell. This gives a low permeability through anion-exchange membranes. On the other hand, protons and hydroxide ions have a very low contribution to the transport of water by electro-osmosis (see later), since their transport does not invoke water transport.

From Eqs. (7.8), (7.9), it can be concluded that the selective permeation of ions through ion-exchange membranes depends on two factors: (1) the mobility of the counterions during permeation, and (2) the affinity between the counterions and the membrane, represented by K_B^A . Based on this conclusion, membranes can be modified in view of obtaining a selective removal of certain ions. For example, a higher removal rate of sulfate ions compared to chloride ions can be obtained by increasing the hydrophilicity of the membrane. For membranes with β -cyclodextrin as additive, a higher hydrophilicity is obtained, which suppresses the transport number of less hydrated ions such as nitrate ions, compared to chloride ions. The transport number of strongly hydrated ions such as sulfate ions increases with increasing hydrophilicity of the membranes (Sata et al., 2001). It is assumed that a more hydrophilic membrane material would allow more strongly hydrated ions, like sulfate, to permeate through the membrane, while less hydrated ions, such as chloride and nitrate, would encounter more resistance, because they have a lower affinity with hydrophilic membranes (Van Geluwe et al., 2011). The higher selectivity for more strongly hydrated ions can be fundamentally explained on the basis of the higher degree of dielectric shielding, that a larger hydration hull provides to the ion (Gärtner et al., 2005). The larger hydration hull reduces the polarity of the ion, so that the ion encounters less resistance while permeating through the membrane. These resistances consist of charge repulsion with the coions in the membrane and resistances from the hydrophobic backbone of the polymers. An ion, shielded by a large and strongly bounded hydration hull, would experience these effects less, than an unshielded ion (Van Geluwe et al., 2011). The current trend, however, is to develop monovalent selective membranes (anion selective as well as cation selective membranes), because the ion mobility is the easiest factor to tune. This is related to the size effect; monovalent ions tend to be smaller and therefore have a benefit in terms of mobility.

For selective membranes, the ratio of transport numbers for a target ion (denoted as an) and a standard ion (denoted as am), which represents the permselectivity between an and am , is:

$$P_{an}^{am} = \frac{t_{am}^D / c_{am}^D}{t_{an}^D / c_{an}^D} = \frac{J_{am}}{J_{an}} \cdot \frac{c_{an}^D}{c_{am}^D} \quad (7.10)$$

in which the superscript D refers to the diluate compartment.

This can be expressed in terms of resistances (Vaselbehagh et al., 2015), by writing the current carried by ion n as:

$$I_n = F \cdot J_n \cdot A = \frac{E}{R_{in}^K + R_{an}^A + R_{dilu,n}} = \frac{E}{R_n} \quad (7.11)$$

R_{in}^K and R_{an}^A denote the electric resistances of cation and anion-exchange membranes for ion transport, respectively. $R_{dilu,n}$ is the electric resistance of the diluted compartment caused by the n th electrolyte. A is the surface area of the membrane.

The permselectivity then becomes:

$$P_{an}^{am} = \frac{R_{in}^K + R_{an}^A + R_{dilu,n}}{R_{im}^K + R_{am}^A + R_{dilu,m}} \cdot \frac{c_{an}^D}{c_{am}^D} \quad (7.12)$$

The resistances can be calculated as follows:

$$R_{dilu,n} = \frac{1}{\lambda_{in} c_{in}^D + \lambda_{an} c_{an}^D} \cdot \frac{I_{dilu}}{A} \quad (7.13)$$

$$R_{in}^K = \frac{I_M^K}{\alpha_{in} U_{in} F A c_{in}^M} \quad (7.14)$$

$$R_{an}^A = \frac{I_M^A}{\alpha_{an} U_{an} F A c_{an}^M} \quad (7.15)$$

where α_k represents the sieving effect of the membrane for ion k .

The selectivity can also be quantified by the separation efficiency S between component A and B , which is calculated as:

$$S(t) = \frac{\left(\frac{c_A(t)}{c_A(0)} \right) - \left(\frac{c_B(t)}{c_B(0)} \right)}{\left[1 - \left(\frac{c_A(t)}{c_A(0)} \right) \right] + \left[1 - \left(\frac{c_B(t)}{c_B(0)} \right) \right]} \cdot 100\% \quad (7.16)$$

The separation efficiency reflects the relative difference in transport rate and ranges from 0 (no separation) to 1 (complete separation, i.e., $c_B(t)=0$; component B removed from the diluate fraction).

In principle, the separation efficiency is a time-dependent function. The separation efficiency is relatively constant as a function of time, after some initial fluctuations, as can be seen from Fig. 7.13 (Van der Bruggen et al., 2004). Thus it is independent of the geometry of the equipment (e.g., size of the membranes), because this only influences the time to reach a given concentration in the diluate or concentrate, but not the actual separation measured as the separation efficiency. However, the separation efficiency may also be influenced by the applied voltage. In order to take fluctuations into account, the average separation efficiency can be calculated to express the selectivity of the membranes during experiments:

$$S = \frac{\sum_j \Delta t_j \cdot S_j}{\sum_j \Delta t_j} \quad (7.17)$$

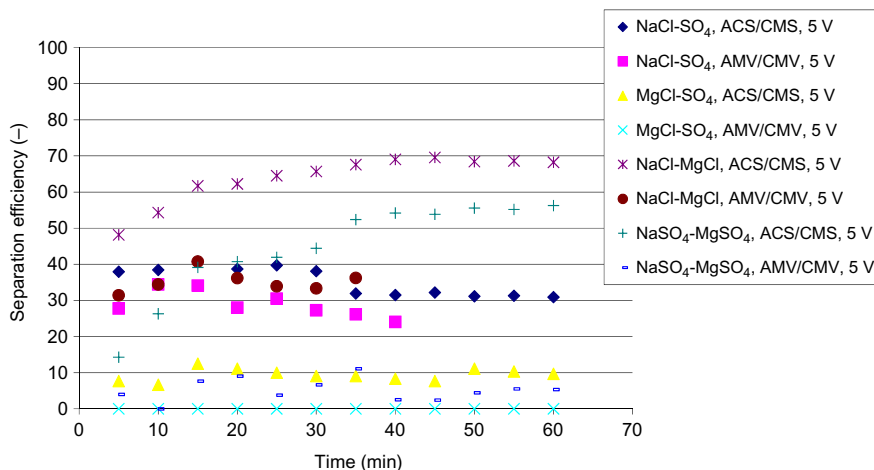


FIG. 7.13

Separation efficiency as a function of time for various combinations of monovalent/divalent ions (Van der Bruggen et al., 2004).

Another method to express the membrane selectivity is by using separation factors (Strathmann, 2004b; Sata et al., 1997):

$$\alpha_B^A(t) = \frac{1 - c_A(t)/c_A(0)}{1 - c_B(t)/c_B(0)} \quad (7.18)$$

where α_B^A is the separation factor, $c_A(0)$, $c_B(0)$, $c_A(t)$, and $c_B(t)$ refer to the concentration of ion A (or B) in the diluate at time 0 and t , respectively.

7.5 ION TRANSPORT THROUGH ION-EXCHANGE MEMBRANES

The transport of ions corresponds to an electrical current, since electrical charges are replaced. This can be described by Ohm's Law:

$$V = R \cdot I \quad (7.19)$$

in which V is the electrical potential between two electrodes, R is the electrical resistance, and I is the current between the electrodes.

In general terms, the electrical resistance can be written as a function of the distance between the electrodes, d , and the surface area of the material, A :

$$R = \rho \frac{d}{A} = \frac{1}{\kappa A} d \quad (7.20)$$

with ρ the specific resistance of the material, and κ the specific conductivity.

This is generally applied for electron conductivity, typically in a solid metal. However, it can also be applied to ion conductivity in an electrolyte solution,

although with conductivities 3–5 orders of magnitude lower, and with an intrinsic effect of mass transport. Furthermore, the conductivity depends on the concentration in the solution, of the temperature in the solution (increasing with temperature, which is opposite to the conductivity in metals) and of the charge number of the ions in the solution. This is sometimes expressed as an equivalent conductivity, as follows:

$$\lambda_{eq} = \frac{\kappa}{C(z_a\nu_a + z_c\nu_c)} \quad (7.21)$$

in which C is the molar concentration of the electrolyte in the solution; z_a and z_c are the charge numbers of the anion and cation, respectively; and ν_a and ν_c are the stoichiometric coefficients of the anion and the cation, respectively.

Thus the number of electrical charges carried by the ions of an electrolyte solution under an electrical potential difference as driving force can be expressed as:

$$N_e = \sum_i z_i u_i \nu_i C F \frac{\Delta\Psi}{d} = \sum_i z_i F N_i = \sum_i z_i \nu_i C \lambda_{eq} \frac{\Delta\Psi}{d} \quad (7.22)$$

in which F is Faraday's constant (96,485 C eq⁻¹), and $\Delta\Psi$ is the electrical potential difference.

The corresponding electrical current is then:

$$I = \sum_i z_i F N_i A = \sum_i z_i \nu_i C \lambda_{eq} \frac{\Delta\Psi}{d} A \quad (7.23)$$

where A is the membrane surface area.

The driving force for transport in electrodialysis is the electrical potential. The two sides of an ion-exchange membrane are in contact with solutions of different composition and of different electrochemical potential. The requirement for equilibrium is that the electrochemical potential is equal on both sides of the membrane, so that ions permeate through the membrane from the compartment with high electrochemical potential to the compartment with low electrochemical compartment. The electrostatic forces remain in balance in this: the number of positive charges and negative charges is always the same.

The electrochemical potential is:

$$\mu_i = \mu_i^\circ + RT \ln a_i + V_i \cdot P + z_i \cdot F \cdot \psi \quad (7.24)$$

where, μ_i is the electrochemical potential of component i , μ_i° is the chemical potential of component i in reference conditions, R is the ideal gas constant, T is the temperature, a_i is the activity of component i , V_i is the molar volume of component i , P is the pressure, z_i is the ion valence ($=0$ in case of uncharged compounds), F is Faraday's constant, and ψ is the electrical potential.

In electrodialysis, the temperature and pressure are assumed constant in the entire stack, which leaves the concentration and electrical potential as driving forces. This assumption, however, is an approximation because the difference in concentration of ions over the membranes, which is intrinsically related to the separation itself, yields an osmotic pressure difference between each two compartments. As a consequence, an osmotic effect will take place, which is described later in this chapter but is neglected in the initial discussion.

The electrical potential is the externally applied driving force, on which the separation relies, but the concentration gradient is inevitable, and is oriented in the opposite direction as the applied electrical potential gradient, so that the effective driving force is decreased. The parallel with the effect of osmotic pressure on the driving force used in pressure-driven membrane processes such as reverse osmosis can be noticed.

Based on Eq. (7.24), mass transport through ion-exchange membranes can be expressed as a function of the gradient of the driving forces:

$$N_i = \sum_k L_{ik} \left(RT \cdot \frac{d \ln a_i}{dz} + z_i F \frac{d\Psi}{dz} \right) \quad (7.25)$$

In Eq. (7.25), the L_{ik} are phenomenological coefficients, and the subscripts i and k refer to components in the system; this assumes that kinetic coupling between individual fluxes may take place.

This can be compared to the extended Nernst-Planck equation (at constant temperature and pressure):

$$N_i = -D_i \left(\frac{dc_i}{dz} + \frac{z_i F c_i}{RT} \frac{d\Psi}{dz} \right) \quad (7.26)$$

which gives an approximation of Eq. (7.25), assuming that no interactions between fluxes take place, and that activity coefficients are close to one. The phenomenological coefficients are then:

$$D_i = \frac{L_{ii} RT}{c_i} \quad (7.27)$$

The current carried by ion i is:

$$i_i = z_i F \left[D_i \left(\frac{dc_i}{dz} + \frac{z_i F c_i}{RT} \frac{d\Psi}{dz} \right) \right] \quad (7.28)$$

The current density i can be written as:

$$i = F \sum_i z_i N_i \quad (7.29)$$

Or

$$i = F 2 \sum_i z_i^2 \frac{c_i D_i}{RT} \left(\frac{RT}{z_i c_i F} \frac{dc_i}{dz} + \frac{d\Psi}{dz} \right) \quad (7.30)$$

This equation shows the electrical flux (current density) as the sum of a contribution from the electrical potential (second term) and the effect of diffusion; the term $\frac{RT}{z_i c_i F} \frac{dc_i}{dz}$ has the units of a potential gradient and reflects this.

By dividing both sides of Eq. (7.28) by the term $z_i F V$ and replacing i_i with $\frac{z_i F Q \Delta c_i}{AN_{cp}}$, the equation becomes (Karimi and Ghassemi, 2016):

$$\frac{Q \Delta c_i}{AN_{cp} V} = \frac{D_i}{V} \left(\frac{dc_i}{dz} \right) + \frac{D_i c_i}{V} \left(\frac{d \left(\frac{z_i F \Psi}{RT} \right)}{dz} \right) \quad (7.31)$$

Q is the total flow rate of dilute stream, ΔC is the difference between the concentrations of the ion in the inlet and outlet of dilute cells that occurs due to ion transport, V is the dilute solution velocity in a cell, and N_{cp} is the number of cell pairs in the stack.

This can be reduced to dimensionless variables:

$$\frac{Q\Delta c_i}{AN_{cp}Vc_{r,i}} = \frac{D_i}{Vh} \left(\frac{d\left(\frac{c_i}{c_{r,i}}\right)}{d\left(\frac{z}{h}\right)} \right) + \frac{D_i}{Vh} \frac{c_i}{c_{r,i}} \left(\frac{d\left(\frac{z_i F \Psi}{RT}\right)}{d\left(\frac{z}{h}\right)} \right) \quad (7.32)$$

where A is the membrane active area, h is the dilute cell thickness, and C_r is the logarithmic average of ion concentration in dilute cells.

$$c_{r,i} = \frac{(c_{F,i} - c_{D,i})}{\ln\left(\frac{c_{F,i}}{c_{D,i}}\right)} \quad (7.33)$$

in which c_F is feed concentration at the inlet of the diluate chamber, and c_D is the diluate concentration at the outlet of diluate chamber.

The following dimensionless numbers can be defined:

Stanton number:

$$St_i = \frac{Q\Delta c_i}{AN_{cp}Vc_{r,i}} \quad (7.34)$$

Dimensionless electrical potential per desalting cell:

$$\Psi_i^* = \frac{z_i F \Psi}{RT} \quad (7.35)$$

Dimensionless direction toward the membrane:

$$z^* = \frac{z}{h} \quad (7.36)$$

Thus Eq. (7.32) can be written as:

$$St_i = \frac{1}{Pe_i} \frac{dc_i^*}{dz^*} + \frac{c_i^*}{Pe_i} \frac{d\Psi_i^*}{dz^*} \quad (7.37)$$

However, an analytical solution of this equation is not possible; empirical equations have been developed (Karimi and Ghassemi, 2016).

Apart from these equations for macroscale modeling, a more detailed description of the potential and charge in the pore is possible by applying the space-charge model, the uniform potential model and the Teorell-Meyer-Sievers model, which calculate the electrical potential profile across cylindrical pores induced by a concentration gradient and/or current density (Kristensen et al., 2017). For details on microscale modeling of membrane pores, the reader is referred to the literature.

In addition to transport of ions, water is also transported through ion-exchange membranes according to the equations shown previously. In the absence of a hydrodynamic pressure difference over the membranes, the water flux in electrodialysis is caused by osmosis and electro-osmosis (Lu et al., 2011). Electro-osmosis refers to

the transport of water molecules in the hydration shell of transported ions and to the water molecules transported by drag. This takes place for all ions apart from H^+ and OH^- (as mentioned before). The second mechanism for water transport is osmosis, that is, the transfer of water through a membrane due to the osmotic pressure difference, which arises due to the different salt concentration on both sides of the membrane. However, studies have indicated that the main cause of water transport is by electro-osmotic rather than osmotic water transfer due to the concentration difference (Jiang et al., 2014a). Apart from this, it has been observed that permeation of organic cosolvents, when present, may also occur (Rottiers et al., 2016). In the application of ion-exchange membranes in methanol fuel cells, for example, the methanol crossover leads to a decrease in fuel cell voltage and efficiency due to the oxidation of methanol (Huang et al., 2008). In general, ion-exchange membranes with low solvent permeability and a dense polymer network are to be preferred, to minimize the ratio of transported water molecules per transported ion. The highest permeability of organic cosolvents was observed for membranes with a low degree of cross-linking; this can be assumed to be the case for water permeation as well. Water transport is also generally low for membranes with a high concentration of fixed charges.

The estimation of water transport due to electro-osmosis is not easy. In an electrolyte solution, an ion (cation or anion) is assumed to be surrounded with two hydration shells consisting of water molecules, that is, the primary and the secondary hydration shells. The primary layer may hold 6 water molecules, while the secondary layer may include about 12 water molecules, depending on the coordination number and the bound force between the ion and the water molecules. The two layers of water molecules are shown in Fig. 7.14 (Lu et al., 2011).

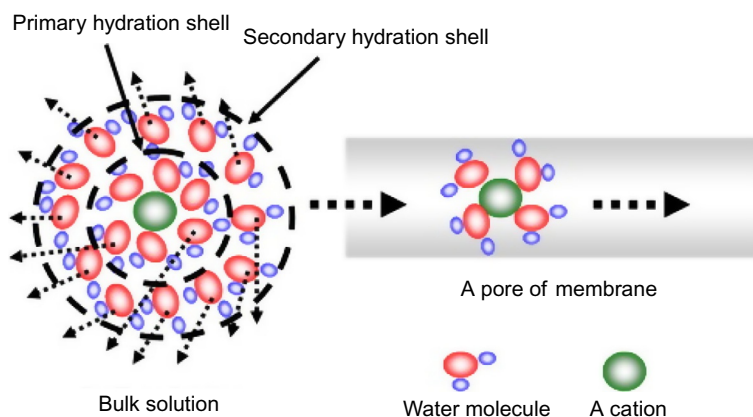


FIG. 7.14

Primary and secondary hydration shell (case of a cation), and the effect of permeation through a membrane (Lu et al., 2011).

In the primary hydration shell, water molecules are bound more strongly than in the secondary hydration shell. When a drag force is exerted by the surrounding fluid during motion of an ion, some hydration water molecules will be separated from the ion, especially water molecules in the secondary hydration shell, and less water molecules remain connected with the central ion; generally this concerns water molecules in the primary hydration shell. The number of remaining water molecules is called “dynamic hydration number” (Lu et al., 2011). As this ion enters into an ion-exchange membrane, some of these remaining water molecules may keep moving with the ion through the membrane; however, some may be separated from the ion, so that fewer water molecules are transported with the ion through the membrane due to the steric effect. How many water molecules would still remain depends on the available free volume for permeation or pore size. As a consequence, the realistic hydration number of the ion when it is transported through the membrane is strongly dependent on its velocity, the pore size of membrane (if any), and the binding force of hydration. In general, the effective hydration number (also the radius of hydrated ion) for ion species is difficult to determine (Lu et al., 2011). As an approximation, an average or effective dynamic hydration number n_{edhn} for all ion species may be used.

The volumetric change in different compartments can be estimated on this basis. For each water molecule migrating to another compartment, the volume change is $18.016/N_A \text{ cm}^3$ (with $N_A = \text{Avogadro's number}$). Thus the volume change due to the migration of ions becomes:

$$\Delta V = \sum_i \frac{N_A}{M_i} \cdot \left(\frac{4}{3} \pi r_i^3 + \frac{18.016 n_{edhn}}{N_A} \right) \cdot \Delta m_i \quad (7.38)$$

with M_i the molar mass of ion i ; Δm_i the mass of ion i transported through the membrane (which can be derived from Eqs. (7.17) or (7.18); n_{edhn} is the effective dynamic hydration number, which was assumed to be 3.5 as a result of an optimization procedure (Lu et al., 2011) (although the variation was very small when values between 3.0 and 4.0 were taken); N_A is Avogadro's number ($6.022141 \cdot 10^{23} \text{ mol}^{-1}$); and r_i is the bare radius of ion i .

7.6 OTHER CONFIGURATIONS OF ELECTRODRIVEN MEMBRANE PROCESSES

7.6.1 DIFFUSION DIALYSIS

Even though not applied with an electrical driving force, diffusion dialysis (DD) is a process closely related to electrodialysis, because it is a separation process using an ion-exchange membrane. The driving force is a concentration gradient instead of an electrical potential; this is shown in Fig. 7.11 as the process located at zero applied potential. Diffusion dialysis is applied for separation and recovery of acid/alkali waste solutions in a cost-effective (low energy cost) and environmentally friendly (no chemicals, energy, or secondary waste) manner (Luo et al., 2011). This is applied

for recovery of sulfuric acid, hydrochloric acid, nitric acid, organic acids, and alkali waste.

Modeling of diffusion dialysis can be carried out in two ways. The solution-diffusion model (Wijmans and Baker, 1995), which is used to describe transport in dialysis, reverse osmosis, gas permeation, and pervaporation, can be used for diffusion dialysis to describe the permeation of strong acids and alkalis. For a detailed description of the solution-diffusion model, the reader is referred to the chapter on pressure-driven membrane processes in this book, and more specifically in the description of reverse osmosis. The resulting equations for the solute flux are:

$$N_i = B(c_{i,o} - c_{i,l}) \quad (7.39)$$

in which B is the permeability of the solute:

$$B = \frac{D_i K_i}{\Delta x} \quad (7.40)$$

in which $c_{i,o}$ and $c_{i,l}$ are the concentration of i at the membrane on either side of the membrane, D_i is the diffusion coefficient of i in the membrane phase, K_i is the distribution coefficient of i in the membrane/liquid phase, and Δx is the membrane thickness.

The use of this model for organic acids in diffusion dialysis may be less accurate since the dissociation degree of organic acids is low and their transport mechanism inside the membrane can be very complex (Palaty et al., 2007).

A second model that has been developed is the three-phase membrane model (Stachera et al., 1998), in which the membrane is assumed to be divided into three separate phases: a hydrophobic polymer, an active region comprising the fixed charge sites and the counterions, and an interstitial region. Water, which is indispensable for the migration of ions, is mainly present in the active and interstitial zones. The ions can be transported through these two regions via different mechanisms: the anions in the active zone may undergo a hopping mechanism, transferring from one exchange site to another; protons and hydrated cations move by a “dragging” mechanism (restricted diffusion) in the interstitial zone, because there is no strong repulsive force in this zone (Luo et al., 2011).

7.6.2 ELECTRO-ELECTRODIALYSIS

Electro-electrodialysis (EED) is a three-compartment electromembrane process, combining electrodialysis and electrolysis. The typical application is to recover an acid from a solution by permselective transport of the acid’s anion through an anion-exchange membrane and electrolysis to provide the protons necessary to form the acid. One example is the recovery of chromic acid from a solution; EED allows the removal of chromic acid from a plating bath in the presence of impurities, and to recover the acid as a pure solution. In this way, EED accomplishes three different tasks in a single process: (i) removal of contaminants, (ii) chromic acid recovery, and (iii) purification of static rinse water (Frenzel et al., 2005a). This is schematically

shown in Fig. 7.15. The diluted compartment is often referred to as the anolyte, while the concentrated solution is the catholyte.

The electro-electrodialysis process is characterized by its efficiency; the overall current efficiency for the product (the acid), Φ^e , is defined as the current carried by acid ions relative to the total current used (Frenzel et al., 2005b):

$$\Phi^e = \frac{m\nu_e F}{Mt} \quad (7.41)$$

where m is the mass of product, M the molar mass, ν_e the stoichiometric number of electrons for the reaction, F the Faraday constant, and It the current quantity.

This can be written as (Luo and Wu, 2000):

$$\Phi^e = \frac{(V_f C_f - V_i C_i) F}{It} \quad (7.42)$$

where V_{f2} and V_{i2} are the final and initial volume of the anolyte; C_{f2} and C_{i2} are the final and initial molarities of formic acid solution in the anolyte.

The specific energy consumption can be calculated as:

$$E_{S,m} = \frac{U_c \nu_e F}{M \Phi^e} \quad (7.43)$$

in which U_c is the applied electrical potential.

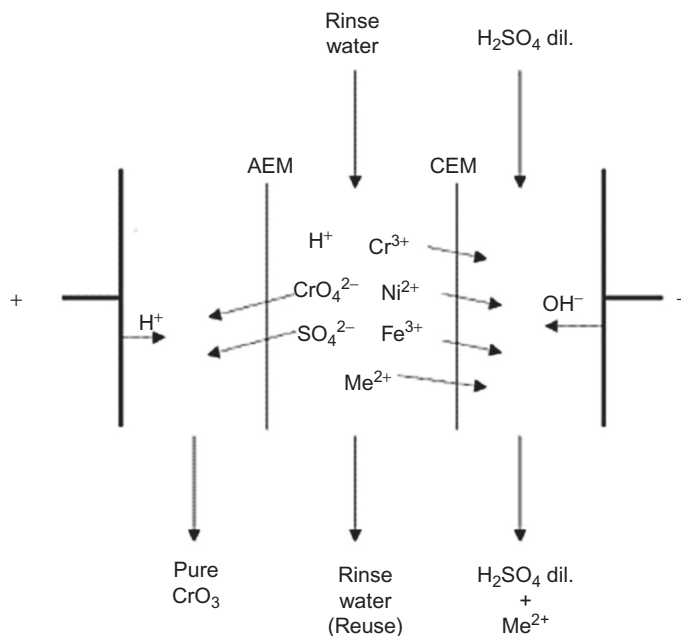


FIG. 7.15

Principle of electro-electrodialysis, applied for the recovery of chromic acid (Frenzel et al., 2005a).

Some variations of the electro-electrodialysis process are to be mentioned:

- two-phase electro-electrodialysis, in which an emulsion (in one case composed of 49.9% kerosene, 49.9% water, and 0.2% Tween) was used as the anolyte instead of an aqueous phase, in order to effectively control electro-osmosis and osmosis (Luo et al., 2005);
- Reverse Electro-Electrodialysis (REED), in which pure and storable hydrogen is produced by using hydrochloric acid and sodium hydroxide as cathode and anode solution, respectively, to reduce the hydrogen evolution potential (Chen et al., 2017);
- electro-electrodialysis with bipolar membrane (EEDBM), which is applied for recovery of lithium from brines as LiOH (Jiang et al., 2014b); this process is shown in Fig. 7.16.

7.6.3 CONTINUOUS ELECTRODEIONIZATION

In continuous electrodeionization (CEDI), an electro dialysis unit is used with the diluate compartment filled with a mixed bed ion-exchange resin. The feed ions are bound on the resin; due to the presence of the resin, the conductivity in the diluate compartment is significantly enhanced. At very low concentrations in the diluate, water dissociates where cation and anion resin beads contact each other, which regenerates the resin in situ. The product is deionized water; the ion-exchange resin is regenerated without the use of chemicals, and not generating a waste stream during regeneration. Thus it is considered a green process for deionized water production. CEDI has been known for many decades (since the 1950s), but it was not until 1987 that commercialization became successful; today, several thousand CEDI systems in commercial operation for the production of high purity water at capacities ranging from <0.1 to $>1500\text{ m}^3/\text{h}$ (Wood et al., 2010). Typical applications are in the pharmaceutical industry, for steam generation, and semiconductor wafer fabrication, manufacturing microelectronic devices, solar panels, or flat-panel display. The process is shown in Fig. 7.17 (Wood et al., 2010).

The removal of ions occurs in two steps: first, diffusion of cations to the strong cation-exchange resin and of anions to the strong anion exchanger; then, ionic conduction of the solid phase to the border of the membranes. Because the ion concentration within the solid is very high, the process that controls ion removal is the ion diffusion rate of the aqueous phase to the surface of the solid ion exchange, which depends on three factors: (1) surface between solid and solution, (2) thickness of the liquid layer through which ions diffuse, and (3) concentration gradient between the solid and liquid phase (Alvarado and Chen, 2014).

Modeling of continuous electrodeionization is similar to electro dialysis; the modification to be made is a correct interpretation of the specific conductivity κ (Eqs. 7.12, 7.13). This can be done with the following porous plug model (Wyllie et al., 1955), considering three parallel conductance elements, corresponding to

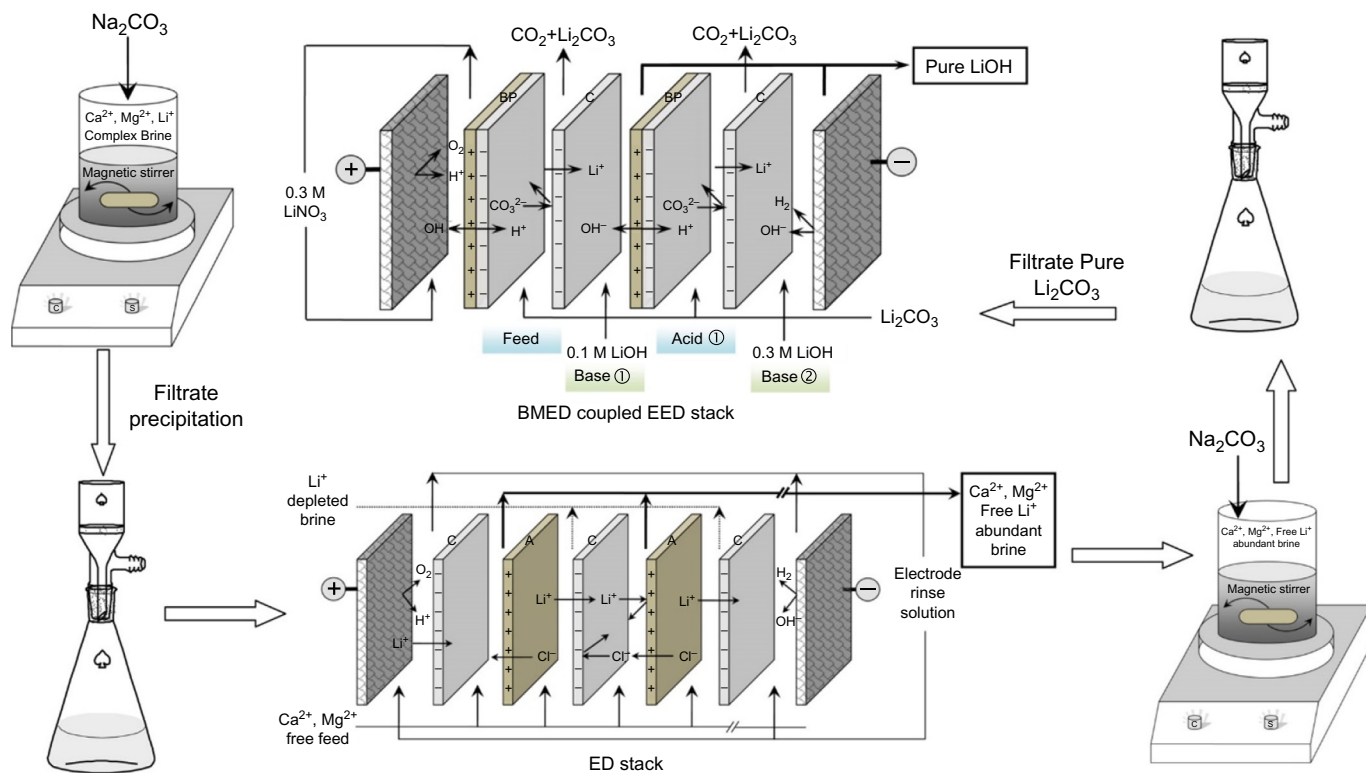


FIG. 7.16

Principle of electro-electrodialysis with bipolar membrane (EEDBM) for lithium recovery (Jiang et al., 2014b).

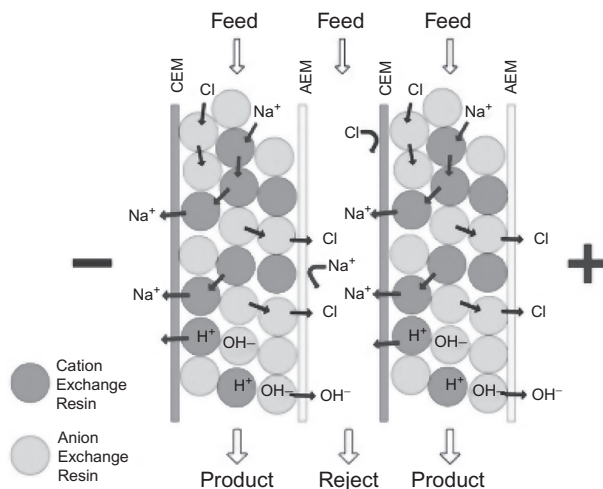


FIG. 7.17
Principle of continuous electrodeionization (Wood et al., 2010).

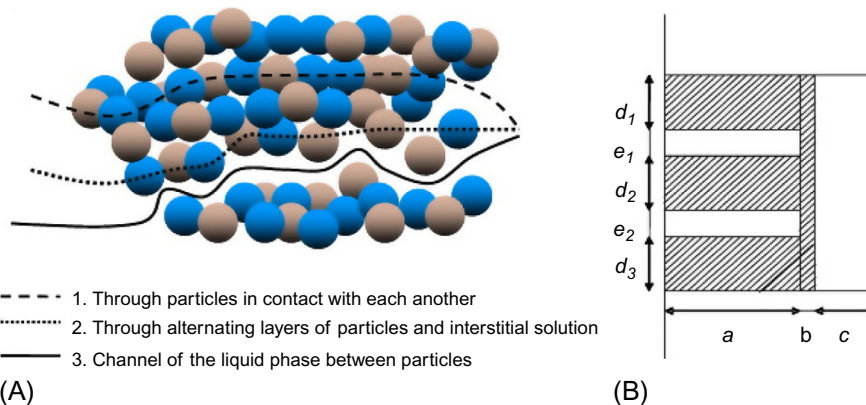


FIG. 7.18
Flow pathways in an ion-exchange resin for continuous electrodeionization (Wyllie et al., 1955).

the three possibilities of flow (shown in Fig. 7.18). The specific conductivity in the resin bed can then be written as (Alvarado and Chen, 2014):

$$\kappa = \kappa_1 + \kappa_2 + \kappa_3 \tag{7.44}$$

with

$$\kappa_1 = \frac{a\kappa\bar{\kappa}}{d\kappa + e\bar{\kappa}} \tag{7.45}$$

$$\kappa_2 = b\bar{\kappa} \quad (7.46)$$

$$\kappa_3 = c\bar{\kappa} \quad (7.47)$$

in which:

κ = specific conductivity of the resin bed.

κ_1 = specific conductivity of the solid and interstitial solution.

κ_2 = specific conductivity of the solid.

κ_3 = specific conductivity of the liquid.

κ = specific conductivity of the interstitial solution.

$\bar{\kappa}$ = resin specific conductance.

a = cross-section fraction in the conductance element: solid and interstitial solution.

b = cross-section fraction in the conductance element: solid.

c = cross-section fraction in the conductance element: liquid solution.

d = fraction in the conductance element κ_1 of solid.

e = fraction in the conductance element κ_2 of solution.

These parameters should fulfill the following summation requirements:

$$a + b + c = 1 \quad (7.48)$$

$$d + e = 1 \quad (7.49)$$

They can be determined from the following boundary conditions:

$$\left(\frac{\kappa b}{\bar{\kappa}}\right)_{\kappa=0} = b \quad (7.50)$$

$$\left(\frac{d\kappa_b}{d\kappa}\right)_{\kappa=0} = \frac{a}{e} + c \quad (7.51)$$

$$\left(\frac{d\kappa_b}{d\kappa}\right)_{\kappa=\bar{\kappa}} = ae + c \quad (7.52)$$

7.6.4 DONNAN DIALYSIS

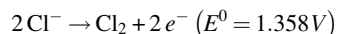
Donnan dialysis makes use of only a cation-exchange membrane (for applications of removal of cations) or anion-exchange membranes (for applications of removal of anions). This membrane is placed between a feed phase and a stripping solution. The most prominent application—although seldom applied in practice—is in water softening, where the membrane is a cation-exchange resin. Calcium and magnesium ions diffuse through the membrane. In this application, the stripping solution would

be a brine containing NaCl. Na^+ ions diffuse through the membrane because of the concentration difference; chloride ions cannot pass the membrane, which generates an electrical potential that serves as the driving force to permeate calcium (and magnesium) cations through the membrane in the direction of the stripping solution. Two Na^+ ions replace one Ca^{2+} ion, and the electroneutrality is thus maintained. The process can be modeled as diffusion dialysis, with the only exception that cations (or in a different application, anions) diffuse through the membrane.

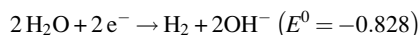
7.6.5 MEMBRANE ELECTROLYSIS

The importance of membrane electro dialysis is not to be underestimated; industrial chlorine and caustic electrolysis units installed during the past two decades are almost exclusively based on membrane electrolysis (Paidar et al., 2016). Membrane electrolysis is a simple process to understand, as it concerns an electrolytic reaction in which the cathode and anode compartment are separated by an ion-exchange membrane. Industrial membrane electrolysis processes require a significantly higher operating current density than used in electro dialysis (typically above 2000 A m^{-2}). The purpose of the membrane is to separate the anode loop (anolyte) from the cathode loop (catholyte) by a fluid, in order to avoid unwanted secondary reactions, and to fractionate the products formed at the electrodes. One important application is water electrolysis, in which the products may be in a gaseous form such as oxygen and hydrogen. In addition, acids (H^+) and bases (OH^-) may be formed on the electrode. In sodium chloride electrolysis, gaseous chlorine and caustic soda are produced as well as hydrogen gas. Thus membrane electrolysis is used for the production of sodium hypochlorite, ozone, chlorine dioxide, and hypochloric acid. The most typical application is in brine electrolysis, in which a saturated (26 wt% NaCl) brine solution is used as a source for the following reactions:

Anode:



Cathode:



This is schematically shown in Fig. 7.19 (Paidar et al., 2016). In this scheme, electrodes are pressed on each side of the membrane to reduce Ohmic potential loss in the electrolyte. This design is referred to as “zero gap.”

The chloride anion is oxidized on the anode to chlorine gas, while sodium ions are transported through the cation-selective membrane from the anode to the cathode compartment. Here they recombine with hydroxyl ions to produce sodium hydroxide.

In the chlor-alkali membrane electrolysis process, titanium anodes coated with a $\text{RuO}_2/\text{TiO}_2$ layer and nickel-based cathodes with a surface modified by a catalytic layer based on high surface Ni compounds doped with platinum metals are used (Paidar et al., 2016).

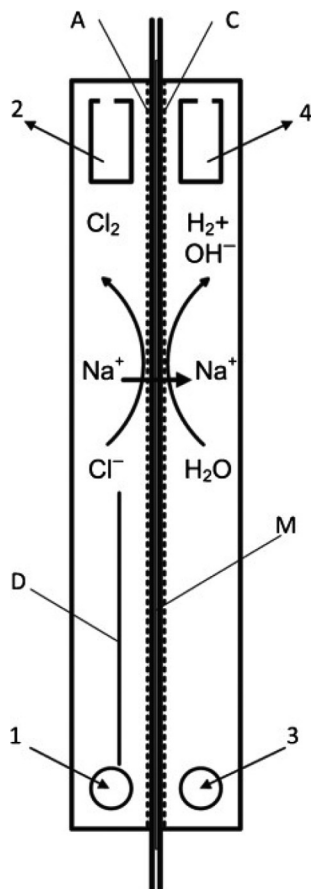


FIG. 7.19

Chlor-alkali process; A—anode (perforated titanium activated by RuO_2), C—cathode (catalyst activated Ni mesh), M—perfluorinated membrane (pressed between anode and cathode), D—downcomer (ensuring brine circulation), 1—brine inlet, 2—depleted brine with chlorine collector (outlet), 3—diluted caustic soda inlet, 4—concentrated caustic soda with hydrogen collector (outlet) (Paidar et al., 2016).

The maximum achievable sodium hydroxide concentration of up to 35 wt% is limited by the water flux between the anode and the cathode compartments, which is primarily connected with hydration of the Na^+ ion. This is estimated to amount to 4 water molecules per Na^+ ion (Wyllie et al., 1955), which is close to the value of 3.5 mentioned previously.

The charge efficiency of the process may be limited by the separation efficiency of the membrane, and specifically the effect of back diffusion of hydroxyl ions from the cathode to the anode compartment, as described before.

Modeling of membrane electrolysis may be based on the description of mass transfer by the Maxwell-Stefan theory (Hogendoorn et al., 2001). However, it should be noted that this is quite tentative since no (reliable) Maxwell-Stefan diffusivities are available for membranes typically used in membrane electrolysis, such as the Nafion membrane.

7.6.6 FUEL CELLS

A fuel cell essentially consists of two electrodes (anode and cathode) and an electrolyte (a thin, conducting layer between the electrodes). The general principle of a (hydrogen) fuel cell is very simple and is in fact the reverse of the electrolysis of water: hydrogen and oxygen are recombined to water and an electric current is produced (Fig. 7.20).

Recombination of O_2 and H_2 occurs at the two electrodes, which are thin and porous so that the electrolyte as well as the gas can penetrate easily. This allows a maximal contact between electrode, electrolyte, and gas.

Acid electrolytes

Depending on the type of electrolyte different reactions take place at the electrodes. For an acid electrolyte the following reactions take place:

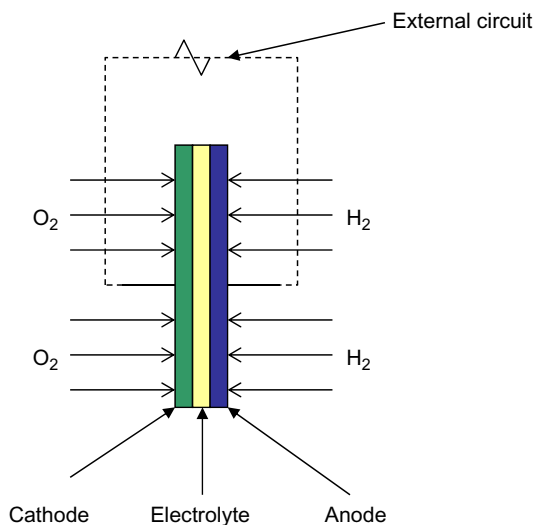
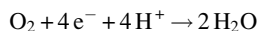


FIG. 7.20

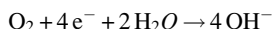
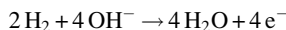
Basic composition of a fuel cell including cathode, electrolyte, and anode.

The electrons produced at the anode are transported to the cathode through an external circuit. In this way, an electrical current is produced from cathode to anode (current is considered to run in the direction of replacement of positive charges, although in fact it concerns a movement of negatively charged electrons—in this case, negative charges are transported from anode to cathode). Protons migrate from the anode through the electrolyte to the cathode. The electrolyte is an acid fluid, containing free H^+ ions migrating from the anode to the cathode (Fig. 7.21). However, only protons and no electrons should pass through the electrolyte; if there is a movement of electrons through the electrolyte, electrons would not migrate through the external circuit and no electrical current would be induced. This is the role of the cation-exchange membrane.

The only side product is water, produced at the cathode. Oxygen can be taken from the air; the anode needs supply of hydrogen.

Alkaline electrolytes

In a fuel cell with alkaline electrolyte the overall reaction is the same, but the reactions taking place at the electrodes are different:



The electrons are transported through an external circuit from the anode to the cathode (identical to the fuel cell with acid electrolyte), but the hydroxyl ions migrate through the electrolyte from the cathode to the anode (Fig. 7.22).

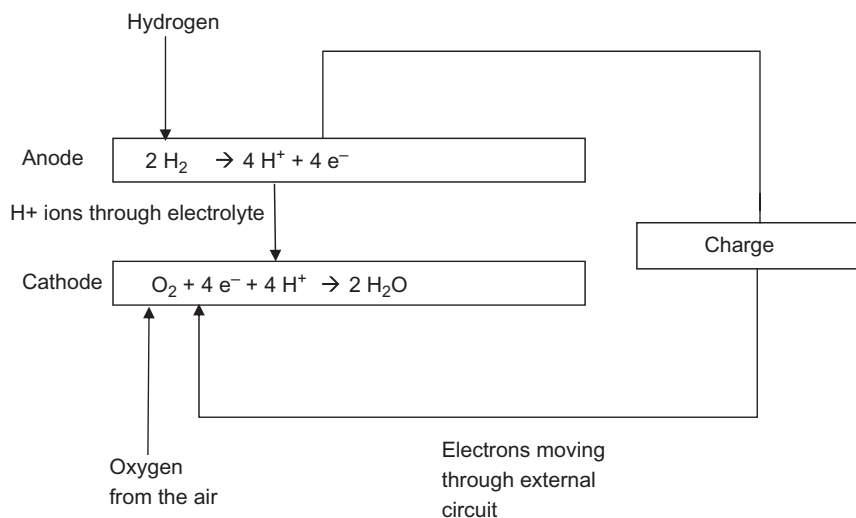
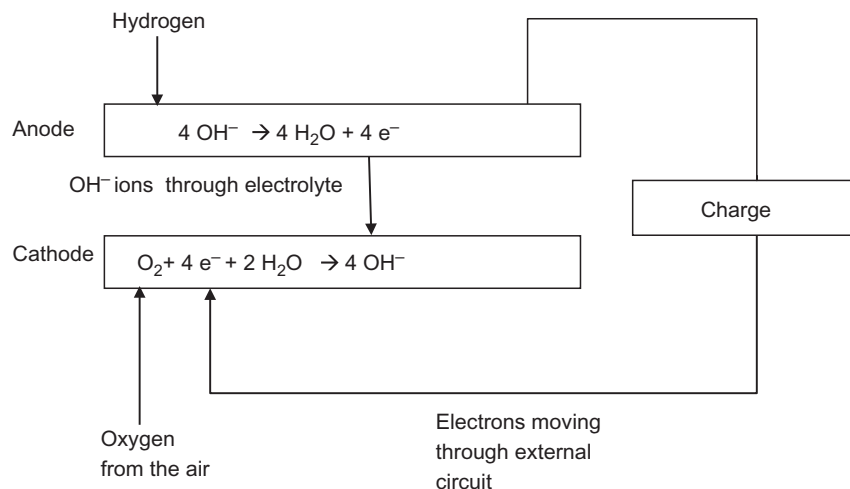


FIG. 7.21

Reactions and migration of charges for a fuel cell with acid electrolyte.

**FIG. 7.22**

Reactions and migration of charges for a fuel cell with alkaline electrolyte.

Water is consumed at the cathode, but is produced at the anode at a rate twice as high as the consumption rate. Thus there is a net production of a side product. Identical to the fuel cell with acid electrolyte, twice as much hydrogen is consumed than oxygen.

Summarizing models for fuel cells is not possible within the scope of this chapter, as there are a large number of different configurations of fuel cells, and the reader is referred to the extensive literature on fuel cells for this specific topic. A small sample of the literature is given in the reference list (Wu, 2016; Salomov et al., 2014; Barbir, 2012; Gou et al., 2017), but a large number of other sources on this topic may be found in addition to this.

7.6.7 CAPACITIVE DEIONIZATION

In capacitive deionization (CDI), the electrode compartments directly participate in the ion removal/concentration process, with oxidation/reduction at the electrodes; electrons are transferred by electrostatic adsorption. Two carbon electrodes are separated by spacer, through which the feed flows. By applying an electrical potential over the electrodes, ions adsorb on the electrodes (electrosorption); when the electrodes are saturated, the electrical potential is reversed (cathode becomes anode and vice versa). This releases the ions from the electrodes so that they can be removed.

An important feature of the process is the adsorption capacity of the electrodes. An enhanced adsorption capacity is obtained by activation of the carbon, by using carbon nanotubes, or carbon aerogels. In this way, a specific surface area of at least $1000 \text{ m}^2/\text{g}$ can be obtained.

In addition, the electrical resistance of the feed solution should be low.

Water dissociation is to be avoided, which requires to operate at a low potential, typically between 0.8 and 1.5 V.

A strong limitation in this concept of capacitive deionization is that counterions adsorb as well, and occupy capacitance within the electrode. This reduces the efficiency. A solution for this is the use of an anion-exchange membrane on the anode, preventing cations to pass, and a cation-exchange membrane on the cathode, preventing anions to pass. In the regeneration step, under reverse polarity conditions, the cation-exchange membrane prevents anions from migrating to the anode, and the anion-exchange membrane prevents cations from migrating to the cathode. This is shown in Fig. 7.23A and B; Fig. 7.23C also suggests the use of a selective cation-exchange membrane, which adds a further feature to membrane capacitive deionization, since it allows for a shift in the ratio of monovalent versus divalent ions (Choi et al., 2016).

Thus a capacitive deionization unit comprises a sequence of electrode-cation-exchange membrane-feed flow channel-anion-exchange membrane-electrode, as a repeating unit in a stack.

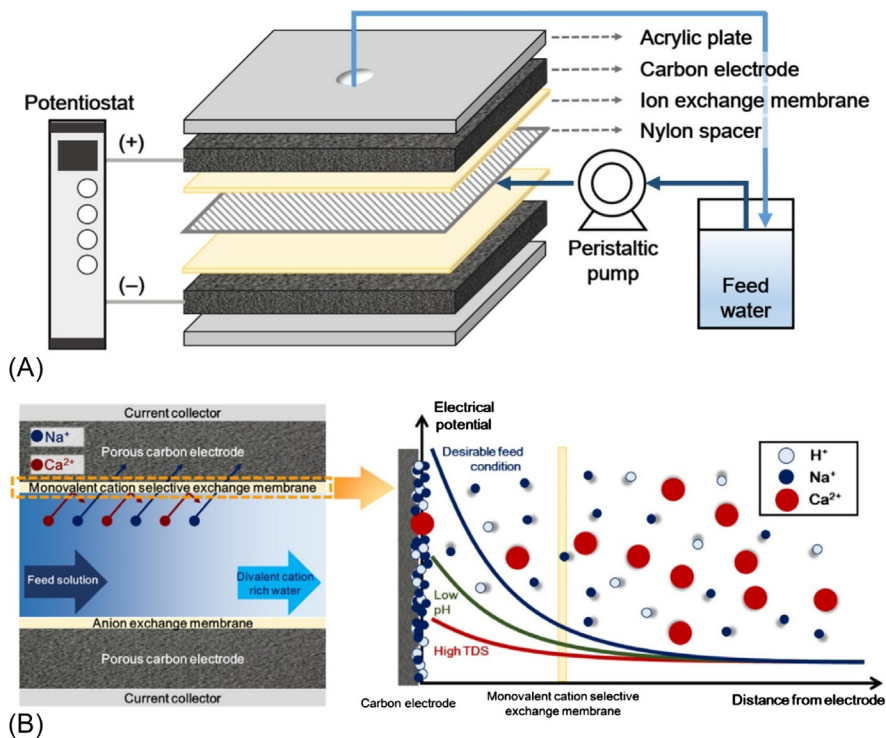


FIG. 7.23

Membrane capacitive deionization (A and B); in (C) the effect of using a monovalent selective membrane is shown (Choi et al., 2016).

A relatively new configuration of CDI is Flow-electrode Capacitive Deionization (FCDI) (Gendel et al., 2014). The static electrodes are replaced by flow electrodes, which consist of carbon particles suspended in an aqueous electrolyte solution. Flow electrodes are pumpable and can be regenerated in a separate module or compartment. This is shown in Fig. 7.24 (Rommerskirchen et al., 2018).

By functionalization of the electrode surfaces with redox polymers in which the charge on the electrodes can be modulated through Faradaic reactions under different cell voltages, an alternative capacitive deionization process denoted as “Faradaic CDI” (FaCDI) is obtained (He et al., 2018). It was shown that equilibrium adsorption capacities 50%–100% higher than attained with CDI systems, and at smaller cell voltages, depending on the redox potentials of the Faradaic moieties (He et al., 2018).

Modeling of membrane capacitive deionization is based on the adsorption capacity (Hassanvand et al., 2018):

$$Q = \frac{\left[\int_0^{t_{ads}} (c_{in} - c_t) dt \right] \cdot \dot{V}}{M_{carbon}} \quad (7.53)$$

Q is the salt adsorption in mmol salt/g carbon, t_{ads} is the adsorption duration, C_{in} is the inlet salt concentration, C_t is the outlet salt concentration at any time t , \dot{V} is the volumetric flow rate, and M_{carbon} is the total mass of carbon in the electrodes.

The total charge (σ) can be obtained by integrating the electrical current (I_e) passed through the cell over the adsorption time:

$$\sigma = \int_0^{t_{ads}} I_e(t) dt \quad (7.54)$$

The energy consumption (Whm^{-3}) during the adsorption step can be calculated based on the applied electrical potential, V_{cell} :

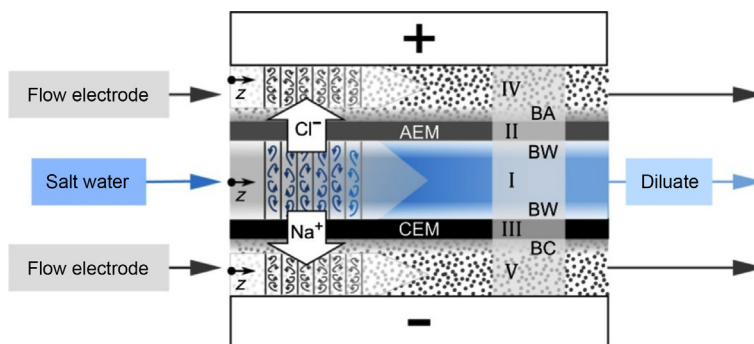


FIG. 7.24

Flow-through membrane capacitive deionization for continuous operation (Rommerskirchen et al., 2018). BA/BC: Boundary layers at interface between IEM and anode/cathode, BW: Boundary layers at interface between IEM and feed water channel.

$$E = \frac{V_{cell}\sigma}{t_{ads}\dot{V}} \quad (7.55)$$

Charge efficiency is defined as the ratio of salt removed over the amount of charge transferred through the cell. The charge is divided by the Faraday constant to be expressed as moles of electrons; and the amount of salt adsorbed is in moles as well:

$$\Lambda = \frac{Q \cdot M_{carbon}}{\sigma / F} \quad (7.56)$$

A normalized charge efficiency can be defined, taking into account the requirement for multiple charges to be transferred for a multivalent salt of valence z :

$$\Lambda_n = \frac{Q_n \cdot M_{carbon}}{\sigma / F} = \frac{z \cdot Q \cdot M_{carbon}}{\sigma / F} \quad (7.57)$$

7.6.8 ELECTRODIALYSIS WITH BIPOLAR MEMBRANES

The configuration of electrodialysis making use of bipolar membranes has already been described earlier in this chapter (see Figs. 7.2 and 7.3). Modeling would depend substantially on the specific application or reaction taking place. A template of a model can be found in the conversion of sodium lactate (NaLac) into lactic acid (HLac) (Roux de Balmann et al., 2002). The system, fluxes, and parameters are shown in Fig. 7.25 (Roux de Balmann et al., 2002).

The two reactions taking place are described by their equilibrium:

$$K_A = \frac{n_H^D(t)n_{Lac}^D(t)}{V_D(t)n_{HLac}^D(t)} \quad (7.58)$$

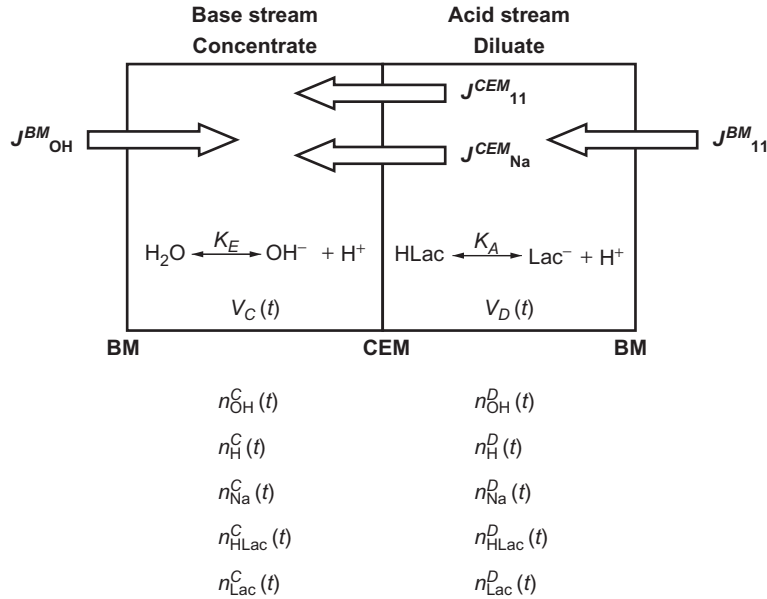
$$K_E = \frac{n_H^C(t)n_{OH}^C(t)}{V_C^2(t)} \quad (7.59)$$

The proton balance in the diluate is as follows:

$$\frac{dn_H^D(t)}{dt} + \frac{dn_{Lac}^D(t)}{dt} = J_H^{BM} - J_H^{CEM} \quad (7.60)$$

If it can be assumed that the water dissociation equilibrium is fast, compared to the transfer of protons through the cation-exchange membrane; and that the flux of hydroxyl ions from the bipolar membrane is larger than that of protons through the cation-exchange membrane, the variation of the OH^- concentration in the concentrate becomes:

$$\frac{dn_{OH}^C(t)}{dt} = J_{OH}^{BM} - J_H^{CEM} \quad (7.61)$$


FIG. 7.25

Fluxes and reactions considered for the model for electrodialysis with bipolar membranes, J_{H}^{BM} and $J_{\text{OH}}^{\text{BM}}$: (mol/s): molar flux of H^+ and OH^- produced by the bipolar membrane; $J_{\text{Na}}^{\text{CEM}}$ and $J_{\text{H}}^{\text{CEM}}$ (mol/s): molar flux of Na^+ and H^+ through the CEM; n_i^j (mol): number of moles of i in compartment j ; V_j : volume in compartment j (Roux de Balmann et al., 2002).

For Na , it can be written:

$$\frac{dn_{\text{Na}}^{\text{D}}(t)}{dt} = -J_{\text{Na}}^{\text{CEM}} \quad (7.62)$$

The mass balance for lactate is:

$$n_{\text{HLac}}^{\text{C}}(t) + n_{\text{HLac}}^{\text{D}}(t) + n_{\text{Lac}}^{\text{C}}(t) + n_{\text{Lac}}^{\text{D}}(t) = n_{\text{Lac},0}^{\text{D}} + n_{\text{HLac},0}^{\text{D}} \quad (7.63)$$

$$n_{\text{Na}}^{\text{D}}(t) + n_{\text{Na}}^{\text{C}}(t) = n_{\text{Na},0}^{\text{D}} + n_{\text{Na},0}^{\text{C}} \quad (7.64)$$

Electroneutrality for the concentrate and diluate compartment:

$$n_{\text{OH}}^{\text{D}}(t) + n_{\text{Lac}}^{\text{D}}(t) = n_{\text{Na}}^{\text{D}}(t) + n_{\text{H}}^{\text{D}}(t) \quad (7.65)$$

$$n_{\text{OH}}^{\text{C}}(t) + n_{\text{Lac}}^{\text{C}}(t) = n_{\text{Na}}^{\text{C}}(t) + n_{\text{H}}^{\text{C}}(t) \quad (7.66)$$

The molar fluxes are:

$$J_{\text{H}}^{\text{CEM}} + J_{\text{Na}}^{\text{CEM}} = J_{\text{H}}^{\text{BM}} \quad (7.67)$$

As described before, the fluxes of ions can be described in terms of transport numbers:

$$\frac{J_{Na}^{CEM}}{J_H^{CEM}} = \frac{t_{Na}^{CEM}}{t_H^{CEM}} = \frac{u_{Na}^{CEM} c_{Na}^{CEM}}{u_H^{CEM} c_H^{CEM}} \quad (7.68)$$

where u refers to mobility and c to concentration.

Furthermore, the concentrations in the membrane are related to those in the solution:

$$\frac{J_{Na}^{CEM}}{J_H^{CEM}} = f \left(\frac{n_{Na}^D}{n_H^D} \right) \quad (7.69)$$

The variation in volume of the diluate compartment is as follows:

$$V_D(t) = V_0 + \int R_v dt \quad (7.70)$$

$$V_C(t) + V_D(t) = 2V_0 \quad (7.71)$$

The fluxes of H^+ and OH^- produced by the bipolar membrane may be the same:

$$J_H^{BM} = J_{OH}^{BM} \quad (7.72)$$

Eqs. (7.58)–(7.72) can be solved in principle, but this gives a set of 14 equations with 14 unknowns comprising strongly nonlinear differential equations, so that numerical methods are required. However, some simplifications can be made. Firstly, the contribution of diffusion to the transfer of target species, HLac and Lac, could be neglected. The transfer of both species from the diluate to the concentrate is then nonexistent, so that the number of mole of HLac and Lac in the concentrate remains constant vs. time and equal to zero. Thus Eq. (7.63) becomes:

$$n_{HLac}^D(t) + n_{Lac}^D(t) = n_0^D \quad (7.73)$$

In Eqs. (7.65), (7.66), $n_{OH}^D(t)$ and $n_H^C(t)$ can be neglected given the pH range:

$$n_{Lac}^D(t) = n_{Na}^D(t) + n_H^D(t) \quad (7.74)$$

$$n_{OH}^C(t) = n_{Na}^C(t) \quad (7.75)$$

For a given current density, the molar flux of sodium through the CEM is assumed to remain constant during the conversion. The constant value of J_{Na}^{CEM} can thus be replaced by the parameter α . Then, Eq. (7.62) can be integrated between $t = 0$ and $t = t_{final}$ and combined with Eq. (7.64):

$$n_{Na}^D(t) = n_{Na,0}^D - \alpha \cdot t \quad (t < t_{final}) \quad (7.76)$$

$$n_{Na}^C(t) = n_{Na,0}^C + \alpha \cdot t \quad (t < t_{final}) \quad (7.77)$$

$$\frac{dn_{Na}^D(t)}{dt} = \frac{dn_{Na}^C(t)}{dt} = 0 \quad (7.78)$$

and

$$n_{Na}^C(t_{final}) = n_{Na,0}^C + n_{Na,0}^D \quad (7.79)$$

Combining Eqs. (7.58), (7.42), and (7.57):

$$n_H^D(t) - \frac{n_0^D K_A V_D(t)}{n_H^D(t) + K_A V_D(t)} + n_{Na}^D(t) = 0 \quad (7.80)$$

So that

$$n_H^D(t) = -\frac{n_{Na}^D(t) + K_A V_D(t)}{2} + \frac{\sqrt{(n_{Na}^D(t) + K_A V_D(t))^2 + 4K_A V_D(t)(n_0^D - n_{Na}^D(t))}}{2} \quad (7.81)$$

And

$$n_H^D(t) = -g(t) + \sqrt{g(t)^2 + 4K_A V_D(t)h(t)} \quad (7.82)$$

$$g(t) = n_{Na,0}^D - \alpha \cdot t + K_A V_D(t) \quad (7.83)$$

$$h(t) = 4K_A V_D(t)(n_0^D - n_{Na,0}^D + \alpha \cdot t) \quad (7.84)$$

The pH in the diluate, $pH_D(t)$, and the corresponding conversion factor, $\tau(t)$, are:

$$pH_D(t) = -\log\left(\frac{n_H^D(t)}{V_D(t)}\right) \quad (7.85)$$

$$\tau(t) = \frac{1}{1 + 10^{(pH_D(t) - pK_A)}} \quad (7.86)$$

7.6.9 REVERSE ELECTRODIALYSIS

The principles of reverse electrodialysis have been outlined earlier in this chapter. Modeling of reverse electrodialysis comprises two aspects:

- the estimation of the power density that can be achieved from the system;
- transport of ions in the system from concentrated to diluted side.

The former aspect is described in the literature based on electromotive force, internal stack resistance, salt and water flux, and concentration gradient (Hong et al., 2013). Often this is elaborated for single salt (NaCl) systems, but it has been shown that magnesium sulfate, sodium sulfate, and magnesium chloride in the feed solutions of the RED system lead to a 15%–43% lower power density than when sodium chloride is the single ion source. Other factors that were found to lead to higher power densities were higher flow rates in the saline water compartment and shorter intermembrane distances in the freshwater compartment (Hong et al., 2013; Hong et al., 2014).

The Nernst equation can be used to estimate the potential differences over the stack; for saline water and freshwater containing NaCl and $MgSO_4$ this would be:

$$\begin{aligned}
E_{cell}(x) = & \alpha_{CEM} \frac{RT}{F} \left[\ln \frac{\gamma_S^{Na^+}(x) c_S^{Na^+}(x)}{\gamma_F^{Na^+}(x) c_F^{Na^+}(x)} \right] + \alpha_{AEM} \frac{RT}{F} \left[\ln \frac{\gamma_S^{Cl^-}(x) c_S^{Cl^-}(x)}{\gamma_F^{Cl^-}(x) c_F^{Cl^-}(x)} \right] + \\
& \alpha_{CEM} \frac{RT}{F} \left[\ln \left(\frac{\gamma_S^{Mg^{2+}}(x) c_S^{Mg^{2+}}(x)}{\gamma_F^{Mg^{2+}}(x) c_F^{Mg^{2+}}(x)} \right)^{\frac{1}{2}} \right] + \alpha_{AEM} \frac{RT}{F} \left[\ln \left(\frac{\gamma_S^{SO_4^{2-}}(x) c_S^{SO_4^{2-}}(x)}{\gamma_F^{SO_4^{2-}}(x) c_F^{SO_4^{2-}}(x)} \right)^{\frac{1}{2}} \right]
\end{aligned} \quad (7.87)$$

Similar equations can be written for other systems. The activity coefficients can be estimated by the Debye-Hückel theory, or more specific thermodynamic equations.

The current density $I(x)$ is

$$I(x) = \frac{E_{cell}(x)}{R_{int}(x) + R_{ext}(x)} \quad (7.88)$$

with $R_{int}(x)$ the internal cell resistance and $R_{ext}(x)$ the external resistance.

The internal cell resistance is:

$$R_{int}(x) = R_S(x) + R_F(x) + R_{AEM} + R_{CEM} \quad (7.89)$$

and

$$R_S(x) = f \cdot \left(\frac{\delta_S}{\frac{\lambda_{m,S}^{AB} (c_{S,ave}^{A^+} + c_{S,ave}^{B^-})}{2} + \frac{\lambda_{m,S}^{CD} (c_{S,ave}^{C^{2+}} + c_{S,ave}^{D^{2-}})}{2}} \right) \quad (7.90)$$

$$R_F(x) = f \cdot \left(\frac{\delta_F}{\frac{\lambda_{m,F}^{AB} (c_{F,ave}^{A^+} + c_{F,ave}^{B^-})}{2} + \frac{\lambda_{m,F}^{CD} (c_{F,ave}^{C^{2+}} + c_{F,ave}^{D^{2-}})}{2}} \right) \quad (7.91)$$

In this equation, f is the obstruction factor, which describes the negative shielding effects of the spacer. For example, if the spacers used in the experiment occupy 46% of the area in a plane projection (Rommerskirchen et al., 2018), the obstruction factor is $1/(1-0.46) = 1.9$.

The power density is:

$$P_d(x) = \frac{1}{2} I^2(x) R_{ext}(x) \quad (7.92)$$

With a maximum power density

$$P_d(x) = \frac{1}{2} \left(\frac{E(x)}{2R_{ext}(x)} \right)^2 R_{ext}(x) \quad (7.93)$$

The second aspect of transport of ions can in principle be described by the same Nernst-Planck transport theory as used for electrodialysis (Tedesco et al., 2016) or can be described by irreversible thermodynamics (Zlotorowicz et al., 2017). The only difference with electrodialysis is in the electrical potential, which is the

driving force in one case and the objective function in the other case; the transport equations, however, are the same.

In a comprehensive approach in which all aspects are integrated (Veerman et al., 2011), the influence of the operational parameters can be assessed; in a comparison between countercurrent and concurrent designs, it was found that cocurrent operation leads to smaller local pressure differences between the freshwater and seawater compartments, and therefore a lower risk of leakages and the possibility to use very thin membranes with high fluxes and very open spacer structures with low hydrodynamic resistance (Veerman et al., 2011).

Furthermore, segmentation of the electrodes was observed to increase the power density (by ca. 15% under realistic operational conditions), and that systems with a shorter flow path have higher power densities (Veerman et al., 2011).

7.7 CONCLUSIONS

Modeling of electrodriven processes has a basis in the use of the Nernst-Planck equation for electrodialysis. This equation includes the influence of electrical potential, concentration differences, and pressure differences, although the latter can typically be neglected. The resulting equations are relatively complex by nature. Phenomenological equations can be used as a pragmatic alternative; the Nernst-Planck equation can be further reduced to dimensionless variables as well, which can then be empirically modeled. As a result, current densities can be related to concentration changes in the diluate and concentrate compartments. The selectivity that can be obtained is expressed in terms of transport numbers, by using resistances, or in a more pragmatic way, by using the separation efficiency.

A large number of variations of electromembrane processes have been developed. Some of these have found a wide entry into industrial practice, such as capacitive deionization (with ion-exchange membranes) and membrane electrolysis. Other processes are currently high on the research agenda, such as reverse electrodialysis, or have reached a stage of sufficient maturity in which wide-scale application depends on other than technical issues (diffusion dialysis, fuel cells, electrodialysis with bipolar membranes). Some processes are very specific by definition (electroelectrodialysis, continuous deionization, Donnan dialysis). Modeling of these processes has a similar basis to electrodialysis, although modifications are necessary in order to highlight the specific aspects of each technology.

REFERENCES

- Alheritiere, C., Ernst, W.R., Davis, T.A., 1998. Metathesis of magnesium and sodium salt systems by electrodialysis. *Desalination* 115 (2), 189–198.
- Alvarado, L., Chen, A., 2014. Electrodeionization: principles, strategies and applications. *Electrochim. Acta* 132, 583–597.

- Arfaoui, M., Ouejhani, A., Hamrouni, B., 2018. Physicochemical characterization of a polymeric conductor: application to defluoridation of industrial effluent by electro dialysis. *Turk. J. Chem.* 42 (1), 121–131.
- Barbir, F., 2012. PEM Fuel Cells. In: *Theory and Practice*, second ed. Elsevier, Waltham, USA.
- Chen, X., Jiang, C.X., Zhang, Y.L., Wang, Y.M., Xu, T.W., 2017. Storable hydrogen production by reverse electro-Electrodialysis (REED). *J. Membr. Sci.* 544, 397–405.
- Chen, Q.B., Ji, Z.Y., Liu, J., Zhao, Y.Y., Wang, S.Z., Yuan, J.S., 2018. Development of recovering lithium from brines by selective-electrodialysis: effect of coexisting cations on the migration of lithium. *J. Membr. Sci.* 548, 408–420.
- Choi, J.M., Lee, H.K., Hong, S.K., 2016. Capacitive deionization (CDI) integrated with monovalent cation selective membrane for producing divalent cation-rich solution. *Desalination* 400, 38–46.
- Cowan, D.A., Brown, J.H., 1959. Effect of turbulence on limiting current in electro dialysis cells. *Ind. Eng. Chem.* 51, 1445–1448.
- Farrokhzad, H., Darvishmanesh, S., Van Gerven, T., Van der Bruggen, B., 2015. Development of bivalent cation selective ion exchange membranes by varying molecular weight of polyaniline. *Electrochim. Acta* 158, 64–72.
- Frenzel, I., Holdik, H., Stamatialis, D.F., Pourcelly, G., Wessling, M., 2005a. Chromic acid recovery by electro-electrodialysis: I. Evaluation of anion-exchange membrane. *J. Membr. Sci.* 261 (1–2), 49.
- Frenzel, I., Holdik, H., Stamatialis, D.F., Pourcelly, G., Wessling, M., 2005b. Chromic acid recovery by electro-electrodialysis: II. Pilot scale process, development, and optimization. *Sep. Purif. Technol.* 47 (1–2), 27–35.
- Frioui, S., Oumeddour, R., Lacour, S., 2017. Highly selective extraction of metal ions from dilute solutions by hybrid electro dialysis technology. *Sep. Purif. Technol.* 174, 264–274.
- Fumatech n.d. Elektrodialysis with bipolar membranes. www.fumatech.com.
- Gärtner, R.S., Wilhelm, F.G., Witkamp, G.J., Wessling, M., 2005. Regeneration of mixed solvent by electro dialysis: selective removal of chloride and sulphate. *J. Membr. Sci.* 259, 113–133.
- Geise, G.M., Cassady, H.J., Paul, D.R., Logan, B.E., Hickner, M.A., 2014. Specific ion effects on membrane potential and the permselectivity of ion exchange membranes. *Phys. Chem. Chem. Phys.* 16, 21673–21681.
- Gendel, Y., Rommerskirchen, A.K.E., David, O., Wessling, M., 2014. Batch mode and continuous desalination of water using flowing carbon deionization (FCDI) technology. *Electrochem. Commun.* 46, 152–156.
- Ghalloussi, R., Chaabane, L., Dammak, L., Grande, D., 2014. Ageing of ion-exchange membranes used in an electro dialysis for food industry: SEM, EDX, and limiting current investigations. *Desalin. Water Treat.* 56 (10), 2561–2566.
- Ghyselbrecht, K., Silva, A., Van der Bruggen, B., Boussu, K., Meesschaert, B., Pinoy, L., 2014. Desalination feasibility study of an industrial NaCl stream by bipolar membrane electro dialysis. *J. Environ. Manag.* 140, 69–75.
- Gonzalez, A., Grageda, M., Ushak, S., 2017. Assessment of pilot-scale water purification module with electro dialysis technology and solar energy. *Appl. Energy* 206, 1643–1652.
- Gou, B., Na, W.K., Diong, B., 2017. *Fuel Cells: Modeling, Control, and Applications*. CRC Press, Boca Raton.
- Gutierrez, L.F., Bazinet, L., Hamoudi, S., Belkacemi, K., 2013. Production of lactobionic acid by means of a process comprising the catalytic oxidation of lactose and bipolar membrane electro dialysis. *Sep. Purif. Technol.* 109, 23–32.

- Hassanvand, A., Chen, G.Q., Webley, P.A., Kentish, S.E., 2018. A comparison of multicomponent electrosorption in capacitive deionization and membrane capacitive deionization. *Water Res.* 131, 100–109.
- He, F., Biesheuvel, P.M., Bazant, M.Z., Hatton, T.A., 2018. Theory of water treatment by capacitive deionization with redox active porous electrodes. *Water Res.* 132, 282–291.
- Hogendoorn, J.A., van der Veen, A.J., van der Stegen, J.H.G., Kuipers, J.A.M., Versteeg, G.F., 2001. Application of the Maxwell–Stefan theory to the membrane electrolysis process. Model development and simulations. *Comp. Chem. Eng.* 25, 1251–1265.
- Hong, J.G., Zhang, W., Luo, J., Chen, Y.S., 2013. Modeling of power generation from the mixing of simulated saline and freshwater with a reverse electro dialysis system: the effect of monovalent and multivalent ions. *Appl. Energy* 110, 244–251.
- Hong, J.G., Zhang, W., Luo, J., Chen, Y.S., 2014. Corrigendum to “Modeling of power generation from the mixing of simulated saline and freshwater with a reverse electro dialysis system: The effect of monovalent and multivalent ions” [*Appl. Energy* 110 (2013) 244–251]. *Appl. Energy* 129, 398–399.
- Huang, C.H., Xu, T.W., Zhang, Y.P., Xue, Y.H., Chen, G.W., 2007. Application of electro dialysis to the production of organic acids: state-of-the-art and recent developments. *J. Membr. Sci.* 288, 1–12.
- Huang, Q.M., Zhang, Q.L., Huang, H.L., Li, W.S., Huang, Y.J., Luo, J.L., 2008. Methanol permeability and proton conductivity of Nafion membranes modified electrochemically with polyaniline. *J. Power Sour.* 184 (2), 338–343.
- Itoh, H., Yoshizumi, T., Saeki, M., 1986. Sieving effect in electro dialysis with an ion exchange membrane. *J. Membr. Sci.* 27, 155–163.
- Jarozsek, H., Lis, A., Dydo, P., 2016. Transport of impurities and water during potassium nitrate synthesis by electro dialysis metathesis. *Sep. Purif. Technol.* 158, 87–93.
- Jiang, C.X., Wang, Y.M., Zhang, Z.H., Xu, T.W., 2014a. Electro dialysis of concentrated brine from RO plant to produce coarse salt and freshwater. *J. Membr. Sci.* 450, 323–330.
- Jiang, C.X., Wang, Y.M., Wang, Q.Y., Feng, H.Y., Xu, T.W., 2014b. Production of Lithium hydroxide from Lake brines through electro-Electro dialysis with bipolar membranes (EEDBM). *Ind. Eng. Chem. Res.* 53 (14), 6103–6112.
- Kariduraganavar, M.Y., Nagarale, R.K., Kittur, A.A., Kulkarni, S.S., 2006. Ion-exchange membranes: Preparative methods for electro dialysis and fuel cell applications. *Desalination* 197 (1–3), 225–246.
- Karimi, L., Ghassemi, A., 2016. An empirical/theoretical model with dimensionless numbers to predict the performance of electro dialysis systems on the basis of operating conditions. *Water Res.* 98, 270–279.
- Khan, M.I., Mondal, A.N., Tong, B., Jiang, C.X., Emmanuel, K., Yang, Z.J., Wu, L., Xu, T.W., 2016. Development of BPPO-based anion exchange membranes for electro dialysis desalination applications. *Desalination* 391, 61–68.
- Kikhavani, T., Farrokhzad, H., Ashrafzadeh, S.N., Van der Bruggen, B., 2014. Nitrate selectivity and transport properties of a novel anion exchange membrane in electro dialysis. *Electrochim. Acta* 144, 341–351.
- Kristensen, M.B., Bontien, A., Tedesco, M., Catalano, J., 2017. Counter-ion transport number and membrane potential in working membrane systems. *J. Colloids Interf. Sci.* 504, 800–813.
- Lu, H.-Y., Lin, C.-S., Lee, S.-C., Ku, M.-H., Hsu, J.-P., Tseng, S., Lin, S.-H., 2011. In situ measuring osmosis effect of Selemion CMV/ASV module during ED process of concentrated brine from DSW. *Desalination* 279 (1–3), 278–284.

- Luo, G.S., Wu, F.Y., 2000. Concentration of formic acid solution by electro-electrodialysis. *Sep. Sci. Technol.* 35 (15), 2485–2496.
- Luo, G.S., Liu, J.G., Lu, Y.C., Pan, S., Wang, J.D., 2005. Two-phase electro-Electrodialysis with an emulsion as Anolyte. *Sep. Sci. Technol.* 39 (6), 1267–1278.
- Luo, J.Y., Wu, C.M., Xu, T.W., Wu, Y.H., 2011. Diffusion dialysis-concept, principle and applications. *J. Membr. Sci.* 366, 1–16.
- Malek, P., Schulte-Herbruggen, H.M.A., 2016. Decentralized desalination of brackish water using an electrodialysis system directly powered by wind energy. *Desalination* 377, 54–64.
- Mei, Y., Tang, C.Y., 2018. Recent developments and future perspectives of reverse electro-dialysis technology: a review. *Desalination* 425, 156–174.
- Paidar, M., Fateev, V., Bouzek, K., 2016. Membrane electrolysis—History, current status and perspective. *Electrochim. Acta* 209, 737–756.
- Palaty, Z., Zakova, A., Prchal, P., 2007. Continuous dialysis of carboxylic acids: permeability of Neosepta-AME membrane. *Desalination* 216, 345–355.
- Prochaska, K., Antczak, J., Regel-Rosocka, M., 2018. Removal of succinic acid from fermentation broth by multistage process (membrane separation and reactive extraction). *Sep. Purif. Technol.* 294, 360–368.
- Ran, J., Wu, L., He, Y., Yang, Z., Wang, Y., Jiang, C., Ge, L., Bakangura, E., Xu, T., 2017. Ion exchange membranes: new developments and applications. *J. Membr. Sci.* 522, 267–291.
- Roblet, C., Doyen, A., Amiot, J., Bazinet, L., 2013. Impact of pH on ultrafiltration membrane selectivity during electro-dialysis with ultrafiltration membrane (EDUF) purification of soy peptides from a complex matrix. *J. Membr. Sci.* 435, 207–217.
- Rommerskirchen, A., Ohs, B., Hepp, K.A., Femmer, R., Wessling, M., 2018. Modeling continuous flow-electrode capacitive deionization processes with ion-exchange membranes. *J. Membr. Sci.* 246, 188–196.
- Rottiers, T., Van der Bruggen, B., Pinoy, L., 2016. Permeability of small alcohols through commercial ion-exchange membranes used in electrodialysis. *Ind. Eng. Chem. Res.* 55 (29), 8215–8224.
- Rottiers, T., Van der Bruggen, B., Pinoy, L., 2017. Synthesis and transport of impurities in electrodialysis metathesis: production of choline dihydrogen phosphate. *J. Membr. Sci.* 541, 550–557.
- Roux de Balmann, H., Bailly, M., Lutin, F., Aimar, P., 2002. Modelling of the conversion of weak organic acids by bipolar membrane electrodialysis. *Desalination* 149, 399–404.
- Salomov, U.R., Chiavazzo, E., Asinari, P., 2014. Pore-scale modeling of fluid flow through gas diffusion and catalyst layers for high temperature proton exchange membrane (HT-PEM) fuel cells. *Comput. Math. Appl.* 67 (2), 393–411.
- Sata, T., 2004. Ion-exchange membranes: Preparation, Characterization, Modification and Application, first ed. The Royal Society of Chemistry, Cambridge.
- Sata, T., Yamaguchi, T., Kawamura, K., Matsusaki, K., 1997. Transport numbers of various anions relative to chloride ions in modified anion-exchange membranes during electro-dialysis. *J. Chem. Soc. Faraday Trans.* 93, 457–462.
- Sata, T., Kawamura, K., Mutsusaki, K., 2001. Electro-dialytic transport of properties of anion-exchange membranes prepared from poly(vinyl alcohol), poly(N-ethyl 4-vinylpyridinium salt) and β -cyclodextrin. *J. Membr. Sci.* 181, 167–178.
- Schäfer, A.I., Hughes, G., Richards, B.S., 2014. Renewable energy powered membrane technology: a leapfrog approach to rural water treatment in developing countries? *Renew. Sust. Energ. Rev.* 40, 542–556.

- Serre, E., Rozoy, E., Pedneault, K., Lacour, S., Bazinet, L., 2016. Deacidification of cranberry juice by electro dialysis: Impact of membrane types and configurations on acid migration and juice physicochemical characteristics. *Sep. Purif. Technol.* 163, 228–237.
- Siebold, M., Vonfrieling, P., Joppien, R., Rindfleisch, D., Schugerl, K., Roper, H., 1995. Comparison of the production of lactic-acid by 3 different lactobacilli and its recovery by extraction and electro dialysis. *Process Biochem.* 30 (1), 81–95.
- Stachera, D.M., Childs, R.F., Mika, A.M., Dickson, J.M., 1998. Acid recovery using diffusion dialysis with poly(4-vinylpyridine)-filled microporous membranes. *J. Membr. Sci.* 148, 119–127.
- Strathmann, H., 2004a. Ion-Exchange Membrane Separation Processes. In: *Membrane Science and Technology*. first ed. Elsevier, Amsterdam.
- Strathmann, H., 2004b. Ion-Exchange Membrane Separation Processes, *Membrane Science and Technology Series*. Vol. 9. Elsevier B.V., Amsterdam.
- Strathmann, H., 2009. Ion Exchange Processes in Water Treatment. (Chapter 6). In: Escobar, I.-C., Schäfer, A.I. (Eds.), *Sustainable Water for the Future: Water Recycling Versus Desalination*. Elsevier.
- Tedesco, M., Hamelers, H.V.M., Biesheuvel, P.M., 2016. Nernst-Planck transport theory for (reverse) electro dialysis: I. Effect of co-ion transport through the membranes. *J. Membr. Sci.* 510, 370–381.
- Tran, A.T.K., Mondal, P., Lin, J., Meesschaert, B., Pinoy, L., Van der Bruggen, B., 2015. Simultaneous regeneration of inorganic acid and base from a metal washing step wastewater by bipolar membrane electro dialysis after pretreatment by crystallization in a pellet reactor. *J. Membr. Sci.* 473, 118–127.
- Valero, D., Garcia-Garcia, V., Exposito, E., Aldaz, A., Montiel, V., 2015. Application of electro dialysis for the treatment of almond industry wastewater. *J. Membr. Sci.* 476, 580–589.
- Van der Bruggen, B., 2017. Membrane Technology. In: *Kirk-Othmer Encyclopedia of Chemical Technology*. John Wiley & Sons.
- Van der Bruggen, B., Koninckx, A., Vandecasteele, C., 2004. Separation of monovalent and divalent ions from aqueous solution by electro dialysis and nanofiltration. *Water Res.* 38 (5), 1347–1353.
- Van Geluwe, S., Braeken, L., Robberecht, T., Jans, M., Creemers, C., Van der Bruggen, B., 2011. Evaluation of electro dialysis for scaling prevention of nanofiltration membranes at high water recoveries. *Resour. Conser. Recycl.* 56 (1), 34–42.
- Vaselbehagh, M., Karkhanechi, H., Takagi, R., Matsuyama, H., 2015. Surface modification of an anion exchange membrane to improve the selectivity for monovalent anions in electro dialysis—experimental verification of theoretical predictions. *J. Membr. Sci.* 490, 301–310.
- Veerman, J., Saakes, M., Metz, S.J., Harmsen, G.J., 2009. Reverse electro dialysis: Performance of a stack with 50 cells on the mixing of sea and river water. *J. Membr. Sci.* 327, 136–144.
- Veerman, J., Saakes, M., Metz, S.J., Harmsen, G.J., 2011. Reverse electro dialysis: a validated process model for design and optimization. *Chem. Eng. J.* 166, 256–268.
- Volodina, E., Pismenskaya, N., Nikonenko, V., Larchet, C., Pourcelly, G., 2005. Ion transfer across ion-exchange membranes with homogeneous and heterogeneous surfaces. *J. Colloids Interf. Sci.* 285, 247–258.
- Wijmans, J.G., Baker, R.W., 1995. The solution-diffusion model: a review. *J. Membr. Sci.* 107, 1–21.

- Wood, J., Gifford, J., Arba, J., Shaw, M., 2010. Production of ultrapure water by continuous electrodeionization. *Desalination* 250, 973–976.
- Wu, H.W., 2016. A review of recent development: Transport and performance modeling of PEM fuel cells. *Appl. Energy* 165, 81–106.
- Wyllie, M.R.J., Sauer, M.C., Southwick, P.F., Spriegler, K.S., 1955. Electrical conductance of porous plugs—ion exchange resin-solution systems. *Ind. Eng. Chem.* 47 (10), 2187–2193.
- Xu, T.W., 2002. Electrodialysis processes with bipolar membranes (EDBM) in environmental protection—a review. *Resour. Conserv. Recycl.* 37, 1–22.
- Xu, T.W., 2005. Ion exchange membranes: State of their development and perspective. *J. Membr. Sci.* 263, 1–29.
- Zhang, Y., 2011. Wastewater Reclamation and Ion Fractionation by Electrodialysis. K.U. Leuven, Belgium. Ph.D. Thesis.
- Zhang, Y., Paepen, S., Pinoy, L., Meesschaert, B., Van der Bruggen, B., 2012. Selectrodialysis: fractionation of divalent ions from monovalent ions in a novel Electrodialysis stack. *Sep. Purif. Technol.* 88, 191–201.
- Zhang, Y.; Pinoy, L.; Meesschaert, B.; Van der Bruggen, B. A natural driven membrane process for brackish and wastewater treatment: photovoltaic powered ED-FO system. *Environ. Sci. Technol.* 2013, 47 (18), 10548–10555.
- Zhang, W., Miao, M.J., Pan, J.F., Sotto, A., Shen, J.N., Gao, C.J., Van der Bruggen, B., 2017. Process economic evaluation of resource valorization of seawater concentrate by membrane technology. *ACS Sustain. Chem. Eng.* 5 (7), 5820–5830.
- Zlotorowicz, A., Strand, R.V., Burheim, O.S., Wilhelmsen, Ø., Kjelstrup, S., 2017. The permselectivity and water transference number of ion exchange membranes in reverse electrodialysis. *J. Membr. Sci.* 402–408.

FURTHER READING

Electrodialysis

- Takagi, R., Vasselbehagh, M., Matsuyama, H., 2014. Theoretical study of the permselectivity of an anion exchange membrane in electrodialysis. *J. Membr. Sci.* 470, 486–493.
- Nikonenko, V., Lebedev, K., Manzanares, J.A., Pourcelly, G., 2003. Modeling the transport of carbonic acid anions through anion-exchange membranes. *Electrochim. Acta* 48, 3639–3650.
- Sata, T., Yamaguchi, T., Kawamura, K., Matsusaki, K., 1997. Transport numbers of various anions relative to chloride ions in modified anion-exchange membranes during electrodialysis. *J. Chem. Soc. Faraday Trans.* 93 (3), 457–462.
- Elattar, A., Elmidaoui, A., Pismenskaia, N., Gavach, C., Pourcelly, G., 1998. Comparison of transport properties of monovalent anions through anion-exchange membranes. *J. Membr. Sci.* 143, 249–261.
- Belashovaa, E.D., Pismenskaya, N.D., Nikonenko, V.V., Sistas, P., Pourcelly, G., 2017. Current–voltage characteristic of anion-exchange membrane in monosodium phosphate solution. Modeling and experiment. *J. Membr. Sci.* 542, 177–185.
- Peters, P.B., van Roij, R., Bazant, M.Z., Biesheuvel, P.M., 2016. Analysis of electrolyte transport through charged nanopores. *Phys. Rev. E.* 93, 053108.
- Saracco, G., 1997. Transport properties of monovalent-ionpermselective membranes. *Chem. Eng. Sci.* 52 (17), 3019–3031.

Electro-Electrodialysis

Cattoir, S., Smets, D., Rahier, A., 1999. The use of electro-electrodialysis for the removal of sulfuric acid from decontamination effluents. *Desalination* 121, 123–130.

Continuous Electrodeionization

Arar, Ö., Yüksel, Ü., Kabay, N., Yüksel, M., 2014. Various applications of electrodeionization (EDI) method for water treatment—a short review. *Desalination* 342, 16–22.

Capacitive Deionization

Liu, P.Y., Yan, T.T., Shi, L.Y., Park, H.S., Chen, X.C., Zhao, Z.G., Zhang, D.S., 2017. Graphene-based materials for capacitive deionization. *J. Mater. Chem. A* 5, 13907–13943.

Electrodialysis With Bipolar Membranes

Hurwitz, H.D., Dibiani, R., 2004. Experimental and theoretical investigations of steady and transient states in systems of ion exchange bipolar membranes. *J. Membr. Sci.* 228, 17–43.

Koter, S., Warszawski, A., 2006. A new model for characterization of bipolar membrane electrodialysis of brine. *Desalination* 198, 111–123.

Jaime-Ferrer, J.S., Couallier, E., Viers, P., Rakib, M., 2009. Two-compartment bipolar membrane electrodialysis for splitting of sodium formate into formic acid and sodium hydroxide: Modeling. *J. Membr. Sci.* 328, 75–80.

Hybrid processes based on membrane technology

Patricia Luis

*Materials & Process Engineering (iMMC-IMAP), Catholic University of Louvain,
Louvain-la-Neuve, Belgium*

CHAPTER OUTLINE

8.1 Introduction	302
8.2 Hybrids Based on Pressure-Driven Processes	302
8.2.1 Example 1: Hybrid Nanofiltration-Distillation for Microalgae Extract Concentration	302
8.2.2 Example 2: Water Desalination	303
8.3 Hybrid Processes Based on Pervaporation	308
8.3.1 Example 1: Production of Ethyl Tert-Butyl Ether	308
8.3.2 Example 2: Separation of Methanol/Tetrahydrofuran Mixtures	309
8.3.3 Example 3 Olefin-Paraffin Separation	314
8.3.4 Example 4 Bioethanol Production	315
8.4 Hybrid Processes Based on Gas Permeation	317
8.4.1 Example 1: Hybrid Absorption-Gas Permeation for CO ₂ Capture	317
8.4.2 Example 2: Hybrid Pressure Swing Adsorption—Gas Permeation for Gas Separation	317
8.4.3 Example 3: Hybrids for Biogas Upgrading	320
8.5 Hybrid Processes Based on Membrane Contactors	322
8.5.1 Example 1: Separation of Organic Acids	322
8.5.2 Example 2: Draw Solution Recovery	324
8.5.3 Example 3: Treatment of Wastewater	325
8.6 Hybrid Processes Based on Membrane Bioreactors	326
8.6.1 Example 1: Wastewater Treatment and Reuse	326
8.6.2 Example 2: Drinking Water Denitrification	329
8.6.3 Example 3: Microbial Fuel Cell and Membrane Bioreactor for Wastewater Treatment	332
8.7 Hybrids Based on Electro-Driven Processes	334
8.7.1 Example 1: Brackish and Wastewater Treatment With Production of Potable Water	334

8.7.2 Example 2: Treatment of Industrial Wastewater	335
8.7.3 Example 3: Electricity Generation	337
References	340

8.1 INTRODUCTION

Membrane technology has shown an undoubtedly interest by the research community and industry due to its large number of advantages, such as the easy scale-up of the membrane systems and relatively low energy consumption. However, the application of only one membrane-based system may not lead to an economically or even technically acceptable solution. The application of hybrid processes that combine different kinds of membrane devices or membranes with conventional processes is a way to overcome any limitation. A hybrid process has been defined in the literature as *a process package consisting of generally different, unit operations, which are inter-linked and optimized to achieve a predefined task* (Lipnizki et al., 1999). From this definition, two kinds of hybrids can be defined (Lipnizki et al., 1999):

- Type S(eparation): hybrid processes consisting of processes which are essentially performing the same function. For example, those processes performing separation, such as the combination ultrafiltration-membrane crystallization, or pervaporation-distillation.
- Type R(eactor): hybrid processes that are an offspring of two different processes. For example reaction-separation, such as the combination reaction-pervaporation.

Hybrid processes are more than just integrated processes. *A true hybrid process circumvents the technical limitations (generally thermodynamic) that apply to at least one of the component unit operations* (Lipnizki et al., 1999). Taking this definition as reference, the following sections show several examples of hybrids based on membrane technology. The output of these studies is basically the evaluation of the technical viability of the process, which is key information before an economic and environmental evaluation can be performed.

8.2 HYBRIDS BASED ON PRESSURE-DRIVEN PROCESSES

8.2.1 EXAMPLE 1: HYBRID NANOFILTRATION-DISTILLATION FOR MICROALGAE EXTRACT CONCENTRATION

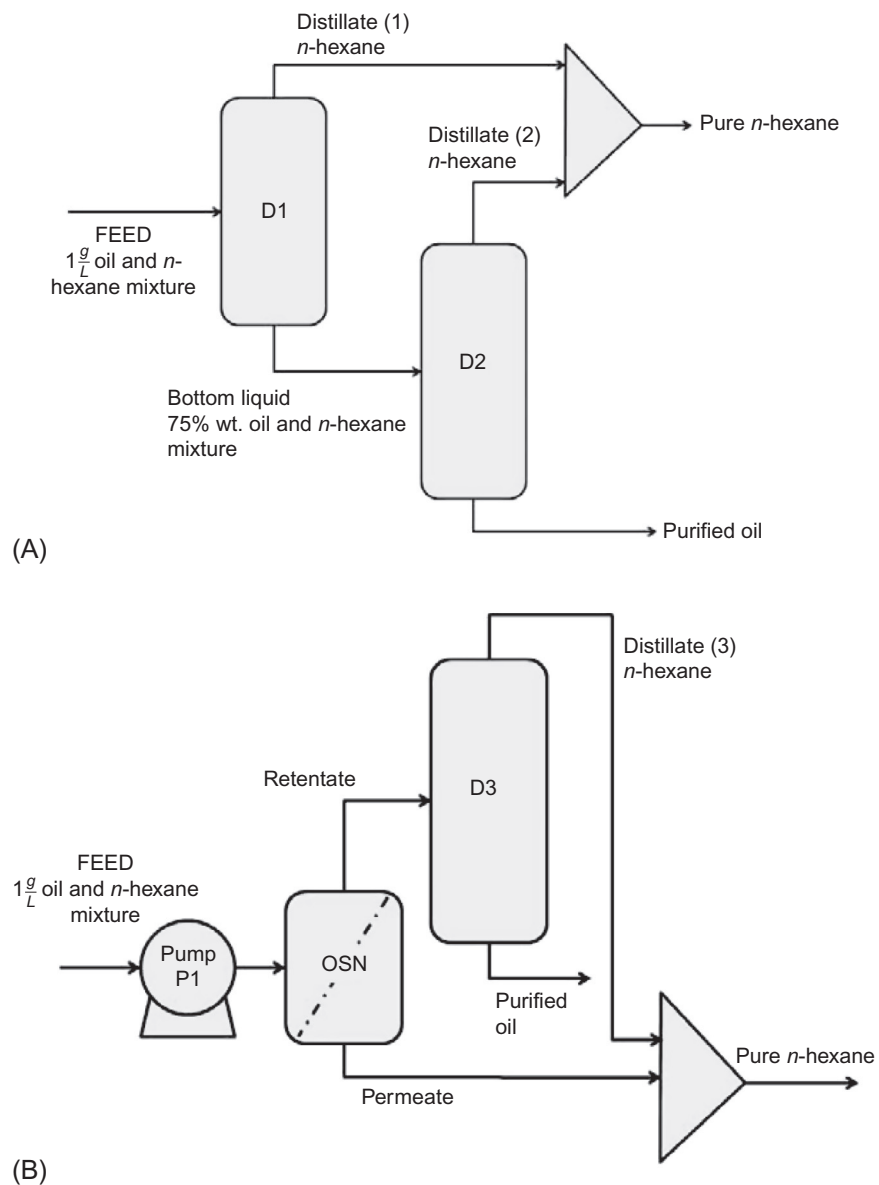
Oil extraction for biofuel production from edible oils such as palm oil, sunflower oil, canola oil, or soybean oil could be questionable since it affects directly the food supply. Microalgae oil has appeared as a new feedstock for the production of biodiesel as well as bioethanol, biosynthesis gas, or bio-oil through thermochemical and biochemical processes (Lopresto et al., 2017). Oil extraction is generally carried out using a solvent, whose recovery is a critical issue in the overall process. Solvent

recovery by organic solvent nanofiltration has been considered in the literature (Lopresto et al., 2017). Lopresto et al. (2017) simulated the conventional process for solvent recovery and a hybrid combining nanofiltration and distillation. The energy consumption and the total cost were calculated. Aspen Plus was used to perform the simulation. The oil component was assumed to be triolein due to the lack of information on algae oil, and UNIFAC was the thermodynamic method to perform the simulation. Fig. 8.1A shows the flowsheet of the conventional process, and Fig. 8.1B the hybrid process. The feed stream consisted of 1000 L/h with 1 g/L of oil.

The conventional process (Fig. 8.1A) includes two distillation columns. The first column concentrates the oil to a concentration of 75 wt.%, which is sent to the second distillation column, which operates under vacuum in order to avoid oil denaturation. In this column, the oil is concentrated to high purity. On the other hand, the hybrid process includes a nanofiltration unit operating at 20 bar that pre-concentrate the oil before being sent to distillation. In the retentate stream, the oil concentration was 10 wt.%. In the permeate stream, the solvent was almost pure. In the distillation column, pure oil was then produced. From the simulation results, it was observed that energy consumption of the hybrid process was much lower than the conventional one. However, in terms of cost, the hybrid process led to a higher overall cost due to the investment on membrane units. For the conventional process, the main cost is due to the heat exchangers of the distillation columns. Thus even though the total cost of the hybrid is larger than the conventional process, the higher cost of utilities in the conventional process is burden over time and the hybrid will become more interesting after 5–10 years of operation.

8.2.2 EXAMPLE 2: WATER DESALINATION

Membrane technology has conquered the application of provision of clean water from sea water desalination. However, the main environmental challenge is brine discharge. Reverse osmosis (RO) was considered the leading technology for this purpose but currently, forward osmosis (FO) has appeared in the picture to lower the energy consumption. In addition, it employs various draw solution recovery methods. Mazlan et al. (2016) simulated several configurations based on reverse osmosis and forward osmosis. The mathematical models used in the simulation and not present in the software library were programmed in Matlab, and embedded in the Aspen Plus environment. The interoperability between the modeling tool, Matlab, and the process simulation suite, Aspen One, was achieved using CAPE-OPEN interface standards (Peshev and Livingston, 2013). Fig. 8.2 shows the two main desalination processes studied in their work: (a) Reverse osmosis (RO) with ultrafiltration (UF) pretreatment; and (b) forward osmosis (FO) with UF pretreatment and varying draw solution recovery methods (nanofiltration (NF) for the recovery of MgSO_4 draw solution; UF for the recovery of polyacrylic acid-nanoparticles (PAA-NP) and, distillation for the recovery of $\text{CO}_2\text{-NH}_3$ draw solution). The main objective was to calculate the specific energy consumption (SEC) of each alternative.

**FIG. 8.1**

Solvent recovery in the concentration of microalgae oil: (A) conventional process; (B) hybrid nanofiltration-distillation process.

Reproduced with permission from Lopresto, C.G., Darvishmanesh, S., Amelio, A., Mazinani, S., Ramazani, R., Calabrò, V., Van der Bruggen, B., 2017. Application of organic solvent nanofiltration for microalgae extract concentration. *Biofuels, Bioprod. Biorefin.* 11(2), 307–324.

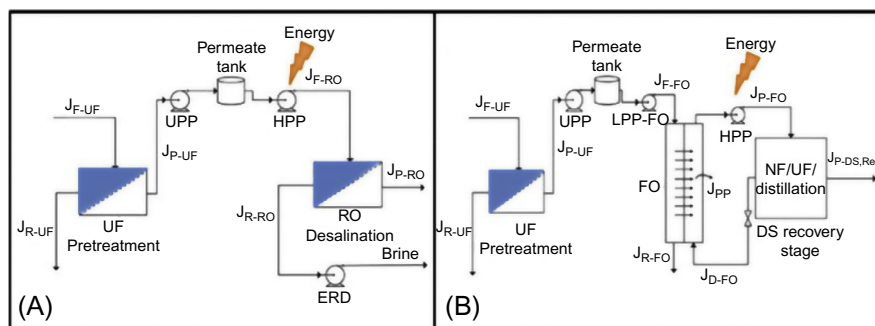


FIG. 8.2

Desalination process flowsheets considered in this study for comparison of specific energy consumption. (A) RO desalination process with UF membrane pretreatment. (B) FO desalination process with UF membrane pretreatment and varying draw solution recovery methods.

Fig. 8.3 shows the comparison of SEC and specific membrane area between a single-stage RO, FO with NF recovery, FO with two-stage NF recovery, two-stage RO, FO-UF and FO-distillation at 50% and 75% product recovery, considering the effects of pretreatment as well. The authors indicated a very low energy consumption for the FO stage (e.g., $\sim 0.11 \text{ kWh m}^{-3}$) at 50% recovery since the process is driven by osmotic pressure instead of hydraulic pressure difference and the low pressure pump (LPP) only needs to overcome the pressure drop in the feed channel (Mazlan et al., 2016). At 75% product recovery, no difference in the specific energy consumption was found between the FO with two-stage NF recovery process and the two-stage RO. The FO with $\text{CO}_2\text{-NH}_3$ DS recovery process utilizing distillation had the lowest specific energy consumption compared to all other processes. As general conclusion, it can be said that there is effectively no difference in SEC between the FO with NF recovery and RO processes. Furthermore, Mazlan et al. (2016) concluded that even if any of the membranes, FO, RO, or NF had infinite permeabilities and 100% rejection, it would not change the SEC significantly. This analysis can be generalized for any pressure-driven membrane process used for the desalination recovery stage.

Valladares Linares et al. (2016) performed an economic analysis on capital and operational expenses (CAPEX and OPEX) for (i) a hybrid forward osmosis-low-pressure reverse osmosis (FO-LPRO) process, (ii) a conventional seawater reverse osmosis (SWRO) desalination process, and (iii) a membrane bioreactor-reverse osmosis-advanced oxidation process (MBR-RO-AOP) for wastewater treatment and reuse. Fig. 8.4A shows the cost of the treatment plants for each scenario, and Fig. 8.4B presents the total cost of water production per cubic meter. It can be observed that the FO-LPRO hybrid membrane system has a 21% higher CAPEX

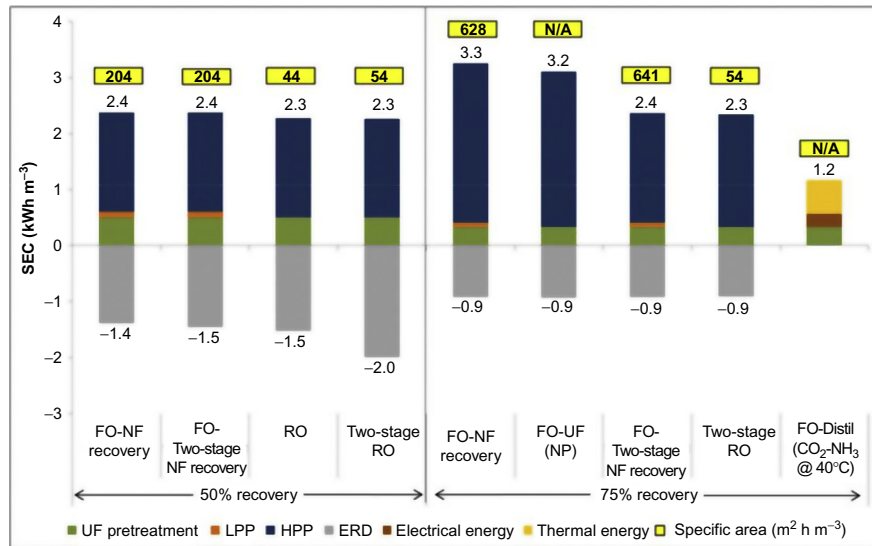


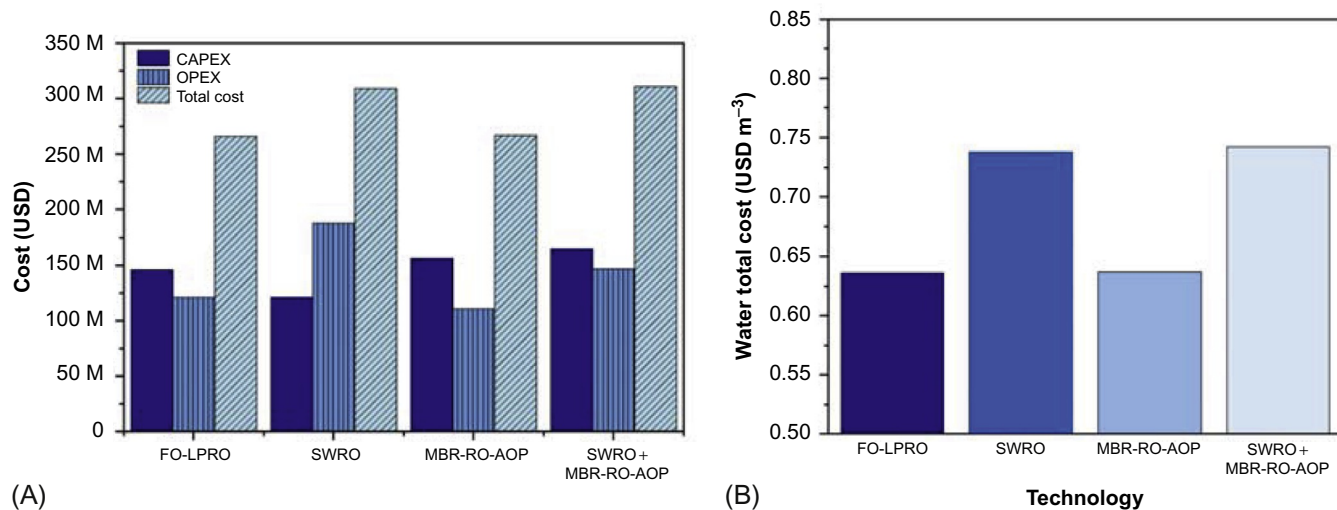
FIG. 8.3

Comparison of SEC and specific membrane area between FO with NF recovery, FO with two-stage NF recovery, single-stage RO, two-stage RO, FO-UF, and FO-distillation at 50% and 75% product recovery. Energy contributions from the pretreatment stage, low pressure pump (LPP), high pressure pump (HPP), energy recovery device (ERD), and distillation are shown in each process.

Reproduced with permission from Mazlan, N.M., Peshev, D., Livingston, A.G., 2016. Energy consumption for desalination—a comparison of forward osmosis with reverse osmosis, and the potential for perfect membranes. *Desalination* 377, 138–151.

and 56% lower OPEX due to saving in energy consumption and fouling control. For the total cost of the project (CAPEX + OPEX), the most economically feasible scenario is the FO-LPRO plant. In addition, the FO-LPRO scenario has the lowest cost of water at USD 0.636 per m³. The MBR-RO-AOP scenario has a very similar cost of USD 0.637 per m³ (Valladares Linares et al., 2016).

Water desalination is becoming more and more necessary in the current global scenario. Seawater is one of the target sources of water but not the only one. Treated wastewater for potable use is an option that may need to be considered seriously due to the current water stress in some parts of the planet. Hybrids based on pressure-driven membrane systems have demonstrated to reach very high quality of water, meeting the standards of the World Health Organization. The social perception is the main barrier that limits the real use of treated wastewater for consumption purposes. The case of direct use of treated wastewater as potable water in Windhoek (Namibia) is the only case in which social acceptance has been achieved (du Pisani, 2006; Wintgens et al., 2005).

**FIG. 8.4**

(A) Capital expenses (CAPEX) and operational expenses (OPEX) for the four water treatment scenarios analyzed for seawater desalination and wastewater recovery and reuse; (B) Total cost of water production per m³ for each water treatment technology. The plant water production capacity is 100,000m³d⁻¹.

Reproduced with permission from Valladares Linares, R., Li, Z., Yangali-Quintanilla, V., Ghaffour, N., Amy, G., Leiknes, T., Vrouwenvelder, J.S., 2016. Life cycle cost of a hybrid forward osmosis e low pressure reverse osmosis system for seawater desalination and wastewater recovery. *Water Res.* 88, 225–234.

8.3 HYBRID PROCESSES BASED ON PERVAPORATION

Pervaporation has been commonly proposed in combination with reaction or distillation. The hybrid pervaporation reactor is of interest to perform reactions that are limited by the equilibrium such as esterification or transesterification reactions. In this case, one of the reaction products (ideally the desired product) is removed from the solution, displacing the equilibrium according to Le-Chatelier principle and increasing the product yield. On the other hand, the hybrid pervaporation-distillation is very common when azeotropic mixtures are present. An azeotrope increases the energy consumption of the distillation process significantly since more advanced distillation, such as azeotropic distillation or pressure swing distillation, is required. Using pervaporation gives the advantage of not having thermodynamic limitations due to the azeotrope, thus that mixture can be separated if the membrane is selective to one of the compounds. Stand-alone pervaporation may not be technically or economically attractive, but its integration with distillation is a very interesting option to minimize energy consumption and respond to the industrial demands.

8.3.1 EXAMPLE 1: PRODUCTION OF ETHYL TERT-BUTYL ETHER

The etherification reaction of isobutene (IB) with ethanol (EtOH) to produce ethyl tert-butyl ether (ETBE) is an equilibrium-limited reaction that is performed industrially using an acid catalyst. The etherification reaction is highly selective so that only isobutene is converted into ether; an excess of alcohol is usually fed to the reactors in order to achieve high conversions of isobutene (Norkobilov et al., 2017). The reaction is performed in two reactors, the first one operating at up to 90°C, while the second reactor operates in the range 50–60°C. In this way, high rates of conversion are achieved. The product of the second reactor is sent to a distillation column for further purification. An azeotrope between ethanol and ETBE can be found at 21.7wt% ethanol at 1 bar and 65.6°C. Thus simple distillation is not able to achieve high product purity and other systems, such as pressure swing distillation, are used. In order to decrease energy consumption, pervaporation has been presented as a technological alternative. However, stand-alone pervaporation may not be technically or economically feasible. Norkobilov et al. (2017) studied the technical and energy performance of several hybrid distillation-pervaporation processes using a PERVAP 2256 membrane. Two main hybrid configurations were evaluated: (i) the pervaporation unit before the distillation column; or (ii) the pervaporation unit after the column on a side stream or directly in the distillate stream of the column. Fig. 8.5 shows the conventional process and the proposed hybrid alternatives.

The Aspen Custom Modeler (ACM) software was used to simulate the pervaporation process. The ACM model was then exported to Aspen Plus software to integrate the pervaporation membrane module into the studied flowsheets. The authors found that the hybrid process designed in case C, in which the pervaporation modules are located on a side stream withdrawn from the distillation column, is more favorable in energy consumption and it shows lower content of ethanol in distillate stream than

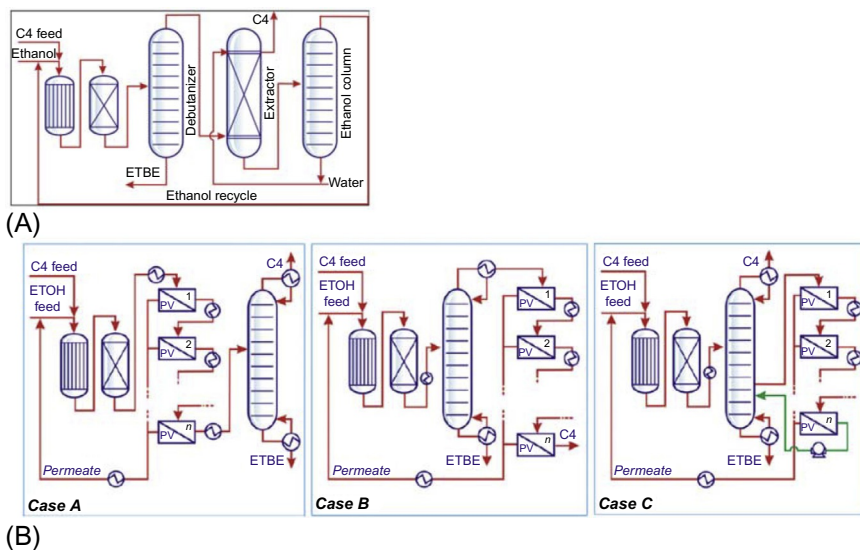


FIG. 8.5

Diagram of the conventional Huels process for ETBE production: (A) conventional process; (B) Three possible hybrid distillation-pervaporation configurations.

Reproduced with permission from Norkobilov, A., Gorri, D., Ortiz, I., 2017. Process flowsheet analysis of pervaporation-based hybrid processes in the production of ethyl tert-butyl ether. *J. Chem. Technol. Biotechnol.* 92, 1167–1177.

other membrane integrated hybrid processes. In addition, recycling the permeate rich in ethanol to the reaction area showed a slight increase in the conversion of isobutene of 0.943.

8.3.2 EXAMPLE 2: SEPARATION OF METHANOL/TETRAHYDROFURAN MIXTURES

Tetrahydrofuran (THF) is commonly used as solvent, reaction medium, and starting material for various syntheses in the chemical industry, for example, for preparing adhesives, special paints, coatings, fibers, in the extraction of specific active substances, for recrystallization of certain compounds or as starting material for various syntheses in a number of reactions. After these uses, the THF is often contaminated with methanol or methanol and water (Krug and Palm, 1996). Recovery of THF could be attractive if a technological solution is proposed (Luis et al., 2014). Conventional distillation is not possible due to a methanol/THF azeotrope. Pressure swing distillation is a conventional technology to perform the separation since the azeotrope is pressure sensitive. The azeotrope contains 31 wt% methanol (boiling point: 59°C) under atmospheric pressure (minimum azeotrope), and 50 wt% methanol (boiling point: 102°C) at 4 atm. Thus two distillation columns working under

different pressures allow the separation of THF and methanol (Fig. 8.6A). However, this process is energetically very demanding. Pervaporation appears as a technology able to minimize the energy consumption. Luis et al. (2014) evaluated the membrane performance and its effect on the recovery of the solvent and energy demand. A pervaporation unit was placed after a conventional distillation so that the feed stream that goes to the pervaporation unit has a concentration closer to the azeotropic point (Fig. 8.2B). In addition to the technical viability, a life cycle assessment (LCA) was performed to quantify the main impacts that the production and recovery of THF and methanol can produce, including impacts from raw material extraction, solvent production, use of energy and ancillaries, as well as waste-solvent treatment. The input data required to perform the LCA is obtained from the simulation of the process, including the requirements of steam, cooling water and electricity for pressure swing distillation, and steam, cooling water, liquid nitrogen, and electricity in the hybrid distillation-pervaporation. The objective was to achieve a purity of 99% for methanol and THF, establishing each time one target compound (methanol or THF) in the mixture, that is, indicating a target recovery of 99% of one of the components in the mixture. The waste stream that was not recovered was sent to a generic incinerator with energy recovery (Luis et al., 2014). Aspen Plus v7.2 and Aspen HYSYS v7.1 were used to simulate pressure swing distillation (two distillation columns) and the hybrid distillation-pervaporation. SimaPro software was used to perform the LCA.

The flowsheet presented in Fig. 8.6A led to energy requirements of 19,875 kJ/h. Instead, when using pervaporation as indicated in Fig. 8.6B, the energy requirements are 2775 kJ/h. Thus a dramatic decrease in energy consumption can be observed when pervaporation is used instead of the second distillation column. The reason was the composition of the recycle stream since the use of pervaporation allows its concentration, decreasing the energy requirements in the first distillation column. Thus from the point of view of energy consumption, the hybrid process presents a large advantage over pressure swing distillation. Nevertheless, the degree of separation caused by the membrane will have a direct impact on the energy consumption. Fig. 8.7 shows the effect of the separation factor on the energy consumption and the product composition. Two kinds of situations are considered: membranes with low flux and high separation factor (Fig. 8.7A) and membranes with high flux and low separation factor (Fig. 8.7B). Membranes that achieve high flux of methanol decrease the energy consumption even though the separation factor is small. In contrast, high methanol-selective membranes with low flux involve high energy consumption unless the separation factor is higher than 1000. This is due to the larger amount of solvent that is recycled to the distillation column if low-flux membranes are used. This thermal energy could be decreased by using more membrane surface, although it would increase the energy consumed by the pervaporation as well as the investment cost (Luis et al., 2014).

From the LCA, the environmental impact of each process can be determined. The first two columns in Fig. 8.8A and B show the results for pressure swing distillation when methanol (first column) or THF (second column) is the target compound to be

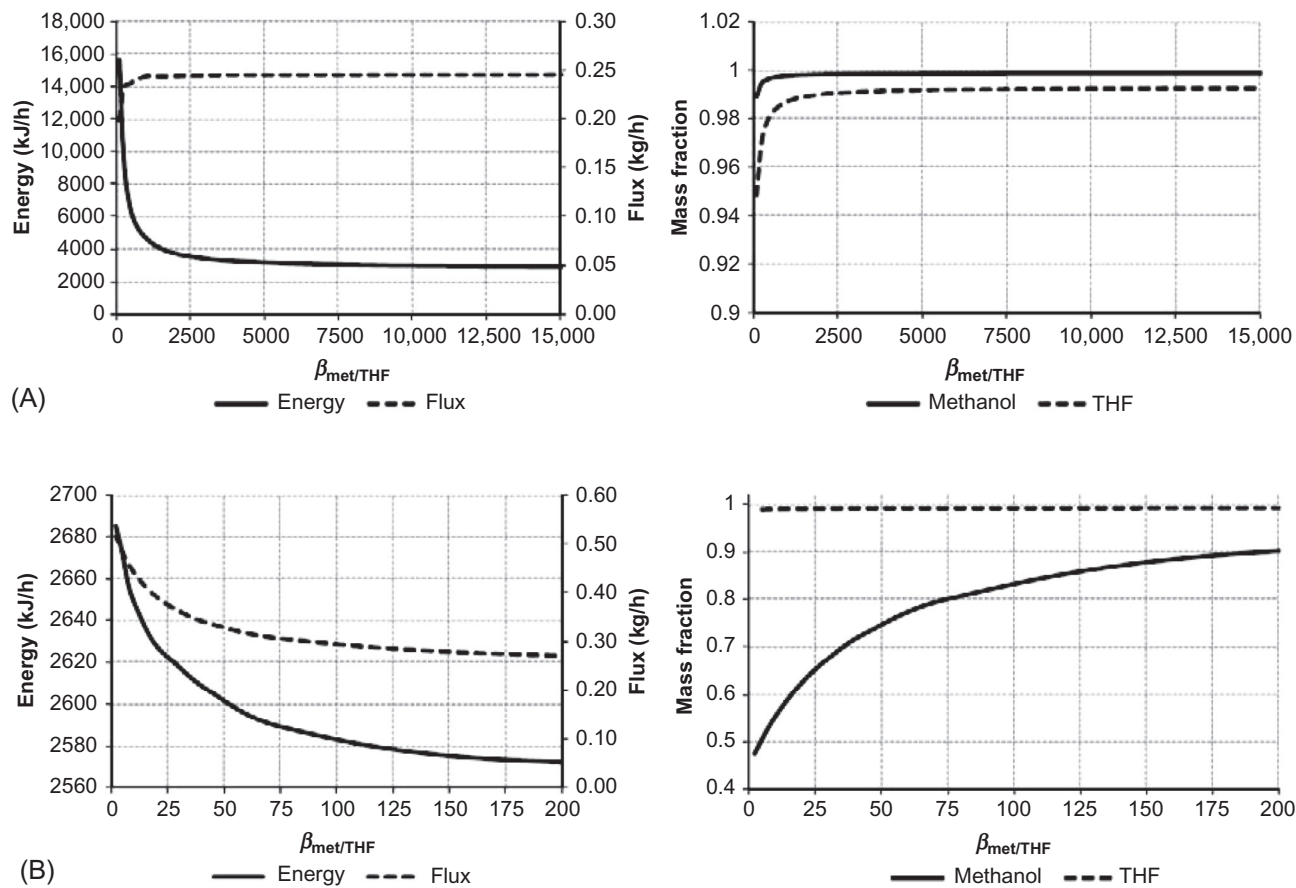


FIG. 8.7

Energy requirement and flux (left) and product composition (right) as a function of the separation factor for a feed of 25wt% methanol/75wt% THF. (A) Low flux—high separation factor; (B) high flux—low separation factor.

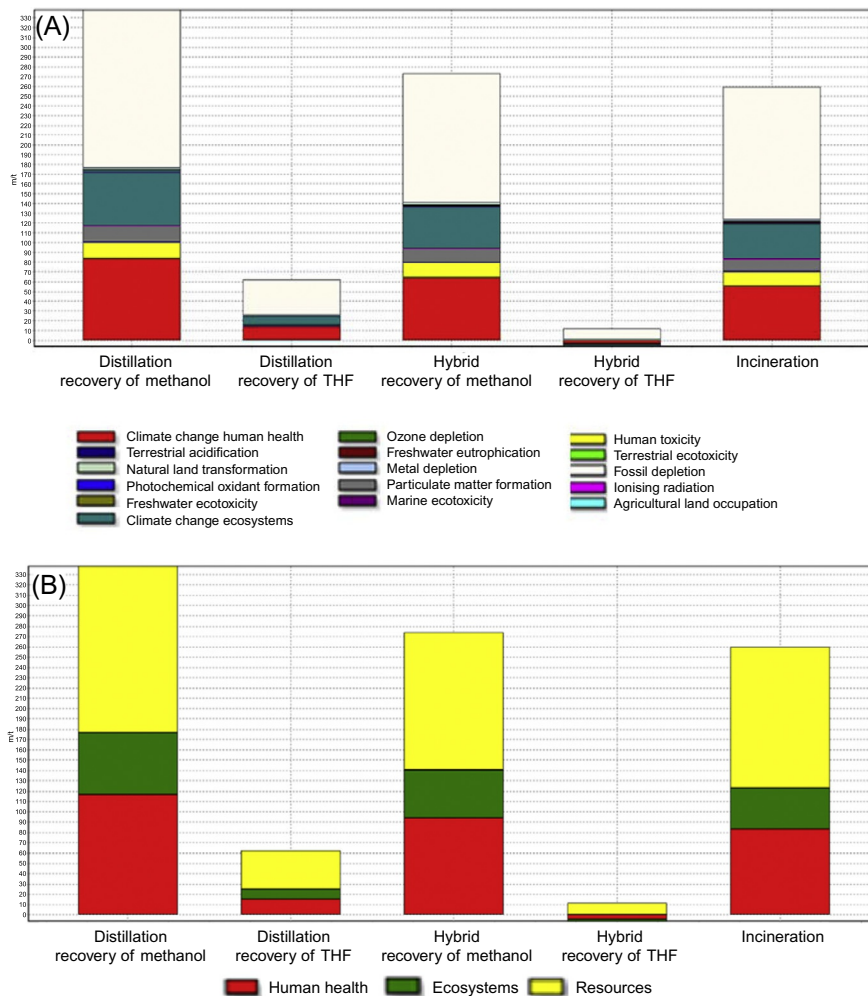


FIG. 8.8

Environmental impact (ReCiPe) when pressure swing distillation (focused on methanol—first column or THF recovery—second column), hybrid distillation-pervaporation (focused on methanol—third column or THF recovery—fourth column), and incineration are considered for a mixture of 25wt% methanol/75wt% THF: (A) mid-points categories; (B) end-points categories (i.e., Human Health, Ecosystem Quality and Resources).

recovered. The same is shown for the hybrid process in the third and fourth columns. The last column refers to incineration. Clearly, the hybrid distillation-pervaporation produces the lowest environmental impacts when THF is the target compound to be recovered. This is due to the high impact caused during the production of this solvent (Luis et al., 2013; Amelio et al., 2014). On the other hand, recovery of methanol

produces higher impact than incineration, which confirms the fact that THF is the only solvent worthy to be recovered (Luis et al., 2014). Combination of the technical and environmental evaluation is thus of utmost importance in the rational design of novel processes or treatment alternatives.

8.3.3 EXAMPLE 3: OLEFIN-PARAFFIN SEPARATION

Olefins, such as ethylene and propylene, are intermediate products in the petrochemical industry. Their separation from paraffin is a very energy-intensive process since it is commonly performed via cryogenic distillation. Very high columns are required (more than 200 trays) due to the close molecular weight and boiling point, as well as their relative volatility (Barakat and Sørensen, 2008; Takht Ravanchi et al., 2009). Thus the development of membrane/distillation hybrid systems has attracted the attention of the research community in order to decrease the energy consumption by locating the membrane unit beside the distillation tower so that a part of the separation is undertaken by the membrane (Pedram et al., 2014). A variation of pervaporation in which a liquid phase is fed into the membrane unit, is vapor permeation, characterized by having a vapor feed stream. Determining the optimal position of the membrane along the column and the minimal energy consumption of the hybrid are the key issues in the design of the hybrid (Kookos, 2003; Olujić et al., 2010; Caballero et al., 2009; Pettersen et al., 1996; Ayotte-Sauve et al., 2010; Moganti et al., 1994). Pedram et al. (2014) evaluated different optimization options for distillation/membrane hybrid systems (Fig. 8.9), minimizing the number of trays and reflux ratio of the distillation column. HYSYS was used as the process simulator and MATLAB as the mathematical tool for modeling the hybrid process.

The four different hybrid configurations shown in Fig. 8.10 present the membrane system located in different positions: (a) at the top of the distillation column (the distillate stream is the membrane feed), (b) at the bottom of the distillation column (the heavy fraction is the membrane feed), (c) the membrane is located in parallel to the distillation column so that the membrane feed is a side stream from the column and its product will feed back into the column, (d) the membrane is located in a front configuration in which the main feed enters the membrane and its products pass to the distillation column to be further purified. In cases (a) and (b), the final purification is performed by the membrane unit and the retentate and permeate streams will feed back into the column, respectively. The membrane feed is supposed to be saturated vapor and the feed into the tower as saturated liquid (Pedram et al., 2014).

The results obtained by Pedram et al. (2014) confirmed that using a membrane along with a distillation tower in a hybrid configuration brings remarkable advantages in terms of reduction of the size of the distillation column and energy consumption. Indeed, the number of trays could be reduced as much as 30% when the reflux ratio is fixed by increasing the feed flow rate to the membrane unit. Thus the investment costs are reduced, with spending the same operating costs. On the other hand, with fixing the number of trays, the reflux ratio can be decreased up to 50%, thus

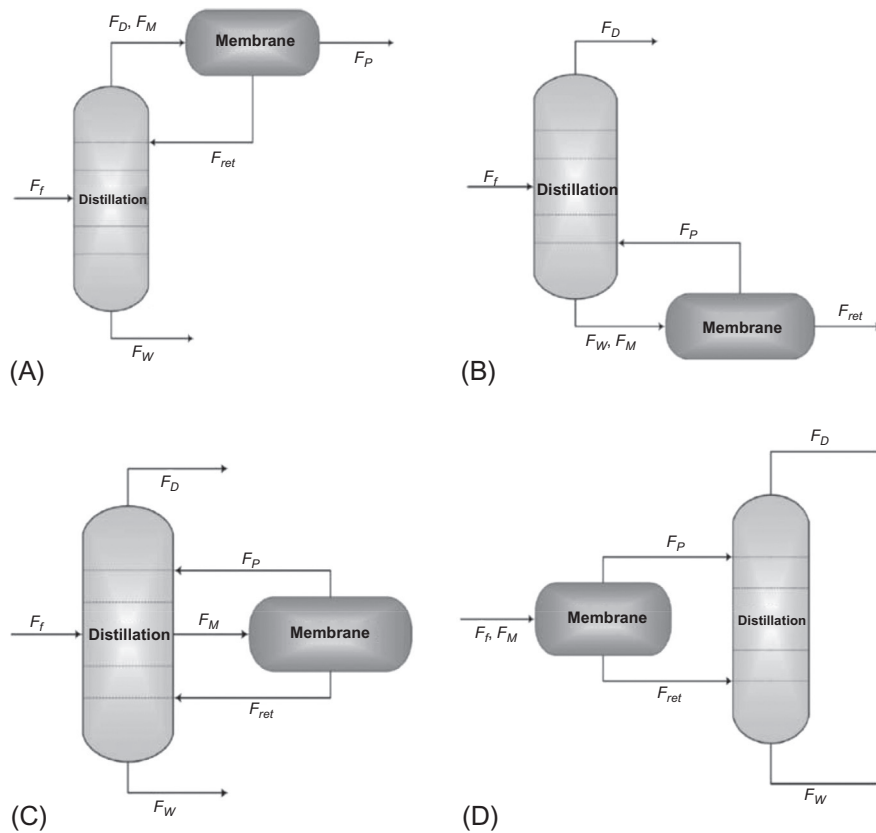


FIG. 8.9

Hybrid system configurations, (A) top, (B) bottom, (C) parallel, and (D) front.

Reproduced with permission from Pedram, S., Kaghazchi, T., Takht Ravanchi, M., 2014. Performance and energy consumption of membrane-distillation hybrid systems for olefin-paraffin separation. *Chem. Eng. Technol.* 37, 4, 587–596.

decreasing the operating costs with keeping the investment cost. In addition, in the hybrid configuration, a more purified product can be obtained. The hybrids membrane/distillation column are thus an excellent alternative to improve conventional separations.

8.3.4 EXAMPLE 4: BIOETHANOL PRODUCTION

Bioethanol is considered as a clean and renewable fuel with major environmental benefits. It can be produced from different kinds of renewable feedstock: sugarcane, corn, wheat, cassava (first generation), cellulose biomass (second generation), and algal biomass (third generation) (Baeyens et al., 2015). The produced bioethanol is very diluted in an aqueous solution, thus it has to be purified. Distillation can

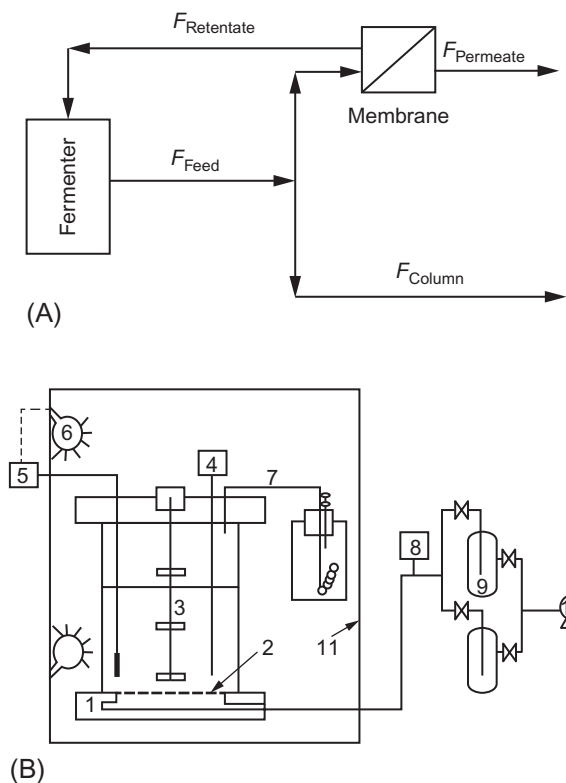


FIG. 8.10

Hybrid reaction-pervaporation for bioethanol production: (A) reaction and pervaporation in different devices; (B) the pervaporation membrane is integrated inside the reactor (1—MBR; 2—Membrane; 3—Feed solution; 4—Sampling port; 5—Temperature controller; 6—Heater; 7—CO₂ outlet; 8—Pirani gauge; 9—N₂ cold trap; 10—Vacuum pump; 11—Temperature preservative box).

concentrate ethanol to the azeotropic mixture, which has a concentration of 95.6 vol% of ethanol. Further concentration of ethanol requires other alternatives than distillation. Baeyens *et al.* (2015) presented a hybrid configuration reaction-pervaporation to reduce the ethanol concentration in the fermenter below the inhibition threshold limit of about 12 vol%. The continuous removal of ethanol would increase the yield of the fermenter. Fig. 8.10A shows the schema of the proposed hybrid. In this case, the pervaporation unit is an independent device (outside the reactor) that receives the fermentation broth but the membrane could be integrated inside the reactor so that no recycle of retentate is required, as indicated in Fig. 8.10B (Esfahanian *et al.*, 2013). The objective of the pervaporation membrane is two-fold: (i) to remove ethanol from the reaction mixture so that the product yield is increased in equilibrium-limited reactions; and (ii) to concentrate ethanol beyond the

azeotropic concentration. Using these configurations may achieve both objectives but the membrane permeability and selectivity will determine the benefit obtained by the use of pervaporation.

8.4 HYBRID PROCESSES BASED ON GAS PERMEATION

8.4.1 EXAMPLE 1: HYBRID ABSORPTION-GAS PERMEATION FOR CO₂ CAPTURE

Capture of carbon dioxide is commonly carried out by absorption-desorption processes using organic solvents, such as diethylamine or monoethylamine. The main concern of this process is the high energy consumption during the regeneration of the solvent (desorption step). Novel processes based on membrane technology are widely studied. One example is the development of hybrids consisting of the conventional absorber and gas permeation. Freeman et al. (2014) presented two different configurations (e.g., in series and in parallel). In the series configuration, the absorber removes approximately half of the CO₂ in the flue gas, followed by additional separation by the membrane contactor to achieve 90% total removal of CO₂ by the hybrid capture system. Boiler combustion air is used as a sweep gas on the membrane permeate side while passing carbon dioxide-rich flue gas at the same pressure across the membrane feed side. In this way, the partial pressure of the carbon dioxide on the permeate side is maintained lower than on the feed side. Carbon dioxide then passes from the flue gas into the sweep air stream that goes to the boiler. The result is to enrich the CO₂ content in the flue gas from a coal-fired power plant from 13% to ~23%. In the parallel configuration, the flue gas leaving the power plant is split and treated by each system in a parallel arrangement. The principal advantage is that the absorber can be around half the size it would normally be. Fig. 8.11 shows both configurations.

As a major conclusion, it was found that the hybrid process offers the potential for two modes of cost savings: a reduction in regeneration energy in the series case and a reduction in capital costs in the parallel case.

8.4.2 EXAMPLE 2: HYBRID PRESSURE SWING ADSORPTION—GAS PERMEATION FOR GAS SEPARATION

Pressure swing adsorption (PSA) is an alternative to cryogenic gas separation that achieves very high purity. Gas permeation using membranes has also become a common technology for gas separation, mainly when product purity requirements are less severe. Esteves and Mota (2002) presented an optimized gas separation process integrating membranes and PSA aiming at the separation of H₂/CH₄ mixtures, improving product purity and/or recovery compared to the stand-alone systems. Fig. 8.12 presents the schematic diagram of the hybrid cyclic process developed for bulk separation of a binary mixture using a membrane device and a dual-bed PSA unit.

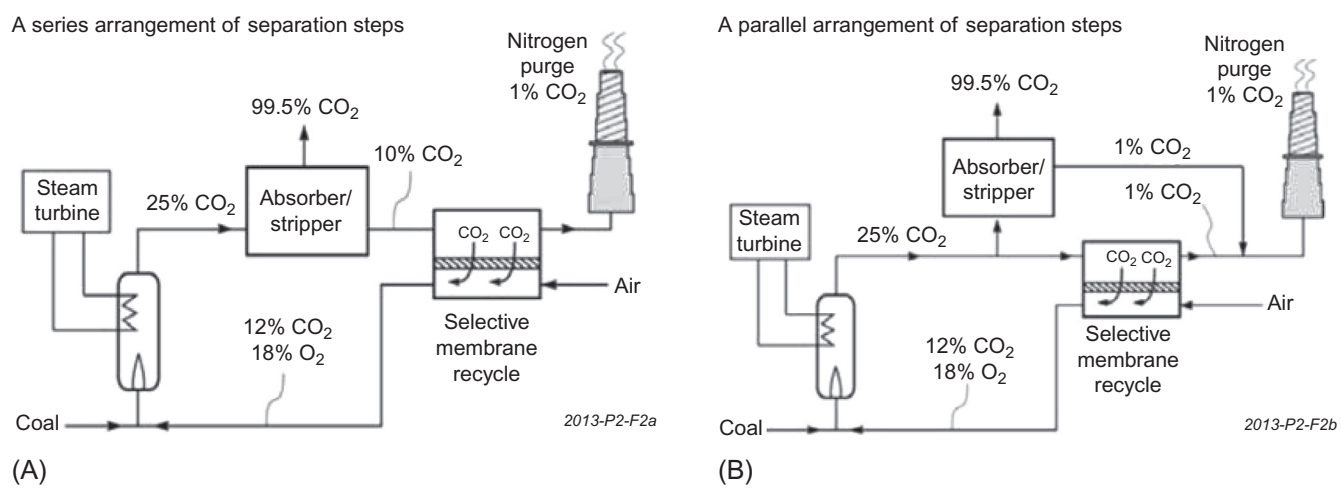


FIG. 8.11

Hybrid design for CO₂ capture: (A) Hybrid series arrangement, and (B) hybrid parallel arrangement.
 Reproduced with permission from Freeman, B., Hao, P., Baker, R., Kniep, J., Chen, E., Ding, J., Zhang, Y., Rochelle, G.T., 2014. Hybrid membrane-absorption CO₂ capture process. *Energy Procedia* 63, 605–613.

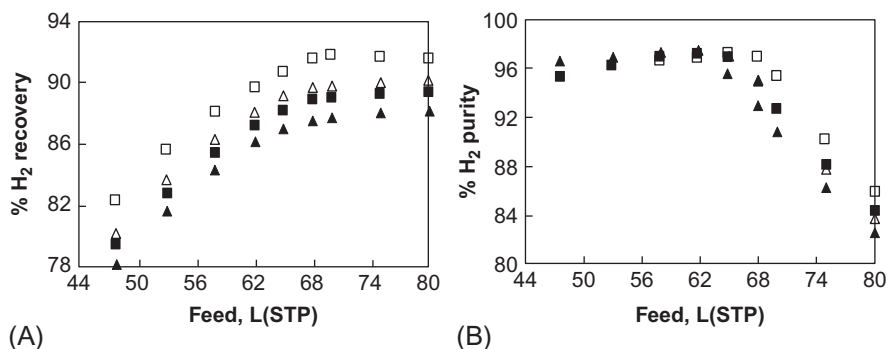


FIG. 8.13

Impact of feed flow rate on H₂ product purity (A) and recovery (B) for stand-alone PSA (△, P , =35 bar; ▲, P , =2.5 bar) and for the hybrid gas permeation-PSA (□, P , =35 bar; ■, P , =25 bar).

Reproduced with permission from Esteves, I.A.A.C., Mota, J.P.B., 2002. Simulation of a new hybrid membrane/pressure swing adsorption process for gas separation. *Desalination* 148, 275–280.

performance. Thus the hybrid using membrane gas permeation increases the treatment capacity of the overall process.

8.4.3 EXAMPLE 3: HYBRIDS FOR BIOGAS UPGRADING

Updated biogas could substitute natural gas for energy supply and as feedstock for chemical synthesis. However, H₂S, water vapor, and mainly CO₂ have to be removed from CH₄ to enhance the heating value of the product gas. The raw gas contains around 60 mol% of CH₄ and it should be increased to more than 96 mol% in order to meet the natural gas requirements (Scholz et al., 2013). Common techniques for biogas upgrading are amine scrubbing, pressurized water scrubbing, pressure swing adsorption, and gas permeation. In addition, hybrids that combine gas permeation with established separation processes would merge the advantages of both technologies. Scholz et al. (2013) analyzed seven different membrane hybrid processes for biogas upgrading. A single gas permeation stage was combined with pressurized water scrubbing, amine absorption, cryogenic separation, and a particular process in which the permeate of the gas permeation stage drives a gas engine. The authors' idea was to consider two main situations: one in which the membrane is used for the bulk removal of CO₂ and the conventional separation equipment performs the final purification, and a second one where the conventional separation technology is used to enhance the CH₄ recovery by separating CO₂ and CH₄ in the permeate stream of the gas permeation stage. Figs. 8.14–8.16 show the proposed hybrids in the study. An economic evaluation was carried out and the results were compared with those obtained considering an individual three-stage membrane process as well as conventional separation processes. The simulation was performed in Aspen Plus.

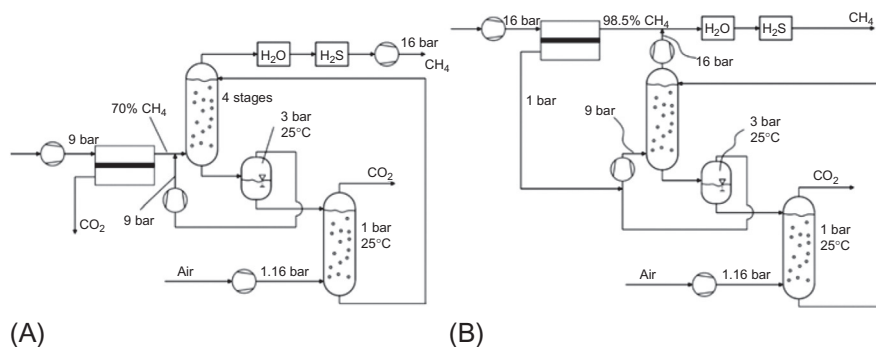


FIG. 8.14

Membrane hybrid processes in which gas permeation technology is combined with pressurized water scrubbing equipment. (A) Membrane hybrid process in which the retentate stream of the membrane is fed to a pressurized water scrubbing absorber which is referred to as *PWS 1*. (B) Membrane hybrid process in which the permeate stream of the membrane is fed to a pressurized water scrubbing absorber which is referred to as *PWS 2*.

Reproduced with permission from Scholz, M., Frank, B., Stockmeier, F., Falß, S., Wessling, M., 2013. Techno-economic analysis of hybrid processes for biogas upgrading. *Ind. Eng. Chem. Res.* 52, 16929–16938.

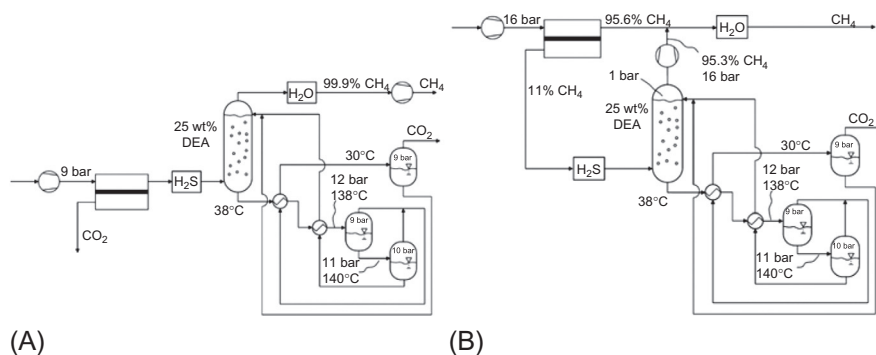


FIG. 8.15

Membrane hybrid processes in which gas permeation technology is combined with amine scrubbing equipment. (A) Membrane hybrid process in which the retentate stream of the membrane is fed to an amine scrubbing absorber. This process is referred to as *Amine 1*. (B) Membrane hybrid process in which the permeate stream of the membrane is fed to an amine scrubbing absorber. This process is referred to as *Amine 2*.

Reproduced with permission from Scholz, M., Frank, B., Stockmeier, F., Falß, S., Wessling, M., 2013. Techno-economic analysis of hybrid processes for biogas upgrading. *Ind. Eng. Chem. Res.* 52, 16929–16938.

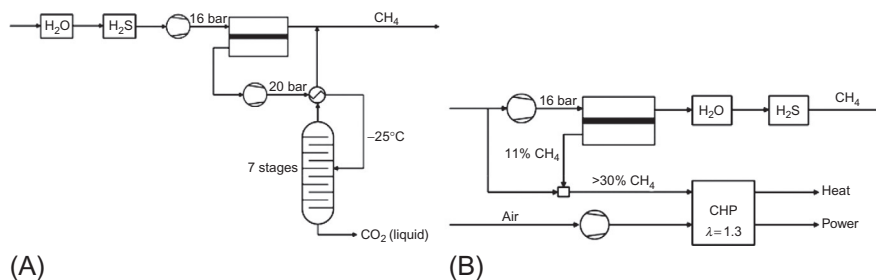


FIG. 8.16

Membrane hybrid processes in which (A) a cryogenic separation separates the gases from the permeate stream of the membrane module; (B) the permeate of the membrane stage is used to drive a combined heat and power engine. (A) Membrane hybrid process in which the permeate of the gas permeation membrane is compressed and separated in a low temperature distillation column. This process is referred to as *Cryogen*. (B) Gas permeation process connected to an engine which used the permeate stream as well as air and a fraction of the raw biogas to provide both, heat and power. This process is referred to as *CHP*.

Reproduced with permission from Scholz, M., Frank, B., Stockmeier, F., Falß, S., Wessling, M., 2013. *Techno-economic analysis of hybrid processes for biogas upgrading*. *Ind. Eng. Chem. Res.* 52, 16929–16938.

The CHP process (hybrid combined heat and power process) shows the lowest CH_4 recovery since a major fraction of the raw gas is used to drive the gas engine. In addition, those processes in which the single gas permeation membrane performs the bulk separation and the conventional process equipment is used for final purification, presented significant CH_4 losses via the permeate of the membrane stage, resulting in low CH_4 recoveries (Scholz et al., 2013)

The specific upgrading costs are lower for the hybrid compared to the conventional scrubbing process, and for the amine absorption process, the process configuration in which the membrane performs the bulk separation and the scrubber does the final gas polishing is the only hybrid that seems to be better than the conventional amine absorption process (Scholz et al., 2013). Thus hybrid processes with membrane technology give competitive alternatives to conventional processes.

8.5 HYBRID PROCESSES BASED ON MEMBRANE CONTACTORS

8.5.1 EXAMPLE 1: SEPARATION OF ORGANIC ACIDS

Enzymatic and biotechnological fermentation processes are alternative routes in the chemical and pharmaceutical industry instead of conventional and well-established chemical methods for the synthesis of target products and their intermediates.

The extraction of components from the reaction media is evolving toward the use of two- and three-phase systems integrated with transformation or even forming hybrid systems with biotransformation and separation occurring in one space (Schlosser et al., 2005). Schlosser et al. (2005) reviewed the recovery and separation of organic acids by membrane-based solvent extraction and pertraction, including interesting examples of hybrid processes using those technologies, such as the extraction of itaconic acid using a hybrid bioreactor with supported liquid membranes (Bressler and Braun, 2000), the extraction of fumaric acid using solvent extraction (Bressler et al., 2002), or the recovery of *s*-phenylethanol using membrane-based solvent extraction (Rissom et al., 1999) among others.

An example of hybrid reactor-membrane-based solvent extraction has been proposed by Trusek-Holownia and Noworyta (2004) for the enzymatic synthesis of taste dipeptides. The enzyme is dissolved in the aqueous phase, where the enzymatic conversion takes place. The membrane contactor with a porous membrane separates the aqueous phase from the organic phase, which is the reservoir of hydrophobic reagents. The reaction product has strongly hydrophobic properties and it has a very low solubility in water under the reaction conditions (60°C, pH 7.0). The high mass transfer area of the membrane contactor for effective mass transport of the product enabled its synthesis without precipitation in the aqueous phase. Fig. 8.17 shows the flowsheet of the hybrid system.

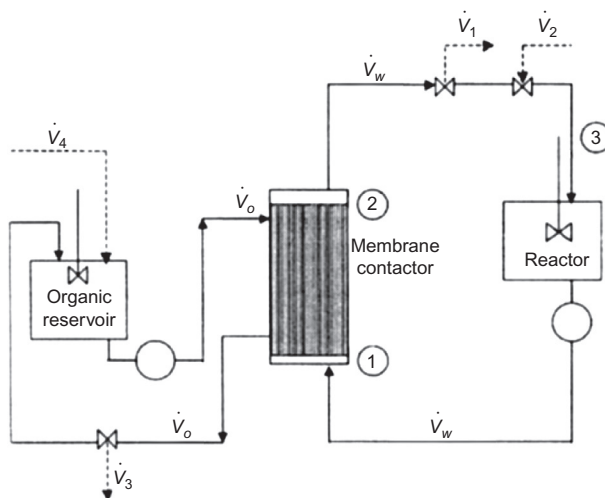


FIG. 8.17

Schematic diagram of a membrane phase contactor applied in enzymatic conversion.

Reproduced with permission from Trusek-Holownia, A., Noworyta, A., 2004. Modelling of the enzymatic synthesis of taste dipeptides with simultaneous extraction in a membrane phase contactor.

Desalination 160, 113.

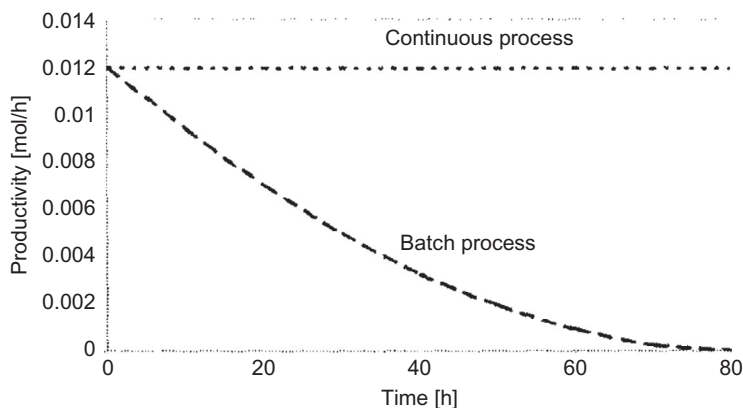


FIG. 8.18

Comparison of process productivity obtained in the continuous and batch process.

Reproduced with permission from Trusek-Holownia, A., Noworyta, A., 2004. Modelling of the enzymatic synthesis of taste dipeptides with simultaneous extraction in a membrane phase contactor. *Desalination* 160, 113.

The advantage of using the hybrid continuous configuration instead of a batch process can be observed in Fig. 8.18. In the continuous process, the reactor operates at high substrate concentrations and a constant, high rate of enzymatic conversion. Thus the productivity remains constant and no precipitation of the product takes place.

8.5.2 EXAMPLE 2: DRAW SOLUTION RECOVERY

Membrane distillation has been proposed as a key technology in the development of processes that involve the use of a draw solution. That is the case of the application of forward osmosis for the concentration of compounds or for water desalination. Forward osmosis uses a concentrated draw solution placed on the other side of a semi-permeable membrane to drive the transport of water molecules from the dilute feed solution to the concentration draw solution. This situation is diluting the draw solution during the operation, thus the dehydration efficacy will decrease over time until there is no enough driving force to lead a feasible process. Membrane distillation can be used to concentrate again the draw solution in a hybrid configuration so that the driving force in the forward osmosis unit is kept constant and a sustainable process is achieved.

Wang et al. (2011) investigated the hybrid forward osmosis (FO)-membrane distillation (MD) in the dehydration of proteins, specifically a bovine serum albumin (BSA) solution. In their hybrid, the FO is used for dewatering protein solutions while the MD was used for draw solution recovery. Fig. 8.19 shows the proposed hybrid. They found that the hybrid FO-MD was working under stable conditions in

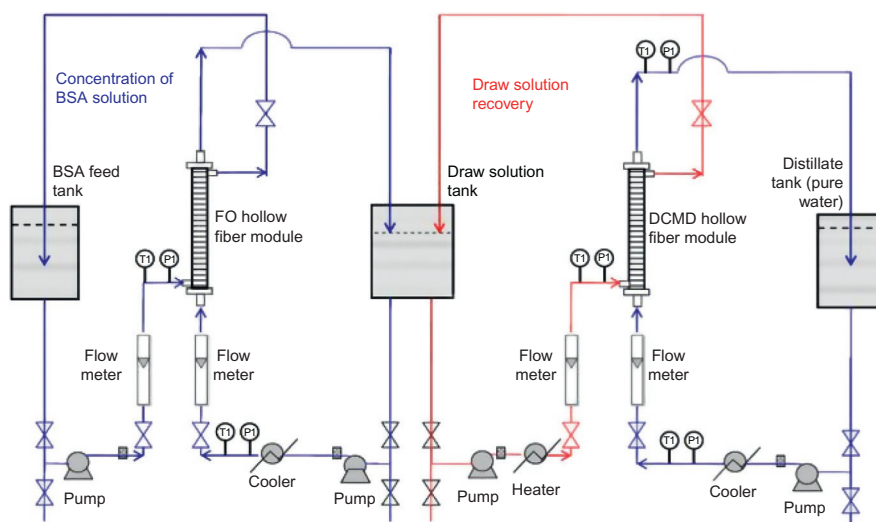


FIG. 8.19

Schematic diagram of the FO-MD hybrid system.

Reproduced with permission from Wang, K.Y., Teoh, M.M., Nugroho, A., Chung, T.-S., 2011. Integrated forward osmosis–membrane distillation (FO–MD) hybrid system for the concentration of protein solutions. *Chem. Eng. Sci.* 66, 2421–2430. <https://doi.org/10.1016/j.ces.2011.03.001>.

continuous operation when the dehydration rate across the FO membrane was the same as the water vapor rate across the MD membrane. Thus a MD unit working between 50°C and 60°C seems to be suitable to balance the FO water transfer rate when using 0.5 M NaCl as draw solution, as shown in Fig. 8.20A. However, it is important to take into account that possible leakage of salts may take place. Fig. 8.20B shows the NaCl leakage and BSA loss in the FO unit. This leakage of draw solutes may be favorable or unfavorable depending on the type of draw solution as well as the protein to be concentrated. The authors concluded that the FO-MD hybrid system is a promising technology for the concentration of pharmaceuticals due to its low temperature and pressure requirements, repeatability, controllability, predictability, and desirable by-product (Wang et al., 2011).

8.5.3 EXAMPLE 3: TREATMENT OF WASTEWATER

Curcio et al. (2010) developed a hybrid nanofiltration–membrane crystallization for the treatment of wastewater containing a high load of sodium sulfate salt produced in the manufacture of rechargeable batteries. The nanofiltration unit is used as a pre-concentration step before the membrane crystallization process in order to decrease the membrane area and energy demand in the downstream membrane crystallization unit, in which sodium sulfate will be crystallized and recovered. The flowsheet of the hybrid is shown in Fig. 8.21. The concentrated solution produced in the

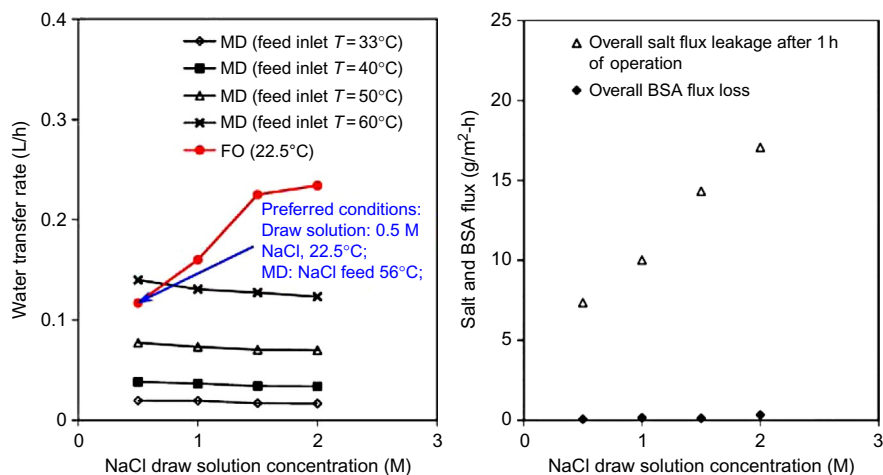


FIG. 8.20

Results for the FO-MD hybrid process for protein concentration: (A) water transfer rate; (B) salt and protein (BSA) flux.

Reproduced with permission from Wang, K.Y., Teoh, M.M., Nugroho, A., Chung, T.-S., 2011. Integrated forward osmosis–membrane distillation (FO–MD) hybrid system for the concentration of protein solutions. *Chem. Eng. Sci.* 66, 2421–2430. <https://doi.org/10.1016/j.ces.2011.03.001>.

nanofiltration unit is sent to membrane crystallization. Both feed and distillate streams are recirculated. Fig. 8.22 shows the dependence of the transmembrane flux of solvent on the feed distillate temperature difference (driving force of the evaporation process). At temperature gradient of 5°C ($T_{\text{feed}}=30^{\circ}\text{C}$ and $T_{\text{distillate}}=25^{\circ}\text{C}$), the water flux scattered around $0.57 \pm 0.07 \text{ kg m}^{-2} \text{ h}^{-1}$, a value not practical for large-scale applications. When feed temperature was increased to 40°C (temperature gradient of 12°C), the transmembrane flux enhanced by 156%, reaching an average value of $1.46 \pm 0.19 \text{ kg m}^{-2} \text{ h}^{-1}$ (Curcio et al., 2010). The produced crystals were the anhydrous form of sodium sulfate. The hybrid nanofiltration–membrane crystallization showed successful results for the recovery of sodium sulfate from wastewater but the idea can be extended to other salts and applications.

8.6 HYBRID PROCESSES BASED ON MEMBRANE BIOREACTORS

8.6.1 EXAMPLE 1: WASTEWATER TREATMENT AND REUSE

Membrane bioreactors (MBR) are widely used for wastewater treatment, but water reuse involves a careful control of water quality and pollutants removal efficiency. The presence of persistent compounds that are not easily biodegradable in the MBR is a limitation of this technology. Song et al. (2018) studied the removal efficiency of

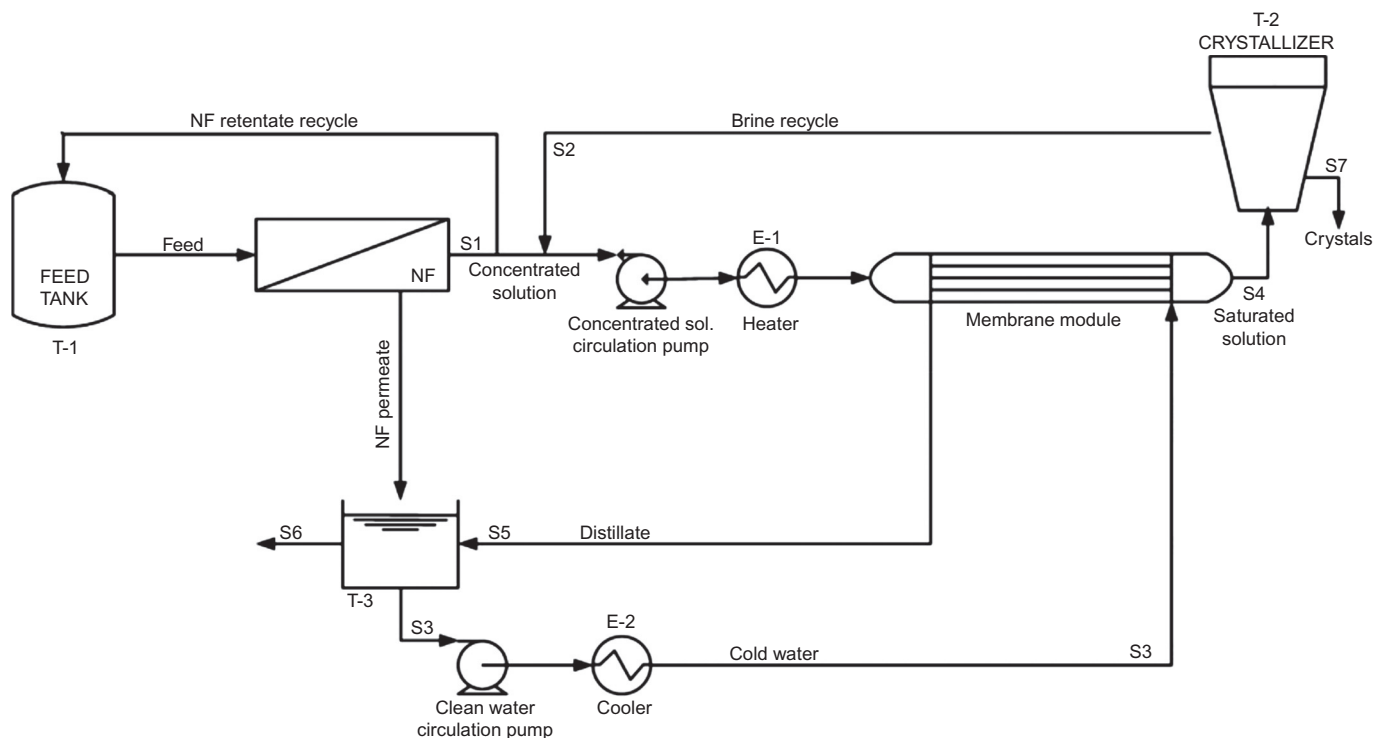


FIG. 8.21

Block flow diagram of the hybrid process (S1: nanofiltration retentate; S2: brine recycle from crystallizer; S3: cold water; S4: saturated solution; S5: distillate stream; S6: clean water; S7: sodium sulfate crystals; T1: wastewater tank; T2: crystallizer; T3: treated water tank; E1: heater; E2: cooler).

Reproduced with permission from Curcio, E., Ji, X., Matin Quazi, A., Barghi, S., Di Profio, G., Fontanovna, E., Macleod, T., Drioli, E., 2010. Hybrid nanofiltration–membrane crystallization system for the treatment of sulfate wastes. *J. Membr. Sci.* 360, 493–498.

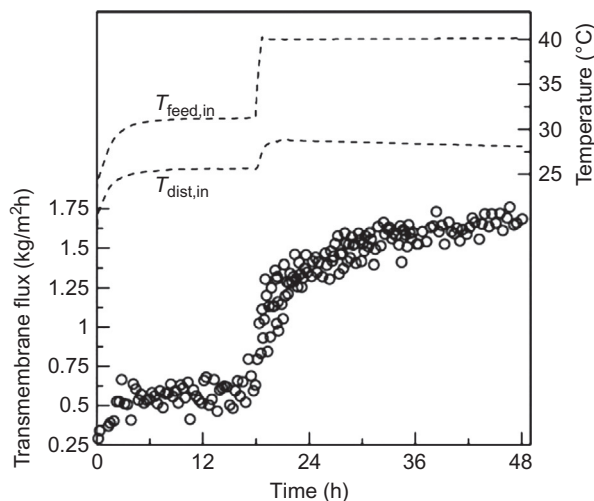


FIG. 8.22

Transmembrane flux and inlet feed and distillate temperature profiles versus time.

Reproduced with permission from Curcio, E., Ji, X., Matin Quazi, A., Barghi, S., Di Profio, G., Fontananova, E., Macleod, T., Drioli, E., 2010. Hybrid nanofiltration–membrane crystallization system for the treatment of sulfate wastes. *J. Membr. Sci.* 360, 493–498.

trace organic contaminants using MBR and proposed a hybrid based on MBR and membrane distillation (MD) to increase the removal efficiency and produce high quality water. Trace organic contaminants are released into the environment by agricultural and industrial activities or human use and have been detected in wastewater in concentrations up to few micrograms per liter (Osorio et al., 2012). The MBR reactor used by Song et al. (2018) worked under anaerobic conditions since it does not require energy input for aeration and even it may lead to a positive energy balance by producing biogas. However, the anaerobic MBR (or AnMBR) has a lower treatment capacity to remove nutrients and persistent compounds. Applying MD after the MBR would allow the removal of those compounds due to their resistance to biodegradation. Fig. 8.23 shows the schematic diagram of the laboratory-scale AnMBR-MD hybrid system. The authors evaluated the hybrid system performance in terms of biogas production, biomass characteristics, contaminant removal, and membrane fouling. The hybrid AnMBR-MD produced 0.3–0.5 L/g COD_{added} biogas with around 65% of methane. The MD process could complement the AnMBR by further enhancing the removal of organic substances and phosphate (Fig. 8.24), reaching a near complete removal. The MD rejects nonvolatile components, thus a considerable accumulation of COD and PO₄³⁻ in the MD feed solution is produced, leading to a significant fouling of the MD membrane that causes a decrease of flux over time. Regarding the removal of NH₄⁺, the MD removed around 90% during the first 20 days of operation but it decreased gradually due to the conversion to ammonia (NH₃) at high feed temperature of 45°C since it is a volatile species that can be transported

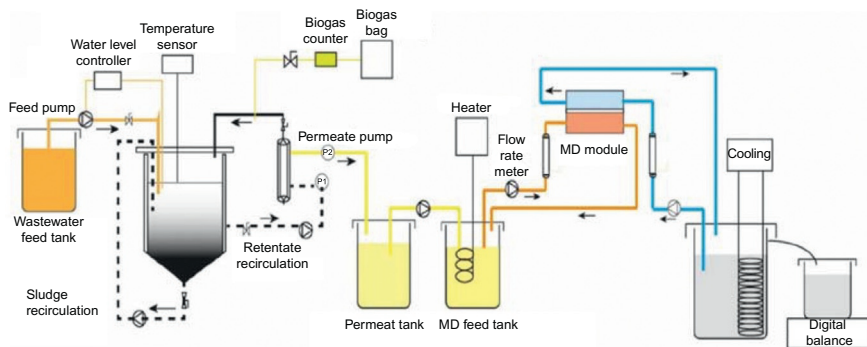


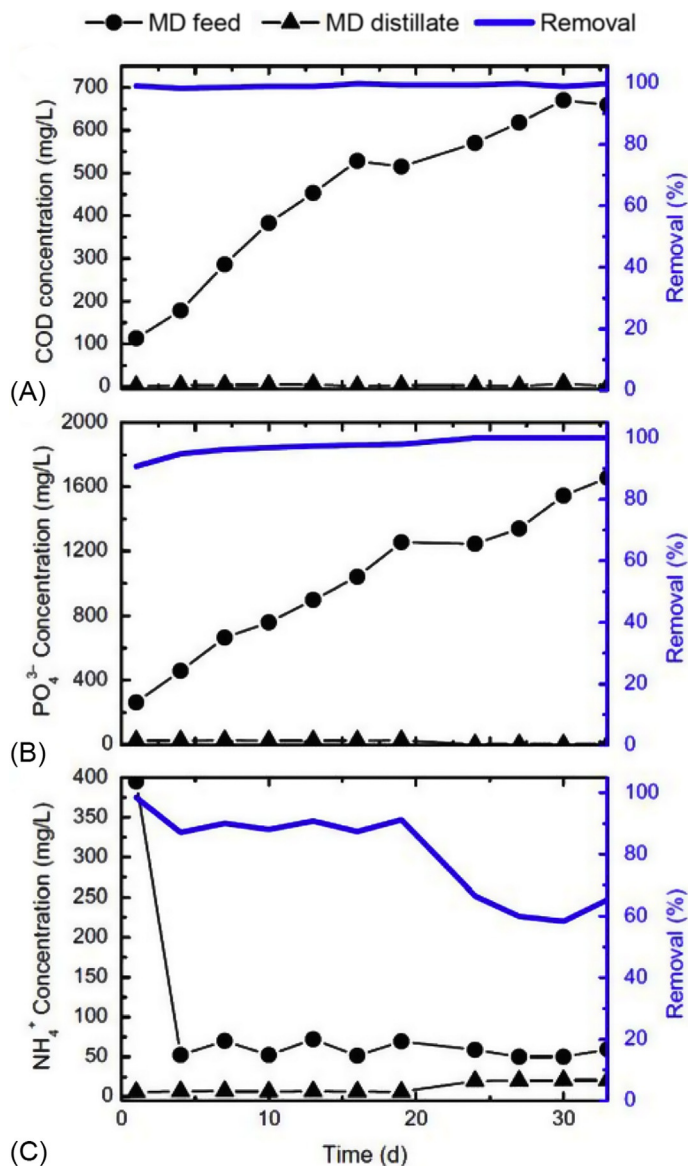
FIG. 8.23

Schematic diagram of the AnMBR-MD hybrid system.

through the MD membrane. NH_4^+ was hence found in the MD distillate, which indicates that ammonia volatilization has to be controlled and further removal of ammonia may be required after the MD process. Finally, concerning the removal of persistent components, the removal efficiency varied significantly with the kind of component, as it can be seen in Fig. 8.25. The MD unit enhanced the overall removal, reaching over 76% removal of all the compounds studied. Thus the hybrid AnMBR-MD is a technological alternative to remove persistent components and produce high quality water, although membrane fouling and ammonia permeation are issues to take into account for further process improvement.

8.6.2 EXAMPLE 2: DRINKING WATER DENITRIFICATION

Nitrate is a pollutant present in groundwater mainly due to the use of nitrogen-rich fertilizers. The maximum contaminant level limited by the World Health Organization for nitrates in drinking water is $50 \text{ mgNO}_3 \text{ L}^{-1}$ (Kapoor and Viraraghavan, 1997). Common technologies used for water denitrification are ion exchange, membrane separation, and biological denitrification. However, these technologies present drawbacks such as the disposal of spent regenerant brine containing nitrate and excess sodium chloride in the case of ion exchange treatment, the addition posttreatment required in order to remove the pollutant completely in the case of membrane separation methods, or the potential risk of microbial contamination of the treated water and presence of residual organics when biological denitrification is performed. An interesting hybrid combining a continuous ion exchange membrane separation (Donnan dialysis) of charged pollutants from water streams and their simultaneous biodegradation has been proposed in the literature (Fonseca et al., 2000; Velizarov et al., 2000/2001). Fig. 8.26A shows the mechanism of nitrate removal in the ion exchange membrane bioreactor (IEMB) and Fig. 8.26B shows the IEMB process used by Velizarov et al. (2000/2001). They used a nonporous mono-anion permselective membrane that prevents direct contact between the polluted water and the

**FIG. 8.24**

Distribution and removal of (A) COD, (B) PO₄³⁻ and (C) NH₄⁺ by the AnMBR-MD hybrid process.

Reproduced with permission from Song, X., Luo, W., McDonald, J., Khan, S.J., Hai, F.I., Price, W.E., Nghiem, L.D., 2018. An anaerobic membrane bioreactor – membrane distillation hybrid system for energy recovery and water reuse: removal performance of organic carbon, nutrients, and trace organic contaminants. *Sci. Total Environ.* 628–629, 358–365.

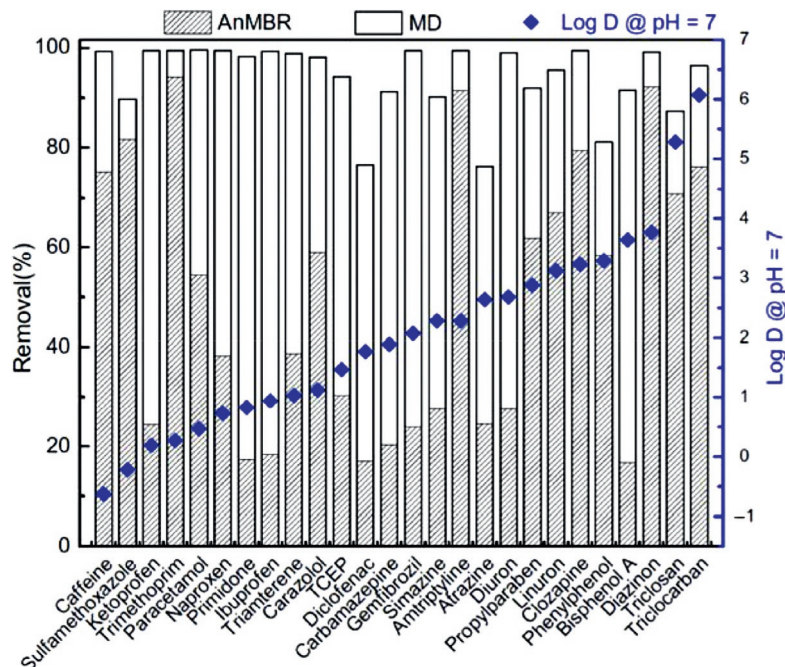


FIG. 8.25

Removal of persistent compounds by the AnMBR-MD hybrid process. The compounds are listed in the order of increasing hydrophobicity.

Reproduced with permission from Song, X., Luo, W., McDonald, J., Khan, S.J., Hai, F.I., Price, W.E., Nghiem, L.D., 2018. An anaerobic membrane bioreactor – membrane distillation hybrid system for energy recovery and water reuse: removal performance of organic carbon, nutrients, and trace organic contaminants. *Sci. Total Environ.* 628–629, 358–365.

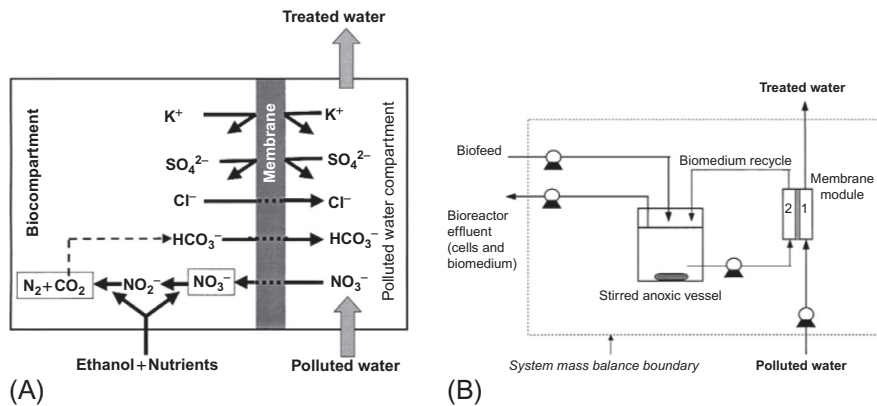


FIG. 8.26

(A) Schematic diagram of ion transport mechanism in the ion exchange membrane bioreactor; (B) schematic diagram of the ion-exchange membrane bioreactor.

Reproduced with permission from Velizarov, S., Rodrigues, C.M., Reis, M.A., Crespo, J.G., 2000/2001. Mechanism of charged pollutants removal in an ion exchange membrane bioreactor: drinking water denitrification. *Biotechnol. Bioeng.* 71, 4.

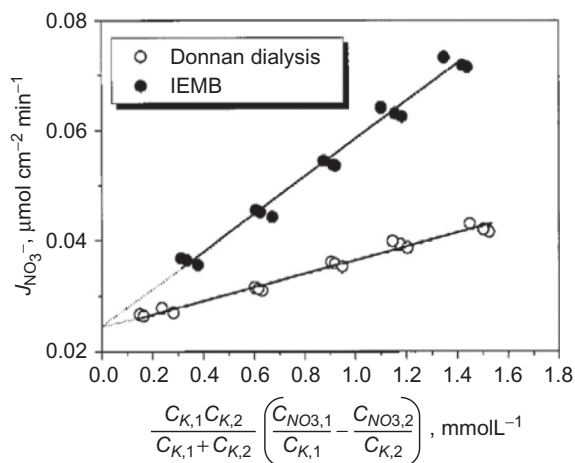


FIG. 8.27

Comparison of the steady-state nitrate fluxes, obtained in Donnan dialysis and in the ion exchange membrane bioreactor, as a function of the driving force. The slope is the overall mass transfer coefficient.

Reproduced with permission from Velizarov, S., Rodrigues, C.M., Reis, M.A., Crespo, J.G., 2000/2001. Mechanism of charged pollutants removal in an ion exchange membrane bioreactor: drinking water denitrification. *Biotechnol. Bioeng.* 71, 4.

denitrifying culture as well as secondary pollution of the treated water with dissolved nutrients and metabolic products. Chloride was added to the bioreactor feed to serve as the main counterion. Ethanol was supplied as a carbon source and electron donor for denitrification. The system achieved complete denitrification without accumulation of NO_3^- and NO_2^- ions in the biocompartment.

Velizarov et al. (2000/2001) achieved a surface denitrification rate of 33 g NO_3^- per square meter of membrane per day was obtained at a nitrate loading rate of $360 \text{ g NO}_3^- \text{ m}^{-3} \text{ d}^{-1}$, resulting in a nitrate removal efficiency of 85%. Fig. 8.27 shows the flux of nitrate as a function of the driving force for the case in which only Donnan dialysis is considered and with the IEMB hybrid. The overall mass transfer coefficient (slope of the line in Fig. 8.27) was 2.8 times higher when the IEMB hybrid was used. That increase was attributed to a reduction of the boundary layer mass transfer resistance in the biocompartment. Thus an efficient nitrate bioreduction reaction was taking place at the biomedium/membrane interface (Velizarov et al., 2000/2001). The hybrid IEMB is hence a technical alternative for water denitrification.

8.6.3 EXAMPLE 3: MICROBIAL FUEL CELL AND MEMBRANE BIOREACTOR FOR WASTEWATER TREATMENT

Membrane bioreactors (MBR) suffer from membrane fouling due to soluble microbial products and extracellular polymeric substances. These compounds have been identified negatively charged. Thus Wang et al. (2013, 2016) proposed the

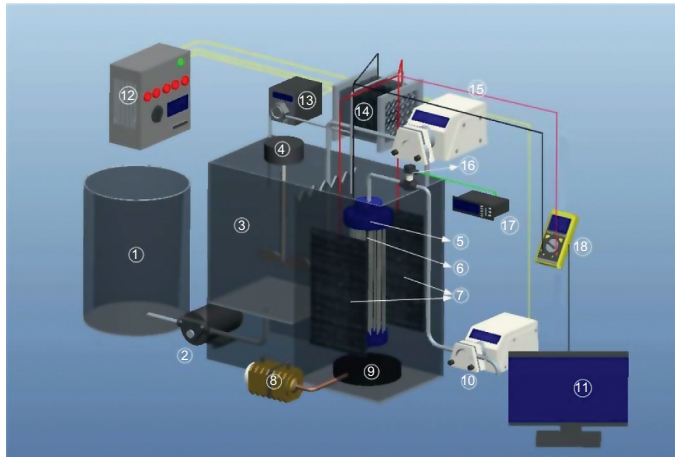


FIG. 8.28

Schematic diagram of the MFC-MBR (① raw tank ② inflow pump for MBR ③ anoxic/oxic membrane bioreactor ④ stirrer ⑤ PVDF hollow fiber membrane module ⑥ graphitic rod ⑦ graphitic plates ⑧ aeration pump ⑨ aeration stone ⑩ effluent pump ⑪ computer ⑫ PLC ⑬ inflow pump for MFC ⑭ membrane-less MFC ⑮ reflux pump ⑯ pressure sensor paperless recorder multimeter).

Reproduced with permission from Wang, J., Bi, F., Ngo, H.-H., Guo, W., Jia, H., Zhang, H., Zhang, X., 2016. Evaluation of energy-distribution of a hybrid microbial fuel cell-membrane bioreactor (MFC-MBR) for cost-effective wastewater treatment. *Bioresour. Technol.* 200, 420–425.

integration of a microbial fuel cell (MFC) with the MBR using the aeration tank of a MBR as cathode chamber, in which the anodic chamber was filled with self-fabricated activated carbon fiber and directly submerged in the membrane bioreactor. Fig. 8.28 shows the schematic representation of the MFC-MBR hybrid. The influent of MFC was supernatant of an anaerobic reactor with low dissolved oxygen. The voltage generated by MFC was appended to the installed electrodes in MBR to reduce the energy consumption of a DC power. The mechanisms of fouling reduction were associated to electrophoresis and electrostatic repulsion against electronegative colloids or particles (Wang et al., 2016).

In order to evaluate the membrane filtration efficiency, Wang et al. (2016) determined the variation of the transmembrane pressure (TMP) over time (Fig. 8.29). An increase in TMP is an indication of membrane fouling. As observed in Fig. 8.29, TMP increased slowly at beginning, potentially due to the attachment of organic matter. Then, the TMP of CMBR increased rapidly, whereas the TMP development of MFC-MBR exhibited considerably slower increase. After physical cleaning, the fouling rate increased more rapidly, which means that the membrane could not be recovered completely after the physical cleaning and the foulants could attach easier on the remained fouling layer. The lower fouling in the hybrid systems indicates that

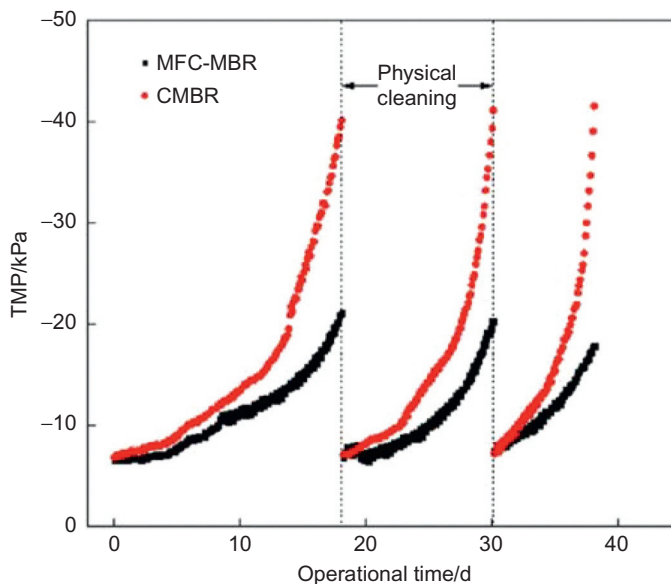


FIG. 8.29

TMP profiles of the MFC-MBR hybrid and conventional MBR (CMBR).

Reproduced with permission from Wang, J., Bi, F., Ngo, H.-H., Guo, W., Jia, H., Zhang, H., Zhang, X., 2016. Evaluation of energy-distribution of a hybrid microbial fuel cell-membrane bioreactor (MFC-MBR) for cost-effective wastewater treatment. *Bioresour. Technol.* 200, 420–425.

the weak electric field was effective to maintain the electrophoresis and electrostatic attraction/repulsion against electronegative sludge particles or colloids (Wang et al., 2016).

8.7 HYBRIDS BASED ON ELECTRO-DRIVEN PROCESSES

8.7.1 EXAMPLE 1: BRACKISH AND WASTEWATER TREATMENT WITH PRODUCTION OF POTABLE WATER

Photovoltaic-driven electro dialysis has appeared as an alternative configuration to reverse osmosis for desalination since it does not need pressure, biofouling is not a dominating problem in the system performance, and the foulants can be removed by chemical cleaning due to the chemical resistance of ion exchange membranes (Zhang et al., 2017). However, it cannot remove uncharged compounds. Thus organic pollutants will remain in the water. Integrating forward osmosis (FO) prior or after the ED unit has been proposed by Zhang et al. (2017) to remove those contaminants from the wastewater. Zhang et al. (2017) developed a novel photovoltaic (PV) hybrid-driven FO-ED system to produce high quality (potable) water from

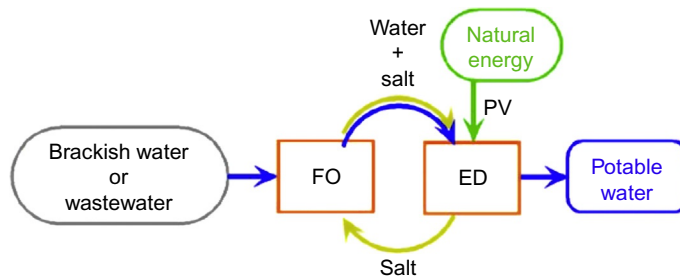


FIG. 8.30

Conceptual diagram on salt-mediated water production by the FO-ED hybrid.

Reproduced with permission from Zhang, Y., Pinoy, L., Meesschaert, B., Van der Bruggen, B., A natural driven membrane process for brackish and wastewater treatment: photovoltaic powered ED and FO hybrid system, *Sep. Purif. Technol.* 174 (2017) 264–274.

secondary wastewater effluent or brackish water. Fig. 8.30 shows the conceptual diagram of the hybrid. The feed water (secondary wastewater effluent or synthetic brackish water) is drawn to the FO draw solution; the organic and inorganic substances (ions, compounds, colloids, and particles) are rejected by the FO membrane. The diluted draw solution is then pumped to the solar energy-driven ED, where high quality water is produced; the concentrate is recycled to the FO unit and reused as the draw solution. NaCl is used as a medium to “carry” water from the brackish water or wastewater to the ED unit. The PV driven FO-ED system can treat streams not applicable to standard NF/RO/ED without pretreatment (Zhang et al., 2017).

According to the authors, the water produced contained low concentration of total organic carbon, carbonate, and cations derived from the feed water; had a low conductivity; and meets potable water standards. The water production cost considering the investment for membranes and solar panel was 3.32–4.92 EUR m⁻³ (for 300 days of production per year) for a small size potable water production system.

8.7.2 EXAMPLE 2: TREATMENT OF INDUSTRIAL WASTEWATER

Industry generates waste effluents with a large number of compounds that could be recovered so that the consumption of new raw material is reduced as well as the toxicity of those streams.

Several examples of using hybrids based on electro-dialysis can be found in the literature. One example is that focused on effluents from metal and surface coating industries (galvanizing, electroplating, anodizing, painting) and other industries such as photography, water softening, textile, and paper manufacturing. Those effluents contain metal ions such as silver, cadmium, copper, zinc, and platinum that contribute largely to their toxic character. Removal of heavy metals is done conventionally by means of precipitation, adsorption, coagulation-flocculation, and solvent extraction, which normally involve the generation of solid wastes or big sludge volumes

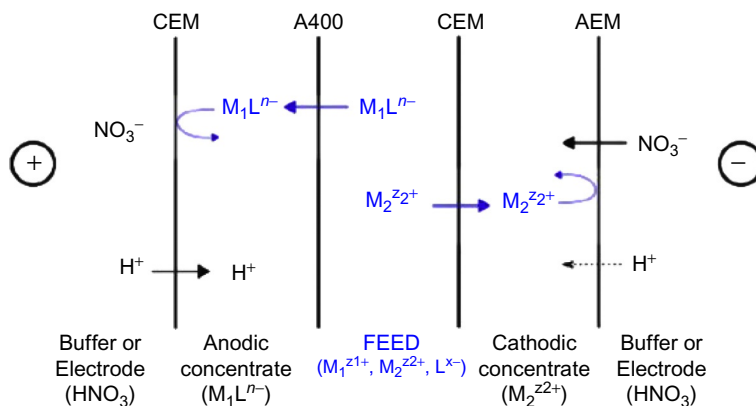


FIG. 8.31

Schematic layout of a unitary cell in the ED-CR process (initial feed solution is composed of $M_1^{Z_1+}$, $M_2^{Z_2+}$, L^{X-} with an in situ complexation reaction: $M_1^{Z_1+}$ is complexed selectively as M_1L^{n-} form).

Reproduced with permission from Frioui, S., Rabah, O., Stella, L., 2017. Highly selective extraction of metal ions from dilute solutions by hybrid electrodialysis technology. *Sep. Purif. Technol.* 174, 264–274.

(Blais et al., 1999). Frioui et al. (2017) proposed the coupling of electrodialysis (ED) with an in situ complexation reaction (CR) step to selectively recover and concentrate various metallic cations with different or similar valences hardly separable by conventional ED. The ED unit is composed of two electrode blocks (platinum plated titanium for anode and stainless steel for cathode) and a membrane stack between them. The stack consists of three cell units; a unitary cell is shown in Fig. 8.31. The diluate compartment contains the metal ion mixture as feed solution, and there are two different concentrate compartments with alternating anion exchange (AEM or A400) and cation exchange (CEM) membranes.

The authors evaluated different chemical ligands (citrate (H_3C), glycine (H_2G^+), phosphate (H_3P), and EDTA (H_4L)) toward binary metallic solutions (Ag/Zn and Cu/Cd). The best complexing agent was found to be EDTA for both metal ion systems, in terms of discriminant metal ion charge modification and complex stability. The process efficiency was very affected by the operating conditions (initial feed concentration and flow rate, feed pH, electric voltage applied, electrolyte concentration in electrode, and buffer compartments) but operating under appropriate conditions would allow achieving an excellent electro-extraction ($\geq 99\%$) together with a total selective metal ion recovery (Frioui et al., 2017).

Another example is the treatment of tannery wastewater by a hybrid electrocoagulation/electrodialysis process (Deghles and Kurt, 2016). The leather industry is making a big effort to minimize the environmental impact of their production processes. Legislation is the driving force for this change and it involves technological advances. The conventional biological treatment does not always achieve acceptable performance since the toxicity of the tannery wastewater affects the bacteria.

A hybrid electrocoagulation (EC)/electrodialysis (ED) process has been proposed for the removal of COD, $\text{NH}_3\text{-N}$, Cr, and color by [Deghles and Kurt \(2016\)](#). EC involves dissolution of metal from the anode with simultaneous formation of hydroxyl ions and generation of hydrogen gas at the cathode. ED is used for the degradation of organic matter. The water treated by EC-ED presented a higher quality than that obtained with only ED ([Table 8.1](#)). The removal efficiency for of ammonium, color, and chromium was 100%. The treated effluent provided water quality values very similar to values of feed water.

A third example is the treatment of textile wastewater, generated during dye production and textile dyeing process. This wastewater contains high salinity ($>6.0\%$ NaCl or $>5.0\%$ Na_2SO_4) and is produced in large quantities since around $200\text{--}350\text{ m}^3$ of pure water is required for producing one ton of dyed textile products ([Lin et al., 2015](#)). Adsorption, coagulation, biological treatment, and advanced oxidation processes are conventional approaches that are used for dye removal or destruction, thus no dye recovery is envisaged. As alternative, [Lin et al. \(2015\)](#) proposed a hybrid based on bipolar membrane electrodialysis (BMED) and nanofiltration (NF). They studied the fractionation of NaCl and diverse dyes in synthetic textile wastewater with high salinity by using loose NF in diafiltration. Then, BMED was applied to remove the remaining salts in the NF permeate and produce acid/base from the salt by fractionation. [Fig. 8.32](#) shows the schema of the studied process. The loose NF membrane presented a good diafiltration performance for the fractionation of dye/salt mixtures, allowing a free passage of salt (rejection $\leq 2.2\%$) and high retention of dyes ($>99.93\%$). The application of a further BMED step led to the production of pure water, acid and base for the salt-containing NF permeate without membrane fouling. In addition, the hybrid process recovered dyes with $>96.6\%$ purity and closed the water loop from textile wastewater ([Lin et al., 2015](#)).

8.7.3 EXAMPLE 3: ELECTRICITY GENERATION

Low-temperature heat source utilization is an alternative solution for electricity generation in remote areas where direct thermal utilization is not applicable. [Long et al. \(2017\)](#) studied a hybrid membrane-based electricity generation system that operates as a heat engine to convert low-grade heat into electricity. The system consists of membrane distillation (MD) and reverse electrodialysis (RED). The MD unit absorbs thermal energy from the heat source and generates high concentrated salty stream, and the RED converts the Gibbs free energy of mixing from the produced salty streams into electricity. [Fig. 8.33](#) shows the proposed hybrid. The thermal separation section is composed of a direct contact membrane distillation along with a regenerator. In the thermal separation section, streams with different NaCl concentrations are produced driven by the low-temperature heat source. In the electricity generation section, RED module harvests the Gibbs free energy of mixing from the produced salty streams to generate electricity ([Long et al., 2017](#)).

Results on the electrical efficiency of the hybrid and relative MD permeate/feed solution flow rate, α , can be seen in [Fig. 8.34](#). The curve has an optimal α leading to

Table 8.1 Characterization of feed water, effluent treated by EC process, and by EC-ED system, as well removal grade obtained using these techniques (Deghles and Kurt, 2016)

Parameter	Results					Legislation
	Effluent Tannery wastewater	Treated effluent (EC)	Removal efficiency %	Treated effluent (EC-ED)	Removal efficiency (%)	
a. In the case of aluminum electrodes (45 min)						
pH	6.0	8.10	–	3.31	–	–
Conductivity (ms/cm)	23.0	22.0	–	0.397	–	–
COD (mg/L)	2800	756	73	224	92	400
Total chrome (mg/L)	570	0.1	100	0.0	100	0.5
NH ₃ -N (mg/L)	180	88.2	51	0.0	100	40
Color (ADMI (10) Pt-Co)	824	49.5	94	0.0	100	Colorless
b. In the case of iron electrodes (75 min)						
pH	7.0	9.0	–	3.95	–	–
Conductivity (ms/cm)	23.0	22.1	–	1.5	–	–
COD (mg/L)	2800	924	67	364	87	400
Total chrome (mg/L)	570	0.1	100	0.0	100	0.5
NH ₃ -N(mg/L)	180	97.2	46	0.0	100	40
Color (ADMI (10) Pt-Co)	824	58	93	0.0	100	Colorless

Characterization of feed water, effluent treated by EC process, and by EC-ED system, as well removal grade obtained using these techniques. (–): unidentified.

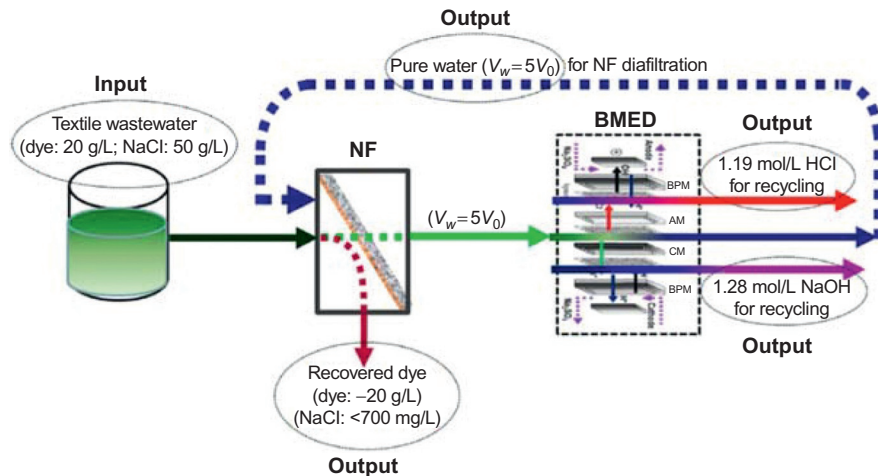


FIG. 8.32

Scheme of resource recovery from textile wastewater by loose NF-BMED hybrid process. Reproduced with permission from Lin, J., Ye, W., Huang, J., Ricard, B., Baltaru, M., Greydanus, B., Balta, S., Shen, J., Vlad, M., Sotto, A., Luis, P., Van der Bruggen, B., 2015. Toward resource recovery from textile wastewater: dye extraction, water and base/acid regeneration using a hybrid NF-BMED process. *ACS Sustain. Chem. Eng.* 3, 1993–2001.

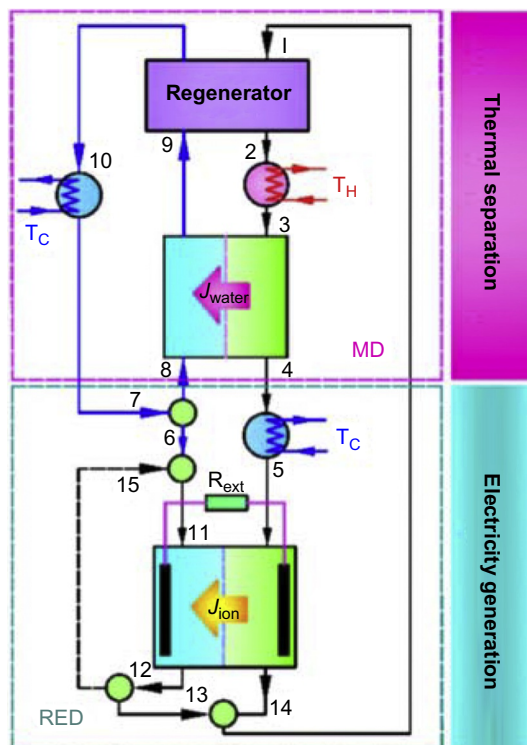


FIG. 8.33

Schematic of the MD-RED hybrid electricity generation system to harvest low-grade thermal energy. Reproduced with permission from Long, R., Li, B., Liu, Z., Liu, W., 2017. Hybrid membrane distillation-reverse electrodialysis electricity generation system to harvest low-grade thermal energy. *J. Membr. Sci.* 525 107–115.

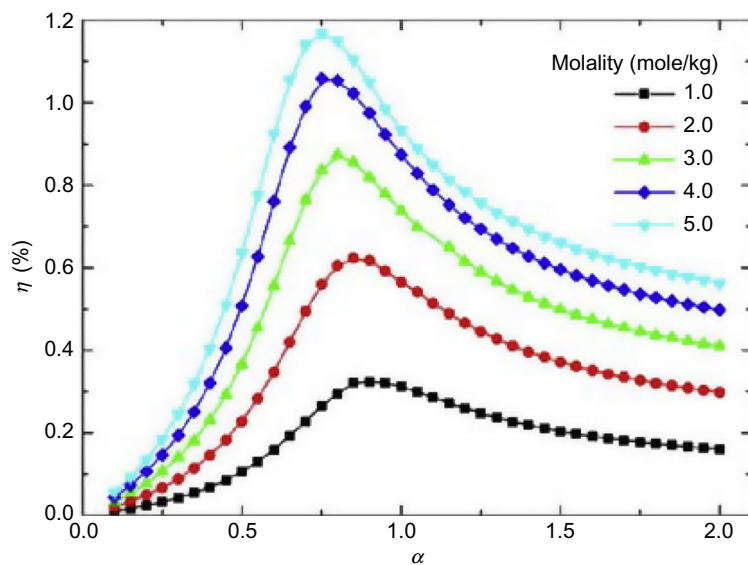


FIG. 8.34

Electrical efficiency of the MD-RED system varies with the relative MD permeate/feed solution flow rate.

Reproduced with permission from Long, R., Li, B., Liu, Z., Liu, W., 2017. Hybrid membrane distillation-reverse electro dialysis electricity generation system to harvest low-grade thermal energy. *J. Membr. Sci.* 525, 107–115.

the maximum electrical efficiency, which corresponds to the minimum value of specific heat duty. In addition, a higher concentration of the MD feed solution induces a higher specific duty, and a higher electrical efficiency. The electricity efficiency of the proposed hybrid system reaches 1.15% operating between 20°C and 60°C with the MD feed NaCl concentration of 5 mol/kg (Long et al., 2017).

REFERENCES

- Amelio, A., Genduso, G., Vreysen, S., Luis, P., Van der Bruggen, B., 2014. Guidelines based on life cycle assessment for solvent selection during the process design and evaluation of treatment alternatives. *Green Chem.* 16, 3045.
- Ayotte-Sauve, E., Sorin, M., Rheault, F., 2010. Energy requirement of a distillation/membrane parallel hybrid: a thermodynamic approach. *Ind. Eng. Chem. Res.* 49, 2295–2305.
- Baeyens, J., Kang, Q., Appels, L., Dewil, R., Lv, Y., Tan, T., 2015. Challenges and opportunities in improving the production of bio-ethanol. *Prog. Energy Combust. Sci.* 47, 60–88.
- Barakat, T.M.M., Sørensen, E., 2008. Simultaneous optimal synthesis, design and operation of batch and continuous hybrid separation processes. *Chem. Eng. Res. Des.* 86, 279–298.
- Blais, J.-F., Dufresne, S., Mercier, G., 1999. State of the art of technologies for metal removal from industrial effluents. *Rev. Sci. Eau* 12 (4), 687–711.

- Bressler, E., Braun, S., 2000. Conversion of citric-acid to itaconic acid in a novel liquid membrane bioreactor. *J. Chem. Technol. Biotechnol.* 75, 66.
- Bressler, E., Pines, O., Goldberg, I., Braun, S., 2002. Conversion of fumaric acid to l-malic by sol-gel immobilized *Saccharomyces cerevisiae* in a supported liquid membrane bioreactor. *Biotechnol. Prog.* 18, 445.
- Caballero, J.A., Grossmann, I.E., Keyvani, M., Lenz, E.S., 2009. Design of hybrid distillation-vapor membrane separation systems. *Ind. Eng. Chem. Res.* 48, 9151–9162.
- Curcio, E., Ji, X., Abdul, M.Q., Shahzad, B., Di, P.G., Enrica, F., Trevor, M., Enrico, D., 2010. Hybrid nanofiltration-membrane crystallization system for the treatment of sulfate wastes. *J. Membr. Sci.* 360, 493–498.
- Deghles, A., Kurt, U., 2016. Treatment of tannery wastewater by a hybrid electrocoagulation/electrodialysis process. *Chem. Eng. Process.* 104, 43–50.
- du Pisani, P.L., 2006. Direct reclamation of potable water at Windhoek's Goreangab reclamation plant. *Desalination* 188 (1–3), 79–88.
- Esfahanian, M., Ghorbanfarahi, A.H., Ghoreyshi, A.A., Najafpour, G., Younesi, H., Ahmad, A.L., 2013. Enhanced bioethanol production in batch fermentation by pervaporation using a PDMS membrane bioreactor. *Int. J. Eng. Trans. B: Appl.* 25, 249–258.
- Esteves, I.A.A.C., Mota, J.P.B., 2002. Simulation of a new hybrid membrane/pressure swing adsorption process for gas separation. *Desalination* 148, 275–280.
- Fonseca, A.D., Crespo, J.G., Almeida, J.S., Reis, A.M., 2000. Drinking water denitrification using a novel ion-exchange membrane bioreactor. *Environ. Sci. Technol.* 34, 1557–1562.
- Freeman, B., Hao, P., Baker, R., Kniep, J., Chen, E., Ding, J., Zhang, Y., Rochelle, G.T., 2014. Hybrid membrane-absorption CO₂ capture process. *Energy Procedia* 63, 605–613.
- Frioui, S., Rabah, O., Stella, L., 2017. Highly selective extraction of metal ions from dilute solutions by hybrid electrodialysis technology. *Sep. Purif. Technol.* 174, 264–274.
- Kapoor, A., Viraraghavan, T., 1997. Nitrate removal from drinking water—review. *J. Environ. Eng.* 123, 371–380.
- Kookos, I.K., 2003. *Ind. Eng. Chem. Res.* 42, 1731–1738.
- Krug J, Palm C, 1996. Separation of a mixture of methanol and tetrahydrofuran into its constituents, United States, BASF. Patent number: 5559254.
- Lin, J., Ye, W., Huang, J., Ricard, B., Baltaru, M., Greydanus, B., Balta, S., Shen, J., Vlad, M., Sotto, A., Luis, P., Van der Bruggen, B., 2015. Toward resource recovery from textile wastewater: dye extraction, water and base/acid regeneration using a hybrid NF-BMED process. *ACS Sustain. Chem. Eng.* 3, 1993–2001.
- Lipnizki, F., Field, R.W., Ten, P.-K., 1999. Pervaporation-based hybrid process: a review of process design, applications and economics. *J. Membr. Sci.* 153, 183–210.
- Long, R., Li, B., Liu, Z., Liu, W., 2017. Hybrid membrane distillation-reverse electrodialysis electricity generation system to harvest low-grade thermal energy. *J. Membr. Sci.* 525, 107–115.
- Lopresto, C.G., Darvishmanesh, S., Amelio, A., Mazinani, S., Ramazani, R., Calabrò, V., Van der Bruggen, B., 2017. Application of organic solvent nanofiltration for microalgae extract concentration. *Biofuels, Bioprod. Biorefin.* 11 (2), 307–324.
- Luis, P., Amelio, A., Vreysen, S., Calabro, V., Van der Bruggen, B., 2013. Life cycle assessment of alternatives for waste-solvent valorization: batch and continuous distillation vs incineration. *Int. J. Life Cycle Assess.*
- Luis, P., Amelio, A., Vreysen, S., Calabro, V., Van der Bruggen, B., 2014. Simulation and environmental evaluation of process design: Distillation vs. hybrid distillation-pervaporation for methanol/tetrahydrofuran separation. *Appl. Energy* 113, 565–575.

- Mazlan, N.M., Peshev, D., Livingston, A.G., 2016. Energy consumption for desalination—a comparison of forward osmosis with reverse osmosis, and the potential for perfect membranes. *Desalination* 377, 138–151.
- Moganti, S., Noble, R.D., Kovalb, C.A., 1994. Analysis of a membrane/distillation column hybrid process. *J. Membr. Sci.* 93, 31–44.
- Norkobilov, A., Gorri, D., Ortiz, I., 2017. Process flowsheet analysis of pervaporation-based hybrid processes in the production of ethyl tert-butyl ether. *J. Chem. Technol. Biotechnol.* 92, 1167–1177.
- Olujic, Z., Behrens, M., Sun, L., Fakhri de Graauw, J., 2010. Augmenting distillation by using membrane based vapor–liquid contractors: an engineering view from Delft. *J. Membr. Sci.* 350, 19–31.
- Osorio, V., Marcé, R., Pérez, S., Ginebreda, A., Cortina, J.L., Barceló, D., 2012. Occurrence and modeling of pharmaceuticals on a sewage-impacted Mediterranean river and their dynamics under different hydrological conditions. *Sci. Total Environ.* 440, 3–13.
- Pedram, S., Kaghazchi, T., Takht Ravanchi, M., 2014. Performance and energy consumption of membrane-distillation hybrid systems for olefin-paraffin separation. *Chem. Eng. Technol.* 37 (4), 587–596.
- Peshev, D., Livingston, A.G., 2013. OSN Designer, a tool for predicting organic solvent nanofiltration technology performance using Aspen One, MATLAB and CAPE OPEN. *Chem. Eng. Sci.* 104, 975–987.
- Petersen, T., Argo, A., Noble, R.D., Kovalb, C.A., 1996. Design of combined membrane and distillation processes. *Sep. Technol.* 6, 175–187.
- Rissom, S., Beliczey, J., Giffels, G., Kragl, U., Wandrey, C., 1999. Asymmetric reduction of acetophenone in membrane reactors: comparison of oxazaborolidine and alcohol dehydrogenase catalysed processes. *Tetrahedron Asym.* 10, 923.
- Schlösser, S., Kertész, R., Marták, J., 2005. Recovery and separation of organic acids by membrane -based solvent extraction and pertraction—an overview with a case study on recovery of MPCA. *Sep. Purif. Technol.* 41, 237–266.
- Scholz, M., Frank, B., Stockmeier, F., Falß, S., Wessling, M., 2013. Techno-economic analysis of hybrid processes for biogas upgrading. *Ind. Eng. Chem. Res.* 52, 16929–16938.
- Song, X., Luo, W., McDonald, J., Khan, S.J., Hai, F.I., Price, W.E., Nghiem, L.D., 2018. An anaerobic membrane bioreactor – membrane distillation hybrid system for energy recovery and water reuse: removal performance of organic carbon, nutrients, and trace organic contaminants. *Sci. Total Environ.* 628–629, 358–365.
- Takht Ravanchi, M., Kaghazchi, T., Kargari, A., 2009. Application of membrane separation processes in petrochemical industry: a review. *Desalination* 235, 199–244.
- Trusek-Holownia, A., Noworyta, A., 2004. Modelling of the enzymatic synthesis of taste dipeptides with simultaneous extraction in a membrane phase contactor. *Desalination* 160, 113.
- Valladares Linares, R., Li, Z., Yangali-Quintanilla, V., Ghaffour, N., Amy, G., Leiknes, T., Vrouwenvelder, J.S., 2016. Life cycle cost of a hybrid forward osmosis e low pressure reverse osmosis system for seawater desalination and wastewater recovery. *Water Res.* 88, 225–234.
- Velizarov, S., Rodrigues, C.M., Reis, M.A., Crespo, J.G., 2000/2001. Mechanism of charged pollutants removal in an ion exchange membrane bioreactor: drinking water denitrification. *Biotechnol. Bioeng.* 71(4).

- Wang, K.Y., Teoh, M.M., Nugroho, A., Chung, T.-S., 2011. Integrated forward osmosis–membrane distillation (FO–MD) hybrid system for the concentration of protein solutions. *Chem. Eng. Sci.* 66, 2421–2430. <https://doi.org/10.1016/j.ces.2011.03.001>.
- Wang, J., Bi, F., Ngo, H.-H., Guo, W., Jia, H., Zhang, H., Zhang, X., 2016. Evaluation of energy-distribution of a hybrid microbial fuel cell-membrane bioreactor (MFC-MBR) for cost-effective wastewater treatment. *Bioresour. Technol.* 200, 420–425.
- Wang, J., Zheng, Y.W., Jia, H., Zhang, H.W., 2013. In situ investigation of processing property in combination with integration of microbial fuel cell and tubular membrane bioreactor. *Bioresour. Technol.* 149, 163–168.
- Wintgens, T., Melin, T., Schaefer, A., Khan, S., Muston, M., Bixio, D., Thoeye, C., 2005. The role of membrane processes in municipal wastewater reclamation and reuse. *Desalination* 178 (1), 1–11.
- Zhang, Y., Luc, P., Boudewijn, M., der Bruggen Bart, V., 2017. A natural driven membrane process for brackish and wastewater treatment: photovoltaic powered ED and FO hybrid system. *Sep. Purif. Technol.* 174, 264–274.

Contributors

João G. Crespo

LAQV - REQUIMTE, Department of Chemistry, Faculty of Sciences and Technology, NOVA University of Lisbon, Caparica, Portugal

Cláudia F. Galinha

LAQV - REQUIMTE, Department of Chemistry, Faculty of Sciences and Technology, NOVA University of Lisbon, Caparica, Portugal

Patricia Luis

Materials & Process Engineering (iMMC-IMAP), Catholic University of Louvain, Louvain-la-Neuve, Belgium

Sandra Sanches

iBET, Institute of Experimental Biology and Technology, Oeiras, Portugal

Bart Van der Bruggen

Department of Chemical Engineering, KU Leuven, Leuven, Belgium;
Faculty of Engineering and the Built Environment, Tshwane University of Technology, Pretoria, South Africa

Index

Note: Page numbers followed by *f* indicate figures, and *t* indicate tables.

A

- Activated sludge models (ASM)
 - BAP, 234
 - CAS processes, 234
 - EPS/SMP, 234–235
 - kinetic models, 233
 - UAP, 234
 - unmodified and modified ASM, 234
 - wastewater treatment, 235
- Activated sludge systems. *See* Microbial mixed cultures
- Air gap membrane distillation (AGMD), 180
- Animal and plant cell bioreactors, 224–225
- Anion-exchange membranes, 251–252
 - acid recovery, 260
 - bipolar membrane, 255
 - capacitive deionization, 287
 - classical electro dialysis stack, 252–253, 253*f*
 - concentration polarization, 255–257, 258*f*
 - Donnan dialysis, 281–282
 - EDBM, 265–266
 - EED, 276–277
 - monovalent selective, 255
 - nonselective, 255
 - selectivity, 266
- AnMBR-MD hybrid system
 - COD, PO_4^{3-} and NH_4^+ distribution and removal, 326–329, 330*f*
 - persistent compounds removal, 326–329, 331*f*
 - schematic diagram, 326–329, 329*f*
- Artificial neural networks (ANN) modeling, 238–239
- ASM. *See* Activated sludge models (ASM)
- Azeotropes separation, 74

B

- Biocatalyst residence time, 210
- Biogas upgrading
 - amine scrubbing, 320, 321*f*
 - chemical synthesis, 320
 - CH_4 recovery, 322
 - common techniques, 320
 - cryogenic separation, 320, 322*f*
 - gas permeation, 320, 322*f*
 - pressurized water scrubbing, 320, 321*f*

- specific upgrading costs, 322
- Biological oxygen demand (BOD_5), 226–227
- Biomass-associated products (BAP), 234
- Bipolar membrane
 - EDBM (*see* Electro dialysis with bipolar membranes (EDBM))
 - EEDBM, 278, 279*f*
 - in electromembrane separations, 255, 255*f*
 - three-compartment electro dialysis cell, 255, 256*f*
- Bipolar membrane electro dialysis (BMED), 337.
 - See also* Electro dialysis with bipolar membranes (EDBM)
- Blue shift, 213

C

- Capacitive deionization (CDI)
 - charge efficiency, 289
 - electrode-cation-exchange-membrane-feed flow channel-anion-exchange membrane-electrode, 287
 - electrostatic adsorption, 286
 - energy consumption, 288–289
 - FaCDI, 288
 - FCDI, 288, 288*f*
 - membrane capacitive deionization, 287, 287*f*
 - modeling, adsorption capacity, 288
 - normalized charge efficiency, 289
 - total charge, 288
- Capillary suction time (CST), 228–229
- Capital expense (CAPEX), 305–306
- Carbon-based membranes, 8–9
- Carbon membranes, 8–9
- Carbon molecular sieve membranes (CMSMs), 8–9
- Carbon nanotubes (CNTs), 8–9
- Cation-exchange membranes (CEM), 251–252
 - alternative stack, 255, 257*f*
 - bipolar membrane, 255
 - capacitive deionization, 287
 - classical electro dialysis stack, 252–253, 253*f*
 - Donnan dialysis, 281–282
 - EDBM, 289
 - selectivity, 266
- CDI. *See* Capacitive deionization (CDI)
- CEDI. *See* Continuous electro deionization (CEDI)
- CEM. *See* Cation-exchange membranes (CEM)

- Ceramic membranes, 7
 - Chemical oxygen demand (COD), 226–227
 - Chilton-Colburn *j*-factor correlations, 13, 13*f*
 - Complexation reaction (CR), 335–336, 336*f*
 - Concentration polarization, 16
 - concentration profile, 17–18, 17*f*
 - in situ monitoring techniques, 20–21
 - in pressure-driven processes, 17–18
 - Contactor membrane reactors, 157
 - forced flow through contactor
 - feed fluid phase through membrane pores, 196, 197*f*, 199–201
 - mass transfer limitations, 201–202
 - performance at different flow rates, 202–203, 203*f*
 - variables effect on reaction rate constant, 201, 202*f*
 - interfacial membrane contactor
 - ceramic membrane contactor, 199, 200*f*
 - phase transfer catalysis, 198, 199*f*
 - separating two immiscible reagents, 196–198, 197*f*
 - using an extracting agent, 196, 197*f*, 198
 - Continuous electrodeionization (CEDI)
 - boundary conditions, 281
 - ion-exchange resin, flow pathways in, 278–281, 280*f*
 - ions removal, 278–281, 280*f*
 - principle, 278, 280*f*
 - specific conductivity, resin bed, 278–281
 - Conventional activated sludge systems (CAS), 215–216, 234
 - Conventional MBR (CMBR), 333–334, 334*f*
 - Coupling effects, pervaporation
 - diffusion coefficient, 88–89
 - Hansen solubility approach
 - application, 96–100
 - dispersion interaction, 92
 - hydrogen bonding, 92
 - interaction radius, 92–96
 - parameters, 91–96, 95–96*t*
 - polar interaction, 92
 - polymeric membrane, 91–92
 - polymers and resins, characteristic parameters, 92–96, 93–94*t*
 - relative energy difference (RED), 96
 - spherical representation, 92–96, 93*f*
 - “trial-and-error” method, 92
 - kinetic coupling, 88–89
 - modified solution-diffusion models
 - binary interaction parameters estimation, 90, 90*t*
 - diffusions coefficients, 90, 91*t*
 - Flory-Huggins interaction parameter, 89
 - Flory-Huggins thermodynamics, 89
 - polymeric membrane, 89–90
 - six coefficients model, 90
 - thermodynamic coupling, 88–89
 - Crystalline polymer, 5–7
- D**
- Darcy’s equation, 80–81
 - Dense membranes
 - gas separation, 7
 - pervaporation, 7, 13
 - solution-diffusion model, 14–15, 14*f*
 - Desalination process. *See* Forward osmosis (FO)
 - Differential equations, membrane contactors
 - axial and radial coordinates of fiber, 160–161, 161*f*
 - lumen side (inside fiber), 163–164
 - membrane, 164–165
 - membrane wetting, 172–174, 173*f*
 - shell side, 161–163
 - Diffusion dialysis (DD), 260, 275–276
 - Direct contact membrane distillation (DCMD), 180
 - Direct pressure measurements, 21
 - Donnan dialysis, 281–282, 332, 332*f*
 - Dynamic hydration number, 275
 - Dynamic transport number, 266–267
- E**
- ED. *See* Electrodialysis (ED)
 - EDBM. *See* Electrodialysis with bipolar membranes (EDBM)
 - EED. *See* Electro-electrodialysis (EED)
 - Electrical impedance spectroscopy, 22
 - Electrocoagulation/electrodialysis (EC-ED) hybrid process, 337, 338*t*
 - Electrodialysis (ED)
 - alternative stack with additional cation-exchange membrane, 255, 257*f*
 - applications
 - bipolar membranes, 264–266, 264*f*
 - brackish water, salt removal from, 260–261
 - coupling electrodialysis, 260–261
 - electrical current and energy production, 262, 263*f*
 - forward osmosis hybrid system, 261, 261*f*
 - green energy, 262
 - hybrid membrane systems, 261
 - renewable energy powered electrodialysis, 261–262, 261*f*

- reverse electrodialysis, 262
- selective membranes, 262–264
- shielding effect, 262
- solar energy-driven electrodialysis, 261
- basic electrodialysis system configuration, 254–255, 254f
- bipolar membrane
 - in electromembrane separations, 255, 255f
 - three-compartment electrodialysis cell, 255, 256f
- classical electrodialysis stack configuration, 252–253, 253f
- ‘concentrate’ compartment, 252–253
- concentration polarization, anion-exchange membrane, 255–257, 258f
- current-voltage curve, Ohmic region, 259–260, 259f
- diffusion dialysis, 260
- ‘diluate’ compartment, 252–253
- electrical potential, 251–253
- electrodriven membrane processes
 - (*see* Electrodriven membrane processes)
- electromigration, 257, 258f
- hemodialysis, 260
- history, 252
- ion-exchange membranes (*see* Ion-exchange membranes)
- LCD, 257–260, 259f
- limiting factors, 252–253
- ‘product’ compartment, 255
- selectivity
 - hydrophilicity, 268
 - membrane potential, 266–267
 - membrane selective permeability, 267
 - permselectivity, 266, 268–269
 - resistances, 268–269
 - selective permeation of ions, 268
 - separation efficiency, 269, 270f
 - separation factors, 270
 - transport number, 266–268
- selectrodialysis stack configuration, 255, 256f
- Electrodialysis with bipolar membranes (EDBM)
 - applications, 265
 - electroneutrality, 290
 - fluidized bed reactor, 265–266
 - HLac and Lac, 291
 - mass balance for lactate, 290
 - molar fluxes, 290–292
 - OH[−] concentration, 289
 - organic acid production, 264–265, 264f
 - pH range, 291–292
 - proton balance in diluate, 289
 - sodium lactate (NaLac) to lactic acid (HLac) conversion, 289
 - system, fluxes, and parameters, 289, 329f
 - ultrafiltration process, 265–266
 - volume variation, diluate compartment, 291
- Electrodriven membrane processes, 252
 - bipolar membranes, 255, 256f, 264–266, 264f
 - CDI (*see* Capacitive deionization (CDI))
 - CEDI (*see* Continuous electrodeionization (CEDI))
 - diffusion dialysis, 275–276
 - Donnan dialysis, 281–282
 - EDBM (*see* Electrodialysis with bipolar membranes (EDBM))
 - EED (*see* Electro-electrodialysis (EED))
 - fuel cells
 - acid electrolytes, 284–285, 285f
 - alkaline electrolytes, 285–286, 286f
 - basic composition, 284, 284f
 - green processes, 252
 - membrane electrodialysis
 - cathode and anode compartment separation, 282
 - charge efficiency, 283
 - chlor-alkali process, 282, 283f
 - modeling, 284
 - water electrolysis, 282
 - zero gap, 282
 - reverse electrodialysis, 292–294
 - selective membranes, 262–264
 - sustainable technology, 262
- Electro-driven processes
 - brackish and wastewater treatment, 334–335, 335f
 - electricity generation, 337–340, 339–340f
 - industrial wastewater treatment
 - EC-ED hybrid, 337, 338f
 - heavy metals removal, 335–336
 - tannery wastewater treatment, 336
 - textile wastewater treatment, resource recovery, 337, 339f
 - unitary cell, ED-CR process, 335–336, 336f
- Electro-electrodialysis (EED)
 - chromic acid recovery, 276–277, 277f
 - contaminants removal, 276–277
 - current efficiency, 277
 - EEDBM, 278, 279f
 - energy consumption, 277
 - REED, 278
 - static rinse water purification, 276–277
 - three-compartment electromembrane process, 276–277
 - two-phase electro-electrodialysis, 278

- Electro-electrodialysis with bipolar membrane (EEDBM), 278, 279*f*
 - Electron diode array microscope, 21
 - Electroneutrality, 290
 - Electro-osmosis, 273–274
 - Enzymatic and biotechnological fermentation processes, 322–323
 - Enzymatic membrane bioreactors
 - blue shift, 213
 - covalent bonding, 212
 - electrostatic interactions, 212
 - entrapment, 214
 - enzymatic enantioselective conversion, 214–215, 215*f*
 - fluorescence anisotropy, 213
 - fluorescence emission, 212–213
 - immobilization, 212, 214
 - mathematical modeling, 215
 - membrane biphasic contactor, 214–215
 - protein-induced denaturation, 213, 213*f*
 - red shift, 213
 - Equimolecular counterdiffusion (EMD), 10, 11*f*
 - Ethanol/water separation factor, 82–83, 83*f*
 - Extended Nernst-Planck equation, 49
 - External concentration polarization (ECP), 58–61
 - Extracellular polymeric substances (EPS), 228–229, 234
- F**
- Facilitated coupled cotransport, 105–108
 - Facilitated coupled counter-transport, 105–108
 - Faradaic CDI (FaCDI), 288
 - Fick's law of diffusion, 9–10
 - Film theory, 158–160, 159*f*
 - Flory-Huggins interaction parameter
 - flux of pure compounds, 98–99, 99*f*
 - hydrophobic ceramic membranes, 98
 - methanol/water separation, 99–100
 - MTBE, 98
 - poly(3-hydroxybutyrate) (PHB) membranes, 99–100
 - R_A and experimental flux, 98–99, 98*f*
 - water-hydrazine separation, 97
 - water-monomethylhydrazine mixtures separation, 97
 - Flory-Huggins thermodynamics, 89
 - Flow-electrode capacitive deionization (FCDI), 288, 288*f*
 - Fluorescence anisotropy, 213
 - Fluorescence spectroscopy, 230–231
 - FO. *See* Forward osmosis (FO)
 - FO-ED hybrid, 334–335, 335*f*
 - FO-MD hybrid process, 324–325, 325–326*f*
 - Forward osmosis (FO), 25–26
 - application, 32, 33*f*
 - concentration polarization
 - concentration profile, 58–60, 60*f*
 - ECP, 58–61
 - ICP, 58–60
 - modulus, 60
 - mass transfer coefficient, 60
 - nonequilibrium thermodynamics, 62
 - PAO, 62
 - pressure-retarded osmosis, 60
 - PRO mode and deionized water, 61–62
 - and reverse osmosis, 58–60, 59*f*
 - salt flux, 61–62
 - solute flux, 61–62
 - transport and structural parameters, 62
 - water flux, 61
 - Fouling, membrane
 - biofouling, 19–20
 - definition, 19–20
 - foulants, 19–20
 - in situ monitoring techniques, 21–22
 - MPBR, 221, 223
 - in pervaporation and gas separation, 19–20, 19*f*
 - transmembrane flux variation, 19–20, 19*f*
 - Fuel cells
 - acid electrolytes, 284–285, 285*f*
 - alkaline electrolytes, 285–286, 286*f*
 - basic composition, 284, 284*f*
- G**
- Gas-liquid membrane contactors, 156, 199, 200*f*
 - Gas permeation, 1–2
 - advantages, 109–110
 - applications, 109–114
 - biogas upgrading (*see* Biogas upgrading)
 - carbon dioxide capture, 317, 318*f*
 - dense membrane, 103–104
 - hybrid pressure swing adsorption
 - cycle sequence, 317–319, 319*f*
 - gas separation, 317–319
 - H₂/CH₄ mixtures separation, 317–319
 - H₂ recovery and product purity, 319–320, 320*f*
 - mass transfer
 - concentration profile of component i , 114, 114*f*
 - through dense membranes, 114–115*f*, 116–118
 - through porous membranes, 114–116, 114–115*f*

multicomponent mixture with N components, 103–104, 104*f*

Gas separation, SLMs

- applications, 111
- CO₂/N₂ mixture separation, 123–125
- CO₂/N₂ selectivity vs. CO₂ permeability, 123–125, 124*f*
- mass transfer, 120–121
- materials and membranes development, 123–125
- membrane area vs. CO₂ permeability, 126, 127*f*
- membrane performance, 126, 128
- membrane stability, 125–126
- polymerized ionic liquids, 123–125
- process performance, 126, 128
- relative membrane weight, 125–126, 126*f*
- separation factor, 128
- solubility effects, 123–125
- temperature effect, upper bound behavior, 125, 125*f*
- transmembrane flux, 126
- two-step vacuum membrane process flow diagram, 128, 129*f*

Gibbs free energy, 88–89

Glass membranes, 7

“Green” energy, 262

Green processes, 252

H

Hagen-Poiseuille’s law, 37

Hansen solubility approach

- application, 96–97
 - flux of pure compounds, 98–99, 99*f*
 - hydrophobic ceramic membranes, 98
 - methanol/water separation, 99–100
 - MTBE, 98
 - poly(3-hydroxybutyrate) (PHB) membranes, 99–100
 - R_A and experimental flux, 98–99, 98*f*
 - water-hydrazine separation, 97
 - water-monomethylhydrazine mixtures separation, 97
- dispersion interaction, 92
- hydrogen bonding, 92
- interaction radius, 92–96
- parameters, 91–92
 - calculation, 92
 - components, 92
 - of various solvents, 92–96, 95–96*t*
- polar interaction, 92
- polymeric membrane, 91–92
- polymers and resins, characteristic parameters, 92–96, 93–94*t*
- relative energy difference (RED), 96
- spherical representation, 92–96, 93*f*
- “trial-and-error” method, 92

Hansen Solubility Parameter (HSP) approach

- components, 51–52
- distribution, 53
- general procedure, 54, 54*f*
- group contribution method, 51–52, 52*t*
- solvent permeabilities, 51
- Teas plot, 52–53, 53*f*

Happel’s free surface model, 160–162

Hemodialysis, 260

Henry’s law constant, 80–81

High performance liquid chromatography (HPLC), 113–114

HRT. *See* Hydraulic retention time (HRT)

HSP approach. *See* Hansen Solubility Parameter (HSP) approach

Hybrid IEMB, 332

Hybrid processes

- definitions, 302
- electro-driven processes
 - brackish and wastewater treatment, 334–335, 335*f*
 - electricity generation, 337–340, 339–340*f*
 - industrial wastewater treatment, 335–337, 336*f*, 338*t*, 339*f*
- gas permeation
 - biogas upgrading (*see* Biogas upgrading)
 - carbon dioxide capture, 317, 318*f*
 - hybrid pressure swing adsorption, 317–320, 319–320*f*
- membrane bioreactors
 - drinking water denitrification, 329–332, 331–332*f*
 - microbial fuel cell, 332–334, 333–334*f*
 - wastewater treatment and reuse, 326–329, 329–331*f*
- membrane contactors
 - draw solution recovery, 324–325, 325–326*f*
 - organic acids separation, 322–324, 323–324*f*
 - wastewater treatment, 325–326, 327–328*f*
- pervaporation
 - bioethanol production, 315–317, 316*f*
 - ethyl tert-butyl ether production, 308–309, 309*f*
 - hybrid pervaporation-distillation, 308
 - hybrid pervaporation reactor, 308
 - methanol/tetrahydrofuran mixtures separation, 309–314, 311–313*f*
 - olefin-paraffin separation, 314–315, 315–316*f*
- pressure-driven processes

- Hybrid processes (*Continued*)
- hybrid nanofiltration-distillation, 302–303, 304*f*
 - water desalination (*see* Water desalination)
 - type R(eactor), 302
 - type S(eparation), 302
- Hydraulic resistance, 36–37
- Hydraulic retention time (HRT), 215–217
- Hydrophilic membranes, 74
- I**
- IEMB. *See* Ion exchange membrane bioreactor (IEMB)
- Inorganic membranes
- application temperature, 5
 - carbon-based membranes, 8–9
 - ceramic membranes, 7
 - glass membranes, 7
 - metallic membranes, 8
 - zeolites, 7–8
- Interfacial membrane contactor
- ceramic membrane contactor, 199, 200*f*
 - phase transfer catalysis, 198, 199*f*
 - separating two immiscible reagents, 196–198, 197*f*
 - using an extracting agent, 196, 197*f*, 198
- Internal concentration polarization (ICP), 58–60
- Ion exchange membrane bioreactor (IEMB)
- ion transport mechanism, 329–332, 331*f*
 - schematic diagram, 329–332, 331*f*
 - steady-state nitrate fluxes, 332, 332*f*
- Ion-exchange membranes
- anion-exchange membranes, 251–252
 - cation-exchange membranes, 251–252
 - charged functional groups, 251–252
 - ion transport
 - applied electrical potential gradient, 272
 - current density, 272
 - dimensionless variables, 273
 - dynamic hydration number, 275
 - electrical current, 271
 - electrical resistance, 270
 - electrochemical potential, 271
 - electro-osmosis, 273–274
 - equivalent conductivity, 270–271
 - extended Nernst-Planck equation, 272
 - mass transport, 272
 - number of electrical charges, 271
 - Ohm's Law, 270
 - osmotic effect, 271
 - phenomenological coefficients, 272
 - primary and secondary hydration shell, 274*f*, 275
 - Stanton number, 273
 - volume change, 275
 - monopolar, 251–252
- Irreversible thermodynamics, 48–49
- K**
- Kinetic coupling, 88–89
- L**
- Laser triangulometry, 21
- LCD. *See* Limiting current density (LCD)
- Life cycle assessment (LCA), 309–310
- Light deflection techniques, 20
- Limiting current density (LCD), 257–260, 259*f*
- Liquid-liquid contact, 154*f*, 199, 200*f*
- Liquid pertraction, SLMs
- carrier concentration effect, 140–142, 141*f*
 - coupled co-/counter-ion transport, 135
 - feed concentration effect, 136–139, 137*f*, 139*f*
 - kind of contactor, 142
 - kind of support effect, 145
 - mass transfer, 121–122
 - mechanisms, 135, 136*f*
 - permeability and selectivity, 135–136
 - separation of toxic metals from water, 135
 - stability, 142–145, 143–144*f*
 - stripping agent concentration effect, 139–140
- Loose Reverse Osmosis, 26
- M**
- Magnetic resonance imaging (MRI), 20
- Mass transfer
- differential equation based modeling (*see* Differential equations, membrane contactors)
 - film theory and resistance-in-series model, 158–160, 159*f*
 - laminar flow/stagnant fluid film
 - concentration profiles, 10, 11*f*
 - EMD, 10, 11*f*
 - mass transfer rates, 9–10
 - UMD, 11–12, 11*f*
 - mechanisms, 9
 - modeling and membrane processes, 16, 16*f*
 - molar flux, 9
 - pervaporation
 - evaluation, 72–73
 - multicomponent mixtures, 75–76
 - pore-flow model, 75–76, 80–81
 - solution-diffusion model, 75–79

- SLMs
 concentration profile of component i , 118, 119 f
 gas feed/gas permeate, 120–121
 liquid/liquid applications, 119–120
 liquid pertraction, 121–122
 permeability, 120
 pervaporation, 121
 transmembrane flux, 120
- through dense membranes
 concentration profile of component i , 114 f , 116–117
 Henry's law, 116–117
 mechanism of transport, 115 f , 116–117
 permeability, 117–118
 permeance, 117
 rate of membrane transport, 117
 selectivity, 118
 separation factor, 117–118
 solution-diffusion model, 116–117
- through membranes
 gas separation, 13
 mass and heat transfer resistances, 15, 15 f
 mass transfer coefficient, 14
 membrane-based liquid extraction, 13
 pervaporation, 13
 pore-flow model, 14–15, 14 f
 resistances-in-series model, 15
 solution-diffusion model, 14–15, 14 f
 transmembrane flux, 14
- through porous membranes
 concentration profile of component i , 114–115, 114 f
 Knudsen diffusion, 115–116
 mechanisms of transport, 115–116, 115 f
 permeability ratio, 116
 permeance, 114–116
 rate of diffusion, 114–115
 turbulent flow, 12–13, 13 f
- Mass transfer coefficient, 186, 187 f
 inside the fibers, 183–184
 in membrane, 184
 at shell side, 184
- Maxwell-Stefan theory, 284
- MBRs. *See* Membrane bioreactors (MBRs)
- McCabe-Thiele diagram, 86–88, 87 f
- MD. *See* Membrane distillation (MD)
- MD-RED hybrid system
 electrical efficiency, 337–340, 340 f
 low-grade thermal energy harvest
 schema, 337, 339 f
- Mechanistic modeling approaches
 biological models
 microbial mixed cultures, 232–235
 production with pure cultures, 235
 physical models
 diffusion models, 235–236
 microfiltration/ultrafiltration, 235
 resistances in series, 236–237
 steps, 235
- Membrane-based absorption
 absorption flux vs. sulfur dioxide logarithmic
 mean molar fraction, 169, 169 f
 experimental setup, 166, 167 f
 individual mass transfer coefficient,
 169–171
 logarithmic mean of driving force, 167
 mass transfer, 169, 170 f
 membrane area vs. overall mass transfer
 coefficient, 168, 168 f
 membrane wetting
 in differential equation based model, 172–174,
 173 f
 in resistance-in-series model, 170 f , 171–172
 removal efficiency, 168
 transmembrane flux, 166
- Membrane-based solvent extraction
 mass transfer resistance analysis for copper (II)
 extraction, 177, 178 f
 membrane-based liquid extraction, 175, 176 f
 processes with immobilized L-L interface(s),
 174, 175 f
 Wilson plot method, 177–178, 179 f
- Membrane bioreactors (MBRs), 1–2, 29–30
 animal and plant cell bioreactors, 224–225
 applications, 211–212
 biocatalyst residence time, 210
 bioreactor uncoupling, 210
 covalent and ionic bonding, 210
 drinking water denitrification
 ion-exchange membrane bioreactor, 329–332,
 331 f
 ion transport mechanism, 329–332, 331 f
 mass transfer coefficient, 332, 332 f
 steady-state nitrate fluxes, 332, 332 f
 enzymatic (*see* Enzymatic membrane
 bioreactors)
 with eukaryotic cells, 211
 in external loop recycle reactor, 210
 hybrid modeling, 241, 242 f
 immobilization, 210
 integrated MBR model, 232, 233 f
 mathematical modeling, 232

- Membrane bioreactors (MBRs) (*Continued*)
 - mechanistic modeling approaches
 - (*see* Mechanistic modeling approaches)
 - microbial (*see* Microbial membrane bioreactors)
 - microbial fuel cell, 332–334, 333–334*f*
 - monitoring and control
 - biological reaction, 225–226
 - fouling, 226
 - membrane separation, 225–226
 - off-line monitoring (*see* Off-line monitoring, MBR)
 - online, real-time monitoring, 230–232, 231*f*
 - wastewater treatment, 226
 - multivariate statistical analysis methods
 - ANN modeling, 238–239
 - data-driven modeling, 238
 - fouling complexity, 237–238
 - multilinear regression tools, 240
 - PCA, 239
 - PLS, 239–240
 - photocatalytic membrane bioreactors, 211
 - physical space restriction, 209–210
 - submerged membrane bioreactors, 210–211
 - wastewater treatment and reuse
 - AnMBR-MD hybrid system (*see* AnMBR-MD hybrid system)
 - membrane distillation, 326–329
- Membrane biphasic contactor, 214–215
- Membrane contactors, 1–2, 5, 14
 - applications, 155, 156*f*, 157–158
 - contactor membrane reactors, 157
 - forced flow through contactor, 196, 197*f*, 199–203, 202–203*f*
 - interfacial membrane contactor, 196–199, 197*f*, 199–200*f*
 - conventional processes, 153–154, 155*r*
 - hybrid process
 - draw solution recovery, 324–325, 325–326*f*
 - organic acids separation, 322–324, 323–324*f*
 - wastewater treatment, 325–326, 327–328*f*
 - mass transfer
 - differential equation based modeling
 - (*see* Differential equations, membrane contactors)
 - film theory and resistance-in-series model, 158–160, 159*f*
 - membrane-based absorption
 - absorption flux vs. sulfur dioxide logarithmic mean molar fraction, 169, 169*f*
 - experimental setup, 166, 167*f*
 - individual mass transfer coefficient, 169–171
 - logarithmic mean of driving force, 167
 - mass transfer, 169, 170*f*
 - membrane area vs. overall mass transfer coefficient, 168, 168*f*
 - membrane wetting, 170*f*, 171–174, 173*f*
 - removal efficiency, 168
 - transmembrane flux, 166
 - membrane-based solvent extraction
 - with immobilized L-L interface(s), 174, 175*f*
 - mass transfer resistance analysis, copper (II) extraction, 177, 178*f*
 - membrane-based liquid extraction, 175, 176*f*
 - Wilson plot method, 177–178, 179*f*
 - membrane distillation-crystallization
 - configurations, 180
 - counter-current mode, 183, 183*f*
 - experimental heat transfer coefficient, 182–183
 - heat transfer, 185
 - heat transfer coefficient, 184–186, 188*f*
 - mass transfer coefficient, 183–184, 186, 187*f*
 - nucleation barrier, 180–181
 - osmotic coefficient, 181–182
 - reduction in free energy, 181, 182*f*
 - transmembrane flux, 181
 - membrane emulsification
 - diffusion coefficient of polymeric surfactant, 195
 - dispersed phase flux, 193
 - droplet diameter vs. wall shear stress, 192, 192*f*
 - lab-scale system, 188–190, 189*f*
 - low wall shear rates, 194
 - membrane material, 190–192
 - moderate wall shear rates, 195
 - oil-in-water (o/w) emulsions, 186–188
 - optical microscope images of drops, 186–188, 189*f*
 - permeability, 193
 - pore size vs. droplet size, 190–192, 191*f*
 - stability, 190
 - steady-state dispersed phase flux vs. transmembrane pressure, 192–193, 193*f*
 - transmembrane pressure, 190, 192–193
 - water-in-oil (w/o) emulsions, 186–188
 - working principle, 186–188, 188*f*
 - pressure calculation, 157
 - working principle, 153–154, 154*f*
 - Membrane crystallization, 155–156
 - Membrane distillation (MD), 155
 - draw solution recovery, 324–325
 - electricity generation, 337
 - MBR, 326–329

- Membrane distillation-crystallization
 configurations, 180
 counter-current mode, 183, 183f
 experimental heat transfer coefficient, 182–183
 heat transfer, 185
 heat transfer coefficient, 184–186, 188f
 mass transfer coefficient, 186, 187f
 inside fibers, 183–184
 in membrane, 184
 at shell side, 184
 nucleation barrier, 180–181
 osmotic coefficient, 181–182
 reduction in free energy, 181, 182f
 transmembrane flux, 181
- Membrane electrodialysis
 cathode and anode compartment separation, 282
 charge efficiency, 283
 chlor-alkali process, 282, 283f
 modeling, 284
 water electrolysis, 282
 zero gap, 282
- Membrane emulsification, 156–157
 diffusion coefficient of polymeric surfactant, 195
 dispersed phase flux, 193
 droplet diameter vs. wall shear stress, 192, 192f
 lab-scale system, 188–190, 189f
 low wall shear rates, 194
 membrane material, 190–192
 moderate wall shear rates, 195
 oil-in-water (o/w) emulsions, 186–188
 optical microscope images of drops, 186–188, 189f
 permeability, 193
 pore size vs. droplet size, 190–192, 191f
 stability, 190
 steady-state dispersed phase flux vs.
 transmembrane pressure, 192–193, 193f
 transmembrane pressure, 190, 192–193
 water-in-oil (w/o) emulsions, 186–188
 working principle, 186–188, 188f
- Membrane photobioreactors (MPBR)
 advantages, 221
 biomass production, 221
 CO₂ transfer rates, 223
 design features, 222
 fouling, 221, 223
 light intensity, 222
 Michaelis-Menten equation, 222–223
 microalgal biomass, 220–221
 rate of mass transfer, 223
 surface-to-ground area ratio, 222
 three-phase system, 222
 wastewater bioremediation, 220
- Membrane technology
 classification, 2
 hybrid processes (*see* Hybrid processes)
 mass transfer modeling, 14
 membrane processes
 characteristics, 1–2, 3–4t
 electro-driven processes, 1–2
 evaluation, 2
 gas permeation, 1–2
 and mass transfer modeling, 16, 16t
 membrane bioreactors, 1–2
 membrane contactors, 1–2
 pressure-driven membrane processes, 1–2
 separation factor, 2
 supported liquid membranes, 1–2
 transmembrane flux, 2
 types, 1–2, 3–4t
- Metallic membranes, 8
- Methyl tertbutyl ether (MTBE), 98
- MF. *See* Microfiltration (MF)
- MFC. *See* Microbial fuel cell (MFC)
- MFC-MBR hybrid
 conventional MBR, 333–334, 334f
 schematic representation, 332–333, 333f
 TMP profiles, 333–334, 334f
- Michaelis-Menten equation, 222–223
- Microalgae extract concentration, 302–303, 304f
- Microbial fuel cell (MFC), 332–334, 333–334f
- Microbial membrane bioreactors
 aerobic vs. anaerobic MBRs, 220
 bio-production and separation, 219–220
 MPBR (*see* Membrane photobioreactors (MPBR))
 wastewater treatment
 activated sludge, 215–216
 aeration flow, 217
 critical flux, 218–219
 cross-flow velocity, 217
 flow velocity, 218
 food-to-microorganism ratio, 218
 fouling, 219
 HRT, 215–217
 industrial wastewaters, 216
 microfiltration/ultrafiltration, 219
 permeate flux, 217–219
 recirculation ratio, 217–218
 side-stream MBR configuration, 216–217, 216–217f
 SRT, 215–217
 submerged MBR configuration, 216–217, 216–217f
 TMP, 217–219

- Microbial mixed cultures, 232–235
- Microfiltration (MF), 25–26
 additional resistance, 38
 application, 29–30
 bulk flow, 37
 cake layer compressibility, 41
 cake layer resistance, 39–40
 constant pressure, 39
 dead-end filtration, 28
 flux, 37–38, 40–41
 equation, 38
 initial flux, 39
 volumetric flux, 38–39
 fouling resistance, 40
 hydraulic diameter, 38
 macroscopic flow, 37
 membrane resistance, 40
 Newtonian liquids, 41
 particle mass balance, 40, 40f
 resistance-in-series model, 39–40
 Reynolds numbers, 37
- Microfiltration/ultrafiltration processes, 5
- Microporous hydrophobic membranes, 155
- Mixed liquor suspended solids (MLSS), 227
- Mixed matrix membranes (MMMs), 7–8
- Modified solution-diffusion models
 binary interaction parameters estimation, 90, 90t
 diffusions coefficients, 90, 91t
 Flory-Huggins interaction parameter, 89
 Flory-Huggins thermodynamics, 89
 polymeric membrane, 89–90
 six coefficients model, 90
- Molecular weight cutoff (MWCO), 41, 42f
- MPBR. *See* Membrane photobioreactors (MPBR)
- Multivariate statistical analysis methods
 ANN modeling, 238–239
 data-driven modeling, 238
 fouling complexity, 237–238
 multilinear regression tools, 240
 PCA, 239
 PLS, 239–240
- MWCO. *See* Molecular weight cutoff (MWCO)
- N**
- Nanofiltration (NF), 25–26, 337
 application, 30–32
 charged solutes, 48–49
 dead-end filtration, 28
 uncharged solutes, 46–48
- Nanopore models, 49
- Nitrate bioreduction reaction, 332
- Nondispersive solvent extraction. *See* Membrane-based solvent extraction
- Nonselective membranes, 5
- Nuclear magnetic resonance (NMR), 20
- O**
- Off-line monitoring, MBR
 biosolids, 227
 environmentally relevant molecules, 228
 filtration performance, 230
 fouling monitoring, 228–229
 ionic species, 227–228
 microbial community, 228, 230
 micropollutants, 228
 mixed microbial cultures, 230
 sum parameters, 226–227
- Oil extraction, 302–303
- Oil-in-water (o/w) emulsions, 186–188
- Online, real-time monitoring, MBR, 230–232, 231f
- Operational expense (OPEX), 305–306
- Optical laser sensor, 21
- Organic membranes. *See* Polymeric membranes
- Organic solvent nanofiltration (OSN), 25–26
 application, 31–32
 aqueous nanofiltration, 49
 HSP approach
 components, 51–52
 distribution, 53
 general procedure, 54, 54f
 group contribution method, 51–52, 52t
 solvent permeabilities, 51
 Teas plot, 52–53, 53f
 hybrid modeling approach, 50–51, 51f
 membrane and solvent properties, 50
 permeability, 50
 permeation, 50
 relative affinity, 53–54
 solute-membrane interactions, 50
- Osmotic membrane distillation (OMD), 155, 180
- OSN. *See* Organic solvent nanofiltration (OSN)
- P**
- Permeability, 14
- Pervaporation, 1–2
 aqueous/organic mixtures and water
 separation, 74
 azeotropic mixture, 75
 bioethanol production, 315–317, 316f
 close-boiling point mixture, 75
 coupling effects (*see* Coupling effects, pervaporation)
 dense membrane, 72

- dense membranes, 7, 13
- ethyl tert-butyl ether production, 308–309, 309f
- hybrid pervaporation-distillation, 308
- hybrid pervaporation reactor, 308
- mass transfer, 13
 - evaluation, 72–73
 - multicomponent mixtures, 75–76
 - pore-flow model, 75–76, 80–81
 - solution-diffusion model, 75–79
- McCabe-Thiele diagram, 86–88, 87f
- membrane fouling, 19–20, 19f
- methanol/tetrahydrofuran mixtures separation
 - energy requirement and flux, 310, 312f
 - environmental impact, 310–314, 313f
 - hybrid distillation-pervaporation, 309–310, 311f
 - LCA, 309–310
 - pressure swing distillation, 309–314, 311f, 313f
 - product composition, 310, 312f
 - THF recovery, 309–310
- multicomponent mixture with N components, 72, 73f
- olefin-paraffin separation
 - advantages, 314–315
 - cryogenic distillation, 314
 - hybrid reaction-pervaporation, 314, 316f
 - investment and operating costs, 314–315
 - membrane/distillation hybrid system
 - configurations, 314, 315f
 - vapor permeation, 314
- organic compounds from aqueous streams
 - removal, 74
- organic/organic mixtures separation, 74
- permeation and evaporation, 71–72
- process vs. membrane performance
 - azeotropes, 84
 - driving force, 84–86
 - equimolar quaternary mixture separation, 84, 85f
 - evaluation, 82
 - liquid and vapor phase, thermodynamic equilibrium, 81–82
 - membrane separation, 81–82
 - methanol/methyl acetate, 85–86
 - methanol/water mixture separation, 83–84, 84f
 - permeabilities and selectivities, 82
 - silicone rubber mixed-matrix membrane, 82–83, 83f
- reactive pervaporation, 75
- retentate, 72
 - as separation technique, 73
- SLMs
 - dense solid membranes, 130
 - downstream pressure effect, 133, 133f
 - feed concentration effect, 130–131, 131f
 - feed temperature effect, 132–133, 132f
 - mass transfer, 121
 - membrane area, 130
 - membrane performance, 130
 - permeation flux and selectivity, 130
 - rate of molecular diffusion, 130
 - stability, 134–135, 134f
 - vapor-liquid equilibrium, 71–72
 - vapor-liquid interface, 72
- Photocatalytic membrane bioreactors, 211
- Polarization
 - concentration polarization, 16
 - concentration profile, 17–18, 17f
 - in situ monitoring techniques, 20–21
 - in pressure-driven processes, 17–18
 - temperature polarization, 16, 18, 19f
- Polymeric membranes
 - application temperature, 5
 - crystalline polymer, 5–7
 - dense membranes, 7
 - linear-chain polymers, 5–7
 - microporous membranes, 7
 - polymer materials, 5–7, 6f
 - thermoplastics, 5–7
 - thermosetting polymers, 5–7
- Polymer-IL membrane, 110–111
- Pore-flow model
 - pervaporation, 75–76
 - flux of component, 81
 - liquid permeation, 80
 - liquid-vapor interface, 80
 - mass transport, 80–81
 - transmembrane flux, 81
 - porous membranes, 14–15, 14f
- Porous membranes
 - membrane-based liquid extraction, 13
 - microfiltration and ultrafiltration, 7
 - nonselective membrane, 13
 - pore-flow model, 14–15, 14f
- Potable water production, 334–335, 335f
- Pressure-Assisted Osmosis (PAO), 62
- Pressure-driven membrane filtration
 - definition, 25–26
 - FO (*see* Forward osmosis (FO))
 - MF (*see* Microfiltration (MF))
 - module performance, 63–64
 - NF (*see* Nanofiltration (NF))
 - operation mode

- Pressure-driven membrane filtration (*Continued*)
- cross-flow filtration, 27–29, 28f
 - dead-end filtration, 27–28, 27f
 - semidead-end operation, 29
 - process modeling, 27
 - RO (*see* Reverse osmosis (RO))
 - system configuration
 - Christmas tree configuration, 34, 35f
 - diafiltration system, 33–34, 34f
 - feed-and-bleed system, 33–34, 34f
 - membrane cascade, 34–36, 35f
 - UF (*see* Ultrafiltration (UF))
- Pressure-driven membrane processes, 1–2
- application scope, 29, 29f
 - hydraulic resistance, 36–37
- Pressure retarded osmosis (PRO), 33
- Pressure swing adsorption (PSA)
- cycle sequence, 317–319, 319f
 - gas separation, 317–319
 - H₂/CH₄ mixtures separation, 317–319
 - H₂ recovery and product purity, 319–320, 320f
- Principal component analysis (PCA), 239
- Projection to latent structures (PLS), 239–240
- Protein-induced denaturation, 213, 213f
- PSA. *See* Pressure swing adsorption (PSA)
- PV driven FO-ED system, 334–335
- ## R
- Raman spectroscopy, 230–231
- Red shift, 213
- Reflection coefficient, ultrafiltration membranes, 46–48
- Resistance-in-series model, 158–160, 159f, 183
- Reverse electrodialysis (RED), 262
- electricity generation, 337
 - electrodriven membrane processes, 292–294
- Reverse electro-electrodialysis (REED), 278
- Reverse osmosis (RO), 25–26
- application, 32
 - dead-end filtration, 28
 - exponential function, 58
 - Fick's law, 57
 - osmotic equilibrium, 57
 - osmotic pressure, 55
 - Pitzer model, 55–56
 - pressure-driven permeation, 56, 57f
 - reflection coefficient, 55
 - solution-diffusion process, 56, 56f, 58
 - van't Hoff equation, 55–56
- ## S
- Selective membranes, 5
- Side-stream MBR, 210
- Silica membranes, 7
- SLMs. *See* Supported liquid membranes (SLMs)
- Solar-driven electromembrane separation, 252
- Solids residence time (SRT), 210
- Solids retention time (SRT), 215–217
- Soluble microbial products (SMP), 228–229, 234
- Solution-diffusion model
- dense membranes, 14–15, 14f
 - pervaporation, 75–76
 - activation energy, 78–79
 - flux of components, 76–77
 - permeability, 76–77
 - selectivity, 78
 - separation factor, 78
 - stages, 76–77
 - temperature dependency, 78–79
 - temperature effect on permeance, 79, 79f
- Solution phase transport number, 267
- Solvent-resistant nanofiltration (SRNF), 25–26
- Spiegler-Kedem model, 41–44
- SRT. *See* Solids retention time (SRT)
- Static transport number, 266–267
- Steric Hindrance Pore (SHP) model, 46
- Submerged membrane bioreactors, 210–211
- Supported ionic liquid membranes (SILMs), 108–109
- Supported liquid membranes (SLMs), 1–2
- advantages, 108–109
 - applications
 - electrochemical applications, 113–114
 - fuel cell applications, 113–114
 - gas separation, 111
 - liquid/liquid extraction, 113–114
 - liquid-phase microextraction, 113–114
 - pervaporation and vapor permeation, 112–113
 - separation of ions, 112
 - separation of organic compounds, 112
 - solid-phase extraction, 113–114
 - solid-phase microextraction, 113–114
 - facilitated coupled cotransport, 105–108
 - facilitated coupled counter-transport, 105–108
 - feed and stripping phases, 105–108
 - gas separation (*see* Gas separation, SLMs)
 - liquid pertraction, 105–108
 - mass transfer
 - concentration profile of component *i*, 118, 119f
 - gas feed/gas permeate, 120–121
 - liquid feed/gas permeate, 121
 - liquid/liquid applications, 119–120
 - liquid pertraction, 121–122
 - permeability, 120
 - transmembrane flux, 120
 - mechanisms, 108–109
 - membrane performance, 122–123

multicomponent gas mixture with N components, 104–105, 105–107*f*
 porous membranes, 104–105
 process performance, 122–123
 SILMs, 108–109
 simple uphill transport, 105–108
 third phase formation, 105–108
 Surface-to-ground area ratio, 222
 Sweep gas membrane distillation (SGMD), 180

T

Temperature polarization, 16, 18, 19*f*
 Tetrahydrofuran (THF), 309–314, 311–313*f*
 Thermodynamic coupling, 88–89
 Thermoplastics, 5–7
 Thermosetting polymers, 5–7
 TMP. *See* Transmembrane pressure (TMP)
 Total suspended solids (TSS), 227
 Transesterification reactions, 74
 Transmembrane pressure (TMP), 217–219, 228
 Triethanolamine (TEA) concentration, 140–141, 141*f*
 Two-phase electro-electrodialysis, 278
 Two-stage membrane cascade, 34–36, 35*f*

U

Ultrafiltration (UF), 25–26
 application, 30
 change in flux, 44–45
 flux equation, 45
 hydrodynamic equations, 42–43
 indicative rejection curves, 41, 42*f*
 membrane pore Péclet number, 43–44
 MWCO, 41, 42*f*
 one minus the retention, 41–42
 permeate flux, 44
 permeate solute concentration density, 45
 probability density function, 44–45
 retention of a solute, 41
 selectivity, 42
 selectivity-permeability trade-off, 42, 43*f*, 44
 sieving coefficient, 41–44
 Ultrasonic time-domain reflectometry (UTDR), 21
 Unimolecular diffusion (UMD), 11–12, 11*f*
 Utilization-associated products (UAP), 234

V

Vacuum membrane distillation (VMD), 180
 Volatile suspended solids (VSS), 227

W

Wall-correction parameter, 46
 Wastewater treatment
 ASM, 235
 brackish water treatment, 334–335, 335*f*
 industrial wastewater treatment
 EC-ED hybrid, 337, 338*r*
 heavy metals removal, 335–336
 tannery wastewater treatment, 336
 textile wastewater treatment, resource recovery, 337, 339*f*
 unitary cell, ED-CR process, 335–336, 336*f*
 membrane bioreactors
 activated sludge, 215–216
 aeration flow, 217
 AnMBR-MD hybrid system (*see* AnMBR-MD hybrid system)
 critical flux, 218–219
 cross-flow velocity, 217
 flow velocity, 218
 food-to-microorganism ratio, 218
 fouling, 219
 HRT, 215–217
 industrial wastewaters, 216
 membrane distillation, 326–329
 microfiltration/ultrafiltration, 219
 permeate flux, 217–219
 recirculation ratio, 217–218
 side-stream MBR configuration, 216–217, 216–217*f*
 SRT, 215–217
 submerged MBR configuration, 216–217, 216–217*f*
 TMP, 217–219
 membrane contactors, 325–326, 327–328*f*
 Water desalination
 brine discharge, 303
 CAPEX and OPEX, 305–306, 307*f*
 forward osmosis, 303, 305, 305*f*
 reverse osmosis, 303, 305, 305*f*
 seawater, 306
 SEC *vs.* specific membrane area, 305, 306*f*
 social perception, 306
 Water-in-oil (w/o) emulsions, 186–188

Z

Zeolite membranes, 7–8